LOHRMANN-OBSERVATORIUM
TECHNISCHE UNIVERSITÄT DRESDEN

OBSERVATOIRE DE PARIS
SYSTÈMES DE RÉFÉRENCE TEMPS-ESPACE
UMR8630 / CNRS

Astrometry, Geodynamics and
Astronomical Reference Systems

Astrométrie, géodynamique et
systèmes de référence astronomiques

JOURNÉES 2008 ☆

SYSTÈMES DE RÉFÉRENCE SPATIO - TEMPORELS

& X. LOHRMANN-KOLLOQUIUM

☆ DRESDEN, 22-24 SEPTEMBER

LOHRMANN-OBSERVATORIUM

TECHNISCHE UNIVERSITÄT DRESDEN
Mommsenstrasse 13, 01062 Dresden, Germany

OBSERVATOIRE DE PARIS

SYSTÈMES DE RÉFÉRENCE TEMPS-ESPACE
UMR 8630 / CNRS
61 avenue de l'Observatoire, F-75014 Paris, FRANCE

Astrometry, Geodynamics and Astronomical Reference Systems

Astrométrie, géodynamique et Systèmes de référence astronomiques

Edited by

Actes publiés par

M. SOFFEL and N. CAPITAINE

JOURNÉES 2008 ☆

SYSTÈMES DE RÉFÉRENCE SPATIO - TEMPORELS

& X. LOHRMANN-KOLLOQUIUM

☆ DRESDEN, 22-24 SEPTEMBER

ISBN 978-2-901057-63-5

TABLE OF CONTENTS

PREFACE

The Journées 2008 "Systèmes de référence spatio-temporels", with the sub-title "Astrometry, Geodynamics and Astronomical Reference Systems", were organized from 22 to 24 September 2008 at Lohrmann Observatory, Technical University in Dresden, Germany. These Journées were the nineteenth conference in this series whose main purpose is to provide a forum for researchers in the fields of Earth rotation, reference frames, astrometry and time. The Journées were organized in Paris each year from 1988 to 1992, and then alternately since 1994 in Paris (in 1996, 1998, 2000, 2004 and 2007) and other European cities, namely Warsaw in 1995 and 2005, Prague in 1997, Dresden in 1999, Brussels in 2001, Bucharest in 2002 and St. Petersburg in 2003. Nine years after the Journées 1999, the Journées 2008 were organized again in Dresden. Such an organization has been the result of an active and continuing cooperation between the Technical University of the Lohrmann Observatory and the "Systèmes de Référence Temps Espace" Department (SYRTE) of Paris Observatory. These "Journées" have been associated with the Xth "Lohrmann colloquium" which is organized, since 1958 at the Lohrmann Observatory. The meeting has been sponsored by the German Science Foundation (DFG) and the ministry of Saxony. The Proceedings are published thanks to a joint financial support from the Department SYRTE of Paris Observatory and Lohrmann Observatory.

The Journées 2008 were focused on the issues related to the recent developments in astronomical reference systems, interrelation of modern astrometry and Earth orientation, numerical standards and their relativistic aspects, and modelling and observations of global geodynamical processes. There have been presentations and discussions related to the Division 1 Commission 52 "Relativity in Fundamental astronomy" and the IAU Working Groups "Numerical standards in Fundamental astronomy" (NSFA) and "The second realization of the ICRF" (ICRF2). Meetings of the IAU Working Group NSFA and the IERS/IVS Working Groups ICRF2 have been organized in association with the Journées.

There were 94 participants from 18 different countries.

We thank here all the colleagues from all countries who have attended our Journées and participated in the scientific discussions. In addition to these scientific activities, the participants met during a social dinner at the "Italienisches Dörfchen" on Tuesday evening September 23.

The scientific programme of the meeting included 10 invited papers, 37 oral communications and 38 posters. It was composed of the five following sessions:

Session 1: Modern astrometry, time and theory of Earth's rotation;
Session 2: Relativity and numerical standards in fundamental astronomy, ephemerides;
Session 3: Global geodynamical modelling;
Session 4: Observations of global geodynamics;
Session 5: Developments in astronomical reference frames.

These Proceedings are divided into five sections corresponding to the sessions of the meeting. The Table of Contents is given on pages iii to v, the list of participants on pages vii and viii, the scientific programme on pages ix to xii and the list of posters on page xiii. The Postface on page 257 gives a preliminary announcement for the "Journées" 2010 that will be held in September 2010 in Paris.

We are very grateful to the Scientific Organizing Committee for its significant role in the elaboration of the scientific programme and to all the authors of the papers for their valuable contributions. On behalf of the SOC, we thank the Local Organizing Committee, and especially its Chair, Anke Theuser, for the very careful and efficient preparation of the meeting, the very kind welcome of the participants, and the very good local conditions and organization. We thank Ralf Langhans for his invaluable help for the preparation of the Proceedings. We are also grateful to O. Becker for his efficient technical help for the publication.

Michael SOFFEL and Nicole CAPITAINE
Chair and co-Chair of the SOC

22 July 2009

List of Participants

Akulenko, Leonid, vadimkin1@yandex.ru, *Institute for Problems in Mechanics RAS (Russia)*
Andrei, Alexandre H., oat1@on.br, *Observatorio Nacional/MCT & Observatorio do Valongo/UFRJ (Brazil)*
Angermann, Detlef, angerman@dgfi.badw.de, *DGFI (Germany)*
Biskupek, Liliane, biskupek@mbox.ife.uni-hannover.de, *Leibniz Universität Hannover (Germany)*
Bizouard, Christian, christian.bizouard@obspm.fr, *SYRTE, Observatoire de Paris (France)*
Boboltz, David, dboboltz@usno.navy.mil, *U.S. Naval Observatory (USA)*
Bolotin, Sergei, bolotin@mao.kiev.ua, *Main Astronomical Observatory (Ukraine)*
Bondarenko, Valery, vvb@miloserdie.msk.ru, *Keldysh Institute of Applied Mathematics RAS (Russia)*
Brzeziński, Aleksander, alek@cbk.waw.pl, *Space Research Center, Polish Academy of Sciences (Poland)*
Capitaine, Nicole, n.capitaine@obspm.fr, *SYRTE, Observatoire de Paris (France)*
Chapanov, Yavor, astro@bas.bg, *Central Laboratory for Geodesy (CLG-BAS) (Bulgaria)*
Damljanović, Goran, gdamljanovic@aob.bg.ac.yu, *Astronomical Observatory Belgrade (Serbia)*
Dill, Robert, dill@gfz-potsdam.de, *GFZ - Helmholtz Centre Potsdam, German RCG (Germany)*
Drewes, Hermann, drewes@dgfi.badw.de, *Deutsches Geodätisches Forschungsinstitut (Germany)*
Dumin, Yurii, dumin@yahoo.com, *Institute of Ionosphere and Radio Wave Propagation of RAS (Russia)*
Débarbat, Suzanne, Suzanne.Debarbat@obspm.fr, *SYRTE, Observatoire de Paris (France)*
Englich, Sigrid, sigrid.englich@tuwien.ac.at, *Vienna University of Technology (Austria)*
Escapa, Alberto, alberto.escapa@ua.es, *University of Alicante (Spain)*
Fetisov, Sergey, gnss.astrometry@gmail.com, *Saint-Petersburg State University (Russia)*
Fey, Alan, afey@usno.navy.mil, *U.S. Naval Observatory (USA)*
Fienga, Agnès, agnes.fienga@obs-besancon.fr, *Observatoire de Besancon (France)*
Folkner, William, william.folkner@jpl.nasa.gov, *Jet Propulsion Laboratory (USA)*
Fukushima, Toshio, Toshio.Fukushima@nao.ac.jp, *National Astronomical Observatory of Japan (Japan)*
Gambis, Daniel, daniel.gambis@obspm.fr, *SYRTE, Observatoire de Paris (France)*
Gaume, Ralph, rgaume@usno.navy.mil, *U.S. Naval Observatory (USA)*
Gerlach, Enrico, enrico.gerlach@tu-dresden.de, *TU Dresden, Lohrmann-Observatory (Germany)*
Graefe, Lutz, Lutz.Graefe@tu-dresden.de, *TU Dresden, Lohrmann-Observatory (Germany)*
Groh, Andreas, groh@ipg.geo.tu-dresden.de, *Institut für Planetare Geodäsie (Germany)*
Gross, Richard, Richard.Gross@jpl.nasa.gov, *Jet Propulsion Laboratory (USA)*
Hadjinicolaou, Christodoulos, odyssy@cytanet.com.cy, *General Constructions Company (Cyprus)*
Hilton, James, jhilton@usno.navy.mil, *U.S. Naval Observatory (USA)*
Hohenkerk, Catherine, catherine.hohenkerk@ukho.gov.uk, *HMNO @ UK Hydrographic Office (UK)*
Horwath, Martin, horwath@ipg.geo.tu-dresden.de, *TU Dresden, Lohrmann-Observatory (Germany)*
Ivanova, Tamara, itv@ipa.nw.ru, *Institute of Applied Astronomy (Russia)*
Jacobs, Christopher, Christopher.S.Jacobs@jpl.nasa.gov, *Jet Propulsion Laboratory (USA)*
Klioner, Sergei, Sergei.Klioner@tu-dresden.de, *TU Dresden, Lohrmann-Observatory (Germany)*
Kolaczek, Barbara, kolaczek@cbk.waw.pl, *Space Research Center of the PAS (Poland)*
Kosek, Wieslaw, kosek@cbk.waw.pl, *Space Research Centre, Polish Academy of Sciences (Poland)*
Krynski, Jan, krynski@igik.edu.pl, *Institute of Geodesy and Cartography (Poland)*
Kuchynka, Petr, kuchynka@imcce.fr, *IMCCE, Observatoire de Paris (France)*
Kudryavtsev, Sergey, ksm@sai.msu.ru, *Sternberg Astr. Institute of Moscow State University (Russia)*
Kudryavtseva, Natalia, natkud@rambler.ru, *Sternberg Ast. Institute of Moscow State University (Russia)*
Langhans, Ralf, ralf.langhans@tu-dresden.de, *TU Dresden, Lohrmann-Observatory (Germany)*
Le Poncin-Lafitte, Christophe, christophe.leponcin-lafitte@obspm.fr, *SYRTE, Observatoire de Paris (France)*
Liu, Jia-Cheng, ljconline@163.com, *Dep. of Astronomy, Nanjing Univ. (People's Republic of China)*
Luzum, Brian, bjl@maia.usno.navy.mil, *U.S. Naval Observatory (USA)*
Ma, Chopo, chopo.ma@nasa.gov, *Goddard Space Flight Center (USA)*
Malkin, Zinovy, malkin@gao.spb.ru, *Pulkovo Observatory (Russia)*
Manche, Hervé, manche@imcce.fr, *IMCCE, Observatoire de Paris (France)*
Markov, Yuri, vadimkin1@yandex.ru, *Moscow Aviation Institute (Russia)*
Miguel, David, davidmig@maf.uva.es, *Universidad de Valladolid (Spain)*
Müller, Jügen, mueller@ife.uni-hannover.de, *Leibniz Universität Hannover (Germany)*
Müller, Malte, malte.mueller@zmaw.de, *University Hamburg (Germany)*
Niedzielski, Tomasz, niedzielski@cbk.waw.pl, *Space Research Centre, Polish Academy of Sciences (Poland)*
Nothnagel, Axel, nothnagel@uni-bonn.de, *Inst. Geodesy and Geoinformation, Univ. Bonn (Germany)*

Olawale Y, Olasupo, whitepetaltravel@yahoo.com, *White Petal Travel Agency Limited (Nigeria)*
Pashkevich, Vladimir, pashvladvit@yandex.ru, *Central (Pulkovo) Astr. Observatory of RAS (Russia)*
Pavlovskaya, Natalya, ne_boo@list.ru, *Saint Petersburg State University (Russia)*
Perepiolkin, Vadim, vadimkin1@yandex.ru, *Moscow Aviation Institute (Russia)*
Petit, Gérard, gpetit@bipm.org, *BIPM (France)*
Petrov, Sergei, petr0v@mail.ru, *St.Petersburg State University (Russia)*
Pitjeva, Elena, evp@ipa.nw.ru, *Institute of Applied Astronomy of Russian Academy of Sciences (Russia)*
Richard, Jean-Yves, jean-yves.richard@obspm.fr, *SYRTE, Observatoire de Paris (France)*
Ron, Cyril, ron@ig.cas.cz, *Astronomical Institute, AS CR (Czech Republic)*
Rothacher, Markus, rothacher@gfz-potsdam.de, *Helmholtz Z. Potsdam Deutsches GFZ (Germany)*
Rykhlova, Lidiya, vadimkin1@yandex.ru, *Institute of Astronomy RAS (Russia)*
Rzeszótko, Alicja, alicja@cbk.waw.pl, *Space Research Center PAS (Poland)*
Rülke, Axel, ruelke@IPG.geo.tu-dresden.de, *TU Dresden (Germany)*
Seitz, Manuela, seitz@dgfi.badw.de, *DGFI (Germany)*
Seitz, Florian, seitz@bv.tum.de, *Institut für Astronomische und Physikalische Geodäsie, TUM (Germany)*
Seoane, Lucia, lucia.seoane@obspm.fr, *SYRTE, Observatoire de Paris (France)*
Sherafati, Nima, nimasherafati@gmail.com, *Teheran Central University (Iran)*
Sidorenkov, Nikolay, sidorenkov@mecom.ru, *Hydrometcenter of Russia (Russia)*
Skurikhina, Elena, sea@ipa.nw.ru, *Institute of Applied Astronomy of RAS (Russia)*
Smirnov, Sergey, microsoft-suxx@mail.ru, *Saint-Petersburg State University (Russia)*
Soffel, Michael, soffel@rcs.urz.tu-dresden.de, *TU Dresden, Lohrmann-Observatory (Germany)*
Souchay, Jean, Jean.Souchay@obspm.fr, *SYRTE, Observatoire de Paris (France)*
Stamatakos, Nick, stamatakos.nick@usno.navy.mil, *US Naval Observatory (USA)*
Štefka, Vojtech, stefka@ig.cas.cz, *Astronomical Institution (Czech Republic)*
Sündermann, Jügen, juergen.suendermann@zmaw.de, *Inst. of Oceanography, Univ. Hamburg (Germany)*
Teyssandier, Pierre, Pierre.Teyssandier@obspm.fr, *SYRTE, Observatoire de Paris (France)*
Theuser, Anke, anke.theuser@tu-dresden.de, *TU Dresden, Lohrmann-Observatory (Germany)*
Thomas, Maik, mthomas@gfz-potsdam.de, *Deutsches GeoForschungsZentrum (Germany)*
Trofimov, Dmitriy, astro.dm.trofimov@gmail.com, *Saint-Petersburg State University (Russia)*
Tsvetkov, Alexander, A.S.Tsvetkov@inbox.ru, *Astr. Inst. of St. Petersburg state University (Russia)*
Verestchagina, Iraida, ver-iraida@yandex.ru, *Central Astronomical Observatory at Pulkovo RAS (Russia)*
Vondrák, Jan, vondrak@ig.cas.cz, *Astronomical Institute (Czech Republic)*
Wallace, Patrick, patrick.wallace@stfc.ac.uk, *STFC Rutherford Appleton Lab (UK)*
Winkelnkemper, Timo, timo@uni-bonn.de, *Meteorological Institute University Bonn (Germany)*
Yagudina, Eleonora I., eiya@ipa.nw.ru, *Institute of Applied Astronomy (Russia)*
Yatskiv, Yaroslav, yatskiv@mao.kiev.ua, *Main Astronomical Observatory of NAS Ukraine (Ukraine)*
Zerhouni, Wassila, wassila.zerhouni@obspm.fr, *SYRTE, Observatoire de Paris (France)*
Zharov, Vladimir, zharov@sai.msu.ru, *Sternberg State Astronomical Institute (Russia)*
Zschocke, Sven, sven.zschocke@tu-dresden.de, *TU Dresden, Lohrmann-Observatory (Germany)*

Scientific programme

Scientific Organizing Commitee: M. Soffel (Germany, Chair), N. Capitaine (France, co-Chair), A. Brzeziński (Poland); P. Defraigne (Belgium), T. Fukushima (Japan), S. Klioner (Germany), D. D. McCarthy (USA), J. Vondrák (Czech Republic), Y. Yatskiv (Ukraine)

Local Organizing Commitee: Anke Theuser (Chair), Lutz Graefe, Ralf Langhans, Sven Zschocke

Monday 22 September

09:00 - 09:15 Opening of Journées 2008 & X. Lohrmann-Kolloquium

Session 1: Modern Astrometry, Time and Theory of Earth's Rotation
Chair: N. Capitaine

Invited presentations

09:15 - 09:45 S. Klioner, M. Soffel
The relativistic reference systems as a tool to model Earth rotation

09:45 - 10:15 H. Schuh, S. Englich
Models for high accurate space geodetic observations

Oral presentations

10:15 - 10:30 V. Brumberg, T. Ivanova
On General Earth's Rotation Theory

10:30 - 11:00 *Coffee Break*

Session 1: continuation
Chair: Ya. Yatskiv

11:00 - 11:15 P. Teyssandier
Some recent developments in relativistic modeling of time and frequency transfers

11:15 - 11:30 T. Fukushima
Canonical and Universal Elements of Rotational Motion of Triaxial Rigid Body

11:30 - 11:45 J. Vondrák et. al.
Towards a long-term parametrization of precession

11:45 - 12:00 V. Pashkevich
Investigation of the short periodic terms of the Rigid and Non-Rigid Earth Rotation Series

12:00 - 12:30 Short Review of Posters (M. Soffel)

12:30 - 14:00 *Lunch Break*

Session 2: Relativity and Numerical Standards in Fundamental Astronomy, Ephemerides
Chair: T. Fukushima

Invited presentations

14:00 - 14:30 B. Luzum et. al.
Current Status of the IAU Working Group for Numerical Standards of Fundamental Astronomy

14:30 - 15:00 G. Petit
Relativistic aspects in Astronomical standards and the IERS Conventions

Oral presentations

15:00 - 15:15 N. Capitaine
Nomenclature and numerical standards for IAU models and IERS Conventions for Earth rotation

15:15 - 15:30 P. Wallace
Recent SOFA Developments

15:30 - 16:00 *Coffee Break*

Session 2: continuation
Chair: S. Klioner

16:00 - 16:15 W. Folkner
The Planetary Ephemeris Reference Frame

16:15 - 16:30 E.V. Pitjeva
Ephemerides EPM2008: the updated model, constants, data

16:30 - 16:45 E.I. Yagudina
Lunar numerical theory EPM2008 ephemeris from analysis of LLR data

16:45 - 17:00 A. Fienga et. al.
New planetary INPOP: from model to observations

17:00 - 17:15 H. Manche et. al.
The de Sitter effect in INPOP ephemerides

17:15 - 19:00 Poster Session

Tuesday 23 September

Session 3: Global Geodynamical Modelling
Chair: T. Vondrák

Invited presentations

09:00 - 09:30 A. Brzeziński
Recent advances in theoretical modeling and observation of Earth rotation at daily and subdaily periods

09:30 - 10:00 R. Gross
An Empirical Model for the Effect of Long Period Ocean Tides on Polar Motion

Oral presentations

10:00 - 10:15 A. Rülke et. al.
Realisation of the Terrestrial Reference System by a global GPS network as a basis for global geodynamic investigations

10:15 - 10:30 A. Escapa, T. Fukushima
Analytical computation of the translational internal motion of a simple non-isobarycentric three-layer Earth model

10:30 - 11:00 *Coffee Break*

Session 3: continuation
Chair: A. Brzeziński

11:00 - 11:15	Y. Yatskiv On optimal detection and estimation of the FCN parameters
11:15 - 11:30	A.K. Sen et. al. Is length of day time series normally distributed?
11:30 - 11:45	T. Winkelnkemper Atmospheric simulations of Earth rotation parameter variations
11:45 - 12:00	R. Dill et. al. Hydrological induced Earth rotation variations from stand-alone and dynamically coupled simulations
12:00 - 12:15	M. Müller Earth rotation parameters obtained from a dynamically coupled atmosphere-hydrosphere model
12:15 - 12:30	F. Seitz et. al. Simulation of Earth rotation parameters with a dynamic Earth system model over a period of 200 years between 1860 and 2059
12:30 - 12:45	A. Groh et. al. Determination of crustal deformations and sea-level changes in the Baltic Sea region
12:45 - 14:00	*Lunch Break*

Session 4: Observations of Global Geodynamics
Chair: J. Souchay

Invited presentations

14:00 - 14:30	C. Bizouard et. al. Combination of EOP observations from different techniques
14:30 - 15:00	M. Rothacher GGOS and the Combination of Space Geodetic Techniques

Oral presentations

15:00 - 15:15	N. Stamatakos Recent Improvements in IERS Rapid Service / Prediction Center Products
15:15 - 15:30	Z. Malkin Improving EOP prediction using combination procedures
15:30 - 16:00	*Coffee Break*

Session 4: continuation
Chair: A. Nothnagel

16:00 - 16:15	W. Kosek et. al. Contribution of wide-band oscillations excited by the fluid excitation functions to the prediction errors of the pole coordinates data
16:15 - 16:30	S. Fetisov et. al. Earth orientation parameters from GLONASS observations
16:30 - 16:45	M. Horwath, R. Dietrich Geophysical mass redistributions from GRACE: the case of the Antarctic and Greenland ice sheets
16:45 - 17:00	N. Sidorenkov The decade fluctuations in the Earth's rotation and in climate characteristics
17:00 - 17:15	Ya. Chapanov et. al. 22-year oscillations of UT1, core angular momentum and geomagnetic field
17:15 - 17:30	L. Biskupek, J. Müller Lunar Laser Ranging and Earth Orientation
17:30 - 17:45	W. Zerhouni et. al. What could bring LLR observations in determining the position of the celestial pole
19:00 -	*Social Dinner*

Wednesday 24 September

Session 5: Developments in Astronomical Reference Frames
Chair: M. Soffel

Invited presentations

09:00 - 09:30 C. Ma
Present and Future Radio Reference Frames

09:30 - 10:00 C. Jacobs
Realizations of the celestial reference system at different wavelengths

Oral presentations

10:00 - 10:15 A.H. Andrei et. al.
Astrometric and Photometric Variability in Quasars

10:15 - 10:30 V. Zharov et. al.
Apparent motion of the radio sources and stability of the celestial reference frame

10:30 - 11:00 *Coffee Break*

Session 5: continuation
Chair: D. Gambis

11:00 - 11:15 S. Bolotin, S. Lytvyn
Investigation of stability of radio sources from arc-length method.

11:15 - 11:30 D. Boboltz et. al.
VLBA Imaging of Celestial Reference Frame Sources at 24 and 43 GHz

11:30 - 11:45 J. Souchay et. al.
The LQAC (Large Quasar Astrometric Catalogue) : principle of compilation and related studies

11:45 - 12:00 R. Gaume
The Joint Milli-Arcsecond Pathfinder Survey (J-MAPS): Introduction and Science Possibilities

12:00 - 12:15 A. Tsvetkov et. al.
The use of wavelet technique for data processing of mass stellar catalogues

12:15 - 12:30 Closing of Journées 2008 & X. Lohrmann Kolloquium

12:30 - 14:00 *Lunch Break*

Meeting of the NSFA IAU WG: 14:00 - 17:30

LIST OF POSTERS

SESSION 1

Yu.V. Dumin *Influence of the Relativistic Lambda-Term on the Measured Values of the Earth's Rotation Deceleration*

V. Stefka et. al. *The Descartes project: Solving the rotational Earths equations in rectangular coordinates for a non-rigid Earth*

SESSION 2

N. Capitaine, B. Guinot *The astronomical units*

S. Débarbat *A new historical view on the fundamental constants*

C. Hohenkerk et. al. *Numerical Standards in The Astronomical Almanac*

S. Kudryavtsev, N. Kudryavtseva *Analytical representation of Pluto ephemeris*

C. Le Poncin-Lafitte *Some remarks about relativistic deep space navigation*

E.V. Pitjeva, E.M. Standish *Values of some astronomical constants proposed for NSFA*

P. Kuchynka et. al. *Improving the asteroid perturbations modeling in planetary ephemerides*

SESSION 3

L. Akulenko et. al. *Multi-frequency Analysis of Oscillation-Rotational Motion of Deformable Earth*

C. Bizouard et. al. *Atmospheric and oceanic normal modes in polar motion*

V. Bondarenko, V. Perepiolkin *Simulation of Irregularity of Deformable Earth Rotation: Interpolation and Forecast*

Ya. Chapanov, D. Gambis *Change of the Earth moment of inertia during the observed UT1 response to the 11-year solar cycles*

L. Cotterau, J. Souchay *An analytical modeling of the rotation of Venus*

V. Dehant et. al. *Rotation and internal dynamics from future geodesy experiment*

S. Englich et. al. *Direct estimation of tidally induced Earth rotation variations observed by VLBI*

L. Karimova et. al. *Non-linear vector ANN predictor for EOP forecast*

D. Miguel et. al. *Contributions of the third degree harmonics to the nutation of a two-layer and a three-layer Earth models*

J. Nastula et. al. *Comparison of regional hydrological excitation of polar motion derived from hydrological models and the GRACE gravity field data.*

T. Niedzielski, W. Kosek *Regional sea level prediction and its relation to El Niño/Southern Oscillation*

A. Rzeszotko et. al. *Comparison of time-frequency characteristics between geodetic and geophysical excitation functions of polar motion*

L. Seoane et. al. *Hydrological excitation of polar motion*

SESSION 4

N. Pavlovskaya et. al. *Atmospheric excitation of diurnal polar motion*

M. Kudryashova et. al. *Contribution of the complete GLONASS constellation to the estimation of nutation rates*

SESSION 5

A. Albert Aguilar et. al. *Photometric identification of QSOs for Astrometric Reduction of CCD Images*

G. Damljanovic *Separation proper motions from orbital one of double or multiple stars by using Hipparcos and ground-based observations*

A. Fey, D. Boboltz *Absolute Astrometry from VLBA RDV Observations*

S. Kurdubov, E. Skurikhina *Source Selection for ICRF2 defining set from Source Position Time Series Analysis*

J. Liu, Z. Zhu *Rotation Curve of Outer Disk from UCAC2 Proper Motion*

V. L'vov et. al. *Forthcoming close approaches of Jupiter and Saturn to geodetic radio sources*

Z. Malkin, E. Popova *Analysis of source motions derived from position time series*

Session 1

MODERN ASTROMETRY, TIME AND THEORY OF EARTH'S ROTATION

ASTROMÉTRIE MODERNE, TEMPS ET THÉORIE DE LA ROTATION DE LA TERRE

THE RELATIVISTIC REFERENCE SYSTEMS AS A TOOL TO MODEL EARTH ROTATION

S.A. KLIONER, M.H. SOFFEL
Lohrmann Observatory,
Dresden Technical University, 01062 Dresden, Germany
e-mail: Sergei.Klioner@tu-dresden.de

ABSTRACT. Relativistic modelling of Earth rotation represents one of the most complicated problems of Applied Relativity. The relativistic reference systems of IAU (2000) give a suitable theoretical framework for such a modelling. Recent developments in the post-Newtonian theory of rigid Earth rotation are reported below. We describe the STF approach to compute the post-Newtonian torque, the framework to compute transformations between all relativistic time scales as the relativistic scaling of various parameters of the theory.

1. EARTH ROTATION IN THE RELATIVISTIC CONTEXT

Early attempts to model rotational motion of the Earth in a relativistic framework (see, e.g., Brumberg, 1972) made use of only one relativistic references system to describe both rotational and translational equations of motion. That reference system was usually chosen to be quite similar to the BCRS. This resulted in a mathematically correct, but physically inadequate coordinate picture of rotational motion. For example, from that coordinate picture a prediction of seasonal variations of the LOD with an amplitude of about 75 microseconds has been put forward.

At the end of the 1980s a better reference system for modelling of Earth rotation has been constructed and after a number of modifications and improvements has been adopted as GCRS in the IAU 2000 Resolutions. The GCRS implements the Einstein's equivalence principle and represents a reference system in which the gravitational influence of external matter (the Moon, the Sun, planets, etc.) is reduced to tidal potentials. Thus, for physical phenomena occurring in the vicinity of the Earth the GCRS represents a reference system, the coordinates of which are, in a sense, as close as possible to physically measurable quantities. This substantially simplifies the interpretation of the coordinate description of physical phenomena localized in the vicinity of the Earth. One important application of the GCRS is modelling of Earth rotation. The price to pay when using GCRS is that one should deal not only with one relativistic reference system, but with several reference systems, the most important of which are BCRS and GCRS. This makes it necessary to clearly and carefully distinguish between parameters and quantities defined in the GCRS and those defined in the BCRS.

2. RELATIVISTIC EQUATIONS OF EARTH ROTATION

The model which is used in this investigation was discussed and published by Klioner *et al.* (2001) and recalled in Klioner *et al.* (2008). Let us, however, repeat these equations one again not going into physical details of the model since we will need them in our subsequent discussion. The post-Newtonian equations of motion (omitting numerically negligible terms as explained in Klioner *et al.* (2001)) read

$$\frac{d}{dT}\left(C^{ab}\,\omega^{b}\right)=\sum_{l=1}^{\infty}\frac{1}{l!}\,\varepsilon_{abc}\,M_{bL}\,G_{cL}+L^{a}(\mathbf{C},\omega,\mathbf{\Omega}_{\rm iner}), \tag{1}$$

where $\mathbf{C}=C^{ab}$ is the post-Newtonian tensor of inertia and $\omega=\omega^{a}$ is the angular velocity of the post-Newtonian Tisserand axes (Klioner, 1996), T = TCG, M_L are the multipole moments of the Earth's gravitational field defined in the GCRS, G_L are the multipole moments of the external tidal gravitoelectric field in the GCRS. In the simplest situation (a number of mass monopoles) G_L are explicitly given by Eqs. (19)–(23) of Klioner *et al.* (2001).

The additional torque L^a depends on $\mathbf{C}$, ω, as well as on the angular velocity $\mathbf{\Omega}_{\rm iner}$ describing the

relativistic precessions (geodetic, Lense-Thirring and Thomas precessions). The definition of $\mathbf{\Omega}_{\rm iner}$ can be found, e.g., in Klioner *et al.* (2001). A detailed discussion of L^a, its structure and consequences will be published elsewhere (Klioner et al. 2009).

The model of rigidly rotating multipoles (Klioner *et al.*, 2001) represents a set of formal mathematical assumptions that make the general mathematical structure Eqs. (1) similar to that of the Newtonian equations of rotation of a rigid body. The assumptions are

$$C^{ab} = P^{ac}\, P^{bd}\, \overline{C}^{cd}, \quad \overline{C}^{cd} = \text{const} \tag{2}$$

$$M_{a_1 a_2 \ldots a_l} = P^{a_1 b_1}\, P^{a_2 b_2} \ldots P^{a_l b_l}\, \overline{M}_{b_1 b_2 \ldots b_l}, \quad \overline{M}_{b_1 b_2 \ldots b_l} = \text{const}, \quad l \geq 2, \tag{3}$$

where the orthogonal matrix $P^{ab}(T)$ is assumed to be related to the angular velocity ω^a used in (1) as

$$\omega^a = \frac{1}{2}\, \varepsilon_{abs}\, P^{db}(T)\, \frac{d}{dT}\, P^{dc}(T). \tag{4}$$

The meaning of these assumptions is that both the tensor of inertia C^{ab} and the multipole moments of the Earth's gravitational field M_L are "rotating rigidly" and that their rigid rotation is described by the same angular velocity ω^a that appears in the post-Newtonian equations of rotational motion. It means that in a reference system obtained from the GCRS by a time-dependent rotation of spatial axes both the tensor of inertia and the multipole moments of the Earth's gravitational field are constant.

No acceptable definition of a physically rigid body exists in General Relativity. The model of rigidly rotating multipoles represent a minimal set of assumptions that allows one to develop the post-Newtonian theory of rotation in the same manner as one usually does within Newtonian theory for rigid bodies. In the model of rigidly rotating multipoles only those properties of Newtonian rigid bodies are saved which are indeed necessary for the theory of rotation. For example, no assumption on local physical properties ("local rigidity") is made. It has not been proved as a theorem, but it is rather probable that no physical body can satisfy assumptions (2)–(4). The assumptions of the model of rigidly rotating multipoles will be relaxed in a later stage of the work when a non-rigid Earth will be discussed. On the other hand, such a model has been always tacitly used in the model of SLR data.

3. POST-NEWTONIAN EQUATIONS OF ROTATIONAL MOTION IN NUMERICAL COMPUTATIONS

Looking at the post-Newtonian equations of motion (1)–(4) one can formulate several problems to be solved before the equations can be used in numerical calculations:

A. How to parametrize the matrix P^{ab}?

B. How to compute M_L from the standard models of the Earth gravity field?

C. How to compute G_L from a solar system ephemeris?

D. How to compute the torque $\varepsilon_{abc}\, M_{bL}\, G_{cL}$ out of M_L and G_L?

E. How to deal with different time scales (TCG, TCB, TT, TDB) appearing in the equations of motion, solar system ephemerides, used models of Earth gravity, etc.?

F. How to treat the relativistic scaling of various parameters when using TDB and/or TT instead of TCB and TCG?

G. How to find relativistically meaningful numerical values for the initial conditions and various parameters?

Question A has been already discussion in Section 3 of Klioner et al. (2008). Questions B–D are considered in Section 4 below. Question E is discussed in Section 5. Question F is the subject of Section 6. An analysis of question G will be published elsewhere.

4. STF MODEL FOR THE TORQUE

The relativistic torque requires computations with STF tensors M_L and G_L. For this project special numerical algorithms for numerical calculations have been developed. The detailed algorithms and their derivation will be published elsewhere. Let us give here only the most important formulas. For each l the component $D_a = \varepsilon_{abc}\, M_{bL-1}\, G_{cL-1}$ of the torque in the right-hand side of Eq. (1) can be computed as ($A_l = 4\,l\,\pi\,l!/(2l+1)!!$, $a^+_{lm} = \sqrt{l(l+1) - m(m+1)}$)

$$D_1 = \frac{1}{A_l}\left(\sum_{m=0}^{l-1} a^+_{lm}\,\left(-\mathcal{M}^R_{lm}\,\mathcal{G}^I_{l,m+1} + \mathcal{M}^I_{l,m+1}\,\mathcal{G}^R_{lm}\right) + \sum_{m=1}^{l-1} a^+_{lm}\,\left(\mathcal{M}^I_{lm}\,\mathcal{G}^R_{l,m+1} - \mathcal{M}^R_{l,m+1}\,\mathcal{G}^I_{lm}\right)\right), \tag{5}$$

$$D_2 = \frac{1}{A_l}\left(\sum_{m=0}^{l-1} a^+_{lm}\,\left(-\mathcal{M}^R_{lm}\,\mathcal{G}^R_{l,m+1} + \mathcal{M}^R_{l,m+1}\,\mathcal{G}^R_{lm}\right) + \sum_{m=1}^{l-1} a^+_{lm}\,\left(-\mathcal{M}^I_{lm}\,\mathcal{G}^I_{l,m+1} + \mathcal{M}^I_{l,m+1}\,\mathcal{G}^I_{lm}\right)\right), \tag{6}$$

$$D_3 = \frac{2}{A_l}\sum_{m=1}^{l} m\,\left(\mathcal{M}^I_{lm}\,\mathcal{G}^R_{lm} - \mathcal{M}^R_{lm}\,\mathcal{G}^I_{lm}\right). \tag{7}$$

The coefficients $\mathcal{G}^R_{lm}$ and $\mathcal{G}^I_{lm}$ characterizing the tidal field can be computed from Eqs. (19)–(23) of Klioner *et al.* (2001) as explicit functions of the parameters of the solar system bodies: their masses, positions, velocities and accelerations. A Fortran code to compute $\mathcal{G}^R_{lm}$ and $\mathcal{G}^I_{lm}$ for $l < 7$ and $0 \le m \le l$ has been generated automatically with a specially written software package for *Mathematica*. It is possible to develop a sort of recursive algorithm to compute $\mathcal{G}^R_{lm}$ and $\mathcal{G}^I_{lm}$ for any l similar to the corresponding algorithms for, e.g., Legendre polynomials.

The coefficients $\mathcal{M}^R_{lm}$ and $\mathcal{M}^I_{lm}$ characterizing the gravitational field of the Earth can be computed as

$$\mathcal{M}^R_{l0} = \frac{l!}{(2l-1)!!}\left(\frac{4\pi}{2l+1}\right)^{1/2} M_E\,R_E^l\,C_{l0}, \tag{8}$$

$$\mathcal{M}^R_{lm} = (-1)^m\,\frac{1}{2}\,\frac{l!}{(2l-1)!!}\left(\frac{4\,\pi}{2l+1}\,\frac{(l+m)!}{(l-m)!}\right)^{1/2} M_E\,R_E^l\,C_{lm},\ 1 \le m \le l, \tag{9}$$

$$\mathcal{M}^I_{lm} = (-1)^{m+1}\,\frac{1}{2}\,\frac{l!}{(2l-1)!!}\left(\frac{4\,\pi}{2l+1}\,\frac{(l+m)!}{(l-m)!}\right)^{1/2} M_E\,R_E^l\,S_{lm},\ 1 \le m \le l, \tag{10}$$

where M_E is the mass of the Earth, R_E its radius, C_{lm} and S_{lm} are usual harmonics (potential coefficients) of the Earth gravitational field. If only Newtonian terms are considered in the torque this formulation with STF tensors is fully equivalent to the classical formulation with Legendre polynomials (e.g., Bretagnon *et al.*, 1997, 1998). If the relativistic terms are taken in account, the only known way to express the torque is that with STF tensors.

5. TIME TRANSFORMATIONS

An important aspect of relativistic Earth rotation theory is the treatment of different relativistic time scales. The numerical code described in (Klioner *et al.*, 2008) contains a subsystem dealing with the transformations between time scales TCB, TCG, TT and TDB. The transformation between TDB and TT *at the geocenter* (all the transformations in this Section are meant to be "evaluated at the geocenter") are computed along the lines of Section 3 of (Klioner, 2008b). Namely,

$$\mathrm{TT} = \mathrm{TDB} + \Delta\mathrm{TDB}(\mathrm{TDB}), \tag{11}$$

$$\mathrm{TDB} = \mathrm{TT} - \Delta\mathrm{TT}(\mathrm{TT}), \tag{12}$$

$$\mathrm{TCG} = \mathrm{TCB} + \Delta\mathrm{TCB}(\mathrm{TCB}), \tag{13}$$

$$\mathrm{TCB} = \mathrm{TCG} - \Delta\mathrm{TCG}(\mathrm{TCG}), \tag{14}$$

so that

$$\frac{d\Delta\mathrm{TDB}}{d\mathrm{TDB}} = A_{\mathrm{TDB}} + B_{\mathrm{TDB}}\,\frac{d\Delta\mathrm{TCB}}{d\mathrm{TCB}}, \tag{15}$$

$$A_{\mathrm{TDB}} = \frac{L_B - L_G}{1 - L_B}, \tag{16}$$

$$B_{\mathrm{TDB}} = \frac{1 - L_G}{1 - L_B} = A_{\mathrm{TDB}} + 1, \tag{17}$$

$$\frac{d\Delta\mathrm{TT}}{d\mathrm{TT}} = A_{\mathrm{TT}} + B_{\mathrm{TT}}\,\frac{d\Delta\mathrm{TCG}}{d\mathrm{TCG}}, \tag{18}$$

$$A_{\mathrm{TT}} = \frac{L_B - L_G}{1 - L_G}, \tag{19}$$

$$B_{\mathrm{TT}} = \frac{1 - L_B}{1 - L_G} = 1 - A_{\mathrm{TT}}, \tag{20}$$

$$\frac{d\Delta\mathrm{TCB}}{d\mathrm{TCB}} = F(\mathrm{TCB}) = \frac{1}{c^2}\,\alpha(\mathrm{TCB}) + \frac{1}{c^4}\,\beta(\mathrm{TCB}), \tag{21}$$

$$\frac{d\Delta\mathrm{TCG}}{d\mathrm{TCG}} = \frac{F(\mathrm{TCG} - \Delta\mathrm{TCG})}{1 + F(\mathrm{TCG} - \Delta\mathrm{TCG})}, \tag{22}$$

where functions α and β are given by Eqs. (3.3)–(3-4) of (Klioner, 2008b) and Eq. (22) represents a computational improvement of Eq. (3.8) of (Klioner, 2008b). Clearly, the derivatives $\frac{d\Delta\mathrm{TCB}}{d\mathrm{TCB}}$ and $\frac{d\Delta\mathrm{TCG}}{d\mathrm{TCG}}$ must be expressed as functions of TDB and TT, respectively, when used in (15)–(18).

The differential equations for ΔTDB and ΔTT are first integrated numerically for the whole range of the used solar system ephemeris (any ephemeris with DE-like interface can be used with the code). The initial conditions for ΔTDB and ΔTT should be chosen according to the IAU 2006 Resolution defining TDB: for $JD_{\mathrm{TT}} = 2443144.5003725$ one has $JD_{\mathrm{TDB}} = 2443144.5003725 - 6.55 \times 10^5/86400$ and vice verse. The results of the integrations for the pairs ΔTDB and $\frac{d\Delta\mathrm{TDB}}{d\mathrm{TDB}}$, and ΔTT and $\frac{d\Delta\mathrm{TT}}{d\mathrm{TT}}$ are stored with a selected step in the corresponding time variable (TDB for ΔTDB and its derivative, and TT for ΔTT and its derivative). A cubic spline on the equidistant grid is then constructed for each of these 4 quantities. The accuracy of the spline representation is automatically estimated using additional data points computed during the numerical integration. These additional data points lie between the grid points used for the spline and are only used to control the accuracy of the spline. The splines precomputed and validated in this way are stored in files and read in by the main code upon request. These splines are directly used for time transformation during the numerical integrations of Earth rotation. Although this spline representation requires significantly more stored coefficients than, for example, a representation with Chebyshev polynomials with the same accuracy, the spline representation has been chosen because of its extremely high computational efficiency. More sophisticated representations may be implemented in future versions of the code.

6. RELATIVISTIC SCALING AND TIME SCALES

Let us again consider the post-Newtonian equations of rotational motion (1)–(4). Obviously, there are two classes of quantities entering these equations that are defined in the BCRS and GCRS and, therefore, naturally parametrized by TCB and TCG, respectively. It is important to realize that the post-Newtonian equations of motion are only valid if non-scaled time scales TCG and TCB are used. If TT and/or TDB are needed, the equations should be changed correspondingly.

The relevant quantities defined in the GCRS and parametrized by TCG are: (1) the orthogonal matrix P^{ab}, angular velocity ω^a and corresponding angles φ, ψ and ω with which they are parametrized (see, Klioner *et al.*, 2008); (2) the tensor of inertia C^{ab}; (3) the multipole moment of Earth's gravitational field M_L. In principle, (a) G_L and (b) Ω^a_{iner} are also defined in the GCRS and parametrized by TCG, but these quantities are computed using positions $\mathbf{x}_A$, velocities $\mathbf{v}_A$ and accelerations $\mathbf{a}_A$ of solar system bodies. The orbital motion of solar system bodies are modelled in BCRS and parametrized by TCB or TDB. The definition of G_L is conceived in such a way that positions, velocities and accelerations of solar system bodies in BCRS should be taken at the moment of TCB corresponding to the required moment of TCG with spatial location taken at the geocenter (Klioner *et al.*, 2001; Klioner, Voinov, 1993; Soffel *et al.*, 2003). Let us recall that the transformation between TCB and TCG is a 4-dimensional one that involves the spatial location of an event.

In all theoretical works aimed to derive and/or analyze the rotational equations of motion in the GCRS one uses TCG as coordinate time scale parametrizing the equations. Although the natural time variable for the equations of Earth rotation is TCG, in principle, using a corresponding re-parametrization any time scale (including TCG, TT, TCB and TDB) can be used as independent time variable. Thus, simple rescaling of the first and second derivatives of the angles entering the equations of rotational motion should be applied to use TT instead of TCG:

$$\frac{d\theta}{d\mathrm{TCG}} = (1 - L_G)\,\frac{d\theta}{d\mathrm{TT}}, \tag{23}$$

$$\frac{d^2\theta}{d\mathrm{TCG}^2} = (1 - L_G)^2\,\frac{d^2\theta}{d\mathrm{TT}^2}, \tag{24}$$

where θ is any of the angles φ, ψ and ω used in the equations of motion to parametrize the orientation of the Earth. If TDB is used as independent variable the corresponding formulas are more complicated:

$$\frac{d\theta}{d\mathrm{TCG}} = (1 - L_G)\left(\left.\frac{d\mathrm{TT}}{d\mathrm{TDB}}\right|_{\mathbf{x}_E}\right)^{-1}\frac{d\theta}{d\mathrm{TDB}}, \tag{25}$$

$$\frac{d^2\theta}{d\mathrm{TCG}^2} = (1 - L_G)^2\left(\left.\frac{d\mathrm{TT}}{d\mathrm{TDB}}\right|_{\mathbf{x}_E}\right)^{-2}\frac{d^2\theta}{d\mathrm{TDB}^2} - (1 - L_G)^2\left(\left.\frac{d\mathrm{TT}}{d\mathrm{TDB}}\right|_{\mathbf{x}_E}\right)^{-3}\left.\frac{d^2\mathrm{TT}}{d\mathrm{TDB}^2}\right|_{\mathbf{x}_E}\frac{d\theta}{d\mathrm{TDB}}, \tag{26}$$

where the derivatives of TT w.r.t. TDB should be evaluated at the geocenter (i.e., for $\mathbf{x} = \mathbf{x}_E$). These relations must be substituted into the equations of rotation motion to replace the derivatives of the angles φ, ψ and ω w.r.t. TCG as appear e.g., in Eqs. (7)–(9) of (Bretagnon *et al.*, 1998). It is clear that the parametrization with TDB makes the equations more complicated.

The values of the parameters naturally entering the equations of rotational motion must be interpreted as unscaled (TCB-compatible or TCG-compatible) values. If scaled (TT-compatible or TDB-compatible) values are used, the scaling must be explicitly taken into account. The relativistic scaling of parameters read (see e.g. Klioner, 2008a):

$$GM_A^{\mathrm{TT}} = (1 - L_G)\,GM_A^{\mathrm{TCG}}, \quad GM_A^{\mathrm{TCG}} = GM_A^{\mathrm{TCB}}, \quad GM_A^{\mathrm{TDB}} = (1 - L_B)\,GM_A^{\mathrm{TCB}}, \tag{27}$$

$$X^{\mathrm{TT}} = (1 - L_G)\,X^{\mathrm{TCG}}, \quad x^{\mathrm{TDB}} = (1 - L_B)\,x^{\mathrm{TCB}}, \tag{28}$$

$$V^{\mathrm{TT}} = V^{\mathrm{TCG}}, \quad v^{\mathrm{TDB}} = v^{\mathrm{TCB}}, \tag{29}$$

$$A^{\mathrm{TT}} = (1 - L_G)^{-1}\,A^{\mathrm{TCG}}, \quad a^{\mathrm{TDB}} = (1 - L_B)^{-1}\,a^{\mathrm{TCB}}, \tag{30}$$

where GM_A is the mass parameter of a body, x, v, and a are parameters represents spatial coordinates (distances), velocities and accelerations in the BCRS, respectively, while X, V, and A are similar quantities in the GCRS.

Now, considering the source of the numerical values of the parameters used in the equations of Earth rotation we can see the following.

a. The position $\mathbf{x}_A$, velocities $\mathbf{v}_A$, accelerations $\mathbf{a}_A$ and mass parameters GM_A of the massive solar system bodies are taken from standard JPL ephemerides and are TDB-compatible.

b. The radius of the Earth comes together with the potential coefficients C_{lm} and S_{lm} from a model of the Earth's gravity field (e.g., GEMT3 was used in SMART). These values come from SLR and dedicated techniques like GRACE. GCRS with TT-compatible quantities is used to process these data. Therefore, the values of the radius of the Earth is TT-compatible. Obviously, C_{lm} and S_{lm} have the same values when used with any time scale. The mass parameter GM_E of the Earth coming with the Earth gravity models is also TT-compatible.

c. From the definitions of $\mathcal{M}^R_{lm}$ and $\mathcal{M}^I_{lm}$ given above and formulas for G_L given by Eqs. (19)–(23) of Klioner *et al.* (2001), it is easy to see that the TCG-compatible torque $F^a = \sum_{l=1}^{\infty} \frac{1}{l!}\,\varepsilon_{abc}\,M_{bL}\,G_{cL}$ can be computed using TDB-compatible values of mass parameters GM_A^{TDB}, positions $\mathbf{x}_A^{\mathrm{TDB}}$, velocities $\mathbf{v}_A^{\mathrm{TDB}}$ and accelerations $\mathbf{a}_A^{\mathrm{TDB}}$ of all external bodies, TDB-compatible value of the mass parameter of the Earth GM_E^{TDB} and the value of Earth radius formally rescaled from TT to TDB as $R_E^{\mathrm{TDB}} = (1 - L_B)\,(1 - L_G)^{-1}\,R_E^{\mathrm{TT}}$. Denoting the resulting torque by F^a_{TDB}, it can be seen that the TCG-compatible value is $F^a_{\mathrm{TCG}} = (1 - L_B)^{-1}\,F^a_{\mathrm{TDB}}$.

d. The values of the Earth's moments of inertia $\mathcal{A}_i$, $i = 1, 2, 3$ can be represented as $G\mathcal{A}_i = GM_E R_E^2 k_i$, where k_i is a factor characterizing the distribution of the matter inside Earth. Clearly, the factors k_i do not depend on the scaling. Therefore, the moments of inertia can be scaled as

$$\mathcal{A}_i^{\rm TT} = (1 - L_G)^3 \, \mathcal{A}_i^{\rm TCG}. \tag{31}$$

The last question is how to interpret the values of the moments of inertia $\mathcal{A}_i = (A, B, C)$ and the initial conditions for the angles φ, ψ and ω and their derivatives given in (Bretagnon *et al.*, 1998). Obviously, the initial angles at J2000 are independent of the scaling. For the other parameters in question it is not possible to clearly claim if the given values are TDB-compatible or TT-compatible. Arguments in favor of both interpretations can be given. The rigorous solution here is only possible when all calculations leading to these quantities are repeated in the framework of General Relativity. In this paper we prefer to interpret the SMART values of $\mathcal{A}_i$, $\dot{\varphi}$, $\dot{\psi}$ and $\dot{\omega}$ as being TT-compatible. Therefore, if TDB is used as independent variable, the values of the derivatives should be changed accordingly. For any of these angles one has

$$\frac{d\theta}{d\mathrm{TDB}} = \left(\left. \frac{d\mathrm{TT}}{d\mathrm{TDB}} \right|_{\mathbf{x}_E} \right) \frac{d\theta}{d\mathrm{TT}} \, . \tag{32}$$

Thus, we have all tools to treat correctly the relativistic scaling of all relevant parameters of the Earth rotation theory as well as relativistic time scales. A numerical integration of Earth rotation over the full range of DE403 shows that the effect of these two factor is relatively small: periodic effects of an amplitude of $0.15 - 0.25$ μas (depending on the angle) and a period of 18 years plus secular trends in φ and ψ (-68.4 and 74.7 μas per century, respectively). Further details will be published elsewhere.

REFERENCES

Bretagnon, P., Francou, G., Rocher, P., Simon, J.L., 1997, "Theory of the rotation of the rigid Earth", A&A , 319, 305–317

Bretagnon, P., Francou, G., Rocher, P., Simon, J.L., 1998, "SMART97: a new solution for the rotation of the rigid Earth", A&A , 329, 329–338

Brumberg, V.A. 1972, Relativistic Celestial Mechanics, Nauka: Moscow, in Russian

Klioner, S.A., 2008a, "Relativistic scaling of astronomical quantities and the system of astronomical units", A&A, 478, 951–958

Klioner, S.A., 2008b, "Relativistic astrometry and astrometric relativity", In: A Giant Step: from Milli- to Micro-arcsecond Astrometry, W.Jin, I.Platais, M.Perryman (eds.) Proc. of the IAU Symposium 248, Cambridge University Press, Cambridge, 356–362

Klioner, S.A., Soffel, M., Xu. C., Wu, X., 2001, "Earth's rotation in the framework of general relativity: rigid multipole moments", In: Influence of geophysics, time and space reference frames on Earth rotation studies (Proc. Journées' 2001), N. Capitaine (ed.), Paris Observatory, Paris, 232–238

Klioner, S.A., Soffel, M., Le Poncin-Lafitte, Chr., 2008, "Towards the relativistic theory of precession and nutation", In: The Celestial Reference Frame for the Future (Proc. of Journes'2007), N. Capitaine (ed.), Paris Observatory, Paris, 139-142

Klioner, S.A., Gerlach, E., Soffel, M., 2009, Rigorous treatment of geodetic precession in the theory of Earth rotation, in preparation

Klioner, S.A., Voinov, A.V., 1993, "Relativistic Theory of Reference Systems in Closed Form", Phys. Rev. D 48, 1451–1461

Soffel, M. *et al.*, 2003, "The IAU 2000 resolutions for astrometry, celestial mechanics and metrology in the relativistic framework: explanatory supplement", AJ , 126, 2687–2706

MODELS FOR HIGH ACCURATE SPACE GEODETIC OBSERVATIONS

S. ENGLICH, H. SCHUH
Vienna University of Technology, Institute of Geodesy and Geophysics, Advanced Geodesy
Gußhausstraße 27-29, 1040 Vienna, Austria
sigrid.englich@tuwien.ac.at

ABSTRACT. Since the introduction of modern space geodetic techniques, such as Very Long Baseline Interferometry (VLBI) and Global Navigation Satellite Systems (GNSS), the precision of instruments and observations has been constantly increasing. Within the process of transferring the observations into results a multitude of assumptions has to be applied for modeling phenomena concerning signal dispersion, site displacement and reference point deformation, earth orientation, geopotential and relativistic effects. Thus it is desirable that the used models are always improved concurrently to the technological development of the space techniques so as to provide the best possible results. The consistent combination and integration of the various space geodetic techniques and their related models is the main task of IAG's Global Geodetic Observing System (GGOS). In this paper we give examples about conventional models and recent progress in modeling. Focus is paid on the characterization of geophysical phenomena related to the Earth's crust, atmosphere, and rotation, and the effects on VLBI and GNSS observations and some relevant results are shown.

1. INTRODUCTION

One of the big challenges for the Global Geodetic Observing System (GGOS) organization is the development of an observing system capable of measuring variations in the Earth's shape, gravity field, and rotation with an accuracy and consistency of 0.1 to 1 ppb, with high spatial and temporal resolution (GGOS, website). For example target accuracy of the terrestrial reference frame is to determine station positions better than 1 mm/year. This is a very ambitious goal which requires, besides the improvement of the observation techniques themselves, highly accurate models. Roughly estimated this implies that if we apply up to let us say ten astronomical and geophysical models during the data processing each model needs to be precise to approximately 0.1-0.2 mm in order to reach the anticipated accuracy for the station position. Depending on the technique a variety of model assumptions has to be considered, which cannot be treated exhaustively in this paper. For a complete register of the conventional models we refer to the Conventions of the International Earth Rotation and Reference Systems Service (IERS Conventions, 2003). The aim of this paper is to highlight some of the current advances in modeling and to discuss necessary steps for the future evolution of the model assumptions related to

- Earth rotation parameter (ERP) variations,
- troposphere modeling - mapping functions,
- site displacements
  - thermal deformation of VLBI antennas and definition of the reference temperature,
  - tectonic plate motion and modeling non-linear effects,
  - atmosphere loading and choice of the reference pressure.

2. EARTH ROTATION PARAMETER VARIATIONS

At present tidally induced variations of the ERP are considered in the parameter estimation. The tidal variations are subclassified to diurnal and sub-diurnal ocean tidal variations in all three ERP (pole coordinates x_p, y_p, and dUT1) and zonal tidal variations with periods from around 5 days to 18.6 years

in dUT1 or the length of day (LOD), respectively. Zonal tidal variations are primarily caused by the deformation of the solid Earth due to the zonal part of the tidal potential from Sun, Moon, and the planets. A minor part of these variations is also generated by the deformation of the world oceans, i.e. by long-period ocean tides. The model for zonal tidal ERP variations recommended in the IERS Conventions currently does not treat these two effects separately. Recent studies (Englich et al., 2008; Gross, 2009) show that this joint model exhibits some deficiencies especially for the fortnightly term. A revision of the modeled contribution of the long-period ocean tides is recommended and also a separation of the two effects in the Conventions would be advisable for the sake of clarity. The present conventional model for the effects of diurnal and sub-diurnal ocean tides is based on empirical ocean tide models deduced from satellite altimetry measurements. In Steigenberger et al. (2008) this model was compared to sub-daily ERP variations derived from observation data of Very Long Baseline Interferometry (VLBI) and the Global Positioning System (GPS). The comparison showed that the space geodetic techniques are sensitive to the effect of the triaxial shape of the Earth on the ERP, which also occurs in the sub-daily frequency band. Deviations to the IERS model, which confirm these results were also found in a study by Englich et al. (2008). The effect of the triaxiality on polar motion is already covered in the IERS Conventions, whereas the effect on the Earth rotation rate, the so-called semi-diurnal spin libration is not yet considered. Keeping in mind the goal to provide the most accurate models, the short-period dUT1 variations should be extended with a model for the semi-diurnal spin libration.

3. TROPOSPHERE MODELING - MAPPING FUNCTIONS

On the occasion of the inclusion of the Vienna Mapping Function 1 (VMF1) and the Global Mapping Function (GMF) to the IERS Conventions we would like to show an example of the advantageous performance of the VMF1 compared to the Niell Mapping Function (NMF) (Boehm et al., 2006a and 2006b). Changes of the station heights due to changes in the mapping functions can very well be predicted by a rule of thumb (Boehm et al., 2006a). The left part of figure 1 shows such predicted station height changes determined on a global 15 ° by 15 ° grid as provided by the European Centre for Medium-Range Weather Forecasts (ECMWF). The right part of figure 1 displays the estimated station height changes determined from the analysis of one year of global GPS observations (Boehm et al., 2007). The largest estimated changes appear at the coast of Antarctica with 1.3 cm, which is in very good agreement with the predictions for this region (dark red in the figure 1 corresponds to a height change of 13-15 mm).

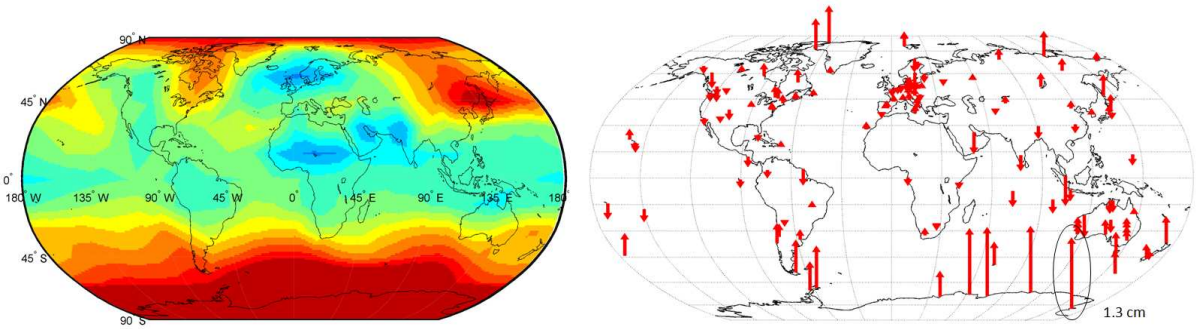

Figure 1: Predicted and estimated station height changes when using VMF1 instead of NMF.

4. SITE DISPLACEMENTS

For the comprehensive treatise of all effects causing a change of the station positions please refer once more to the IERS Conventions. Here we only pick out some interesting new approaches or indicate open questions, starting with the thermal deformation of VLBI telescopes and the need for a clear definition of the reference temperature.

4.1 Thermal deformation of VLBI antennas

VLBI antennas are subject to structural deformations due to temperature variations, which can cause

variations of the coordinates of the reference point of several millimeters. Therefore a model for VLBI antenna thermal deformation is proposed in the IERS Conventions to be used in routine VLBI processing. This model requires thermal expansion coefficients of the material the antenna is built of and usually the surrounding temperature as input. In a paper by Wresnik et al. (2007) it could be illustrated for two exemplary antennas that the application of the surrounding temperature is not always appropriate, but that it would be preferable to use the real structure temperature. In the normal case the structure temperature of the telescopes is not available. The alternative to providing all sites with temperature sensors to collect the structure temperature would be the development and application of temperature penetration models, as shown in the paper referred above. Another important input to a thermal deformation model is the already mentioned reference temperature. For the definition of the reference temperature (which has still not been defined by the international community) there are three options:

- mean air temperature from temperature records of stations,
- mean temperature during a certain time period from numerical weather models,
- temperature according to the Global Pressure and Temperature model (GPT), see Boehm et al. (2007b).

For further details and a discussion of these three options see Boehm et al. (2008a).

4.2 Tectonic plate motion

As a second example we present a work by Heinkelmann et al. (2008), which deals with modeling of tectonic plate motion in reference frame solutions. Conventionally, tectonic plate motion is modeled within a terrestrial reference frame (TRF) solution by a constant velocity, i.e. as linear motion or piecewise linear function of the observing sites. This approach is not always appropriate, especially in case of episodic events such as large earthquakes. These incidents are often followed by co- and post-seismic deformations causing local site displacements, which are not necessarily linear. In special cases TRF solutions could be improved by non-linear deformation models for stations suffering from the consequences of an earthquake. In the study a post-seismic relaxation model for the 2002 Denali earthquake from GPS deformation analysis was applied to VLBI data. One TRF solution including a refined non-linear model for the motion of the VLBI site GILCREEK was compared to other TRF solutions and to the ITRF2005 (using linear deformation models) and to single VLBI session solutions. The root mean square of the coordinates with respect to the single VLBI solutions is given in table 1. IGG07R04 denotes a former VLBI TRF solution with a linear deformation model for station GILCREEK, whereas IGG08R01 stands for the new solution comprising the refined non-linear station model. The application of such a refined model is especially mandatory when fixing station coordinates or developing a time-dependent solution.

RMS	ITRF2005	IGG07R04	IGG08R01	GPS data
Latitude (mm)	3.8	6.1	3.1	13.8
Longitude (mm)	3.8	5.1	3.1	17.6
Height (mm)	8.3	7.8	7.5	10.5
3D (mm)	9.8	11.2	8.7	24.7

Table 1: RMS w.r.t. single VLBI solutions (Heinkelmann et al., 2008)

4.3 Atmosphere loading

Atmosphere loading can cause vertical crustal displacements of up to 25 mm (the horizontal displacement amounts to about 1/3 of the vertical). In principle there are two methods to calculate the effect of atmosphere loading on the station coordinates:

- using geophysical models (Green's functions, numerical weather models, load Love numbers, ...),
- using empirical models based on site-dependent data.

One simple form of such an empirical model is e.g. $dh = (p - \underline{p}) \cdot r$, with p: pressure at the station, $\underline{p}$: reference pressure and r: empirically determined regression coefficient. Currently atmosphere loading is applied in VLBI but not in GNSS solutions. For reasons of consistency it would be important to find a common way of considering atmosphere loading by both communities. Basically, there are various options concerning the application of atmosphere loading corrections. It can either be accounted for at the observation level or considered as a posteriori corrections to the final coordinate time series. If normal equations of different space techniques are to be combined, atmosphere loading could also be applied at the so-called "stacking" level, which requires very careful book-keeping and data treatment. A very detailed investigation of this issue can be found in Boehm et al. (2009). Another open question related to this issue is the definition of the reference pressure to which given or computed station coordinates are related. Referring to the ambitious accuracy goals stated at the beginning the following estimations can be made for the reference pressure: 1. If we consider the simple model for the atmosphere loading and assume a regression coefficient of -0.5 mm/hPa then the reference pressure has to be known to at least 2 hPa to reach the millimeter level; 2. Since a pressure difference of 1 hPa corresponds to approximately 10 m height difference, the heights to which the pressure values refer have to be known better than 20 m. General requirements for the reference pressure field are:

- It should be "accurate enough" (mostly < 2 hPa).
- The mean pressure should refer to a height field.
- Easy calculation for any point on the Earth surface (subroutine for coordinates).
- Unambiguously determinable now and in future.

One possible option for the realization of the reference pressure would be the usage of a rather simple model for global pressure and also temperature like the GPT (Global Pressure and Temperature model, Boehm et al., 2007b), which has already been mentioned in section 4.1. For a more detailed treatment on reference pressure refer to Boehm et al. (2008b).

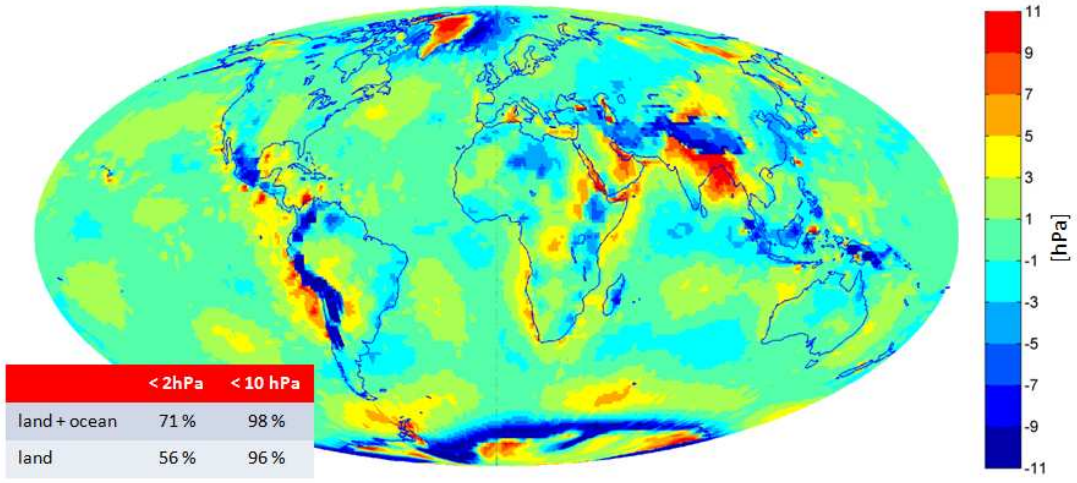

Figure 2: 2.0 ° x 2.5 ° grid of mean surface pressure values (ECMWF) vs. GPT model (differences in hPa)

5. CONCLUDING REMARKS

- We gave an overview and examples about models for highly accurate geodetic observations without claiming the list to be exhaustive.
- Having the sights on the sub-millimeter there are still pending tasks and open questions to deal with regarding the applied models.

- It is of major importance for GGOS that the same geophysical model constants and standards are applied consistently for all geodetic techniques.
- It is advisable to agree on the treatment of surface loading effects and to clearly define reference pressure and temperature.

6. REFERENCES

Boehm J., Werl B., and Schuh H., 2006a, "Troposphere mapping functions for GPS and very long baseline interferometry from European Centre for Medium-Range Weather Forecasts operational analysis data", J. Geophys. Res. , 111, B02406, doi:10.1029/2005JB003629.

Boehm J., Niell A. E., Tregoning P., and Schuh H., 2006b, "Global Mapping Function (GMF): A new empirical mapping function based on numerical weather model data", Geoph. Res. Letters, 33, L07304, doi:10.1029/2005GL025546.

Boehm J., Mendes-Cerveira P. J., Schuh H., and Tregoning P., 2007a, "The impact of mapping functions for the neutral atmosphere delay based on numerical weather models in GPS data analysis", in Dynamical Planet - Monitoring and Understanding a Dynamic Planet with Geodetic and Oceanographic Tools, IAG Symposium Series, 130, Springer-Verlag, Rizos C. and Tregoning P. (eds.), pp. 837-843.

Boehm J., Heinkelmann R., and Schuh H., 2007b, "Short note: A global model of pressure and temperature for geodetic applications", Journal of Geodesy, Vol. 81, No. 10, pp. 679-683.

Boehm J., Heinkelmann R., Schuh H., and Nothnagel A., 2008a, "Validation of mean temperature values as provided by GPT", IVS Memorandum 2008-003v01, ftp://ivscc.gsfc.nasa.gov/pub/memos/ivs-2008-003v01.pdf.

Boehm J., Schuh H., Mendes Cerveira P. J., and Heinkelmann R., 2008b, "Reference Pressure for the Global Geodetic Observing System (GGOS)", IVS Memorandum 2008-002v01, ftp://ivscc.gsfc.nasa.gov/pub/memos/ivs-2008-002v01.pdf.

Boehm J., Heinkelmann R., Mendes Cerveira P. J., Pany A., and Schuh H., 2009, "Atmospheric loading corrections at the observation level in VLBI analysis", Journal of Geodesy (under review).

GGOS, website, http://www.iag-ggos.org/,(status April 2009).

IERS Conventions (2003), IERS Technical Note 32, D.D. McCarthy and G. Petit (eds), Frankfurt am Main: Verlag des Bundesamts für Kartographie und Geodäsie, 2004.

Englich S., Weber R., and Schuh H., 2008, "Empirical validation of the conventional model for length of day variations due to zonal tides", Proceedings of the Journes 2007 "Systèmes de Référence Spatio-Temporels", N. Capitaine (ed.), Observatoire de Paris, pp. 184-187.

Englich S., Heinkelmann R., and Schuh H., 2008, "Re-Assessment of Ocean Tidal Terms in High-Frequency Earth Rotation Variations Observed by VLBI", Proceedings of the 5th IVS General Meeting 2008, A. Finkelstein and D. Behrend (eds.), Saint Petersburg, pp. 314-318.

Gross R. S., 2009, "Ocean tidal effects on Earth rotation", Submitted to the Proceedings of the 16th International Symposium on Earth Tides "New Challenges in Earth's Dynamics".

Heinkelmann R., Freymueller J., and Schuh H., 2008, "A Postseismic Relaxation Model for the 2002 Denali Earthquake from GPS Deformation Analysis Applied to VLBI Data", Proceedings of the 5th IVS General Meeting 2008, A. Finkelstein and D. Behrend (eds.), Saint Petersburg, pp. 335-340.

Steigenberger P.,Tesmer V., MacMillan D., Thaller D., Rothacher M., Fritsche M., Rlke A., and Dietrich R., 2008, "Subdaily Earth rotation observed by GPS and VLBI", Geophysical Research Abstracts, Vol. 10, EGU2008-A-03739, EGU General Assembly 2008.

Wresnik J., Haas R., Boehm J., and Schuh H., 2007, "Modeling thermal deformation of VLBI antennas with a new temperature model", Journal of Geodesy, Vol. 81, No.6-8, pp. 423-431.

ON GENERAL EARTH'S ROTATION THEORY

V.A. BRUMBERG, T.V. IVANOVA
Institute of Applied Astronomy
10, Kutuzov quay, St. Petersburg, 191187, Russia
e-mail: itv@ipa.nw.ru

This paper dealing with the general problem of the rigid–body rotation of the three–axial Earth represents a straightforward extension of (Brumberg and Ivanova, 2007) where the simplified Poisson equations of rotation of the axially symmetrical Earth have been considered. The aim of the present paper is to reduce the equations of the translatory motion of the major planets and the Moon and the equations of the Earth's rotation around its centre of mass to the secular system describing the evolution of the planetary and lunar orbits (independent of the Earth's rotation) and the evolution of the Earth's rotation (depending on the planetary and lunar evolution). In doing so, the techniques of the General Planetary Theory (GPT) (Brumberg, 1995) and the Poisson Series Processor (PSP) (Ivanova, 1995) have been used. The complete equations in terms of the planetary–lunar eccentric and oblique Laplace–type variables $a_i, \bar{a}_i, b_i, \bar{b}_i$ $(i = 1, 2, \ldots, 9)$ and the Earth's rotation parameters $p = (p_i)$, $\bar{p} = (\bar{p}_i)$ $(i = 1, \ldots, 4)$ being the functions of the Euler angles, have the form

$$\dot{X} = i\,\mathcal{N}[PX + R(X,t)], \tag{1}$$

where X and R standing for the vectors of the variables and right–hand members, respectively,

$$X = (a, \bar{a}, b, \bar{b}, p, \bar{p}), \qquad R = (R_1, \ldots, R_6) \tag{2}$$

are vectors with 44 components (a, b and R_i with $i = 1, 2, 3, 4$ for the planets and the Moon are 9–vectors, p and R_5, R_6 for the Earth's rotation are 4–complex–value vectors). $\mathcal{N}$ and P are 44×44 diagonal matrices of the structure

$$\begin{aligned} \mathcal{N} &= \mathrm{diag}(N, N, N, N, n, n, n, n, n, n, n, n), \\ P &= \mathrm{diag}(E_{(9)}, -E_{(9)}, E_{(9)}, -E_{(9)}, E_{(4)}, -E_{(4)}), \end{aligned} \tag{3}$$

$n = -\dfrac{1}{2}\Omega$, Ω being the mean Earth's rotation velocity, N is 9×9 diagonal matrix of the mean motions of the major planets and the Moon, $E_{(9)}$ and $E_{(4)}$ are the unitary matrices of dimension 9×9 and 4×4, respectively. The transformation from X to new variables $Y = (a, \bar{a}, b, \bar{b}, q, \bar{q})$

$$X = Y + \Gamma(Y,t) \tag{4}$$

results in a new system

$$\dot{Y} = i\,\mathcal{N}\big[PY + F(Y,t)\big]. \tag{5}$$

Functions Γ and F are found by iterations as series in powers of Y with quasi–periodic coefficients of t

$$U = R - \mathcal{N}^{-1}\Gamma_Y \mathcal{N} U^*\,, \tag{6}$$

$$\Gamma_t + i\,(\Gamma_Y \mathcal{N} P Y - \mathcal{N} P \Gamma) = i\,\mathcal{N} U^+\,, \tag{7}$$

$$U = U^* + U^+\,, \qquad F = U^*\,. \tag{8}$$

The splitting of U is aimed to ensure the integration of (7) without t–secular terms. Since planetary and lunar secular system was already constructed in GPT, the transformation

$$p_i = q_i + \Gamma_{4+i} \qquad (i = 1, \ldots, 4) \tag{9}$$

transforms the Earth's rotation equations into the secular system

$$\dot{q}_i = i\; n(q_i + F_{4+i}) \tag{10}$$

with

$$F_\kappa = U^*_\kappa(q, \bar{q}, \alpha, \bar{\alpha}, \beta, \bar{\beta}). \tag{11}$$

Here $\alpha, \bar{\alpha}, \beta, \bar{\beta}$ are 9–vectors of slowly changing Laplace–type elements for the major planets and the Moon. Expressions (9) describe the short–period nutation depending on the mean longitudes of the Sun, the Moon and major planets. System (10) is responsible for precession and long–period nutation since it includes lunar evolutionary variables α_9 and β_9 related to the motions of the lunar perigee and node.

The work is now in progress and the final results will be published elsewhere in the future.

REFERENCES

Brumberg, V.A., 1995, "Analytical techniques of celestial mechanics", Springer, Heidelberg, 236 pp.

Ivanova, T.V., 1995, "PSP: A New Poisson series processor", The Proceedings of the IAU Symposium 172, Paris, 1995, eds. S.Ferraz-Mello, B.Morando and J. -E. Arlot), pp. 283–284.

Brumberg, V.A., Ivanova, T.V., 2007, "Precession/nutation solution consistent with the general planetary theory", Celest. Mech. Dyn. Astr. 97, pp. 189–210.

SOME RECENT DEVELOPMENTS IN RELATIVISTIC MODELING OF TIME AND FREQUENCY TRANSFERS

P. TEYSSANDIER
SYRTE, Observatoire de Paris, CNRS, UPMC
61, avenue de l'Observatoire, 75014 Paris, France
e-mail: Pierre.Teyssandier@obspm.fr

ABSTRACT. We determine the relativistic effects of the tidal potentials on the time and frequency transfers between an atomic clock orbiting round the Earth and a ground clock. These effects are estimated for ESA Atomic Clocks Ensemble in Space (ACES) mission planned to be launched in 2012.

1. INTRODUCTION

The ACES mission is planned to compare a cold atom clock PHARAO onboard the ISS with terrestrial clocks by the mean of a microwave link. PHARAO is expected to reach a frequency stability of $1 \cdot 10^{-16}$ for an integration time of ten days, with a relative accuracy of $1 \cdot 10^{-16}$ (see Blanchet et al. 2001 and Duchayne et al. 2007). A primary objective of ACES will be to compare ground clocks in common view below the $1 \cdot 10^{-17}$ level after one day of integration. This level of performance requires to determine the influence of the tidal potentials on the frequency shifts in the vicinity of the Earth.

2. GENERAL FORMULA GIVING THE FREQUENCY SHIFT

We assume that space-time can be covered by a global coordinate system $x^\alpha = (x^0, x^i) \equiv (ct, \boldsymbol{x})$, in which the metric

$$ds^2 = g_{\mu\nu} dx^\mu dx^\nu \tag{1}$$

is such that

$$g_{\mu\nu} = \eta_{\mu\nu} + h_{\mu\nu}, \qquad \eta_{\mu\nu} = \text{diag}\,(1, -1, -1, -1). \tag{2}$$

The coordinate travel time $t_B - t_A$ of a photon between an emission point $x_A = (ct_A, \boldsymbol{x}_A)$ and a reception point $x_B = (ct_B, \boldsymbol{x}_B)$ may be considered as a function of $\boldsymbol{x}_A, t_B$ and $\boldsymbol{x}_B$, so that we can write

$$t_B - t_A = \mathcal{T}_r(\boldsymbol{x}_A, t_B, \boldsymbol{x}_B), \tag{3}$$

where $\mathcal{T}_r(\boldsymbol{x}_A, t_B, \boldsymbol{x}_B)$ represents what we call the "reception time transfer function". For the decomposition of the metric given by Eq. (2), the function $c\mathcal{T}_r(\boldsymbol{x}_A, t_B, \boldsymbol{x}_B)$ may be written in the form

$$c\mathcal{T}_r(\boldsymbol{x}_A, t_B, \boldsymbol{x}_B) = |\boldsymbol{x}_B - \boldsymbol{x}_A| + \Delta_r(\boldsymbol{x}_A, t_B, \boldsymbol{x}_B), \tag{4}$$

where $\Delta_r(\boldsymbol{x}_A, t_B, \boldsymbol{x}_B)$ is of the order of the gravitational perturbation $h_{\mu\nu}$.

The knowledge of $\Delta_r(\boldsymbol{x}_A, t_B, \boldsymbol{x}_B)$ enables to treat both the problems of time transfers and of frequency transfers. Indeed, consider a light signal emitted at point x_A by an observer A moving with a unit 4-velocity vector $u_A^\alpha = dx_A^\alpha/ds_A$ and received at point x_B by an observer B moving with a unit 4-velocity vector $u_B^\alpha = dx_B^\alpha/ds_B$. Let ν_A be the frequency of the signal as measured by A at x_A and ν_B the frequency of the signal as measured by B at x_B. A simple reasoning shows that within the geometric optics approximation the frequency shift between x_A and x_B is given by the formula

$$\frac{\nu_A}{\nu_B} = \frac{u_A^0}{u_B^0} \frac{1 - \boldsymbol{N}_{AB} \cdot \frac{\boldsymbol{v}_A}{c} + \frac{\partial \Delta_r}{\partial x_A^i} \frac{v_A^i}{c}}{1 - \boldsymbol{N}_{AB} \cdot \frac{\boldsymbol{v}_B}{c} - \frac{\partial \Delta_r}{c \partial t_B} - \frac{\partial \Delta_r}{\partial x_B^j} \frac{v_B^j}{c}}, \qquad \boldsymbol{N}_{AB} = \frac{\boldsymbol{x}_B - \boldsymbol{x}_A}{|\boldsymbol{x}_B - \boldsymbol{x}_A|}, \tag{5}$$

where $\boldsymbol{v}_A = (d\boldsymbol{x}/dt)_A$ and $\boldsymbol{v}_B = (d\boldsymbol{x}/dt)_B$ are the coordinate velocities of observers A and B, respectively. It follows from $g_{\mu\nu} u^\mu u^\nu = 1$ that u_A^0 and u_B^0 may be calculated by the relation

$$u^0 = \frac{dx^0}{ds} = \left[1 + h_{00} + 2h_{0i}\frac{v^i}{c} - (\delta_{ij} - h_{ij})\frac{v^i v^j}{c^2}\right]^{-1/2} \tag{6}$$

applied to the observers A and B, respectively.

The formula (5) shows that it is sufficient to determine $\Delta_r(\boldsymbol{x}_A, t_B, \boldsymbol{x}_B)$ at the order $1/c^2$ when the frequency shift is required at the order $1/c^3$.

3. EFFECT OF THE TIDAL POTENTIALS

Since we are concerned here by time and frequency transfers between a satellite of the Earth and a ground station, we now suppose that the coordinate system $(ct, \boldsymbol{x})$ constitutes a local nonrotating geocentric reference system (GCRS). Then it may be assumed with a sufficient approximation that the gravitational potentials are given by (see Klioner & Soffel 2000):

$$G_{00} = 1 - \frac{2}{c^2}W + O(1/c^4), \tag{7}$$

$$G_{0i} = O(1/c^3), \tag{8}$$

$$G_{ij} = -\left(1 + \frac{2\gamma}{c^2}W\right)\delta_{ij} + O(1/c^4), \tag{9}$$

where γ is the well-known post-Newtonian parameter involved in light deflection ($\gamma = 1$ in general relativity) and W may be decomposed as

$$W(t, \boldsymbol{x}) = W_\oplus(t, \boldsymbol{x}) + W^{(T)}(t, \boldsymbol{x}) + Q_i x^i + O(1/c^2), \tag{10}$$

where $W_\oplus(t, \boldsymbol{x})$ is the potential of the Earth , $W^{(T)}(t, \boldsymbol{x})$ is the tidal potential and Q_i is the non geodesic acceleration of the Earth center of mass with respect to the GCRS. At the order $O(1/c^3)$, the ratio ν_A/ν_B is given by

$$\frac{\nu_A}{\nu_B} = \frac{1 - \boldsymbol{N}_{AB}\cdot\frac{\boldsymbol{v}_A}{c}}{1 - \boldsymbol{N}_{AB}\cdot\frac{\boldsymbol{v}_B}{c}}\left(1 + \frac{v_A^2 - v_B^2}{2c^2}\right) + \left(\frac{\delta\nu}{\nu}\right)_g, \tag{11}$$

where $(\delta\nu/\nu)_g$ contains all the contributions of the gravitational field:

$$\begin{aligned}\left(\frac{\delta\nu}{\nu}\right)_g =& \frac{1}{c^2}(W_A - W_B)\left[1 - \frac{1}{c}\boldsymbol{N}_{AB}.(\boldsymbol{v}_A - \boldsymbol{v}_B)\right] \\ &+ \frac{\partial\Delta_r}{\partial x_A^i}\frac{v_A^i}{c} + \frac{\partial\Delta_r}{c\partial t_B} + \frac{\partial\Delta_r}{\partial x_B^j}\frac{v_B^j}{c} + O(c^{-4}).\end{aligned} \tag{12}$$

It follows from Eq. (8) that the contributions of G_{0i} may be neglected. So the expression of $\Delta_r(\boldsymbol{x}_A, t_B, \boldsymbol{x}_B)$ reduces to (see Linet & Teyssandier 2002):

$$\Delta_r(\boldsymbol{x}_A, t_B, \boldsymbol{x}_B) = \frac{1}{c^2}(\gamma + 1)|\boldsymbol{x}_B - \boldsymbol{x}_A|\int_0^1 W(z_-^\alpha(\lambda))d\lambda + O(1/c^3), \tag{13}$$

the integral being taken along the null straight line in Minkowski space-time defined by the parametric equations

$$z_-^0(\lambda) = -\lambda|\boldsymbol{x}_B - \boldsymbol{x}_A| + x_B^0, \quad z_-^i(\lambda) = -\lambda(x_B^i - x_A^i) + x_B^i.$$

At the order $1/c^3$, the potentials $W_\oplus$ and $W^{(T)}(t, \boldsymbol{x})$ involved in Eqs. (12) and (13) may be replaced by their respective Newtonian expressions. Moreover the contribution of the non geodesic acceleration to $(W_A - W_B)/c^2$ is completely negligible since $|c^{-2}Q_i x^i| < 10^{-20}$.

The contributions of $W_\oplus(t, \boldsymbol{x})$ were analyzed in Blanchet et al. (2001), Duchayne et al. (2007), Le Poncin-Lafitte & Lambert (2007), and Linet & Teyssandier (2002). So we discuss only the contributions of the tidal potentials. The dominant effects are due to the Moon ($\leftmoon$) and to the Sun ($\odot$). Putting

$$h = r_B - r_A, \quad \zeta_A = \frac{h}{r_A}, \quad \kappa_A = \frac{|\boldsymbol{x}_B - \boldsymbol{x}_A|}{r_A}, \tag{14}$$

we get to a sufficient approximation:

$$\left(\frac{\delta\nu}{\nu}\right)_{g,T} \approx \sum_{K=(\!|,\odot} \frac{GM_K}{2c^2 D_K}\frac{r_A^2}{D_K^2}\left\{\zeta_A(2+\zeta_A)\right.$$
$$\left.-3\kappa_A(\boldsymbol{d}_K\cdot\boldsymbol{N}_{AB})[2(\boldsymbol{d}_K\cdot\boldsymbol{n}_A)+\kappa_A(\boldsymbol{d}_K\cdot\boldsymbol{N}_{AB})]\right\}, \tag{15}$$

where

$$\boldsymbol{n}_A=\frac{\boldsymbol{x}_A}{r_A},\quad \boldsymbol{n}_B=\frac{\boldsymbol{x}_B}{r_B},\quad \boldsymbol{d}_K=\frac{\boldsymbol{D}_K}{D_K}, \tag{16}$$

$\boldsymbol{D}_K$ being the vector position of the body K exerting a tidal influence. Since they are slowly varying with respect to time, the values of $\boldsymbol{D}_{(\!|}$ and $\boldsymbol{D}_\odot$ may be taken at any instant in the range $t_A \le t \le t_B$.

For the ACES mission, we have $h \approx 400$ km. So $\zeta_A \approx 0.063$. Moreover, we may admit that a comparison of clocks will be acceptable only when the elevation angle of the ISS over the horizon of the ground station will be greater than 20°. Then, $0.063 \le \kappa_A \le 0.154$. Under these conditions, Eq. (15) leads to inequalities as follow

$$\left|\left(\frac{\delta\nu}{\nu}\right)_{g,T}\right|_{(\!|} \le 2.6\cdot10^{-17}, \qquad \left|\left(\frac{\delta\nu}{\nu}\right)_{g,T}\right|_{\odot} \le 9.6\cdot10^{-18}. \tag{17}$$

We conclude that the influence of the tidal potentials will be negligible in the comparison of PHARAO with a ground clock. However, a more detailed discussion will be necessary for the comparison of ground clocks in common view.

4. REFERENCES

Blanchet et al., 2001, A&A 370, pp. 320-329.
Duchayne, L., Wolf, P., Mercier, F., 2007, ArXiv: 0708.2387 (24pp).
Klioner, S., Soffel, M., 2000, Phys. Rev. D 62, 024019 (29 pp).
Le Poncin-Lafitte, C., Lambert, S., 2007, Class. Quantum Grav. 24, pp. 801-808.
Linet, B., Teyssandier, P., 2002, Phys. Rev. D 66, 024045 (14 pp).

CANONICAL ELEMENTS OF ROTATIONAL MOTION

T. FUKUSHIMA
National Astronomical Observatory of Japan
2-21-1, Ohsawa, Mitaka, Tokyo 181-8588, Japan
e-mail: Toshio.Fukushima@nao.ac.jp

ABSTRACT. We present a new set of canonical variables to describe general rotation of a triaxial rigid body. Explicit are both the forward and backward transformations from the new variables to the Andoyer canonical variables, which are universal. The rotational kinetic energy is expressed as a quadratic monomial of one new momentum. Consequently, the torque-free rotations are expressed as a linear function of time for the conjugate coordinate and constants of time for the rest two coordinates and three momenta. This means that the new canonical variables are universal elements in a broad sense.

1. BACKGROUND

Triggered by a recent review article on the analytical treatise on rotational motions (Gurfil et al. 2007), we initiated a series of researches on the theme. At the beginning, we intended to establish an all-purpose analytical tool such as the canonical and universal elements for the rotation of a general triaxial rigid body (Fukushima 2008d) which we summarize here. However, this was far more difficult than we expected. In order to find a clue, we changed our strategy so as to seek for a non-canonical formulation deploying the force function, U, like Lagrange's planetary equation in case of orbital motions. Again, this was too complicated to be realized.

Then, we shifted our target to a Gaussian formulation using non-canonical elements. Here the term 'Gaussian' means that not the partial derivatives of U but the torque vector components directly appear in the time evolution equations of the elements. Although we could obtain such a formulation (Fukushima 2008c), we were not fully sure of the correctness of the obtained formulation, especially whether the time evolution equation of non-canonical elements are analytically correct. A simple and independent check would be a comparison with the direct numerical integration of the equations of motion which are well established such as Euler's kinematical and dynamical equations of rotation in terms of Euler angles in the 3-1-3 convention, (ψ, θ, ϕ), and the angular velocity vector components referred to the body-fixed reference frame, $(\omega_A, \omega_B, \omega_C)$ (MacMillan 1936). We thought this an easy task. However, we immediately faced numerical difficulties in conducting simulations to examine the correctness of the analytical formulation.

The reason is clear; the kinematical equation in terms of the 3-1-3 Euler angles contain a singular point, $\theta = 0$. The singularity remains whichever convention of Euler angles we choose (Hughes 1986). Thus, we had to make an investigation on robust numerical formulations. In the course, we confirmed that Euler parameters, (q_0, q_1, q_2, q_3), are suitable substitutes to Euler angles. We succeeded to stabilize the method adopting $(q_0, q_1, q_2, q_3; \omega_A, \omega_B, \omega_C)$ as main variables by enforcing their normalization condition, $q_0^2 + q_1^2 + q_2^2 + q_3^2 = 1$, at every integration step. To our surprise, this method is the fastest and most precise (Fukushima 2008b).

After confirming the correctness of the Gaussian element formulation, we reformed it into a Lagrangian one by replacing the torque vector components by the corresponding partial derivatives of force function. Next we compared the obtained equation of non-canonical elements in the Lagrangian manner with those of canonical equations of motion in terms of the Andoyer variables and found the explicit relations between them. After some trials and errors of the formula manipulation of the obtained analytical relations, we arrived at a new set of canonical elements (Fukushima 2008d). However, it was difficult to prove their canonicity from the transformed relations. Thus, we searched for a suitable generating function, which is not always available for arbitrary canonical transformation. Fortunately, we could find such a function. Therefore, we will begin with the generating function.

2. A CANONICAL TRANSFORMATION OF FREEDOM TWO

Consider a following function of four variables, S, Z, ℓ, and g,

$$W(S,Z,\ell,g) \equiv Zg + \int_{\pi/2}^{\ell} \left(\sqrt{\frac{\left(a\sin^2\theta + b\cos^2\theta\right) Z^2 - aS^2}{(a-c)\sin^2\theta + (b-c)\cos^2\theta}} \right) \mathrm{d}\theta, \tag{1}$$

where a, b, and c are arbitrary positive constants satisfying the magnitude relations; $a \geq b \geq c$ and $a > c$. Regard S and Z as the new canonical momenta and ℓ and g as the old canonical coordinates. Then, by treating W as a generating function, we obtain a new canonical transformation of freedom two;

$$(L, G; \ell, g) \to (S, Z; s, z) \tag{2}$$

where the old momenta L and G and the new coordinates s and z are determined from W (Golstein et al. 2002) as

$$L \equiv \left(\frac{\partial W}{\partial \ell}\right)_{S,Z,g}, \qquad G \equiv \left(\frac{\partial W}{\partial g}\right)_{S,Z,\ell} = Z, \qquad s \equiv \left(\frac{\partial W}{\partial S}\right)_{Z,\ell,g}, \qquad z \equiv \left(\frac{\partial W}{\partial Z}\right)_{S,\ell,g}. \tag{3}$$

Conducting these partial derivatives, we obtain the explicit form of the canonical transformation as

$$S = \left(\sqrt{\frac{d}{a}}\right) G, \; s = \left(\sqrt{\frac{ad}{(a-d)(b-c)}}\right) F(\varphi|m), \; z = g - \left(\frac{cF(\varphi|m) + (a-c)\Pi(\varphi, -f|m)}{\sqrt{(a-d)(b-c)}} \right). \tag{4}$$

and $Z = G$. Here $F(\varphi|m)$ and $\Pi(\varphi, -f|m)$ are the incomplete elliptic integrals of the first and third kind with the argument φ, the parameter m, and the characteristic $-f$ (Byrd & Friedman 1971, Wofgram 2003), and

$$d \equiv \left(a\sin^2\ell + b\cos^2\ell\right)\left(\frac{G^2 - L^2}{G^2}\right) + c\left(\frac{L^2}{G^2}\right), \qquad \varphi \equiv \frac{\pi}{2} - \ell - \tan^{-1}\left(\frac{f\sin\ell\cos\ell}{\sqrt{1+f}+1+f\sin^2\ell}\right),$$
$$m \equiv \frac{(a-b)(d-c)}{(a-d)(b-c)}, \qquad f \equiv \frac{a-b}{b-c}. \tag{5}$$

3. NEW CANONICAL VARIABLES OF ROTATION

Apply the transformation (2) to the Andoyer canonical variables (Andoyer 1923), $(L, G, H; \ell, g, h)$, while interpret the constants a, b, and c as the inverse of principal moments of inertia, $A \equiv I_1$, $B \equiv I_2$, and $C \equiv I_3$;

$$a = \frac{1}{A}, \qquad b = \frac{1}{B}, \qquad c = \frac{1}{C}. \tag{6}$$

Then, we obtain a new set of canonical variables to describe rotational motions, $(S, Z, H; s, z, h)$. The transformation from the Andoyer canonical variables to the new ones are explicit as provided in Equation (4). Also explicit is the transformation from the new variables to the Andoyer ones as

$$L = \left(\sqrt{\frac{a-d}{a-c}}\right) Z\mathrm{dn}(u|m), \qquad \ell = \frac{\pi}{2} - \mathrm{am}(u|m) - \tan^{-1}\left(\frac{f\mathrm{sn}(u|m)\mathrm{cn}(u|m)}{\sqrt{1+f}+1+f\mathrm{sn}^2(u|m)}\right),$$
$$g = z + \left(\frac{cu + (a-c)\mathrm{pn}(u, -f|m)}{\sqrt{(a-d)(b-c)}}\right), \tag{7}$$

and $G = Z$ where

$$d = a\left(\frac{S^2}{Z^2}\right), \qquad u = \left(\sqrt{\frac{(a-d)(b-c)}{ad}}\right) s, \tag{8}$$

and m is computed from this d by the second last of Equation (5). Meanwhile $\mathrm{am}(u|m)$, $\mathrm{sn}(u|m)$, $\mathrm{cn}(u|m)$, and $\mathrm{dn}(u|m)$ are the Jacobian elliptic functions with the argument u and the parameter m, and

$$\mathrm{pn}(u, n|m) \equiv \Pi(\mathrm{am}(u|m), n|m), \tag{9}$$

is the pi amplitude function which we recently introduced (Fukushima 2008c). Using these transformation formulas, we obtain the expression of the Hamiltonian in terms of the new variables as

$$\mathcal{H} = \frac{1}{2}\left[\left(G^2 - L^2\right)\left(a\sin^2\ell + b\cos^2\ell\right) + cL^2\right] - U = \frac{1}{2}aS^2 - U, \tag{10}$$

where U is the perturbing force function. As a result, the canonical equations of motion become as simple as

$$\begin{aligned}
&\frac{\mathrm{d}S}{\mathrm{dt}} = \left(\frac{\partial U}{\partial s}\right)_{S,Z,H,z,h}, \qquad \frac{\mathrm{d}Z}{\mathrm{dt}} = \left(\frac{\partial U}{\partial z}\right)_{S,Z,H,s,h}, \qquad \frac{\mathrm{d}H}{\mathrm{dt}} = \left(\frac{\partial U}{\partial h}\right)_{S,Z,H,s,z}, \\
&\frac{\mathrm{d}s}{\mathrm{dt}} = aS - \left(\frac{\partial U}{\partial S}\right)_{Z,H,s,z,h}, \qquad \frac{\mathrm{d}z}{\mathrm{dt}} = -\left(\frac{\partial U}{\partial Z}\right)_{S,H,s,z,h}, \qquad \frac{\mathrm{d}h}{\mathrm{dt}} = -\left(\frac{\partial U}{\partial H}\right)_{S,Z,s,z,h}.
\end{aligned} \tag{11}$$

In case of torque-free rotations, $U = 0$. Therefore, the solutions are plainly given as

$$S = S_0, \qquad Z = Z_0, \qquad H = H_0, \qquad s = s_0 + aS_0t, \qquad z = z_0, \qquad h = h_0, \tag{12}$$

where the quantities with the suffix 0 are their values when $t = 0$. This means that the new variables are elements in a broad sense (Fukushima 2008a). The Andoyer canonical variables are universal in the sense they can describe all three modes of rotation; the short-, the middle-, and the long-axis modes. Therefore, the new canonical elements are also universal.

4. PARTIAL DERIVATIVES

Let us describe how to evaluate the partial derivatives of the force function with respect to the new variables, $\partial U/\partial(S, Z, H, s, z, h)$. Assume that already available are the partial derivatives with respect to the Andoyer canonical variables, $\partial U/\partial(L, G, H, \ell, g, h)$, the calculation of which has been extensively discussed in the literature. Then, the resulting procedure to compute $\partial U/\partial(S, Z, H, s, z, h)$ is to give the Jacobian matrix of the transformation, namely the 6×6 matrix of partial derivatives of the Andoyer canonical variables with respect to the new ones, $\partial(L, G, H, \ell, g, h)/\partial(S, Z, H, s, z, h)$. Among 36 components of the Jacobian matrix, (1) zero are 23 of them; $(\partial L/\partial H)$, $(\partial L/\partial z)$, $(\partial L/\partial h)$, $(\partial G/\partial S)$, $(\partial G/\partial H)$, $(\partial G/\partial z)$, $(\partial G/\partial h)$, $(\partial H/\partial S)$, $(\partial H/\partial Z)$, $(\partial H/\partial s)$, $(\partial H/\partial z)$, $(\partial H/\partial h)$, $(\partial \ell/\partial H)$, $(\partial \ell/\partial z)$, $(\partial \ell/\partial h)$, $(\partial g/\partial H)$, $(\partial g/\partial z)$, $(\partial g/\partial h)$, $(\partial h/\partial H)$, $(\partial h/\partial S)$, $(\partial h/\partial Z)$, $(\partial h/\partial s)$, and $(\partial h/\partial z)$, (2) unity are four of them; $(\partial G/\partial Z)$, $(\partial g/\partial z)$, $(\partial H/\partial H)$, and $(\partial h/\partial h)$, and (3) non trivial are the rest nine components, which are explicitly expressed as

$$\begin{aligned}
&\left(\frac{\partial L}{\partial S}\right) = \left(\frac{\partial L}{\partial d}\right)\left(\frac{\partial d}{\partial S}\right), \qquad \left(\frac{\partial \ell}{\partial S}\right) = \left(\frac{\partial \ell}{\partial d}\right)\left(\frac{\partial d}{\partial S}\right), \qquad \left(\frac{\partial g}{\partial S}\right) = \left(\frac{\partial g}{\partial d}\right)\left(\frac{\partial d}{\partial S}\right), \\
&\left(\frac{\partial L}{\partial Z}\right) = \left(\frac{\partial L}{\partial Z}\right)^* + \left(\frac{\partial L}{\partial d}\right)\left(\frac{\partial d}{\partial Z}\right), \qquad \left(\frac{\partial \ell}{\partial Z}\right) = \left(\frac{\partial \ell}{\partial d}\right)\left(\frac{\partial d}{\partial Z}\right), \qquad \left(\frac{\partial g}{\partial Z}\right) = \left(\frac{\partial g}{\partial d}\right)\left(\frac{\partial d}{\partial Z}\right), \\
&\left(\frac{\partial L}{\partial s}\right) = \left(\frac{\partial L}{\partial u}\right)\left(\frac{\partial u}{\partial s}\right), \qquad \left(\frac{\partial \ell}{\partial s}\right) = \left(\frac{\partial \ell}{\partial u}\right)\left(\frac{\partial u}{\partial s}\right), \qquad \left(\frac{\partial g}{\partial s}\right) = \left(\frac{\partial g}{\partial u}\right)\left(\frac{\partial u}{\partial s}\right),
\end{aligned} \tag{13}$$

where

$$\begin{aligned}
&\left(\frac{\partial L}{\partial d}\right) = \left(\frac{\partial L}{\partial d}\right)^* + \left(\frac{\partial L}{\partial m}\right)\left(\frac{\partial m}{\partial d}\right) + \left(\frac{\partial L}{\partial u}\right)\left(\frac{\partial u}{\partial d}\right), \qquad \left(\frac{\partial \ell}{\partial d}\right) = \left(\frac{\partial \ell}{\partial m}\right)\left(\frac{\partial m}{\partial d}\right) + \left(\frac{\partial \ell}{\partial u}\right)\left(\frac{\partial u}{\partial d}\right), \\
&\left(\frac{\partial g}{\partial d}\right) = \left(\frac{\partial g}{\partial d}\right)^* + \left(\frac{\partial g}{\partial m}\right)\left(\frac{\partial m}{\partial d}\right) + \left(\frac{\partial g}{\partial u}\right)\left(\frac{\partial u}{\partial d}\right), \qquad \left(\frac{\partial d}{\partial S}\right) = \frac{2d}{S}, \qquad \left(\frac{\partial d}{\partial Z}\right) = \frac{-2d}{Z}, \\
&\left(\frac{\partial u}{\partial s}\right) = \sqrt{\frac{(a-d)(b-c)}{ad}}, \qquad \left(\frac{\partial L}{\partial Z}\right)^* = \left(\sqrt{\frac{a-d}{a-c}}\right)\mathrm{dn}(u|m), \qquad \left(\frac{\partial L}{\partial d}\right)^* = \frac{-L}{2(a-d)}, \\
&\left(\frac{\partial L}{\partial m}\right) = \frac{1}{2}\left(\sqrt{\frac{a-d}{a-c}}\right)Z\mathrm{sn}(u|m)\left[\mathrm{cn}(u|m)\left\{u - \mathrm{pn}(u,m|m)\right\} - \left(\frac{\mathrm{sn}(u|m)}{\mathrm{dn}(u|m)}\right)\right], \\
&\left(\frac{\partial L}{\partial u}\right) = -\left(m\sqrt{\frac{a-d}{a-c}}\right)Z\mathrm{sn}(u|m)\mathrm{cn}(u|m), \qquad \left(\frac{\partial \ell}{\partial m}\right) = \frac{\left(\sqrt{1+f}\right)\mathrm{dn}(u|m)\left[u - \mathrm{pn}(u,m|m)\right]}{2m\left[1 + f\mathrm{sn}^2(u|m)\right]},
\end{aligned}$$

$$\left(\frac{\partial \ell}{\partial u}\right) = \frac{-\left(\sqrt{1+f}\right)\mathrm{dn}(u|m)}{1+f\mathrm{sn}^2(u|m)}, \qquad \left(\frac{\partial g}{\partial d}\right)^* = \frac{c+(a-c)\mathrm{pn}(u,-f|m)}{2(a-d)\sqrt{(a-d)(b-c)}},$$

$$\left(\frac{\partial g}{\partial m}\right) = \left(\frac{a-c}{2\sqrt{(a-d)(b-c)}}\right)\left[u + \frac{\mathrm{pn}(u,m|m) - \mathrm{pn}(u,-f|m)}{m+f}\right],$$

$$\left(\frac{\partial g}{\partial u}\right) = \frac{1}{\sqrt{(a-d)(b-c)}}\left[c + \frac{a-c}{1+f\mathrm{sn}^2(u|m)}\right], \qquad \left(\frac{\partial m}{\partial d}\right) = \frac{(a-b)(a-c)}{(a-d)^2(b-c)},$$

$$\left(\frac{\partial u}{\partial d}\right) = -\left(\frac{1}{2d}\sqrt{\frac{a(b-c)}{d(a-d)}}\right)s. \tag{14}$$

5. CONCLUSION

By utilizing a new generating function, we obtain a new set of canonical variables of rotation from the Andoyer canonical variables. The new set is superior to the existing sets of canonical variables of rotation in the sense that (1) the unperturbed Hamiltonian remains finite while it vanishes in the case of Serret's canonical elements (Serret 1866), (2) the new variables are the rotational elements for any triaxial rigid body while the Andoyer canonical variables (Andoyer 1923) become elements only when the body is oblately spheroidal and while their 1-2-3 variations (Fukushima 1994) do so only when the body is prolately spheroidal, (3) the new set is universal while Sadov's canonical elements (Sadov 1970) as well as Kinoshita's similar elements (Kinoshita 1972) are well-defined only for the short-axis mode rotation, and (4) the transformation to the Andoyer variables is explicit while it is implicit for Sadov's and Kinoshita's canonical elements. In short, the new canonical elements are a universal counterpart, in the rotational dynamics, of the Delaunay canonical elements for elliptic orbital motion.

6. REFERENCES

Andoyer, H. 1923, Mécanique Céleste, Gauthier-Villars, Paris

Byrd, P.F., & Friedman, M.D. 1971, Handbook on Elliptic Integrals for Engineers and Physicists, 2nd ed. (Berlin: Springer-Verlag)

Fukushima, T. 1994, Celest. Mech. Dyn. Astron., 60, 57.

Fukushima, T. 2008a, AJ , 135, 72.

Fukushima, T. 2008b, AJ , 135, 2298.

Fukushima, T. 2008c, AJ , 136, 649.

Fukushima, T. 2008d, AJ , 136, 1728.

Goldstein, H., Poole, C.P., & Safko, J.L. 2002, Classical Mechanics, 3rd ed., (Reading, MA: Addison-Wesley)

Gurfil, P., Elipe, A., Tangren, W., & Efroimsky, M. 2007, Regular and Chaotic Dynamics, 12, 389.

Hughes, P.C. 1986, Spacecraft Attitude Dynamics, (New York: John Wiley & Sons)

Kinoshita, H. 1972, Publ. Astron. Soc. Japan, 24, 423.

MacMillan, W.D. 1936, Dynamics of Rigid Bodies, reprinted 1960 (New York: Dover)

Sadov, Y.A. 1970, Keldysh Inst. Appl. Math. Acad. Sci. USSR, Preprint No.22

Serret, J.A. 1866, Mem. Acad. Sci. Paris, 35, 585.

Wolfram, S. 2003, The Mathematica Book, 5th ed., (Cambridge: Wolfram Research Inc./Cambridge Univ. Press)

TOWARDS A LONG-TERM PARAMETRIZATION OF PRECESSION

J. VONDRÁK[1], N. CAPITAINE[2], P. WALLACE[3]
[1]Astronomical Institute, Acad. Sci. Czech Rep.
Boční II, 141 31 Prague 4, Czech Republic
e-mail: vondrak@ig.cas.cz
[2]SYRTE, Observatoire de Paris, CNRS, UPMC
61, Ave. de l'Observatoire, 75014 Paris, France
e-mail: n.capitaine@obspm.fr
[3] STFC / Rutheford Appleton Laboratory
Harwell Science and Innovation Campus, Didcot, Oxfordshire OX11 0QX, UK
e-mail: patrick.wallace@stfc.ac.uk

ABSTRACT. The IAU 2000/2006 precession-nutation model is designed to provide the coordinates X, Y of the Celestial Intermediate Pole (CIP) with respect to the Geocentric Celestial Reference System (GCRS), with microarcsecond precision for several centuries around the central epoch J2000. Its precessional part is expressed in terms of polynomial developments of the time elapsed from this epoch. However, when extrapolated to more distant epochs (comparable to the basic 26000-yr period of CIP motion around the ecliptic pole), it starts to diverge rapidly from reality. The aim of this paper is to estimate the accuracy of the present model as function of the length of the interval, and to propose new developments for X, Y, based on long-periodic functions of time. The goal is to obtain accuracy that approaches the present IAU developments for epochs close to J2000, and a better fit to reality for longer intervals.

1. INTRODUCTION

The position of the Celestial Intermediate Pole (CIP) in the Geocentric Celestial Reference System (GCRS) at any given date includes the motion due to precession-nutation together with a frame bias (of about 23 mas) between the GCRS and the J2000 equatorial system. Expressions for predicting the CIP directions, based on the IAU 2000A precession-nutation, can be found in Capitaine et al. (2003a), in the IERS Conventions (2003) and in the IAU SOFA software (Wallace 1998). Expressions based on the IAU 2006 precession have been provided by Capitaine et al. (2003b) and Wallace and Capitaine (2006). The developments of the CIP's GCRS X, Y coordinates are given as polynomials of t which originate mainly from precession, plus a series of Fourier and Poisson terms representing the contribution from nutation. These developments, which ensure a microarcsecond accuracy valid over an interval of several centuries, aim to meet the requirements of high-accuracy applications. Outside this interval the errors quickly grow with time. In reality, precession represents a complicated and very long-periodic process, with periods equal to hundreds of centuries; this can be demonstrated by numerical integration of the respective equations of motion of the Earth in the solar system and its rotation (see below).

It appears necessary to develop expressions that would allow more realistic long-term behavior, comparable to that of the Euler angle approaches. The purpose of this paper is to provide a development for these quantities for use in the long term (covering several precession cycles) and to evaluate their accuracy through numerical comparison with precession-nutation ephemerides based on other precession formulations. A first such attempt was made by one of us (Vondrák 2007), where long-term developments of the precession of the ecliptic and equator were derived separately. This long term study will be mainly based on precession only, the nutation part being the short-periodic (i.e., with periods shorter than several tens of years) component of the motion.

2. NUMERICAL INTEGRATION AND X, Y POLE COORDINATES

In order to obtain the long-term behavior of Earth's orientation in space we use the numerical integration of both Earth's motion in solar system (precession of the ecliptic) and its rotational motion

(general precession and obliquity of the ecliptic).

A. Precession of the ecliptic (angles Π_A, π_A):
The basis for this is the numerical integration of the motion of the solar system, using the integrator package Mercury 6 (Chambers, 1999), in the interval 2000cy with step equal to 1cy.

B. General precession, obliquity (angles p_A, ε_A):
The basis is the numerical integration of general precession and obliquity LA93 (Laskar et al. 1993) available for the interval 1My with step equal to 10cy. Additional corrections are applied to account for the secular change of dynamical ellipticity ($\dot{J}_2$) and the secular change of obliquity.

The relations of these four angles to other parameters describing precession are shown in Fig. 1. To calculate the precession part of X, Y we obtain first the auxiliary angles α, β, γ from the triangle $\Upsilon\Upsilon_o$N:

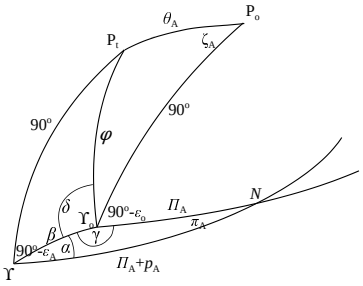

$$
\begin{aligned}
\cos\beta &= \cos\Pi_A\cos(\Pi_A+p_A)+\sin\Pi_A\sin(\Pi_A+p_A)\cos\pi_A\\
\sin\beta\cos\alpha &= \cos\Pi_A\sin(\Pi_A+p_A)-\sin\Pi_A\cos(\Pi_A+p_A)\cos\pi_A\\
\sin\beta\sin\alpha &= sin\Pi_A\sin\pi_A\\
\sin\beta\sin\gamma &= \sin(\Pi_A+p_A)\sin\pi_A\\
\sin\beta\cos\gamma &= \sin\Pi_A\cos(\Pi_A+p_A)-\cos\Pi_A\sin(\Pi_A+p_A)\cos\pi_A,
\end{aligned}
\tag{1}
$$

Figure 1: Precession quantities

then the angles φ, δ by solving the triangle $\Upsilon\Upsilon_o P_t$

$$
\begin{aligned}
\cos\varphi &= \sin\beta\sin(\varepsilon_A+\alpha)\\
\sin\varphi\cos\delta &= -\cos\beta\sin(\varepsilon_A+\alpha)\\
\sin\varphi\sin\delta &= \cos(\varepsilon_A+\alpha)
\end{aligned}
\tag{2}
$$

and finally, from triangle $\Upsilon_o P_t P_o$ and accounting for small celestial pole and equinox offsets, we get

$$
\begin{aligned}
X &= \sin\theta_A\cos\zeta_A + 0.0146''\sin\theta_A\sin\zeta_A - 0.016617''\\
Y &= -\sin\theta_A\sin\zeta_A + 0.0146''\sin\theta_A\cos\zeta_A - 0.006951'',
\end{aligned}
\tag{3}
$$

where $\sin\theta_A\cos\zeta_A = \cos\varphi$, $\sin\theta_A\sin\zeta_A = \sin\varphi\cos(\gamma+\delta-\varepsilon_o)$. We used these formulas to calculate X, Y in the interval $\pm$2000cy with 1cy step.

Next we compared these long-term integrated values with different models, in the interval of $\pm$200 centuries (about 1.5 precession cycles) around J2000 (see Fig. 2). The first three models – by Lieske et al. (1977), designated Lieske; by Simon et al. (1994), designated Simon; and by Capitaine et al. (2003b), designated Capitaine I – are such that the values X, Y are calculated from polynomial expressions for the angles θ_A, ζ_A. In the last model (Capitaine II) the values X, Y are directly calculated from their polynomial expressions provided in (Capitaine et al. 2003b). It is evident that the models are not graphically distinguishable in the interval $\pm$50cy around J2000, but they start to differ significantly outside the interval $\pm$100cy. Generally speaking, a better fit is obtained if X, Y values are calculated from the polynomial expressions for θ_A, ζ_A, using Eqs. (3) rather than from the direct development of X, Y.

3. ESTIMATION OF PERIODIC TERMS OF THE MODEL

To develop a long-term precession formula, valid over several precession cycles, the expressions for X, Y must contain long-periodic terms. Therefore, we made a spectral analysis of integrated coordinates X, Y, based on a least-squares approach, to find hidden periodicity. The most pronounced ones were then compared with the periods found by Laskar (1993, 2004) from much longer interval. We identified our periods with Laskar's whenever possible and made a least-squares estimation of 14 dominant sine/cosine amplitudes plus a cubic parabola (to account for missing longer periods).

In order to obtain a model as close to P03 as possible near the epoch J2000, we used numerical integration outside the interval $\pm$10cy, and P03 values inside this interval, with much higher weights.

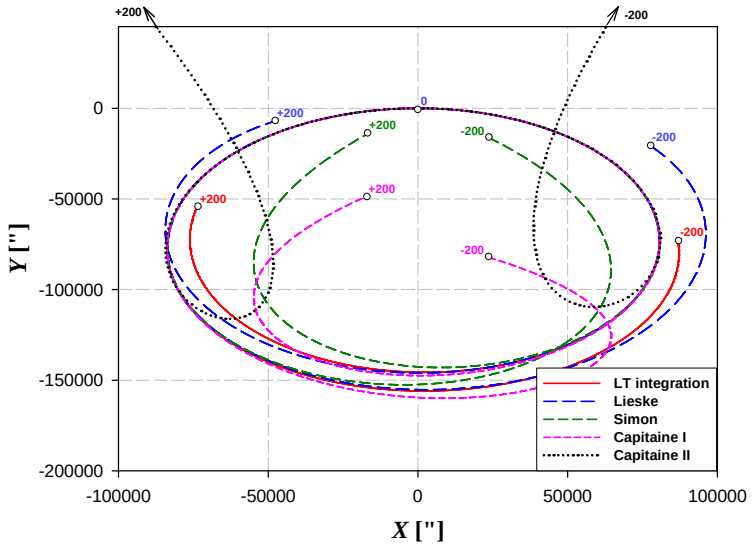

Figure 2: Different models of precession X, Y in the interval ±200cy around J2000

Small additional corrections were then applied to the constant, linear and quadratic terms to keep the derivatives up to the 2nd order identical with P03 model. The results (in arcseconds) are given as

$$\begin{aligned} X =& 5452.121068 + 0.4936640T - 0.00037051T^2 - 188 \times 10^{-9}T^3 + \\ &+ \sum_{i=1}^{14} \left(C_{xi} \cos 2\pi T/P_i + S_{xi} \sin 2\pi T/P_i\right) \\ Y =& -73748.904862 - 0.7300392T - 0.00018363T^2 + 212 \times 10^{-9}T^3 + \\ &+ \sum_{i=1}^{14} \left(C_{yi} \cos 2\pi T/P_i + S_{yi} \sin 2\pi T/P_i\right). \end{aligned} \tag{4}$$

The periodic terms of Eqs. (4), where T counts in centuries from J2000.0, are given in Table 1 below.

Table 1: Periodic terms in long-term expressions for X, Y

term	P[cy]	C_x	S_x	C_y	S_y
p	256.75	-890.392958	81486.055678	74993.013701	1624.771025
σ_3	708.15	-8442.032827	786.472556	623.634003	7772.231028
$p - g_2 + g_5$	274.20	2645.487483	1175.748879	1183.101287	-2262.613844
$p + g_2 - g_5$	241.45	2799.283269	-1163.092273	-1010.239126	-2564.893806
s_1	2309.00	-165.543689	-3021.082069	-2654.217193	217.164493
s_6	492.20	872.202300	639.204007	699.627348	-846.622884
$p + s_4$	396.10	45.589521	129.102969	152.109075	-1394.137691
$p + s_1$	288.90	-523.682245	-419.460618	-926.684032	379.173891
$p - s_1$	231.10	-827.551724	529.877488	444.781911	757.410362
	1610.00	-539.346941	-60.246349	-151.914565	462.551085
	620.00	-193.676517	524.751903	557.485310	239.959374
$2p + s_3$	157.87	-403.471752	-13.830660	-26.992841	374.350053
	220.30	180.209107	-196.580144	-147.305110	-172.499874
	1200.00	-9.210712	-52.971311	12.498143	-28.484470

The differences of both integrated values and model defined by Eqs. (4) in the interval ±20cy are depicted in Fig. 3. A similar comparison in much longer interval (±2000cy) shows that the integration and our new model differ only very slightly (not more than several arcminutes), while their difference from P03 grows extremely rapidly.

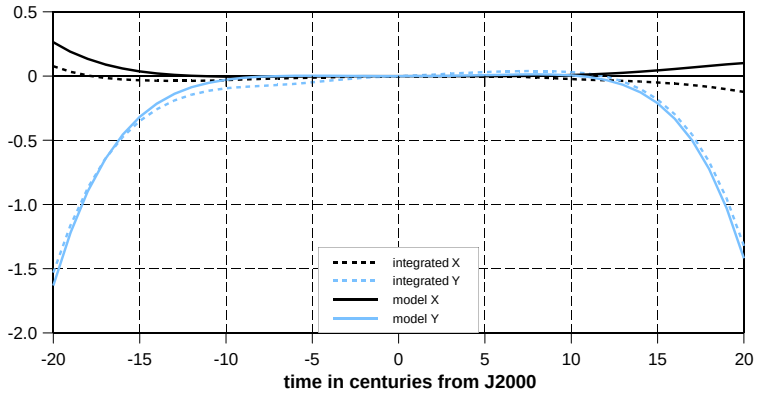

Figure 3: Differences of integrated and modeled values $X, Y[''']$ from P03

4. DISCUSSION

Most of the precession models used so far, being expressed as polynomials of time, are valid, with a high accuracy, only for a few centuries around J2000). Their errors grow rapidly outside this interval – more than 10° 200 centuries from J2000. Generally speaking, models based on polynomials for the classical precession angles give better results than those obtained from the time polynomials for the GCRS CIP coordinates X, Y.

We demonstrate the possibility of constructing a model of precession for predicting the CIP direction in the GCRS that yields results comparable to P03 in a short-time interval (a few centuries) around J2000, and follows the periodical character of precession in a long-term sense (hundreds of millennia), with only very slowly decreasing accuracy (several arcminutes) ± 0.2My away from J2000.

5. REFERENCES

Capitaine, N., Chapront, J., Lambert, S. and Wallace, P.T., 2003a, "Expressions for the Celestial Intermediate Pole and Celestial Ephemeris Origin consistent with the IAU 2000A precession-nutation model" A&A , 400, pp. 1145–1154.

Capitaine, N., Wallace, P.T. and Chapront J., 2003b, "Expressions for IAU 2000 precession quantities", A&A , 412, pp. 567–586.

Chambers, J.E., 1999, "A hybrid symplectic integrator that permits close encounters between massive bodies", MNRAS , 304, pp. 793-799.

IERS Conventions 2003, IERS Technical Note 32, D.D. McCarthy and G. Petit (eds), Frankfurt am Main: Verlag des Bundesamts für Kartographie und Geodäsie, 2004.

Laskar, J., Joutel, F. and Boudin, F., 1993, "Orbital, precessional, and insolation quantities for the Earth from −20 Myr to +10 Myr", A&A , 270, pp. 522-533.

Laskar, J., Robutel, P., Joutel, F., Gastineau, M., Correia, A.C.M. and Levrard, B., 2004, "A long-term numerical solution for the insolation quantities of the Earth", A&A , 428, pp. 261–285.

Lieske, J.H., Lederle, T., Fricke, W. and Morando, B., 1977,"Expressions for the precession quantities based upon the IAU (1976) system of astronomical constants", A&A , 58, pp. 1–16.

Simon, J.L., Bretagnon, P., Chapront, J., Chapront-Touzé M., Francou G. and Laskar J., 1994, "Numerical expressions for precession formulae and mean elements for the Moon and the planets", A&A , 282, pp. 663–683.

Vondrák J., 2007, "Long-periodic precession parametrization", Highlights of Astronomy Vol. 14, K.A. van der Hucht (ed.), Cambridge University Press, p. 467.

Wallace, P.T., 1998, "SOFA: Standards of Fundamental Astronomy", Highlights of Astronomy Vol. 11A, J. Andersen (ed.), Kluwer Academic Publishers, 11, p. 191.

Wallace, P.T. and Capitaine, N., 2006, "Precession-nutation procedures consistent with IAU 2006 resolutions", A&A , 459, pp. 981–985.

INVESTIGATION OF THE SHORT PERIODIC TERMS OF THE RIGID AND NON-RIGID EARTH ROTATION SERIES

V.V. PASHKEVICH
Central (Pulkovo) Astronomical Observatory of Russian Academy of Science
Pulkovskoe Shosse 65/1, 196140, St. Petersburg, Russia
e-mail: pashvladvit@yandex.ru

ABSTRACT. The aims of this research are the investigation of the short periodic terms in a long time new high-precision series of the rigid (S9000A) and non-rigid Earth rotation (SN9000A). Choice of the optimal spectral analysis scheme for this investigation is carried out. The previous version of the rigid Earth rotation series S9000 has been updated the new version the high-precision rigid Earth rotation series S9000A, which contained the short periodic terms (diurnal and sub-diurnal). The high-precision non-rigid Earth rotation series SN9000A containing the short periodic terms (diurnal and sub-diurnal), which is expressed as a function of the three Euler angles with respect to the fixed ecliptic plane and equinox J2000.0 and is dynamically adequate to the ephemerides DE404/LE404 over 2000 years, has been constructed.

1. INTRODUCTION

In the previous investigations were constructed the high-precision rigid S9000 and non-rigid Earth rotation series SN9000, which are expressed as functions of Euler angles and are dynamically adequate to the ephemeris DE404/LE404 over 2000 years. The main purpose of this research is the construction a new high-precision rigid S9000A and non-rigid Earth rotation series SN9000A, which will include the short periodic terms (diurnal and sub-diurnal).

The method of this investigation is following:

1.To update the previous version of the high-precision numerical solution of the rigid Earth rotation (V.V. Pashkevich, G.I. Eroshkin and A.Brzezinski, 2004), (V.V. Pashkevich and G.I. Eroshkin, Proceedings of "Journees 2004") by using the integration step of 1 day and the interpolation step of 0.1 day. All calculations have been carried out with the quadruple precision (Real 16) on PC Intel®Core™2 Duo E6600 (2.4GHz). In this investigation is considered only the Kinematical (relativistic) case.

2.The initial conditions have been calculated from the model of the rigid Earth rotation SMART97 (P.Bretagnon, G.Francou, P.Rocher, J.L.Simon, 1998). The discrepancies between the numerical solution of the rigid Earth rotation and the semi-analytical solution SMART97 were expressed in Euler angles over 2000 years with 0.1 day spacing.

3.Investigation of the discrepancies, which contained the diurnal and sub-diurnal periodic terms, has been carried out by the least squares (LSQ) and by the refined spectral analysis (SA) algorithms (V.V. Pashkevich and G.I. Eroshkin, 2005), (V.V. Pashkevich and G.I. Eroshkin, Proc. "Journees 2005").

4.The high-precision rigid Earth rotation series S9000 (V.V. Pashkevich and G.I. Eroshkin, 2005) has been update by including the short periodic terms (diurnal and sub-diurnal).

5.The new high-precision non-rigid Earth rotation series (SN9000A) has been constructed. This series is expressed in the function of the three Euler angles and containing the short periodic terms. For it is applied the method of P. Bretagnon et al. (1999) and the transfer function of P.M. Mathews et al. (2002).

2. INVESTIGATION RIGID AND NON-RIGID EARTH ROTATION SERIES

In order to choice of the optimal spectral analysis scheme for the investigation of the short periodic terms will consider two algorithms (Figure 1) and (Figure 2). The ALGORITHM - 1 (Figure 1) (V.V. Pashkevich and G.I. Eroshkin, Proc. "Journees 2005") have only one iteration, which investigated the discrepancies D between numerical solution and semi-analytical solution of the rigid Earth rotation for all periodical terms. This procedure is accomplished in the following manner. After the removal of the

secular trend from discrepancies and the compute the new precessional and GMST polynomials by scheme of V.V.Pashkevich and G.I. Eroshkin, (2005), the spectra of the discrepancies are constructed by using the set of nutation terms of SMART97 solutions. The amplitudes of the spectra of the discrepancies are computed by the LSQ method for each harmonic of SMART97. The spectra of the discrepancies are bounded by the periods from 0.3284255 days to 1000 years for the time interval of 2000 years. The determination of the coefficients of the harmonics is accomplished successively starting from the maximum term in the power spectra by the LSQ method:

a) The amplitude of the largest harmonic is determined by the LSQ method.

b) If the absolute value of the amplitude Am of a harmonic exceeds the absolute value σ of its mean square error then this harmonic is removed from the discrepancies. The new harmonic is determined as a sum of the calculated periodic term and the corresponding harmonic of SMART97.

c) The steps a) and b) are performed up to the end of the spectra.

The new series S9000A1 are constructed in the result of summing the determined periodic terms and the corresponding harmonics of SMART97.

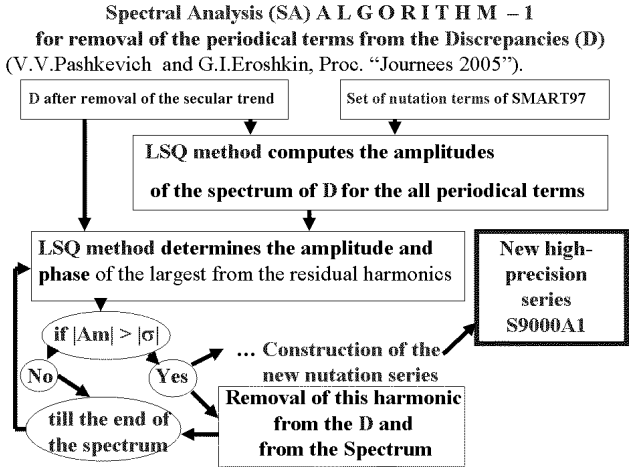

Figure 1: Algorithm 1

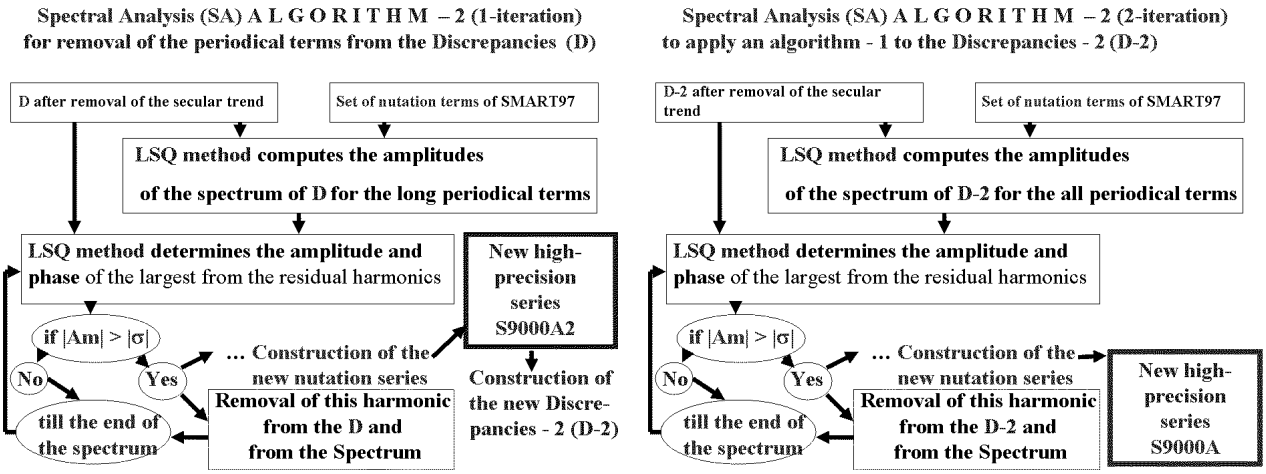

Figure 2: Algorithm 2

The ALGORITHM - 2 (Figure 2) have two iterations. The first iteration investigated the discrepancies D for only the long periodical terms. (This procedure is similar procedure of the ALGORITHM - 1. Only the spectra of the discrepancies are bounded by the periods from 1.0003 days to 1000 years for the time interval of 2000 years.) The second iteration is the ALGORITHM - 1, which investigated the

new construction (after the first iteration) discrepancies D-2 between new numerical solution and new semi-analytical solution of the rigid Earth rotation for all periodical terms. The residuary discrepancies (Figure 3) between numerical solution and semi-analytical solution of the rigid Earth rotation for case of the ALGORITHM - 2 are better than for case of the ALGORITHM - 1. So, in this investigation the ALGORITHM - 2 is better than the ALGORITHM - 1. The investigation of the discrepancies, which contained the diurnal and sub-diurnal periodic terms, has been carried out by the least squares (LSQ) and by the new spectral analysis (SA) ALGORITHM - 2. As the result of this research is the new high-precision rigid Earth rotation series S9000A, which including the short periodic terms (diurnal and sub-diurnal).

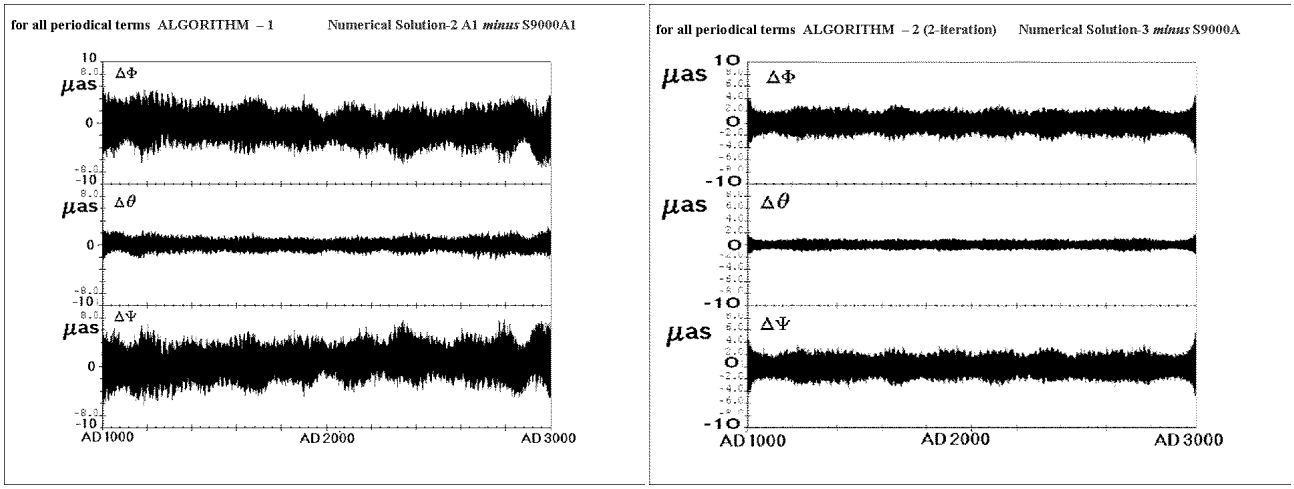

Figure 3: The residuary discrepancies between numerical solution and semi-analytical solution of the rigid Earth rotation after formal removal of the secular trends in the proper rotation angle

For the construction of the non-rigid Earth rotation series (SN9000A) in this investigation applied the method of P. Bretagnon et al. (1999) and the transfer function (MHB) and geophysical model of P.M. Mathews et al. (2002). The comparison of different Earth rotation solutions for selected diurnal periodical terms in the Euler angels are demonstrated Table 1. Others the diurnal and semidiurnal periodic terms have very small difference or have not difference.

Period (days), Argument	Solution rigid Earth rotation	ψ(sin) μas	ψ(cos) μas	θ(sin) μas	θ(cos) μas	ϕ(sin) μas	ϕ(cos) μas
1.03474	SMART97	-0.0133	0.0016	-0.0010	-0.0085	-0.0129	0.0016
$3\lambda_3 + 3D - 2F - \phi$	S9000A	-0.0806	-0.0612	0.0073	-0.0065	-0.0754	-0.0564
0.99758	SMART97	-19.8544	2.4906	-0.9877	-7.8729	-18.2334	2.2873
$\lambda_3 + D - l - \phi$	S9000A	-19.8521	2.4941	-0.9891	-7.8720	-18.2314	2.2908
Period (days), Argument	Solution non-rigid Earth rotation	ψ(sin) μas	ψ(cos) μas	θ(sin) μas	θ(cos) μas	ϕ(sin) μas	ϕ(cos) μas
1.03474	SMN	-0.0225	-0.0100	-0.0044	-0.0006	-0.0213	-0.0090
$3\lambda_3 + 3D - 2F - \phi$	SN9000A	-0.0898	-0.0728	0.0039	0.0014	-0.0838	-0.0670
0.99758	SMN	-19.8316	-1.0929	0.4389	-7.8522	-18.2125	-1.0005
$\lambda_3 + D - l - \phi$	SN9000A	-19.8293	-1.0894	0.4375	-7.8513	-18.2105	-0.9974

Table 1: The Comparison of different Earth rotation solutions for selected diurnal periodical terms in the Euler angels. Here $\lambda_3 + D - F = \Omega + 180^o$; λ_3 is the mean longitude of the Earth; D is the difference between the mean longitudes of the Moon and the Sun; Ω is the mean longitude of the ascending node of the lunar orbit; F is the mean argument of the Moon's latitude; l is the mean anomaly of the Moon; SMN=SMART97+MHB; SN9000A=S9000A+MHB; MHB- Mathews et al., 2002.

3. CONCLUSIONS

1. The optimal spectral analysis scheme for this investigation (with respect to the accuracy) has been determined. It is algorithm-2, which used two iterations. The first iteration investigated the discrepancies for only the long periodical harmonics, while the second iteration investigated the discrepancies for all harmonics.

2. The new version the high-precision rigid Earth rotation series S9000A has been constructed. It contains the short periodic terms (diurnal and sub-diurnal).

3. The high-precision non-rigid Earth rotation series SN9000A (containing the short periodic terms) has been constructed. This series is expressed in the function of the three Euler angles with respect to the fixed ecliptic plane and equinox J2000.0 and is dynamically adequate to the ephemerides DE404/LE404 over 2000 years.

Acknowledgements. The author highly appreciates for very useful discussions with Prof. A. Brzeziński. The investigation was carried out at the Central (Pulkovo) Astronomical Observatory of the Russian Academy of Sciences and at the Space Research Centre of Polish Academy of Science, under a financial support of the Cooperation between Russian and Polish Academies of Sciences, Theme No 31.

4. REFERENCES

Bretagnon, P., Francou, G., 1988, "Planetary theories in rectangular and spherical variables", A&A 202, pp. 309–315.

Bretagnon, P., Francou, G., Rocher P., Simon J.L., 1998, "SMART97: A new solution for the rotation of the rigid Earth", A&A 329, pp. 329–338.

Bretagnon, P., Mathews, P.M.,Simon, J.-L., 1999, "Non Rigid Earth Rotation", in Proc. of Journees 1999: Motion of Celestial Bodies, Astrometry and Astronomical Reference Frames Les Journees 1999 & IX. Lohrmann - Kolloquium, (Dresden, 13-15 September 1999), pp. 73–76.

Brumberg, V.A., Bretagnon, P., 2000, "Kinematical Relativistic Corrections for Earths Rotation Parameters", in Proc. of IAU Colloquium 180, eds. K.Johnston, D. McCarthy, B. Luzum and G. Kaplan, U.S. Naval Observatory, pp. 293–302.

Dehant, V., Defraigne, P., 1997, "New transfer functions for nutations of a non-rigid Earth", J. Geophys. Res. 102, pp. 27659–27688.

Mathews, P.M., Bretagnon, P., 2003, "Polar Motions Equivalent to High Frequency Nutations for a Nonrigid Earth with Anelastic Mantle" A&A 400, pp. 1113–1128.

Mathews, P. M., Herring, T. A., and Buffett B. A., 2002, "Modeling of nutation and precession: New nutation series for nonrigid Earth and insights into the Earth's Interior", J. Geophys. Res. 107, B4, 10.1029/2001JB000390.

Pashkevich, V.V., Eroshkin, G.I. and Brzezinski, A., 2004, "Numerical analysis of the rigid Earth rotation with the quadruple precision", Artificial Satellites, Vol. 39, No. 4, Warszawa, pp. 291–304.

Pashkevich, V.V. and Eroshkin, G.I., 2004, "Spectral analysis of the numerical theory of the rigid Earth rotation", in Proc. of Journees 2004: Fundamental Astronomy: New concepts and models for high accuracy observations (Observatoire de Paris, 20-22 September 2004.), pp. 82–87.

Pashkevich, V.V. and Eroshkin, G.I., 2005, "Choice of the optimal spectral analysis scheme for the investigation of the Earth rotation problem", in Proc. of Journees 2005: Earth dynamics and reference systems: five years after the adoption of the IAU 2000 Resolutions (Space Research Centre of Polish Academy of Sciences, Warsaw, Poland, 19-21 September 2005), pp. 105–109.

Pashkevich, V.V. and Eroshkin, G.I., 2005, "Application of the spectral analysis for the mathematical modelling of the rigid Earth rotation", Artificial Satellites, Vol. 40, No. 4, Warszawa, pp. 251–260.

Pashkevich, V.V., 2008, "Construction of the Non-Rigid Earth Rotation Series", Artificial Satellites, in press.

Shirai, T., Fukushima, T, 2001, "Construction of a new forced nutation theory of the nonrigid Earth", AJ 121, pp.3270–3283.

Wahr, J.M., 1981, "The forced nutations of an elliptical, rotating, elastic and oceanless Earth", Geophys. J. R. Astron. Soc. 64, pp.705–727.

INFLUENCE OF THE RELATIVISTIC LAMBDA-TERM ON THE MEASURED VALUES OF THE EARTH'S ROTATION DECELERATION

Yu.V. DUMIN
Institute of Terrestrial Magnetism, Ionosphere, and Radio Wave Propagation,
Russian Academy of Sciences, 142190 Troitsk, Moscow region, Russia
e-mail: dumin@yahoo.com

ABSTRACT. It is shown that one of the possible ways to resolve the long-standing discrepancy between the values of secular deceleration of the Earth's rotation derived from astrometric observations (9×10^{-6} sec/yr) and by the lunar laser ranging (LLR, 2.1×10^{-5} sec/yr) may be based on a more accurate treatment of the Earth–Moon dynamics in the framework of General Relativity with an account for the relativistic Λ-term, whose existence is well supported now by the cosmological data. In such a case, any additional corrections for ancient observations of solar eclipses and secular decrease in the Earth's moment of inertia would be unnecessary.

1. DATA ON SECULAR DECELERATION OF THE EARTH'S ROTATION

It is well-known that the values of secular deceleration of the Earth's proper rotation $\dot{T}_{\rm E}$ derived from various data sets considerably differ from each other, namely:

- 0.9×10^{-5} sec/yr from telescopic observations during the last ~350 years (e.g. the time series compiled by Sidorenkov 2002);
- 1.4×10^{-5} sec/yr from the telescopic data supplemented by ancient observations of solar eclipses (Stephenson & Morrison 1984);
- 2.1×10^{-5} sec/yr from the rate of secular increase in the Earth–Moon distance measured by the lunar laser ranging (Dickey et al. 1994).

The most popular way to reconcile these data, proposed about 25 years ago, was based on taking into account a secular decrease in the polar moment of inertia due to the viscous rebound of the solid Earth from the decrease in load caused by the last deglaciation. (Namely, a huge amount of ice in the polar regions during the glacial period resulted in the overdeformed state of the solid Earth. Next, when the ice have melted, the Earth gradually restores its spherical shape, leading to the decrease in the polar moment of inertia and the respective speed-up of the Earth's rotation.) The first data on secular change in the Earth's moment of inertia, characterized by the zonal gravitational harmonic coefficient J_2, gave the value $\dot{J}_2 = -3 \times 10^{-11}$ yr^{-1} (Yoder et al. 1983), which apparently confirmed the above-mentioned mechanism. In other words: $\dot{T}_{\rm E}$ *from the telescopic observations + correction for the ancient data on solar eclipses + correction for secular decrease in the polar moment of inertia* = $\dot{T}_{\rm E}$ *from LLR.*

Unfortunately, the most recent studies have shown that the secular trend in J_2 has a less amplitude (Bourda & Capitaine 2004) or even the opposite sign in some time intervals (Cox & Chao 2002). As a result, the value of long-term trend is still poorly known: for example, the various estimates discussed in Sec. 3.5. of the paper by Cheng & Tapley (2004) are scattered from -2.75×10^{-11} yr^{-1} to -1.0×10^{-11} yr^{-1}. Moreover, reliability of the ancient data on solar eclipses is also doubtful. Therefore, the problem of disagreement between the astrometric and LLR data remains now as acute as 25 years ago.

The aim of the present report is to show that the astrometric and LLR data can be well reconciled by using only the series of telescopic observations for the last ~350 years and taking into account the effect of relativistic Λ-term (whose existence at large scales is well confirmed now by the cosmological data). In other words: $\dot{T}_{\rm E}$ *from telescopic observations + correction for* Λ*-term* = $\dot{T}_{\rm E}$ *from LLR.*

2. EFFECT OF THE LAMBDA-TERM

The basic idea of our approach is that the rate of secular increase in the Earth–Moon distance measured

by LLR (3.8 cm/yr, e.g. Dickey et al. 1994) consists actually of the two parts. The first of them is caused by the well-known tidal exchange of angular momentum between the Earth and Moon (for more details see, for example, Dumin 2003), and only this part should be taken into account in the calculation of $\dot{T}_{\rm E}$; while the second part is the "local" Hubble expansion, which does not affect the actual value of $\dot{T}_{\rm E}$.

Next, we assume that the rate of the "global" Hubble expansion (at intergalactic scales) is caused both by the uniformly-distributed Λ-term ("dark energy") with density $\rho_{\Lambda 0}$ and the irregularly-distributed dust-like matter $\rho_{\rm D0}$: $H_0 = \sqrt{8\pi G/3}\,\sqrt{\rho_{\Lambda 0} + \rho_{\rm D0}}$; while the local Hubble expansion is produced only by the perfectly-uniform Λ-term: $H_0^{\rm (loc)} = \sqrt{8\pi G/3}\,\sqrt{\rho_{\Lambda 0}}$ (Dumin 2008). Taking the standard values $H_0 = 71$ km/sec/Mpc and $\rho_{\Lambda 0}/\rho_{\rm D0} \approx 3$, we find that the Λ-term is responsible for a considerable part of the secular increase in the Earth–Moon distance: $\dot{R}_\Lambda = 2.2$ cm/yr; while the remaining part should be attributed to the tidal influence: $\dot{R}_{\rm tid} = 1.6$ cm/yr.

At last, using the well-known relation $\dot{R}_{\rm tid} = k\,\dot{T}_{\rm E}$ with $k = 1.81 \times 10^5$ cm/sec (Kaula 1968), we get $\dot{T}_{\rm E} = 0.9 \times 10^{-5}$ sec/yr, which is in perfect agreement with the value of secular increase in the length of day derived from the series of telescopic observations for the last ∼350 years (e.g. Sidorenkov 2002). Therefore, any further corrections (for the ancient solar eclipses etc.) become unnecessary.

Of course, the above semi-empirical estimates must be verified by a rigorous analysis of the General Relativity (GR) equations "from the first principles". In general, the problem of local Hubble expansion is discussed for a long time, starting from the early 1930's (e.g. review by Bonnor 2000); the main problem being a reverse influence of the local gravitating masses on the background cosmological matter distribution. The situation is much simplified for the case of the Λ-dominated (de Sitter) cosmology, and the respective GR metric was found long time ago by Kottler (1918). Unfortunately, there is still a large controversy regarding a correct choice of coordinates for the interpretation of observational data. For example, Soffel & Klioner (2004) and Klioner & Soffel (2005) constructed the local coordinates around the barycenter and concluded that the effects of the Λ-term within the solar system, manifesting themselves as tidal forces, should be completely negligible. On the other hand, when we tried to reduce the local Kottler metric to the correct Robertson–Walker cosmological asymptotics (Dumin 2007), the contributions from Λ-term looked appreciable. This contradiction should be resolved by a detailed analysis of the equations of planetary motion and light propagation in the above-cited metrics. This work is currently under way.

I am grateful to Profs. N. Capitaine and S.A. Klioner for valuable suggestions and critical comments on the present work.

3. REFERENCES

Bonnor, W.B., 2000, Gen. Rel. Grav., 32, 1005–1007.
Bourda, G., Capitaine, N., 2004, A&A, 428, 691–702.
Cheng, M., Tapley, B.D., 2004, J. Geophys. Res., 109, B09402.
Cox, C.M., Chao, B.F., 2002, Science, 297, 831–833.
Dickey, J.O. et al., 1994, Science, 265, 482–490.
Dumin, Yu.V., 2003, Adv. Space Res., 31, 2461–2466.
Dumin, Yu.V., 2007, Phys. Rev. Lett., 98, 059001.
Dumin, Yu.V., 2008, Proc. 11th Marcel Grossmann Meeting on General Relativity 2006, eds. H. Kleinert, R.T. Jantzen & R. Ruffini, World Scientific, Singapore, pp. 1752–1754.
Kaula, W.M., 1968, "An Introduction to Planetary Physics: The Terrestrial Planets", J. Wiley & Sons, New York.
Klioner, S.A., Soffel, M.H., 2005, Proc. Symp. "The Three-Dimensional Universe with Gaia", 4-7 Oct. 2004, Paris, France (ESA SP-576), eds. C. Turon, K.S. O'Flaherty & M.A.C. Perryman, ESA Publ. Div., Noordwijk, Netherlands, pp. 305–308.
Kottler, F., 1918, Ann. Phys. (Leipzig), 56, 401–462.
Sidorenkov, N.S., 2002, "Physics of the Earth's Rotation Instabilities", Nauka-Fizmatlit, Moscow (in Russian).
Soffel, M., Klioner, S., 2004, Proc. Journées 2003 Systèmes de Référence Spatio-Temporels, eds. A. Finkelstein & N. Capitaine, Inst. Appl. Astron., St.Petersburg, pp. 297–301.
Stephenson, F.R., Morrison, L.V., 1984, Philos. Trans. R. Soc. London, A313, 47–70.
Yoder, C.F. et al., 1983, Nature, 303, 757–762.

SOLVING THE ROTATIONAL EARTH'S EQUATIONS IN RECTANGULAR COORDINATES FOR A NON-RIGID EARTH

V. ŠTEFKA[1], M. FOLGUEIRA[2,3], S. LAMBERT[3] and N. CAPITAINE[3]

[1] Astronomical Institute, Academy of Sciences of the Czech Republic,
Boční II, 14131 Prague 4, Czech Republic
e-mail: stefka@ig.cas.cz
[2] Instituto de Astronoma y Geodesia (UCM-CSIC), Facultad de Ciencias Matemáticas,
Ciudad Universitaria, ES-28040 Madrid, Spain
e-mail: marta_folgueira@mat.ucm.es
[3] SYRTE, Observatoire de Paris, CNRS, UPMC,
61 avenue de l'Observatoire, 75014 Paris, France
e-mail: n.capitaine@obspm.fr and sebastien.lambert@obspm.fr

ABSTRACT. The Descartes prize 2003 was awarded by the European Union to the IAU/IUGG Working Group on 'Nutation for a nonrigid Earth'. One of the Descartes-nutation projects following this prize is named "Advances in the integration of the equations of the Earth's rotation in the framework of the new parameters adopted by the IAU 2000 Resolutions". The first paper devoted to this project has been published by Capitaine at al. (2006) (it will be denoted $XYRE06$ in the following) and the second one (denoted $XYRE08$ in the following) is about to be submitted by Capitaine and Folgueira (2008). This poster contains a brief report of Sub-project entitled *"Solving the rotational Earth's equations in rectangular coordinates for a non-rigid Earth"* which is currently under development as an extension to a non-rigid Earth model of the two previous works ($XYRE06$ and $XYRE08$) considered for the rigid Earth.

1. BACKGROUND

The aim of $XYRE06$ and $XYRE08$ consisted in obtaining the coordinates of the celestial intermediate pole CIP, (X,Y), in the geocentric celestial reference system ($GCRS$), from the direct integration of the differential equations in the terms of these coordinates.

1. The rigorous rotational equations (see Capitaine at al. 2006) were developed for a rigid Earth in terms of $(X, Y)_R$ and were then simplified for an axially symmetric Earth ($A = B$) as follows:

$$\begin{aligned} -\ddot{Y} + \tfrac{C\Omega}{A}\dot{X} &= \tfrac{L}{A} + F'' \\ \ddot{X} + \tfrac{C\Omega}{A}\dot{Y} &= \tfrac{M}{A} + G'', \end{aligned} \tag{1}$$

   where F'' and G'' are functions, at the 2nd order of X, Y and their 1st and 2nd time derivatives, L and M are the components of the torque in the Celestial intermediate reference system (denoted $CIRS'$) linked to the CIP and the point Σ (see Capitaine et al. 2006) and A, C are the principal moments of inertia of the rigid Earth.

2. The most complete semi-analytical developments of the solutions for the Moon (ELP2000), the Sun and the planets (VSOP97), were used to to compute the semi-analytical development of the external torque.

3. The equations were integrated using the method of variations of parameters and a semi-analytical integration with successive approximations to obtain the X, Y solution.

2. RESEARCH DESIGN OF THE PROJECT

The main goal of this work is to use the same method as in $XYRE08$, but with a non-rigid Earth model in order to obtain the solution for the $GCRS$ coordinates of the CIP (X,Y) for a non-rigid Earth.

1. We will first consider a deformable Earth for which the dynamical equations have been provided by Capitaine at al. (2006) in terms of $(X, Y)_{DE}$:

$$\begin{aligned} -\ddot{Y} + \Gamma \dot{X} &= \tfrac{L}{A} + d\psi_1^L + d\psi_1^{TD} + F'' \\ \ddot{X} + \Gamma \dot{Y} &= \tfrac{M}{A} + d\psi_2^L + d\psi_2^{TD} + G'' \,, \end{aligned} \tag{2}$$

with :

$$\Gamma = (C\Omega/A) / \left(1 + \tfrac{k_1}{k_S} \tfrac{C-A}{A}\right), \tag{3}$$

where, $\psi = \psi_1 + i\psi_2$ is the excitation function, $d\psi_L$ is the contribution due to the secular variation of the dynamical ellipticity of the Earth, $d\psi_{TD}$ is the contribution due to the tidal deformation of the Earth and L and M are components of the external torque which could be obtained as in the case for rigid Earth. The differential equations (2) will be solved semi-analytically by the method of variation of parameters in a similar way as for a rigid Earth, but taking into account (i) the new frequency for a deformable Earth, $\Gamma = f(\sigma, k_2, k_S)$, and (ii) the additional contributions $d\psi_L$ and $d\psi_{TD}$.

2. Then, the computed solutions $(X, Y)_{DE}$ will be checked by comparison with the solutions obtained in a classical way :

$$(\Delta\psi,\, \Delta\varepsilon)_{\text{REN2000}} \xrightarrow{\text{Transfer Function (DE)}} (\Delta\psi,\, \Delta\varepsilon)_{DE} \xrightarrow{\text{(Capitaine at al. 2003)}} (X, Y)^1_{DE}.$$

3. The model will be improved step by step taking into account different non-rigid effects (elasticity, fluid core, anelasticity, etc.). Figure (1) displays the values taken by the so-called *transfer function* (see Mathews et al. 2002) for tidal frequencies in the diurnal band for increasingly complex Earth models. Anelasticity has weak effects, making it non distinguishable on the plot from elasticity.

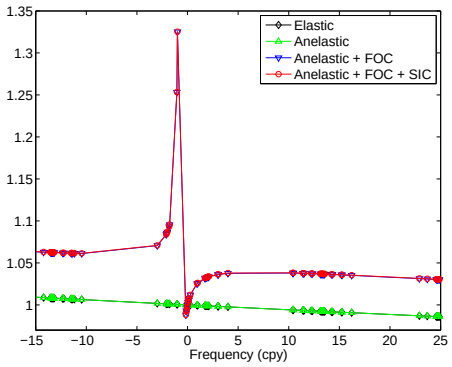

Figure 1: Values of the transfer function for various Earth models where *FOC* and *SIC* are free core nutation and solid inner core, respectively.

Acknowledgements. This research was made possible thanks to the Descartes-nutation project and two research stays V. Stefka and M. Folgueira at Paris Observatory (SYRTE Department).

3. REFERENCES

Capitaine, N., Chapront, J., Lambert, S., Wallace, P., 2003, "Expressions for the Celestial Intermediate Pole and Celestial Ephemeris Origin consistent with the IAU 2000A precession-nutation model", A&A , 400, 1145

Capitaine, N., Folgueira, M. & Souchay, J., 2006, "Earth rotation based on the celestial coordinates of the celestial intermediate pole I. The dynamical equations", A&A , 445, 347

Capitaine, N., Folgueira, M., 2008, "Earth rotation based on the celestial coordinates of the celestial intermediate pole II. The solutions for a rigid Earth", (to be submitted to A&A)

Mathews, P. M., Herring, T. A. & Buffett B. A., 2002, J. Geophys. Res. , 107, B4, 10.10292001JB000390

Session 2

RELATIVITY AND NUMERICAL STANDARDS IN FUNDAMENTAL ASTRONOMY, EPHEMERIDES

RELATIVITÉ ET STANDARDS NUMÉRIQUES EN ASTRONOMIE FONDAMENTALE, EPHÉMÉRIDES

CURRENT STATUS OF THE IAU WORKING GROUP FOR NUMERICAL STANDARDS OF FUNDAMENTAL ASTRONOMY

B. LUZUM, U.S. Naval Observatory, USA, N. CAPITAINE, Observatoire de Paris, France, A. FIENGA, Observatoire de Besançon, France, W. FOLKNER, Jet Propulsion Laboratory, USA, T. FUKUSHIMA, National Astronomical Observatory, Japan, J. HILTON, U.S. Naval Observatory, USA, C. HOHENKERK, HM Nautical Almanac Office, UK, G. KRASINSKY, Institute of Applied Astronomy RAS, Russia, G. PETIT, Bureau International des Poids et Mesures, France, E. PITJEVA, Institute of Applied Astronomy RAS, Russia, M. SOFFEL, Dresden Technical University, Germany, P. WALLACE, Rutherford Appleton Laboratory, UK

ABSTRACT. At the 2006 International Astronomical Union (IAU) General Assembly (GA), a proposal was adopted to form the Working Group (WG) for Numerical Standards of Fundamental Astronomy. The goal of the WG is to update the "IAU Current Best Estimates" conforming with IAU Resolutions, the International Earth Rotation and Reference Systems Service (IERS) Conventions, and the Système International d'Unités (SI). Changes to the numerical standards have been precipitated by the adoption of a new precession model, the redefinition of Barycentric Dynamical Time (TDB), and the significant improvement of the accuracy of recent estimates for a number of constants. To date, eleven additional constants have been added to the provisional list of Current Best Estimates (CBEs), one has been superseded, one has been removed, and the numerical values for ten previous constants have been replaced by newer values. In addition, the working group has looked into larger issues such as identifying the best methods for maintaining an IAU list of CBEs, the best ways of properly documenting the CBE list, and whether a new IAU System of Constants should be recommended to the IAU General Assembly. The current status of WG activities and anticipated future directions are presented.

1. INTRODUCTION

The International Astronomical Union (IAU) Working Group (WG) on Numerical Standards for Fundamental Astronomy has been tasked with updating the IAU Current Best Estimates (CBEs), conforming with the IAU Resolutions, IERS Conventions and Système International d'Unités whenever possible. As part of its effort to achieve this, the WG is working in close cooperation with IAU Commissions 4 and 52, the IERS, and the BIPM Consultative Committee for Units.

This is the third IAU WG to be tasked with producing CBEs and is adding to the legacy of the two previous WGs. The first Sub-group on Numerical Standards of the IAU WG on Astronomical Standards was headed by E.M. Standish and the WG report (Standish, 1995) established the rules which are still used today. For instance, this group decided on the two-tiered approach to the astronomical constants that we are currently using (*i.e.* having both an official system of constants and a set of CBEs), specified the content of the file of the current best estimates, and also created the first CBEs for a list of IAU constants.

This work was continued by T. Fukushima and his IAU WG on Astronomical Standards (Fukushima, 2000; Fukushima, 2003). Many of the updates concerned work on constants in a general relativistic framework and improved estimates of the precession constant. This revised list of CBEs remains the currently adopted list of IAU CBEs. The excellent work of both these WGs has helped to establish the precedent and allows us to improve incrementally the values for which there are now better estimates.

2. CHANGES SINCE THE LAST CURRENT BEST ESTIMATES

In addition to the need to update the CBEs because of improved estimates, there have also been significant changes that impact the IAU CBEs. Since the IAU CBEs were adopted, the IERS Conventions 2003 (McCarthy and Petit, 2004), a document widely used by the astronomical and geodetic communities, has been produced. This reference contains estimates of many of the constants included in the IAU CBEs.

One significant development was the adoption of a new precession model with IAU 2006 Resolution

B1. This resolution accepted the conclusion of the IAU Division I Working Group on Precession and the Ecliptic (Hilton *et al.*, 2006) and adopted the P03 precession theory of Capitaine *et al.* (2003). This resolution also replaced the terms "lunisolar precession" and "planetary precession" with "precession of the equator" and "precession of the ecliptic." Another change is the redefinition of Barycentric Dynamical Time (TDB) that occurred with the adoption of IAU 2006 Resolution B3. Moreover, IAU 2000 Resolution B1.8 introduced a conventional relationship that defines UT1 from the Earth Rotation Angle (ERA). In doing so, it introduced two defining constants for UT1.

These resolutions fundamentally alter the status of the associated constants. For instance, the general precession found in the IAU CBEs is no longer the appropriate quantity to describe precession. Also, the status of the relativistic constant L_B was changed to a defining constant.

3. CHANGES TO THE CURRENT BEST ESTIMATES

The current WG started where the previous IAU WG tasked with providing CBEs left off, by using the existing IAU CBEs as the starting draft. From this starting point, the WG has proceeded to update the CBEs based on internationally adopted values and recent research. Some examples are adopting values:

- from IAU Resolutions;
- from the Committee on Data for Science and Technology (CODATA) 2006;
- based on recent research to modify most of the planetary masses and adding masses for Ceres, Pallas, Vesta, and Eris. These improvements are possible due to years of high-precision observations of spacecraft as they near planets and their satellites.

The interim CBEs serve two significant purposes. First, they keep the IAU CBEs consistent, where possible, with international standards. Second, they also keep the constants consistent with the most accurate estimates currently available, which is vital for enabling progress in research.

For the latest draft version, eleven additional constants have been added to the initial list (L_B, TDB_0, θ_0, $\dot{\theta}$, au, M_S/M_{Eris}, M_{Ceres}/M_S, M_{Pallas}/M_S, M_{Vesta}/M_S, GM_S), one value has been removed (τ), one constant has been superseded (p by ψ_{J2000}), and the numerical values for ten additional constants have been replaced by more current, accurate values (G, L_C, M_M/M_E, M_S/M_V, M_S/M_{Ma}, M_S/M_J, M_S/M_{Sa}, M_S/M_P, GM_E, ϵ_0).

4. ADDITIONAL CONCERNS

In addition to updating the list of CBEs, the WG is addressing the larger issues surrounding the adoption of IAU CBEs. These include the mechanism to keep the CBEs current and the way in which these constants will be provided, the procedure to document the theoretical context of the constants, and whether the IAU should revise its current list of adopted constants to be consistent with the new list of CBEs.

The mechanism for maintaining the IAU CBEs has been discussed and to date, three options have been considered. The current method is for the IAU to form a WG when it believes that the CBEs need to be updated. This method has worked in the past and there is no reason to believe that it would not work in the future. Another possibility would be to enlist the aid of the IERS Conventions Product Center to maintain the IAU CBEs. Since the IERS is an IAU service organization and it already has a mechanism in place to maintain CBEs, it is possible that the IERS Conventions could be used to maintain the IAU CBEs as well. The biggest problem with this method is that the user communities and the areas of research of the IERS and the IAU are slightly different and there is a possibility that these differences could be problematic. A third option is to create a permanent body within the IAU that would maintain the list of CBEs. One potential problem with this option is that currently, the IAU has no mechanism to maintain a standing body to handle this task. The general consensus of the WG is to request that IAU Commission 4 (Ephemerides) revise its terms of reference so that standards would fall under its purview.

When considering the way in which the IAU System of Constants will be provided, a few options have been suggested. The current method is to provide the Constants with the maximum accuracy provided by the supporting scientific research. However, another option has been suggested to provide the Constants with a decreased accuracy — essentially truncate the digits at the level where disagreement between estimates exists. This would allow for a longer "shelf life" for the constants. This method has the

advantage of keeping a list of constants with the highest possible accuracy (CBEs) while also creating a list of constants that will be more universally acceptable and have longer life. The latter point is particularly appropriate since the acceptance of any new System of Constants by the IAU General Assembly would be facilitated if the values to be adopted agreed (at least to the number of digits provided) with all reasonable research results and the longer life would be consistent with the long span between the adoption of new IAU System of Constants.

The way in which the constants GM_S, au, and k are treated have been debated extensively. While a majority agree that the preferable way to treat these constants is to set au as a defining constant, estimate GM_S, and eliminate k, there is a vocal minority that does not agree with this option. The discussion to resolve this issue is still ongoing.

There are multiple relativistic time scales (TCB, TCG, TDB, TT) that are appropriate for various applications. In order to meet the needs of these users, values that are compatible with different time scales will be provided for the CBEs. Providing values for multiple relativistic time scales will also warn users implicitly that they need to be careful to use the appropriate value for their specific task.

Another question that has been discussed is what constitutes an acceptable reference for documenting a numerical estimate. In this age of rapid analysis of data, it is possible to create estimates frequently in an electronic format. In order to ensure that the estimation process is based on scientifically accepted procedures, it will be required that all values be published in refereed journals.

Electronic information will play a much greater role with the CBEs than with the astronomical constants. While it might be useful to have the astronomical constants provided on the IAU web page, it is expected that in the future the CBEs will be maintained in electronic form only. In order for this to be feasible, it will be necessary to establish a formal approval process, implement version control on the electronic document, and maintain past version of the CBEs in a publicly accessible location. To make best use of the electronic media, it would be desirable to have the web page hosting the CBEs provide extensive background information, references, and possibly information regarding the interrelation of the constants.

5. UPDATE OF IAU SYSTEM OF CONSTANTS

There are now significant differences between the CBEs and the current IAU System of Constants. This is due to both increasing accuracy of estimates and to changes in astronomical theory. As a result of this, there is a consensus of the NSFA WG to recommend to the 2009 IAU General Assembly that the IAU System of Constants be updated.

It is anticipated that the IAU System of Constants will continue to be a set of numbers that are changed infrequently and will be used by people looking for definitive numbers from an authoritative source. It is anticipated that the recommended new System of Constants will be provided to the accuracy that different estimates are in agreement. Because of this, the values for the System of Constants are expected to be correct and only need to be updated as additional digits of accuracy become available.

Currently, the plan is to provide the CBEs as an electronic document since the consensus is that this is the best way to facilitate the most accurate estimates being available to the user community in a timely fashion. In order to ensure the integrity of the CBEs, a formal procedure for the adoption of new values and the archiving of older versions of the CBEs will need to be developed.

The NSFA WG will be recommending to the IAU General Assembly that IAU Commission 4 (Ephemerides) revise its terms of reference so that standards would fall under its purview. This will allow the IAU to have a standing body that will be responsible for maintaining standards including numerical values.

6. REFERENCES

Capitaine, N., Wallace, P. T., and Chapront, J., 2003, "Expressions for IAU 2000 precession quantities," A&A , 412, pp. 567–586, doi: 10.1051/0004-6361:20031539.

Fukushima, T., 2000, "Report on Astronomical Constants," Proc. IAU Colloquium 180, Johnston, K. J., McCarthy, D. D., Luzum, B. J., Kaplan, G., pp. 417–427.

Fukushima, T., 2003, "Report on Astronomical Constants," Highlights of Astronomy, 13, International Astronomical Union, 2002, H. Rickman (ed.), pp. 107–112.

Hilton, J. L., Capitaine, N., Chapront, J., Ferrandiz, J. M., Fienga, A., Fukushima, T., Getino, J., Mathews, P., Simon, J.-L., Soffel, M., Vondrak, J., Wallace, P., William, J., 2006, "Report of the

International Working Group on Precession and the Ecliptic," Celest. Mech. Dyn. Astr., 94, pp. 351–367.

McCarthy, D.D. and Petit, G. (eds.), 2004, "IERS Conventions (2003)," IERS Technical Note 32, Frankfurt am Main, 127 pp.

Standish, E.M., 1995, "Report of the IAU WGAS Sub-group on Numerical Standards," Highlights of Astronomy, 12, International Astronomical Union, 1994, I. Appenzeller (ed.), pp. 180–184.

RELATIVISTIC ASPECTS IN ASTRONOMICAL STANDARDS AND THE IERS CONVENTIONS

G. PETIT
Bureau International des Poids et Mesures
92312 Sèvres France
e-mail: gpetit@bipm.org

ABSTRACT. In the last years, the definition of reference systems and their application to astronomy and geodesy has been passed into Resolutions of the scientific unions, following work of several working groups and of the community at large. However some work remains to be done to disseminate the information and to resolve a few residual questions. We review some topics that are still debated in the ad-hoc working groups and commissions. The IAU framework for relativity has also been introduced in the IERS Conventions, but some work remains to be done to obtain full consistency and conformity throughout the document, as will be reviewed. Finally, several updates under realization or under consideration for the IERS Conventions are presented.

1. THE RELATIVISTIC FRAMEWORK

In order to describe observations in astronomy and geodesy, one has to choose the proper relativistic reference systems best suited to the problem at hand. A barycentric celestial reference system (BCRS) should be used for all experiments not confined to the vicinity of the Earth, while a geocentric celestial reference system (GCRS) is physically adequate to describe processes occurring in the vicinity of the Earth. These systems have been defined in a series of Resolutions passed by scientific Unions, mostly the International Astronomical Union (IAU), in the past 20 years, see a more complete description of the work until year 2000 in (Soffel et al., 2003).

1.1 1991 and the following years

The reference systems were first defined by the IAU Resolution A4 (1991) which contains nine recommendations, the first four of which are summarized below.

In the first recommendation, the metric tensor for space-time coordinate systems $(t, \mathbf{x})$ centered at the barycenter of an ensemble of masses is recommended in the form

$$\begin{aligned} g_{00} &= -1 + 2U(t,\mathbf{x})/c^2 + \mathcal{O}(c^{-4}), \\ g_{0i} &= \mathcal{O}(c^{-3}), \\ g_{ij} &= \delta_{ij}\left(1 + 2U(t,\mathbf{x})/c^2\right) + \mathcal{O}(c^{-4}), \end{aligned} \tag{1}$$

where c is the speed of light in vacuum ($c = 299792458$ m/s) and U is the Newtonian gravitational potential (here a sum of the gravitational potentials of the ensemble of masses, and of a external potential generated by bodies external to the ensemble, the latter potential vanishing at the origin). The recommended form of the metric tensor can be used, not only to describe the barycentric reference system of the whole solar system, but also to define the geocentric reference system centered in the center of mass of the Earth with U, now depending upon geocentric coordinates.

In the second recommendation, the origin and orientation of the spatial coordinate grids for the barycentric and geocentric reference systems are defined.

The third recommendation defines TCB (Barycentric Coordinate Time) and TCG (Geocentric Coordinate Time) as the time coordinates of the BCRS and GCRS, respectively, and, in the fourth recommendation, another time coordinate named TT (Terrestrial Time), is defined for the GCRS as

$$\mathrm{TT} = \mathrm{TCG} - \mathrm{L_G} \times (\mathrm{JD_{TCG}} - T_0) \times 86400, \tag{2}$$

where $\mathrm{JD_{TCG}}$ is the TCG Julian date, $T_0 = 2443144.5003725$ and where $L_G = U_G/c^2$ with U_G being the gravity potential on the geoid.

Note that the International Union for Geodesy and Geophysics (IUGG), in its Resolution 2 (1991), endorsed the IAU Recommendations and explicitly based its definition of Terrestrial Reference Systems on the IAU relativistic framework.

In 1997 the IAU has supplemented the framework by one more recommendation stating that no scaling of spatial axes should be applied in any reference system, even if scaled time coordinate like TT is used for convenience of an analysis (this is in relation with e.g. discussions on the VLBI model, see Section 3.3).

1.2 2000 and the recent years

In the years following the adoption of the IAU'1991 Resolution, it became obvious that this set of recommendations was not sufficient, especially with respect to planned astrometric missions with μas-accuracies and with respect to the expected improvement of atomic clocks and the planned space missions involving such clocks and improved time transfer techniques. For that reason the IAU WG "Relativity for astrometry and celestial mechanics" together with the BIPM-IAU Joint Committee for relativity suggested an extended set of Resolutions that was finally adopted at the IAU General Assembly in Manchester in the year 2000 as Resolutions B1.3 to B1.5 and B1.9.

Resolution B1.3 concerns the definition of Barycentric Celestial Reference System (BCRS) and Geocentric Celestial Reference System (GCRS). The Resolution recommends to write the metric tensor of the BCRS in the form

$$\begin{aligned} g_{00} &= -1 + 2w/c^2 - 2w^2/c^4 + \mathcal{O}(c^{-5}), \\ g_{0i} &= -4/c^3 w^i + \mathcal{O}(c^{-5}), \\ g_{ij} &= \delta_{ij}\left(1 + 2w/c^2\right) + \mathcal{O}(c^{-4})\,. \end{aligned} \tag{3}$$

where w is a scalar potential and w^i a vector potential. This extends the form of the metric tensor given in (1), so that its accuracy is now sufficient for all applications foreseen in the next years, including those involving accurate space clocks. For the GCRS, Resolution B1.3 also adds that the spatial coordinates are kinematically non-rotating with respect to the barycentric ones.

Resolution B1.4 provides the form of the expansion of the post-Newtonian potential of the Earth to be used with the metric of Resolution B1.3.

Resolution B1.5 applies the formalism of Resolutions B1.3 and B1.4 to the problems of time transformations and realization of coordinate times in the solar system. Resolution B1.5 is based upon a mass monopole spin dipole model. It provides an uncertainty not larger than 5×10^{-18} in rate and, for quasi-periodic terms, not larger than 5×10^{-18} in rate amplitude and 0.2 ps in phase amplitude, for locations farther than a few solar radii from the Sun. The same uncertainty also applies to the transformation between TCB and TCG for locations within 50 000 km of the Earth.

Some shortcomings appeared in the definition of TT (2) when considering accuracies below 10^{-17}: the uncertainty in the determination of U_g is limited, the surface of the geoid is difficult to realize so that it is difficult to determine the potential difference between the geoid and the location of a clock, and in addition the geoid varies with time. Therefore it was decided to dissociate the definition of TT from the geoid while maintaining continuity with the previous definition. The constant L_g was turned into a defining constant with its value fixed to $6.969290134 \times 10^{-10}$ in Resolution B1.9, which therefore removes the limitations mentioned above when realizing TT from clocks onboard terrestrial satellites.

Finally in 2006 it was decided to redefine the coordinate time TDB, which had been introduced by the IAU in 1976 as a dynamical time scale for barycentric ephemerides. As it had not been unambiguously defined, multiple realizations of TDB were possible. Because such realizations are still widely used for barycentric ephemerides, IAU Resolution B3 (2006) was passed to define TDB as the following linear transformation of TCB:

$$\mathrm{TDB} = \mathrm{TCB} - \mathrm{L_B} \times (\mathrm{JD_{TCB}} - T_0) \times 86400 + TDB_0, \tag{4}$$

where $\mathrm{JD_{TCB}}$ is the TCB Julian date and where $L_B = 1.550519768 \times 10^{-8}$ and $TDB_0 = -6.55 \times 10^{-5} s$ are defining constants. Figure 1 shows graphically the relationships between the time scales following the IAU Resolutions of 1991, 2000 and 2006.

2. RELATIVISTIC ASPECTS IN ASTRONOMICAL STANDARDS

The main task of the IAU Working Group on Numerical Standards for Fundamental Astronomy (Luzum et al., 2008) is to update the IAU Current Best Estimates, eventually defining a new official system of constants. In doing so, it has to apply the relativistic framework defined above, and to disseminate the information on the consequences.

Without duplicating work of the Working group, we here remind the principal items where the application of the relativistic framework has direct impact on the astronomical standards. One concerns the definitions of the constants related to the rates between time coordinates L_C, L_G and L_B. In the present situation (since 2006) the last two are *defining* constants, where $\mathrm{d}TT/\mathrm{d}TCG = 1 - L_G$ and $\mathrm{d}TDB/\mathrm{d}TCB = 1 - L_B$, while L_C is *measured* as $1 - L_C =< \mathrm{d}TCG/\mathrm{d}TCB >$. Thus the relation $1 - L_B = (1 - L_G).(1 - L_C)$, which was used to define L_B, is no more (strictly) valid. Equivalently this means that TT and TDB dont have (strictly) the same rate at the geocenter.

Also of importance to this field is the discussion on the nomenclature (see section 3.1) and the choices to be made on the statute of the Sun's gravitational constant $GM_\odot$ and (correspondingly) that of the Gaussian constant K and the astronomical unit.

3. RELATIVISTIC ASPECTS IN THE IERS CONVENTIONS

In the current work to update the IERS Conventions (2003), relativistic aspects cover three topics. The first is to review the nomenclature throughout the document. The second concerns chapter 10 (models for space-time coordinates and equations of motion) where, in a recent update (see `http://tai.bipm.org/iers/convupdt/convupdt.html`) the transformation from proper time to coordinate time in the vicinity of the Earth is treated and numerical examples are provided for the different terms in the relativistic expression for the acceleration of an Earth satellite. The third concerns chapter 11 (models for signal propagation) and covers models for VLBI and (radio and laser) ranging techniques.

3.1. Nomenclature

Nomenclature issues in the IERS Conventions can be loosely classified in three categories, although several issues are interconnected. The first type concerns the designation of coordinate quantities, the second type relates to the transformation between celestial and terrestrial reference systems, the third type relates to the definition and realization of terrestrial reference systems.

In the first category, we must mention the wording used to designate coordinate quantities (e.g. space coordinates, gravitational constants GM, etc...). In the Conventions (2003) three types of wording are used:

- One wording uses the word "unit", like in "[so-called] TDB unit" (for cases when a scaled coordinate time is used, here TDB), or in "TCB (SI) units" TCB (SI) units (for cases when an unscaled coordinate time is used).
- One uses the word "scale", like in "ITRF ... uses the TT scale".
- One uses a full set of words in a sentence, like in " ... coordinates consistent with TDB".

It is one goal of the IAU Commission "Relativity in fundamental astronomy" (RIFA) to propose a conventional wording (Klioner, 2008).

The second category mostly concerns Chapter 5 (transformation between celestial and terrestrial systems) and is in the process of being reviewed following the work of the IAU Division I Working Group "Nomenclature for Fundamental Astronomy" (NFA), see `http://syrte.obspm.fr/iauWGnfa/NFA_Glossary.html` and (Capitaine, 2008).

Finally the nomenclature to name terrestrial reference systems and frames is to be set consistently throughout the Conventions, mostly in Chapter 4 (Terrestrial Reference System) and Chapter 5 (Transformation between celestial and terrestrial frames). Most of the terms have been considered in the Glossary of the NFA working group. Note also that the IUGG Resolution 2 (2007) was passed to provide updated definitions and terminology concerning Terrestrial Reference Systems. Nevertheless, an IAG Inter-commission Working Group (WG 1.3) has been formed to finalize a complete recommended nomenclature in the field of Geodetic Reference Systems.

3.2. Models for space-time coordinates and the equations of motion

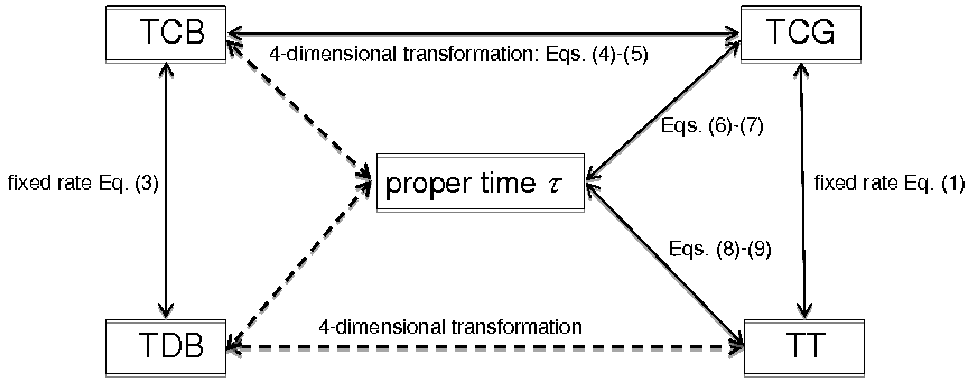

Figure 1: Various relativistic time scales and their relations. Each of the coordinate time scales TCB, TCG, TT and TDB can be related to the proper time τ of an observer, provided that the trajectory of the observer in the BCRS and/or GCRS is known. Transformations shown as dashed lines are not explicitly described in this document.

Chapter 10 (Models for space-time coordinates and the equations of motion) has been updated recently (October 2008) and the presentation of coordinate time scales now accounts for all IAU Resolutions (see section 1). The relationship between all time scales used in this context is shown on Figure 1, as taken from the IERS Conventions.In addition, a new section covers the transformation between proper time and coordinate time in the vicinity of the Earth (typically up to geosynchronous orbit or slightly above). Evaluating the contributions of the higher order terms in the metric (3) applied to the geocentric reference system GCRS, it is found that the IAU'1991 metric (1) is sufficient for time and frequency applications in the GCRS in the light of present clock accuracies.

When considering TT as coordinate time, the proper time of a clock A located at the GCRS coordinate position $\mathbf{x}_A(t)$, and moving with the coordinate velocity $\mathbf{v}_A$, is

$$\frac{d\tau_A}{dTT} = 1 + L_G - 1/c^2 \left[\mathbf{v}_A^2/2 + U_{\rm E}(\mathbf{x}_A) + V(X_{\rm A}) - V(X_{\rm E}) - x_A^i \partial_i V(X_{\rm E})\right] \tag{5}$$

Here, $U_{\rm E}$ denotes the Newtonian potential of the Earth at the position $\mathbf{x}_A$ of the clock in the geocentric frame, and V is the sum of the Newtonian potentials of the other bodies (mainly the Sun and the Moon) computed at a location X in barycentric coordinates, either at the position $X_{\rm E}$ of the Earth center of mass, or at the clock location $X_{\rm A}$. The last three terms are tidal terms and their contribution will be limited to below 1×10^{-16} in frequency and 1 ps in time amplitude up the GPS orbit, so they may be skipped depending on the uncertainty required. Nevertheless, some care needs to be taken when evaluating the Earth's potential $U_{\rm E}$ at the location of the clock as the uncertainty in $U_{\rm E}$ should be consistent with the uncertainty expected on (5). Analytical formulas may be specified e.g. for GPS (Kouba, 2004), however a numerical integration of equation (5) using the proper development for the potential is always worth using. This is specially the case for low Earth orbit satellites (see *e.g.* Larson et al., 2007), where analytical expressions may be significantly in error or even completely misleading.

3.3. Models for signal propagation

The chapter 11 of the Conventions (2003) "Models for signal propagation" describes the relativistic model for VLBI time delay and for Laser ranging.

While no change is expected in the VLBI model, except possible changes linked to the nomenclature, is is worth reminding the past history of this model since its introduction in 1990. In 1990, the so-called "Consensus model" was adopted at a USNO workshop. This was in a "pre-1991" era so that, although relativity was carefully accounted for, the currently agreed notations did not exist at that time. The model appeared in IERS Standards (1992), but was modified in the IERS Conventions (1996), erroneously intending to comply with IAU/IUGG Resolutions, stating that "as the time argument is now

based on TAI ...., distance estimates from these conventions will now be consistent 'in principle' with physical distances". However the change would have produced coordinates which would have differed from the usual "TT-compatible" coordinates by a scale change of 1.4×10^{-9}. Furthermore the stated goal is not achievable as no coordinate quantity can be consistent with a physical (proper) quantity over the extension of the Earth. The change was never implemented and the model was eventually restored in its original form in the IERS Conventions (2003) with additional explanations: Indeed the consensus model can provide either "TT-compatible" space coordinates when used with raw VLBI (TT) delays (as is the usual case in VLBI analysis), or it could provide "TCG-compatible" space coordinates if used with delays transformed to TCG. These issues are examined whenever the scale of the terrestrial reference frame is discussed, however it should be stressed that no ambiguity exists in the present model of the Conventions.

The section on laser ranging is to be expanded to cover all ranging techniques by electromagnetic signals in the vicinity of the Earth (up to the Moon). As it has been shown (Klioner, 2007) that post-post Newtonian terms are not required in view of the present uncertainty, no significant model change is expected.

4. CONCLUSIONS

The relativistic framework specified by IAU Resolutions in 1991 and 2000, and supplemented by additional Recommendations, is now complete and adapted to the current and planned applications in astrometry and space geodesy. Work remains to be done to apply it in all fields and, in some cases, a conventionally adopted nomenclature is still missing. This work is under way in IAU working groups (NSFA) and commissions (RIFA) and in the IERS Conventions center and should be concluded in the near future.

5. REFERENCES

Capitaine, N., 2008, "Nomenclature and numerical standards for IAU models and IERS Conventions for Earth rotation", these proceedings.

Klioner, S.A., 2007, "Relativistic aspects of the IERS Conventions", IERS Workshop on Conventions.

Klioner, S.A., 2008, "Relativistic scaling of astronomical quantities and the system of astronomical units", A&A 478-3, pp. 951–958.

Kouba, J., 2004, "Improved relativistic transformations in GPS," *GPS Solutions* 8,3, pp. 170–180.

Larson,] K. M., Ahsby, N., Hackman, C., Bertiger, W., 2007, "An assessment of relativistic effects for low Earth orbiters: the GRACE satellites," *Metrologia* 44, pp. 484–490.

Luzum, B.J. et al., 2008, "Current Status of the IAU Working Group for Numerical Standards of Fundamental Astronomy", these proceedings.

McCarthy, D.D. (ed.), 1992, "IERS Standards (1992)", IERS TN13, Observatoire de Paris, 150 p.

McCarthy, D.D. (ed.), 1996, "IERS Conventions (1996)", IERS TN21, Observatoire de Paris, 95 p.

McCarthy, D.D., Petit, G. (eds.), 2004, "IERS Conventions (2003)", IERS TN32, Verlag des BKG, 127 p.

Soffel M. et al., 2003, "The IAU2000 resolutions for astrometry, celestial mechanics and metrology in the relativistic framework: explanatory supplement", AJ 126(6), 2687–2706.

NOMENCLATURE AND NUMERICAL STANDARDS FOR IAU MODELS AND IERS CONVENTIONS FOR EARTH ROTATION

N. CAPITAINE
SYRTE, Observatoire de Paris, CNRS, UPMC
61, avenue de l'Observatoire, 75014 – Paris, France
e-mail: n.capitaine@obspm.fr

ABSTRACT. Important resolutions regarding Earth rotation have been adopted by IAU and IUGG since 2000, which include new concepts, a new nomenclature and new models for the quantities necessary for expressing the celestial orientation of the Earth. This presentation summarizes the consequences of the joint IAU 2000/2006 resolutions on the IAU models and the IERS Conventions that implement those models. It then looks at the changes in the status and numerical values for the constants associated with the IAU models for precession, nutation and the angle for Earth rotation, with respect to those of the previous IAU System of astronomical constants and previous lists of Current Best Estimates.

1. INTRODUCTION

The high accuracy observations of Earth rotation require a coordinated use of IAU-approved formulations, numerical standards and software that implement the IAU models. Several IAU resolutions on reference systems that are related to Earth's rotation have been passed in 2000 and 2006 including new nomenclature, models and standards. The IERS Conventions provide a practical and fully detailed implementation of these models and standards, expressed in terms of the new nomenclature, while the authoritative algorithms for implementing the IAU resolutions are provided by SOFA (Standards Of Fundamental Astronomy).

The aim of this paper is to review the changes resulting from the joint IAU 2000/2006 resolutions in the status and the numerical values for the constants associated with the new IAU models for precession, nutation and the angle for Earth rotation with respect to those of the current (1976) IAU System of astronomical constants and previous lists of Current Best estimates. The role of SOFA will be considered in the following paper of these Proceedings (cf. Wallace 2009, this Volume).

2. THE IAU 2000/2006 RESOLUTIONS FOR EARTH ROTATION

The IAU 2000 Resolutions have refined the definition of the astronomical reference systems and transformations between them and adopted the IAU 2000 precession-nutation. Those resolutions came into force on 1 January 2003 and were endorsed by IUGG in July 2003. The IAU 2006 Resolutions have adopted a new precession model and have addressed definition, terminology or orientation issues relative to reference systems and time scales. These have been endorsed by IUGG in 2007 with additional refinements for the definition of terrestrial reference systems.

The major points on Earth's rotation of the IAU 2000/2006 and IUGG 2003/2007 resolutions are:

- The systems of space-time coordinates for the solar system and the Earth within the framework of General Relativity have been specified (i) by IAU 2000 Resolution B1.3 (i.e. the Barycentric and Geocentric Celestial Reference Systems, BCRS and GCRS, respectively) and (ii) by IUGG 2007 Resolution 2 for the terrestrial systems (i.e. the Geocentric and Terrestrial Reference Systems, GTRS and ITRS, respectively).

- A high precision model for precession and nutation has been adopted in two stages. The first stage (IAU 2000 Resolution B1.6) was the adoption of the IAU 2000 precession-nutation (Mathews et al. 2002), which has been implemented in the IERS Conventions 2003. The second stage (IAU 2006 Resolution B1) was the adoption of the P03 Precession (Capitaine et al. 2003; Hilton et al. 2006) (i.e. the IAU 2006 precession) as a replacement for the precession part of the IAU 2000A precession-nutation, beginning on 1 January 2009.

- The definition of the Earth's Pole has been refined (IAU 2000 Resolution B1.7), so that the Celestial Intermediate Pole, CIP, is the intermediate pole, separating nutation from polar motion by a convention in the frequency domain. The GCRS direction of the CIP has been recommended as a replacement for the classical precession-nutation angles (IAU 2000 Resolution B1.8).

- The definition of the Earth's rotation around the CIP axis has been provided by the Earth Rotation Angle (ERA) between the "non-rotating origins" (Guinot, 1979) on the CIP equator (IAU 2000 Resolution B1.8). The diurnal rotation is expressed through a conventional linear transformation of UT1.

- The names of the pole and origins at date t have been harmonized to "intermediate" by IAU 2006 Resolution B2, i.e. celestial and terrestrial "intermediate" origins, CIO and TIO (instead of CEO and TEO, respectively, as originally named in the IAU 2000 resolutions).

3. NEW PARAMETERS AND NOMENCLATURE RELATED TO EARTH ROTATION

According to the new concepts adopted by IAU 2000 Resolution B1.8, the GCRS coordinates X, Y of the CIP unit vector and the Earth rotation angle, ERA, replace the classical precession and nutation angles and Greenwich sidereal time, GST, respectively (see more details in Capitaine et al. (2003)). Two recommendations from the IAU Working Group on "Nomenclature for Fundamental Astronomy" (NFA) (Capitaine et al. 2008) have been endorsed by IAU 2006 Resolution B2 while the detailed IAU 2006 nomenclature for fundamental astronomy are provided in the IAU 2006 NFA Glossary that is available at `http://syrte.obspm.fr/iauWGnfa`. A few examples of that Glossary are given in the following:

Celestial Intermediate Origin (CIO): origin for right ascension on the intermediate equator in the celestial intermediate reference system. It is the non-rotating origin in the GCRS that is recommended by the IAU 2000 Resolution B 1.8, where it was designated the Celestial Ephemeris Origin. The CIO was originally set close to the GCRS meridian and throughout 1900-2100 stays within 0.1 arcseconds of this alignment.

Celestial Intermediate Pole (CIP): geocentric equatorial pole defined by IAU 2000 Resolution B1.7 as being the intermediate pole, in the transformation from the GCRS to the ITRS, separating nutation from polar motion. It replaced the CEP on 1 January 2003. Its GCRS position results from (i) the part of precession-nutation with periods greater than 2 days, and (ii) the retrograde diurnal part of polar motion (including the free core nutation, FCN) and (iii) the frame bias. Its ITRS position results from (i) the part of polar motion which is outside the retrograde diurnal band in the ITRS and (ii) the motion in the ITRS corresponding to nutations with periods less than 2 days. The motion of the CIP is realized by the IAU precession-nutation plus time-dependent corrections provided by the IERS.

Earth Rotation Angle (ERA): angle measured along the intermediate equator of the Celestial Intermediate Pole (CIP) between the Terrestrial Intermediate Origin (TIO) and the Celestial Intermediate Origin (CIO), positively in the retrograde direction. It is related to UT1 by a conventionally adopted expression in which ERA is a linear function of UT1 (see IAU 2000 Resolution B1.8). Its time derivative is the Earth's angular velocity. Previously, it has been referred to as the stellar angle.

4. IAU MODELS FOR EARTH ROTATION AND THEIR IERS IMPLEMENTATION

The precession-nutation model is composed of a nutation part and a precession part. In addition are frame bias values between the J2000 mean pole and equinox and the Geocentric Celestial Reference System (GCRS).

The IAU 2000 semi-analytical series for nutation is composed of 1365 lunisolar and planetary terms with "in-phase" and "out-of-phase" components with amplitudes from $17''.2$ to $0.1\,\mu$as and periods between 3 d and 101 cy. This series is based on the REN2000 solution (Souchay et al. 1999) for the nutation of a rigid Earth model, transformed to nutation of a non-rigid Earth model with the MHB2000 "transfer function" (Mathews et al. 2002) expressed as function of seven Basic Earth Parameters (BEP) fitted to VLBI data. The IAU 2000 precession part consists only of corrections to the precession rates of the IAU 1976 precession; this is why IAU 2000 Resolution B1.6 recommended the development of new expressions for precession consistent with dynamical theories and with IAU 2000A nutation.

The IAU 2006 precession (Capitaine et al. 2003) provides improved polynomial expressions up to the 5th degree in time, t, both for the precession of the ecliptic and the precession of the equator, the latter

being consistent with dynamical theory while matching the IAU 2000A precession rate for continuity reasons. The precession of the equator was derived from the dynamical equations expressing the motion of the mean pole about the ecliptic pole with the value $\epsilon_0 = 84381''.406$ (Chapront et al. 2002) for the mean J2000 obliquity of the ecliptic. This includes various contributions from the non-rigidity of the Earth as well as corrections for the perturbing effects in the observed quantities.

The coordinate transformation from the ITRS to the GCRS at the date t of the observation that is considered in Chapter 5 of the IERS Conventions (2003) is written as:

[GCRS] = $Q(t)R(t)W(t)$ [ITRS],

where $Q(t)$, $R(t)$ and $W(t)$ are the transformation matrices arising from the GCRS motion of the CIP, the ERA and the ITRS motion of the CIP, respectively.

The IERS implementation of the ITRS-to-GCRS coordinate transformation compliant with the latest IAU resolutions should be based (i) for $Q(t)$: on the IAU 2006/2000 precession-nutation model plus IERS estimated celestial pole offsets, (ii) for $R(t)$: on the IAU 2000 expression for ERA(UT1) and the IERS estimated UT1, and (iii) for $W(t)$: on the IERS estimated pole coordinates, plus a modeled part of polar motion (cf. IERS Conventions 2003). The IAU 2000/2006 implementation of the precession-nutation model has been provided by Capitaine & Wallace (2006) and Wallace & Capitaine (2006).

5. NUMERICAL STANDARDS FOR EARTH ROTATION QUANTITIES

Numerical standards for Earth rotation in previous systems

In the first system of fundamental astronomical constants (adopted by the "Conférence internationale des étoiles fondamentales", Paris, 1896), the constants associated with precession-nutation, were (1) the "constant of precession", p, for the yearly amount of precession of the equinox, (2) the "constant of nutation", N_0, for the amplitude of the 18.6-yr nutation in obliquity, and (3) the obliquity of the ecliptic, ϵ. In the IAU 1976 System of astronomical constants, the precession-nutation constants have been unchanged, though they have been called "general precession in longitude at standard epoch 2000", p, "obliquity of the ecliptic at standard epoch 2000", ϵ, and "constant of nutation at standard epoch 2000", N; their numerical values have been updated to the best estimates at that time. In the Numerical Standards of the IERS Conventions (2003), the constants, ϵ_0 and ψ_1 associated with precession corresponds to a change of status for precession, i.e. replacing the classical constant of precession that was related to the general precession at J2000 with the precession rate ψ_1 of the equator at J2000 (with the IAU 2000 numerical value). There is no longer a constant associated with nutation, which corresponds to a change of status for nutation. This is due to the fact that, since the IAU 1980 nutation model, the nutation amplitudes are no longer related to the amplitude of the 18.6-yr term (as it was the case in the past). There is an additional IERS constant for Earth's rotation, i.e. ω, for the "nominal mean angular velocity of the Earth", the numerical value of which is the International Association of Geodesy (IAG) value.

Numerical standards for the IAU 2000/2006 model for Earth rotation

(i) Precession: The IAU 2006 precession of the equator is based on the expressions for the precession quantities ψ_A, and ω_A, which have been directly derived from the precession equations; it also includes expressions for a number of derived precession quantities, such as the GCRS CIP's X, Y. The numerical standards associated with the IAU 2006 precession are those for the coefficients of the polynomial expressions for the precession quantities. Those coefficients are dependent on (1) the J2000 precession rates of the equator, (2) the J2000 obliquity of the ecliptic, (3) the precession of the ecliptic and (4) the J_2 rate.

One option for representing the IAU 2006 precession with a very few numerical standards would be to consider only the IAU 2006 values for the J2000 precession rates X_1, Y_1, of the equator; this would correspond to retaining the same number of constants for precession in the list of numerical standards for fundamental astronomy, but with a change of status. Another option would be to consider the IAU 2006 values for the most relevant physical parameters associated with precession, such as the dynamical flattening, H_d and the J_2 rate (i.e. $H_d = 3.27379448\ \ 10^{-3}$ and $dJ_2/dt = -3.0 \times 10^{-11}$/yr), plus the J2000 obliquity of the ecliptic ($\epsilon_0 = 84381''.406$). These few constants could only provide a first order approximation for precession and it should be clear that the complete IAU 2006 precession expressions must be used for high accuracy needs.

(ii) Nutation: there is a large number of numerical standards associated with the IAU 2000 nutation. The fundamental values are the numerical values for the nutation amplitudes, which are directly related to the numerical values for (1) the REN2000 amplitudes and (2) the MHB2000 Basic Earth parameters, BEP (e.g. the dynamical ellipticities, e, of the whole Earth, and e_f of its fluid core, respectively).

Hence, the numerical standards associated with nutation could be either the IAU 2000 nutation amplitudes, or the REN2000 nutation amplitudes plus the MHB2000 Basic Earth parameters, which in both cases, would correspond to a very large number of values. A few numerical values out of this series can only provide a very poor approximation of nutation.

(iii) Earth's rotation: the conventional relationship defining UT1 (which is intended to be a representation of the hour angle of the "fictitious mean" Sun) from the ERA is:

$ERA(\mathrm{UT1}) = 2\pi \times [0.7790572732640 + 1.00273781191135448\ (\text{Julian UT1 date} - 2451545.0)]$,
where 0.7790572732640, 1.00273781191135448 rev/day are"defining constants".

The "nominal" mean angular velocity of the Earth, $\omega = 7.292\ 115 \times 10^{-5}$ rad/s (cf. IERS Conventions 2003), has been chosen to have the number of significant digits limited to those for which the value can be considered a constant; that value is "significantly" different from the actual value for the true Earth's angular velocity, which is known to have relative variations of the order of 10^{-7}.

Therefore, the numerical standards associated with the Earth's rotation angle and rate, and compliant with the IAU 2000/2006 resolutions, consist of values for two conventional constants for the relationship that defines UT1 from ERA and one conventional constant for the nominal mean angular velocity of the Earth. The observed variations in the Earth's angular velocity must refer to that nominal value.

The IAU 2000/2006 Resolutions have modified the status and numerical values of the constants associated with Earth rotation. A few constants for representing precession and nutation are no longer appropriate. The IAU precession-nutation model is necessary to ensure a precision compliant with that of the current observations. For continuity reasons, two numerical values can be provided for precession, but with making clear that those values are only a part of the constants of the IAU 2006 precession that in fact includes expressions as functions of time of various quantities. Nutation cannot be represented by a few constants, except for low precision needs; it must be represented by the IAU 2000 nutation model. A very few numerical values for conventional constants provide a model for the Earth's rotation angle and rate, which must be completed with their observed variations.

6. REFERENCES

Capitaine, N., Wallace, P.T., Chapront, J., 2003, "Expressions for IAU 2000 precession quantities", A&A 412, 567–586.

Capitaine, N., Wallace, P.T., 2006, "High precision methods for locating the celestial intermediate pole and origin", A&A 450, 855–872.

Capitaine, N., Andrei, A., Calabretta, M. Dehant, V., Fukushima, T., Guinot, B., Hohenkerk, C., Kaplan, G., Klioner, S., Kovalevsky, J., Kumkova, I., Ma, C., McCarthy, D., Seidelmann, K., and Wallace, P., 2007, "Proposed terminology in fundamental astronomy based on IAU 2000 resolutions", in *Transactions of the IAU* XXVIB, van der Hucht, K.A. (ed), 14, pp. 474–475.

Chapront, J., Chapront-Touzé, M. and Francou, G., 2002, "A new determination of lunar orbital parameters, precession constant and tidal acceleration from LLR measurements", A&A 387, 700–709.

Guinot, B., 1979, "Basic Problems in the Kinematics of the Rotation of the Earth", in *Time and the Earth's Rotation*, McCarthy, D.D. and Pilkington, J.D. (eds.), D. Reidel Publishing Company, pp. 7–18.

Hilton, J., Capitaine, N., Chapront, J., et al., 2006, "Report of the International Astronomical Union Division I Working Group on Precession and the Ecliptic", Celest. Mech. Dyn. Astr. 94, 3, 351.

IAU 2006, *Transactions of the IAU* XXVIB; van der Hucht, K.A. (ed).

IERS Conventions (2003), *IERS Technical Note 32*, D.D. McCarthy and G. Petit (eds), Frankfurt am Main: Verlag des Bundesamts für Kartographie und Geodäsie, 2004.

IUGG 2007, IUGG Resolutions, http://www.iugg.org/resolutions/perugia07.pdf .

Mathews, P.M., Herring, T.A., Buffet, B.A., 2002, "Modeling of nutation and precession: New nutation series for nonrigid Earth and insights into the Earth's interior", J. Geophys. Res. , 107(B4), doi: 10.1029/2001JB000390.

Souchay, J., Loysel, B., Kinoshita, H., and Folgueira, M., 1999, "Corrections and new developments in rigid Earth nutation theory: III. Final tables REN-2000 including crossed-nutation and spin-orbit coupling effects", A&AS 135, 111.

Wallace P.T., 2009, "Recent SOFA Developments", This Volume.

Wallace P.T., Capitaine, N., 2006, "Precession-nutation procedures consistent with IAU 2006 resolutions", A&A 459, 3, 981.

RECENT SOFA DEVELOPMENTS

P.T. WALLACE
Space Science & Technology Department, Rutherford Appleton Laboratory,
Harwell Science and Innovation Campus, Didcot, Oxfordshire, OX11 0QX, UK
e-mail: patrick.wallace@stfc.ac.uk

ABSTRACT. SOFA is an IAU Division 1 service that provides authoritative fundamental-astronomy algorithms, including models for precession-nutation and Earth rotation. The selection of algorithms and the development of computer code is supervised by an international panel called the SOFA Review Board, and the resulting software collection is published through a dedicated website. The collection at present comprises 108 astronomy routines, 41 of which implement canonical models, plus 52 vector/matrix routines, all written in Fortran 77. Recent developments include (i) an explanatory document covering the facilities for calculating Earth orientation, (ii) a second version of the Collection, written in the C programming language, and (iii) a relaxation of the licensing conditions to facilitate use by industry. The presentation looks at aspects of the 2006 changes in the IAU precession-nutation, the increasing importance of software in the implementation of IAU models, and plans for strengthening SOFA's links with other components of IAU Division 1 and with the IERS.

1. INTRODUCTION

SOFA, which stands for *Standards of Fundamental Astronomy,* is a service operated by IAU Division 1 to provide authoritative fundamental-astronomy algorithms. It is run by an international panel, the *SOFA Reviewing Board,* and reports through Commission 19 (Rotation of the Earth). To reflect the breadth of the inputs needed for SOFA to perform its function effectively, the Board includes experts in fundamental astronomy and software, and its membership overlaps with relevant IAU working groups and the IERS Conventions effort. The present membership is John Bangert (USNO, USA), Mark Calabretta (ATNF, Australia), Anne-Marie Gontier (Observatoire de Paris, France), Catherine Hohenkerk (HMNAO, UK), Wen-Jing Jin (Shanghai Observatory, China), Brian Luzum (USNO, USA), Zinovy Malkin (Pulkovo Observatory, Russia), Jeffrey Percival (University of Wisconsin, USA) and Patrick Wallace (RAL, UK, chair). Board members who participated in the work discussed in this paper but who stepped down during 2007 were Wim Brouw (University of Groningen, Netherlands) and Dennis McCarthy (USNO, USA).

2. THE SOFA SOFTWARE COLLECTION

SOFA's output is in the form of a collection of computer codes, distributed through a website.[1] At the time of writing, the SOFA Software Collection comprises 160 Fortran subprograms. Two-thirds of these routines perform astronomical actions, the remainder providing support for vectors, rotation matrices and angular coordinates. Excluding pro forma license statements, the number of lines of code is just under 25,000, roughly half of which are comments.

A great many SOFA routines implement successive IAU precession-nutation models. Other topics include calendars, time scales, ephemerides (low precision), Earth rotation, polar motion, star space motion and certain star catalog transformations. A distinction is made between SOFA routines that implement specific models and ones that help knit these together into useful tools. 41 of the astronomy routines have the designation "canonical model", while the other 67 are classed as "support routines" (supplemented in turn by the 52 vector-matrix routines). These distinctions are important to some end

[1]The SOFA URL is currently http://www.iau-sofa.rl.ac.uk/; the website is hosted by the UK Hydrographic Office and maintained by staff of H.M. Nautical Almanac Office.

users, and are clearly specified in the preamble comments to each routine.

3. RECENT DEVELOPMENTS

The SOFA work during the year starting mid-2007 reflect decisions and recommendations made at a meeting of the Board held in Paris during April 2007. The main developments have been as follows:

- A new software release (Number 4, August 2007) was made that contains 39 additional Fortran SOFA routines to implement the IAU 2006 (P03, Capitaine et al. 2003) precession model that comes into force on 2009 January 1. In order to support the methods specified in IERS Conventions 2003, the SOFA routines include implementations of the precession-nutation based on direct series for CIP X, Y as well as implementations using spherical angles.[2]

- SOFA's software documentation consists mainly of the preamble comments that begin each routine. These are quite detailed and offer a good resource for "reference" purposes, but lack any kind of tutorial qualities. The Board decided to supplement this material with a 38-page "cookbook", called *SOFA Tools for Earth Attitude*.[3] While concentrating on Earth-attitude applications, the cookbook contains detailed examples that touch upon a wide range of SOFA capabilities.

- A version of the SOFA software in a second programming language, namely ANSI C, has been developed. See Section 4 for details.

- Fortran and C testbed programs have been developed. (The Fortran testbed was kindly contributed by Beth Stetzler of USNO.) These allow an end user to verify that he or she has successfully built the SOFA library, and that every routine can be called and passes simple tests.

- The licensing conditions for SOFA routines have been relaxed, to permit free use for all classes of user while at the same time protecting against unapproved modifications. Further details are given in Section 5.

- Consultations have been made concerning SOFA's role and its relationships with IAU Division 1 and IERS Conventions. This topic is developed in Sections 6 & 7.

4. SOFA/C

The SOFA Board's original decision to use Fortran 77 was conservative, but consistent with practices in fundamental astronomy at that time (1997). However, the development of versions of the SOFA software written in other programming languages was planned from the start.

The ultimate decision that the second version would be in ANSI C was reached after much debate, with some Board members favouring a modern object oriented (OO) language such as Java or C++. The further possibility was discussed of developing a special SOFA macro language which would capture algorithms once and for all, and allow automatic translation into multiple languages for distribution. However, after informal polls of the community, and having due regard for the available effort and expertise, it was decided to opt for plain ANSI C, and moreover to retain much the same structure (argument lists etc.) as the existing Fortran. However, internally the functions use C idiomatically, and features missing from Fortran such as a portable "include" are used to the full.

Apart from being a useful resource in its own right, the resulting C library is a good starting point for applications written in Java, C++, Python and so on, and it can be argued that the low-level approach SOFA has adopted avoids eroding the user's freedom of choice when designing the OO classes. At the time of writing, SOFA/C is complete, and release is imminent.

5. SOFTWARE LICENSING

The original license conditions for the SOFA software were drawn up with considerable care. The SOFA Board asserted ownership of the software and granted free use for non-profit research purposes, but

[2] This mixed canonical basis is a potential danger, and the end user is warned not to develop applications that use both methods and are sensitive to the microarcsecond-level differences between them.

[3] See http://www.iau-sofa.rl.ac.uk/2007_0810/sofa/sofa_pn.pdf

retained the right to charge a fee for commercial use. However, when enquiries from aerospace companies about acquiring SOFA licenses began to be received – there have been a handful of such cases to date – the obstacles to commercial exploitation became clear. The whole concept went against the grain of IAU (and IERS) activities in general, and none of the institutes of individual Board members was in a position to administer such a scheme. Consequently, the Board agreed it would be best to make the SOFA Collection "free software".

This left two problems to be solved. The first was that some of the standard free-software licenses, notably the GNU General Public License (GPL),[4] contain what has been called a "viral" element, that effectively prevents commercial use: when a company incorporates GPL items in its own products, the latter inherit the license conditions, which is usually not acceptable. The second difficulty was that whereas the world of free software approves of, and actively encourages, modification and enhancement by end users, as a way of harnessing "free" effort, this is anathema to SOFA: the circulation of "improved" versions, under the IAU banner, would be certain to lead to endless confusion. These rather unusual considerations made it necessary for SOFA once again to develop its own license conditions.

In the new SOFA license, free use is granted to all classes of user. Users may develop and distribute "derived works", but subject to these conditions (among others):

- Such derived works must say they use SOFA techniques but must not contain straight copies of what SOFA distributes;
- The source code must describe its relationship to SOFA;
- Routine names must be different from SOFA originals, and use of the *iau* prefix is prohibited;
- There must be no misrepresentation or false authorship claims, and no patent applications for SOFA algorithms;
- SOFA requirements must be reproduced intact and apply to users of the derived work.

6. USER CONFIDENCE

During the year covered by this report, the Board looked into complaints from one or two potential users that the official status of the SOFA software was unclear. SOFA has a very low profile as far as the IAU web site is concerned, and software products from such authorities as IERS Conventions appear to differ in subtle ways from what SOFA has provided. The user is thus faced with competing products, all claiming to be IAU-consistent, and all supposedly authoritative. What defines an IAU approved model?

- The wording of the Resolution?
- A Working Group report?
- A piece of software?
- A published paper?

...or some combination of the above? The related question is what the user is expected to do when shortcomings and differences surface.

A case in point is the IAU 2000A precession-nutation. The IAU Resolution (B1.6, 2000) adopted something that was at the time awaiting publication. The first authoritative realization available to the SOFA Board was the MHB_2000 Fortran code that was in circulation; SOFA adopted this code as its reference: SOFA's implementation must match to bit accuracy the numbers produced by MHB_2000. However:

- MHB_2000 treated the frame bias and the precession rate adjustments as if they were nutation components, applied in the mean system of date rather than of epoch. SOFA instead applies them directly to the appropriate classical precession angles.
- Only two components of the frame bias (ΔX and ΔY) were specified: SOFA added the missing third component, $\Delta\alpha$.

[4] http://www.gnu.org/licenses

- The MHB_2000 code used different Delaunay argument expressions for the luni-solar and planetary terms respectively; this oddity was retained by SOFA.
- The planetary argument expressions used in MHB_2000 were not quite the same as in the original references quoted; SOFA retained the MHB_2000 versions.
- The 1365 nutation terms included 38 duplicated and 3 triplicated frequencies; these were not noticed in time and appear in the SOFA code.
- The MHB_2000 code omitted certain small terms (the t term in the out-of-phase luni-solar amplitudes) that appeared in the tables subsequently published (and adopted by IERS Conventions).

There is in addition the problem (for users) that there are two different methods of implementing the IAU 2000A precession-nutation: via the classical angles, used by MHB_2000 and by SOFA, and via direct series for X, Y, used by IERS Conventions.

Most of these differences have only a small effect, undetectable by VLBI, but enough to be noticed by users comparing results from SOFA, IERS Conventions, the USNO NOVAS software and so on, all of which made different choices. And when the IAU replaced the precession part of the model with the P03 theory (2006, Resolution B.1) nothing was said explicitly about the tiny adjustments needed when combining the new precession model, with its revised obliquity and inclusion of $\dot{J}_2$, with the existing IAU 2000A nutation.

In the author's view, imperfections, ambiguities and omissions are inevitable when drawing up IAU Resolutions, and the problem for the community is how to deal with that fact of life. The questions to be answered include (i) Should the process of establishing IAU recommended models for fundamental astronomy be revised? (ii) Is the 3-year cycle too long? and (iii) Should a computer algorithm be a part of future Resolutions? The last suggestion would be a radical departure, but would eliminate uncertainty and ambiguity almost completely. Where the issue is less about algorithmic complication and more about the sheer size of a model, the alternative is for the IAU Resolution to refer to electronic tables that can be accessed through the Internet.

7. SOFA IN THE IAU HIERARCHY

The difficulties raised in the previous Section lead naturally to questions about SOFA's role and standing, and how it relates to the IAU and IERS. Does SOFA's status need to be more visibly endorsed by the IAU (and also the IERS)? For one thing, Board members need to convince their institutes that their SOFA work is important, and a more visible endorsement by the IAU would help. But more crucially the community must be able to trust the SOFA software, be confident of its long-term availability and support, and be convinced that the underlying review procedures are sound.

Another issue is SOFA's relationship to the IERS Conventions effort. The links between the two have grown over the years. Prior to the 2003 uptake of the IAU 2000A precession-nutation, SOFA-compatible software was supplied for the IERS Conventions website, and when designing new software to support the introduction of the IAU 2006 precession SOFA made decisions with IERS requirements specifically in mind (notably the implementation of the direct series for X, Y). More recently, there have been moves to harmonize IERS Conventions with SOFA programming standards. Possibilities for further strengthening the SOFA/IERS links have been raised by the IAU representative on the IERS Directing Board.

8. THE FUTURE

The completion of the SOFA algorithms for IAU 2006 precession and the imminent release of the C version have eased the pressure on SOFA to develop new software. The next technical area to consider might be the transformation between the barycentric and geocentric reference systems: parallax, light deflection and aberration. This means that the most important SOFA activities at present are to review and reform its constitution.

The immediate questions for IAU Division 1 are whether the SOFA Board should be enlarged, whether its constitution should be more formally defined, and whether it should be obliged to consult more widely than it does at present. The possibility of raising SOFA's profile on the IAU website needs to be raised. And, assuming SOFA is to continue its IAU Division 1 role, could it do so as part of a larger group of standards-related activities, located in an appropriate Commission?

THE PLANETARY EPHEMERIS REFERENCE FRAME

W.M. FOLKNER, J.S. BORDER
Jet Propulsion Laboratory, California Institute of Technology
4800 Oak Grove Dr., Pasadena, CA, 91109 USA
e-mails: William.M.Folkner@jpl.nasa.gov; James.S.Border@jpl.nasa.gov

ABSTRACT. The JPL planetary ephemeris is aligned to the ICRF through use of VLBI observations of spacecraft in orbit about Mars and Venus. VLBI measurements using DSN and ESA tracking stations have been supplemented by use of the Very Long Baseline Array for specific measurement campaigns. Currently the planetary ephemeris is aligned to the ICRF with an accuracy of 0.25 milli-arcseconds, nearing the accuracy of current quasar catalogs. The ephemeris dynamics are most accurately determined by range measurements to spacecraft, including spacecraft currently in orbit about Mars, Venus, and Saturn. Because the orbit of Mars is significantly perturbed by asteroids, a continued program of measurements is planned in order to support increasing ephemeris accuracy needs for Mars landers, including the upcoming Mars Science Laboratory.

1. THE CURRENT JPL PLANETARY EPHEMERIS

The current JPL planetary and lunar ephemeris is DE421 (Folkner et al. 2008). The DE421 ephemeris has been fit to a large number of spacecraft range and very-long- baseline interferometry (VLBI) measurements, most of which were not available for the widely used ephemeris DE405 (Standish et al. 1997).

Most notably the DE405 ephemeris preceded the wave of spacecraft to Mars starting with the Mars Pathfinder lander in 1997, followed by Mars Global Surveyor, Mars Odyssey, Mars Express, and Mars Reconnaissance Orbiter. The dynamics of the Earth and Mars orbits were thus based mainly on range measurements to the Viking landers between 1976 and 1982, with the orbits of Mercury and Venus determined primarily by radar ranging from Earth to the planetary surfaces. The DE405 ephemeris was aligned to the International Celestial Reference Frame mainly through VLBI observations of the Magellan spacecraft in orbit about Venus between 1990 and 1995. Unfortunately the Magellan spacecraft radio system did not support range measurements.

Starting in 1997 range measurement to Mars have been made regularly, with an accuracy about ten times better than the Viking lander range data due to improved radio measurement systems and use of higher radio frequency than used for Viking, reducing the effects of charged particles in the heliosphere. The recent Mars spacecraft also support regular VLBI observations. The VLBI measurement accuracy has improved by a factor of ten from Magellan through improved calibration techniques and changes to the spacecraft radio systems.

The ephemerides of the other planets have also benefited from recent space missions. The Venus Express spacecraft has provided accurate range measurements greatly improving the accuracy of the orbit of Venus. The Galileo and Cassini spacecraft measurements have significantly improved the orbit accuracy for Jupiter and Saturn. The orbit of Mercury will shortly be improved from measurements from the MESSENGER spacecraft. The orbits of Neptune and Uranus have been improved by modern astrometric observations.

2. SPACECRAFT VLBI MEASUREMENTS FOR PLANETARY EPHEMERIDES

Spacecraft VLBI measurements used for planetary ephemeris estimation have primarily been made for spacecraft in orbit about other planets. Measurements of the Doppler shift of the spacecraft radio signal determine the spacecraft positions relative to the planet center of mass with an accuracy as good as $1m$ for spacecraft in low-altitude orbits (e.g. Konopliv et al. 2006) and less accuracy for high-altitude orbits such as Galileo about Jupiter. The VLBI measurements are performed using two or more tracking antennas on Earth. Most measurements to date have been made with the NASA Deep Space Network, with an antenna at Goldstone California used to co-observe with either an antenna in Madrid, Spain or in Canberra, Australia. The measurements are made by determining the difference in arrival time at

the Earth tracking antennas of a radio signal transmitted by the spacecraft spanning a wide bandwidth, often two narrow-band tones separated by about $40MHz$. The separation between tracking stations and station clock differences are calibrated by observing the difference in arrival time of the radio signal from an extra-galactic radio source shortly before or after the spacecraft observation. The difference in delay time divided by the baseline length gives a measurement of one component of the direction to the spacecraft. Since the Goldstone and Madrid stations are at nearly the same latitude, VLBI measurement made on the Goldstone-Madrid baseline are largely aligned with right ascension. Measurements on the Goldstone- Canberra baseline are about mid-way between right ascension and declination. (More details on the VLBI measurement technique are given in Thornton and Border, 2000).

Figure 1 shows the differences between measured and estimated angular position of Venus from the ephemeris DE421 on the two DSN baselines from the Magellan spacecraft in orbit about Venus. These measurements were used to align the DE405 ephemeris to the ICRF. The average of the residuals is about 3 mas (milli-arcsecond) and largely represents the errors in the Magellan VLBI measurements and the difference in orientation of DE421 and DE405.

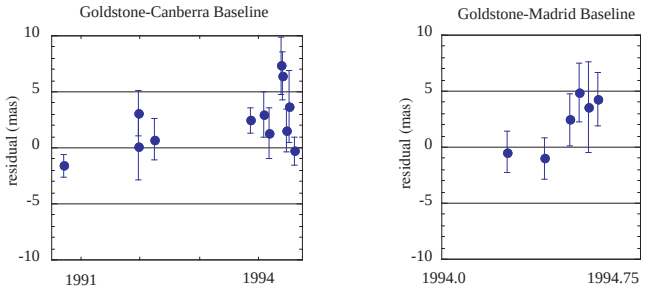

Figure 1: Residuals of VLBI measurements of the Magellan spacecraft in orbit about Venus, relative to the JPL planetary ephemeris DE421.

Figure 2 shows the VLBI measurement residuals of recent Mars-orbiting spacecraft relative to the DE421 ephemeris. The average of the residuals is about 0.25 mas and may be limited by the different quasar catalogs used to reduce the VLBI measurements from different periods. The uncertainty in the Mars ephemeris is thus currently thought to be about 0.25 mas. The orbit uncertainty predicted into the future increases with time since the interaction of asteroids with unknown masses limits the dynamical modeling accuracy. Thus to maintain the ephemeris accuracy requires an on-going measurement campaign, which is required for the upcoming Mars Science Laboratory project.

3. FUTURE PROSPECTS

Since the Mars spacecraft VLBI measurement residuals appear to be limited, at least in part, by changes in quasar catalog, the current measurement set will shortly be adjusted to a common quasar catalog. Further measurements are expected to be acquired at the rate of about one per month at least until the Mars Science Laboratory arrival at Mars.

4. REFERENCES

Folkner, W.M., Williams, J.G., Boggs, D.H., 2008, "The Planetary and Lunar Ephemeris DE 421", JPL Memorandum 343R-08-003 (ftp://ssd.jpl.nasa.gov/pub/eph/planets/ioms/de421.iom.v1.pdf)

Konopliv, A., Yoder, C., Standish, E.M., Yuan, D.-N., Sjogren, W.L., 2000, "A global solution for the Mars static and seasonal gravity, Mars orientation, Phobos and Deimos masses, and Mars ephemeris", Icarus 182, pp. 23-50

Standish, E.M., Newhall, X.X., Williams, J.G., Folkner, W.M., 1997, "JPL Planetary and Lunar Ephemerides", Willmann-Bell, Richmond, Virginia

Thornton, C.L., Border, J.S., 2000, "Radiometric Tracking Techniques for Deep-Space Navigation", Monograph 1, Deep-Space Communications and Navigation Series, Jet Propulsion Laboratory, California Institute of Technology, (http://descanso.jpl.nasa.gov)

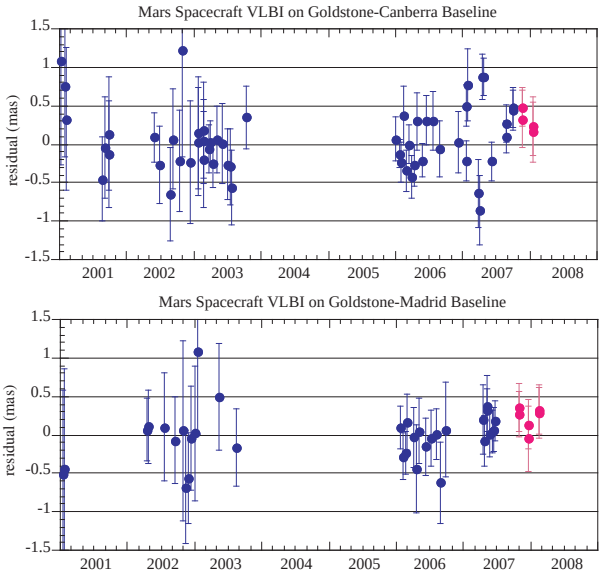

Figure 2: Residuals of VLBI measurements of Mars Global Surveyor, Mars Odyssey, and Mars Reconnaissance Orbiter in orbit about Mars, relative to the JPL planetary ephemeris DE421. Measurements prior to December 2007 (in blue) were included in the estimation process leading to the DE421 ephemeris, measurement taken later (in red) were not used in the estimation process.

Acknowledgements. The research described in this paper was carried out at the Jet Propulsion Laboratory, California Institute of Technology, under a contract with the National Aeronautics and Space Administration.

EPHEMERIDES EPM2008: THE UPDATED MODEL, CONSTANTS, DATA

E.V. PITJEVA
Institute of Applied astronomy RAS
Kutuzov Quay 10, 191187 St.-Petersburg
e-mail: evp@ipa.nw.ru

The EPM ephemerides of IAA RAS originated in seventies of the last century and have been developed since that time. The renovation of the planet part of the EPM ephemerides includes the constants, model, observation data.

Recent years of high-precision data of spacecraft have yielded significant improvements of a whole set of constants for planet ephemerides. Masses of planets have been determined by different authors from data of spacecraft orbiting and passing near planets or from observations of satellites of these planets. Other constants like the value of the Astronomical Unit (AU) in meters, masses of the largest asteroids, the ratio of the masses of the Earth and the Moon, etc. have been obtained inside the EPM2008 ephemeris fitting process.

The updated model of EPM2008 includes Eris which surpasses Pluto in the mass and the other 20 largest trans-Neptunian objects into a process of the simultaneous numerical integration in addition to other bodies. The simultaneous numerical integration of the equations of motion of the nine major planets, the Sun, 301 biggest asteroids and 21 TNO, the Moon, and the lunar physical libration has performed in the Parameterized Post-Newtonian metric for General Relativity taking into account perturbations due to the solar oblateness and perturbation from the massive ring of small asteroids.

Moreover, some tests have been made for estimating influence other TNO on the motion of planets. Their perturbations have been modeled by the perturbation from a circular ring having a radius 43 AU and different masses. The minimum mass of this ring is equal to the mass of 100000 bodies with 100 km in diameter and density is equal 2 g/cm^3, it is 110 masses of Ceres or 1.5 mass of the Moon. The maximum mass of the ring is expected the minimum mass by 100 times. Influence of the ring is noticeable for more accurate observations — data from spacecraft. The rms residuals and the weight unit errors for these date after fitting standard and test EPM ephemerides are given in Table 2.

Ephemeris	Viking-1	Viking-2	MGS	Odyssey	σ_0
EPM	9.15	3.0	1.45	1.34	0.764
EPM$_{MmaxTNO}$	10.85	5.54	1.98	1.70	0.786

Table 1: The rms residuals in m and the weight unit errors σ_0 for EPM and EPM$_{MmaxTNO}$

It is seen that the maximal mass of the TNO ring is too large, but perhaps, its value may be estimated in future.

Database, to which EPM2008 have been adjusted (more 550000 measurements), includes in addition to previous observations since 1913, recently spacecraft measurements (Odyssey, Cassini, VEX, MRO) (see below). As for optical data, we use observations of satellites for all the outer planets which are more accurate than the observations of their parent planets and are practically free from the phase effect. We are developing numerical theories of main satellites of the outer planets and are improving them to the observations.

Observations used for constructing EPM2008

Optical data of outer planets and satellites 1913–2008, 49890

$USNO$
$Pulkovo$
$Nikolaev$
$Tokyo$
$Bordeaux$
$LaPalma$
$Flagstaff$
TMO

Types	Years	*A priori* accuracy
optical transit	1913–1994	$1'' \rightarrow 0\farcs5$
photoelectric transit	1963–1998	$0\farcs8 \rightarrow 0\farcs25$
photographic	1913–1998	$1'' \rightarrow 0\farcs2$
CCD	1995–2008	$0\farcs2 \rightarrow 0\farcs06$

Radar observations of Mercury, Venus, Mars, 58112

$Millstone$
$Haystack$
$Arecibo$
$Goldstone$
$Crimea$

Types	Years	*A priori* accuracy
ranging	1961–1997	100 km → 150 m

Spacecraft data obtained by DSN 1971–2008, 437613

$Mariner-9$	$Venus$
$Pioneer-10,11$	$Jupiter$
$Voyager$	$Jupiter$
$Phobos$	$Mars$
$Ulysses$	$Jupiter$
$Magelan$	$Venus$
$Galileo$	$Jupiter$
$Viking-1,2$	$Mars$
$Pathfinder$	$Mars$
MGS	$Mars$
$Odyssey$	$Mars$
$Cassini$	$Saturn$
VEX	$Venus$
MRO	$Mars$

Types	Years	*A priori* accuracy
ranging	1971–2008	6 km → 1 m
differenced range	1976–1997	1.3 → 0.1 mm/sec
radial velocity	1992–1994	0.1 → 0.002 mm/sec
Δ VLBI	1990–2007	12 mas → 0.3 mas

More 260 parameters have been determined while improving the planetary part of EPM2008. As compared with our previous version EPM2006 described in the paper of Pitjeva (2008), the orbital] elements of the addition 4 satellites of the outer planets, velocities for three orientation angles of the EPM2008 ephemerides relative to the International Celestial Reference Frame (ICRF), masses of the addition three asteroids, constant bias for the new VEX and MRO spacecrafts were estimated also.

EPM2008 have been oriented to ICRF with the accuracy better than 1 mas by including into the total solution the 118 ICRF-base VLBI measurements of spacecraft (Magellan, Phobos, MGS, Odyssey, Venus Express, and Mars Reconnaissance Orbiter) 1989 – 2007 near Venus and Mars.

Mean values and rms data residuals obtained from the adjustment of the EPM2008 ephemerides are shown in Tables 2–3, plots of some observations are given on Fig. 1–3. For example, it is seen from Table 2, the rms residuals of ranging for Viking are 8.8 m, for Pathfinder 2.8 m, for MGS 1.4 m, and for Odyssey 1.2 m.

The values of some parameters are given below. The Astronomical Unit = 149597870697(3) m, the Earth-Moon mass ratio $M_{Earth}/M_{Moon} = 81.300568(3)$, the masses of Ceres, Pallas, Vesta: $M_{Ceres}/M_{\odot} = 4.71(3) \cdot 10^{-10}, M_{Pallas}/M_{\odot} = 1.03(2) \cdot 10^{-10}, M_{Vesta}/M_{\odot} = 1.34(2) \cdot 10^{-10}$, where the real errors are shown, obtained from comparison with different fitting versions of DE and EPM ephemerides.

REFERENCES

Pitjeva, E.V., 2008, "Recent models of planet motion and fundamental constants determined from position observations of planets and spacecraft" Journées 2007: "The Celestial Reference Frame for the Future", N. Capitaine (ed), Paris, pp. 65–69.

Planet	Type of data	Time interval	N	$< O-C >$	σ
MERCURY	τ [m]	1964–1997	746	0	575
VENUS	τ [m]	1961–1995	1354	-2	584
	Magellan dr [mm/s]	1992–1994	195	0	0.007
	MGN,VEX VLBI [mas]	1990–2007	22	1.6	3.0
	Cassini τ [m]	1998–1999	2	4.0	2.4
	VEX τ [m]	2006–2007	547	0.0	2.45
MARS	τ [m]	1965–1995	402	0	738
	Viking τ [m]	1976–1982	1258	0	8.8
	Viking $d\tau$ [mm/s]	1976–1978	14978	-0.02	0.89
	Pathfinder τ [m]	1997	90	0	2.8
	Pathfinder $d\tau$ [mm/s]	1997	7569	0	0.09
	MGS τ [m]	1998–2006	7342	0	1.4
	Odyssey τ [m]	2002–2008	5682	0	1.2
	MRO τ [m]	2006–2007	378	0	1.6
	spacecraft VLBI [mas]	1984–2007	96	0.0	0.7
JUPITER	spacecraft τ [m]	1973–2000	7	0.0	11.8
	spacecraft VLBI [mas]	1996–1997	24	-1.8	9.5
SATURN	spacecraft τ [m]	1979–2006	33	1.0	20.2
URANUS	VGR2 τ [m]	1986	1	1.9	105
NEPTUNE	VGR2 τ [m]	1989	1	0.0	14

Table 2: Mean values and rms residuals for radiometric observations

Planet	N	$< O-C >_\alpha$	σ_α	$< O-C >_\delta$	σ_δ
VENUS*	4	1.5	2.0	1	6.5
JUPITER	12518	15	187	-30	199
JUPITER*	16	0.1	1.9	-4.1	6.1
SATURN	14296	-1	167	-3	160
SATURN*	68	2.2	2.9	4.2	5.9
URANUS	11446	6	178	2	208
URANU*	2	-45	9	-25	12
NEPTUNE	10982	7	160	9	205
NEPTUNE*	2	-11	3.5	-14	4.0
PLUTO	5134	1	191	6	197

Table 3: Mean values and rms residuals for optical observations and spacecraft encounters* (α and δ in mas, 1913–2008)

Time interval	Number of obs.	ε_x mas	ε_y mas	ε_y mas	ω_x mas/cy	ω_y mas/cy	ω_z mas/cy
1989–1994	20	4.5±0.8	−0.8±0.6	−0.6±0.4			
1989–2003	62	1.9±0.1	−0.5±0.2	−1.5±0.1			
1989–2007	118	1.2±0.2	1.1±0.2	0.5±0.1	−49.6±3.0	−4.5±3.5	16.0±2.0

Table 4: The rotation angles for the orientation of EPM2008 onto ICRF

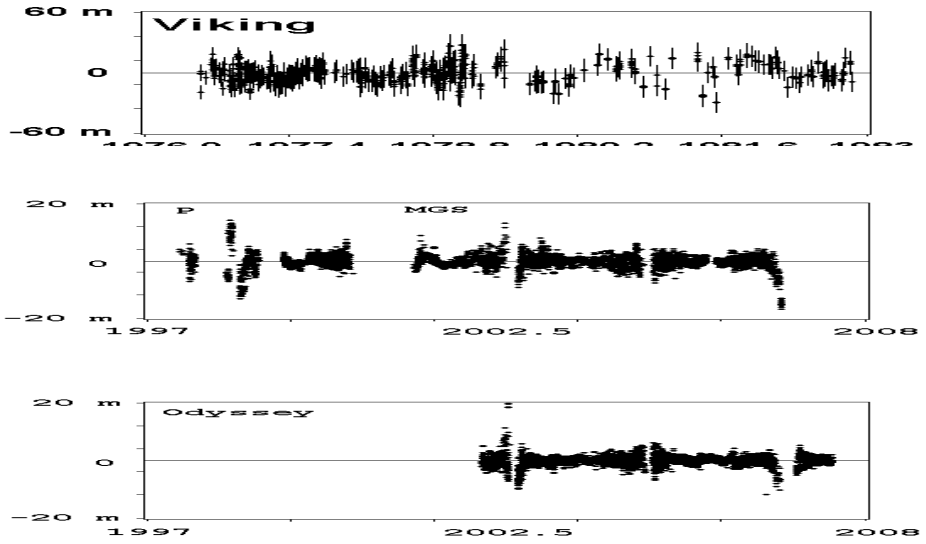

Figure 1: Viking, Pathfinder (P), MGS, Odyssey range residuals

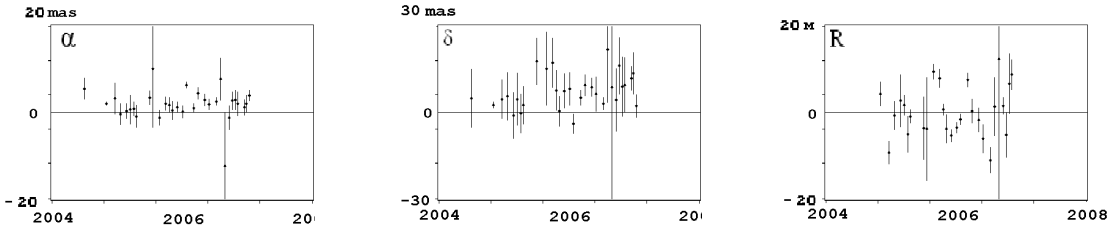

Figure 2: Saturn residuals from Cassini encounters

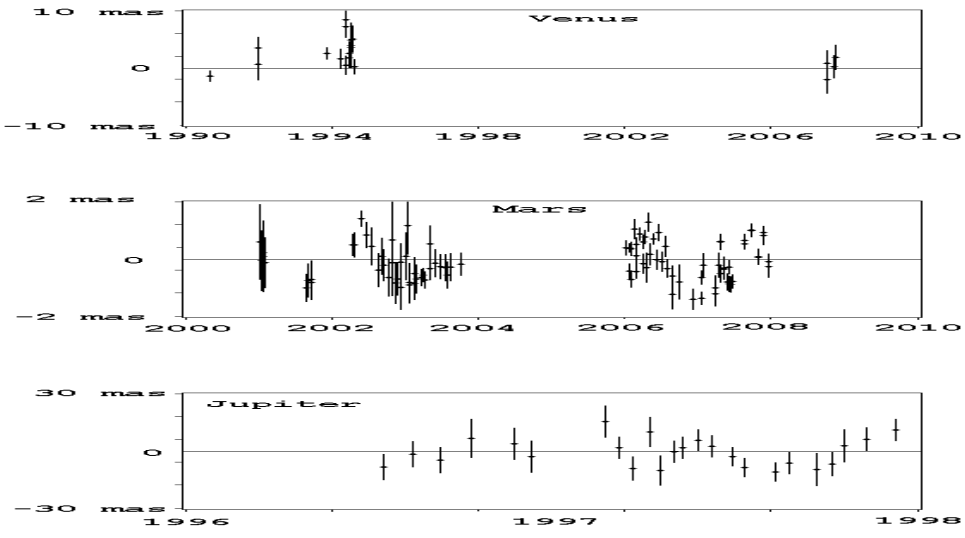

Figure 3: Venus, Mars, Jupiter spacecraft VLBI residuals

LUNAR NUMERICAL THEORY EPM2008 FROM ANALYSIS OF LLR DATA

E.I. YAGUDINA
IAA, RAS, St-Petersburg, Russia
10 Kutuzov quay, St-Petersburg, 191187, Russia
e-mail: eiya@ipa.nw.ru

ABSTRACT. The analysis of Lunar Laser Ranging (LLR) data from 1970 till 2008 has been carried out to improve the lunar part of the luni-solar ephemerides EPM2008 under developing. The dynamical model of the lunar rotation takes into account the effects of elasticity of the lunar body and the tidal dissipation in the Moon. The orbital parameters of the Moon, parameters of the physical libration and coordinates of the retro-reflectors have been estimated. The new ephemeris are compared with DE403, DE405 and DE421 versions of the JPL ephemerides. All the calculations have been carried out in the framework of the universal software package ERA developed for scientific research in the ephemeris and dynamical astronomy.

1. INTRODUCTION

The very precise now days LLR observations are the basis for construction of the modern lunar ephemeris. The high accuracy of the modern LLR data demands dynamical theories of a adequate precision. Such theories are developed and supported by JPL, USA (DE403, DE405, DE421); by IMCCE (INPOP06), Observatoire de Paris and is under developing in IAA RAS (Russia Institute of Applied Astronomy)-EPM-Ephemerides Planets and Moon. The application of EPM to planets is very known and are in use. The preliminary version of lunar numerical theory has been presented (for example, in Krasinsky, 2002), where analysis of 14612 LLR observations of time interval 1970-2001 was fulfilled, the selenodynamical parameters have been obtained. At present analysis of 16320 LLR observations (time interval is 1970-2008) has been included in processing for improving ephemeris of the Moon and obtaining some selenodynamical parameters. To estimate the precision of our EPM2008 ephemeris the result has been compared with three versions of DE ephemerides.

2. OBSERVATIONS

In the present analysis 16320 LLR observations have been included in the processing . They have been carried out mainly at McDonald (Texas), where at different epochs three different sites were activated as McDonald, MLRS1 and MLRS2; Cerga station (France) and a set of observations of two years duration made at Haleakala Observatory (Hawai). Number of observations at each site is shown in Table 1. In LLR

Station	Time interval	Number of LLR observations
McDonald	1970 Mar - 1985 Jun	3439
MLRS1	1985 Jan - 1988 Jan	275
MLRS2	1988 Aug - 2008 Jan	2933
HALEAKALA	1989 Nov - 1990 Aug	694
CERGA	1985 Jan - 2008 Jan	8979
TOTAL	1970 Mar- 2008 Jan	16320

Table 1: Distribution of LLR observations

analysis a number of parameters appear to be strongly correlated and may be only estimated because four reflectors could be observed: 1-Apollo 11, 2-Apollo 14, 3-Apollo 15, 4-Lunahod2. The number

of ranging to Apollo 11, Apollo 14, Apollo 15, Lunahod2 are 1585, 1557, 12724 and 452, respectively. Unfortunately such disparity of the observations distribution deteriorates the reliability of the estimates of a number of selenodynamical parameters. Before 1998 the observations are obtained by request from observatories, later on they have been retrieved from FTP server *ccdisa.gsfc.nasa.gov/pub/slr*, partly from *oca.eu/gemini/donnees/las_lune*, some of them have been obtained by private correspondence.

3. MODEL, EPHEMERIDES AND PARAMETERS

In this paper only a brief summary of the used model is described. The precise dynamical model of the Moon motion has been constructed under Krasinsky by simultaneous numerical integration the equations of orbital and rotational motions of the Moon, major planets, five biggest asteroids (the integration includes reduced equations of 295 asteroids, it is important for the major planets but not for the Moon). Potential of the Moon is calculated up to 4-th order of the zonal index, that of the Earth includes the 2th order harmonics C_{20} and C_{22}. Tidal perturbations in the lunar orbital motion caused by tidal dissipation on the Earth's body is computed by the model with a constant lag, the effects of elasticity of the lunar body has been taken into account. The integration was carry out by Everhart's method with the automatically operated choice of the step of integration. Partials of ranging respectively to dynamical parameters of the orbital and rotational model of the Moon are computed mostly by integration of variational equations; in a few cases they have been obtained by integration of the rigorous system of equations with slightly varied values of the parameters under study. The set of parameters includes the lunar initial coordinates and velocities, libration angles and their velocities, Stocks coefficients of the selenopotential, the angle of tide delay, the coordinates of reflectors, observational stations etc. The LLR data set has been also processed with a help of DE403, DE405 and DE421 lunar ephemerides making use of the partials obtained with EPM (these partials are not distributed along with DE ephemerides). However nominal values of many of the estimated parameters in DE ephemerides are not known; that is why only corrections to such parameters could be determined. Then we might implement the improved values of dynamical parameters only to EPM, but not to DE ephemerides. In Table 2 the list of 65 parameters have been improved , all of them being then fed back to EPM by iteration. As lunar rangings

N	Parameters estimated
1-6	Lunar orbital state vector for the epoch JD 2446000.5
7-12	Euler's angles and their time derivatives for the same epoch
13	Lag of the Moon's body tides
14-16	Lunar Love numbers k1, h2,l2
17	Lag of the Earth's body tides
18-29	Harmonics of lunar potential from c_{20} to s_{33}
30-38	Coordinates of reflectors A11, A14, L2
39	Coordinate X for Appollo 15
40-54	Coordinates of 5 stations
55-56	Corrections to orientation of the Earth's equator ϵ, ϕ
57-58	Secular trends $\dot{\epsilon}$, $\dot{\phi}$
59-60	Secular trends in siderial angles of the Earth and Moon
61	Undimentional lunar moment of inertia $g = C/mR^2$
62-64	Moon's core-mantle factors v_1, v_2, v_3
65	Moon's core-mantle coupling factor k

Table 2: List of estimated parameters

are invariant relatively to the rotation of the Earth-Moon system as a whole, all set of parameters of orientation of this system cannot be determined simultaneously. Due to this reason two coordinates of the most often observable reflector Apollo15 have been fixed (longitude and latitude). Values of these two parameters were obtained from a simplified solution made as the first step, in which lunar libration have not been improved. LLR observations are sensitive to the Earth's gravitational constant Gm_E. The investigation shows that the observable effect cannot be reliably separated from corrections to X

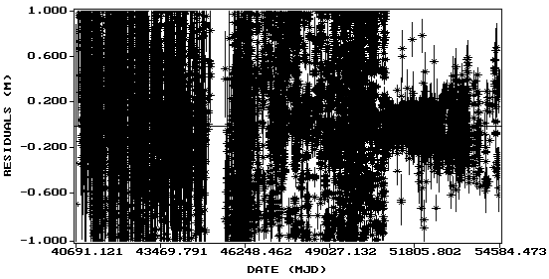

Figure 1: DE403

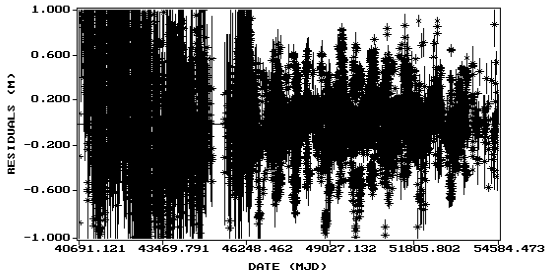

Figure 2: DE405

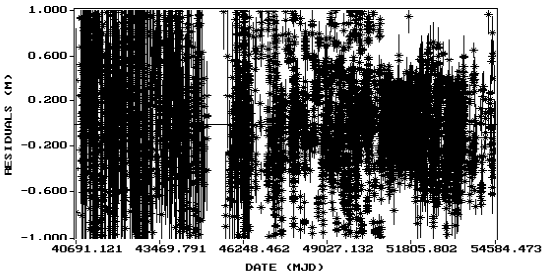

Figure 3: DE421

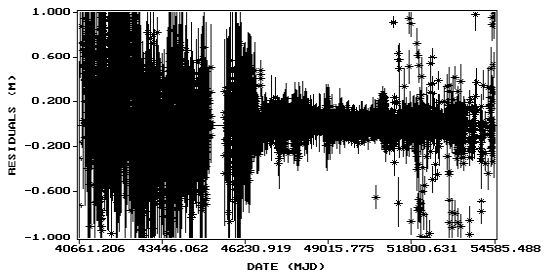

Figure 4: EPM2008

coordinate of the reflectors. Thus the value Gm_E has not been included to the list of parameters.

4. DISCUSSION OF RESULTS

Using the derivatives from EPM all calculations have been made by help of three versions of DE ephemerides: DE403, DE405, De421. The pre-fit, post-fit residuals and number of included LLR observations in the processing of DE ephemeredes along with EPM one can see in Table 3.

ephemeris	pre-fit cm	post-fit cm	Number of obs.
DE403	23.66	5.24	16105
DE405	23.20	5.10	16102
DE421	22.96	5.06	16087
EPM2008	6.32	6.32	16115

Table 3: Internal precision of DE ephemerides compared with EPM

Because the EPM model has been implemented by the obtained corrections the post-fit residuals practically coincide with difference $O - C$ computed with the improved model equal 0.422ns (6.32 cm). For now days version of EPM post-fit and pre-fit residuals is coincide. For DE ephemerides a similar work could not be carried out in the full scale and only estimated of coordinated of reflectors and Love numbers h2, l2 of the Moon have been incorporated. The plots of Fig1, Fig2, Fig3, Fig4 shows us the residuals. In tables 4 corrections to initial coordinates and velocities of the Moon for all DE versions are presented. The plots of Fig1, Fig2, Fig3, Fig4 shows us the residuals. In table 5 the corrections to parameters of Moon's libration are shown. One can see that the corrections to the parameters of libration in all versions of DE ephemerides are big enough but they cannot be feed in ephemeris because the values of these parameters are not known (they are not distributed with the ephemerides).

5. CONCLUSION

1. The investigation has proved a necessity to refine the model of dissipative effect of the lunar

Corrections to coordinates of the Moon	DE403 m	DE405 m	DE421 m
dX	-0.346 ± 0.094	2.625 ± 0.092	0.021 ± 0.091
dY	-0.320 ± 0.055	-1.516 ± 0.054	-0.232 ± 0.053
dZ	0.988 ± 0.088	0.509 ± 0.086	0.342 ± 0.085
Corrections to velocities of the Moon	DE403 m/sec	DE405 m/sec	DE421 m/sec
dV_x	-0.043 ± 0.009	0.247 ± 0.008	-0.004 ± 0.008
dV_y	0.105 ± 0.022	0.560 ± 0.027	0.024 ± 0.022
dV_z	0.006 ± 0.009	0.228 ± 0.008	0.001 ± 0.008

Table 4: The corrections to the DE ephemerides parameters

Corrections to Euler's angles	DE403	DE405	DE421
$d\phi$	0.137 ± 0.030	-0.439 ± 0.029	0.922 ± 0.028
$d\theta$	-0.299 ± 0.010	-0.169 ± 0.009	-0.546 ± 0.009
$d\psi$	-1.502 ± 0.022	0.756 ± 0.022	-5.659 ± 0.022
Corrections time derivatives of Euler's angles	DE403 arc/year	DE405 arcs/year	DE421 arcs/year
$\mathrm{d}\dot{\phi}$	-0.182 ± 0.005	-0.103 ± 0.005	-0.327 ± 0.005
$\mathrm{d}\dot{\theta}$	-0.007 ± 0.002	0.031 ± 0.002	-0.081 ± 0.002
$\mathrm{d}\dot{\psi}$	0.167 ± 0.005	0.095 ± 0.005	0.301 ± 0.005

Table 5: The corrections to the DE ephemerides parameters

rotation for EPM ephemeris by integration the equations of orbital and rotation motions with retarded argument. We used the simplified model of dissipation tides of the Moon. This is the main source of errors the present model.

2. The outward accuracy of DE ephemerides is about 22-24 cm. The inward accuracy of DE ephemerides cannot be used by independent researcher because it is not possible to feed back the correction values.

The study has been carried out by the software package ERA for Ephemeris Astronomy.

6. REFERENCES

Aleshkina E.Yu, Krasinsky G.A., Vasiliev M.V., 1997, "Analysis of LLR data by the program ERA", Proceedings of IAU Colloquium 165, 1996, Poznan, Poland, pp.228-232.

Krasinsky G.A.,2002, "Selenodynamical parameters from analysis of LLR observations of 1970-2001", Comminications of the IAA RAS, N 148, 2002, pp. 1-27.

Krasinsky G.A., Vasiliev M.V.,1997, "ERA: knowledge base for Ephemeris and dynamical astronomy", Proceedings of IAU Colloquium 165, 1996, Poznan, Poland, pp.239-244.

EVOLUTION OF INPOP PLANETARY EPHEMERIDES

A. FIENGA[1,2], J. LASKAR[2], P. KUCHYNKA[2], H. MANCHE[2], M. GASTINEAU[2], L. SOMENZI[2]
[1] Observatory of Besançon, France
e-mail: agnes.fienga@obs-besancon.fr
[2] IMCCE, Paris Observatory, France

ABSTRACT The last version of the planetary ephemerides developed at the Paris Observatory and at the Besançon Observatory is presented here. INPOP08 is a 4-dimension ephemerides since it provides to users positions, velocities of planets and relation between TT and TDB. Investigations leaded to improve the modelling of asteroids are described as well as the new sets of observations used for the fit of INPOP08. New observations provided by the European Space Agency (ESA) deduced from the tracking of the Mars Express (MEX) and Venus Express (VEX) missions are presented as well as the normal point deduced from the Cassini mission. We show the huge impact brought by these observations in the fit of INPOP08, especially in term of Venus and Saturn orbits, Sun oblateness adjustment and PPN parameter β estimations.

1. INTRODUCTION

Since INPOP06 (Fienga et al. 2008), several improvements were brought to the planetary ephemerides developed at the Paris Observatory and at the Besançon Observatory. First, we now integrate at each step the TT-TDB relation defined by IAU 2006. Such integration makes the planetary ephemerides and TT-TDB totally consistent. INPOP08 can then be seen as the first 4-D planetary ephemerides (Klioner 2008). Besides this time-scale aspect, new independent constraints for asteroid modelling were established. New data are used in the fit of INPOP08. These new data are Cassini normal points of Saturn and MEX and VEX tracking observations provided by ESOC.

2. TT-TDB AND ASTEROID MODELLINGS

2.1 TT-TDB

As defined by IAU 2006, TT is such as

$$TT = TCB - L_G.(JD_{TCG} - T_0), \tag{1}$$

and TDB is such as

$$TDB = TCB - L_B.(JD_{TCB} - T_0) + TDB_0. \tag{2}$$

So estimating TT-TDB is equivalent to integrate at each step of the integration of the equation of planet motion:

$$\begin{cases} TT - TDB = F(TDB) \\ \dfrac{dF}{dTDB} = f(\vec{x}, \vec{\dot{x}}, \vec{\ddot{x}}, \mu, \beta, \gamma, c^2, c^4) \end{cases} \tag{3}$$

with TDB_0 estimated at T_0.

Such integration is implemented in INPOP08 and we then can provide to users positions and velocities of planets as well as the differences between TT and TDB as defined in the IAU 2006 recommendations. Such differences are provided under the form of Chebychev polynomials as positions and velocities of planets. Adjustment of INPOP08 is done by using the new TT-TDB relation as estimated during the integration of INPOP planet equations of motion. As no differences are noticeable in the residuals estimated using the Fairhead and Bretagnon (1990) relation or the INPOP08 relation, no iteration is necessary in the estimation of the TT-TDB.

Table 1: Residuals obtained from INPOP06 and INPOP08

Planet	Type of Data [unit]	Nbr	INPOP06 1σ	INPOP08 1σ
Saturn Cassini	ra [mas]	31	11	4
Saturn Cassini	de [mas]	31	10	7
Saturn Cassini	range [m]	31	1851	21
Venus	VLBI [arcsec]	18	0.003	0.003
Venus	range [m]	488	1400	1400
Venus Vex	range [m]	10768	174.829	3.194
Mars MGS	range [m]	10410	3.70	1.371
Mars MEX	range [m]	4704	15.40	1.998
Mars Path	range [m]	90	7.633	7.647
Mars Vkg	range [m]	1245	17.396	19.916
Mars	VLBI [arcsec]	44	0.000	0.001

2.2 ASTEROID MODELLINGS

We have studied individual accelerations on Earth-Mars distances induced by about 25000 known asteroids (ASTORB/Tesdesco et al. 2005 /SIMPS). ¿From there, we have shown that after 300 asteroids, the effects can be averaged and represented by a ring. We have estimated by Monte Carlo simulations on albedo errors, than the mass of this ring is $GM_{ring} = (0.34 \pm 0.1).10^{-10}\ M_\circ$ at 3.14 AU . This study gives new independent constraints for asteroids in INPOP because the mass of this ring is obtained independently from the planetary ephemerides. We also stress that such independent constraints help for the Sun oblateness J2 determination because the effects of the asteroid ring and the Sun J2 have very similar impact on the inner planet distances to Earth. For more details, see Kuchynka et al. (2008) in the same volume.

3. MEX,VEX AND CASSINI NEW DATASETS

Cassini normal points are the first tracking data about Saturn. They are synthetic observations deduced from the navigation tracking of the Cassini spacecraft orbiting the Saturn satellite system. These observations are synthetic is the sense that they are estimated after the adjustment of the Saturn satellite orbits to Cassini tracking data. We then have to deal with differences in Earth-Saturn distances, geocentric angles between DE405 and synthetic positions of Saturn deduced from Cassini tracking. These observations have a few meter and few milliarcsecond (mas) accuracy. This accuracy has to be compared to the 100 mas accuracy of optical observations used to fit the planetary ephemerides. Thanks to these data, a huge improvement in the Saturn orbit was done as one can see on table 1.

The VEX data are the first Venus observations since Magellan (VLBI) in 1994. They are deduced from the tracking data of the VEX spacecraft orbiting Venus. They are provided by ESOC navigation team and they are one-way range residuals of the VEX probe after accurate determination of its orbit. The remaining signature in such residuals is induced by systematic errors in the Venus orbit itself (see for instance red curve on figure 1). The VEX data have a few meter accuracy compared to about 1 km accuracy of direct range used to fit INPOP06. The improvement of the Venus orbit is very important as one can see on table 1 and on figure 1. Before VEX, the orbit of Venus was accurate of about 200 m thanks to 18 VLBI Magellan data (1994). With VEX, Venus orbit has a few meter accuracy over the VEX time interval.

The MEX data are the first data with VEX tracking one-way range provided by ESOC from navigation processes. The MEX dataset represents now 30 % of the Mars INPOP08 dataset. They are the same level of accuracy that the MGS and Mars Odyssey data provided by JPL. With the MEX data, we have been able to test the correlation between the JPL navigation procedures and the adjustment of the planetary ephemerides used by the same navigation softwares. The fact that the MEX observations provide the same type of residuals as the JPL MGS and MO do tells us that no systematic effects are introduced in the JPL reduction procedures. Furthermore, in a more political point-of-view, the MEX data and the VEX data are a unique chance for European teams to develop fully independent planetary ephemerides.

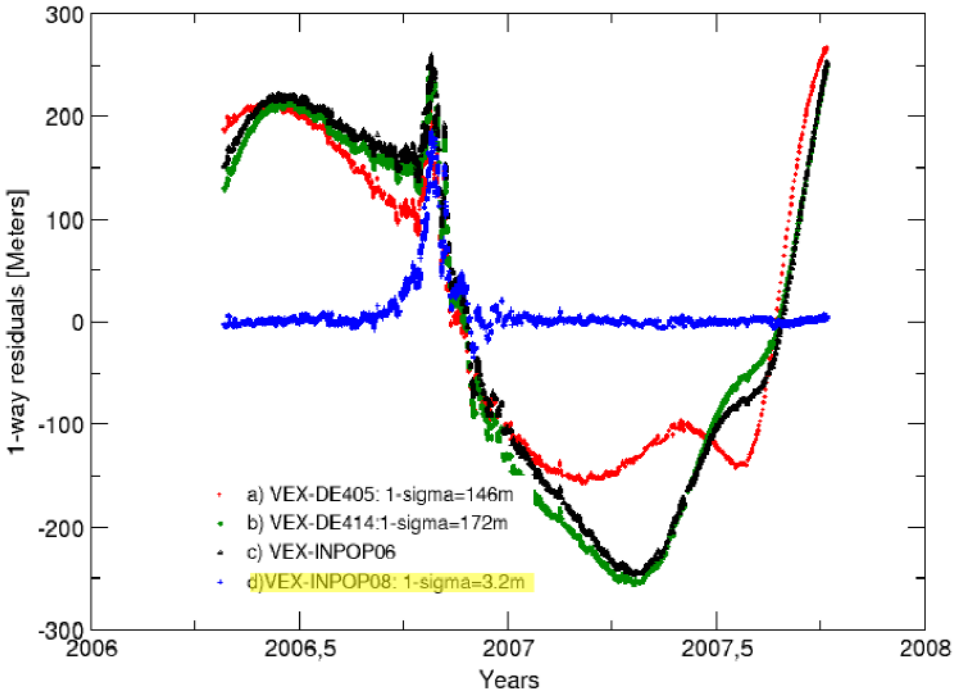

Figure 1: VEX 1-way residuals with the new INPOP08 fitted to VEX and MEX data, and other ephemerides not fitted on VEX observations (INPOP06, DE405, DE414). The solar conjunction is clearly identified with the pick of residuals in October 2006.

4. RESULTS

As it is described previously, the new data used in INPOP08 fitting procedure bring a lot of improvement in the estimation of the planet orbits. Besides these improvements, 33 asteroid masses as well as Earth-Moon ratio, Astronomical Unit, Sun J2 and PPN parameter β are estimated. The most important fitted parameters are presented on table 2. As Venus is 7 times more sensitive to general relativity than Mars, the use of the new VEX data allow to decorrelate the J2 and the PPN β with a good accuracy. Tests of sensitivity of the most accurate datasets (Mercury range, Mars tracking, VEX tracking, Saturn Cassini normal points) to the determination of the Sun J2 and PPN β have been done. They show that the most sensitive data are the Mars and VEX tracking data because even if the two planets are less sensitive to J2 and β than Mercury, their tracking observations are far more accurate than the Mercury direct range. Furthermore they indicate a limit of $|1-\beta| < 5.10^{-4}$: if β is such as $|1-\beta| > 5.10^{-4}$, then residuals of MGS, MEX and VEX are changed significantly. However if β is such as $|1-\beta| < 5.10^{-4}$, then no modification in the residuals are noticeable. We can then conclude than INPOP is not sensitive to β upto $|1-\beta| < 5.10^{-4}$.

5. REFERENCES

Fairhead, L. Bretagnon, P.,1990, "An analytical formula for the time transformation TB-TT" ,A&A , 229, 240, 247

Fienga, A., Manche, H., Laskar, J.,Gastineau, M., 2008, "INPOP06: a new numerical planetary ephemeris", A&A , 477, 315, 327

Klioner, S. A., 2008, IAU Symposium, 248, 356

Tedesco, E. F., Cellino, A., Zappala, V., 2005, "The Statistical Asteroid Model. I. The Main-Belt Population for Diameters Greater than 1 Kilometer",AJ , 129, 2869

Table 2: Physical parameters fitted in INPOP08. Other values deduced from planetary ephemerides are presented for comparisons.The given uncertainties are given at 5-sigma for the GMs and 1 formal sigma for others. NC stands for non-considered and NE as non-estimated. For AU, the presented values are the differences in meters between the fitted values and the AU value of the IERS conventions 2003, AU_{IERS03} = 149597870.691 km.

	Unit	DE414	DE421	INPOP06	INPOP08
Mass of Ceres	$10^{-10}M_\odot$	4.699 ± 0.028	4.685	4.756 ± 0.020	4.658 ± 0.045
Mass of Vesta	$10^{-10}M_\odot$	1.358 ± 0.016	1.328	1.348 ± 0.015	1.392 ± 0.015
Mass of Pallas	$10^{-10}M_\odot$	1.026 ± 0.028	1.010	1.025 ± 0.005	1.076 ± 0.010
Mass of Juno	$10^{-10}M_\odot$	0.149 ± 0.015	0.116	NE	0.075 ± 0.015
Mass of Iris	$10^{-10}M_\odot$	0.060 ± 0.010	0.060	0.058 ± 0.005	0.050 ± 0.010
Mass of Bamberga	$10^{-10}M_\odot$	0.047 ± 0.007	0.048	0.046 ± 0.003	0.056 ± 0.004
Mass of Ring	$10^{-10}M_\odot$	3.12 ± 0.27	NE	0.34 ± 0.1	1.0 ± 0.3
Distance of Ring	UA	2.8	NE	2.8	3.14
Density of the C class		1.62 ± 0.07	1.09	1.56 ± 0.02	1.54 ± 0.07
Density of the S class		2.08 ± 0.19	3.45	2.18 ± 0.04	1.94 ± 0.14
Density of the M class		4.32 ± 0.37	4.22	4.26 ± 0.12	4.98 ± 0.50
Sun J2	10^{-7}	2.34 ± 0.49	2.0	2.46 ± 0.40	1.82 ± 0.47
EMRAT		81.300568	81.300569	NE	81.300540 ± 0.00005
AU-AU_{IERS03}	m	8.62	8.62	NE	8.22 ± 0.11

THE GEODESIC PRECESSION IN THE INPOP EPHEMERIDES

H. MANCHE[1], J. LASKAR[1], A. FIENGA[2], N. CAPITAINE[3], S. BOUQUILLON[3],
G. FRANCOU[3], M. GASTINEAU[1]
[1] ASD, IMCCE, UMR8028, Observatoire de Paris, UPMC
77 avenue Denfert-Rochereau, 75014 Paris
e-mail: manche@imcce.fr
[2] Observatoire de Besançon
41 bis av. de l'Observatoire, 25000 Besançon
[3] SYRTE, Observatoire de Paris, CNRS, UPMC
61 avenue de l'Observatoire, 75014 Paris

ABSTRACT. The INPOP ephemerides include the eight planets, Pluto and the Moon, and are fitted to planetary observations (and to Lunar Laser Ranging data for the version currently in development). They also integrate the Earth orientation. Compared to INPOP06 (Fienga et al., 2008), the next version takes into account the geodesic precession for the Earth and for the Moon. We present here some comparisons with analytical theories of the Earth rotation and the consequences on LLR computations.

Warning: All the INPOP solutions presented here, except INPOP06, are working versions. The numbering from INPOP08_b1 to INPOP08_b5 is valid only inside this paper, to facilitate comparisons. In particular, the following INPOP08_bx solutions are not exactly the one that is described in this volume by Fienga et al. in "Evolution of INPOP planetary ephemerides".

1. THE GEODESIC PRECESSION FOR THE EARTH

Together with the equations of motion of the bodies of the Solar System, INPOP integrates a model of Earth orientation for the computations of interactions between the Earth and other bodies due to its non spherical potential (figure effects). It should be noted that for the reduction of the observations, the more precise IAU2000 model is used. By integrating a spin model for the Earth, the precession-nutation evolution is consistent with the planetary and lunar motions, and integrations are not limited by the polynomial development of the precession.

The orientation of the Earth in the dynamical part of INPOP08_b1 (solution close to INPOP06) is modellized by its angular momentum $\vec{G}$. Its time derivative is equal to the sum of all external torques exerted upon the Earth, and then is solution of the differential equation:

$$\dot{\overrightarrow{G}} = \sum_{bodies} \left(\overrightarrow{M}_2 + \overrightarrow{M}_3 + \overrightarrow{M}_4 + \overrightarrow{M}_{tides} \right) \tag{1}$$

In this expression, $\overrightarrow{M}_i$ are the torques due to the zonal coefficients J_i of the Earth potential ($\overrightarrow{M}_3$ and $\overrightarrow{M}_4$ were neglected in INPOP06) and $\overrightarrow{M}_{tides}$ is the torque due to the deformation of the Earth raised by the Moon and the Sun (solid tides).

Initial conditions and the C/MR^2 ratio are fitted to the CIP-P03 coordinates over a period of 200 years around J2000. The CIP-P03 is the unit vector computed with the precession of Capitaine et al. (2003) and the nutations of Mathews et al. (2002).

The left side of Fig.1 (black curves) shows the differences between the orientation of the Earth integrated in INPOP08_b1 (X and Y coordinates of the unit vector $\overrightarrow{G}/\|\overrightarrow{G}\|$) and the CIP-P03.

The discrepancies between INPOP08_b1 and CIP-P03 are mainly due to the transformation function of Mathews from solid to non-rigid Earth and to the different nature of the pole compared: the CIP-P03 is related to the figure-axis of the Earth, whereas $\overrightarrow{G}$ is the angular momentum. Instead of comparing $\overrightarrow{G}$ to the CIP-P03, one defines REN2000-P03 as the pole computed with the precession of Capitaine et al. (2003) and with the angular momentum nutations of REN2000 (Souchay et al., 1999), converted to the

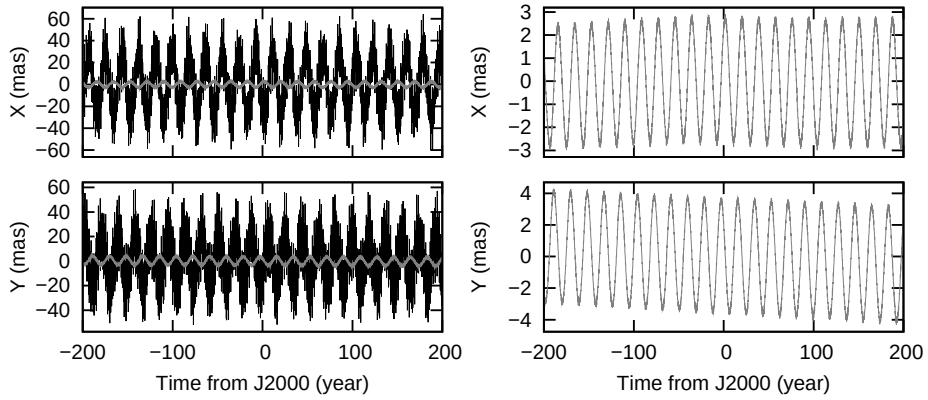

Figure 1: These curves show the discrepancies between INPOP08_b1 (or INPOP06) and analytical solutions for the Earth rotation (CIP-P03 in black, REN2000-P03 in grey). On the right side, the discrepancies between INPOP08_b1 and REN2000-P03 are plotted with a more convenient scale than on the left side. X and Y are the GCRS coordinates of the Earth's pole, expressed in milliarcsecond over a period of 200 years around J2000.

same dynamical ellipticity as IAU2000/P03. REN2000 is the rigid Earth theory on which the IAU 2000 nutation is based.

On Fig.1 (grey curves), one can see that the pole computed in INPOP08_b1 is much closer to REN2000-P03 than to CIP-P03. But there is still a small periodic signal, whose period is 18.6 years.

To reduce this signal, we introduced the geodesic precession, which was omitted in INPOP08_b1. If the Earth is considered as a point mass gyroscope, the geodesic precession can be modelized as an additional torque in the angular momentum equation (see Misner et al., 1973):

$$\dot{\overrightarrow{G}} = \sum_{bodies} \left(\overrightarrow{M}_2 + \overrightarrow{M}_3 + \overrightarrow{M}_4 + \overrightarrow{M}_{tides} \right) + \frac{1+\gamma}{2} \sum_{bodies} \frac{\mu}{c^2 r^3} \left(\vec{v}_E \wedge \vec{r} \right) \wedge \overrightarrow{G} \tag{2}$$

In this expression, μ is the product of the gravitational constant G by the mass of the body, c is the light velocity, $\vec{r}$ is the Earth-Body position vector and $\vec{v}_E$ is the barycentric velocity vector of the Earth. In fact, only the Solar contribution is taken into account, the next one (Lunar), which is 1000 times lower, has been neglected. Without any change of parameter (same initial conditions and C/MR^2 value), the solution INPOP08_b2 is built from INPOP08_b1 by adding the geodesic precession.

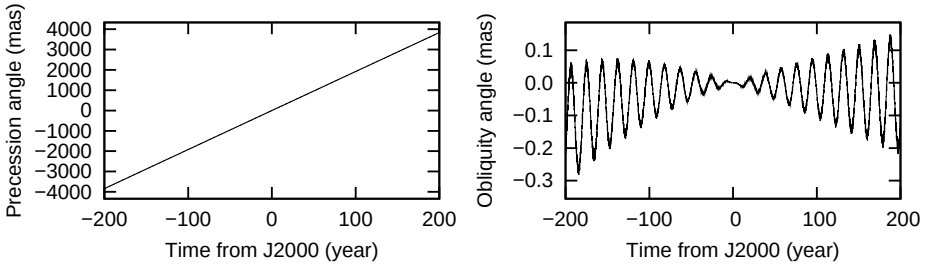

Figure 2: Comparison between the INPOP solutions for Earth rotation with and without the geodesic precession (respectively INPOP08_b2 and INPOP08_b1). The precession angle and the obliquity angle are expressed in milliarcsecond over a period of 200 years around J2000.

The main effect is observed on the precession angle, where the geodesic precession induces a linear drift (see Fig. 2). The slope is measured to 1.9193 arcsecond per century, and is close to the value from Brumberg et al. (1992). Because of this drift, initial conditions, and mainly the C/MR^2 ratio need to be changed. After a new fit on REN2000-P03 coordinates, one obtains INPOP08_b3, and the curves Fig.3 show the improvement.

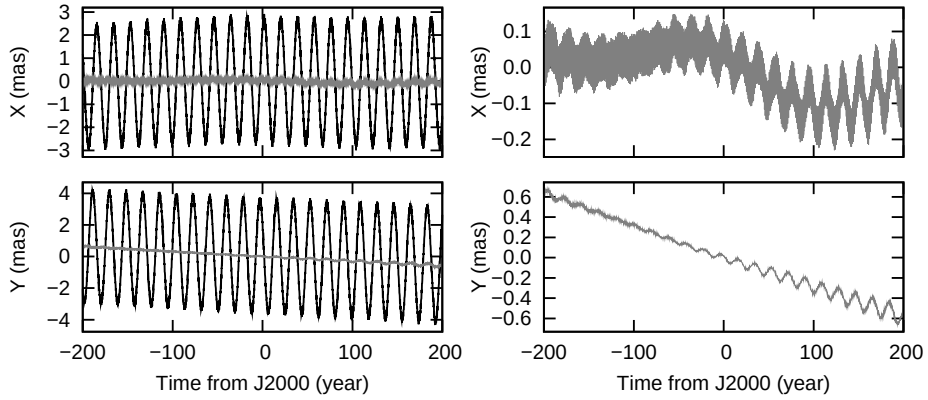

Figure 3: These curves show the discrepancies between REN2000-P03 and INPOP08_b1 (in black), and between REN2000-P03 and INPOP08_b3 (in grey, both on left and right sides). X and Y are the GCRS coordinates of the Earth's pole, expressed in milliarcsecond over a period of 200 years around J2000.

2. THE GEODESIC PRECESSION FOR THE MOON

Once the geodesic precession has been taken into account for the Earth, similar torques can be added to the angular momentum equation of the Moon:

$$\dot{\overrightarrow{G}} = \sum_{bodies} \left(\overrightarrow{M}_{C_{nm}} + \overrightarrow{M}_{S_{nm}} + \overrightarrow{M}_{tides} \right) + \frac{1+\gamma}{2} \sum_{bodies} \frac{\mu}{c^2 r^3} \left(\vec{v}_M \wedge \vec{r} \right) \wedge \vec{G} \tag{3}$$

In this expression, $\overrightarrow{M}_{C_{nm}}$ and $\overrightarrow{M}_{S_{nm}}$ are the torques exerted by bodies upon the Moon due to the potential coefficients C_{nm} and S_{nm} (the Moon is not considered to have a revolution symmetry), $\overrightarrow{M}_{tides}$ is the torque due to the deformation of the Moon raised by the Earth and the Sun (solid tides), and the last term is similar to the one seen earlier for the Earth. The contributions of both the Sun and the Earth (only 100 times lower) are here taken into account. INPOP08_b4 is built from INPOP08_b3, with the geodesic precession for the Moon, without any change of parameter.

The effect on LLR residuals depends on the location of the reflector, as it is shown on Fig.4. For Apollo XI (and for Apollo XIV, which is not shown in the figure), one can see that the effect of the geodesic precession (upper center plot) is not significant compared to the residuals (upper left corner). But for Lunakhod2 (the results are similar for Apollo XV), the geodesic precession induces a signal (see bottom center plot) that is not negligible when compared to LLR residuals (bottom left corner). Therefore, a new fit of parameters on LLR data is needed, leading to INPOP08_b5. After fit, the differences between INPOP08_b1 and INPOP08_b5 (right side of Fig.4) are small when compared to LLR residuals (left side of Fig.4).

Finally, Fig.5 shows the INPOP08_b1 LLR residuals for the Grasse and MLRS2 ground stations (black dots). The discrepancies between INPOP08_b1 and INPOP08_b5 (both fitted to LLR data) do not exceed 2 millimeters (gray dots), and the two solutions have the same standard deviation (4.75 cm for Grasse, 4.07 cm for MLRS2 before J2000 and 6.60 cm for MLRS2 after J2000).

3. CONCLUSION

In conclusion, taking into account the geodesic precession for the Earth is necessary as it is shown by comparing with analytical solutions like REN2000-P03. The same correction applied to the Moon librations does not improve the LLR residuals: the effect is not negligible, but can be fitted with a change of parameters.

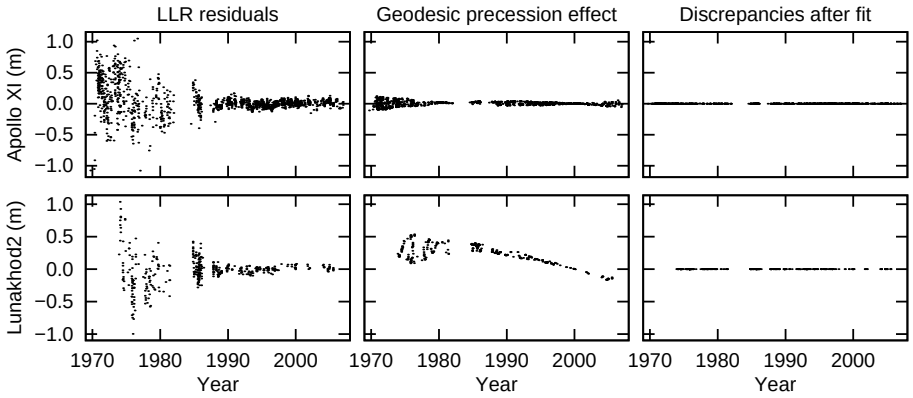

Figure 4: On the left side are shown the LLR residuals (in meter) for Apollo XI and Lunakhod2 reflectors computed with INPOP08_b1 (same as for INPOP08_b3). On the center column is shown, at the same scale and for the same dates of observations, the effect of the geodesic precession for the Moon (difference between INPOP08_b3 and INPOP08_b4). The right column show the differences between the two solutions fitted to LLR observations INPOP08_b1 and INPOP08_b5, respectively without and with the geodesic precession for the Moon.

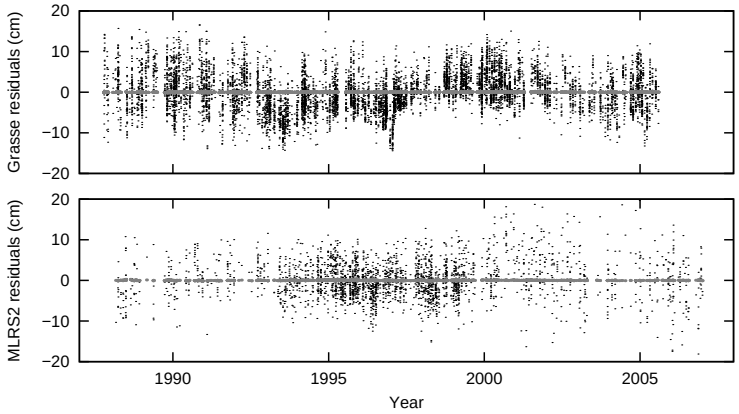

Figure 5: LLR residuals (in centimeters) for Grasse and MLRS stations, computed with INPOP08_b1 (in black). The discrepancies between INPOP08_b1 and INPOP08_b5 are shown in gray.

4. REFERENCES

Brumberg, V. A., Bretagnon, P., Francou, G., 1992, Proceedings of the Journées 1991 "Systèmes de référence spatio-temporels", N. Capitaine ed., Observatoire de Paris, pp. 141-148

Capitaine, N., Wallace, P. T., Chapront, J., 2003, "Expressions for IAU2000 precession quantities", A&A 412, pp. 567-586

Fienga, A., Manche, H., Laskar, J., Gastineau, M., 2008, "INPOP06: a new numerical planetary ephemeris", A&A 477, pp. 315-327

Fienga, A., Laskar, J., Kuchynka, P., Manche, H., Gastineau, M., Somenzi, L., 2009, "Evolution of INPOP planetary ephemerides", this volume

Mathews, P. M., Herring, T. A., Buffett, B. A., 2002, "Modeling of nutation-precession: New nutation series for non-rigid Earth, and insights into the Earth's interior", J. Geophys. Res. , 107 (B4), doi: 10.1029/2001JB000390

Misner, C. W., Thorne, K. S., Wheeler, J. A., 1973, "Gravitation", San Francisco: W.H. Freeman and Co, pp. 1118-1119

Souchay, J., Loysel, B., Kinoshita, H., Folgueira, M., 1999, "Corrections and new developments in rigid Earth nutation theory", A&AS 135, pp. 111-131

THE ASTRONOMICAL UNITS

N. CAPITAINE, B. GUINOT
SYRTE, Observatoire de Paris, CNRS, UPMC,
61, avenue de l'Observatoire, 75014 – Paris, France
e-mail: n.capitaine@obspm.fr; guinot.bernard@wanadoo.fr

ABSTRACT. The IAU-1976 System of astronomical constants includes three astronomical units (i.e. for time, mass and length). This paper reports on the status of the astronomical unit of length (ua) and mass (M_{Sun}) within the context of the recent IAU Resolutions on reference systems and the use of modern observations in the solar system. We especially look at a possible re-definition of the ua as an astronomical unit of length defined trough a fixed relation to the SI metre by a defining number.

1. INTRODUCTION

The IAU-1976 System of astronomical constants includes three astronomical units, namely the astronomical unit of time, the day, D, which is related to the SI by a defining number (D=86400 s), the astronomical unit of mass, i.e. the mass of the Sun, M_{Sun}, and the astronomical unit of length, ua. Questions related to the definition, numerical value and role of the astronomical units have been discussed in a number of papers, e.g. (Capitaine & Guinot 1995), (Guinot 1995), (Huang et al. 1995), (Standish 1995, 2004) and (Klioner 2007). The aim of this paper is to report on recent views on these topics.

The role of the astronomical unit of time, which (as is the Julian century of 36 525 days) is to provide a unit of time of convenient size for astronomy, does not need further discussion. In the dynamics of the solar system, the unit of mass appears only through the products GM (dimension $\mathrm{L}^3\mathrm{T}^{-2}$). The gravitational constant G having a relative uncertainty of about 10^{-5}, only relative masses are obtained accurately. For these reasons we restrict our discussion to the unit of length. We recall first its historical basis and current use, then we consider a reform which might be desirable.

2. THE SI AND THE ASTRONOMICAL UNIT OF LENGTH (UA)

Physicists and astronomers have a common goal: transferring the quality of the measurement of time to that of length. This can be achieved by assigning conventional values to physical constants whose dimensions are only time and length. However an essential condition is the possibility of a realization of the unit of length with a satisfactory accuracy.

In physics, the metre of the SI has been defined in 1983 from a fixed value of the speed of light. This was made possible by the progress in the measure of optical frequencies providing wavelengths and then lengths in metre by interferometry. Of course the direct use of the definition is especially useful for distances encountered in geodesy and astronomy.

In astronomy, the unit of length (ua) is, in fact, defined by the adoption of a conventional value of GM_{Sun} [The official definition in the IAU-1976 System of astronomical constants, rather obscure, refers to the Gaussian gravitational constant, k (with $k^2 = G$ in astronomical units), whose value has never been changed]. The realization of the ua was based on the measurement of mean motions and on the laws of Newtonian dynamics (i.e. Kepler's third law: $n^2a^3 = GM_{Sun}$ for a planet of negligible mass).

This conceptual difference between physicists and astronomers can be explained by the poor accuracy of evaluation of distances in SI through classical astrometric measurements: parallaxes, radial velocities, annual aberration leading to relative uncertainties of order 10^{-4}. As long as the value GM_{Sun} remains conventional, the link between the ua and the SI metre is subject to measurement and has an uncertainty.

3. EVOLUTION OF MEASUREMENTS AND MODELS, CONSEQUENCES

High accuracy positioning in the solar system is now based mainly on range and Doppler measurements, especially for telluric bodies (Moon, Mercury, Venus, Mars, ...) (Standish 2004, Pitjeva, 2005, Fienga et al. 2006, Folkner et al. 2008). Moreover, the space-time references have been defined in General

Relativity framework in 1991, with further improvements from 2000 to present. In the adopted metrics, the GMs of celestial bodies remain meaningful quantities.

For the telluric bodies, for which there are precise range and Doppler measurements, coordinates are obtained in metres with a very high accuracy and GM_{Sun} is obtained in SI units with a relative uncertainty of 4 $\times 10^{-9}$ (according to IERS Conventions 2003). For the planets for which observations are mainly angular measurements (Jupiter, Saturn, etc.), the relative distances are determined as with old observations and the scale in SI of the global solution is provided by the GM_{Sun} value obtained from telluric bodies, as above. If very precise angular measurements for some bodies of the solar system are available, it may happen that the use of the experimental value for GM_{Sun} leads to less precise absolute distance in SI than the relative distances. This is quite similar to the effect of the use of the experimental value for the ua on distances expressed in ua as it is currently defined.

4. POSSIBLE REFORM IN THE STATUS OF THE ASTRONOMICAL UNITS

Basically there are two possibilities, both valid in the Newtonian context as well as in general relativity:

- GM_{Sun} conventionally fixed in astronomical units and the SI value of the ua estimated, which corresponds to the current official status of the ua,

- GM_{Sun} estimated in SI from the observations and the ua, if needed, conventionally expressed as a fixed number of SI metres, which would correspond to a reform in the status of the ua.

In the latter case, the use of the ua is a simple change of unit. This ua has the same character as the metre: it is defined as a unit of proper length (Huang et al. 1995). Therefore its relation to the metre is not affected by changes in the relativistic metric (introduction of scaling factors).

5. CONCLUSION

A re-definition of the ua through a fixed relation to the SI metre by a defining number (whose value should be in agreement with the current best estimate of the ua for continuity reasons) appears desirable for modern dynamics of the solar system. This would mean:

- determining experimentally GM_{Sun} which would cease to have a "fixed" value in astronomical units,
- limiting the role of the ua to that of a unit of length of "convenient" size for some applications.

Such a change of status of the ua would

- be a great simplification for the users of the astronomical constants,
- let possible variations of the mass of the Sun, and/or G, appear directly,
- avoid an unnecessary deviation from the SI.

6. REFERENCES

Capitaine, N., Guinot, B., 1995, "Astronomical units and constants in a relativistic framework", *Highlights of Astronomy*, Vol 10, IAU, 1994, I. Appenzeller (ed), 201.

Fienga A., Manche H., Laskar J., Gastineau M., 2008, INPOP96, "A new numerical planetary ephemeris", A&A 477, 315.

Folkner W.M., Williams J.G., Boggs D.H., 2008, Memorandum IOM 343R-08-003, Jet Propulsion Laboratory.

Guinot B., 1995, "Le système international d'unités (SI) et les unités astronomiques", Proc. Journées 1994 "Systèmes de référence spatio-temporels", N. Capitaine (ed), 21.

Huang T.-Y., Han C.-H., Yi Z.-H., Xu B.-X., 1995, "What is the astronomical unit of length?", A&A 298, 629.

IERS Conventions (2003), *IERS Technical Note 32*, D.D. McCarthy and G. Petit (eds), Frankfurt am Main: Verlag des Bundesamts für Kartographie und Geodäsie, 2004.

Klioner S., 2007, "Relativistic scaling of astronomical quantities and the system of astronomical units", A&A 478, 951.

Pitjeva, E.V., 2005, "High-Precision Ephemerides of Planets EPM and Determination of Some Astronomical Constants", Solar System Research, Volume 39, Issue 3, pp.176-186.

Standish E.M. 1995, "Report of the IAU WGAS Sub-Group on Numerical Standards", *Highlights of Astronomy*, Vol 12, IAU 1994, Appenzeller, I. (ed), 180.

Standish E.M., 2004, "The Astronomical Unit now", in "Transits of Venus, New views of the Solar System and Galaxy", Proc. IAU Coll. 196, D.W. Kurtz (ed), 183.

ON THE HISTORY OF THE ASTRONOMICAL CONSTANTS

S. DÉBARBAT
SYRTE, Observatoire de Paris, CNRS, UPMC
e-mail: suzanne.debarbat@obspm.fr

1. INTRODUCTION.

This paper summarizes, historical developments concerning star catalogues and the unification of astronomical constants, as well as related decisions about time. The text is mainly presented as a chronological list.

2. CONNAISSANCE DES TEMPS (CDT) AND THE NAUTICAL ALMANAC (NA)

The French ephemerides, CDT, created under Dalencé (1640-1707), was published, for the first time, for the year 1679. It was a very small book. Due to the duration of voyages, the navigators were used to employ the Desplaces'ephemerides established for ten years. After some time, the CDT appeared a few years in advance, which was not sufficient for navigators, but very appropriate to astronomers's uses. The reference meridian was the symmetry axis of the newly built *Observatoire Royal* of Louis the 14th, fixed on 1667 June 21. The NA appeared almost one century later, in 1767, under Maskelyne (1732-1811), the *Astronomer Royal* of the King of England.

Some major constants used in *Connaissance des Temps* up to 1868, have been, in chronological order:

1679: Data resulting from observations performed by astronomers; as examples: refraction studies from Picard (1620-1680), Cassini I (1625-1712), solar and lunar data from observations (various observers), satellites of Jupiter by Cassini I.

1785: Data issued from observations, catalogues, calculations; as examples: refraction after studies by Cassini I, Flamsteed (1646-1719), Bradley (1693-1762), La Caille (1713-1762), Le Monnier (1715-1799), catalogues of stars from La Caille, Tobias Mayer (1723-1762).

1868: CDT values for: *Precession* (discovered by Hipparchus (II cy BC)), further studies by Picard, Cassini I (17th century) and others (18th and 19th centuries): **50.2401"**; *Nutation*, discovered, by Bradley (1726): **9.2236"** from Peters (1806-1880); *Aberration*, discovered by Bradley (1729): **20.463"**; *Refraction* tables by Laplace (1749-1827). Satellites of Jupiter: tables by Damoiseau (1768-1846).

3. THE FIRST UNIFICATION OF STAR CATALOGUES AND CONSTANTS

1887: The *Carte du Ciel*, an international enterprise for cataloguing the sky, is launched by Mouchez (1821-1892), then director of *Observatoire de Paris*, and Gill (1843-1914), the director of The Cape Observatory.

1895: In view of a general catalogue of stars, the unification of constants to reduce the observations appeared necessary. Downing (1850-1917), the Superintendant of NA, requested the opinion of Lœwy (1833-1907), the director of the CDT, placed under the responsibility of the *Bureau des Longitudes* in Paris; the Bureau agreed about the necessity of unification for astronomy, navigation and geodesy.

1896: *Conférence internationale des étoiles fondamentales* (Paris, *Bureau des longitudes*). Participants: Bauschinger (1860-1934, Berliner Jachbuch), Newcomb (1835-1909, Nautical Almanac, USA), Downing (1850-1897, Nautical Almanac, GB), Lœwy (CDT), Tisserand (1845-1896, *Observatoire de Paris*), Backlund (1846-1916, Pulkovo Observatory), Gill (Southern hemisphere Observatories), Faye (1814-1902, president of the *Bureau des longitudes*); invited and secretariat: Sande Bakhuysen (1838-1923, Leiden) and Trépied (1845-1907, Algiers Observatory).

The discussed and adopted values were: *Nutation*: Gill 9.2068"; Newcomb 9.214"; Chandler 9.198"; value suggested by Lœwy and adopted : **9.21"**. *Aberration*: Lœwy and Puiseux : 20.46"; Gill 20.467"; Newcomb 20.48"; value suggested by Lœwy and adopted: **20.47"**. *Precession*: needed more research by Newcomb; by the end, adopted value: **50.2564"**. The decision was to apply the adopted values starting from 1901.

4. INTERNATIONAL MEETINGS FROM 1900 TO WORLD WAR I

1911: Upon invitation of B. Baillaud (1848-1934), then director of the *Observatoire de Paris*, a *Congrès international des éphémérides astronomiques* was held, in Paris (October 23-26). Among participants: Backlund (Pulkovo), Cohn (Berliner Jachbuch), Dyson (Greenwich), Eichelberger (American Ephemeris), Gill (UK), Perrine (Cordoba Observatory). *French side* : André, Baillaud, Bigourdan, Deslandres, Picard, Poincaré, Radau, with Andoyer and La Baume-Pluvinel as secretaries.

After the unification of time over the French territory (1891), the Airy Greenwich meridian line became the time reference (1911) in France, following meetings (Roma 1883 and Washington 1884). The *Système métrique décimal* (called sometimes MKS) included *Mètre, Kilogramme*, and the *seconde* (a fraction of the mean solar day), the second being added after a proposal said to be from Gauss (1777-1855).

1912: *Conférence internationale de l'heure* (Paris, *Bureau des longitudes*) after, in 1899, the first successful time signals by wireless telegraphy from Hamburg, later from *Observatoire de Paris* and the *Tour Eiffel* summit, up to 5000 kilometers (1910). A project is established (*Association internationale de l'Heure*, including a *Bureau international de l'heure*), with statutes and *Convention diplomatique*.

1913: *Conférence diplomatique* (Paris, October 20-26). Project accepted, signed by participants when approved by their governments. Limit for other signatures: 1914 February 1. The Convention (October 25), had to be in force up to 1920 December 31. B. Baillaud is at the head of the Bureau, to become "BIH" located at *Observatoire de Paris*. During the war, the *Observatoire de Paris Service de l'heure* and the BIH were maintained by B. Baillaud and Bigourdan (1851-1932). After the war, everything was more or less forgotten and new ideas came up.

1919: A meeting (Brussels, July 18-19) creates a *Conseil international des recherches*, including several international unions and, among them, the International Astronomical Union (UAI/IAU), divided into 32 commissions including number 4, *Commission des éphémérides*, and number 31, *Commission de l'heure*, the by-laws of which are signed on July 26. An official character is given to the BIH, at the *Observatoire de Paris*. Commissions 4 and 31 will, in the future take care of the fundamental astronomical constants and of the units. But, World War II was not far and a new cut came.

5. THE IAU 1964 AND 1976 SYSTEMS OF ASTRONOMICAL CONSTANTS

1950: *Colloque international* by the *Centre national de la recherche scientifique* (Paris Observatory, March 27-April 1) on the fundamental astronomical constants. Among the participants: Ambarzumian, Batrouchevitch, Brouwer, Clemence, Jeffreys, Kopff, Kilokov, Morgan, Nemiro, Sadler, Spencer Jones, Oort, Zverev. For France: Chazy, Danjon, Fayet, Mineur, Stoyko. The recommendation of the conference to the IAU on the System of astronomical constants was to apply no change to their conventional values.

1950, 1953, 1954, 1955, 1958: Five successive meetings concerning astrometry connected with time, ephemerides, constants, fundamental units and references for space and time. During the General Assemblies (GA) of the IAU, incoherences in the fundamental constants are pointed out (Dublin 1955) and news about the catalogue for fundamental stars (to be FK4) are given (Moscow 1958).

1961: GA of the IAU (Berkeley), Danjon (1890-1967) director of *Observatoire de Paris*, suggests an IAU symposium on *Le système de constantes astronomiques* to be held in 1963.

1963: IAU symposium N° 21 (Paris, May 27-31). Adoption of new values.

1964: GA of the IAU in Hamburg, during which the FK4 and the proposed set of constants are adopted by the IAU; their use is recommended in the national and international ephemerides as soon as possible; this was from 1968.

1976: GA of the IAU (Grenoble). After discussions (1964-1976), another complete set of constants associated to a model of precession is adopted in the "IAU 1976 System of astronomical constants". In parallel, evolution of the time unit: the second, related to the rotation of the Earth (UT) up to 1960, was replaced by its revolution with ET (*temps des éphémérides*) up to 1967, when the second was based upon a Caesium frequency. The first name, *temps atomique intégré*, was changed into *Temps atomique international*, after its new modern realization in 1972 and under its official name TAI in 1976.

Note: All the references can be found in: - Débarbat, S., Les fondements historiques d'un système de constantes unifiées (Journées 1994 "Systèmes de référence spatio-temporels", Paris, pp. 3–10); - Capitaine, N., Les constantes astronomiques fondamentales de 1896 à nos jours (in press in Actes des Journées Lalande-Lœwy, Paris 2007); - Symposium "The origins, achievement and influence of the Royal Observatory, Greenwich: 1675–1975" (Greenwich, 13–18 July 1975); - Lévy, J., La création de la Connaissance des temps (Vistas in Astronomy, 20, pp 75–77, 1977).

NUMERICAL STANDARDS IN THE ASTRONOMICAL ALMANAC

C.Y. HOHENKERK[1], S.A. BELL[1], S.E. URBAN[2], J.L. HILTON[2]
[1] H.M. Nautical Almanac Office
U.K. Hydrographic Office, Admiralty Way, Taunton, TA1 2DN, UK
e-mail: Catherine.Hohenkerk@ukho.gov.uk and Steve.Bell@ukho.gov.uk
[2] U.S. Naval Observatory
3450 Massachusetts Avenue NW, Washington, DC 20392-5420, USA
e-mail: seu@usno.navy.mil and jhilton@usno.navy.mil

ABSTRACT. *The Astronomical Almanac* (AsA), a joint publication of Her Majesty's Nautical Almanac Office (HMNAO) and the Nautical Almanac Office of the U.S. Naval Observatory (USNAO), is a worldwide reference standard for astronomy. As such, the offices strive to adhere to the standards set forth by the larger astronomical community. However, sometimes the astronomical community is not clear as to what standards should be followed. There are standards that are promulgated formally, such as via IAU resolutions, some are informal but generally recognized as customary and common practice, while others seem to be adopted only within a particular field. This paper looks at various ephemerides, constants, parameters and models used in the AsA and the decision-making process that determines how they are selected for inclusion in the book.

1. THE MAIN STANDARDS FOR *THE ASTRONOMICAL ALMANAC*

The standards to which the AsA adheres may be divided into four areas. These are formal standards, informal but widely recognized standards, informally recognized practices and lastly the requirement to be consistent. Clearly, there should not be competing formal standards.

Our aim is to always follow formal standards. These are set down by the International Astronomical Union (IAU) via its resolutions and working groups (WG) and the *Technical Notes* of the International Earth Rotation and Reference Systems Service (IERS). The International Association of Geodesy (IAG) also provide various formal standards which are relevant to astronomy (e.g., the radius of the Earth).

Examples of pertinent IAU resolutions are those on the use of the International Celestial Reference System (ICRS) and ICRS-based catalogues and ephemerides, time scales, and precession-nutation. In recent years there have been WGs that have reported on "nomenclature" and "precession and the ecliptic". This work and the resulting resolutions all feed into the almanac. There is also the IAU-SOFA software which provides definitive algorithms for many of these models. Then there are examples like photometric standards and the rotational elements for the planets. The latter come from the IAU inter division WG on Cartographic and Coordinates and Rotational Elements.

There are many data sources and computational techniques that are not formalized within resolutions, but are world-recognized; most have been documented in refereed journals. Choosing between competing standards is done via numerical comparisons, usability, origin, and wider astronomical community acceptance. For example there is no IAU resolution that prescribes which planetary ephemeris to use. We have been using the Jet Propulsion Laboratory's (JPL) ephemeris since the 1984 edition (DE200/LE200). This was updated, for the 2003 AsA prepared in 2001, to JPL's DE405/LE405 ephemeris. This not only provided improvement in planetary positions but was also referred to the ICRS. Other recognized standards relate to satellite orbital parameters and magnitude coefficients. Similarly, rise and set times are only given to the nearest minute of time and the standard amount of refraction at the horizon is $34'$.

The requirements of astronomers, our customers, also matter. Often there are similar data sources and computational methods that have scientific justification. Other times new, formally recognized techniques have not been fully accepted by users. Selection of which to use and maintain is made by customary practices within HMNAO and USNAO, or a clearly-defined user need to maintain past data sets.

An example where the user community have specific requirements, which maintains links with the past, is for the solar physical ephemeris. Here Carrington's elements and reference system is still the reference system of choice. On the other hand, currently, the almanac is still publishing apparent places,

i.e. right ascension and declination with respect to the true equator and equinox of date. This is despite the fact that the IAU has recommended that right ascension should be measured from the celestial intermediate origin (CIO).

Within all these standards and practices it is necessary to try to be consistent. An example of inconsistency occurs in eclipse calculations, where old constants and IAU values are still being used as they are the required standard. On the other hand, with the requirements of more accurate positions and need to include relativity, it is becoming clear that constants must be scaled so that their units are consistent within the system that is being used.

The following table contains a selection of some of the standards that the AsA follows. A full list, valid for the 2009 edition of the AsA may be found on HMNAO's website at http://www.hmnao.com.

Quantity		**Reference, Comment**
Reference systems: ICRS	IAU 1997	Resolution B2, T*rans. IAU*, **XXIIIB**.
BCRS, GCRS	IAU 2000	Resolutions B1.3 and B1.4, respectively, *Trans. IAU*, **XXIVB**.
Time scales: TAI	IAU 1967	Adopted 1971.
TT	IAU 2000	Resolution B1.9, TT = TAI + $32^{s}.184$.
TDB	IAU 2006	Resolution B3.
Standard epoch; century; day; secs	IAU 1976	J2000·0 , JD2451545·0 TT, 2000 Jan 1 12^{h} TT, Julian cy=36525 ^{d}, day of 86400^{s}.
Software		USNO/HMNAO, NOVAS v3, IAU-SOFA library.
Vector/Matrix approach	IAU 1976	
Positions		Apparent (not intermediate) places tabulated at 0^{h} TT.
		Minor planets and Pluto astrometric positions tabulated at 0^{h} TT.
Stars space motion		No light time included; NOVAS v3 includes simple light time formulation.
		IAU-SOFA uses Stumpff, P., A&A **144**, 232-240, 1985.
Transit times		Transit over the ephemeris meridian.
Magnitudes: Mercury & Venus		Hilton, J.L., AJ, **129**, 2902, 2005, AJ, **130**, 2928, 2005.
Mars - Pluto		Harris, D.L., *Planets & Satellites*, eds. Kuiper, G.P.& Middlehurst, B.L., **272**, 1961.
Planetary & lunar ephemerides		JPL DE405/LE405 ephemerides Standish, E.M., JPL IOM 312.F-98-048, 1998.
T_{eph}		Standish, E.M., A&A, **336**, 381-384.
Light time, unit distance		$\tau_A = 499{\cdot}0047\,8380\,61$ ms^{-1}, $c\tau_A = 1495\,9787\,0691$ m.
Categorizing Pluto	IAU 2006	Resolutions 5 & 6; Pluto is a dwarf planet.
Minor planet ephemerides	USNO	AE98, AJ, **117**, 1077, 1999. Also USNO ephemeris AE2001.
ICRS star catalogues	ESA, USNO	Hipparcos, Tycho-2, UCAC2, USNO-B; many other object catalogues are used.
Physical ephemerides, ...	IAU 2006	WG Cartographic Coordinates & Rotational Elements, Report 10,
Sun, Planets and Pluto;		Seidelmann, P.K., et al., *Celest. Mech.*, **98**, 155-180, 2007.
and for Sun	1863	Based on Carrington, R.C., *Observations of the Spots of the Sun* and updated by
	1992	Seidelmann P.K., et al., *Explanatory Supplement to the AsA*, p 397.
Lunar librations	Eckhardt	*The Moon and the Planets*, **25**, 3, 1981; High Precision Earth Rotation &
(but using IAU inclination)	1982	Earth-Moon Dynamics , ed. Calame, O., 193-198, 1982.
Earth rotation angle / UT1	IAU 2000	Resolution B1.8, Trans. IAU, **XXIVB**.
GMST / UT1	IAU 2006	Capitaine, N., Wallace, P.T., and Chapront, J., A&A, **432**, 355-367, 2005.
Equation of Origins	IAU 2006	IAU WG on Nomenclature, Trans IAU, **XXVIB**.
Precession; variety of angles;	IAU 2006	Resolution B1, *Celest. Mech.*, **94**, 351-367, 2006,
ϵ_A, ψ_J, ϕ_J, γ_J χ_A, ω_A, ψ_A, ϵ_0		P03: Capitaine, N., Wallace, P.T., & Chapront, J., A&A, **412**, 567-586, 2003, and
z_A, θ_A, ζ_A		Wallace, P.T., and Capitaine, N., A&A, **459**, 981-985, 2006.
Nutation $\Delta\psi$, $\Delta\epsilon$	IAU 2000A	Resolution B1.6, Trans. IAU, **XXIVB**. Implementations:
		IERS Conventions 2003, *Technical Note 32*, eds. McCarthy, D.D. & Petit, G.,
		USNO Circular 179, Kaplan, G., and IAU-SOFA routine NUT00A.
adjustments at the μas level	IAU 2006	Resolution B1: due to IAU 2006 precession, included by IAU-SOFA in NUT06A.
CIP & CIO Locator; X, Y, & s	IAU 2006	Resolution B1 & B2. Capitaine, N., & Wallace, P.T., A&A, **450**, 855-872, 2006.
Eclipses	IAU 1982	$k = 0{\cdot}272\,5076$, Moon's apparent SD= $\sin^{-1}(k \sin\pi)$,
k also used for occultations	1963	consistent with Watts datum APAE, XVII, 1963. Lunar radius = 1737·97 km.
	IAU 1976	Sun's SD at 1 au $15'59''.64$.
Rise/Set phenomena	IAU	Nearest minute of time. Upper limb on the horizon with $34'$ of refraction.
Phases of Moon, Lunation		Brown, E. W., MNRAS, **93**, 603, 1933. No. 1 - 1923 January 16.

Figure 1: Some of the main standards for *The Astronomical Almanac*

ANALYTICAL REPRESENTATION OF PLUTO MODERN EPHEMERIS

S.M. KUDRYAVTSEV, N.S. KUDRYAVTSEVA
Sternberg Astronomical Institute of Moscow State University
13, Universitetsky Pr., Moscow, 119992, RUSSIA
e-mail: ksm@sai.msu.ru, natkud@rambler.ru

ABSTRACT. A high-accurate analytical representation of the latest JPL's numerical ephemeris of Pluto, DE421 (Folkner et al. 2008), by Fourier series is obtained. The maximum difference between barycentric positions of Pluto given by the new analytical series and the numerical ephemeris over 1900–2050 (the entire time interval covered by DE421) is 1.3 km. To get Pluto heliocentric positions, a development of heliocentric coordinates of the Solar system barycenter to Poisson series is made. The heliocentric positions of the barycenter given by the new analytical series and by DE421 numerical ephemeris differ by less than 5 km over 1900–2050.

1. INTRODUCTION

An accurate ephemeris of Pluto is of a great interest now because of the NEW HORIZONS mission recently launched to that dwarf planet. The spacecraft should reach Pluto in 2015, and by anticipating that encounter, the Pluto ephemeris is essentially updated in recent JPL's planetary ephemerides; the latest and most accurate of them is DE421 (Folkner et al. 2008). It is important to note, that all modern ephemerides of Pluto are numerical ones. There is also a number of analytical series representing Pluto coordinates (Goffin et al. 1986; Chapront & Francou 1995, 1996; Simon 2004); their advantage over the numerical ephemerides is an essential compactness. However, all the available analytical series are adjusted to now outdated numerical ephemerides of Pluto that differ from its modern ephemerides by several thousand km (Folkner et al. 2007). Therefore, the task of obtaining the new analytical series for Pluto coordinates that accurately approximate the latest Pluto ephemeris is an actual one.

2. DEVELOPMENT OF PLUTO COORDINATES TO ANALYTICAL SERIES

To obtain new analytical series for barycentric coordinates of Pluto we used a method by Chapront & Vu (1984). Following their approach, Pluto coordinates are first calculated over at least one orbital period of this dwarf planet with a small sampling step. In our study we used the latest JPL's numerical planetary ephemeris DE421 as a source of Pluto coordinates. As an approximating analytical function, the method suggests a Fourier series with the frequencies being successive multiples of the main frequency of Pluto's motion ν plus a constant term and a term proportional to time t:

$$X(t) = X_0^c + X_0^s t + \sum_{k=1}^{N} (X_k^c \cos k\nu t + X_k^s \sin k\nu t) \qquad (1)$$

The amplitudes $X_0^c, X_0^s, \ldots, X_N^c, X_N^s$ are found with help of the least-mean-square algorithm. This form of expansion by us is used to represent rectangular barycentric ICRF coordinates of Pluto: X, Y and Z.

However, the method is only effective when the expansion is made over a time interval not shorter than the Pluto's orbital period. It is equal to about 248 years, but DE421 ephemeris only covers 150 years (1900–2050). Thus DE421 by us has been preliminary expanded over the time interval 1850–2150 with help of ERA software (Krasinsky & Vasilyev 1997).

Table 1 presents the main characteristics of the new development of the rectangular barycentric ICRF coordinates of Pluto to series of form [1]. The comparison of the new analytical series with DE421 numerical ephemeris is done over 1900–2050, the entire time interval covered by the ephemeris. The complete set of numerical values for all the coefficients of the expansion [1] for rectangular barycentric coordinates of Pluto can be found at http://lnfm1.sai.msu.ru/neb/ksm/pluto/pluto_ssb.zip. The archive also includes a relevant Fortran subroutine for calculation of Pluto barycentric coordinates.

Coordinate	Number of Fourier terms	Maximum error of approximation
X	153	0.83 km
Y	153	0.96 km
Z	153	0.41 km

Table 1: Analytical approximation of DE421 barycentric coordinates of Pluto over 1900–2050.

Coordinate	Number of Poisson terms	Maximum error of approximation
X	128	4.17 km
Y	129	4.12 km
Z	130	1.36 km

Table 2: Analytical approximation of DE421 heliocentric coordinates of the SSB over 1900–2050.

To get Pluto positions relative to the Sun, a development of heliocentric coordinates of the Solar system barycenter (SSB) to Poisson series is additionally made. For that we used the expansion method by Kudryavtsev (2007). The development is made over 1000AD–3000AD; as a source of the SSB heliocentric coordinates we used the latest long-term JPL's ephemeris DE406 (Standish 1998). According to the method, the development is directly done to Poisson series, where both amplitudes and frequencies of the series' terms are high-degree time polynomials. This allows one to make the expansion over long-term intervals, and therefore the series' terms of close frequencies can be better separated.

Table 2 presents the main characteristics of our development of the rectangular heliocentric ICRF coordinates of the SSB to Poisson series. All coefficients of the Poisson series for the SSB coordinates and a relevant Fortran subroutine can be found at http://lnfm1.sai.msu.ru/neb/ksm/ssb/ssb_sun.zip.

Acknowledgements. The authors are grateful to Prof. G.A. Krasinsky and Dr. E.V. Pitjeva for their valuable consultations on ERA software. A travel grant provided to us by the LOC of the Journées 2008 is sincerely appreciated.

3. REFERENCES

Chapront, J., Vu, D.T., 1984, "A new compact representation of ephemerides: application to the motion of Pluto, the Sun and the Gallilean satellites of Jupiter", A&A , 141, pp. 131–143.

Chapront, J., Francou, G., 1995, "Ephemerides of Pluto between 1700 and 2100", http://cdsarc.u-strasbg.fr/viz-bin/Cat?VI/88.

Chapront, J., Francou, G., 1996, "Ephemerides of planets between 1900 and 2100", http://cdsarc.u-strasbg.fr/viz-bin/Cat?VI/87.

Folkner, W.M., Standish, E.M., Williams, J.G., Boggs, D.H., 2007, "Planetary and lunar ephemeris DE418", Jet Propulsion Laboratory, Memorandum IOM 343R-08-003.

Folkner, W.M., Williams, J.G., Boggs, D.H., 2008, "The planetary and lunar ephemeris DE 421", Jet Propulsion Laboratory, Memorandum IOM 343R-07-005.

Goffin, E., Meeus, J., Steyaert, C., 1986, "An accurate representation of the motion of Pluto", A&A , 155, pp. 323–325.

Krasinsky, G.A., Vasilyev, M.V., 1997, "ERA: Knowledge Base for Ephemeris and Dynamical Astronomy", In: Proceedings of IAU Colloquium 165, Poznan, Poland, July 1-5, 1996 (Eds.: I.M. Wytrzyszczak, J.H. Lieske, R.A. Feldman), Dordrecht, Boston, Kluwer Academic Publishers, p. 239.

Kudryavtsev, S.M., 2007, "Long-term harmonic development of lunar ephemeris", A&A , 471, pp. 1069–1075.

Simon, J.-L., 2004, "Représentation analytique du mouvement de Pluton", Notes scientifique et techniques de l'IMCCE, S081, pp.53–58.

Standish, E.M., 1998, "JPL planetary and lunar ephemerides DE405/LE405", Jet Propulsion Laboratory, Memorandum IOM 312.F-98-048.

REMARKS ABOUT RELATIVISTIC DEEP SPACE NAVIGATION

C. LE PONCIN-LAFITTE[1], V. LAINEY[2]
[1] SYRTE, Observatoire de Paris, CNRS, UPMC
61, avenue de l'Observatoire, 75014 – Paris, France
e-mail: christophe.leponcin-lafitte@obspm.fr
[2] IMCCE, UMR8028, Observatoire de Paris, UPMC
77 Avenue Denfert Rochereau, F75014 – Paris, France
e-mail: Valery.Lainey@imcce.fr

ABSTRACT. The principal objective of spacecraft navigation is to determine the present and future trajectory of a probe. This is done by measuring the spacecraft's radial velocity and/or ranging to further improve the predicted spacecraft trajectory. Many intricate relativistic effects are involved all the way through the data analysis: Einstein-Infeld-Hoffmann equations in the predicted equations of motion, Shapiro delay in the calculation of precision light times during the tracking and finally relativistic time scales when we confront the global modelling with raw data of observation. We present here some remarks concerning that modelling by studying the order of magnitude of neglected terms.

1. FORMULATION OF DEEP SPACE NAVIGATION

One of the first task is to produce a spacecraft ephemeris usually done by a numerical integration. It gives a file of spacecraft positions and velocities as functions of the satellite ephemeris time. The equations of motion of a spacecraft are based on the well-known Einstein-Infeld-Hoffmann equations. In addition, one needs to solve the relativistic light propagation equation in order to get the solution for the total light time travel. In the solar system, this equation is given in a barycentric reference frame as follow

$$c\,(t_2-t_1)=|\boldsymbol{x}_2-\boldsymbol{x}_1|+\sum_A\frac{2\,\mu_A}{c^2}\,\ln\frac{|\boldsymbol{r}_{1A}|+|\boldsymbol{r}_{2A}|+|\boldsymbol{r}_{21}|}{|\boldsymbol{r}_{2A}|+|\boldsymbol{r}_{1A}|-|\boldsymbol{r}_{21}|}+\mathcal{O}(c^{-4}),\tag{1}$$

where μ_A is the gravitational constant and index 1 and 2 correspond to an emission and reception of a signal, respectively. The last interesting observable is the Doppler shift, $\delta\nu/\nu$, which can be calculated as follows:

$$\frac{\delta\nu}{\nu}=\frac{d\,\rho}{d\,t}\,,\tag{2}$$

where ρ is the two-ways precision light time (so taking into account Eq. (1), see Eq. (7)) and dt is here related to a terrestrial time scale. Because the old IAU definition of time coordinate in the barycentric frame, the only difference between TDB (dynamical barycentric time) and TT (terrestrial time) are due to periodic terms. Indeed, the difference between the International Atomic Time, TAI, and the satellite Ephemeris Time, T_{eph}, generally used (Moyer, 2003) is given by:

$$\frac{dT_{eph}}{dTAI}=1-\frac{U}{c^2}-\frac{1}{2}\frac{v^2}{c^2}+L\,,\quad\text{with } L=\tfrac{1}{c^2}\Big\langle U+\tfrac{v^2}{2}\Big\rangle,\tag{3}$$

$<>$ denoting the long-term average value of the quantity contained within them, U and v being the external gravitational potential of the Earth and its orbital velocity, respectively. To maintain unchanged equations of motion, light time and Doppler shift, the spatial coordinates in the barycentric frame have to be rescaled by the factor L (order of magnitude $\approx 10^{-8}$) to keep the speed of light unchanged. As μ_A/c^2 have also the dimension of length, they have to be rescaled by the factor L. Then, we have three scaling laws as follow:

$$t=(1+L)\tilde{t},\quad \boldsymbol{x}=(1+L)\tilde{\boldsymbol{x}},\quad \mu_A=(1+L)\tilde{\mu}_A\,.\tag{4}$$

2. TIME SCALE UP TO THE ORDER $1/c^4$

It is obvious that from Eq. (3), terms of order $1/c^4$ are neglected. The correct time dilation equation between the IAU conventional barycentric coordinate time TCB and the geocentric coordinate time TCG is given as follows:

$$\frac{dTCG}{dTCB} = 1 + \frac{1}{c^2}\mathcal{A}(TCB) + \frac{1}{c^4}\mathcal{B}(TCB) + \mathcal{O}\left(\frac{1}{c^6}\right). \tag{5}$$

It immediately produces another scaling factor $\bar{L}$ because we can expect a supplementary linear drift due to these terms. To quantify this possible additional linear drift, we can compute Eq. (5) with a planetary ephemerides. Hervé Manche, from the INPOP group, provided us the difference between Eqs (3) and (5). The additional linear drift $\bar{L}$ is something about 10^{-17}. What are the consequences on the equations of motion, the light time (1)? On the scaling of mass, time and position, we thus obtain:

$$\tilde{t} = \left(1 + \frac{\bar{L}}{1 + L + \bar{L}}\right)\bar{t} = (1 + \bar{L})\,\bar{t} + \mathcal{O}(L\bar{L}), \tag{6}$$

$\tilde{\mu}_A \approx (1+\bar{L})\,\bar{\mu}_A$ and $\tilde{\boldsymbol{x}} \approx (1+\bar{L})\,\bar{\boldsymbol{x}}$, the Taylor expansion being truncated at $\mathcal{O}(L\bar{L})$ because $L\bar{L} \approx 10^{-25}$ which is really negligible. We see immediately that these equations will not be affected by this factor. However we can suspect a possible impact on the calculation of the Doppler shift (2). Indeed it needs the evaluation of the two-ways precision light times which are given by (Moyer, 2003):

$$\begin{aligned}\rho = &(t_3 - t_2) + (t_2 - t_1) - (T_{eph} - TAI)_{t_3} + (T_{eph} - TAI)_{t_1} - (TAI - UTC)_{t_3} + (TAI - UTC)_{t_1} \\ &-(UTC - ST)_{t_3} + (UTC - ST)_{t_1} + ...,\end{aligned} \tag{7}$$

where indexes 1 and 3 correspond to the emission and reception of a signal on Earth, respectively, and index 2 refers to the spacecraft. Here $UTC - ST$ represents a time scale transformation from the local time ST at tracking station to UTC. In practice, we see that the relation $T_{eph} - TAI$ is required; so we have two additional terms $\Delta(T_{eph} - TAI)_{t_3}$ and $\Delta(T_{eph} - TAI)_{t_1}$ because of the modification due to $\bar{L}$. It leads to a drift in the time-tagging. However the Doppler shift is calculated from $d\rho/dt$, which means that we finally have only a constant offset of order 10^{-17} in the Doppler data, fully negligible.

3. MODIFY THE SHAPIRO DELAY?

It is well known that Eq. (1) is obtained from the gravitational field of motionless mass-monopole bodies. We can imagine to take into account some gravitomagnetic effects due to their motion. In that case, the spacetime metric has a g_{0i} contribution as follow

$$g_{0i}(c\,t, \boldsymbol{x}) \propto \frac{1}{c^3}\sum_A \frac{\mu_A}{|\boldsymbol{x} - \boldsymbol{x}_A|} v_A^i, \tag{8}$$

where v_A^i is the velocity of body A. In a simple situation, we can suppose that the bodies are moving with a constant velocity. The solution of this problem is known but usually expressed by means of retarded potentials, not so convenient to use in practice. However, we can derive quite easily an order of magnitude. One of the main gravitomagnetic contribution will be a modification of the usual Shapiro delay by a factor $\boldsymbol{v}_A.(\boldsymbol{x}_2 - \boldsymbol{x}_1)/|\boldsymbol{x}_2 - \boldsymbol{x}_1|$. For the Earth, we have $GM_E|\boldsymbol{v}_E|/c^4 \approx 10^{-15}$. Maybe it will be interesting in the future to study in details the impact of these extra-terms on the precision two-ways light time, and consequently on the Doppler shift.

4. REFERENCES

Moyer, T. D., 2003, Formulation for Observed and Computed Values of Deep Space Network Data Types for Navigation, (John Wiley & Sons: Hoboken)

VALUES OF SOME ASTRONOMICAL CONSTANTS PROPOSED FOR NSFA

E.V. PITJEVA[1], E.M. STANDISH[2]
[1] Institute of Applied astronomy RAS
Kutuzov Quay 10, 191187 St.-Petersburg
e-mail: evp@ipa.nw.ru
[2] 519 Birchbark Court
Seneca, SC 29672, USA
e-mail: ems@jpl.nasa.gov

Improved values for the masses of Ceres, Pallas, Vesta, the Earth-Moon mass ratio, and the Astronomical Unit are hereby proposed to the NSFA WG (the IAU Working Group on Numerical Standards for Fundamental Astronomy) as current best estimates. These value are based upon the improvements of planetary ephemerides carried out by the authors at IAA RAS and at Caltech/JPL, respectively; comparisons of the values with those of other researchers ensure their reliability and provide realistic estimates of their uncertainties.

Many asteroids are massive enough so that direct dynamical determinations of their masses may come from their perturbations upon other solar system bodies. Unfortunately, the classical example, where the perturbed body is some other asteroid, often leads to inaccurate or poorly-determined estimations. However, masses of the largest asteroids, Ceres, Pallas, and Vesta, may be reliably estimated using modern planetary ephemerides to analyze the highly accurate ranging data of spacecraft orbiting Mars or landed upon its surface.

We have proposed to the NSFA the following mean representative values and realistic uncertainties for the masses of the three largest asteroids (Ceres, Pallas, Vesta), to be used as the current best estimates:

$$M_{Ceres}/M_\odot = 4.72(3)\cdot 10^{-10},$$
$$M_{Pallas}/M_\odot = 1.03(3)\cdot 10^{-10},$$
$$M_{Vesta}/M_\odot = 1.35(3)\cdot 10^{-10}.$$

Unlike the values adopted in the Astronomical Almanac of 2006, these are consistent with nearly all of the twenty or so modern accurate determinations from various authors, being based mainly on spacecraft ranging data. (See Table 1 of Pitjeva & Standish, 2009)

We also have proposed improved values for the Moon-Earth mass ratio and the astronomical unit, also obtained from the ephemeris improvement processes at JPL and at IAA RAS:

$$M_{Moon}/M_{Earth} = 0.0123000371(4) \text{ and } AU = 149597870700(3) \text{ m}.$$

This value for the AU is consistent with the value of GM_{Sun}, proposed to the NSFA WG by W. Folkner:

$$GM_{Sun}=1.32712442099(10)\cdot 10^{20}[\mathrm{m}^3 s^{-2}].$$

All of the main ephemerides of JPL and IAA RAS have been constructed in the TDB time scale. It is noted here that the AU, expressed in meters, has the same numerical value for ephemerides based upon the TDB or upon the TCB time scale, assuming one uses the conversion proposed by Irwin and Fukushima, Brumberg and Groten, Brumberg and Simon.

The detailed description of this paper was published (Pitjeva & Standish, 2009).

REFERENCES

Pitjeva, E.V., Standish, E.M., 2009, "Proposals for the masses of the three largest asteroids, the Moon-Earth mass ratio and the Astronomical Unit", Celest. Mech. Dyn. Astr. 2009, 103(4), 356-372, DOI 10.1007/s10569-009-9203-8.

IMPROVING THE ASTEROID PERTURBATIONS MODELING IN PLANETARY EPHEMERIDES

P. KUCHYNKA[1], J. LASKAR[1], A. FIENGA[1,2], H. MANCHE[1], L. SOMENZI[2]
[1] ASD, IMCCE, UMR8028, Observatoire de Paris, UPMC, Paris, France
[2] Observatoire de Besançon-CNRS UMR6213, Besançon, France
e-mail: kuchynka@imcce.fr

ABSTRACT. The objective of this study is to investigate the advantages of modeling the large numbers of weakly perturbing asteroids present in the main belt by a solid ring. With a simple model we perform various Monte Carlo experiments and show that a ring is indeed able to represent a global effect. We estimate at 200 the number of asteroids that need to be eliminated before the global effect becomes dominant and calculate with the Monte Carlo method an independent estimate of the ring's mass.

1. INTRODUCTION: Asteroids are considered as the major obstacle for achieving a satisfactory long-term prediction accuracy in ephemerides. There are hundreds of asteroids whose perturbations on Mars are above the precision limit of available observations ($\sim$1 m for modern ranging data) and there are many more asteroids whose perturbations though individually weak add up to a significant global effect. Krasinsky et al. 2002 proposed to model the effect of a large number of weakly perturbing asteroids by a solid ring, the purpose of this work is to gain further insight into the advantages of such a model in a planetary ephemeris.

2. METHODOLOGY: We chose 24635 asteroids from the ASTORB database for an initial model of the main-belt, this selection was based on the asteroids' semi-major axes (required to be bellow 3.5 AU) and absolute magnitudes (required brighter than 14). A simple model allows us to assign each asteroid with a set of "reasonable" random masses. The model is based on a simplified version of the Statistical Asteroid Model (Tedesco et al. 2005); SIMPS data, taxonomies and dynamical family memberships are used to assign to each asteroid a mean albedo ρ and an albedo uncertainty $\Delta\rho$, in the most common case where no data at all is available, the asteroid is randomly assigned one of four albedo classes and a corresponding ρ and $\Delta\rho$ (see Tedesco et al. 2005 for details). At this point we are able to calculate a diameter for every asteroid: we pick randomly an albedo from the $[\rho - \Delta\rho, \rho + \Delta\rho]$ interval and use the absolute magnitude to obtain a diameter. In order to obtain a mass, we assign a density interval to each of the albedo classes : $[0.5, 2.5]$ for low albedo (class C), $[1.6, 3.8]$ for moderate albedo (class S) and $[1, 5]$ for intermediate and high albedos (classes E and M). By randomly picking diameters together with corresponding albedo class densities, we obtain for each asteroid a reasonable distribution of masses.

In order to test the ability of a solid ring to represent a large number of weakly perturbing asteroids we compare perturbations on the Earth-Mars distance exerted by a ring to perturbations arising from all of the 24635 selected asteroids but the N most perturbing ones. By performing this comparison for different values of N we can estimate the ability of the ring to model a global effect and we can also estimate a limit from which this global effect is dominant. We devised a scheme that allows fast testing of many possible mass configurations of the 24635 asteroids. For each of the selected asteroids, the Solar system is integrated between 1969 and 2010 with and without the asteroid. These integrations are made with the INPOP integrator (Fienga et al. 2008). We can thus obtain for each asteroid the perturbation on the Earth-Mars distance $\Delta D = D_{\text{with}} - D_{\text{without}}$, this perturbation is proportional to the asteroid's mass and it also gives an estimation of $\partial D/\partial M$ $(= \Delta D/M)$. The proportionality relation can be verified empirically by comparing different ΔD for a whole range of the asteroid's mass values. Our scheme is based on the expansion to the first order in asteroid masses of a perturbation generated by all 24635 asteroids: $D(M_1, ..., M_{24635}) - D(0, ..., 0) = \Delta D_1 + ... + \Delta D_{24635}$. The expansion allows to calculate the global perturbation for any given set of asteroid masses by simply adding perturbations calculated once and applying corresponding mass proportionality relations. As it was the case with the proportionality relation, the validity of the expansion can be verified empirically.

3. RESULTS: We denote by ΔD_{ring} the perturbation on the Earth-Mars distance caused by a solid ring centered at the Sun. The perturbation is proportional to the mass of the ring, the dependency of the perturbation on the ring's radius is not linear, but for a radius between 2.5 AU and 3.5 AU it can be properly compensated by a variation of the ring's mass. We denote by $\Delta D_{\text{glob}}(N)$ the perturbation from all the asteroids but the N most perturbing ones (in terms of amplitude). The ability of the ring to model a global effect on the Earth-Mars distance is estimated by comparing ΔD_{ring} to $\Delta D_{\text{glob}}(N)$, in order to account for the possibility to adjust the ring's mass, we normalize ΔD_{ring} and $\Delta D_{\text{glob}}(N)$. Figure 1 shows the evolution of $R(N) = |\frac{\Delta D_{\text{ring}}}{|\Delta D_{\text{ring}}|} - \frac{\Delta D_{\text{glob}}(N)}{|\Delta D_{\text{glob}}(N)|}|$ for a particular set of asteroid masses as well as an average over 100 different sets. We observe two drops in $R(N)$, one for $N \sim 20$ and another one for $N \sim 125$, this shows that from $N \sim 200$ a ring represents indeed well the remaining asteroids, though the similarity is not perfect because $R(N)$ doesn't reach 0.

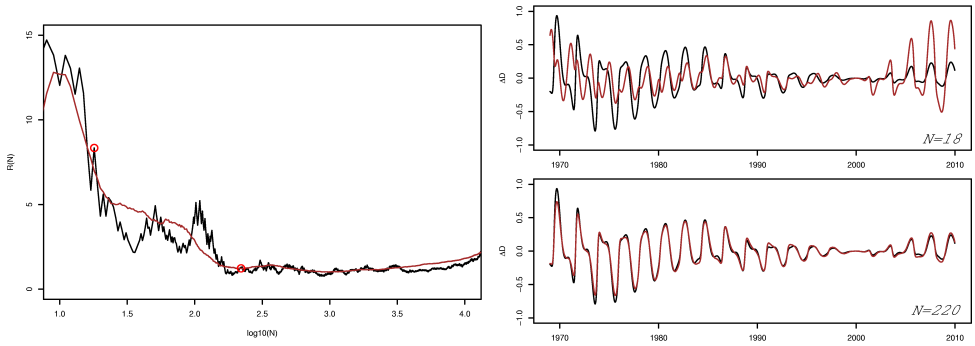

Figure 1: Evolution of $R(N)$, the brown curve is an average over 100 different sets of masses. On the right side are shown the normalized perturbations ΔD_{ring} and ΔD_{glob} for two particular values of N.

The random masses sets allow us to use the Monte Carlo method to estimate an average mass of a ring representing perturbations of all but the 300 most perturbing asteroids: fitting the ring's mass so as to minimize $|\Delta D_{\text{ring}} - \Delta D_{\text{glob}}(N = 300)|$ for 1000 different sets of asteroid masses leads to the estimate $M_{\text{ring}} = 0.6 \pm 0.2 \times 10^{-10} M_{\odot}$ for a ring with radius of 2.8 AU (the estimate becomes $M_{\text{ring}} = 1 \pm 0.3 \times 10^{-10} M_{\odot}$ for a radius of 3.14 AU). The corresponding perturbation $\Delta D_{\text{glob}}(N = 300)$ reaches on average 250 m whereas the residuals after fitting the ring reach 40 m (on the 1969-2010 interval). We emphasize that these estimations are dependent only on the model for assigning masses described in the methodology part, they are obtained independently from a fit to observations of a ring mass as an ephemeris parameter. One should note that the obtained estimation of M_{ring} is close to the value of $0.34 \pm 0.15 \times 10^{-10} M_{\odot}$ fitted for a ring at 2.8 AU in INPOP06 (Fienga et al. 2008).

Besides allowing for an independent estimation of the ring's mass, the Monte Carlo method can also be used to find the most probable list of the top 300 perturbing asteroids in terms of amplitude of the perturbation on the Earth-Mars distance on the 1969-2010 interval. Such a list is quite similar to the list of the 300 asteroids taken individually into account in INPOP06, a notable difference being the presence of 60 Echo, 516 Amstherstia and 585 Bilkis, which have large estimated amplitudes (the perturbation of 60 Echo reaches 170 m) and are absent from INPOP06.

4. CONCLUSION: We showed through a simple Monte Carlo study the ability of a ring to model a global perturbation caused by large numbers of weakly perturbing asteroids. We were also able to give an independent estimate of the ring's mass.

5. REFERENCES

Krasinsky, G.A., Pitjeva, E.V., Vasilyev, M.V., Yagudina, E.I., 2002, "Hidden mass in the asteroid belt", Icarus 158, pp. 98–105.

Tedesco, E.F., Cellino, A., Zappala, V., 2005, "The Statistical Asteroid Model. I. The Main-Belt Population for Diameters Greater than 1 Kilometer", A&A 129, pp. 2869–2886.

Fienga, A., Manche, H., Laskar, J., Gastineau, M., 2008, "INPOP06: a new numerical planetary ephemeris", A&A 477, pp. 315–327

Session 3

GLOBAL GEODYNAMICAL MODELLING

MODÉLISATION GÉODYNAMIQUE GLOBALE

RECENT ADVANCES IN THEORETICAL MODELING AND OBSERVATION OF EARTH ROTATION AT DAILY AND SUBDAILY PERIODS

A. BRZEZIŃSKI[1,2]
[1] Department of Geodesy and Cartography, Warsaw University of Technology
[2] Space Research Centre, Polish Academy of Sciences, Warsaw, Poland
e-mail: alek@cbk.waw.pl

ABSTRACT. This paper gives an overview of the recent advances in theoretical modeling and observation of Earth rotation at daily and subdaily periods. The dominant part of this group, with the size up to 1 mas, is due to the gravitationally forced ocean tides. There is also a small variation (about 0.03 mas) due to the direct influence of the tidal gravitation on the triaxial structure of the Earth. The remaining part (up to 0.1 mas) is a geophysical effect driven by the daily cycle in solar heating giving rise to high frequency variations of the atmospheric and oceanic angular momenta (AAM, OAM). The observational evidence of diurnal and semidiurnal signals in polar motion and UT1 concerns mostly the purely harmonic ocean tide effects. The variations of geophysical origin have been detected in the high resolution AAM and OAM data, though there are still significant differences between results from various models. Recent developments of technologies used to monitor Earth rotation, the space geodetic techniques - VLBI, GNSS, SLR, but also the ring laser gyroscope, rises a question about observability of diurnal and subdiurnal components of Earth rotation. Of particular importance is the possibility of monitoring high frequency geophysical signals which are irregular to some extent therefore cannot be described by a simple harmonic model.

1. INTRODUCTION

Polar motion and UT1 contain physical signals within the diurnal and subdiurnal frequency bands. A common feature, besides the high frequency, is their small size: the total peak-to-peak size is only up to about 1 milliarcsecond (mas) corresponding to 3 cm at the Earth surface. Such variations could not be observed by the methods of optical astrometry and early space geodetic measurements, because the observations were not sufficiently accurate and their sampling interval was significantly longer than 1 day. Hence all earlier predictions were purely theoretical based on the knowledge about the shape and internal constitution of the Earth. All observational evidence of diurnal and subdiurnal variations in Earth rotation has been gathered during the last two decades. The high resolution observations of Earth orientation are still under development. For instance, one purpose of the VLBI 2010 system is continuous measurement of the Earth Orientation Parameters (EOP). Another example which will be discussed in a more detailed way in Sec. 3 is determination of high frequency polar motion by the ring laser. An important and independent method of modeling diurnal/subdiurnal variations in Earth orientation is by the high resolution estimation of the total angular momentum of geophysical fluids, primarily the atmosphere and the oceans.

Despite the small size, the diurnal and subdiurnal signals in Earth rotation are important for understanding the high frequency global dynamics of the solid Earth and the overlying fluid layers. The research concerning such signals is also important for validation of the high resolution determinations of Earth rotation parameters and of the procedures applied for data reduction. A possible benefit from such research could be empirical verification of the equations of Earth rotation at high frequencies.

In the next section we will give a brief systematic review of the known diurnal and subdiurnal signals in Earth rotation. For each effect we will describe the physical mechanism, the method of mathematical modeling and the observational evidence. A separate part, Sec. 3, will be devoted to the observations of diurnal polar motion by the ring laser, and their relation to standard determinations of the EOP.

2. DIURNAL/SUBDIURNAL COMPONENTS OF POLAR MOTION AND UT1

In this section we will briefly discuss all known perturbations of Earth rotation with daily and subdaily periods. The perturbations are divided into several groups based on their physical cause. For each group we describe the way of modeling and the observational evidence gathered so far. We also report about own research and estimation efforts.

Astronomical variations. The underlying physical mechanism are the lunisolar and planetary torques exerted upon the rotating Earth. Such torques are regular and predictable. A standard mathematical model consists of a sum of polynomial and (quasi)harmonic terms. The main corresponding effect in Earth rotation is the astronomical precession-nutation which is due to the influence of tidal gravitation on those features of the Earth's mass distribution which are expressed by the zonal terms of geopotential. This component of perturbation is expressed by the conventional a priori model, currently the IAU 2000 precession-nutation model (IERS, 2004). All possible imperfections of the conventional model as well as geophysical signals such as the free core nutation (FCN) contribute to the celestial pole offsets $\delta X, \delta Y$ which are determined by very long baseline interferometry (VLBI). In case of other space geodetic techniques, such as global navigation satellite system (GNSS), satellite laser ranging (SLR), all unmodeled effects can contribute to polar motion as a retrograde diurnal variation.

A minor part of the astronomical variation, called "subdiurnal nutation" or libration, is due to the influence of the tidal gravitation on the non-zonal terms of geopotential. In case of polar motion it contains both the long periodic terms and the prograde diurnal variation with total amplitude up to 50 microarcseconds (μas). The corresponding theoretical model is a part of the IERS Conventions 2003 (IERS, 2004; Table 5.1). In case of UT1, the perturbation is semidiurnal with total amplitude up to 75 μas. The model has been developed in several works (Wünsch, 1991; Chao et al., 1991; Brzeziński and Capitaine, 2002) but is not included in the IERS Conventions.

Ocean tide contributions. The underlying physical mechanism is the influence of the gravitationally-forced ocean tides with diurnal and semidiurnal periods, upon the rotating Earth via the angular momentum exchange. This effect is also regular and predictable. The model of the Ocean Tidal Angular Momentum (OTAM) consists of a sum of harmonic terms with tidal frequencies. The frequencies are well known from the tidal developments, while the amplitudes and phases can be derived from the ocean tide models and/or from the observations of Earth rotation. The ocean tides contribute to all three components of Earth rotation, including precession-nutation, polar motion and UT1. In case of polar motion and UT1 this is dominant effect in the diurnal and semidiurnal frequency bands. The current OTAM model recommended by IERS Conventions 2003 is based on hydrodynamic ocean tide model constrained by TOPEX/Poseidon altimetry data (Chao et al., 1996). The equatorial retrograde diurnal component of the OTAM which contribute to nutation has been accounted for in the IAU 2000 precession-nutation model. In case of polar motion the ocean tide influence consists of semidiurnal and prograde diurnal variation with amplitudes up to 330 μas and 150 μas, respectively (IERS 2004; Table 8.2). In case of UT1, the ocean tide influence appears as semidiurnal and diurnal variations with amplitudes up to 260 μas and 240 μas, respectively (IERS 2004; Table 8.3).

Parameters of the model of the ocean tide effect in polar motion and UT1 have been estimated from the space geodetic observations: VLBI solutions – (Herring and Dong, 1994; Gipson, 1996); SLR solution – (Watkins & Eanes, 1994) with later updates by R. Eanes; GPS solution – (Rothacher et al., 2001). Our recent analysis (Bolotin and Brzeziński, 2006) using VLBI data spanning 1984.0–2006.2 revealed significant corrections to the conventional model, the largest in each group being:

polar motion, prograde diurnal – 30±5 μas (K_1);
polar motion, retrograde semidiurnal – 16±4 μas (M_2);
polar motion, prograde semidiurnal – 14±4 μas (S_2);
UT1, diurnal – 34±5 μas (K_1);
UT1, semidiurnal – 20±4 μas (M_2).

Here in parentheses are given standard codes of the tidal constituents. Our recommendation is that the model of the OTAM should be recomputed using the recent estimates from space geodesy and the available data sets from the satellite altimetry.

Diurnal atmospheric tides. The influence of diurnal atmospheric tides on Earth rotation was discussed in details by Brzeziński (2008). Here we will recall some basic facts. The diurnal cycle in solar heating give rise to variations in AAM with main components S_1, S_2 of periods 24 and 12 hours, and their side lobes due to seasonal modulations. These harmonic components are superimposed on the background variation of stochastic character. Similar effect can be seen in the nontidal OAM due to the ocean response

to the atmospheric forcing. All diurnal and semidiurnal harmonics of AAM and OAM expressing the atmospheric thermal tides are added to the harmonics with the same frequencies but produced by the gravitational ocen tides. With exception of S_1, in all cases the ocean tide contributions are significantly larger than the corresponding thermal effects expressed by AAM and OAM.

The diurnal and semidiurnal variations of AAM and OAM excite small perturbations in all three components of Earth rotation, including precession-nutation, polar motion and UT1. So far, only the S_1 contributions to Earth rotation could be detected in both the space-geodetic observations and geophysical models:

precession-nutation – prograde annual term, amplitude about 100 μas from VLBI data and roughly the same magnitude from AAM and OAM;

polar motion – prograde 24-hour harmonic, amplitude between 30 and 40 μas from space geodesy and below 10 μas from AAM and OAM;

UT1 – 24-hour harmonic, amplitude between 25 and 40 μas from space geodesy and below 20 μas from AAM and OAM.

There were also several attempts to estimate the S_3 harmonic of thermal origin from the continuous observation campaigns (Haas and Wünsch, 2006; Salstein et al., 2008), but they have been not conclusive so far. Finally we note that the thermal contribution to the S_2 component in polar motion and UT1 has been included in the conventional model of the ocean tide effect. In case of S_1, only the contribution to prograde annual nutation has been modeled as a so-called Sun-synchronous empirical correction. The contributions of S_1 to polar motion and UT1 are still not included in the conventional models, though significantly exceed the level of detectability. In addition, the stochastic component of excitation by the atmospheric diurnal tides needs regular monitoring in the time domain.

Atmospheric normal modes. An important feature of the global-scale dynamics of the atmosphere is the presence of the so-called normal modes. Three of them could be detected as pseudoharmonic oscillations in the equatorial components of AAM, hence contributing to polar motion. Their standard codes and central periods are the following:

ψ_3^1 Rossby-Haurwitz wave (toroidal mode), retrograde period about 10 days;

ψ_1^1 mixed Rossby-gravity wave (the Yanai wave), retrograde period about 1.2 days;

ξ_2^1 gravity wave (spheroidal mode), prograde period about 0.6 days.

Brzeziński *et al.* (2002) investigated these three atmospheric normal modes using the NCEP-NCAR reanalysis AAM data with 6-hourly resolution. They estimated the mean amplitudes of the corresponding polar motion to be: ψ_3^1 – 0.54 mas (pressure term) and 0.15 mas (wind term); ψ_1^1 – 30 μas (wind term) and 2 μas (pressure term); and ξ_2^1 – 2 μas (wind term) and 2 μas (pressure term). (Here by "mean amplitude" we understand square root of the total variance of oscillation). Brzeziński and Ponte (2005) extended the estimation by taking account the ocean response to the atmospheric forcing, expressed by the barotropic OAM model with hourly resolution. They derived the following combined influence of the atmosphere-ocean system: ψ_3^1 – 0.32 mas (matter term) and 0.27 mas (motion term); ψ_1^1 – 45 μas (motion term) and 15 μas (matter term); and ξ_2^1 – 5 μas (motion term) and 2 μas (matter term).

Among the two normal modes which are in the diurnal/subdiurnal frequency band, only the ψ_1^1 is significant. However, due to its broadband nature, it can only be expressed as time series of Earth rotation parameters with subdiurnal resolution.

3. DIURNAL POLAR MOTION OBSERVED BY RING LASER

Ring laser gyroscope is a promising emerging technology for directly and continuously measuring changes in Earth rotation; see (Schreiber et al., 2004) for details. A single instrument is capable to determine the polar motion of the instantaneous rotation axis, in contrast to the space geodetic techniques which report the terrestrial and celestial motions of the conventional Celestial Intermediate Pole (CIP); see (IERS, 2004) for details. However, due to the instrumental drift, the measurements of ring laser are not stable over periods longer than a few days. Therefore only the diurnal and subdiurnal variations in polar motion can be estimated. Among several instruments which have been developed so far, the most accurate for monitoring high frequency polar motion is the G ring laser in Wettzell (Germany). As shown in Fig. 1, its measurements are quite well correlated with prediction from the theoretical model of the forced diurnal polar motion (Brzeziński, 1986).

Here we will address the question about the possible benefits from the use of the ring laser data for monitoring variations of Earth rotation. We start from recalling some definitions and elementary kinematical relationships.

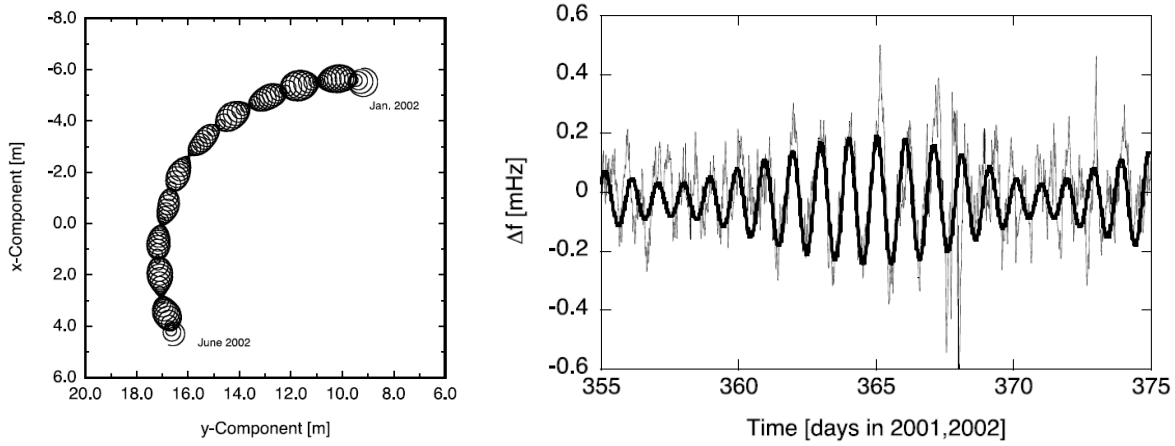

Figure 1: Model of the forced diurnal polar motion of the IRP (Brzeziński, 1986) – left, and its comparison to the measurements of the G ring laser in Wettzell, Germany – right; from (Schreiber et al., 2004).

Let $\vec{\omega} = \Omega\,[m_1, m_2, 1+m_3]^T$ be the rotation vector of the Earth, where $\Omega = 7\,292\,115 \times 10^{-11}$ rad/s denotes the average angular velocity of rotation, and m_ℓ, $\ell = 1, 2, 3$, are unitless parameters describing small departures from the uniform rotation (from observations $|m_\ell| < 10^{-6}$). The instantaneous rotation pole (IRP) which is identified with the unit vector $\vec{\omega}/|\vec{\omega}| \approx [m_1, m_2, 1]^T$, is usually expressed by the complex parameter $m = m_1 + i m_2$, with $i = \sqrt{-1}$. The time variations of m are described as polar motion of the IRP.

The space geodetic techniques express time variations of Earth rotation by the so-called Earth Orientation Parameters (EOP) $\{x_p, y_p, \delta X, \delta Y, \delta UT1\}$. The first two of EOP's, x_p, y_p, describe the terrestrial orientation of the axis defining the CIP, the next two parameters $\delta X, \delta Y$, describe small difference between the observed celestial direction of this axis and the direction predicted by the conventional precession-nutation model, and finally $\delta UT1$ expresses changes in the rotation angle around the CIP axis; see (IERS, 2004) for definition. The complex parameter $p = x_p - i y_p$ is used to describe polar motion of the CIP, while $P = \delta X + i\delta Y$ describe the nutation. Each perturbation in the direction of the CIP axis is treated either as polar motion, or as nutation, depending on frequency. If the space-referred period of perturbation is longer than 2 days, then the perturbation is treated as nutation P, for other periods it is considered as polar motion p. The corresponding perturbations in polar motion of the IRP can be expressed by the following first-order relationships (Brzeziński and Capitaine, 1993)

$$m = p - i\,\frac{\dot{p}}{\Omega}; \qquad m = i\,\frac{\dot{P}}{\Omega}\,e^{-i\theta}, \tag{1}$$

where $\theta = \Omega t + \theta_o$ denotes the sidereal rotation angle with $\theta_o \approx$ const.

Assuming harmonic form of perturbation $p = p(\sigma)e^{i\sigma t}$, $P = P(\sigma')e^{i\sigma' t}$, where $p(\sigma)$ and $P(\sigma')$ are the complex amplitudes, the relationships (3) take the following form

$$m = p(\sigma)\left(1+\frac{\sigma}{\Omega}\right)e^{i\sigma t}; \qquad m = \frac{\sigma'}{\Omega}\,P(\sigma')\,e^{i[\sigma' t-(\theta+\pi)]} \approx \frac{\sigma'}{\Omega}\,P(\sigma')\,e^{i[(-\Omega+\sigma')t-(\theta_o+\pi)]}\,. \tag{2}$$

According to the definition of the CIP (IERS, 2004), $|\sigma'| \le 0.5\Omega$ and from eq.(2) the frequency of the corresponding perturbation of m, $\overline{\sigma} = -\Omega + \sigma'$, is nearly diurnal retrograde: $\overline{\sigma} \in < -1.5\Omega, -0.5\Omega >$. The perturbations of the CIP having the Earth-referred frequencies outside the diurnal retrograde band, $\sigma \in (-\infty, -1.5\Omega) \cup (-0.5\Omega, \infty)$, are treated as polar motion.

Having regular determinations of m by the ring laser, we could easily combine them with standard observations of p and P by space geodesy, using the linear relationships (3). One obvious benefit would be the interpolation of EOP's with subdiurnal sampling. Below, we will make a quantitative discussion taking into account various known equatorial components of Earth rotation, and using the estimates derived by Brzeziński (2004). The low frequency polar motion will be disregarded because it can not be observed by the ring laser.

Precession-nutation of the CIP. The corresponding terrestrial perturbation of the IRP, expressed by m, is nearly diurnal retrograde. The total size is below 28 mas (Brzeziński, 1986) which is much smaller than the observed precession-nutation of the CIP. This is the main signal in polar motion m which can be derived from the ring laser observation; see Fig. 1. From eq.(2) one can deduce that the total difference between the precession-nutation models IAU 2000 and IAU 1980, which amounts to about 10 mas, corresponds to less than 25 μas in m. This is by more than one order of magnitude below the current accuracy of m from the ring laser data which is at the level of 1 mas (Paulo Mendes Cerveira, private communication). The geophysical signal in P, which is primarily the free core nutation, has the amplitude below 0.4 mas. The corresponding signal in m is below 1 μas, hence completely negligible.

Prograde diurnal polar motion. We have $\sigma \approx \Omega$ and from eq.(2) the corresponding relationship between m and p is $m \approx 2p$. When taking into account the size of p, one can see that the amplitudes of m will be below 0.3 mas.

Semidiurnal polar motion. For the retrograde component $\sigma \approx -2\Omega$ we derive $m \approx -p$. The maximum amplitude of m is the same as for p, that is up to about 0.3 mas. For the prograde component $\sigma \approx +2\Omega$ the relationship is $m \approx 3p$ and the amplitude of the ocean tide influence can reach the level of 1 mas.

One should bear in mind that after removing the a priori harmonic model, the size of diurnal and semidiurnal variations in polar motion will be probably by one order of magnitude smaller than assumed in the above analysis, that is below the level of 0.1 mas. The analysis shows that the observations of the ring laser are potentially useful for continuous monitoring of the prograde diurnal and retrograde/prograde semidiurnal signals in polar motion. However, as these signals are extremely small, the uncertainty of the estimated position of the IRP should be better than 0.1 mas.

4. CONCLUDING REMARKS

We presented in this work a systematic review of the perturbations in Earth rotation with daily and subdaily periods. Below, we summarize the most important conclusions and recommendations concerning each group of effects considered here.

- Astronomical variations: Model of the semidiurnal variation in UT1 due to the influence of tidal gravitation upon the triaxiality of the Earth should be included in the IERS Conventions.
- Ocean tide contributions: Observations of space geodesy revealed significant differences with the conventional model. The model recommended by the IERS Conventions 2003 should be recomputed using the available data sets from satellite altimetry and from space geodesy.
- Diurnal atmospheric tides and high frequency normal modes: The 24-hour S_1 component of thermal origin should be added to the conventional a priori model of diurnal variations in polar motion and UT1. Also the side lobes of S_1 and S_2 should be accounted for in the model. A search for the S_3 thermal component should be continued using the high frequency geophysical models and geodetic observations of Earth rotation. Regular subdiurnal observations of Earth rotation are needed to express the influences of the stochastic component of S_1 and of the ψ_1^1 mode.
- Polar motion observations of ring laser: The observations of ring laser are much less accurate than VLBI in determining those components of rotation which are currently expressed as precession-nutation of the CIP, but are potentially useful for continuous monitoring of the prograde diurnal and retrograde/prograde semidiurnal signals in polar motion. However, for significant results the uncertainty of the estimated position of the IRP should be better than 0.1 mas. The observations of ring laser can be combined with space geodetic polar motion data using the first-order kinematical relationships between the motions of the CIP and IRP.

Acknowledgements. This research was supported by the Polish national science foundation 2007-2009 under grant No. N526 037 32/3972. The Deutsche Forschungsgemeinschaft is acknowledged for covering the participation costs.

5. REFERENCES

Bolotin, S., and Brzeziński, A., 2006, "A search for geophysical signals in diurnal and semidiurnal polar motion from analysis of the routine VLBI observations", Geophys. Res. Abstracts, Vol.8, abstract No. EGU06-A-01665.

Brzeziński, A., 1986, "Contribution to the theory of polar motion for an elastic earth with liquid core", Manuscripta Geodaetica, 11, pp. 226–241.

Brzeziński, A., 2004, "Forced polar motion of the instantaneous rotation axis", paper presented at FGS Workshop 2004 on "Ringlaser Gyroscopes and Earth Rotation", Höllenstain/Wettzell, Germany.

Brzeziński, A., 2008, "On the influence of diurnal atmospheric tides on Earth rotation", Proc. Journées Systèmes de Référence Spatio-Temporels 2007, N. Capitaine ed., Paris Observatory, pp. 180–183.

Brzeziński, A., and Capitaine, N., 1993, "The use of the precise observations of the Celestial Ephemeris Pole in the analysis of geophysical excitation of earth rotation", J. Geophys. Res. , 98(B4), pp. 6667–6675.

Brzeziński, A., and Capitaine, N., 2002, "Lunisolar perturbations in Earth rotation due to the triaxial figure of the Earth: geophysical aspects", Proc. Journées Systèmes de Référence Spatio-Temporels 2001, N. Capitaine ed., Paris Observatory, pp. 51–58.

Brzeziński, A., and Ponte, R. M., 2005, "A search for the high frequency atmospheric and oceanic modes in the excitation of polar motion", Geophys. Res. Abstracts, Vol. 7, abstract No. EGU05-A-09840.

Brzeziński, A., Bizouard, Ch., and Petrov, S. D., 2002, "Influence of the atmosphere on Earth rotation: what new can be learned from the recent atmospheric angular momentum estimates?", Surveys in Geophysics, 23, pp. 33–69.

Chao, B. F., Dong, D. N., Liu, H. S., and Herring, T. A., 1991, "Libration in the Earth's rotation", Geophys. Res. Letters, 18(11), pp. 2007–2010.

Chao, B. F., Ray, R. D., Gipson, M. J., Egbert, G. D., and Ma, C., 1996, "Diurnal/semidiurnal polar motion excited by oceanic tidal angular momentum", J. Geophys. Res. (Solid Earth), 101(B9), pp. 20,151–20,163.

Gipson, J. M., 1996, "Very long baseline interferometry determination of neglected tidal terms in high-frequency Earth orientation variations", J. Geophys. Res. , 101(B12), pp. 28,051–28,064.

Haas, R., and Wúnsch, J., 2006, "Sub-diurnal earth rotation variations from the VLBI CONT02 campaign", J. Geodynamics, 41, pp. 94–99.

Herring, T. A., and Dong, D., 1994, "Measurement of diurnal and semidiurnal rotational variations and tidal parameters of Earth", J. Geophys. Res. , 99(B9), pp. 18,051–18,071.

IERS, 2004, "IERS Conventions 2003", D. McCarthy and G. Petit (eds.), IERS Technical Note No. 32, Verlag des Bundesamts für Kartographie und Geodäsie, Frankfurt am Main.

Rothacher, M., Beutler, G., Weber, R., and Hefty, J., 2001, "High-frequency variations in Earth rotation from Global Positioning System data", J. Geophys. Res. , 106(B7), pp. 13,711–13,738.

Salstein, D. A., Nastula, J., Quinn, K., MacMillan, D., and Mendes Cerveira, P. J., 2008, "Atmospheric excitation of Earth rotation/polar motion at high temporal resolution", Proc. Journées Systèmes de Référence Spatio-Temporels 2007, N. Capitaine ed., Paris Observatory,, pp. 177–179.

Schreiber, K. U., Velikoseltsev, A., Rothacher, M., Klügel, T., and Stedman, G. E., 2004, "Direct measurement of diurnal polar motion by ring laser gyroscopes", J. Geophys. Res. (Solid Earth), 109(B06405), doi: 10.1029/2003JB002803.

Watkins, M. W., and Eanes, R. J., 1994, "Diurnal and semidiurnal variations in Earth orientation determined from LAGEOS laser ranging", J. Geophys. Res. , 99(B9), pp. 18,073–18,079.

Wünsch, J., 1991, "Small waves in UT1 caused by the inequality of the equatorial moments of inertia A and B of the Earth", Astron. Nachr., 312(5), pp. 321–325.

OCEAN TIDAL EFFECTS ON EARTH ROTATION

R.S. GROSS
Jet Propulsion Laboratory, California Institute of Technology
4800 Oak Grove Drive, Pasadena, CA 91109, USA
e-mail: Richard.Gross@jpl.nasa.gov

ABSTRACT.

The second-degree zonal tide raising potential, which is responsible for tidal changes in the Earths rotation rate and length-of-day, is symmetric about the polar axis and hence can excite the Earths polar motion only through its action upon nonaxisymmetric features of the Earth like the oceans. Ocean tides excite polar motion in the diurnal, semidiurnal, and long-period tidal bands. Here, ocean tidal excitation of polar motion in the long-period tidal band, specifically at the Mm (monthly), Mf (fortnightly), and Mt (9-day) tidal frequencies, is studied. Spectra of observed polar motion excitation functions exhibit peaks at the prograde and retrograde fortnightly tidal frequencies. In fact, except at seasonal and longer periods, these are the largest peaks in the observed spectra after atmospheric and nontidal oceanic effects are removed from the observations. An empirical model for the effect of the monthly, fortnightly, and 9-day ocean tides upon polar motion excitation is obtained by least-squares fitting periodic terms at these tidal frequencies to observed polar motion excitation from which atmospheric and nontidal oceanic effects have been removed. The resulting empirical model is compared with predictions from hydrodynamic ocean tide models.

REALISATION OF THE TERRESTRIAL REFERENCE SYSTEM BY A GLOBAL GPS NETWORK AS A BASIS FOR GLOBAL GEODYNAMIC INVESTIGATIONS

A. RÜLKE[1], M. FRITSCHE[1], R. DIETRICH[1], P. STEIGENBERGER[2], M. ROTHACHER[3]
[1] Institut für Planetare Geodäsie, Dresden Technical University, Germany
[2] TU Müchen, Institut für Astronomische und Physikalische Geodäsie, Germany
[3] GFZ Potsdam, Department of Geodesy and Remote Sensing, Germany
e-mail: ruelke@ipg.geo.tu-dresden.de

ABSTRACT.

For the investigation of global geodynamics a consistent and log-term stable realisation of the International Terrestrial Reference System (ITRS) is crucial. We present a GPS-only reference frame, based on the results of a homogeneous reprocessing of a global GPS network. The reference frame is realised in the center of mass system. This implies that a self-consistent model considering the reference frame and loading dynamics has been applied. The determined station coordinates and their linear rates are evaluated in terms of self-consistency and are compared to other realisations of the ITRS, such as ITRF2000, ITRF2005, IGb00 and IGS05. The results show the high potential of homogeneously reprocessed GPS observations for the realisation of the ITRS. Finally, we will use the determined station velocities to validate models of glacial isostatic adjustment.

ANALYTICAL COMPUTATION OF THE TRANSLATIONAL INTERNAL MOTION OF A SIMPLE NON-ISOBARYCENTRIC THREE-LAYER EARTH MODEL

A. ESCAPA[1], T. FUKUSHIMA[2]
[1] Dpto. Matemática Aplicada. Escuela Politécnica Superior
Universidad de Alicante. E-03080 Alicante. Spain
e-mail: alberto.escapa@ua.es
[2] National Astronomical Observatory
Ohsawa, Mitaka, Tokyo 181-8588, Japan
e-mail: Toshio.Fukushima@nao.ac.jp

ABSTRACT. In this investigation, we start the study of the dynamics of non-isobarycentric three-layer celestial bodies, that is to say, of bodies whose internal layers have barycenters located in different points of the space. Due to the complexity of the problem, our first step focuses on determining the translational internal motions of a simple three-layer body composed by a spherical rigid mantle, a homogeneous fluid outer core and a spherical rigid inner core. To this end, we construct the Lagrangian of the system by considering an irrotational fluid motion. On the basis of assuming a small relative motion of the mantle with respect to the inner core, the analytical expression of its associated free frequency, usually referred as Slichter mode, is found. This expression is in agreement with others provided by quite different approaches. Finally, we discuss the dependence of the frequency with the rheological parameters that characterize the Earth model.

1. INTRODUCTION

Usually, Earth rotation studies assumes isobarycentric models, that is to say, models for which the barycenters of all the components, or layers, are located always at the same point. This is an approximation, since the rigid motions around the barycenter of the Earth also contain a translational part. In this way, we face the problem to consider non-isobarycentric bodies, in such a way that the rigid internal motions around the barycenter of the body is composed of rotational and translational motions. This is the case, for example, of a three layer Earth model composed of a solid mantle, a fluid core and a solid inner core that we will study in this investigation.

One possibility to tackle this problem is to apply the normal modes techniques (Rogister 2003). However, they present some disadvantages. For example: (1) they provide numerical solutions, what makes difficult to interpret the interdependence between the different internal motions and to analyze the influence of the Earth model characteristics in them; (2) a precise data set describing the rheology of the body is need, this information is not available for the main part of the celestial bodies. Therefore, it becomes evident a need to develop complementary analytical treatments to these kind of approaches.

As far as we know, currently there is not any analytical approach that considers the whole internal dynamics of a non-isobarycentric three–layer Earth model. The only exceptions are referred, on the one hand, to Earth rotation studies that do not consider the translation among the barycenter of the layers. On the other hand, there have been developed two investigations, due to Busse (1974) and Grinfeld & Wisdom (2005), which worked out the translational motions by constructing the linear momentum equations of the inner core with the help of vectorial mechanics by different Earth models. Busse (1974) considers an Earth model composed of a motionless spherical rigid mantle, an homogeneous fluid outer core and a spherical rigid inner core. Grinfeld & Wisdom (2005) discussed the translational internal motion of an Earth model composed of a spherical rigid mantle, an homogeneous fluid outer core and a spherical rigid inner core, neglecting the effect of the rotation. These translational motions have geophysical interest since it has been proposed (Slichter, 1961) that the internal translational motion of the inner core barycenter could be observed in precise gravimeter records after great earthquakes, providing information about the rheology in the fluid–inner core boundary. In fact, this is a simplified model since one should consider the effects of the Earth rotation.

In this note, we start the study of the dynamics of the internal motion by means of Analytical Mechanics methods, since these approaches have provided competitive Earth rotation models (e.g. Getino & Ferrándiz, 2001). The first step in this task is to give a proper description of the internal translational motion in this framework.

2. LAGRANGIAN OF THE SYSTEM

Next, we will consider a three-layer Earth model similar to that of Grinfeld & Wisdom (2005), that is to say, a body isolated in the space and composed of an external rigid spherical shell (mantle) and an internal rigid sphere (inner core). The space between these layers is filled with a perfect fluid (fluid outer core); all the components of the system are assumed to have constant densities distributions (see figure 1). In addition, we will only consider the translational motion of the rigid layers. To describe the dynamics of the system, we will construct the Lagrange equations

$$\frac{d}{dt}\left(\frac{\partial L}{\partial \dot{q}_i}\right) - \frac{\partial L}{\partial q_i} = 0,\ i = 1, \ldots, n, \tag{1}$$

being $L = T - V$ the difference between the kinetic and potential energy. The dynamical system is properly described by considering six generalized coordinates: three, $\vec{\xi}_M$, are the components of the mantle barycenter O_M with respect to a reference frame whose origin is located at barycenter of the Earth, O, and the remaining ones, $\vec{\xi}_S$, the components of the inner core barycenter O_S referred to the same frame. With respect to the motion of the fluid, let us point out that under the above mentioned conditions it is generated by that of the solids layers (Lamb, 1932). In these circumstances, the fluid velocity $\vec{v}_F$ is irrotational and we can introduce a velocity potential f , $\vec{v}_F = \vec{\nabla} f$, such as

$$\vec{\nabla}^2 f = 0 \tag{2}$$

with the boundary conditions

$$\vec{v}_F \cdot \vec{n} = \vec{V}_M \cdot \vec{n} \text{ at } \partial D_M,\ \vec{v}_F \cdot \vec{n} = \vec{V}_S \cdot \vec{n} \text{ at } \partial D_S, \tag{3}$$

being $\vec{V}_M = d\vec{\xi}_M/dt$ and $\vec{V}_S = d\vec{\xi}_S/dt$, and $\vec{n}$ the normal vector on the boundaries ∂D_M and ∂D_S (see figure 2). Anyway, it is possible a further reduction in the number of the degrees of freedom of our system. Namely, we have the two relationships

$$m_M\vec{\xi}_M + m_F\vec{\xi}_F + m_S\vec{\xi}_S = \vec{0};\ m_F\vec{\xi}_F = m_F\vec{\xi}_M + \frac{\rho_F}{\rho_S}m_S\vec{\xi}_M - \frac{\rho_F}{\rho_S}m_S\vec{\xi}_S, \tag{4}$$

being m_i the mass of each layer, m the mass of the Earth and $\vec{\xi}_F$ the components of the fluid barycenter with respect to $\mathcal{R}$. The first one reflects the fact that the barycenters of the layers are referred to O; the second one is due to the simple geometry of our model (see figure 3). Hence, our model can be described with three generalized coordinates. The most expedient choice is to take $\vec{\eta}_S = \vec{\xi}_S - \vec{\xi}_M$. In this way, the mantle and the inner core barycenters can be written as

$$\vec{\xi}_M = \frac{m_S}{m}\left(\frac{\rho_F}{\rho_S} - 1\right)\vec{\eta}_S = \alpha_M\vec{\eta}_S,\ \vec{\xi}_S = (1 + \alpha_M)\,\vec{\eta}_S. \tag{5}$$

To construct the Lagrange equations, we will assume that the instantaneous configuration (figure 2) remains always close enough to the reference configuration (figure 1). It will allow a simpler mathematical treatment of the problem, since all the functions which involves the fluid motion will be developed up to the first order in the perturbation-like parameter $e = \left|\vec{\xi}_M - \vec{\xi}_S\right|/R_S$.

The kinetic energy of the system is $T = T_M + T_S + T_F$. Since the mantle and the inner core are rigid bodies, the expression of their kinetic energy is straightforward and with the help of 5 can be written as

$$T_M + T_S = \frac{1}{2}\left[m_M\alpha_M^2 + m_S\,(1 + \alpha_M)^2\right]\left(\frac{d\vec{\eta}_S}{dt}\right)^2. \tag{6}$$

The kinetic energy of the fluid is given by

$$T_F = \frac{1}{2}\int_{fluid}\vec{v}_F^2\rho_F\,dV = \frac{1}{2}\int_{fluid}\left(\vec{\nabla} f\right)^2\rho_F\,dV. \tag{7}$$

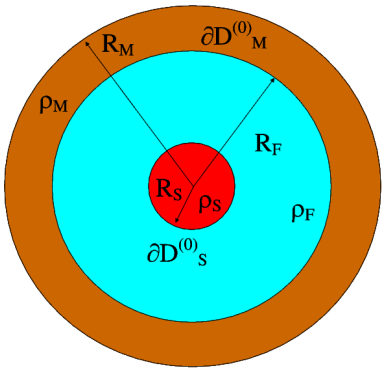

Figure 1

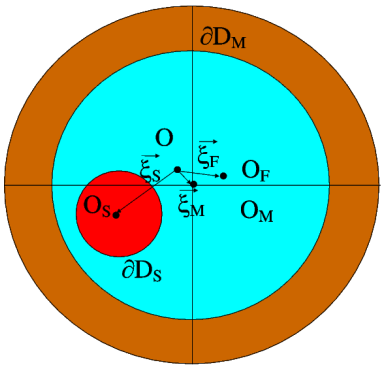

Figure 2

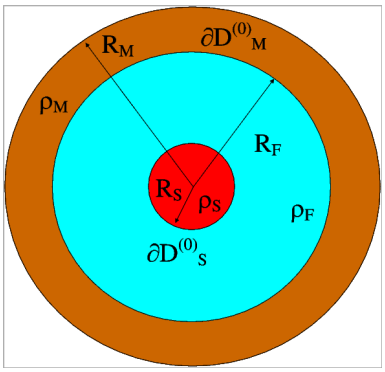

Figure 3

By considering the solution of equations 2 and 3, expressed in terms of an spherical harmonics expansion, and Gauss theorem, it can be shown (Escapa & Fukushima, 2009) that, at the first order in e, this expression has the value

$$T_F = \frac{1}{2}\left(\frac{2}{3}\pi\rho_F c\right)\left(\frac{d\vec{\eta}_S}{dt}\right)^2 = \frac{1}{2}\left\{\frac{2}{3}\pi\rho_F\left[2\alpha_M^2 R_F^3 - 2\left(1+\alpha_M\right)^2 R_S^3 + 3\frac{R_F^3 R_S^3}{R_F^3 - R_S^3}\right]\right\}\frac{d\vec{\eta}_S}{dt}^2 . \tag{8}$$

The potential energy of the system is due to the gravitational interaction among the layers. However, since the mantle is an rigid spherical shell of constant density the gravitational potential inside it takes a constant value, so it does not play any role in the dynamics of the system. Hence, the gravitational potential energy of our model arises from the fluid–solid inner core interaction. Its expression can be computed by considering the the potential gravitational energy of a homogeneous sphere and the decomposition sketched in the figure 3. Namely, we have

$$V = \frac{2\pi}{3} G\rho_F\, m_S \left(1 - \frac{\rho_F}{\rho_S}\right)\left(\vec{\eta}_S\right)^2 . \tag{9}$$

Taking into account the equations 6, 8 and 9, the Lagrangian of the system turns out to be

$$L = \frac{1}{2}\left[m_M\alpha_M^2 + m_S\left(1+\alpha_M\right)^M + \frac{3}{2}\pi\rho_F c\right]\left(\frac{d\vec{\eta}_S}{dt}\right)^2 - \frac{1}{2}\left[\frac{4\pi}{3}G\rho_F\, m_S\left(1-\frac{\rho_F}{\rho_S}\right)\right]\left(\vec{\eta}_S\right)^2 . \tag{10}$$

3. DISCUSSION

Equation 10 shows that the dynamics of the system is completely specified since it is the same as that of a harmonic oscillator of frequency. Therefore, the barycenter of the solid inner core performs harmonics oscillations with respect to the mantle barycenter, being the equilibrium position the reference configuration. The dependence of this translational internal motion with the characteristics of the Earth model is clearly reflected in the functional dependence of the frequency, ω_0, which with the aid of the equations 5 and 8 can be written as

$$\omega_0^2 = \frac{4\pi}{3}G\rho_F\left(1-\frac{\rho_F}{\rho_S}\right)\frac{1}{\left[1+\frac{1}{2}\frac{\rho_F}{\rho_S}+\frac{3}{2}\left(\frac{\rho_F}{\rho_S}\right)^2\frac{m_S}{m_F}\right] - \left[\frac{m_S}{m_M+m_F+m_S}\left(1-\frac{\rho_F}{\rho_S}\right)^2\right]} . \tag{11}$$

This expression allows easy comparisons with the previous investigations by Busse (1974) and Grinfeld & Wisdom (2005). In particular, we can recover the results of Busse by equating the rotation to 0 in his formula, and by taking $m \to +\infty$ (mantle rest condition) in equation 11. This is also the case for the expression of Slichter mode of Grinfeld & Wisdom (2005) which, after some tedious algebra, agrees with equation 11 in spite of the quite different methods employed.

On the other hand, the derived expression of the Slichter frequency ω_0 makes possible to discuss the influence of the model on it. In particular, we can compute for different three-layer celestial bodies the

effect that has the motion of the mantle in the frequency. The contribution of this effect appears in the denominator of equation 11 through the term

$$\Delta = \frac{m_S}{m_M + m_F + m_S} \left(1 - \frac{\rho_F}{\rho_S}\right)^2 . \tag{12}$$

By considering some numerical data given in Grinfeld & Wisdom (2005) for the Earth and Mercury, we can compute the period T_{ω_0} associated to the frequency ω_0; its counterpart when considering a mantle in rest $T_{\omega_0|_{\vec{\xi}_M=\vec{0}}}$ and the absolute value of the relative difference between these two periods. The results are displayed in the next table.

Body	T_{ω_0}	$T_{\omega_0\|_{\vec{\xi}_M=\vec{0}}}$	Rel. dif.%	m_S/m	$1-\rho_F/\rho_S$
Earth	4.2356	4.2358	.003	.016	.077
Mercury	8.3900	8.3977	.091	.598	.158

As it can be seen, the contribution of the mantle motion to the period in the case of the Earth is completely negligible. This is due to two factors. On the one hand, to the small mass of the inner core with respect to the mass of the whole planet. On the other one, the relative density contrast between the fluid an the inner core, $1-\rho_F/\rho_S$, is also small. So, as Busse (1974) did rightly the effect of the mantle motion in the case of the Earth can be safely disregarded when computing the value of the Slichter mode. In addition, following Grinfeld & Wisdom (2005), we can examine the Slichter mode of Mercury. For this planet the mass of the inner core is more than the half of the total mass, so one could expect the effect of the mantle motion to be significant (Grinfeld & Wisdom, 2005). However, that is not the case. With help of equation 12 derived following our analytical treatment, the reason is clear since also for Mercury the relative density contrast between the fluid an the inner core is very small, so when taking its square in equation 12 the value of Δ still remains small.

To summarize, it has been developed a model to describe Earth translational internal motions with the methods of Analytical Mechanics, providing an analytical expression of Slichter mode. In particular, it have been shown that the effect of the mantle motion in the value of the Slichter mode should be considered depending both on the existence of a heavy inner core and the value of the density contrast, conditions that are not fulfilled by the planets Earth and Mercury but that could be verified in the case of other celestial bodies. Future steps of this investigation should consider the joint effects of the rotational and translational internal motions, as well as improvements in the rheological characterization of the Earth model.

Acknowledgements. AE's contribution has been partially supported by the Descartes–Nutation project and the Spanish projects I+D+I, AYA2004-07970 and AYA2007-67546 and *Junta de Castilla y León* project VA070A07.

4. REFERENCES

Busse, F.H., 1974. "On the free oscillation of the Earths inner core". J. Geophys. Res. 79, 753–757.

Escapa, A. and Fukushima, T., 2009, "Translational modes of a simple three-layer body through Lagrange's equations" (in preparation).

Getino, J. and Ferrándiz, J. M., 2001, "Forced nutation of a two-layer Earth model". MNRAS 322, 785–799.

Grinfeld, P. and Wisdom, J., 2005, "Motion of the mantle in the translational mode the Earth and Mercury". Phys. Earth Planet. Int., 151, 77–87.

Lamb, H., 1932, "Hydrodynamics", 6th ed. Dover Publications, New York.

Rogister, Y., 2003, "Splitting of seismic free oscillations and of the Slichter triplet using the normal mode theory of a rotating, ellipsoidal earth". Phys. Earth Planet. Int. 140, 169–182.

Slichter, L., 1961. "The fundamental free mode of the Earths inner core". Proc. Natl. Acad. Sci. U.S.A. 47, 186-190.

ON OPTIMAL DETECTION AND ESTIMATION OF THE FCN PARAMETERS

Y.S. YATSKIV
Main Astronomical Observatory of the NAS of Ukraine
27 Akad. Zabolotnoho St.
Kyiv 03680 Ukraine
mailto:yatskiv@mao.kiev.ua
http://www.mao.kiev.ua

ABSTRACT. Statistical approach for detection and estimation of parameters of short-term quasi-periodic processes was used in order to investigate the Free Core Nutation (FCN) signal in the Celestial Pole Offset (CPO). The results show that this signal is very unstable and that it disappeared in year 2000. The amplitude of oscillation with period of about 435 days is larger for dX as compared with that for dY.

1. INTRODUCTION

Free Core Nutation (FCN) is a free motion of the Celestial Intermediate Pole (CIP) in space due to the interaction of the mantle and the fluid, ellipsoidal core of the Earth. FCN signal is the most significant oscillation in the Celestial Pole Offset (CPO) residuals with respect to the IAU 2000A nutation model. It was investigated by many authors (for references see Malkin, 2004, Kalarus et al., 2006) which have showed that this signal was non-stationary one. Supposing the space-referred retrograde period of the FCN is constant (about 430 days) the variations of amplitude and phase of oscillation were determined (see, for example, Brzezinski, 2005). Studies were performed to understand possible causes of the FCN, in particular the diurnal variability in the system of atmosphere-oceans. Nevertheless, there is no final conclusion on this matter and a search for possible sources of excitation of the FCN has to be continued. For this reason additional study of the FCN time-varying signal in the CPO through the use of new methods could be of some interest. In this study a new statistical approach for detection and estimation of parameters of quasi-periodic processes proposed by Panasenko and Chernogor (2007) was used for analyzing the CPO included in the IERS C04 (IAU 2000).

2. METHOD OF ANALYSIS

Method for detection and estimation of the parameters of quasi-periodic processes proposed by Panasenko and Chernogor (2007) was used in order to determine areas of the FCN signal i.e. time of appearance of the signal and duration of its existence. This method is based on the theory of optimal detection and optimal estimation of quasi-periodic processes (QPP) of the type

$$s(t) = A\cos(\omega + \varphi)[\theta(t-\tau) - \theta(t-\tau-t_p)],$$

where $\omega = 2\pi/T$; T is the period of QPP; t and t_p are time of appearance and duration of existence of QPP, respectively;

$$\theta(t) = \begin{cases} 0, t < 0 \\ 1, t \geq 0 \end{cases}$$

In case of additive noise $w(t)$ we have

$$x(t) = s(t) + w(t).$$

Optimal detection criterion is defined by equation

$$L = \frac{W_w[x(t)]}{W_s[x(t)]} > L_n,$$

where $W_w[x(t)]$ and $W_s[x(t)]$ are the likelihood functional in cases of absence of signal $s(t)$ and its presence respectively; L_n is adopted limit value of L.

3. DATA AND RESULTS OF ANALYSIS

The CPO time series dX and dY (IERS CO4 1984-2006) with the sampling interval of 1 day where used in the analysis. From previous studies of the FCN we know that there is significant power in the retrograde period range from 300 to 600 days. Therefore for the analysis of this period range and for decreasing an amount of computation the 30 days average values of dX and dY were used in what follows. The results of this computation are shown in Fig.1 and Fig.2.

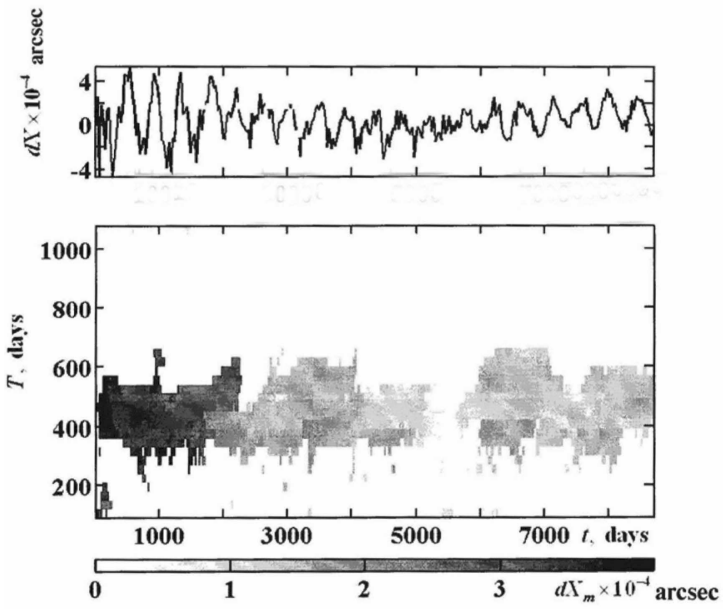

Figure 1: Optimal detection and estimation of amplitude (dX_m) of the FCN signal in the dX of the CPO.

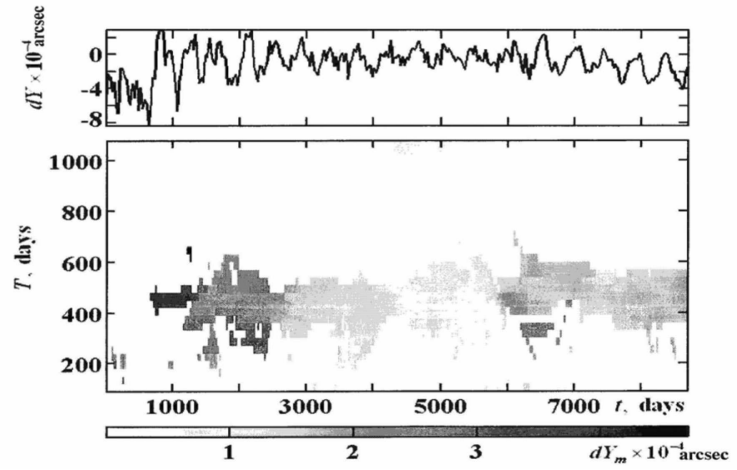

Figure 2: Optimal detection and estimation of amplitude (dY_m) of the FCN signal in the dY of the CPO.

These results were compared with those obtained by the adaptive Fourier transform and the Morlet wavelet analysis of the CPO. Because of the results of these computations for dX and dY are similar ones we show here (Fig. 3) the result for dX only.

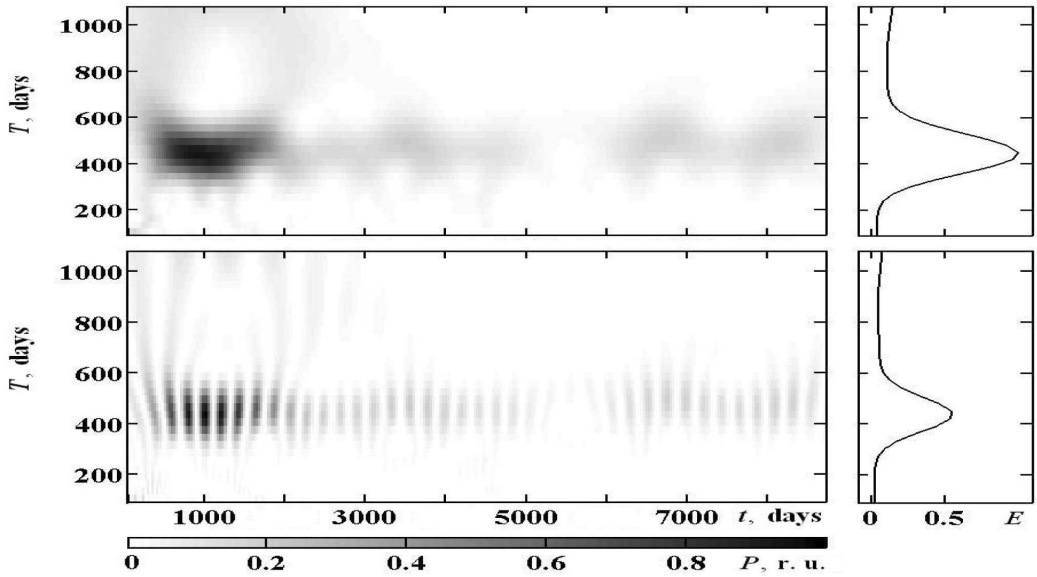

Figure 3: Adaptive Fourier transform (upper picture) and the Morlet wavelet (bottom picture) of the dX, where E is energy spectrum of process.

These figures show that there is a significant variation of amplitude of the FCN signal. One of striking results is the absence of signal in the year 2000. This fact could be used for search of possible source of the FCN excitation.

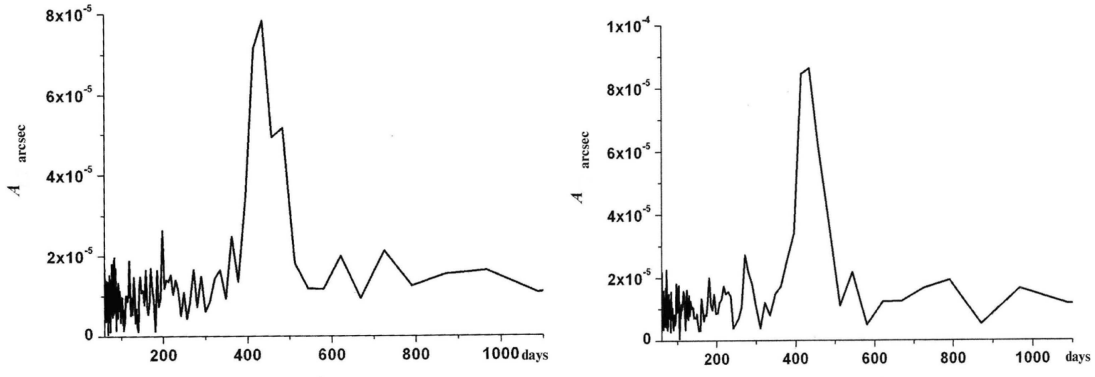

Figure 4: Amplitude spectrum of dX (left) and dY (right).

We have also computed the amplitude spectra of dX and dY (Fig 4). One can see that the average value of period of the FCN is of about 435 days which differs from what is used in the FCN model by Colarus et al. (2006). The FCN looks like as slightly elliptical motion because of the amplitudes for dX and dY are not equal.

4. CONCLUSION

The FCN which looks like as a quasi-periodic process is slightly elliptical motion with variable amplitude and period of about 435 days. There is a strong damping of this process in some interval of time resulting in a disappearance of the FCN signal in close proximity to the year 2000.

Acknowledgements. The author expresses his gratitude to Prof. L. Chernogor and Dr. S. Panasenko for their valuable comments and support of this work.

5. REFERENCES

Brzeziński A., 2005, "Chandler Wobble and free core nutation: observation, modeling and geophysical interpretation", Artif. Satellites., 40, pp. 21–33.

Kalarus M., Luzum B.I., Lambert and Kosek W., 2006, in the Proceedings of the Journées 2005 "Systèmes de Réfŕence Spatio-Temporels", A. Brzezinski, N. Capitaine and B. Kolaczek (eds.), Space Research Centre PAS, Warsaw, Poland, pp. 181–184.

Malkin Z., 2004, "A New Free Core Nutation Model with Variable Amplitude and Period", in IVS 2004 General Meeting Proceedings, pp. 388–392.

Panasenko S.V. and Chernogor L.F., 2007, "Optimal Detection and Optimal Estimation of the parameters of short-term Quasi-Periodic Processes", Radiofisika i Radioastronomiya, vol. 12., N1. pp. 61–75.

IS THE LENGTH-OF-DAY TIME SERIES NORMALLY DISTRIBUTED?

A.K. SEN[1], T. NIEDZIELSKI[2,3], W. KOSEK[2]
[1]Department of Mathematical Sciences, Indiana University
402 N. Blackford Street, Indianapolis, IN 46202, USA
e-mail: asen@iupui.edu
[2]Space Research Centre, Polish Academy of Sciences
Bartycka 18A, 00-716 Warsaw, Poland
e-mail: niedzielski@cbk.waw.pl, kosek@cbk.waw.pl
[3]Institute of Geography and Regional Development, University of Wrocław
pl. Uniwersytecki 1, 50-137 Wrocław, Poland

ABSTRACT. The non-tidal LOD data are analysed (data span 01.01.1962-09.01.2008) in order to provide the probabilistic characteristics of the Earth rotation rate fluctuations. The skewness of the LOD probability distribution is of -0.31 indicating that the probability distribution is asymmetrical. Moreover, the residual non-tidal LOD data is considered (after removal of the semiannual, annual, 9.3-years, and 18.6-years oscillations, and linear trend). The skewness of this residual data equals to -0.64 and indicates an increased asymmetry in the distribution. For the non-transformed LOD data the kurtosis is of 2.31 and it shows that the distribution is flattened. The kurtosis for the residuals is 5.64 indicating that the distribution is more peaked than a normal distribution. For the non-transformed LOD data, the Jonhson SB distribution provides the best fit. For the residual LOD data, the Johnson SU distribution is found to be the most appropriate model. Both the LOD and it's residual time series are appropriately modeled by probability laws that are different from a normal distribution.

1. INTRODUCTION

Many applications of time series analysis, e.g. prediction methods, require the assumption that the data are normally distributed. If the time series consists of the extreme values, the underlying probability law of data is rather different that a normal (or Gaussian) distribution. In particular, the large-scale El Niño/Southern Oscillation (ENSO) causes the extreme stochastic fluctuations in the Earth rotation rate. The Earth rotation rate is described by length-of-day (LOD, also denoted by Δ) or its integral, i.e. UT1-UTC Universal Time. The LOD increases during El Niño (due to the collapse of the tropical easterly winds), and decreases during La Niña.

The fluctuations in Δ (or equivalently UT1-UTC) are of tidal and non-tidal origins. The oscillations caused by the tides with periods from 5 days to 18.6 years are caused by gravitational interactions among the Earth, the Moon, the Sun, and - less significantly - other planets of our solar system. The tidal correction $\delta\Delta$ is determined using the model defined by the International Earth Rotation and Reference Systems Service (IERS) Conventions 2003 (McCarthy and Petit, 2004).

We consider the two time series: (1) the non-tidal length-of-day time series ($\Delta - \delta\Delta$) for the period from 01.01.1962 to 09.01.2008 computed by removing the tidal model $\delta\Delta$ from Δ time series eopc04_IAU2000.62-now (IERS, 2008) (Fig. 1(a)), and (2) the residual $\Delta - \delta\Delta$ time series denoted by $\varepsilon(\Delta - \delta\Delta)$ (after removal of the least-squares model which consists of semiannual, annual, 9.3-year, and 18.6-year oscillations, and the linear trend) (Fig. 1(b)).

Many researchers analysed $\Delta - \delta\Delta$ time series using the data processing techniques (Kosek, 1997; Kosek et al., 1998; Schuh et al., 2002; Akyilmaz and Kutterer, 2004; Niedzielski and Kosek, 2008). The predictions of $\Delta - \delta\Delta$ determined by time series methods are based upon the decomposition of $\Delta - \delta\Delta$ time series into deterministic components and stochastic residuals. Several forecasting methods assume that the residuals are normally distributed (Kosek et al., 2005; Niedzielski and Kosek, 2008).

A normal distribution is characterized by the mean and standard deviation. This distribution exhibits the zero skewness and a kurtosis value of 3. First, we discuss if a normal distribution fits both $\Delta - \delta\Delta$

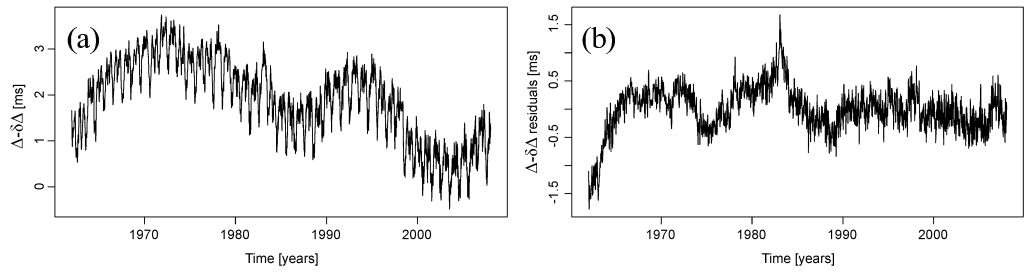

Figure 1: The $\Delta - \delta\Delta$ (a) and the $\varepsilon(\Delta - \delta\Delta)$ (b) time series.

and its residuals. Second, several non-Gaussian probability distributions are fitted to these time series.

2. FITTING A NORMAL DISTRIBUTION

Table 1 shows that the distributions of both $\Delta - \delta\Delta$ and $\varepsilon(\Delta - \delta\Delta)$ time series are skewed. The probability distribution of $\varepsilon(\Delta - \delta\Delta)$ reveals the increased asymmetry in respect to the asymmetry of $\Delta - \delta\Delta$ distribution. In both cases, the heavy-tail is present in the left-hand side of the probability density function. The analysis of kurtosis shows that the distribution of $\Delta - \delta\Delta$ is more flat than the normal distribution. In contrast, the probability density function of $\varepsilon(\Delta - \delta\Delta)$ is more peaked than the Gaussian one.

	Skewness	Kurtosis
$\Delta - \delta\Delta$	-0.31	2.31
$\varepsilon(\Delta - \delta\Delta)$	-0.64	5.64

Table 1: The skewness and kurtosis of the non-tidal LOD time series and its residuals.

The departure of $\Delta - \delta\Delta$ from the normal distribution is also detected (a) by comparing the probability density function (pdf) with the histogram of the data, (b) by comparing the cumulative distribution function (cdf) with the cdf of the data, (c) using a Probability-Probability (P-P) plot, and (d) using a Quantile-Quantile (Q-Q) plot (Fig. 2). The P-P plot is a plot of the empirical cdf values depicted against the theoretical cdf values. The Q-Q plot is a graph of the data plotted against the quantiles of the theoretical distribution. Both the P-P plot and the Q-Q plot are widely used to evaluate the goodness-of-fit (Gilchrist, 2000; Holmgren, 1995; Reiss & Thomas, 2007; Wasserman, 2002). These plots can be used to test how closely a theoretical distribution compares with the empirical distribution of the data, and to compare several fitted distributions. Figures 2(a) and 2(b) show that the empirical distribution of $\Delta - \delta\Delta$ differs from the normal distribution. The analysis of both the P-P plot (Fig. 2(c)), and the Q-Q plot (Fig. 2(d)) supports the above-mentioned conclusions.

The similar analyses confirm that the distribution of the residual time series $\varepsilon(\Delta - \delta\Delta)$ differs from the normal probability law. Indeed, Figures 3(a) and 3(b) indicate that the pdf (cdf) of the normal distribution does not fit the histogram (empirical distribution function) of $\varepsilon(\Delta - \delta\Delta)$. Similarly, the P-P plot (Fig. 3(c)) and the Q-Q plot (Fig. 3(d)) confirm the inadequacy of the normal distribution.

In the case of $\Delta - \delta\Delta$ time series, the departure from the normal distribution can be caused by the long-term oscillations driven by geological processes acting between the core and the Earth's mantle. However, the non-Gaussian distribution of $\varepsilon(\Delta - \delta\Delta)$ data is probably due to ENSO episodes which are recorded as extreme spikes in this time series.

3. FITTING NON-GAUSSIAN DISTRIBUTIONS

Following the fact, that the distributions of both $\Delta - \delta\Delta$ and $\varepsilon(\Delta - \delta\Delta)$ are different than a normal probability law, several non-Gaussian distributions are examined.

In the case of $\Delta - \delta\Delta$ time series, the 3-parameter generalized extreme value (GEV) distribution

(Kotz & Nadarajah, 2001), 4-parameter Beta (Gupta & Nadarajah, 2004), and Johnson SB distributions (Bowman & Shenton 1983) provide good fit (Fig. 2). Among them, the Johnson SB distribution appears to provide the best fit to $\Delta - \delta\Delta$ data.

The analysis of the Q-Q plot (Fig. 2(d)) shows that for small quantiles, the Johnson SB distribution provides the best fit to the empirical distribution of $\Delta - \delta\Delta$ time series. The Johnson SB distribution is rather the best in modeling the probabilities around the mode (Fig. 2(a)). However, for high quantiles both GEV and 4-parameter Beta probability distributions provide the best fit to the histogram of $\Delta - \delta\Delta$.

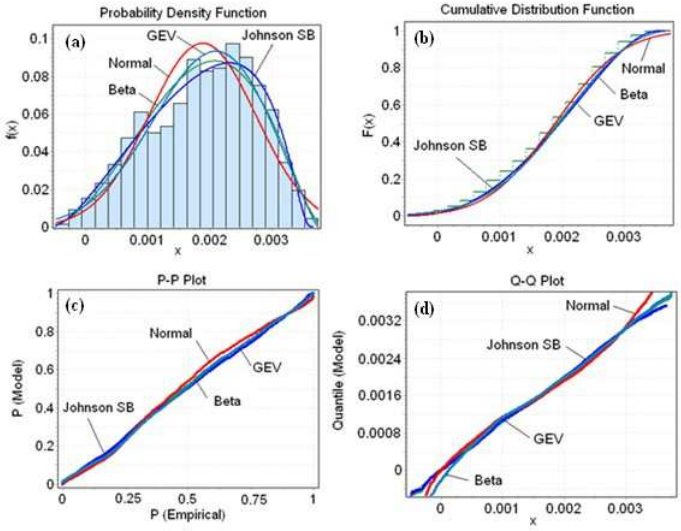

Figure 2: The analysis of $\Delta - \delta\Delta$ time series; the pdf vs. the histogram of the data (a), the cdf vs. the cdf of the data (b), the P-P plot (c), the Q-Q plot (d).

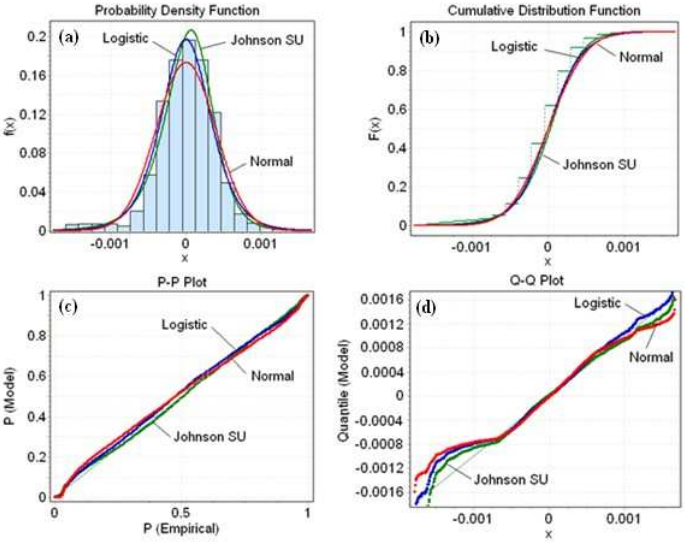

Figure 3: The analysis of $\varepsilon(\Delta - \delta\Delta)$ time series; the pdf vs. the histogram of the data (a), the cdf vs. the cdf of the data (b), the P-P plot (c), the Q-Q plot (d).

Regarding the residual $\varepsilon(\Delta - \delta\Delta)$ time series, the logistic distribution (Balakrishnan, 1991) and Johnson SU distribution (Bowman & Shenton, 1983) provide the appropriate fit (Fig. 3). In particular, the Q-Q plot (Fig. 3(d)) reveals that for high quantiles, the logistic distribution is more accurate than the Johnson SU distribution. The Johnson SU distribution outperforms the logistic distribution in the

vicinity of the mode (Fig. 3(a)). For the low quantiles, however, the Johnson SU distribution provides the best fit.

4. CONCLUSIONS

The probability distribution of the non-tidal length-of-day time series cannot be accurately modeled by a normal distribution. Similarly, the distribution of the residual non-tidal length-of-day data differs from a normal probability law. We argue that these findings may be interpreted twofold. First, the departure from a normal distribution in the case of the non-tidal length-of-day time series is caused by the long-term oscillations with high amplitudes, probably due to the interactions between the core and the Earth's mantle. Second, the distribution of the residual non-tidal length-of-day data is different than a normal probability law probably due to ENSO events recorded as spikes in the residuals.

Several non-Gaussian probability distributions fit to the analysed time series. The best overall goodness-of-fit is provided by the family of the Johnson distribution. In the case of the non-tidal length-of-day time series and its residuals the Johnson SB and SU distributions, respectively, are found to be the most appropriate.

Acknowledgements. The research is supported by the Polish Ministry of Education and Science under the project No 4 T12E 039 29. Tomasz Niedzielski is supported by the Foundation for Polish Science within the Start Program (stipends for young researchers) and by the European Union within the Marie-Curie Actions. Tomasz Niedzielski and Wiesław Kosek are supported by the organizers of the Journées "Systèmes de référence spatio-temporels" 2008 and X. Lohrmann-Kolloquium, September 2008, Dresden, Germany.

5. REFERENCES

Akyilmaz, O., Kutterer, H., 2004, Prediction of Earth rotation parameters by fuzzy inference systems, J. Geodesy 78, pp. 82–93.

Balakrishnan, N., 1991, Handbook of the Logistic Distribution, Marcel Dekker, New York.

Bowman, K.O., Shenton, L.R., 1983, Johnson's system of distributions, Encyclopedia of Statistical Sciences, John Wiley & Sons, New York, 4, pp. 303–314.

Gilchrist, W., 2000, Statistical Modelling with Quantile Functions, Chapman and Hall, New York.

Gupta, A.K., Nadarajah, S., 2004, Handbook of beta functions and its applications, CRC Press, Boca Raton, Florida.

Holmgern, E.B., 1995, The P-P plot as a method of comparing treatment effects, J. Am. Stat. Assoc. 90, pp. 360–365.

IERS 2008, http://hpiers.obspm.fr/iers/eop/eopc04_05.

Kosek, W., 1997, Autocovariance prediction of short period Earth rotation parameters, Artif. Satell. 32, pp. 75–86.

Kosek, W., McCarthy, D.D., Luzum, B., 1998, Possible improvement of earth orientation forecast using autocovariance prediction procedures, J. Geodesy 72, pp. 189–199.

Kosek, W., Kalarus, M., Johnson, T.J., Wooden, W.H., McCarthy, D.D., Popiski, W., 2005, A comparison of LOD and UT1-UTC forecasts by different combined prediction techniques, Artif. Satell. 40, pp. 119–125.

Kotz, S., Nadarajah, S., 2001, Extreme Value Distributions: Theory and Applications, World Scientific, Singapore.

McCarthy, D.D., Petit, G., (Eds.), 2004, IERS Conventions, IERS Technical Note No. 32.

Niedzielski, T., Kosek, W., 2008, Prediction of UT1-UTC, LOD and AAM X3 by combination of the least-squares and multivariate stochastic methods, J. Geodesy 82, pp. 83–92.

Reiss, R.D., Thomas, M., 2007, Statistical Analysis of Extreme Values: with applications to Insurance, Finance, Hydrology and Other Fields, Birkhuser, Basel, Switzerland.

Schuh, H., Ulrich, M., Egger, D., Mueller, J., Schwegmann, W., 2002, Prediction of Earth orientation parameters by artificial neural networks, J. Geodesy 76, pp. 247–258.

Wasserman, G., 2002, Reliability Verification, Testing and Analysis in Engineering Design, CRC Press, Boca Raton, Florida.

A PHYSICALLY CONSISTENT SYSTEM MODEL FOR THE STUDY OF THE EARTH'S ROTATION, SURFACE DEFORMATION AND GRAVITY FIELD PARAMETERS

J. SÜNDERMANN[1], A. HENSE[2]
[1] Institute of Oceanography, University Hamburg
Bundesstr. 53, 20146 Hamburg, Germany
e-mail: juergen.suendermann@zmaw.de
[2]Meteorological Institute, University of Bonn[2]
Auf dem Hügel 20, 53121 Bonn, Germany
e-mail: ahense@uni-bonn.de

ABSTRACT. The coupling of models of different subsystems of the Earth forms a necessary step towards a dynamic Earth system model which is physically consistent with respect to Earth rotation, gravity and surface deformation. In a cooperative project with contributions from meteorology, oceanography, hydrology and geodesy the fluxes of momentum, energy and mass between atmosphere, ocean, continental hydrosphere and rigid Earth have been jointly simulated for centennial periods. The corresponding variations of the Earth's rotation, gravity and shape have been calculated and compared with satellite data. This paper and the following four ones are closely linked.

1. INTRODUCTION

This article gives an overview about a series of projects which studied the Earth's rotational parameters (ERP) angular momentum, tensor of inertia as well as related variables of the Earth's gravitational field. A system view has been taken by trying to incorporate the contributions from the various subsystems of the Earth system in a physically consistent way. These subsystems concern the atmosphere, the continental hydrosphere, the ocean and the rigid Earth; accordingly the next four papers are presenting the respective contributions from the fields of meteorology, hydrology, oceanography and geodesy.

We started from a couple of stand-alone models for the subsystems: ECHAM for the atmosphere (Roeckner et al., 1992), HDM for the continental hydrosphere (Hagemann & Dümenil, 1998), OMCT for the ocean (Thomas et al., 2001) and DyMEG for the Earth's dynamics (Seitz, 2004). We did know from previous runs of these models that

- decadal scale variations in axial relative angular momentum variations do exist in the ECHAM simulations which are obviously forced by sea surface temperature (SST);
- the same holds for OMCT and the oceans contribution. We got first indications that the interaction of ocean currents and tides might be important;
- the length-of-day variations on time scales from a few days to several years could be almost completely explained by atmospheric torques (Seitz, 2005);
- the Chandler wobble is excited by temporally stochastic but spatially coherent modes (Seitz et al., 2004).

Our main objective in the recent working phase was the step from stand-alone simulations to a representation of subsystems within one coupled Earth system model. Such a model would exchange the mass-, energy- and stress-fluxes interactively between the atmospheric, oceanic and any other necessary submodel conserving those fundamental quantities. Even the global climate models used in the last IPCC assessment report (No.4 in 2007) are only coupled in their energy and water cycles but not with respect to angular momentum. Lastly, it had become clear that the Earth rotation components determined by astrometrical-geodetical methods are the only measurable globally integrated variables of the Earth's systems. This is in contrast e.g. to the globally mean surface temperature which has to be aggregated from individual pointwise measurements using specific model assumptions. Therefore one has to admit

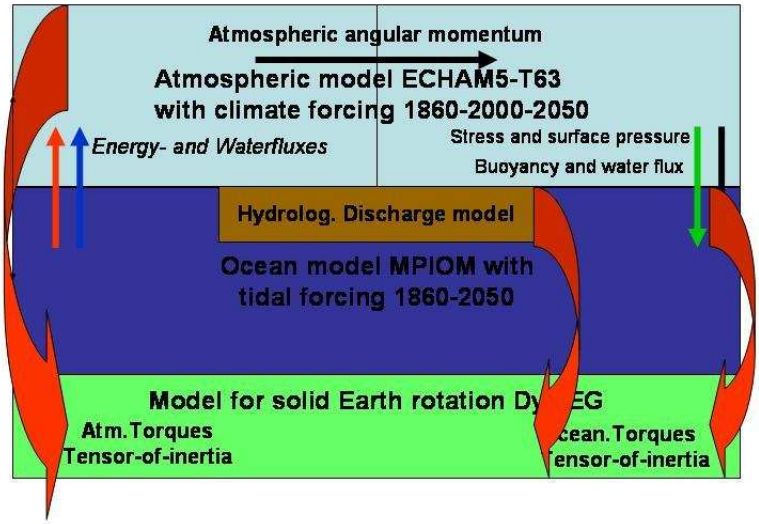

Figure 1: Symbolic layout of the modelling approach.

that the ERP have the potential for monitoring specific changes of the Earth system related to global climate change. However, as the measured ERP are variables of the solid Earth, the conclusions from the monitored ERP signal with respect to the atmosphere or the ocean require a modelling approach to disintegrate the measured signal. Therefore a prerequisite question for quantifying the monitoring potential are modelling studies using fully coupled atmosphere-ocean-land surface models to derive the changes due to anthropogenic and natural climate forcing influences on the atmospheric and oceanic torques and integrate them using the dynamic rotational model of the solid Earth. These are in effect the aims of the project which will be reported here:

- The development of a fully and self-consistently coupled atmosphere-ocean model ECOCTH based on the state-of-the-art ECHAM5-T63 atmosphere and the MPIOM ocean model including ephemeridical tidal forcing (Jungclaus et al., 2006).
- A detailed land surface hydrology model fitted into the fluxes of the internal ECHAM5/MPIOM hydrological discharge model HDM for calculating offline the sub-terrain water levels and their contributions to the tensor of inertia.
- Simulations of the 20th century under observed climate forcing from anthropogenic and natural sources of the coupled model as well as the atmospheric model ECHAM5/T63 forced with the observed SST/SIC and climate change simulations for the 21th century with the coupled model under the assumed A1b scenario for the future man-made climate forcing.
- Calculation of the influence of atmosphere and hydrosphere on rotation, shape and gravity of the Earth.
- Comparison with satellite data.

The type of modelling approach is sketched in Fig. 1.
Partners cooperating in the project are: in the field of meteorology Andreas Hense and Timo Winkelnkemper from the University of Bonn, in the field of hydrology Maik Thomas, Claudia Walter and Robert Dill from the Geo Research Centre Potsdam, in the field of oceanography Jürgen Sündermann, Xueen Chen and Malte Müller from the University of Hamburg, in the field of geodesy Hermann Drewes from the German Geodetic Research Institute Munich and Florian Seitz from the Technical University of Munich.

2. MODELS OF SUBSYSTEMS

First, it should be reemphasized that the main objective of the project was to develop an integrated model of the subsystems atmosphere, ocean and continental hydrosphere (ECOCTH). Thereafter, on the basis of the obtained spatial and temporal data fields the dynamical Earth model DyMEG should calculate the respective rotation parameters, the gravity field and the shape of the Earth and their variabilities (see Fig. 1). Only such a coupled model can guarantee the mass, energy and momentum fluxes between the subsystems to be steady and the Earth system parameters to be consistent. Differently from the singular treatment of a subsystem (where the influence of another subsystem will be prescribed by observed boundary values) the integrated approach does not use data assimilation; so principally the approximation of real nature might be somewhat inferior. On the other side, the fundamental physical properties are conserved in the coupled system and this is necessary for a consistent calculation of Earth system parameters. Moreover, only such a model can be run in a prognostic way for decades, because it does not need boundary conditions at interfaces (with the exception of the solar radiation, emission scenarios and the gravitational influence of Moon and Sun which, of course, must be prescribed).
Nevertheless, for different reasons a preceding or partially simultaneous treatment of separate subsystems made still sense. Firstly, the pioneering development of a free coupled model including ephemeridic tides represented a certain risk while the submodels had been already successfully tested. Indeed, initial difficulties arose when applying the OASIS coupling code. Together with the high computational effort for the five 200 years runs this delay allowed a common analysis and evaluation of results only in the final phase of the project. Moreover, one scientific attraction of the study was just the comparison of the classical stand-alone models of the atmosphere, the continental hydrosphere and the ocean with the new integrated model, with respect to both, specific meteorological, hydrological and oceanographical parameters, and simulations with the DyMEG model. So specifically the working groups meteorology and hydrology performed own experiments with the submodels ECHAM and HDM. The working group oceanography has focused its activities on the coupled model ECOCTH.

3. MAIN RESULTS

The results of the subsystem studies are given in the following four papers. Here some major findings will be noted.

Tidal mixing

For a long time it has been assumed that barotropic ocean tides have minor influence on the general circulation. During the last 10-15 years it has been recognized that tides induce small-scale mixing processes and therefore interact substantially with thermohaline ocean currents. Baroclinic tides are generated at topographical barriers as deep sea trenches, middle oceanic ridges and islands and breaking internal waves are causing vertical mixing. This mechanism has been mostly ignored in global ocean circulation models, sometimes it has been roughly parameterized. ECOCTH is the first model of the World Ocean's thermohaline and wind driven motion which explicitly contains the astronomical tides. The tidally induced vertical current shear enters the Richardson number of the flow modifying locally the vertical exchange of momentum, heat and salt. In the Atlantic Ocean this mechanism leads to a significant improvement in modelling the North Atlantic Current. This subsequently has influence on the structure of climate changes in scenario simulations of climate changes in the North Atlantic. Presently it is discussed whether future IPCC model runs should include ocean tides.

Anthropogenic impact on atmospheric angular momentum

Basing on the ECOCTH runs and on an ensemble of simulations with the coupled atmosphere-ocean model ECHO-G (Legutke & Voss, 1999) the possible anthropogenically induced variation of the axial component of the atmospheric angular momentum AAM has been investigated. With both models an increase of AAM due to higher mean zonal wind velocities is obtained corresponding to an increase in length-of-day (see Figure 4 in the following article by Winkelnkemper & Hense). Comparable effects have been shown also by other coupled models, but with quite different amplitudes. It is an open question whether oceanic torques and their changes - caused by a redistribution of mass from lower to higher latitudes - can compensate this effect.

Chandler wobble excitation by white noise forcing

The dynamical gyro-model of the solid Earth DyMEG has been forced by the simulated torques (matter and motion term) of the geo-fluids atmosphere, ocean and continental hydrosphere aimed at an explanation of the permanently existing Chandlerian motion of the angular momentum vector. Without these external variations of the atmospheric and oceanic angular momentum the Chandler wobble would disappear within 30-40 years due to rheological damping in the Earth's interior. This is not observed, and consequently there must be a continuous process which feeds in energy in the spectral band of the Chandlerian motion (period 430 days). Until now quasi-periodic processes in the atmosphere and the ocean close to the resonance period of the free Chandlerian oscillation have often been assumed as forcing. Now the analysis of the excitations obtained from the ECOCTH simulations have shown that the stochastic part of the forcing (mainly the variations of the off-diagonal elements of the tensor of inertia) in the period range of 400-460 days represents the essential component for the conservation of the Chandler wobble. It even turned out that a white noise forcing with an amplitude similar to the calculated geo-fluid torques is sufficient to conserve the Chandlerian motion over 1000 years, and this with characteristics as observed in 1900-2000. That means that random fluctuations of atmospheric and oceanic bottom pressure could be identified as forcing factors of the simulated by DyMEG Chandler wobble (see Figure 4 in the following article by Seitz).

4. CONCLUSIONS AND OUTLOOK

The project performs considerable progress in connecting integral parameters of the Earth as vector of rotation, surface shape or gravity field and their temporal variability with small-scale processes within the Earth system proper. Terrestrial and satellite observations provide the first mentioned planetary quantities, geological data from the atmosphere, ocean and solid Earth the variable state of the globe. It was and is the general objective of the research programme to understand and quantify this fundamental interconnection by means of model conceptions learning thereby from the total system about its components and vice versa (see Figure 1 in the following article by Seitz). From the view point of physics, we consider fluxes of momentum and energy between the Earth and extraterrestrial bodies as well as between the geophysical system parts of the Earth itself (for the latter ones also mass fluxes exist). This exchange happens on different time scales ranging from geological periods (eons) down to tidal and weather dynamics (hours). The above formulated balance must be always fulfilled.

Naturally at the beginning of the research work about forty years ago we firstly considered the long time scales (Brosche & Sündermann, 1978). Existing geological data (growth rhythms of fossil organisms; time range 500 mio years) and astronomical observations (eclipses, orbits of planets; time range 3000 years) have been used and interpreted in terms of geophysical processes on the Earth. Within the last decades more and more new astronomical and geodetical data (LLR, VLBI, altimetry, gravity) became available. They have achieved meanwhile a high degree of accuracy and density allowing analysis from the decadal and annual scale down to seasonal, daily and tidal signals. The planetary data have firstly been focused on Earth rotation parameters (mainly LOD) and supplemented in recent years by measurements of the shape and the gravity of the Earth and their variations. At the same time modelling has been advanced from separate and rough studies of the system parts to high-resolving and coupled simulations of the total Earth system.

In the current project some major progresses have been achieved on the sketched way: For the first time a free, coupled model of the partial systems atmosphere, ocean and terrestrial hydrosphere has been realized and applied. The global ocean model comprises the wind- and thermohaline driven circulation as well as ephemeridic tides and their nonlinear interaction. Basing on this data a physically consistent dynamic Earth model is run and provides simultaneously rotation parameters, surface deformation and gravity field of the Earth. The numerical results are directly compared with satellite data. 'Free' model means that on the rotating Earth with real topography - like in nature - only solar radiation and gravitational potential of Moon and Sun are acting. Atmosphere and ocean circulations as well as the hydrological cycle are freely developing under this forcing. No observational data are assimilated resulting in an independent numerical data set. This set is physically consistent in the sense that momentum, energy and mass are conserved in the total system and that fluxes between the system parts are steady.

The developed model type is necessary for the synthetical interpretation of existing and newly gained geophysical, geodetical and astronomical data, although it still may have some deficiencies for operational use. Restricted spatial resolution, insufficient parameterisation of processes or numerical artefacts must

cause inaccuracies which may be greater than in a 'bounded' (by data assimilation) model. Nevertheless, for the theoretical interpretation of remote sensing data, its correction and for deducing information on the geophysical system parts, specifically for future scenarios, our model type is the only appropriate approach.

Further research activities could now focus on

- refinement of the model resolution;
- improvement of process parameterisations;
- simulations of the past millennium to assess secular changes;
- scenario runs under global change.

The last item includes the monitoring of climate change. There are strong indications that climate change is reflected in time series of planetary parameters (e.g. LOD). This opens the innovative possibility of an integral climate monitoring - independent of local geophysical observations.

5. REFERENCES

Brosche, P., and J. Sündermann (eds.), 1978, "Tidal friction and the Earth's rotation", Springer-Verlag, 241 pp.

Hagemann, S., and Dümenil, L., 1998, "A parametrization of the lateral waterflow for the global scale". Climate Dynamics,14, 17–31

IPCC (Intergovernmental panel on climate change) (2007) Climate Change 2007, "The science of climate change. Working Group I: The Physical Basis of Climate Change", Cambridge University Press, 996 pp.

Jungclaus, J.H., Keenlyside, N., Botzet, M., Haak, H. , Luo, J.-J., Latif, M., Marotzke, J., Mikolajewicz, U. and Roeckner, E., 2006, "Ocean circulation and tropical variability in the coupled model ECHAM5/MPI-OM", J. Climate, 19, 3952–3972

Legutke, S., and Voss, R., 1999, "The Hamburg Atmosphere-Ocean Coupled Circulation Model ECHO-G", Technical report, DKRZ, Hamburg, 62 pp.

Roeckner, E., Arpe, K., Bengtsson, L., Brinktop, S. Dümenil, L., Esch, M., Kirk, E., Lunkeit, F., Ponater, M., Rockel, B., Sausen, R. Schlese, U., Schubert, S., Windelband, M., 1992, "Simulation of the present-day climate with the ECHAM model: impact of model physics and resolution", Max-Planck-Institute for Meteorology, Rep. 93, Hamburg, 171 pp.

Seitz, F., 2004, "Atmosphärische und ozeanische Einflüsse auf die Rotation der Erde - Numerische Untersuchungen mit einem dynamischen Erdsystemmodell", Deutsche Geodätische Kommission, C 578, München

Seitz, F., Stuck, J. and Thomas, M., 2004, "Consistent atmospheric and oceanic excitation of the Earth's free polar motion", Geophys. J. Int., 157, 25–35

Seitz, F., 2005, "Zur Anregung der Chandler-Schwingung. Zeitschrift für Vermessungswesen", 130(3), 166–173

Thomas, M., Sündermann, J. and Maier-Reimer,E., 2001, " Consideration of ocean tides in an OGCM and impacts on subseasonal to decadal polar motion excitation", Geophys. Res. Lett, 28, 2457–2460

ATMOSPHERIC SIMULATIONS OF EARTH ROTATION PARAMETER VARIATIONS

T. WINKELNKEMPER
Meteorological Institute University Bonn, Germany
e-mail: timo@uni-bonn.de

ABSTRACT.

Atmospheric general circulation models are able to explain variations in the Earth rotation parameters to a certain extent. Their ability to simulate mass movements and mass concentrations on a global scale in a realistic way allows for analyzing their impact on Earth rotation. Due to enormous mass displacements and relative movements (to the rotating Earth) the atmosphere has an important impact on Earth rotation parameters. On a subdaily to decadal scale the atmosphere and the oceanic hydrosphere explain nearly all variance of Earth rotation parameters.

An Earth system model has been developed by our interdisciplinary project group which has realized an entire coupling of the subsystems atmosphere, ocean and continental hydrosphere with respect to conservation of mass, energy and momentum. Tides are implemented as well. The coupled model consists of the ECHAM 5.3 GCM, OMCT 3.0 ocean model and HDM hydrospheric dispersion model. This talk will focus on the atmospheric model. A detailed structure analysis of observed and simulated Earth rotation parameters and atmospheric forcing factors like solar variability, ENSO or greenhouse gas will be presented.

To examine a possible future increase in the length of day associated with a decrease in Earth angular velocity, future long term trends have been calculated under a climate change scenario.

HYDROLOGICAL INDUCED EARTH ROTATION VARIATIONS FROM STAND-ALONE AND DYNAMICALLY COUPLED SIMULATIONS

R. DILL, M. THOMAS, C. WALTER
Helmholtz Centre Potsdam, GFZ German Research Centre for Geosciences
Telegrafenberg, D-14473 Potsdam
e-mail: dill@gfz-potsdam.de

ABSTRACT. The impact of continental water mass redistributions on Earth rotation is deduced from stand-alone runs with the Hydrological Discharge Model (HDM) forced by ERA40 re-analyses as well as by the unconstrained atmospheric climate model ECHAM5. The HDM is attached in three different approaches to the atmospheric forcing models. First, ECHAM5 and its embedded land surface model generates directly runoff and drainage appropriate for the subsequent processing with HDM, like it is realized in the dynamically coupled model system ECOCTH, too. Second, an intermediate Simplified Land Surface scheme (SLS) is used to separate ERA40 precipitation into runoff, drainage, and evaporation. Third, precipitation and evaporation are used as input for the Land Surface Discharge Model (LSDM), which estimates runoff and drainage internally for its HDM-like discharge scheme. The individual models are validated by observed river discharges. The induced rotational variations represent mainly the different forcing from precipitation-evaporation and trends from inconsistent mass fluxes. The dynamical coupling of atmosphere and ocean has only a subordinated influence.

1. HYDROLOGICAL MODEL APPROACHES

Water mass redistributions within the global hydrological cycle affect the Earth's rotation and its gravity field, especially on seasonal to interannual timescales. Since Earth rotation variations and particularly Length-of-Day are sensitive for deficiencies in the global water balance, consistent mass exchanges among the atmosphere, oceans and continental hydrology are mandatory for realistic simulations of hydrospheric induced global integral Earth parameters. The continental water mass redistributions have been simulated with the Hydrological Discharge Model (HDM) from the Max-Planck-Institute for Meteorology (MPI-M) in Hamburg (Hagemann & Dümenil, 1998a) which has been applied in three different configurations (Fig. 1).

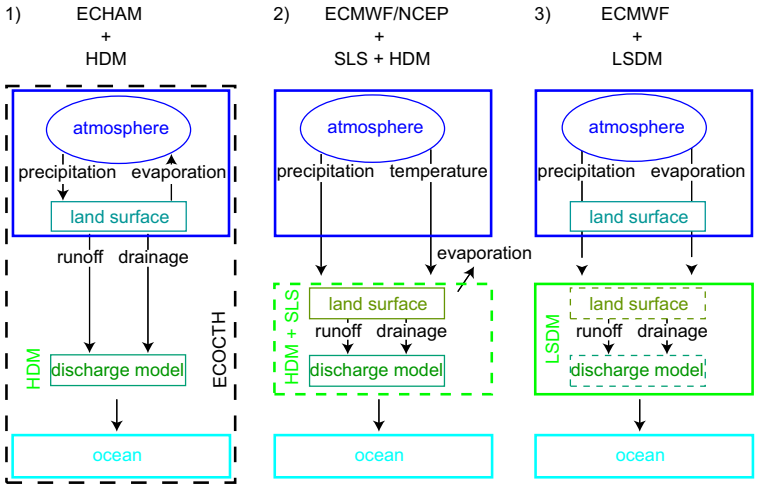

Figure 1: Three approaches to pass the input from the atmospheric models to the hydrological discharge model HDM.

HDM classifies the lateral water flow processes into three parallel types of flows. Water produced within a catchment, reaching the land surface by rain or snowmelt, enters the HDM as surface runoff or groundwater drainage. Surface runoff feeds the fast overland flow. Groundwater drainage is passed laterally as slow base flow. The water is transferred from gridcell to gridcell by the river flow network. Retention of water in each flow process is represented by a cascade of equal linear reservoirs with spatially distributed lag times depending mainly on topography. Wetlands and lakes are included by an extended renewal rate concept (Hagemann & Dümenil, 1998b). Within the DFG project TH864/3 the initial version of HDM has been improved to calculate hydrological angular momentum (HAM) functions and low degree gravity coefficients.

Since HDM exclusively describes the lateral flow processes, it requires input data separated in runoff and drainage. To split precipitation into snow accumulation, soil moisture, runoff, groundwater drainage, and evaporation a land surface model is interposed between atmosphere and HDM (Fig. 2). Most atmo-

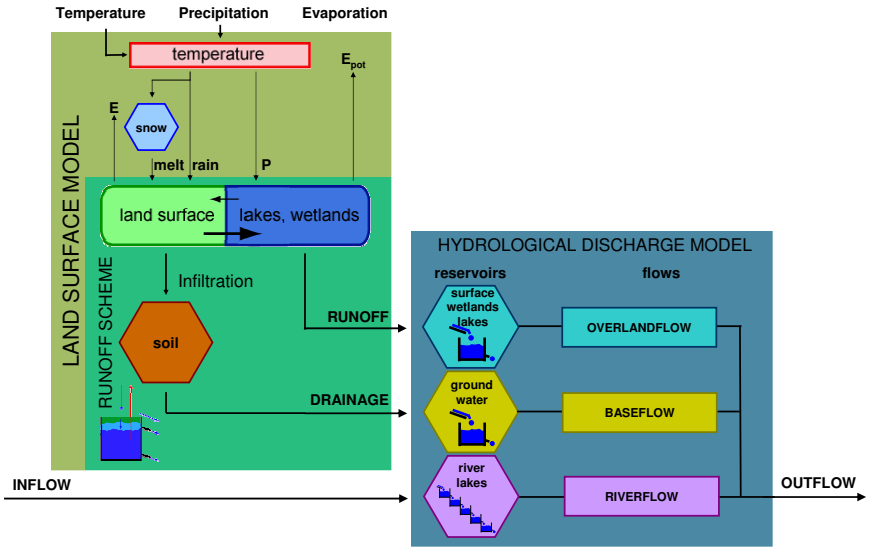

Figure 2: Connecting land surface model to hydrological discharge model HDM via runoff and drainage.

spheric models comprise their own land surface model to obtain correct atmosphere-land boundary conditions. Unfortunately, the weather models from the European Centre for Medium-Range Weather Forecasts (ECMWF) and the National Centers for Environmental Prediction (NCEP) do not provide appropriate runoff and drainage data for HDM. Only the output from the atmospheric climate model ECHAM fits directly for HDM (approach 1). The dynamically coupled model ECOCTH (ECHAM+OMCT+HDM) follows also approach 1. To use HDM with atmospheric data from ECMWF's re-analyses ERA40 or analogous data from NCEP the Simplified Land Surface scheme (SLS; Hagemann & Dümenil, 2003) has been implemented (approach 2). SLS processes precipitation and temperature to generate runoff, drainage and also its own evaporation estimates. In long term studies the SLS+HDM combination exposes several deficiencies concerning mass conservation. Consequently, a new model setup, based on SLS and HDM, has been developed. This Land Surface Discharge Model (LSDM; Dill, 2008) ensures internally consistent water mass fluxes between land surface and HDM. Further, it implies the incorporation of glaciated regions, the option to import evaporation rates from the weather model, and conservative mass exchanges among the connected Earth's sub-systems and models avoiding standard interpolation schemes. It turned out that evaporation rates consistent with precipitation are crucial in the atmosphere-land coupling. Estimating precipitation and evaporation within two different land surface models, as in approach 2, provokes critical errors in the global water budget due to unsynchronized land surface water balances. Therefore, LSDM operates with evaporation rates from the same atmospheric model as precipitation (approach 3). Compared to the simple temperature based evaporation modelling in SLS the ECMWF evaporation benefit notable from the more sophisticated treatment of wind, radiation, and humidity in their land surface scheme TESSEL (Beljaars & Viterbo, 1999). The ECMWF evaporation correlates higher to local precipitation events and can compensate precipitation overestimations.

2. DISCHARGE VALIDATION

The continental discharge of HDM strongly depends on the atmospheric forcing, primarily on the precipitation data. This dependency is more pronounced in models using the SLS land surface module for evaporation (approach 2) than in models using ECHAM runoff and drainage (approach 1) or the ECMWF's evaporation (approach 3). ECHAM and ECMWF comprehend a much more complex land surface modelling. The monthly precipitation means of atmospheric weather models indicate generally a slight overestimation compared to observed climatological values from the Global Precipitation Climate Centre (GPCC). In contrast, the climate model ECHAM produces too low annual precipitation amplitudes, i.e., only 40% of that suggested by GPCC, coming along with less variability. In total, the correlation of monthly mean precipitation rates from GPCC with NCEP is 0.9, with ECMWF 0.8 and with the unconstrained climate model ECHAM 0.4. Detailed analyses of all atmospheric forcing fields can be found in Walter (2008).

Due to the lack of globally distributed water storage measurements the HDM has been validated indirectly by comparing modelled river discharges with in-situ river runoff observations from the Global Runoff Data Centre (GRDC) at 142 selected stations. In general, HDM shows a very good agreement for all Arctic river catchments. In contrast, some African rivers are not satisfactorily reproduced due to especially high evaporation rates and anthropogenic influences not represented by the atmospheric nor by the hydrological model (e.g., irrigation, dams). The various atmospheric forcing data result in significant differences in the simulated river discharges. Forcing with re-analyses data from ECMWF or NCEP naturally leads to more realistic discharges than simulations driven by the climatological ECHAM data. The coupled model ECOCTH produces slightly lower annual runoff amplitudes than the corresponding ECHAM5+HDM stand-alone simulations. In Middle- and South-America, in the Congo basin and in the monsoon regions of South-East-Asia these differences reach up to 20%. A comprehensive verification based on statistical analyses has been done by Griesbach (2004).

3. HYDROLOGICAL ANGULAR MOMENTUM (HAM)

Unlike the oceanic angular momentum (OAM) and the atmospheric angular momentum (AAM) the HAM time series are dominated by mass variations, the matter term, while relative motions of water masses in rivers are subordinated. Contributions from the motion term come mainly from seasonal variations in river flows with magnitudes three orders lower than the matter term. The most significant annual amplitudes in HAM reflect the different magnitudes of the precipitation forcing fields. Differences in the corresponding phases might be associated with the use of different land surface models resulting in diverse snow melting seasons and soil moisture capacities.

Inconsistencies in the hydrological modelling appear as long-term trends in the HAM functions. Fig. 3 gives the three components of the HAM matter term ERA40 forced simulations using approach 2 and 3. The positive trend in SLS+HDM (blue) is eliminated when using LSDM. ECHAM5+HDM or ECOCTH results show less seasonal variability in HAM but they are also free of linear trends. Daily updated HAM functions and low degree gravity coefficients from LSDM, forced by ERA40 and operational ECMWF analyses, are routinely produced and can be accessed via anonymous FTP from:

FTP.GFZ-POTSDAM.DE public/ig/dill.

4. CONCLUSIONS

The hydrological discharge model HDM is capable of reproducing continental water mass variations on a global scale. On seasonal time scales the good agreement of modelled gravity field variations with estimates based on GRACE observations suggest that the HDM realistically represents variations of continental water mass storage. Using the HDM in a closed model system to simulate water mass exchanges among the three Earth subsystems atmosphere, ocean and continental hydrosphere offers the possibility to assess deficiencies in the global hydrological cycle, in particular inconsistencies in the mass fluxes between the sub-models are detected by long term trends in the hydrological angular momentum functions caused by accumulated water mass losses. We recommend the use of inter-coordinated atmospheric forcing fields and a mass-conservative remapping to obtain well balanced mass fluxes among atmosphere and land surface. The ECOCTH (approach 1) and the LSDM model (approach 3) satisfy these requirements for the generation of long term global geodetic parameters. However, over glaciated regions both models

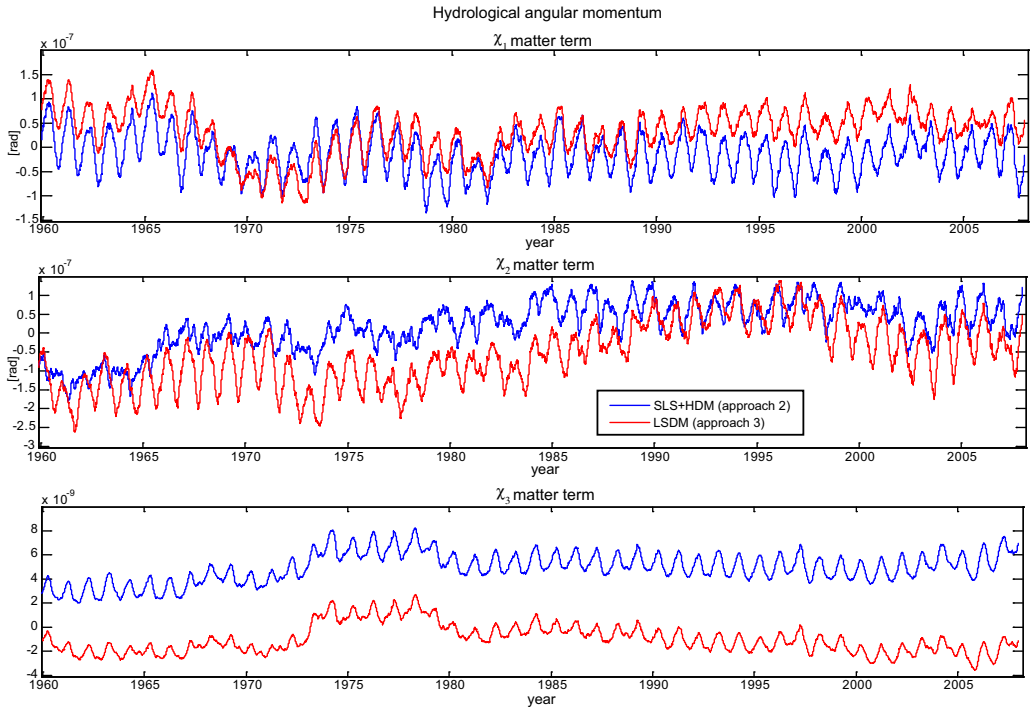

Figure 3: Three components of HAM matter term, simulated with ERA40 forced SLS+HDM (approach 2) in blue and LSDM (approach 3) in red.

still suffer from the absence of a sophisticated ice model. The dominant impact on continental water mass distributions arises from atmospheric forcing conditions, mainly from the precipitation-evaporation budget. Forced simulations with reanalysis data from atmospheric weather models have naturally a more realistic real-time relation than unconstrained atmospheric climate models, such as ECHAM5 and ECOCTH. The dynamical coupling of atmosphere and ocean in ECOCTH has only subordinated influence on the continental hydrosphere resulting in a slightly lower variability and better seasonal time relation compared to ECHAM5 forced HDM stand-alone simulations.

5. REFERENCES

Beljaars, A.C.M., Viterbo, P., 1999. Soil moisture-precipitation interaction: Experience with two land surface schemes in the ECMWF model. In: Browning, K., Gurney, R. (ed) Global energy and water cycles, Cambridge University Press, Cambridge, 223-233.

Dill, R., 2008. Hydrological model LSDM for operational Earth rotation and gravity field variations. Scientific Technical Report STR08/09, GFZ Helmholtz-Zentrum Potsdam.

Griesbach, I., 2004: Validierung modellierter kontinentaler Wassertransporte, TU-Dresden, Institut für Planetare Geodäsie - Astronomie, p.157, 2004

Hagemann, S., Dümenil, L., 1998a. A parametrization of the lateral waterflow for the global scale. Climate Dynamics 14, 17-31, Springer Verlag 1998.

Hagemann, S., Dümenil, L., 1998b. Documentation for the Hydrological Discharge Model, Technical Report No. 17. Max Planck Institute for Meteorology, Hamburg, Germany.

Hagemann, S., Dümenil Gates, L., 2003. Improving a subgrid runoff parameterization scheme for climate models by the use of high resolution data derived from satellite observations. Clim. Dyn. 21, 349-359.

Walter, C., 2008. Simulation hydrologischer Massenvariationen und deren Einfluss auf die Erdrotation. PhD-thesis, p. 195, TU Dresden, Germany.

EARTH ROTATION PARAMETERS OBTAINED FROM A DYNAMICALLY COUPLED ATMOSPHERE-HYDROSPHERE MODEL

M.MÜLLER [1], X. CHEN[2], J. SÜNDERMANN[3]
[1] Max Planck Institute for Meteorology
Bundesstr. 53, 20146 Hamburg
e-mail: malte.mueller@zmaw.de
[2] Ocean University of China
238 Songling Road, 266100 Qingdao, China
e-mail: xueen.chen@zmaw.de
[3] Institute of Oceanography, University Hamburg
Bundesstr. 53, 20146 Hamburg
e-mail: juergen.suendermann@zmaw.de

ABSTRACT. A state-of-the-art climate model has been modified in order to obtain an Earth system model with consistent mass, energy and momentum fluxes. Five climate future scenarios from 1860 till 2059 are performed. Till the year 1999 the model is forced by observed greenhouse gas emissions and pre-calculated sulfate aerosols. For future climate predictions the model is forced by the IPCC A1B scenario. The influence of all parts of the Earth near-surface system, namely the atmosphere, the oceans and the continental hydrology, on the Earth's rotation can be consistently analyzed on daily to decadal timescales. We present first model results, i.e. Long periodic length of day variations induced by climate events and short-term length of day variations induced by lunisolar tides.

1. INTRODUCTION

Variations of the Earth's rotation are determined by mass redistributions within the Earth's system. As parts of the Earth's system atmosphere and hydrosphere (ocean and continental hydrology) contribute largely to these variations. It is of considerable interest to estimate the contribution of these subsystems. Studying each of these subsystems separately leads to inconsistencies in energy, mass and angular momentum transfer between the subsystems and thus in conservation of these quantities. However, for analyses of Earth rotation it is substantial to allow for mass and angular momentum conservation. Thus, coupling the subsytems of atmosphere, continental hydrology and ocean is necessary to allow for an improved simulation of variations of the Earth's rotation induced by atmospheric and hydrospheric mass redistributions.
We used a state-of-the-art dynamically coupled atmosphere-hydrosphere model suited for climate predictions to determine Earth rotation parameters. Several modifications of the climate model, described in Chapter 2, were necessary for a sufficient conservation of mass and angular momentum. In Chapter 3 we present first results from this Earth system model approach.

2. MODEL

The model chosen in the present study is the climate model of the Max Planck Institute for Meteorology in Hamburg. The atmospheric component of the model (ECHAM5; Roeckner et al., 2003) has a spatial resolution of T63 (corresponding to a grid box size of 1.875°x1.875°) with 31 vertical layers. The oceanic component (MPI-OM; Marsland et al., 2003] is a z-coordinate ocean general circulation model with integrated sea-ice model and it utilizes horizontally a bipolar orthogonal grid where the positions of the North and South pole can freely be chosen. Thus, the singularity at the geographical North pole can be avoided by replacing the grid North pole on land. In this configuration the North pole is centered on Greenland (30°W, 80°N) and the South pole on Antarctica (30°W, 80°S). The horizontal resolution of the grid ranges from three to one degree, between 12 km near Greenland and 180 km in the tropical Pacific. Vertically the grid has 40 layers, where 20 layers are distributed over the upper 700 m. The ECHAM5 is coupled via the OASIS interface (Terray et al., 1998) without any flux correction to the

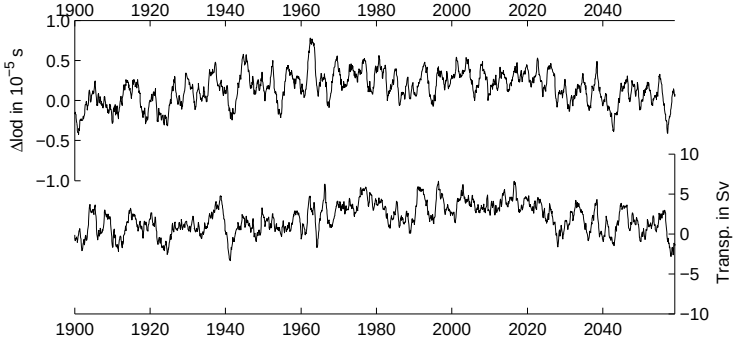

Figure 1: Time series from 1900 till 2059: (top) The variation of LOD (detrended, 12-month running mean) caused by variations of the oceanic motion term. (bottom) Time series of the variation in transport of the Antarctic circumpolar current (detrended, 12-month running mean) in the Drake Passage. The correlation of the two time series amounts to 0.68.

MPI-OM. Further, the climate model consists of a land hydrology model, embedded in ECHAM5. This climate model version was used for the 4th IPCC assessment report simulations.
Several modifications are done in order to improve the conservation of mass, energy and momentum within the climate model. Firstly, in the standard version of the model the coupling interface between ocean surface and atmosphere neglects the atmospheric pressure on top of the ocean. We implemented the 'dynamic pressure' to the coupling variables of the OASIS interface. The 'dynamic pressure' is defined as the atmospheric pressure on the ocean surface and thus the ocean gets explicitly forced by atmospheric pressure. Secondly, the steric sea level correction is implemented in order to allow for mass conservation. This correction is necessary since the ocean model is a z-coordinate model and thus the model is volume conserving rather than mass conserving. In order to allow for mass conservation a correction term was implemented according to Greatbatch (1994). And thirdly, the ocean tides are implemented in the ocean model. The ocean tides are essential when considering Earth rotation parameters, but are still missing in all state-of-the-art climate models. We extended the MPI-OM by the implementation of the complete lunisolar tidal forcing of second degree. This real time forcing describes the tidal potential of second degree in terms of ephemerides (Thomas et al., 2001). Thus, all tidal harmonics of second degree are forced in the model explicitly. Further, routines are included into the model to compute online the Earth rotation parameters of atmosphere, ocean and continental hydrology. The time resolution of atmosphere and ocean model are 720 s and 2160 s, respectively. The time-step of the ocean model is reduced compared to the standard MPI-OM version (3600 s) for the reliable representation of semi-diurnal and diurnal ocean tides. Five 200 year experimental runs are performed, with simulation periods from 1860 to 2059. Till the year 1999 the model is forced by observed greenhouse gas emissions and pre-calculated sulfate aerosols. For future climate predictions the model is forced by the A1B scenario. For the initial conditions we are using the 500 year IPCC pre-industrial control experiment, where the model was run with fixed pre-industrial GHG conditions. The state of the Earth system is taken in one hundred year intervals from the control experiment, and each of these five states are used to initialize the five experimental runs.

3. INTER-DAILY AND INTER-ANNUAL VARIATIONS IN LOD

In this section we present variations of the Earth rotation parameters as obtained by five climate model experiments. We are focusing on the length of day (LOD) variations, which are caused through pressure torque induced by zonal pressure gradients on the solid Earth, through changes in the moment of inertia of the coupled system (matter term) and through changes in the angular momentum stored in the ocean and atmosphere (motion term). The motion term is defined by the angular momentum stored in the ocean and atmosphere:

$$L_1 = R \int_V \rho u(\phi, \lambda) \cos\phi dV$$

there u are the zonal velocities of fluid elements with density ρ, R is the distance to the earth's center and ϕ and λ are geographical coordinates. Solely the zonal ocean currents and atmospheric winds cause

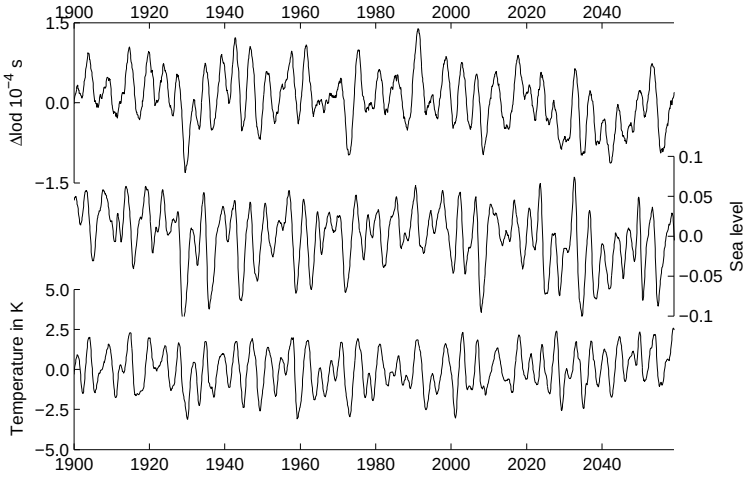

Figure 2: Time series from 1900 till 2059: (top) The variation of LOD (detrended, 12-month running mean) caused by variations of the oceanic matter term. (middle) The variations in sea level (detrended, 12-month running mean) averaged over the equatorial Pacific region extending from 9°S-9°N and 150°W-270°W. (bottom) Time series of the sea surface temperature anomalies in the Niño3.4 region. The correlation beween the temperature (sea level) anomalies and the LOD variations amounts to 0.7 (0.6).

changes in LOD. The LOD is written as

$$\Delta LOD = 86164s \frac{L_1 - L_{1(t=0)}}{L_1^E + L_1},$$

where L_1^E is the angular momentum of the solid earth. The matter term depends on the moment of inertia I_{33} relative to the Earth's axis of rotation, defined through

$$I_{33} = R^2 \int_V \rho(\phi, \lambda) \cos^2 \phi dV.$$

The variations of the matter term (or the moment of inertia) induced by the ocean, the atmosphere and the continental hydrology is determined through the meridional and vertical redistribution of mass. The induced change in LOD is written as

$$\Delta LOD = 86164s \frac{I_{33} - I_{33(t=0)}}{I_{33}^E + I_{33}}.$$

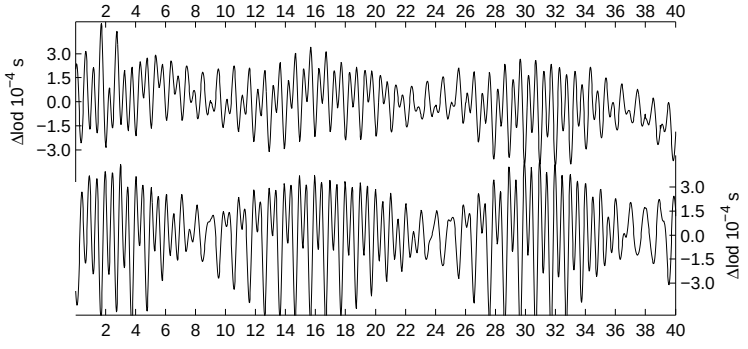

Figure 3: Time series of 40 days in 1900 : The LOD time series caused variations of the oceanic matter term (top) and motion term (bottom).

LOD variations induced by the oceanic motion term are determined by variations of oceanic zonal currents. The major zonal ocean current is the Antarctic Circumpolar Current (ACC) and indeed inter-annual variations in the motion term are mainly controlled by changes in the magnitude of the ACC (Brosche & Sündermann, 1985). In Fig. 1 the variation of the ACC, in the Drake Passage, and the LOD variation induced by the motion term are shown. The magnitude of the ACC shows an inter-annual variability with an amplitude of around $5Sv$ and induces LOD variations of up to $10^{-5}s$. The correlation between these two time- series amounts to 0.7, indicating that the ACC determines to a large extent the LOD variations induced by the oceanic motion term.
The inter-annual variations of LOD induced by the oceanic matter term are shown in Fig. 2 (top). Further, the temperature anomaly in the Niño 3.4 Region is shown Fig. 2 (bottom). This region is in the western equatorial Pacific, bounded by 120°W-170°W and 5°S- 5°N. El Niño events are accompanied by warming the central and eastern tropical Pacific Ocean, thus are indicated by positive temperature anomalies in Niño 3.4 Region. The El Niño episodes are often followed by La Niña events, indicated through negative temperature anomalies in the tropical Pacific Ocean. Obviously the temperature anomaly of the Niño3.4 region correlates well with the ocean induced LOD variation (correlation 0.7). El Niño events lead to positve LOD changes with values up to $1.5 \cdot 10^{-4}s$ and La Niña events lead to negative LOD changes, vice versa.
The variation in the motion term can either result from redistribution of density in the ocean water column or through changes in sea level. The averaged sea level change in the equatorial Pacific region, extending from 9°S to 9°N and 150°W to 270°W, is shown in Fig. 2 (middle). It is well correlated with the LOD and thus with the Niño 3.4 temperature anomalies, as well (correlation 0.6). It seems that the sea level variation, and not the density redistribution, is mainly responsible for inter-annual LOD variations. To clarify the role of the sea level variation, the contribution of the sea level variation to the total moment of inertia is determined in the following. As in Fig. 2 shown, the averaged amplitude in sea level is around 5 cm. The size of the region (9°S-9°N, 150°W-270°W) amounts to $2.6 \cdot 10^{13}m^2$. This corresponds to a water mass of around $1.4 \cdot 10^{15}kg$, which in turn is equivalent to a variation of the moment of inertia of about $5.6 \cdot 1028kg \cdot m^2$. This variation of moment of inertia results in a LOD variation of around $0.7 \cdot 10^{-4}s$, comparable with the LOD variations shown in Fig. 2. This clearly suggests that the inter-annual LOD variations induced by the oceanic matter term are due to the sea level anomaly in the tropical Pacific interconnected with the ENSO variability.
In Fig.3 sub- to inter-daily LOD variations induced by the matter and motion term are shown. Lunisolar ocean tides are the dominant in exciting these harmonic oscillations. The semi-diurnal and diurnal oscillations and their longer period modulations can clearly be identified. The amplitude of these oscillations in LOD are up to $3.5 \cdot 10^{-4}s$ and similar in size for motion and matter term.

4. REFERENCES

Brosche, P., Sündermann, J., 1985, "The Antarctic Circumpolar Current and its influence on the Earths rotation", Dt. Hydrogr. Z., 38 , 1–6.

Greatbatch, T. J., 1994, "A note on the representation of steric sea level in models that conserve volume rather than mass", J. Geophys. Res. , 99, 12767–12771.

Marsland, S. J., Haak, H., Jungclaus, J., Latif, M., Röske, F., 2003 "The Max-Planck-Institute global ocean-sea ice model with orthogonal curvilinear coordinates", Ocean Modelling, 5, 91–127.

Roeckner, E., Büml, G., Bonaventura, L., Brokopf, R., Esch, M., Giorgetta, M., Hagemann, S., Kirchner, I., Kornblueh, L., Manzini, E., Rhodin, A., Schlese, U., Schulzweida, U., Tompkins A., 2003, "The atmospheric general circulation model ECHAM5, part I: Model description", Technical Report 349, Max-Planck-Institute for Meteorology, 127pp.

Terray L., Valcke, S., Piacentine, A., 1998, "The OASIS coupler user guide, Version 2.2" Techn. Rep. TR/CMGC/98-05, CERFACS, 85pp.

Thomas, M., Sündermann, J., Maier-Reimer, E., 2001, "Consideration of ocean tides in an OGCM and impacts on subseasonal to decadal polar motion excitation". Geophys. Res. Lett, 28, 2457–2460.

SIMULATION OF POLAR MOTION WITH A DYNAMIC EARTH SYSTEM MODEL OVER A PERIOD OF 200 YEARS (1860-2060)

F. SEITZ[1], H. DREWES[2]
[1] Earth Oriented Space Science and Technology (ESPACE), TU Munich
Arcisstr. 21, D-80333 Munich, Germany; e-mail: seitz@bv.tum.de
[2] Deutsches Geodätisches Forschungsinstitut (DGFI)
Alfons-Goppel-Str. 11, D-80539 Munich, Germany

ABSTRACT. On time scales between months and decades the Earth's polar motion is mainly influenced by redistributions and motions of atmospheric and hydrospheric masses. Here we report the results of a long-term simulation of polar motion with the dynamic Earth system model DyMEG which is forced by the consistently coupled atmosphere-hydrosphere model ECOCTH. Simulations are performed for five ensemble members of ECOCTH and cover a period of 200 years between 1860 and 2060. Since rotational deformations of the Earth are regarded in DyMEG, forced variations of Earth rotation due to atmospheric and hydrologic angular momenta influence the free polar motion (Chandler oscillation) of DyMEG. The 200-year forcing allows for long-term studies of the excitation mechanism of the Chandler oscillation as well as for the prediction and statistical evaluation of polar motion variations until 2060. Statistical comparisons of modelled and observed polar motion time series over 200 years verify a realistic weather variability of ECOCTH.

1. DYNAMIC EARTH SYSTEM MODEL

Geometric and gravimetric space geodetic techniques, such as Very Long Baseline Interferometry (VLBI), Satellite Laser Ranging (SLR), Global Navigation Satellite Systems (GNSS) and the gravity field missions CHAMP and GRACE observe the Earth system since many years and map it into time series of geodetic parameters related to geometry, gravity field and orientation of our planet. Temporal variations of these parameters reflect a broad spectrum of exogenous and endogenous forces which are the hurriers of continuous geophysical processes within and between individual Earth system components. In order to interpret the geodetic time series in terms of underlying geophysical processes, the connection between the parameters and individual geophysical processes has to be ascertained.

Geodetic parameters are integral quantities, what implies that specific features in the time series cannot be related to particular causative processes and contributions of individual system components without knowledge from additional observations or from independent theoretical models.

In the following we discuss forward-modelled time series of geodetic parameters which are based on simulations with the dynamic Earth system model DyMEG (Dynamic Model for Earth Rotation and Gravity). DyMEG integrates rotation, gravity field and geometry of the Earth and is consistent with respect to applied model parameters, the reference system and geophysical forcing. The set-up of DyMEG has been described and extensively discussed in various publications and shall not be repeated here (see, e.g., Seitz 2004, Seitz and Schmidt 2005). Its set-up is depicted in Figure 1.

DyMEG is forced by the fully coupled and self-consistent model of the subsystems atmosphere, ocean and continental hydrosphere ECOCTH which covers a period of 200 years between 1860 and 2060. ECOCTH has been developed in interdisciplinary co-operation between groups at the University of Hamburg, the University of Bonn, and the Deutsches GeoForschungsZentrum GFZ (Potsdam). Its set-up is described in detail by Jungclaus et al. (2006) and in other articles in this volume.

Modelled variations of the distribution and motions of mass elements from five ensemble runs of ECOCTH are introduced as forcing into DyMEG. Variations of Earth rotation and gravity field are computed simultaneously with solid Earth deformations due to loading effects. In this article we concentrate on the discussion of numerical model results for polar motion, i.e. the variations of the position of the Earth rotation axis with respect to an Earth-fixed coordinate system.

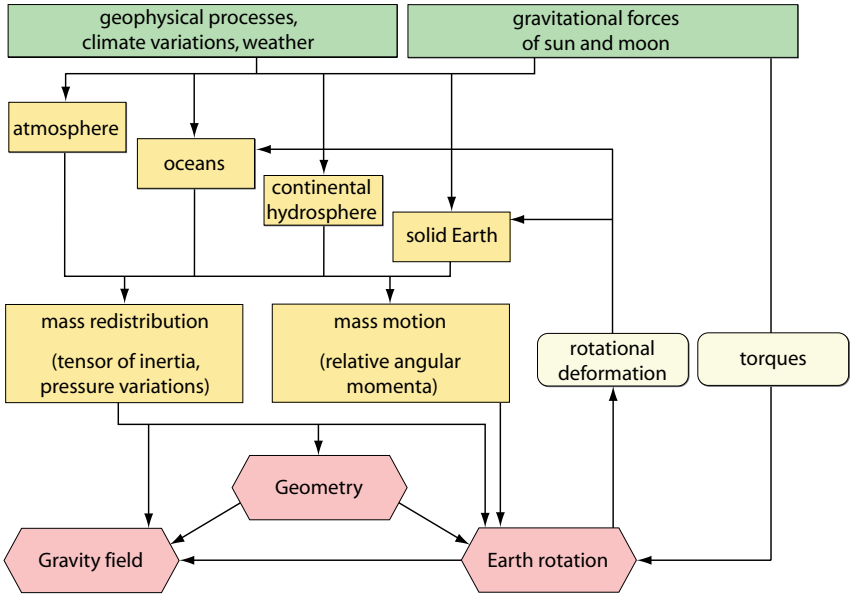

Figure 1: Set-up of the Earth system model DyMEG.

2. RESULTS FOR POLAR MOTION

On time scales from months to decades polar motion is mainly influenced by the variability of angular momentum within and between the atmosphere and the hydrosphere. Model time series of variations of the Earth's tensor of inertia and relative angular momenta due to the motion of atmospheric and hydrospheric mass elements with respect to an Earth-fixed reference frame are introduced into DyMEG and numerically balanced with the Earth rotation vector according to the Liouville differential equation (see Seitz 2004 for details). The resulting time series of polar motion is displayed in Figure 2 for each of the five runs (x-components). For comparison the time series C01 of astrometrical and geodetic observations of polar motion as released by the International Earth Rotation and Reference Systems Service (IERS) is displayed, too.

There are significant differences between the runs that reflect the internal variability of the five ensemble members of ECOCTH. In all cases a clear beat between the two prominent signals, the annual and the Chandler oscillation, is obvious. Signal analysis by means of wavelet filtering (Seitz and Schmidt 2005) reveals, that the annual components of all runs are characterised by rather stable amplitudes over the entire time span of 200 years. However the mean annual amplitudes of all runs amount to 0.16 as (arc seconds), which is almost twice as much as observed (0.09 as). This implies that the annual cycle is overestimated by ECOCTH. While the annual oscillations of the five results are very similar, there are large discrepancies between the modelled Chandler oscillations (Figure 3).

While the annual component of polar motion is a forced phenomenon due to the annual variability of atmosphere and hydrosphere, the Chandler oscillation is a free rotational mode of the Earth which is caused by misalignment of figure axis and rotation axis. However since the Earth's body is deformable this misalignment would diminish, until both axes would coincide after few decades if no counteracting mechanism would perpetuate the Chandler oscillation. The deformations of the Earth's body which occur as a consequence of polar motion (so-called rotational deformations) are a back-coupling mechanism of polar motion on mass redistributions within the solid Earth as a consequence of centrifugal potential variations.

In DyMEG the Chandler oscillation is modelled as a damped oscillation on the basis of rotational deformations and complex Love-Numbers. This way forced variations of Earth rotation due to atmospheric and hydrologic excitations influence the Chandler oscillation of DyMEG. Obviously all runs of ECOCTH allow for the excitation of the Chandler oscillation, even though the shapes of the resulting curves are very different. But concerning the general signal characteristics (distribution of nodes and maxima) the runs are similar and agree well with the observations. Since the Chandler frequency is a resonance frequency of the Earth, energy is required in a spectral band close to the Chandler frequency

in order to excite the oscillation. But since there are no periodic or quasi-periodic signals present in the Chandler frequency band of the spectra of the atmospheric and hydrospheric forcing, the question arises where the necessary excitation energy emerges.

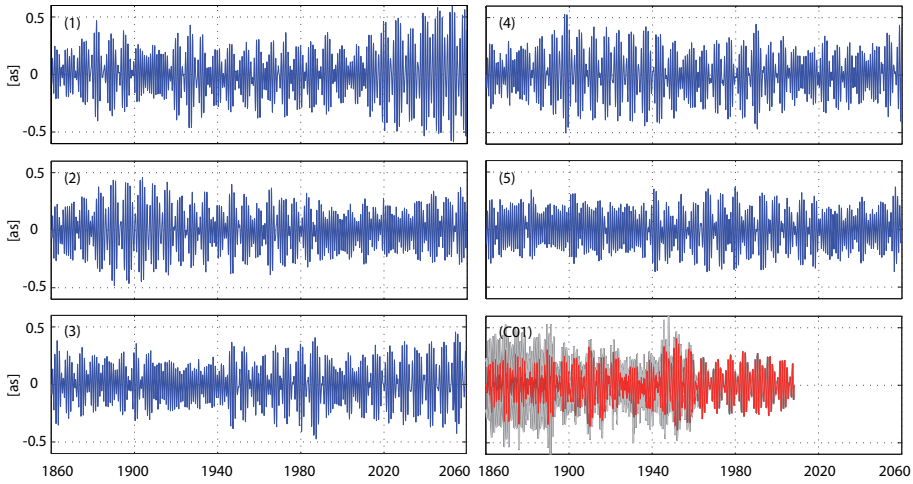

Figure 2: Model results from DyMEG for polar motion (x-components) over 200 years for the five scenario runs (1-5) in comparison with the geodetic observations of the C01-series of the IERS (red). The 3σ-error margin of the observations is diplayed in gray.

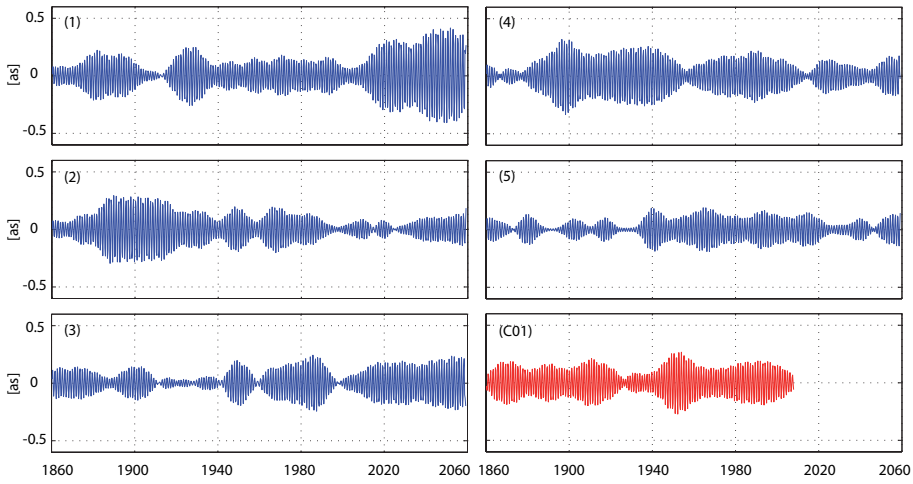

Figure 3: Chandler oscillation (x-components) of the model results and the C01-series determined by wavelet filtering.

3. WHITE NOISE EXPERIMENT

It is assumed that the Chandler oscillation of DyMEG is excited by atmospheric and hydrospheric background noise which is caused by stochastic weather phenomena. Furthermore it is assumed that the noise level (i.e. the amount of excitation energy) is high enough to induce the observed Chandler amplitude variations. Due to the stochastic trait of the simulated weather variations of ECOCTH the five runs lead to results that are quite different at particular points in time, but similar with respect to their general characteristics. In order to corroborate the assumption that the Chandler oscillation can be excited by the stochastic background signal, an experiment is conduced in which the ECOCTH excitations are replaced by white noise. This procedure is similar to runs performed by Seitz et al. (2005), however in the following the experiment is extended to a period of 1000 years between 1900 and 2900.

The model values of the off-diagonal tensor elements $\Delta\mathbf{I}_{xz}$ and $\Delta\mathbf{I}_{yz}$ as well as the equatorial components of the relative angular momentum vector are substituted by synthetic time series of equally distributed random numbers (white noise) from the interval $[-1, +1]$ multiplied by a constant factor l in

order to vary the noise level. It has been shown by Seitz et al. (2005) that for a factor of $l = 1 \cdot 10^{29}$ the noise level of the random number time series is just as high as the noise level of the background signal of the atmospheric and hydrospheric tensor variations. Figure 4 displays the result for the model Chandler oscillation (x-component) when DyMEG is forced with respective random excitations. The first 100 years of the time series are compared with the observed Chandler oscillation.

Again model result and observation show the same characteristics, and the alternation of the Chandler amplitude (increasing and dying down) keeps on going for the entire simulation period of one millennium. The maximum amplitude which can be attained is limited by the noise level. Since the noise level of the applied random excitations is just as high as the noise level of the ECOCTH forcing, we conclude that the stochastic atmospheric fluctuations due to weather variations are indeed the prominent hurriers of the Earth's free polar motion.

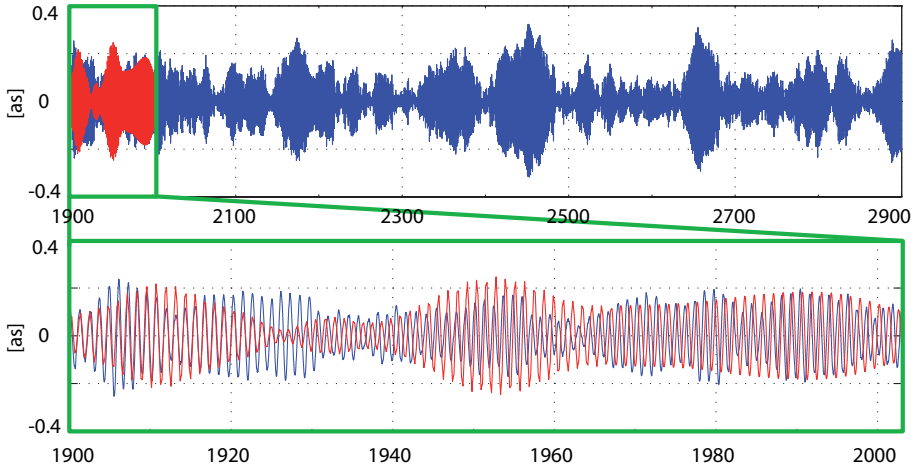

Figure 4: Model result from DyMEG for polar motion (x-components) over 1000 years with white noise forcing instead of atmospheric and hydrospheric excitations (top panel) and comparison with the geodetic observations of the C01-series of the IERS (red) during the last century (lower panel).

4. RÉSUMÉ

From the numerical model results of DyMEG for polar motion quality and potential of the atmosphere-hydrosphere model ECOCTH can be assessed. While the annual cycle turns out to be overestimated in ECOCTH, the physically consistent and fully coupled model has been shown to be a valuable tool for long-term studies of the Chandler oscillation since the five equiprobable ensemble members feature a statistically realistic weather variability over 200 years.

5. REFERENCES

Jungclaus, J.H., M. Botzet, H. Haak, et al., 2006. Ocean circulation and tropical variability in the coupled model ECHAM5/MPI-OM. J. Climate 19 (16), pp. 3952-3972.

Seitz, F., 2004. Atmosphärische und ozeanische Einflüsse auf die Rotation der Erde - Numerische Untersuchungen mit einem dynamischen Erdsystemmodell, Deutsche Geodätische Kommission, C 578, Munich (in German).

Seitz, F., Schmidt, M., 2005. Atmospheric and oceanic contributions to Chandler wobble excitation determined by wavelet filtering, J. Geophys. Res. , 110, B11406, doi: 10.1029/2005JB003826.

Seitz, F., Stuck, J., Thomas, M., 2005. White noise Chandler wobble excitation, In: Forcing of Polar Motion in the Chandler Frequency Band: A Contribution to Understanding Interannual Climate Variations, H.-P. Plag, et al. (Eds.), Cahiers du Centre Européen de Géodynamique et de Séismologie, Vol. 24, pp. 15-21, Luxembourg.

DETERMINATION OF CRUSTAL DEFORMATIONS AND SEA-LEVEL CHANGES IN THE BALTIC SEA REGION

A. GROH, R. DIETRICH, A. RICHTER, C. KNÄFEL
Institut für Planetare Geodäsie, Dresden Technical University, Germany
e-mail: ruelke@ipg.geo.tu-dresden.de

ABSTRACT.

The Baltic Sea region is affected by different geodynamic and oceanographic processes. Global eustatic sea-level change due to thermal expansion and freshwater influx from melting glaciers and ice caps effects the level of the Baltic Sea too and is of special climatological interest. Recent crustal deformations in the region under investigation are dominated by glacial isostatic adjustment arising from the surface load change due to the deglaciated Fennoscandian ice-sheet.

Tide-gauge measurements for a period of more than 150 years provide a sound base to derive secular sea-level changes. The mean sea-level and its changes determined from homogeneous long-term time series are related to the Earth's crust. Therefore, tide-gauge records are not capable to infer eustatic sea-level change, because the vertical movement of the Earth's crust has to be taken into account. These deformations of the solid Earth are observable by GPS. The extraction of geophysical signals from GPS-derived time series relies upon homogeneously processed observations and a stable realization of the terrestrial reference system. Here we benefit from the results of a reprocessed global GPS network.

We determined relative sea-level changes for approximately 60 tide-gauge stations around the Baltic Sea and the adjacent North Sea. In addition we inferred crustal deformations for 44 stations of a densified regional GPS network. For stations where both techniques are collocated the combination of these results allows the determination of the eustatic sea-level change. The so inferred sea-level change rates in the Baltic Sea region are in good agreement with global change rates.

MULTI-FREQUENCY ANALYSIS OF OSCILLATION-ROTATIONAL MOTION OF DEFORMABLE EARTH

L.D. AKULENKO[1], Yu.G. MARKOV[2], L.V. RYKHLOVA[3]
[1] Institute for Problems in Mechanics of RAS
prosp. Vernadskogo 101, block 1, Moscow 119526, Russian Federation
e-mail: kumak@ipmnet.ru
[2] Moscow Aviation Institute (State Technical University)
Volokolamskoe Shosse 4, 125993,GSP-3, Moscow, Russia
e-mail: vadimkin1@yandex.ru
[3] Institute of Astronomy of RAS
48 Pyatnitskaya St. 119017, Moscow, Russia
e-mail: rykhlova@inasan.ru

ABSTRACT. We have considered an extended theoretical model of the Earth's Pole oscillations in order to study the influence of terms with higher frequencies, based on six fundamental parameters of the model for the Earth's Pole oscillations of Akulenko et al. (2005); that model contains Chandler and annual components and an irregular slow drift (trend) of the average Earth's Pole. The generalization of the model has been realized on the base of celestial mechanical approaches with spectral analysis of the time series of the International Earth Rotation and Reference Systems Service (IERS). The identification of the model parameters has been carried out by the method of least squares.

A theoretical model for multi-frequency oscillation process of the Earth's Pole has been built. The generalization of the main mathematical model of Akulenko et al. (2005), which includes two frequencies (Chandler and annual), has been carried out with the help of celestial-mechanical approaches and oscillation theory methods. The influence of high-frequency actions - both regular (lunar) and irregular - that appears during maximal and minimal (extremal) deviations of the Pole trajectory (x_p, y_p) has been studied. The estimation of the amplitudes has been obtained and the explanation for a few high-frequency harmonics is given. The anomaly in the effects in the Pole motion during the beatings with six-year intervals has been investigated. The relations based on a model of oscillations with forced frequency of lunar-solar precession and parametric disturbances with double Chandler and combined frequencies used for the analysis of irregular motions of the Earth's Pole are presented.

A model based on celestial-mechanical for the irregularities in the rotation of a deformable Earth that fits IERS data adequately has been obtained.

The thin resonance structure of interaction between long-period zone tides (annual, semi-annual, monthly, fortnightly) and diurnal and semi-diurnal ones has been adjusted. This appreciable property is confirmed reliably by spectral analysis of IERS measurements data. The numerical simulation of tidal irregularities of the Earth's axis of rotation has been carried out. The analysis of variations of the length of the day (l.o.d.) on short time intervals with one-year period and less (inter-annual oscillations) and their forecast have been presented. The data set of the differences between the interpolation/forecast and UT1-UTC according to obtained mathematical model has been provided.

REFERENCES

Akulenko L.D., Kumakshev S.A., Markov Yu.G., Rykhlova L.V., 2005, "Gravitational-tidal mechanism of the Earth Pole oscillations", Astronomical Journal, vol. 82, No. 10, pp. 950–960.

MODELLING IRREGULARITIES OF THE EARTH'S ROTATION

V.V. BONDARENKO[1], V.V. PEREPIOLKIN[2]
[1] Keldysh Institute of Applied Mathematics
Miusskaya sq., 4 Moscow, 125047, Russia
e-mail: vvb@saintdmtr.comcor.ru
[2] Moscow Aviation Institute (State Technical University)
Volokolamskoe Shosse 4, 125993,GSP-3, Moscow, Russia
e-mail: vadimkin1@yandex.ru

ABSTRACT. The methods of celestial mechanics can be used to construct a mathematical model for the perturbed rotational motions of the deformable Earth that can adequately describe the astrometric measurements of the International Earth Rotation Service. This model describes the gravitational and tidal influences of the Sun and Moon. Fine resonant interactions of long period zonal tides (annual, semiannual, monthly and biweekly) with the diurnal and semidiurnal tides are revealed. These interactions can be reliably confirmed via a spectral analysis of the IERS data. Emphasis is placed on the variations of the day duration on short time intervals with periods of one year and less (interaannual fluctuations).

To study the axial rotation of the deformable Earth, we will use the classical dynamical EulerLiouville equations with a varying inertia tensor:

$$J\dot{\boldsymbol{\omega}} + \boldsymbol{\omega} \times J\boldsymbol{\omega} = \mathbf{M}, \quad \boldsymbol{\omega} = (p,q,r)^T, \quad J = J^* + \delta J, \quad J^* = const,$$
$$J^* = diag(A^*, B^*, C^*), \quad \delta J = \delta J(t), \quad \|\delta J\| \ll \|J^*\|, \tag{1}$$
$$\mathbf{M} = \mathbf{M}_K + \mathbf{M}^S + \mathbf{M}^L.$$

Here, $\boldsymbol{\omega}$ is the angular-velocity vector in a coordinate system (reference frame) fixed to the Earth. The axes of this frame approximately coincide with the main central inertia axes J^* of the "frozen" Earths figure allowing for the equatorial bulge. The reference frame chosen agrees qualitatively and quantitatively with the ITRF coordinates. The small variations in the inertia tensor δJ can contain harmonics due to regular perturbations exerted by the solar and lunar gravitational diurnal tides, and probably some other harmonics as well (annual, semiannual, monthly, biweekly, etc). Additional perturbations result from differentiating the vector of the kinetic moment of the deformable Earth. These terms are included in the vector $\mathbf{M}_K$, which has a very complex structure and is, in turn, additively included in $\mathbf{M}$. Note that the equations for the components p and q were examined during analyses of the Earths polar oscillations.

Let us rewrite the third equation of (1) for the Earths axial rotation component $r(t)$:

$$C^*\dot{r} + (B^* - A^*)pq + (J_{qr}p - J_{pr}q)r = M_r^S + M_r^L. \tag{2}$$

Here, J_{pr} and J_{qr} are small nondiagonal elements of the inertia tensor, and $M_r^{S,L}$ are the gravitational tidal solar and lunar perturbing moments, respectively [1]. For example, M_r^S includes:

$$M_r^S = 3\omega_0^2[(B^* + \delta B - (A^* + \delta A))\gamma_p\gamma_q + \delta J_{pq}(\gamma_p^2 - \gamma_q^2) +$$
$$+\delta J_{qr}\gamma_p\gamma_r - \delta J_{pr}\gamma_q\gamma_r], \tag{3}$$
$$\gamma_p = \sin\theta\sin\varphi, \quad \gamma_q = \sin\theta\cos\varphi, \quad \gamma_r = \cos\theta.$$

where ω_0 is the frequency of the orbital motion; γ_p, γ_q, and γ_r the direction cosines of the radius-vector in the fixed frame; ψ, θ, and φ the Euler angles; and A^*, B^*, and C^* the effective main central moments of inertia, allowing for deformations of the "frozen" Earth, which can be calculated accurately. The coefficients δA, δB, δJ_{pq}, δJ_{qr}, and δJ_{pr} are due to the tidal diurnal and semidiurnal gravitational influences of the Moon and Sun, which cannot be measured directly. These coefficients can be indirectly

estimated using measurements of the characteristics of the process themselves. Averaging over the fast variable φ (φ is the angle of the proper rotation) yields the simple expression for M_r^S

$$M_r^S = 3\omega_0^2[\chi_{1r}^S \sin^2\theta + \chi_{2r}^S \sin\theta\cos\theta]. \tag{4}$$

The quantities χ_{1r}^S and χ_{2r}^S in (4) are due to the semidiurnal and diurnal tides, respectively, and these result from the φ-averaging of the coefficients of $\sin^2\theta$ and $\sin\theta\cos\theta$ in the solar gravitational force moment components:

$$\chi_{1r}^S = \frac{1}{2}\left\langle \frac{\delta B - \delta A}{C^*}\sin 2\varphi \right\rangle_\varphi - \left\langle \frac{\delta J_{pq}}{C^*}\cos 2\varphi \right\rangle_\varphi, \tag{5}$$

$$\chi_{1r}^S = \frac{1}{2}\left\langle \frac{\delta J_{qr}}{C^*}\sin\varphi \right\rangle_\varphi - \left\langle \frac{\delta J_{pr}}{C^*}\cos\varphi \right\rangle_\varphi.$$

Integrating (2), we obtain the *l.o.d.* fluctuations:

$$l.o.d.(\tau) = c + a_c^S\cos(2\pi\tau) + a_s^S\sin(2\pi\tau) + b_c^S\cos(4\pi\tau) + b_s^S\sin(4\pi\tau) +$$
$$+ a_c^L\cos(2\pi\nu_m\tau) + a_s^L\sin(2\pi\nu_m\tau) + b_c^L\cos(2\pi\nu_f\tau) + b_s^L\sin(2\pi\nu_f\tau). \tag{6}$$

Here, ν_m and ν_f are the frequencies of the monthly and biweekly oscillations due to the lunar perturbation, while the unknown quantities c, $a_{c,s}^{S,L}$, and $b_{c,s}^{S,L}$ must be determined from the IERS measurements via least-squares fitting. These coefficients are uniquely related to the unknowns contained in (2). The parameter τ in (6) and below is measured in standard years.

With account for the spectral analysis of the IERS data, the model parameters are identified by means of the least squares method. A statistically reliable interpolation of the measured data over a time interval of one year (and longer) is obtained, and the nonuniformities of the Earths rotation (that is, the variations of the day duration and the UT1-UTC correction) are predicted on an interval of 4 to 10 months. A comparison of the real and theoretical trajectories for the irregularity of tidal oscillations of the rotational angular velocity indicates agreement between the constructed model and the IERS observations.

The theoretical model constructed demonstrates a good agreement with the IERS forecast, according to the accuracy of the approximation.

REFERENCES

Akulenko L.D., Markov Yu.G.,Perepiolkin V.V. Rykhlova L.V., 2008, "Intrayear Irregularities of the Earth's Rotation", Astronomical Journal, vol. 52, No. 7, pp. 590–597.

CHANGE OF THE EARTH MOMENT OF INERTIA DURING THE OBSERVED UT1 RESPONSE TO THE 11-YEAR SOLAR VARIATION

Ya. CHAPANOV[1], D. GAMBIS[2]
[1] Central Laboratory for Geodesy of Bulgarian Academy of Sciences
Acad. G. Bonchev Str., Bl.1, Sofia 1113, Bulgaria
e-mail: chapanov@clg.bas.bg
[2] SYRTE, Observatoire de Paris, CNRS, UPMC
61, avenue de l'Observatoire, 75014 Paris, France
e-mail: daniel.gambis@obspm.fr

ABSTRACT. The observed oscillation in UT1 with the period 10.47a and amplitude of 60 ms, are highly correlated with the delayed variations of smoothed Wolf's numbers. These oscillations are connected with corresponding changes of the principal Earth moment of inertia C, due to the conservation of angular momentum. The necessary changes of the Earth moment of inertia, during the solar maxima, are considered in two cases - first by an axial-symmetric deformation and uniform decrease of the mean earth equatorial radius, simultaneously with the solar cycles, and second - by a decrease of mean sea level, due to additional water evaporation, and corresponding increase of polar ice thickness, due to the global water redistribution. The observed 11-year UT1 oscillation, due to changes in the Earth moment of inertia, is connected in the first case with the earth equatorial radius variations with an amplitude of about 2 mm, and in the second case - with mean sea level oscillations with mean amplitude of about 5 mm. The only climatic reason of the first case is adequate variations of atmospheric temperature and pressure over the equatorial regions, but according the matter term of the atmospheric angular momentum AAM, no such atmospheric variations exist. The second case is confirmed by a 11-year mean sea level oscillation in some maregraph stations. The necessary energy of additional sea water evaporation during the solar cycles is connected with the total solar irradiance changes with mean magnitude of about 1 Watt per square meter.

ANALYSES. The decadal variations of the Earth rotation are strongly affected by the 11-year cycle of the solar activity and the UT1 response to these cycles is delayed by $1.5a$ with amplitude of about 60 ms (Chapanov and Gambis, 2008). The explanation of the delayed UT1 response to the sunspot cycles is the appropriate change of the axial Earth moment of inertia, due to climatic variations, connected with the total solar irradiance change. Let us consider a homogeneous sphere with radius $R = 6364km$, density $5.6g/cm^3$, inertial moment C, angular velocity ω and constant mass M. From the conservation of angular momentum, any change of inertial moment ΔC is compensated with a corresponding change of angular velocity $\Delta\omega$ according the following expression

$$\Delta C\omega + C\Delta\omega = 0 \tag{1}$$

The variation ΔC depends on the variation of the radius ΔR according the formula

$$C + \Delta C = 1/2(R^2 + 2R\Delta R + \Delta R^2) \tag{2}$$

and from (1) and (2), after neglecting the second order term ΔR^2, we obtain

$$2\Delta R\omega + R\Delta\omega = 0 \tag{3}$$

The formula (3) expresses the relationship between the variations of the radius and the angular velocity of an ideal elastic homogeneous sphere without external moments, hence the necessary change of radius ΔR, which corresponds to the observed variation of time angle ΔUT for time interval P is

$$\Delta R = -\frac{1}{2}R\frac{\Delta UT}{P} \tag{4}$$

In case of periodical variations of time angle ΔUT with observed amplitude A_{UT} and period P, the necessary amplitude A_R of the periodical oscillations of the radius is

$$A_R = \frac{1}{2} R \frac{A_{UT}}{P} \tag{5}$$

In case of a sunspot cycle with $A_{UT} = 0.06 s and P = 10.47a = 3.3 \times 10^8 s$, we obtain $A_R = 0.6mm$. The corresponding deformation of the real Earth is represented by oscillations of the equatorial and polar Earth radii with opposite phases and amplitudes of about 2 mm. The only possible reason of such oscillation is climatic, due to adequate variations of atmospheric temperature and pressure over the equatorial regions, but according the matter term of the atmospheric angular momentum AAM, no such atmospheric variations exist. Another source of Earth inertial moment oscillations, without significant deformations of the Earth crust, are the periodical variations of the mean sea level, followed by polar ice thickness changes, due to global water redistribution. The free global ocean surface is approximately 68% of the Earth surface and the mean density of sea water is $1.025 g/cm^3$. Thus, the necessary change of the Earth axial moment of inertia during a sunspot cycle is provided by mean sea level oscillation with 8 times higher mean amplitude A_{MSL} than A_R, which yields $A_{MSL} = 4.8mm$. The change of inertial moment of polar caps, due to the ice thickness variations during a single sunspot cycle is approximately 5% of ΔC, which need to increase A_{MSL} by 2.5% to the value $4.9mm$. The necessary energy to evaporate a $9.8mm$ thin layer of sea water with surface of $1m^2$, salinity 3.5% and mean temperature 15°C is $9.8l \times 0.989kg \times 2440kJ/kg = 23.6MJ$, collected for time interval of $1/2 \times 10.47a$, or $1.65 \times 10^8 s$. The corresponding deviation of the total solar irradiance is $0.14 W/m^2$ only, which is 7 times less than the total solar irradiance variations due to the solar activity. The mean amplitude of the 11-year oscillations

Table 1: Amplitudes A_{MSL} of the 11-year oscillations of the mean sea level for some maregraph stations.

Station	Period	$A_{MSL}[mm]$	Station	Period	$A_{MSL}[mm]$
Fremantle	1897–1990	16.6	Kabelvag	1880–2005	9.6
Sydney	1886–1994	8.1	Barencburg	1948–2006	14.1
Stockholm	1774–2001	7.3	Honolulu	1905–2006	14.7
Port Adelaide	1941–2005	9.0	Mumbay	1878–1994	6.8
Prince Rupert	1909–2006	10.5	Genova	1884–1998	11.8

of the mean sea level, determined from 10 maregraph stations (Table1), is $11 \pm 3mm$. We may conclude that:

1. The 11-year solar activity cycles strongly affect earth climatic variations by the variations of the total solar irradiance with mean magnitude of about $1 W/m^2$. These variations provide additional amount of energy ($1.7 \times 1017 MJ$ for the whole Earth and $165 MJ$ per square meter on the equator) during a single sunspot cycle. This energy is capable of the evaporation $66l$ of water from 1 square meter equatorial ocean surface and $25l$ of water from 1 square meter ocean surface from the north latitudes.

2. The necessary change of the Earth axial moment of inertia during the 11-year cycle of the $UT1$ with an amplitude of about $60ms$ is provided by synchronized global mean sea level oscillations with mean amplitude of about $5mm$ and corresponding change of the ice thickness at the polar caps, due to the global water redistribution.

3. The observed 11-year oscillations of the mean sea level at 10 maregraph stations are with mean amplitude about 11 mm and opposite phase relative to the sunspot oscillations with a delay of about 1.5a. The reason of these oscillations is the additional evaporation due to the variations of the total solar irradiance during the solar activity cycles and next global water redistribution. The greater part of evaporated water (60–80%) returns back to the ocean. The rest part of the evaporated water is periodically redistributed over the continents and polar caps. A minor part of redistributed water (about 40%) periodically changes snow and ice cover over the polar caps and causes the observed $UT1$ response to the sunspot cycles.

REFERENCES

Chapanov Ya., Gambis D., 2008, "Correlation between the solar activity cycles and the Earth rotation", Proceedings of the Journées 2007 "Systèmes de Référence Spatio-Temporels", N. Capitaine (ed.), Observatoire de Paris, 206–207.

AN ANALYTICAL THEORY OF THE ROTATION OF VENUS

L. COTTEREAU, J. SOUCHAY
SYRTE, Observatoire de Paris, CNRS, UPMC
61, avenue de l'Observatoire, 75014 – Paris, France
e-mail: laure.cottereau@obspm.fr

ABSTRACT. Although a full and detailed discussion of the effects of the Venus atmosphere and Venus interior on its rotation has already been done by several authors (Correia & Laskar, 2001; Yoder, 1995), a precise analytical determination of its precession and nutation coefficients has been poorly investigated. In that aim, we use the same theoretical framework as Kinoshita (1977) for the Earth, in order to construct the tables of nutation of Venus, together with its precession constant. A comparative study with the Earth is done, which shows that two fundamental characteristics of Venus lead to very specific rotational properties: its very long sidereal retrograde rotation (243 d) and its very small flattening.

1. INTRODUCTION

One of the important results of Venus' radar ranging observations was the discovery of its retrograde rotation, with a period of -243.16 days. Various efforts were made to explain this particular rotational mode. Soon after the discovery, Goldreich & Peale (1970) explained that thermally driven atmospheric tidal torque and dissipation of energy at the boundary between a rigid mantle and a differentially rotating liquid core are possible mechanics for maintaining the retrograde spin. Lago & Cazenave (1979) have studied the past evolution of the rotation of Venus using the hypothesis that only solar tidal torques and core-mantle coupling have been active since formation. They have found quite conceivable that Venus had originally a rotation quite similar to the other planets and had evolved in 4.5 x 10^9 years from a rapid and direct rotation to the slow retrograde one. Yoder (1995) has made a full account of the various internal mechanisms acting on Venus' obliquity, as core friction, CMB (core-mantle boudary) ellipticity, and resonant excitations. More recently Correia & Laskar (2001) showed that the atmospheric torque on Venus is large enough for a synchronous rotation to become unstable. Then two configurations appear, one prograde and the other retrograde. From numerical simulations they investigated four possible scenari of change of the obliquity, one leading to the present state. Although these various studies concern the evolution of Venus' rotation at very long time scales, few attempts were made to modelize accurately the rotation for a short time span. An analytical study of the rotation of rigid Venus was carried out by Habibullin (1995) with rather uncommon parametrization, showing that Venus rotates almost uniformly with libration harmonics being negligible. In the following we propose an alternative construction of a rigid Venus rotation contradicting in some extent these last results.

2. MODELING VENUS' ROTATION

In Table 1 we present the various orbital, rotational and physical characteristics of Venus together with the corresponding values for the Earth. Some elements tend to make the amplitudes of the precession constant and the coefficients of nutation larger for Venus than for the Earth : these are the smaller heliocentric distance as well as the very long period of rotation. On the opposite the comparative small value of the dynamical ellipticity should reduce these amplitudes. The fact that the Venus eccentricity is significantly smaller than the Earth's should also lead to a smaller number of coefficients for a given level of amplitude. The moments of inertia A, B, and Chave been taken from Habibullin (1995).

In our study, Venus is considered as a rigid body. Therefore in order to construct the analytical theory of its rotation, we use the same analytical framework as Kinoshita (1977) when computing the coefficients of nutation of the Earth for a rigid model. Thus we use the Andoyer variables (Andoyer, 1923) allowing a full description of the rotation, by considering three different and close axis : the axis of figure, the axis of angular momentum and the axis of rotation. The precession-nutation angles in longitude and obliquity are respectively given by h and I with : $H = G\cos I$.

Table 1: Results of cross-identification between A–H and HB.

	Earth	Venus
Semi-major axis	1.000000 U.A	0.723332 U.A
Eccentricity	0.0167	0.0068
Density	5.51 g/cm^3	5.25 g/cm^3
Equatorial radius	6378 km	6051 km
Mass	$5.97 \times 10^{24} kg$	$4.87 \times 10^{24} kg$
Period of revolution	365.25 d	224.70 d
Inclination	0	3°.39
Obliquity	23°.43	2°.63
Period of rotation	0.997 d	-243.02 d
Ascending node	174°.87	76°.67
Triaxiality $\frac{A-B}{4C}$	-5.34×10^{-6}	-2.67×10^{-6}
Dyn. Flattening : $\frac{2C-A-B}{2C}$	3.27×10^{-3}	1.7×10^{-5}
$\frac{B-A}{2*(2*C-A-B)}$	-0.0016	-0.15

Then the Hamiltonian for the Venus' rotation becomes : $K = F_0 + U + E$, where F_0 stands for the Hamiltonian of the free motion of rotation, U is the perturbing potential and E is a part of the Hamiltonian corresponding to a change of reference plane, from Venus' orbital plane at the fundamental epoch J2000.0 (the equivalent of the ecliptic of J2000.0 for the Earth) to the orbital plane at the date t. At the first order U can be divided into two parts, one involving the Venus' dynamical flattening (term depending on $2C - A - B$) and the other one Venus' triaxiality (term depending on $A - B$): $U = U_1 + U_2$ with :

$$\mathtt{U_1} = \frac{\mathtt{k^2 M'}}{\mathtt{r^3}}[\frac{\mathtt{2C - A - B}}{\mathtt{2}}\mathtt{P_2}(\sin\delta)] \qquad \mathtt{U_2} = \frac{\mathtt{k^2 M'}}{\mathtt{r^3}}[\frac{\mathtt{A - B}}{\mathtt{4}}\mathtt{P_2^2}(\sin\delta)\cos 2\alpha] \tag{1}$$

Where M' is the mass of the Sun, r its distance from Venus geocenter and α et δ its planetocentric coordinates (respectively the longitude et latitude of the Sun with respect to a meridian origin. The P_n^m are the classical Legendre functions.

The basic canonical equations are (Kinoshita, 1977) :

$$\frac{\mathtt{d}}{\mathtt{dt}}(\mathtt{L,G,H}) = -\frac{\partial \mathtt{K}}{\partial(\mathtt{l,g,h})} \qquad \frac{\mathtt{d}}{\mathtt{dt}}(\mathtt{l,g,h}) = \frac{\partial \mathtt{K}}{\partial(\mathtt{L,G,H})} \tag{2}$$

Where K is obtained by integrating directly U. Following the same methodology as Kinoshita (1977) we have computed the precession constant as well as the nutation coefficients of Venus. Complete results will be published soon (Cottereau & Souchay, in prep.) The scaling factor k for these computations is given by $k_{Venus} = 3(n^2/\omega) \times (2C - A - B/2C)$. Although the dynamical flattening $(2C - A - B/2C)$ at the nominator is much smaller than for the Earth, this is compensated by the fact that the angular rotational velocity ω at the denominator is itself much smaller. Thus we have calculated that the precession constant is $\dot{\psi} = 6133.7$ "/cy by taking the same values of A, B, and C as Habibullin (1995). It is roughly 3.5 times larger than the solar part of the precession constant of the Earth. The largest nutation coefficients has a 3" amplitude and a period (112.35 d) half the period of revolution of Venus. Complete computations are on the way (Cottereau & Souchay, in prep.)

3. REFERENCES

Andoyer, H., 1923, *Cours de Mécanique Céleste*, Paris, Gauthier-Villars ed.
Correia, A. C., Laskar, J., 2001, Nature 411,767
Goldreich, P., Peale, S.J., 1970, AJ 75, No. 3, 273
Habibullin, S.T., 1995, Earth, Moon and Planets 71, 43
Kinoshita, H., 1977, Celest. Mech. 15, 277
Lago, B., Cazenave, A., 1979, The Moon and the Planets 21, 127
Yoder, 1995, Icarus 117, 250

ROTATION AND INTERNAL DYNAMICS OF MARS FROM FUTURE GEODESY EXPERIMENTS

V. DEHANT[1], W. FOLKNER[2], A. CHICARRO[3],
THE LARA TEAM[4] AND THE MARSNEXT SCIENCE DEFINITION TEAM[5]
[1] Royal Observatory of Belgium
Avenue Circulaire 3, B1180 Brussels, Belgium
e-mail: v.dehant@oma.be
[2] Jet Propulsion Laboratory
m/s 301-150; 4800 Oak Grove Drive, Pasadena CA 91109, USA
e-mail: william.folkner@jpl.nasa.gov
[3] Research and Scientific Support Department, ESA/ESTEC
PO Box 299; 2200 AG Noordwijk, The Nederlands
e-mail: achicarro@rssd.esa.int

ABSTRACT. The LaRa (Lander Radioscience) experiment on the lander platform of the ExoMars mission (the Humboldt Payload) on the surface of Mars is designed to obtain coherent two-way Doppler measurements from the radio link between the ExoMars lander and the Earth over at least one third of a Martian year. We have set up a design for LaRa and realized a breadboard.

Complementary to LaRa, in the future network-science Mars-NEXT mission, there will be radio links between other landers at the surface of Mars and the orbiter and a radio link between the orbiter and the Earth. The Mars-NEXT mission to Mars addresses different fields of investigation, of which an important part is related to planetary rotation and interior structure as for LaRa.

With the objectives to determine interior properties of Mars as well as angular momentum changes induced by CO2 sublimation/condensation process, we have simulated these Doppler measurements and developed a strategy for reaching these goals.

1. INTRODUCTION

In the last decades, several missions and observations have brought new insight on the inner structure of the terrestrial planets. This information is a big challenge for the planet interior models; these data are also our best chance to improve our knowledge of the interior. Data obtained through new space missions are the basis of the future progress in this field. Classically, as done for the Earth, the interior models are constrained through seismic data provided from an extended network of seismometers. However, for planets, in the absence of such a network, gravitation and rotation studies are the most efficient ways to learn about the interior of the planets. Practically, our study is based on the analysis of the precise orbits of spacecrafts around the planets and on the positions of landers. Our experiments will allow us to answer some of the most debated questions of the moment: the atmospheric dynamics and the state and dimension of the core.

2. EXPERIMENTS

The paper presents the concept, the objectives, the approach used, and the expected performances and accuracies of radioscience experiments based on radio links between the Earth and the surface of Mars, between the Earth and an orbiter around Mars and between this orbiter and the landers on the surface of Mars. These experiments involve radioscience equipment installed on a lander at the surface of Mars and on a spacecraft orbiting around Mars, as well as dedicated ground stations on Earth. The

[4]The LaRa team: V. Dehant (PI), W. Folkner (Co-PI), D. Orban (IM), E. Renotte (PM), L. Rossi (DPM); S. Asmar, J. Benoist, R. Biancale, J. Biele, F. Budnik, O. de Viron, J.P. Halain, B. Haeusler, S. Le Maistre, P. Lognonné, M. Menvielle, M. Mitrovic, M. Paetzold, P. Rosenblatt, G. Schubert, T. Spohn, P. Tortora, T. Van Hoolst, O. Witasse

[5]The Mars-NEXT Science Definition Team: A. Chicarro (PS) , D. Breuer, J. Carpenter, E. Chassefiere, V. Dehant, R. Fisackerly, M. Grady, L. Marinangeli, P. Pinet, A. Rossi, A. Santovincenzo

experiments are not fictive as there are at least two possibilities in the future. The first, with the generic name LaRa (Lander Radioscience), consists of an X-band transponder that has been designed to obtain, over at least 180 days (minimum guaranteed mission) and more probably over one Martian year, two-way Doppler measurements from the radio link between the ExoMars lander and the Earth (ExoMars is an ESA mission to Mars within the Aurora Exploration Programme and due to launch in 2016).

The second possibility is MarsNEXT also called MarsNet consisting in several landers at the surface of Mars and an orbiter around Mars. This mission is studied in the frame of the Next Exploration Science and Technology (NEXT) mission opportunity, as part of ESA's Aurora Exploration Programme. Following the Mars-Express Orbiter and the ExoMars rover-lander, MarsNEXT offers a unique opportunity to produce a global picture of the geophysics of Mars. The Network Mission concept addresses key science goals on a given terrestrial planet (in this case, Mars) that can only be achieved by simultaneous (or quasi-simultaneous) measurements from a number of landers, which are spaced across the surface of the planet. The primary objectives of such a mission concern a planet's internal geophysics and its meteorology. A Mars Network Mission also allows for a significant improvement to our understanding of the rotational parameters of the planet. This can be achieved by means of radio transmission between the various landers and the Earth and between these landers and a single orbiter. Studies into the rotational parameters of Mars are an important complement to internal geophysical studies. Thus important science objectives at Mars cannot be achieved by any means other than Network Science and by a Mars Network Science mission.

As mentioned above, radioscience measurements are Doppler measurements that are used to obtain Mars' orientation in space and rotation (precession and nutations, and length-of-day variations). More specifically, the relative position of a lander on the surface of Mars with respect to the Earth ground stations or of a lander with respect to an orbiter and of the orbiter with respect to Earth allows reconstructing Mars' time varying orientation and rotation in space.

3. FUTURE RESULTS

Radioscience using landers-Orbiter-Earth links will provide important constraints on the rotation of Mars and on its deformations. Analytical and numerical simulations confirm the feasibility of LaRa and emphasize the potential of future radioscience experiments.

- From Length-of-day variations it will be possible to obtain information on the mass transfer in the sublimation/condensation process of CO2;
- From precession and nutation, it will be possible to obtain the moments of inertia of the whole planet, of its core and its mantle, as well as Mars' core state and dimension;
- From tidal effects on the orbiter, it will be possible to better constrain de tidal Love number k2 and therewith further constrain the models of Mars' interior;
- Precession, nutation, moments of inertia of the core and the mantle, dimension of the core, and tidal Love number are constraints for interior modeling, which will allow a better understand of Mars evolution and habitability.

In particular, LaRa radioscience on ExoMars will improve our knowledge on the core and the rotation of Mars; LaRa feasibility has been demonstrated on a poster (Le Maistre et al.) presented yesterday. MarsNet/MarsNEXT will further improve this knowledge and will provide the possibility to further precisely determine the physical properties and dimension of the core (and possible inner core). This will allow us to obtain global properties of Mars. It will be perfectly complementary with seismic measurements, heat flow measurements, and magnetic measurements; these data will be jointly used for obtaining the best knowledge of Mars interior.

The ultimate objectives of the proposed experiments are to obtain information on Mars' interior and on the sublimation/condensation of CO2 in Mars' atmosphere. Improved knowledge of the interior will help us better understand the formation and evolution of Mars.

Improved knowledge of the CO2 sublimation/condensation cycle will enable better understanding of the circulation and dynamics of Mars' atmosphere. For further detail, see the paper on LaRa (Dehant et al., 2008, Planet. Space Sci., doi: 10.1016/j.pss.2008.08.009) and on MarsNEXT (Chicarro et al., Science Definition Document, ESA publication).

DIRECT ESTIMATION OF TIDALLY INDUCED EARTH ROTATION VARIATIONS OBSERVED BY VLBI

S. ENGLICH, R. HEINKELMANN, J. BÖHM, H. SCHUH
Vienna University of Technology, Institute of Geodesy and Geophysics, Advanced Geodesy
Gußhausstraße 27-29, 1040 Vienna, Austria
sigrid.englich@tuwien.ac.at

ABSTRACT. The subject of our study is the investigation of periodical variations induced by solid Earth tides and ocean tides in Earth rotation parameters (ERP: polar motion, UT1)observed by VLBI. There are two strategies to determine the amplitudes and phases of Earth rotation variations from observations of space geodetic techniques. The common way is to derive time series of Earth rotation parameters first and to estimate amplitudes and phases in a second step. Results obtained by this means were shown in previous studies for zonal tidal variations (Englich et al., 2008a) and variations caused by ocean tides (Englich et al., 2008b). The alternative method is to estimate the tidal parameters directly within the VLBI data analysis procedure together with other parameters such as station coordinates, tropospheric delays, clocks etc. The purpose of this work was the application of this direct method to a combined VLBI data analysis using the software packages OCCAM (Version 6.1, Gauss-Markov-Model) and DOGSCS (Gerstl et al., 2001). The theoretical basis and the preparatory steps for the implementation of this approach are presented here.

1. DERIVATION OF TIDAL ERP VARIATIONS

Earth rotation parameters or Earth orientation parameters (ERP+precession-nutation), respectively, are usually estimated as linking elements between Earth-fixed and space-fixed reference frames, within the normal adjustment procedure. Periodical variations of the ERP are thereby introduced to get best possible a priori ERP, the values are taken from conventional models. The actually estimated quantities are small corrections to the a priori ERP values. ERP time series obtained in this way can then be used to determine the inherent periodical variations in a second adjustment independent from the general data analysis. The disadvantage of this strategy is that it is necessary to reduce signals with frequencies that are not of interest in the special case. For example, if the signals of interest are daily and sub-daily variations caused by ocean tides, a smoothed ERP series (i.e. low-frequency signal) has to be reduced from the original one. Thus additional a priori information is introduced. This step might insert artificial signal and hence influences the estimation of the tidal parameters.
In the direct approach the ERP are represented as a sum of the parameter in the absence of tidal effects and the variations due to solid Earth tides or ocean tides (e.g. Sovers & Jacobs, 1996). The partial derivatives of the unknown parameters of the variations are formulated (considering their periods as known) and are integrated into the functional model of the adjustment. New parameters are set up for ocean tidal variations with diurnal and semi-diurnal periods in all ERP and for zonal tidal variations with periods from around 5-365 days in UT1 only (the term zonal tidal variations comprises effects of solid Earth tides and long period ocean tides here). We use an extended parameterization for polar motion

$$x_p = x_{p_0} + \delta x_{p_{ot}}$$

$$y_p = y_{p_0} + \delta y_{p_{ot}}$$

and accordingly for Universal Time

$$UT1 = UT1_0 + \delta UT1_{zt} + \delta UT1_{ot}.$$

Quantities with the subscript 0 label the slowly varying parameter in the absence of ocean/zonal tidal variations, whereas δ and the subscripts ot or zt mark the corresponding variations. The representation

(we write ERP substitutional for all parameters) for the ocean tidal variations reads

$$\delta ERP_{ot} = \sum_{i=1}^{n} [A_{i_{ot}} cos\xi_i + B_{i_{ot}} sin\xi_i] \quad with \quad \xi_i(t) = \sum_{j=1}^{6} N_{ij} F_j(t)$$

and similar for the zonal tidal variations

$$\delta UT1_{zt} = \sum_{i=1}^{m} [A_{i_{zt}} cos\xi_i + B_{i_{zt}} sin\xi_i] \quad with \quad \xi_i(t) = \sum_{j=1}^{5} N_{ij} F_j(t)$$

Where n and m specify the number of considered tidal terms, A_i and B_i denote the amplitudes corresponding to tidal wave i and ξ_i are the so-called fundamental arguments.
The software OCCAM still uses the transformation based on ecliptic and equator for the transfer from the celestial to the terrestrial reference frame. This means there is a rotation matrix for x_p and y_p and one for Greenwich sidereal time and therewith implicitly for UT1. If we name the corresponding matrix for each ERP R_{ERP} then the partial derivatives with respect to the tidal amplitudes can be simply written as follows

$$\frac{\partial R_{ERP}}{\partial A_i} = \frac{\partial R_{ERP}}{\partial ERP} \cdot \frac{\partial ERP}{\partial A_i} \quad with \quad \frac{\partial ERP}{\partial A_i} = sin\xi_i$$

and correspondingly w.r.t. B_i

$$\frac{\partial ERP}{\partial B_i} = cos\xi_i$$

2. DISCUSSION AND FUTURE TASKS

The intention of this work was to estimate coefficients of tidal ERP variations directly from VLBI group delay observations. The main advantage of this approach is that no additional information has to be introduced, which could distort the results. In this paper the basic formulation of the problem and the partial derivatives were presented. Within this study the above described approach was implemented and tested with the quoted software packages. We conducted a global solution which yielded preliminary results for 16 zonal tidal terms (UT1) and 13 ocean tidal terms (UT1, x_p, y_p). The results are not given here, because the realization of the method requires further examination before resulting values can be compared to conventional models.
The first tests were accomplished using a rather simple approach. It is intended to consider other periodic effects (such as atmospheric tides) in follow-up studies. Another future issue is the correlation between the newly introduced unknowns and other parameters of the adjustment which has to be investigated in more detail and handled appropriately.

3. REFERENCES

Englich S., Weber R., Schuh H., 2008, "Empirical validation of the conventional model for length of day variations due to zonal tides". Proceedings of the Journes 2007 "Systèmes de Référence Spatio-Temporels", N. Capitaine (ed.), Observatoire de Paris, pp. 184-187.

Englich S.,Heinkelmann R.,Schuh H., 2008, "Re-Assessment of Ocean Tidal Terms in High-FrequencyEarth Rotation Variations Observed by VLBI", in International VLBI Service for Geodesy and Astrometry 2008 General Meeting Proceedings, edited by Dirk Behrend and Karen Baver, Russian Science Series.

Gerstl M., Kelm R., Müller H., Ehrnsperger W., 2001, "DOGSCS Kombination und Lösung großer Gleichungssysteme", Deutsches Geodätisches Forschungsinstitut, DGFI Interner Bericht Nr. MG/01/1995 /DGFI.

Sovers O.J., Jacobs C.S., 1996, "Observation Model and Parameter Partials for the JPL VLBI Parameter Estimation Software "Modest"-1996", JPL Publication 83-39, Rev. 6, California Institute of Technology, Pasadena, California.

NON-LINEAR VECTOR ANN PREDICTOR FOR EARTH ROTATION PARAMETERS FORECAST

D.A. MILKOV[1], L.KARIMOVA[2], Z.M. MALKIN[1],
[1] The Central Astronomical Observatory RAS
Russia, Saint-Petersburg
e-mail: milkov@yandex.ru
[2] Institute of Mathematics, Alma-Ata, Kazakhstan

ABSTRACT. Many approaches are developed for the forecasting of the Earth rotation parameters. In this work, we consider long-term vector prediction scheme realized on the artificial neural network. Learning set is formed on basis of the Taken' algorithm. Our approach allows us to obtain the vector of the parameter values and escape the exponential growth of the prediction errors. The versions of the prediction enhancement based on the using for nonlinear corrector are discussed.

1. INTRODUCTION

So far as Artificial Neuron Network (ANN) is representation "in-out" signal and entering vector is distributed in multidimensional space of attributes, we realized the procedure of learning table building for which the main constructing concepts bases on the dynamic features. In this case the space of attributes transforms qualitative into phase space of dynamic system which, as we suppose, generates the concerned time series (Ott et al. 1994a; Abarbanel et al. 1994; Tribelsky et al. 2002; Sauer et al. 1991; Rapp et al. 1999). The ANN realizes (or very close approximates) representation in the space. Correspondingly it is structural changed the representation of probability measure with a glance dynamic system behavior (Ott et al. 1994b). And the learning vector becomes the points of phase space which belongs the phase system trajectory.

A method of the building of learning set was developed for prediction using ANN where the main destination is modeling the asymptotic behavior of phase trajectory and extrapolation in time, i.e. prediction service.

The building of learning set consists in several stages.

The first stage consists in estimation of the dynamic features of the considering time series. In the first stage we obtain the dimension of embedding and time lag (τ) (Ott et al. 1994b; Parker et al. 1989). In the second stage, we construct the vectors using method which is described above. The obtaining vectors is filled the rows in learning table of ANN step-by-step in compliance with movement in the line of time series (Ott et al. 1994b; Parker et al. 1989).

The application of this method leads to interesting effect. The ANN which is learned on such sample realized the vector scheme of prediction. In contrast to a one-step scheme of prediction, the error of prediction is not accumulated through iterative using prediction-following counts.

2. RESULTS AND CONCLUSION

In this work, we used the following scheme of ANN: 10-5-1.

The dimension of embedding is $m = 10$. For 10, 100, 200, 300 day forecast the time lag was correspondingly $\tau = 10$, $\tau = 100$, $\tau = 200$, $\tau = 300$.

It was done several forecast series. For every forecast (10, 100, 200, 300 days) ANN started $k = 10$ times. Then we moved back on the time line through 30 days. And so on in the past altogether was $n = 11$.

The 100, 200, 300 days forecast was done for X_p, Y_p, $UT1$. The 10 day forecast was done only for X_p.

On figure, 1 it is shown the MAE and RMS statistics for 10-, 200- and 300-day forecast for X_p:

$$MAE = \frac{1}{n}\sum_{i=1}^{i=n} |forecastaverage_i - realvalue_i|, RMS = \sqrt{\frac{1}{n-1}\sum_{i=1}^{i=n}(forecastaverage_i - realvalue_i)^2}.$$

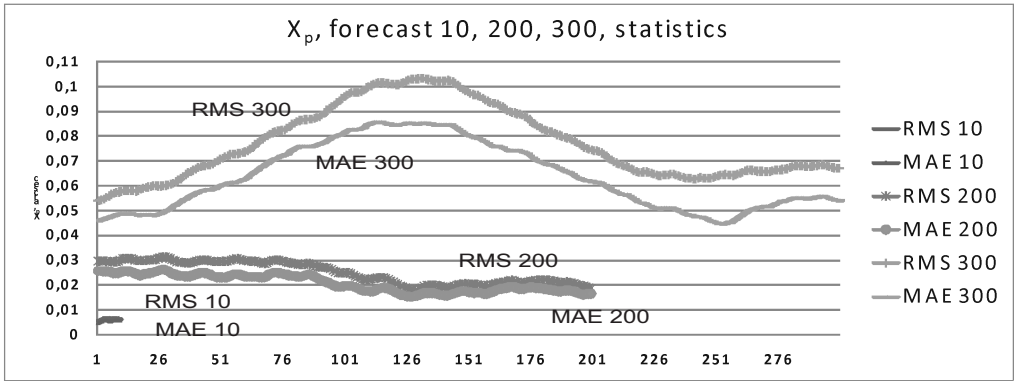

Figure 1: 10, 200, 300 day statistics for X_p forecast.

From our results we see that it was complicate drawn a conclusion about quality of our forecast. It is need more detailed statistics on greater sample.

However, we can say that 200 day forecast results are very interesting between 100 and 200 days if we compare with ((figure 2).

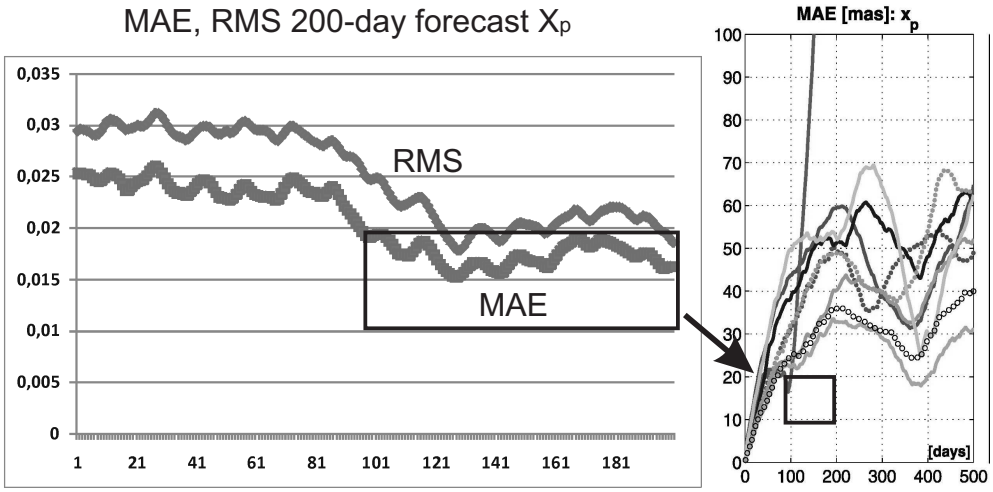

Figure 2: Example of our results as compared with those available at `http://www.cbk.waw.pl/EOP_PCC/.`

3. REFERENCES

Abarbanel H.D.I., Carroll T.A., Pecora L.M., Sidorowich J.J., Tsimring L.S., 1994, Predicting physical variables in time-delay embedding, Phys. Rev. E, V.49, N. 3, pp.1840–1853.

Ott E., Sauer T., Yorke J.A., 1994b, Coping with chaos: Analysis of chaotic data and the exploitation of chaotic systems, John Wiley and Sons, p. 432.

Parker, T. S., Chua, L. O., 1989, Practical Numerical Algorithms for Chaotic Systems, Springer, p. 348.

Rapp P.E., Schmah T.I., Mees A.I. Models of knowing and investigation of dynamical systems, 1999, Physica D 132, pp. 133–149.

Sauer T., Yorke J.A., Casdagli M. Embedology, 1991 J.Statist.Phys. v.65, N3/4, pp. 579–616.

Tribelsky M., Harada Y., Kuandykov Y., Makarenko N., 2002 Predictability of Market Prices, In Empirical Science of Financial Fluctuations: The Advent of Econo-physics, pp. 241-249.

http://www.cbk.waw.pl/EOP_PCC/

CONTRIBUTIONS OF THE THIRD DEGREE HARMONICS TO THE NUTATION OF TWO-LAYER AND THREE-LAYER EARTH MODELS

D. MIGUEL[1], J. GETINO[1], A. ESCAPA[2], J.M. FERRÁNDIZ[2]
[1] Dpto. Matemática Aplicada. Facultad de Ciencias
Universidad de Valladolid. E-47005. Valladolid. Spain
e-mail: davidmig@maf.uva.es
[2] Dpto. Matemática Aplicada. Escuela Politécnica Superior.
Universidad de Alicante. E-03080. Alicante. Spain

ABSTRACT. In this work, the contribution to the nutation due to the third degree spherical harmonics of the geopotential expansion is obtained within the framework of the Hamiltonian theory. To reach this goal, we extend previous works by Getino *et al.* (2001) on the basis of a three-layer Earth model described in Escapa *et al.* (2001). The main aim of this investigation is to evaluate the contribution of the solid inner core on these nutations, which are usually computed by considering a two-layer Earth model.

1. INTRODUCTION

Accurate knowledge of the Earth orientation is of great importance for studies in space navigation, geophysics and astronomy. In the last decade remarkable advances have taken place in the construction of theories that model the Earth rotational motion. In the present work, forced nutations have been obtained by considering a three-layer Earth model (Escapa *et al.* 2001) and following the Hamiltonian framework established by Getino & Ferrándiz developed to study the rotation of the non-rigid Earth (Getino & Ferrándiz 2001). Nutations are obtained by means of a generating function that is found as $W = \int H_{1Per} dt$, where H_{1Per} is the periodic part of H_1, which in this case coincides with the third order harmonics $V_3 = \sum_{m=0}^{3} V_{3m}$. This integral is performed along the solution of unperturbed part of the free problem. Nutations can be computed by taking into account that $m = 0$ corresponds to long period terms, $m = 1$ to diurnal, $m = 2$ to semi-diurnals and $m = 3$ to ter-diurnals respectively.

Neglecting second-order quantities, we have obtained the same values for Poisson terms as in Folgueira *et al.* (1998), where a rigid model was used. This agrees with the fact that motion of the angular momentum axis does not depend on the internal constitution of the Earth at the first order. Nutations of the figure plane are related to the Oppolzer terms which depend on the previous Earth model considered, the contributions are given by

$$\begin{aligned}
\Delta(\lambda_f - \lambda) &= \frac{k_{nm}}{M \sin I} \sum_{\tau=\pm 1} \sum_i \left[\Gamma_i^{(n,m,m-1)} \hat{F}_1^{a,m-1} + \Gamma_i^{(n,m,m+1)} F_1^{a,m+1} \right] \sin(\Phi_A^{n,m,m} - \rho_{nm}) \\
\Delta(I_f - I) &= \frac{k_{nm}}{M} \sum_{\tau=\pm 1} \sum_i \left[\Gamma_i^{(n,m,m-1)} \hat{F}_1^{a,m-1} - \Gamma_i^{(n,m,m+1)} F_1^{a,m+1} \right] \cos(\Phi_A^{n,m,m} - \rho_{nm})
\end{aligned} \tag{1}$$

where $\hat{F}_1^{a,m-1}$ and $F_1^{a,m+1}$ depend on the rheological properties of Earth and for a two layer Earth model they are obtained by equaling to zero all the parameters related to SIC. $\Gamma_i^{(n,m,q)}$ plays a similar role as the B_i, C_i and D_i for the second order harmonics. $\Phi_A^{n,m,m} = m(\nu + \mu) - \tau\Theta_i - (m - n)\frac{\pi}{2}$ a function of the Andoyer variables and the perturbing bodies. ρ_{nm} is a phase shift to refer the Andoyer variables to the Greenwich prime meridian and k_{nm} are related to the geopotential coefficients.

2. RESULTS

As it can be seen from Tables 1, 2 and 3, values corresponding to the two-layer Earth model do not not exceed, in absolute value, $1\mu as$ for the nutation in obliquity as compared to those of IERS, 2003. This fact can be viewed as a check of the validity of our computations, in spite of the different methods

employed.
On the other hand, the differences between the values of two-layer and three-layer Earth models are practically negligible, so for operative purposes these nutations terms can be worked out from the easier two layer Earth model. However, it should be mentioned that accordingly the values of the parameters, diurnal terms should be affected by the presence of the inner core, since in this case the normal mode corresponding to the inner core Chandler wobble lies in the diurnal band.

Table 1: **Long terms** (μas) $m = 0$

l_M	l_S	F	D	Ω	Nutation Period	Longitude [3-layer]	Longitude [3-layer]-[2-layer]	Obliquity [3-layer]	Obliquity [3-layer]-[2-layer]
-1	0	1	0	1	3231.49565	107.291	-0.533	90.581	0.211
-1	0	1	0	2	6159.13567	-37.018	0.053	-17.710	-0.019
-1	0	1	0	0	2190.35011	-33.303	-0.055	0.066	0.026
0	0	1	0	1	27.32158	-19.369	-0.019	15.100	-0.010
0	0	1	0	0	27.21222	-8.487	-0.065	-0.372	0.017

Table 2: **Diurnal terms** (μas) $m = 1$

l_M	l_S	F	D	Ω	Period of PM	Nutation Period	Longitude [3-layer] sin	Longitude [3-layer] cos	Longitude [3-layer]-[2-layer] sin	Longitude [3-layer]-[2-layer] cos	Obliquity [3-layer] sin	Obliquity [3-layer] cos	Obliquity [3-layer]-[2-layer] sin	Obliquity [3-layer]-[2-layer] cos
0	0	-1	0	0	1.03521	-27.21222	6.308	0.775	0.178	0.022	0.312	-2.542	0.009	-0.072
-1	0	1	0	0	0.99682	2190.35011	-6.248	-0.768	0.053	0.006	-0.306	2.487	0.003	-0.021
0	0	-1	0	-1	1.03505	-27.32158	41.097	5.048	1.161	0.143	1.940	-15.791	0.055	-0.446
-1	0	-1	0	-1	1.07545	-13.71879	3.680	0.452	0.104	0.013	0.168	-1.367	0.005	-0.039
1	0	-1	0	-1	0.99758	-3231.49565	29.412	3.613	0.719	0.088	1.434	-11.671	0.035	-0.285
-1	0	-1	2	-1	1.00243	-193.55971	2.031	0.249	0.056	0.007	0.099	-0.802	0.003	-0.022
0	0	-1	0	-2	1.03489	-27.43183	1.966	0.241	0.056	0.007	0.109	-0.887	0.003	-0.025
1	0	-1	0	-2	0.99743	-6159.13568	1.594	0.196	0.038	0.005	0.079	-0.639	0.002	-0.015
0	0	1	0	0	0.96201	27.21222	6.801	0.835	0.193	0.024	0.329	-2.676	0.009	-0.076
1	0	-1	0	0	0.99772	-2190.35011	4.472	0.549	0.112	0.014	0.219	-1.781	0.005	-0.045
0	0	1	0	1	0.96215	27.32158	43.131	5.298	1.227	0.151	2.102	-17.110	0.060	-0.487
1	0	1	0	1	0.92969	13.71879	3.305	0.406	0.094	0.012	0.161	-1.307	0.005	-0.037
-1	0	1	0	1	0.99696	3231.49565	-37.252	-4.576	-0.532	-0.065	-1.821	14.821	-0.026	0.212
1	0	1	-2	1	0.99216	193.55971	5.775	0.709	0.168	0.021	0.282	-2.297	0.008	-0.067
0	0	1	0	2	0.96229	27.43183	2.240	0.275	0.064	0.008	0.109	-0.890	0.003	-0.025
-1	0	1	0	2	0.99711	6159.13568	-1.814	-0.223	-0.036	-0.004	-0.089	0.722	-0.002	0.014
0	0	3	0	3	0.89884	9.10719	1.042	0.128	0.030	0.004	0.051	-0.414	0.001	-0.012

Table 3: **Semi and terci-diurnal terms** (μas) $m = 2$, $m = 3$

l_M	l_S	F	D	Ω	Period of PM	Nutation Period	Longitude [3-layer] sin	Longitude [3-layer] cos	Longitude [3-layer]-[2-layer] sin	Longitude [3-layer]-[2-layer] cos	Obliquity [3-layer] sin	Obliquity [3-layer] cos	Obliquity [3-layer]-[2-layer] sin	Obliquity [3-layer]-[2-layer] cos
0	0	-1	0	-1	0.50790	-27.32158	-0.254	-0.370	-0.007	-0.011	0.130	-0.089	0.004	-0.003
0	0	-3	0	-3	0.52752	-9.10719	-0.208	-0.304	-0.006	-0.009	-0.021	0.015	-0.001	0.000
-1	0	-3	0	-3	0.53781	-6.84486	-0.060	-0.087	-0.002	-0.002	-0.006	0.004	0.000	0.000
0	0	1	0	1	0.48970	27.32158	-0.079	-0.115	-0.002	-0.003	0.045	-0.031	0.001	-0.001
0	0	-1	0	-1	0.33652	-27.32158	-0.058	-0.113	-0.002	-0.003	-0.049	0.025	-0.001	0.001
0	0	-3	0	-3	0.34502	-9.10719	0.072	0.142	0.002	0.004	0.057	-0.029	0.002	-0.001

Acknowledgements. This work has been partially supported by Spanish projects I+D+I, AYA2004-07970 and AYA2007- 67546 and *Junta de Castilla y León* project VA070A07.

3. REFERENCES

Escapa, A., Getino, J. and Ferrándiz, J. M., 2001, J. Geophys. Res. (Solid Earth), 106, pp. 11387-11397.
Folgueira, M., Souchay, J. and Kinoshita, H., 1998, Celest. Mech. , 69, pp. 373–402.
Getino, J. and Ferrándiz, J.M., 2001, Mon. Not. R. Astron. Soc., 322, pp. 785–799.
Getino, J., Ferrándiz, J.M. and Escapa, A., 2001, A&A , 370, pp. 330–341.
IERS Conventions 2003, eds. McCarthy, D. D. and Petit, G., 2003, IERS Technical Notes 32.

COMPARISON OF REGIONAL HYDROLOGICAL EXCITATION OF POLAR MOTION DERIVED FROM HYDROLOGICAL MODELS AND THE GRACE GRAVITY FIELD DATA

J. NASTULA[1],B. KOLACZEK[1], D.A. SALSTEIN[2]
[1] Space Research Center of the PAS
Bartycka 18a, 00-716 Warsaw, Poland
e-mail:nastula@cbk.waw.pl
e-mail:kolaczek@cbk.waw.pl
[2]Atmospheric and Environmental Research, Inc.
Lexington, MA 02421, USA
e-mail: dsalstei@aer.com

EXTENDED SUMMARY

1. ANALYSES AND RESULTS

Global geophysical excitation functions of polar motion do not explain fully the observed polar motion as determined by geodetic techniques. The impact of continental hydrologic signals, from land water, snow, and ice, on polar motion excitation HAM (Hydrological Angular Momentum), is still inadequately estimated and not known so well as atmospheric and oceanic ones. Recently the GRACE (Gravity Recovery and Climate Experiment) satellite mission monitoring Earth's time variable gravity field has allowed us to determine global mass term of the polar motion excitation functions, which inherently includes the atmospheric, oceanic and hydrological portions. We use these terms to make comparisons with the mass term of the geodetic and geophysical excitation functions of polar motion on seasonal scales. Global GRACE excitation function of polar motion and hydrological excitation function of polar motion have been determined and were studied earlier (Nastula et al., 2008, Chen & Wilson, 2008, Brzezinski et al., 2008).

For comparison of regional hydrological excitation of polar motion derived from hydrological models and the GRACE gravity field, data variances and residuals of these data from polar motion excitations were computed.

The following models of the HAM were considered in these studies: CPC–LDAS (Fan et al., 2003), LaD (Milly & Shamkin, 2002), GLDAS (Rodell et al., 2004). Regional and global gravimetric excitation functions over land were computed from the GRACE data based on equivalent water thickness, determined by D. P. Chambers from the RL04 solution of data processed at the GeoforschungsZentrum (GFZ), Jet Propulsion Laboratory (JPL), and Center for Space Research (CSR and available at `http://grace.jpl.nasa.gov`. The $1^o \times 1^o$ grids are an implementation of the destriping of Chambers (2006) who calibrated his results against sea surface height corrected for climatological steric expansion and contraction.

Variances of the data of regional GRACE gravimetric excitation functions of the solutions mentioned were computed over the globe with high spatial resolution, at $1^o \times 1^o$ (64800 sectors). These variances reach maxima of the order of 3×10^{-4} (mas/sector) over Southeast and South Asia, the Amazon Basin of South America, the Southeast United States and areas north of the Mediterranean Sea.

Residuals of the variances between the GFZ and CSR solutions show good agreement. Differences between other GRACE solutions are greater, however, and reach a value of the order of $1.5 - 2.0 \times 10^{-4}$ (mas/sector) in the regions of maximum variance.

Variances of the regional hydrological excitation functions computed from the LaD, CPC and GLDAS models reach maximum values of 3×10^{-4} (mas/sector). These occur in similar regions as in earlier studies; however, in regions of Southeast Europe and West Siberia only the LaD model has strong maxima.

Residuals of variances between regional hydrological excitation functions computed from the LAD and the CPC models reach maximum values of 2×10^{-4} (mas/sector)in some regions. Such values appear in the residuals of LaD and GRACE hydrological excitation functions in some regions, indicating that they are likely connected with the LaD model. Residual variations computed as differences between variances

of the regional hydrological excitation functions of the CPC model and GFZ solution of the GRACE - RL04 gravimetric variances are smaller than others.

2. CONCLUSIONS

Variances of regional excitation functions of polar motion computed from the GRACE gravity fields and from the hydrological models show similar geographic patterns, reaching maximum values in the regions Southeast and South Asia, the Amazon Basin of South America, the Southeast United States and areas north of the Mediterranean Sea.

Residuals of the variances between the GFZ and CSR indicate good agreement between these series. Differences between other solutions are greater. Comparison of residuals between the variances of regional excitation functions of polar motion from LaD and from GRACE with the residuals between the variances of regional excitation functions of polar motion from CPC and GRACE shows that the CPC has better agreement with the GRACE data.

The GRACE regional excitation functions of polar motion have larger magnitudes than the regional hydrological excitation functions.

Acknowledgements. We acknowledge the support of Grant NNG04GF93G from US NASA's GRACE program and National Science Foundation Grant ATM-0429975 and of Grants N526 037 32/3972 and N526140735 from the Polish Ministry of Science and Higher Education. We thank Mr. M. Sawicki for preparation of the graphics of the poster.

3. REFERENCES

Brzeziński, A., Nastula, J., Kolaczek, B., 2008, "Seasonal excitation of Earth rotation estimated from recent geophysical models and observations", Presented at ETS 2008 New Challenges in Earths Dynamics, Jena, Germany.

Chambers, D.P., 2006, "Evaluation of New GRACE Time-Variable Gravity Data over the Ocean", Geophys. Res. Lett., 33(17), LI7603.

Chen, J.L, Wilson, C.R., 2008, "Low degree gravity changes from GRACE, Earth rotation , geophysical models and satellite laser ranging", Journal of Geophysical Research, vol. 13, B06402, doi: 10.1029/2007JB005397.

Fan, Y., van den Doll, H., Mitchel, K., Lohmann, D., 2003, "A 51-year reanalysis of the US land-surface hydrology", GEWEX News, 13(2), pp.6, 10.

Milly, P.C.D., Shmakin, A.B., 2002, "Global modeling of land water and energy balances, Part I: The Land Dynamics (LaD) model", Journal of Hydrometeorology, v. 3, no.3, p. 283-299.

Nastula, J., Kolaczek B., Salstein, D.A., 2008, "Regional Differences of hydrological excitation of polar motion computed from hydrological models and from the GRACE gravity field data", Presented at EGU General Assembly, Vienna, Austria.

Rodell, M., Houser, P.R., Jambor, U., Gottschalck, J., Mitchell, K., Meng, C.J., Arsenault, K., Cosgrove, B., Radakovich, J., Bosilovich, M., Entin, J. K., Walker, J.P., Lohmann, D. Toll, D., 2004, "The Global Land Data Assimilation System", Bull. Amer. Meteor. Soc., 85 (3), 381-394.

REGIONAL SEA LEVEL PREDICTION AND ITS RELATION TO EL NIÑO/SOUTHERN OSCILLATION

T. NIEDZIELSKI[1,2], W. KOSEK[1]
[1] Space Research Centre, Polish Academy of Sciences
Bartycka 18A, 00-716 Warsaw, Poland
e-mail: niedzielski@cbk.waw.pl (T. Niedzielski), kosek@cbk.waw.pl (W. Kosek)
[2]Institute of Geography and Regional Development, University of Wrocław
pl. Uniwersytecki 1, 50-137 Wrocław, Poland

ABSTRACT. The study focuses on forecasting sea level anomaly (SLA) data (the entire data span is 1993-2002) in the rectangular area: 20 S - 20 N, 70 W - 130 W covering the equatorial sections of west coasts of South, Middle, and North America. First, the polynomial-harmonic least-squares model (LS) consisted of annual, semiannual oscillations and the linear trend was extrapolated. Second, the above-mentioned extrapolation was combined with the autoregressive prediction (LS+AR) of stochastic SLA residuals. The second approach leads to more accurate SLA data predictions, both in ENSO conditions and in normal conditions. The LS+AR technique reveals the root mean square errors (RMSEs) of regional SLA 1-month predictions to be approx. three times smaller than the maximum amplitudes of the signal (El Niño 1997/1998 validation period). For La Niña 1998/1999, the 1-month RMSEs determined by the LS+AR technique are four times smaller than the amplitudes of the signal obtained from maximum amplitudes of the annual and semiannual cycles. In normal conditions, the corresponding ratio is of 1/6.

1. INTRODUCTION

The problems related to sea level fluctuations are in the scope of Global Geodetic Observing System (GGOS) project. The essential and highly unpredictable reason of regional sea level change in the equatorial Pacific is El Niño/Southern Osciallation (ENSO). El Niño event causes an increase in sea level in the vicinity of the east equatorial Pacific, whereas La Niña phenomenon leads to the decrease of the sea level in this region. The sea level may rise in the east equatorial Pacific even several tens of centimeters. For instance, the dynamic sea level change expressed by the sea level anomaly (SLA) recorded by TOPEX/Poseidon (T/P) altimetric satellite is shown to be of approx. 40 cm during El Niño 1997/1998. Thus, the predictions of SLA time series may be applied to forecast the ENSO signal.

The SLA gridded time series obtained from TOPEX/Poseidon and Jason-1 satelite altimetry provides the insight into the large-scale ocean circulation. Kosek (2001) detected several oscillations in SLA data with periods of 365 days, 183 days, 120 days, 90 days, 62 days, 37 days, and 30 days. The maxima of amplitudes corresponding to those oscillations may cause that - theoretically - the maximum amplitudes of entire SLA signal may be very high, especially during El Niño. Niedzielski & Kosek (2008) predicted the SLA time series in the east equatorial Pacific and discussed the accuracy of the predictions in respect to the maximum amplitudes of annual and semiannual terms. In this article, we discuss the results obtained by Niedzielski & Kosek (2008).

2. RESULTS

The SLA time series covering the area of the east equatorial Pacific (20 S - 20 N, 70 W - 130 W) and the period 1993-2003 were examined. The temporal resolution of these data is 9.9140625 days and the spatial resolution if of $1^o \times 1^o$.

The two prediction techniques were applied. First, the extrapolation of the polynomial-harmonic least-squares model (LS method) was utilized. This model was used to capture the annual and semiannual oscillations, and the linear inclining trend. Second, we combined the above mentioned extrapolation and the autoregressive prediction of SLA residuals (LS+AR method). The residuals, however, were computed as the difference between the data itself and the LS model. The accuracy of forecasts was evaluated by means of the root mean square error (RMSE) of predictions.

These two methods were used to determine the 1-month SLA predictions in the east equatorial Pacific. Three experiments were planned, i.e. forecasting SLA during El Niño 1997/1998, during La Niña 1998/1999, and during normal conditions. The T/P cycles which respectively correspond to these events are the following: 163-213, 213-263, 285-335. For instance, during El Niño 1997/1998 the maxima of amplitudes of the SLA oscillations in the considered region were of approximately 20 cm and 14 cm, for the annual and semiannual terms, respectively.

In the first experiment (Niño 1997/1998), the RMSE values of 1-month SLA predictions computed by the LS technique for the east equatorial Pacific reached even 19 cm in the vicinity of the Equator. The application of the LS+AR technique allowed us to reduce the prediction errors during El Niño 1997/1998, i.e. the RMSE values were smaller than 12 cm. Hence, the LS+AR method decreased the prediction errors due to the autoregressive modelling of the stochastic component of the signal.

In the second experiment (La Niña 1998/1999), the RMSE values of the 1-month forecasts obtained by the LS technique were smaller than 14 cm. The reduction of the prediction errors (LS vs. LS+AR techniques) was also noticed in the case of La Niña 1998/1999. Indeed, the RMSE values were not higher than 6 cm.

In the third experiment (normal conditions), for the LS-based predictions the maximum RMSE inaccuracy was smaller than 6 cm. The predictions determined by means of the LS+AR technique were more accurate, i.e. RMSE values were found to be smaller than 4 cm in the Pacific.

The overall satisfactory performance of the LS+AR method is enhanced by the comparison between the RMSE values and the maximum amplitudes of the most energetic annual and semiannual oscillations. In what follows, the ratios between the RMSE values and the sums of the two maxima (of annual and semiannual terms) justify a good performance of the LS+AR prediction approach (see conclusions).

3. CONCLUSIONS

The LS+AR technique was applied to predict SLA in the east equatorial Pacific. The performance of the method is acceptable, particulary in respect to the maximum amplitudes of the signal. Indeed, the LS+AR technique leads to the RMSE values of regional SLA 1-month predictions to be approx. three times smaller than the maximum amplitudes of the signal (El Niño 1997/1998 validation period). For La Niña 1998/1999, the RMSE values determined by the LS+AR technique were four times smaller than the amplitudes of the signal obtained from maximum amplitudes of the annual and semiannual cycles. In normal conditions, this ratio was of 1/6.

Acknowledgements. The research is supported by the Polish Ministry of Education and Science under the project No 4 T12E 039 29. Tomasz Niedzielski is supported by the Foundation for Polish Science within the Start Program (stipends for young researchers) and by the European Union within the Marie-Curie Actions. The authors thank the Center for Space Research, University of Texas at Austin, USA for providing the T/P and J-1 data. The authors of R 2.0.1., a Language and Environment 2004 and the additional packages are acknowledged. Wiesław Kosek are supported by the organizers of the Journées 2008 "Systèmes de référence spatio-temporels" and X. Lohrmann-Kolloquium, September 2008, Dresden, Germany.

4. REFERENCES

Kosek, W., 2001, Long-term and short period global sea level changes from TOPEX/Poseidon altimetry, Artif. Satell. 36, pp. 71-84.

Niedzielski, T., Kosek, W., 2008, Forecasting sea level anomalies from TOPEX/Poseidon and Jason-1 satellite altimetry, Journal of Geodesy, doi: 10.1007/s00190-008-0254-5.

DETECTION OF TIME-FREQUENCY RELATIONS BETWEEN GEODETIC AND GEOPHYSICAL EXCITATION FUNCTIONS OF POLAR MOTION

A. RZESZÓTKO[1], W. KOSEK[1], W. POPIŃSKI[2]
[1] Space Research Centre, Polish Academy of Sciences, Warsaw, Poland
[2] Central Statistical Office, Warsaw, Poland
e-mail: alicja@cbk.waw.pl

1. INTRODUCTION AND DATA

The redistribution of mass in the atmosphere, oceans and hydrology and the changes of the wind and ocean currents velocities are important sources of polar motion excitation. Relations between the geodetic excitation function and the effective angular momentum functions of the atmosphere, oceans and hydrology are examined in the time-frequency domain by means of coherence and phase synchronization. Coherence may be interpreted as a correlation coefficient between oscillations with the same frequencies present in two time series whereas phase synchronization allow to investigate the phase agreement between these oscillations.

The following data sets were used in the analysis: 1) equatorial component χ^{GEOD} of geodetic excitation function, 2) equatorial component χ^{AAM} of effective angular momentum function of the atmosphere from aam.ncep.reanalysis.*, 3) equatorial component χ^{OAM} of effective angular momentum function of the ocean from c20010701.oam and ECCO_kf049f.oam, 4) equatorial component $\chi^{\mathrm{HAM\ (NCEP)}}$ of effective angular momentum function of the hydrology from chi_ncep_water_*, 5) equatorial component $\chi^{\mathrm{HAM\ (ECMWF)}}$ of effective angular momentum function of the hydrology obtained by numerical integration of the water storage data from water_ECMWF_*.nc.

2. ANALYSIS, RESULTS AND CONCLUSIONS

Intuitive generalisation of correlation coefficient between two time series $x(t')$ and $y(t')$ is a correlation coefficient between their wavelet transform coefficients $X(t,T_0)$ and $Y(t,T_0)$ for a given value of period T_0. The absolute value of the generalised correlation coefficient is called wavelet coherence and is given by the formula:

$$\gamma_{x,y}(T_0) = \frac{|\sum_{t=1}^{N} X(t,T_0)\overline{Y(t,T_0)}|}{\sqrt{\sum_{t=1}^{N}|X(t,T_0)|^2 \sum_{t=1}^{N}|Y(t,T_0)|^2}}. \quad (1)$$

Phase agreement of the oscillations can be investigated by dividing the wavelet transform coefficients by their moduli and then calculating the coherence. The corresponding function is called phase synchronization and is given by the formula:

$$\gamma^{\phi}_{x,y}(T_0) = \frac{1}{N}\left|\sum_{t=1}^{N} \frac{X(t,T_0)\overline{Y(t,T_0)}}{|X(t,T_0)||Y(t,T_0)|}\right|. \quad (2)$$

Spectro-temporal coherence $\kappa_{x,y}(t,T_0)$ and phase synchronization $\kappa^{\phi}_{x,y}(t,T_0)$ (not shown in this paper) can be obtained by replacing correlation coefficients by running correlation coefficients.

The greatest coherence and phase synchronization occur between χ^{GEOD} and χ^{AAM} as well as between χ^{GEOD} and χ^{OAM}. Coherence and phase synchronization between χ^{GEOD} and $\chi^{HAM(NCEP)}$ and between χ^{GEOD} and $\chi^{HAM(ECMWF)}$ are similar and significant only for the annual and semiannual oscillations. Phase synchronization between χ^{GEOD} and χ^{AAM} (χ^{OAM}) is smaller than coherence between them. It shows that the variable phases of the high frequency oscillations in χ^{GEOD} and χ^{AAM} (χ^{OAM}) can not explain the observed coherence between them which is caused also by variable amplitudes of these oscillations. Coherence and phase synchronization between χ^{GEOD} and $\chi^{AAM}+\chi^{OAM}$ are greater than the coherence between χ^{GEOD} and χ^{AAM}. Adding $\chi^{HAM(NCEP)}$ or $\chi^{HAM(ECMWF)}$ to $\chi^{AAM}+\chi^{OAM}$ causes the increase or the decrease of coherence and phase synchronization depending of the frequency and polarisation of the oscillations being compared.

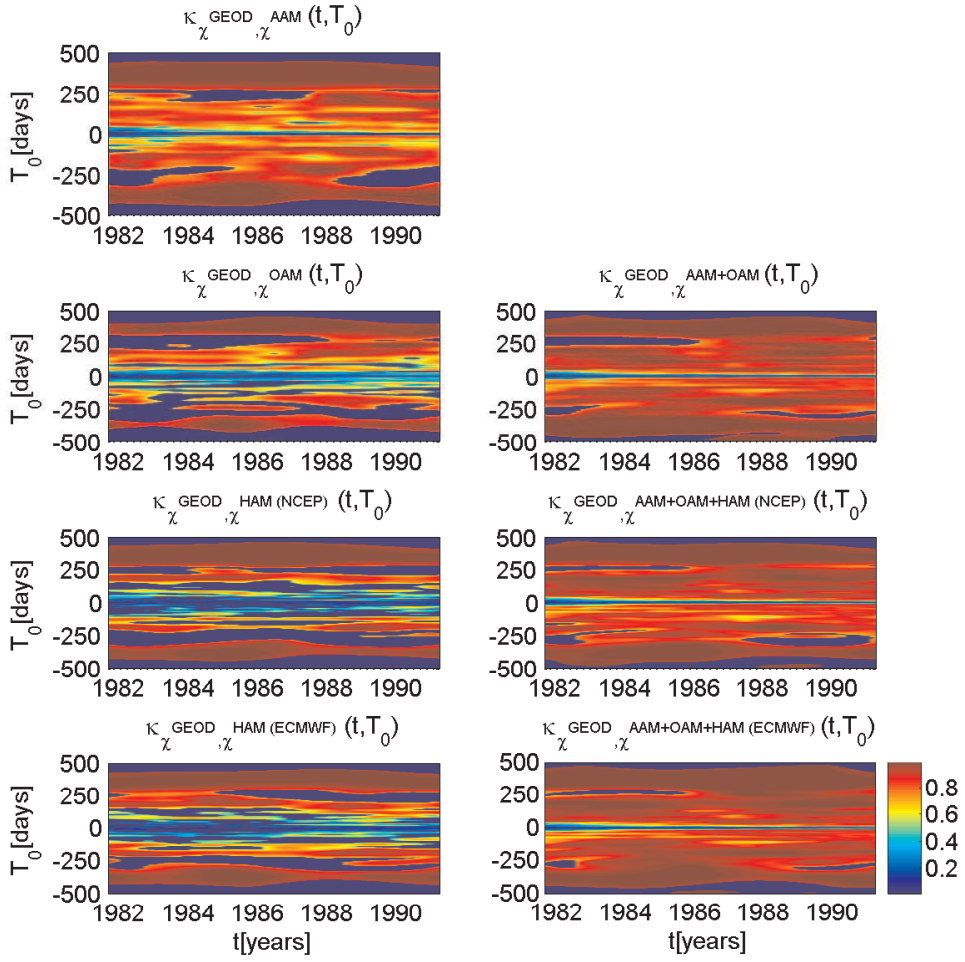

Figure 1: Spectro-temporal coherence between the equatorial component of geodetic excitation function and the equatorial components of geophysical excitation functions (letf) as well as their sums (right).

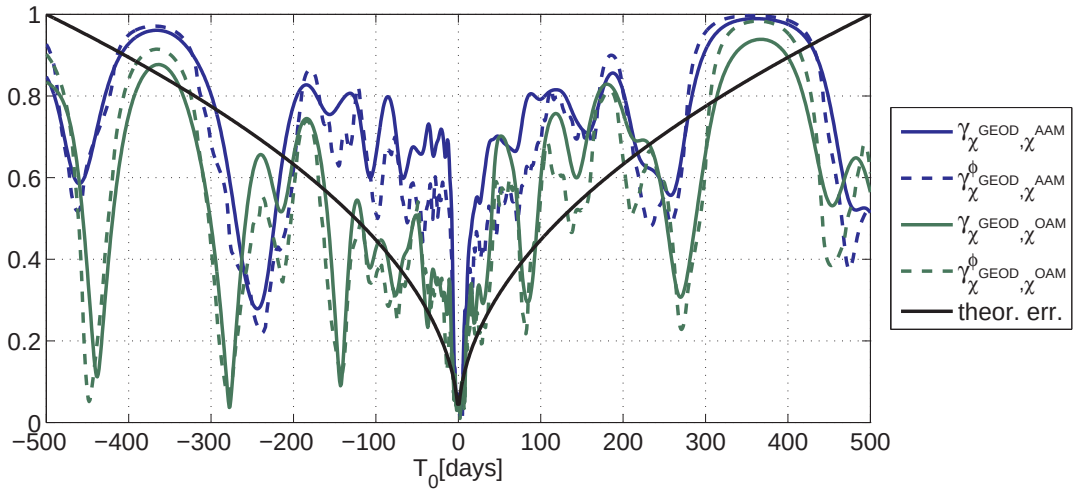

Figure 2: Coherence (solid line) and phase synchronization (dashed line) between the equatorial component of geodetic excitation function and the equatorial components of the effective angular momentum of the atmosphere (blue) and ocean (green).

HYDROLOGICAL EXCITATION OF POLAR MOTION

L. SEOANE[1], J. NASTULA[2], C. BIZOUARD[1], D. GAMBIS[1]
[1] SYRTE, Observatoire de Paris, CNRS, UPMC
61 avenue de l'Observatoire, 75014 Paris, France
e-mail: lucia.seoane@obspm.fr
[2] Space Research Center
Bartycka 18a, 00-716 Warsaw, Poland

ABSTRACT. First harmonics of the gravity field (C_{21} and S_{21}), derived from the Gravity Recovery and Climate Experiment (GRACE), and processed at different institutes, are used to determine the hydrological equatorial excitation function of polar motion. For that purpose time-variable gravity field solutions are made tidal free and free from modelled non-tidal atmospheric and oceanic effects. The residuals reflect unmodelled variations like hydrological processes, snow cover, post-glacial rebound or possibly earthquakes. They are compared to the hydrological excitation computed from hydrological models. They are also compared to the residual geodetic excitation after removing the atmospheric and oceanic effects. We find that seasonal variations of the excitation computed from gravimetric data and geodetic residuals are in good agreement. Annual signal is not well represented by hydrological models. All series show common biennial oscillations with periods of nearly 1.7 and 2.6 years.

1. INTRODUCTION

The excitation of polar motion is to a large extent related to the mass redistribution of geophysical fluids. The importance of atmospheric and oceanic signals at monthly and seasonal periods are well known. The role of the continental hydrology, originated from land water, snow, and ice, is however less known. It is possible to estimate the hydrological excitation from global models. The hydrological part of polar motion excitation, can also be obtained, as a residual series, by removing atmospheric and oceanic signals from the mass term of the geodetically determined excitation of polar motion. It is accepted that the change in continental water storage plays a major role in the seasonal polar motion. However, the models do not agree among themselves and with the observed polar motion. This is mainly due to the lack of global measurements of related hydrological parameters. Thanks to the Gravity Recovery and Climate Experiment (GRACE) mission, the mass redistribution is determined over the period February 2003 to December 2007. Data are tide free and non-tidal atmospheric and oceanic effects have been taken into account in the processing of the data. It means that gravity field solution is mostly of hydrological nature. This allows to compare "gravimetric"-based excitation to the existing hydrological models, differences being possibly due to other Earth phenomena, for example, earthquakes.

2. METHODOLOGY

The determination of the GRACE satellites data is provided by four centres: Center for Space Research (CSR), GeoForschungsZentrum (GFZ), Jet Propulsion Laboratory (JPL) and Groupe de Recherche de Géodésie Spatiale (GRGS). Polar motion excitation is deduced from the relation between the C_{21} and S_{21} coefficients and off-diagonal inertia moments of the Earth in the terrestrial frame. We have used Chen et al. (2003) formulation for computing excitation from GRACE solutions. Time series of C_{21} and S_{21} are tide free and also corrected from non tidal atmospheric and oceanic signals. The International Earth rotation and Reference systems Service provides combined time series of the Earth Orientation Parameters at daily interval, in particular the pole coordinates x and y, which allows us to compute the "geodetic" polar motion excitation according to $G = \chi_1 + i\chi_2 = p + i\frac{\dot{p}}{\sigma_c}$. Where $p = x - iy$ is the complex pole coordinate and σ_c is the Chandler frequency. Hydrological variations are obtained after removing atmospheric and oceanic signals from geodetic excitation (G-A-O: geodetic - atmospheric - oceanic excitations). We use the atmospheric excitation functions of the NCEP/NCAR reanalysis and oceanic excitation from ECCO. On the other hand latitude-longitude grids providing the charge

	CSR	GFZ	JPL	GRGS	CPC	GLDAS
χ_1 G-A-O	0.54	0.14	0.66	0.23	0.57	0.25
χ_2 G-A-O	0.39	0.49	0.39	0.38	0.63	0.56

Table 1: Correlation coefficients between the residual geodetic observations and the excitation from hydrological models or from gravimetric data.

of continental water by surface unit at monthly intervals are available for the period 2003-2008. By integrating the grids of the Climate Prediction Center (CPC) and Global Land Assimilation System (GLDAS) hydrological models we have reconstituted the hydrological excitation function reduced to its mass term. Time series of the CSR, GFZ and JPL solutions present common sampling of about 30 days, but the GRGS solution is given at approximately 10-day intervals. On the other hand our geodetic excitation function presents variations up to 2 days. Applying Vondrák smoothing, which transmits 95% of the signal at 121 days, we make GRGS, geodetic series and modelled mass excitation spectrally consistent with the CSR, GFZ and JPL solutions. All those solutions are then interpolated at common dates, i.e. at 30 day intervals.

3. RESULTS

In Table 1 we note that CPC leads to the highest correlation for geodetic excitation. The gravimetric-based excitation functions derived from CSR and JPL are also significantly correlated with observations. Hydrological model GLDAS and gravimetric excitation from GFZ and GRGS are poorly correlated with geodetic observations in χ_1. The annual and semi-annual variations of hydrological modelled excitations, gravimetric-based excitations and residual geodetic excitation are show in Tab. 2. The annual signals are the most significant and the semi-annual oscillation is generally determined at the level of their significance. Annual variations of the excitation computed from gravimetric data and geodetic residuals are in agreement, especially for CSR and JPL. But there are phase discrepancies for the annual signal of χ_2. The annual signal amplitude is not well represented by hydrological models. Concerning interannual variations (larger than 1 year), a spectral analysis of all series show common biennial oscillations except for CPC hydrology model. They have a period of nearly 2.6 years possibly corresponding to Amazon and Mississippi water storage variations (Schmidt et al. 2007). We also find an oscillation with a period of 1.7 year period. Further study is required.

	χ_1				χ_2			
	Annual		Semiannual		Annual		Semiannual	
	Amplitude mas	phase degree	Amplitude mas	phase degree	Amplitude mas	phase degree	Amplitude mas	phase degree
G-A-O	7.8 ± 1.3	66.7 ± 9.7	1.2 ± 1.4	129.0 ± 66.7	8.5 ± 1.6	72.4 ± 11.1	3.8 ± 1.3	1.8 ± 20.2
CPC	3.6 ± 0.4	89.6 ± 6.8	1.1 ± 0.6	330.1 ± 28.5	13.4 ± 1.0	70.9 ± 4.2	2.1 ± 1.0	298.4 ± 27.5
GLDAS	2.4 ± 0.6	137.6 ± 15.3	1.0 ± 0.6	340.1 ± 33.6	2.4 ± 0.8	93.7 ± 19.3	1.8 ± 1.0	319.9 ± 32.5
CSR	5.7 ± 2.5	71.9 ± 25.4	3.5 ± 2.8	148.2 ± 44.6	8.7 ± 2.1	4.8 ± 13.6	2.7 ± 2.5	340.1 ± 51.8
GFZ	2.6 ± 2.0	20.1 ± 44.0	2.6 ± 2.1	206.6 ± 46.3	8.7 ± 1.8	3.2 ± 11.7	4.1 ± 2.3	336.2 ± 31.5
JPL	8.6 ± 1.2	87.7 ± 7.9	2.7 ± 1.2	86.9 ± 25.3	6.1 ± 1.3	23.9 ± 11.7	3.1 ± 1.3	300.9 ± 24.6
GRGS	5.5 ± 2.9	16.2 ± 29.0	1.9 ± 2.6	261.0 ± 80.1	15.8 ± 2.2	1.9 ± 7.9	1.7 ± 2.4	277.8 ± 80.1

Table 2: Annual and semiannual variations of hydrological excitations functions

4. REFERENCES

Chen, J.L., Wilson, C.R., 2003. Low degree gravitational changes from Earth rotation and geophysical models, Geophys. Res. Lett., 30(24), 2257, doi:10.129/2003GL018688.

Schmidt, R., Petrovic, S, Güntner, A., Wünsch, J., Barthelmes, F., Kusche, J., 2007, Estimating periodic components of water stock changes from GRACE and global hydrology models. 2007 GSTM Symposium.

Session 4

OBSERVATIONS OF GLOBAL GEODYNAMICS

OBSERVATIONS GÉODYNAMIQUES GLOBALES

COMBINATION OF EOP FROM DIFFERENT TECHNIQUES

Ch. BIZOUARD, D. GAMBIS, O. BECKER, J.-Y. RICHARD
SYRTE, Observatoire de Paris, CNRS, UPMC
61, Av. de l'Observatoire, 75014 Paris FRANCE
e-mail: christian.bizouard@obspm.fr

ABSTRACT. We describe the state of the art of the combination of the Earth Orientation Parameters at Paris Observatory/IERS Earth Orientation Centre. We sum up the characteristics of the classical C04 combination. After the algorithm's description, we try to assess its accuracy by comparison with other EOP series. Then the multi-technique combination "GINS-DYNAMO" is presented. We assess its capability to contribute to C04 in the future and its performances for high frequencies determination of the Earth Orientation.

1. INTRODUCTION

The Earth Orientation Parameters (EOP) describe the irregularities of the Earth rotation with respect to a non-rotating reference frame. Two parameters (dPsi, dEps), the celestial pole offsets, correct the precession-nutation model of the celestial pole, one parameter (UT1-UTC) gives the irregularities of the rotation angle, and the two last one (x,y) describe the polar motion with respect to the crust. They give the full transformation between the International Terrestrial Reference Frame (ITRF) and the International Celestial Reference Frame (ICRF). The reference EOP series computed at the Earth Orientation Centre at Paris Observatory is obtained from the combination of "operational" EOP series derived from the various astro-geodetic techniques : Laser Ranging to the Moon (LLR) and to dedicated artificial satellites (SLR), Very Long Baseline Interferometry on extra-galactic sources (VLBI) and more recently from Global Positioning System (GPS) and Doppler Orbitography by Radio-positioning Integrated on Satellite (DORIS) (Gambis, 2004). The objective of this paper is threefold : 1) present the C04 combination procedure and the recent improvements brought in the software code; 2) present the new EOP C04 solution, its accuracy, and how it is made consistent with ITRF 2005; 3) present multi-technique combination implemented recently at Paris Observatory and the way it could contribute to the future C04 combination.

2. DESCRIPTION OF THE PROCEDURE

Step 1 : Selection of a set of operational series. In the past, EOP combined series were based on individual solutions derived by the analysis centres for the different techniques. Nowadays, Technique Centres, i.e. IVS, ILRS, IGS and IDS are deriving combined solutions based on analysis centres which are used in our combinations. In some cases of inaccuracy or instability of some specific series, individual series have been privileged as long as problems have not been solved. This was the case for the IVS combined solution for UT1 and nutation offsets which were initially not used on contrary to individual VLBI series. The IVS solution is now currently used since it is based on SINEX combinations. Table 1 gives the list of the contributed series relatively to the EOP components used as of 1 January 2009.

Step 2 - Computation of the differences between operational and intermediate reference series. We do not directly combine the values of the series. The more these values will present large variations, the larger will be the errors introduced in the successive steps: interpolation, filtering in addition to any instability in the numerical computations. Therefore, we preliminary remove a known reference containing most of the signal, from the operational EOP series. This reference is nothing else that the former combined solution previously obtained and extended by preliminary values extrapolated by predictions. To achieve this, the reference series is interpolated at each date of the operational series applying a Lagrange interpolation over 4 points. The difference between operational series and reference series is then computed. The combinations are applied on these differences. Let us remind, by the way, that the combined C04 solution is so far given at one-day intervals and does not contain any

EOP	x, y, LOD	$UT1$	dX, dY
	EOP (IGS) 07 P 01	EOP (IVS) 07 R 01	EOP (IVS) 07 R 01
	EOP (IGS) 96 P 02	intensive VLBI solutions	Individual standard
	EOP (IVS) 07 R 01	UT(GPS)	VLBI solutions
	EOP (ILRS) 05 L 01		

Table 1: Table 1 - EOP series currently used in the combination as of 1 January 2009

diurnal/sub-diurnal information due to ocean tides. Concerning the offsets of nutation, the parameters of the reference series are dPsi and dEps referred to IAU 2000 precession-nutation model. Therefore all operational celestial pole offsets are transformed into (dX, dY)/IAU 2000, before constituting the difference.

Step 3 - UT1 and LOD computation. VLBI is unique technique in its ability to make accurate measurements of Universal Time in a quasi-inertial frame realized through extragalactic sources coordinates. On the other hand, the celestial frame realized through satellite techniques like SLR and GPS are linked on orbits and is not accurate for UT1 determination. Still, on time scales limited to a couple of weeks, errors in the orbit are limited so that the high-frequency signal contained in the GPS UT determination can be used for densification of UT1 derived by VLBI (Gambis et al, 1993). High frequency GPS LOD estimates calibrated by VLBI are thus integrated in the combined 05C04 solution as a separate series. This additional contribution is of main importance when intensive VLBI are missing, what happens from time to time over several days and as well when estimates obtained from intensive sessions are erroneous (sometimes larger than 100 microseconds). An alternative approach which is now successfully applied is based on the simultaneous combination of UT1 and its rate LOD using a method of combined smoothing (Vondrák & Cepek, 2000). As a control to test the impact of the GPS LOD estimates, a separate analysis was made. Combinations have been compared to an independent time series of atmospheric excitations of the Earth's axial angular momentum variations.

Step 4 - Sorting by increasing dates. For each EOP, the whole set of values of the different series are sorted by chronological dates.

Step 5 - Running average. Data are averaged over successive time intervals of 0.5 day. By using Lagrange interpolation we propagate the observed values to the averaged date. The average is weighted by the formal errors of the observed values. The averaged error or weight is also calculated.

Step 6 - Weighting change. EOP estimated for the combinations are available with associated formal errors. These errors are issued from analyses based for instance on least square or Kalman processes. They are thus reflecting internal precisions and consequently are usually not realistic. Most of the time, they are optimistic (better than real). Still, the combination process requires an estimation of the real accuracy (or inaccuracy). This can be achieved by rescaling the formal uncertainties using an external procedure. The community of Time and frequency uses a variety of stability metrics in order to characterize frequency standards, clocks and oscillators. Allan variance (Gray & Allan, 1974) is currently used for estimation of the stability of primary frequency standards. It is also applied in the time domain for characterization of the stability of atomic time scales. More recently, the Allan variance analysis was applied to the field of earth orientation metrology (Gambis, 2002). Considering three or more time series of similar quality and time resolution, the noise of each series can be evaluated, provided that their errors are assumed to be statistically independent. It means that there is no correlation between these series (the covariance is equal to zero). Tests concerning the various analyses we made (not in the present note) are sustaining this hypothesis. This procedure provides an estimation of a scaling factor of the formal error on which the weighting of the combined individual results is based.

Step 7 - High frequency filtering. Vondrák smoothing (Vondrák & Cepek, 2000) is applied in order to remove high frequency variations. Characteristics of the smoothing, according to the epoch of the solution, are reported in Table 2. It is remarkable that nowadays in view of the accuracy reached by the EOP the smoothing is extremely weak.

Time interval		x,y	UT1	LOD	dPsi, dEps
1984-1993	Smoothing coefficient	10^2	$10^{0.7}$		$10^{0.5}$
	1% remaining amplitude	2.9 d	4.8 d		5.2 d
	99% remaining amplitude	6.2 d	10.3 d		11.2 d
1994-1999	Smoothing coefficient	10^5	10^2	10^2	$10^{0.5}$
	1% remaining amplitude	0.92 d	1.3 d	1.3 d	2.4 d
	99% remaining amplitude	2 d	6.3 d	6.3 d	11.2 d
2000-2008	Smoothing coefficient	10^5	10^5	10^3	$10^{0.5}$
	1% remaining amplitude	0.92 d	0.92 d	2 d	2.4 d
	99% remaining amplitude	2 d	2 d	4.3 d	11.2 d

Table 2: Characteristics of the smoothing coefficient (Vondrak, 1977) adopted for EOP (IERS) 05C 04. Specific percentage of the signal relatively to 1% and 99% remaining amplitude are given.

Step 8 - Interpolation. The filtered series are interpolated at 1 day intervals using a Lagrange polynomial on four points. This step is extremely critical to avoid to deteriorate the accuracy of the estimates.

Step 9 - Adding back the intermediate series. The final values are obtained by adding to the filtered and interpolated values the "intermediate" reference series, which was removed in step 2 as well as the removed models (zonal tides on UT1-TAI/LOD, precession-nutation offsets).

Step 10 - Archiving in the database. The final 05C04 is archived in the ORACLE database and made available to users via ftp/web processes.

3. RESET OF THE C04 COMBINED SOLUTION IN THE ITRF REFERENCE FRAME.

One of the main tasks of the Earth Orientation Centre is to produce EOP consistent with both the International Celestial Reference Frame (ICRF) and the International Terrestrial Reference Frame (ITRF). The operational series are not perfectly aligned with the ITRF and ICRF since they are referred to different terrestrial and celestial systems, realized by the Analysis Centres. This inconsistency of the EOP series with respect to the ITRF and ICRF produce systematic shift between series (Zhu & Mueller, 1983). Due to the separate determination of both celestial and terrestrial reference frames and EOP, there had been a slow degradation with time of the overall consistency. For instance, for pole components, in the late 2005, discrepancies at the level of 300 micro-arc-seconds were present between the current IERS C04 and the ITRF realization. This was solved in the new solution by re-aligning the C04 on the system linked to the newly issued ITRF2005 (Altamimi et al., 2007). Historically, for the first time, the ITRF2005 input data were time series solutions, provided in a weekly production by the IAG International Services of satellite techniques (the International GNSS Service, IGS, the International Laser Ranging Service, ILRS and the International Doris Service, IDS) and in a daily (VLBI session-wise) basis by the International VLBI Service, IVS. Each intra-technique time series is indeed a weekly combination of the individual Analysis Centre (AC) solutions of the technique, except for DORIS for which two individual analysis centre time series were submitted for the ITRF2005 computation. Local tie vectors at about 87 sites were used in the ITRF2005 combination allowing the connection between the four techniques. The ITRF2005 is composed of 608 stations located at 338 sites, with an imbalanced distribution between the northern (268 sites) and the southern hemisphere (70 sites). The 05C04 series is supposed to be consistent with the current IRTF as well as ICRF realization. Therefore, before the process of combination of EOP, all series have to be translated into the system consistent with ITRF. For this purpose, we assume that some specific series are already consistent with ITRF and ICRF:

- The celestial pole offsets (UT1, dPsi, dEps) provided by the IVS are consistent with the ICRF from 1984 to 2006.
- The polar motion components associated with the ITRF 2005 solution gives the direction of the CIP in the ITRF without any linear trend since 1993.

The trends between ITRF/ICRF consistent series and operational series are not perfectly linear over several years, and we have to model them as broken lines, i.e. as consecutive linear trends using a Least

EOP	Time interval	Reference Series
UT1/ dX / dY	1984-1993	IVS combined solution
	1994-2008	id
x,y	1984-1993	Former C04 solution
	1994-2007	EOP ITRF 2005 (IGN)

Table 3: Reference series used according the epoch of the solution.

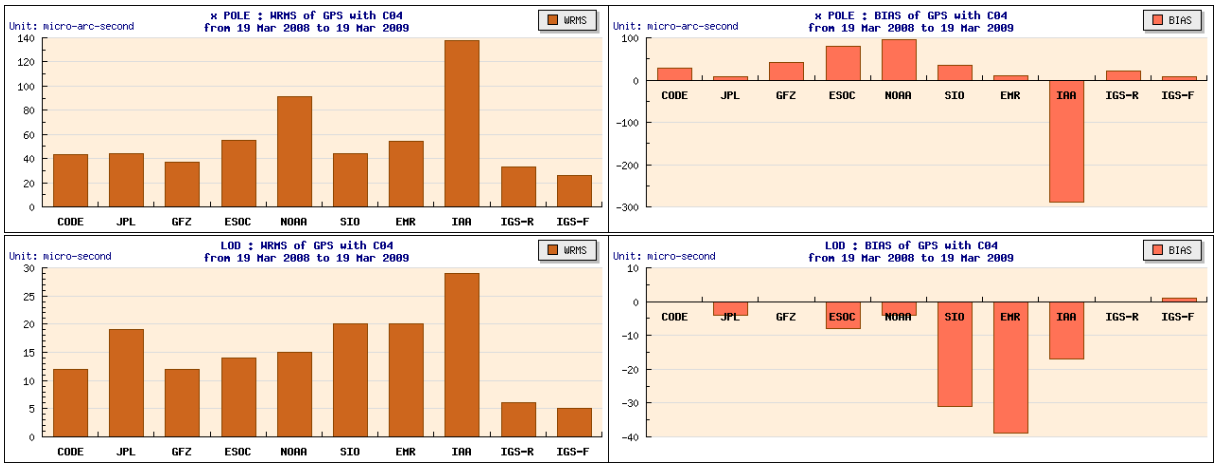

Figure 1: The agreement of C04 EOP with individual GPS solutions is illustrated for x pole coordinates and LOD.

Square fit. For each operational series linear drifts (bias + trend) are estimated according to Table 3. The estimated drifts are then removed from the operational EOP, then consistent with the ITRF and ICRF, and ready to be combined.

4. OTHER IMPROVEMENTS

The description of the previous algorithm leading to the combined C04 EOP series was presented in Gambis (2004). The numerical code was recently upgraded (Bizouard & Gambis, 2009) to take advantage of the evolution of the precision of EOP derived from the various techniques as well as to benefit from the dramatic improvement of computational resources: i) the model for nutation and UT1/LOD tidal variations have been updated according to the last IERS Conventions 2003 ii) the dimensions of tables have significantly been increased and double precision generalized to all parameters ; this allows solutions to be performed over 30 years in one run iii) the formal errors associated with the computed EOPs are estimated and made available. Performances are significantly improved. This is illustrated by better RMS agreements of the differences between individual and the combined solutions. We gain about 3-4 μs for UT1, and 50 μas for nutation offsets. The possibility to make long-term computation over 20 years leads to an improved consistency and long-term stability of the solution.

5. COMBINATION STRATEGY AND COMPARISONS WITH OTHER SERIES

The C04 series is maintained fixed from 1962.0 to the date of today 30 days back. The recent 30 days are regularly updated twice a week. They are considered as preliminary values. It should be noticed that between 2000.0 and 2006.0, C04 solution for x-pole and y-pole almost corresponds to the EOP ITRF 2005. This was achieved by weighting the ITRF 2005 polar motion about 10 times larger than other operational series. Starting at 2006.0 we attributed a regular weighting to ITRF 2005 polar motion. In the initial C04 solution, instabilities in the IVS combined solution prevented us to use it until the solution was available in SINEX format where EOP and terrestrial frame is present. It appeared that the IVS solution greatly improved. Since, it is used in our combinations. We do not combine exclusively IGS or IGS-R (rapid) solutions because the last IGS-R values are available with a one day delay. The CODE and GFZ provide the pole coordinates and LOD for the quasi real-time preliminary solution. To investigate the accuracy of the C04 solution, we can compute the difference of that solution with other operational series, of which are computed WRMS and biases. The results are illustrated over 1 year by figure 1 for

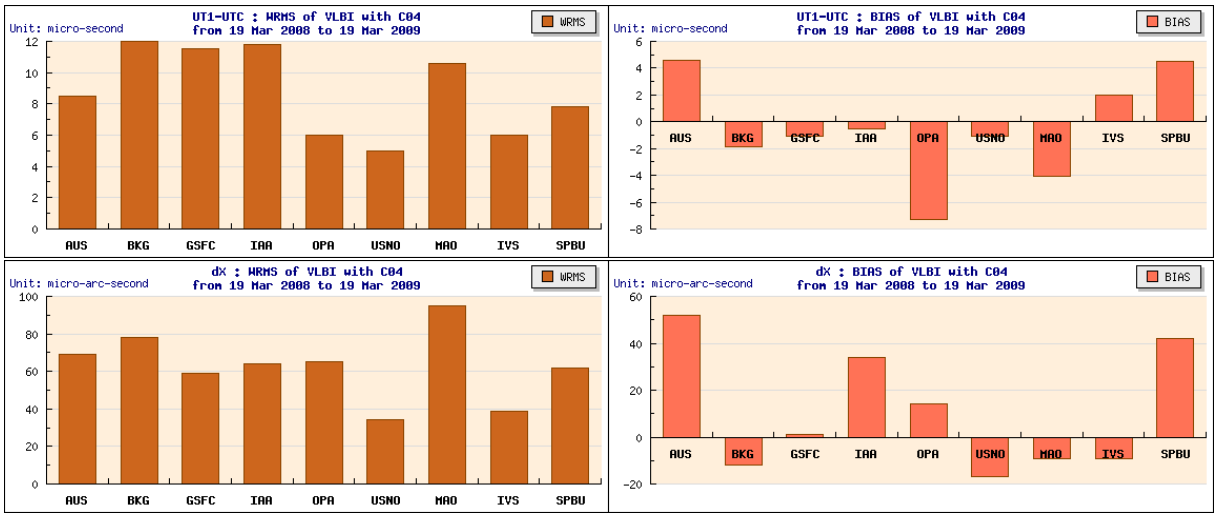

Figure 2: The agreement of C04 EOP with individual VLBI solutions is illustrated UT1 and celestial pole offset dX.

pole coordinates (x) and LOD. The typical WRMS is 40 μas for pole coordinates and 20 μs for LOD. According to the figure 2 the typical WRMS for UT1 is 10 μs and 40 μas for nutation offsets.

6. THE MULTI-TECHNIQUE COMBINATION

The determination of Earth Orientation is now considered in a more global way, incorporating any geodetic observations, related to the parameters to be estimated. What are combined are the normal equations associated with all parameters needed for modelling the observations obtained by VLBI, GPS, SLR and DORIS techniques. After forming a set of normal equations, it is inverted for obtaining the parameters in which we are interested in. The normal equations are produced using a common software and a common set of standard and models, related to the instruments and the propagation of the electromagnetic signal in the atmosphere. That procedure has been set up in France by the GRGS, as an extension of the GINS software initially designed for orbitography. To the 4 techniques and the related production of their normal equations are also assigned 4 different teams : G. Bourda, P. Charlot (Bordeaux Observatory) for VLBI, S. Loyer, F. Perosanz (CNES, CLS, Toulouse) for GPS, F. Deleflie, P. Exertier (OCA, Grasse) for SLR, L. Soudarin (CNES, Toulouse) for DORIS. The GRGS is now organized for a routine production of weekly SINEX files since 2005, which are stored at IERS as inter-technique products. In 2007 the processing has been upgraded and includes common tropospheric biases. At Paris Observatory is set up the inversion of the normal equation, for determining EOP as well as terrestrial station coordinates (software DYNAMO). Our multi-technique combination, based upon the whole sets of VLBI, GPS, SLR, and DORIS observations over the period 2005-2008, does not reach the performance of the "classical" series. However the DYNAMO procedure, restricted to GPS observations, give pole coordinates of quality comparable of the best EOP series (results of March 2009). What may be the most interesting feature of the multi-technique combination is its time resolution of 6 hours. As shown in figure the spectrum of the obtained pole coordinates (GPS combination) shows, besides the retrograde diurnal oscillation corresponding to classical nutation offset, extra peaks both in retrograde and prograde bands to be validated. If validated those series will be a powerful mean for investigating atmospheric-oceanic excitation at diurnal and sub-diurnal scale. For instance in the prograde band the daily prograde peaks stress either defect in the model of the oceanic tidal effect or atmospheric effect to be estimated. Another advantage of GRGS series is that they allow us to densify nutation offsets, which are usually determined at 5-day mean interval.

7. CONCLUSIONS

Over these last years Paris Observatory / IERS Earth Orientation Centre has improved the combined C04 solution. Pole motion and LOD accuracies are 50 μas for pole motion, 10 μs for UT1, 20 μas for LOD and 60 μas for nutation offsets. It is consistent with ICRF and ITRF 2005 to less than 30 μas for pole components, less than the real accuracy. In the future multi-technique combination GINS-DYNAMO

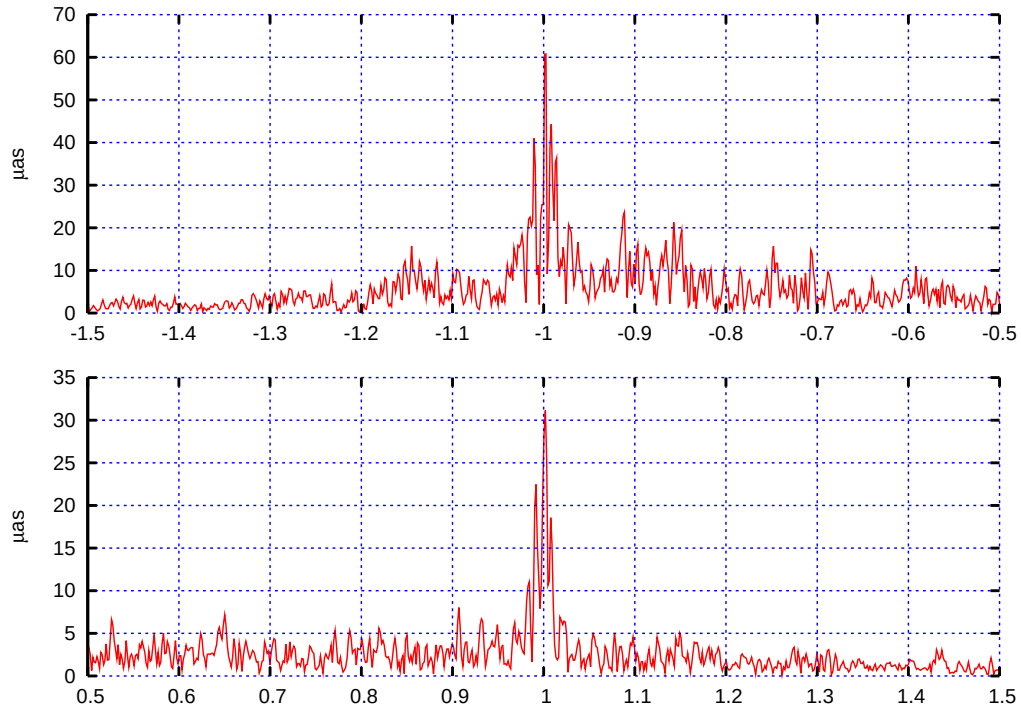

Figure 3: Complex spectrum of the GRGS pole coordinates determined by GPS intra-technique combination over [2007.0, 2009.0]. Notice the several diurnal peaks to be validated by independent solution and further tests of the GINS-DYNAMO procedure.

could become the future realisation of C04 solution and give 6 hourly pole coordinates and daily UT1 and celestial pole offsets.

8. REFERENCES

Altamimi, Z., Collilieux, X., Legrand, J., Garayt, B. and C. Boucher, 2007, ITRF2005, "A New Release of the International Terrestrial Reference Frame based on time series of station positions and Earth Orientation Parameters", J. Geophys. Res. 112, B09401, DOI: 10.1029/2007JB004949.

Bizouard, C. and D. Gambis, 2009, "The combined solution C04 for Earth Orientation Parameters, recent improvements", in print in Springer Verlag series, ISBN:978-3-642-00859-7

Gambis D., Essaifi N., Eisop E. and M. Feissel, 1993, "Universal Time derived from VLBI, SLR and GPS, IERS technical note 16, Dickey and Feissel (eds)", Observatoire de Paris, IV15-20.

Gambis D., 2002, "Allan Variance analysis applied to Earth Orientation Analysis, Adv. Space Research", 30/2, 207-212.

Gambis D., 2004, "Monitoring Earth orientation using space-geodetic techniques: state-of-the-art and prospective", J. of Geodesy, Volume 78, Issue 4-5, pp. 295-303, doi 10.1007/s00190-004-0394-1

Gray J.E. and D.W. Allan, 1974, "A Method for Estimating the Frequency Stability of an Individual Oscillator", Proceedings of the 28th Annual Symposium on Frequency Control, pp. 243-246. IAU, 1998: "Transactions of the International Astronomical Union, Vol. XXIIIB, Proceedings of the 23rd General Assembly, Kyoto, Japan.

Vondrák, J., 1977, Bull. Astron. Inst. of Czechoslovakia, 28, 84.

Vondrák J., Cepek A.: 2000, "Combined smoothing method and its use in combining Earth orientation parameters measured by space techniques", A&AS 147, 347-359

Zhu S.Y., Ivan I. Mueller, 1983, "Effects of adopting new precession, nutation and equinox corrections on the terrestrial reference frame", Bull. Geod. 57, 29–42.

GGOS AND THE COMBINATION OF SPACE GEODETIC TECHNIQUES

M. ROTHACHER
Department of Geodesy and Remote Sensing, GFZ Potsdam, Germany
e-mail: rothacher@gfz-potsdam.de

ABSTRACT.

The Global Geodetic Observing System (GGOS) is the contribution of geodesy to a global Earth monitoring system. In particular, it provides the metrological basis and the reference systems and frames, which are crucial nowadays for all Earth observing systems. GGOS is built on the IAG Services (IGS, IVS, ILRS, IDS, IERS, IGFS, ...) and the products they derive on an operational basis for Earth monitoring, making use of a large variety of space and ground-based geodetic techniques such as VLBI, SLR/LLR, GNSS, DORIS, altimetry, InSAR and gravity satellite missions, gravimetry, etc. All these observation techniques are considered integral parts of GGOS, allowing the monitoring of the Earth's shape and deformation (including water surface), the Earth's orientation and rotation and the Earth's gravity field and its temporal variations with an unprecedented accuracy.

GGOS, already now, is more than just an observing system. Its future vision and goal is the development of a complete chain from the acquisition, transfer and processing of a tremendous amount of observational data over the consistent combination and integration of all space geodetic techniques to the assimilation of the resulting geodetic and geophysical parameters into complex numerical models of the Earth system.

This presentation will concentrate on just one part of this chain, namely the issue of a rigorous combination and integration of the various space geodetic techniques in order to obtain unique highly accurate reference frames and consistent long time series of geodetic and geophysical parameters crucial for the assessment and prediction of global change phenomena. In future, this integration should not only include geometry, but also gravimetry and, in the more distant future, even observation techniques like altimetry, InSAR and seismology. The challenges on the way to such a combination will be discussed and examples will be given for the results already achieved.

RECENT IMPROVEMENTS IN IERS RAPID SERVICE/PREDICTION CENTER PRODUCTS

N. STAMATAKOS, B. LUZUM, STETZLER, W. WOODEN, E. SCHULTZ

U.S. Naval Observatory
3450 Massachusetts Avenue, N.W., Washington, D.C. 20392, USA
e-mail: Stamatakos.Nick@usno.navy.mil e-mail: Brian.Luzum@.usno.navy.mil
e-mail: Stetzler.Beth@.usno.navy.mil e-mail: Wooden.William@usno.navy.mil
e-mail: Schultz.Emily@usno.navy.mil

ABSTRACT. The International Earth Rotation and Reference Systems Service (IERS) Rapid Service/Prediction Center (RS/PC) has made several improvements to its combination and prediction products since the last Journées conference in 2007. These improvements are due to the inclusion of new input data sources as well as modifications to the combination and prediction algorithms. These changes and their impact on the users of the RS/PC data are presented.

1. INTRODUCTION

The IERS RS/PC provides daily Earth Orientation Parameters (EOP) which are used in determining the terrestrial to celestial transformation matrix. These EOP values include polar motion, UT1-UTC, and celestial pole offsets, which can be obtained from the Bulletin A or finals data series located at tt http://maia.usno.navy.mil. After an overview of the RS/PC solution is given, a review of the UTGPS (Universal Time-like quantity using Global Position System data) processing and its usage in the combination and prediction software is presented. Recent and future improvements to the combination and prediction process include a new UTGPS solution with an improved filtering process, an increase in the number of Atmospheric Angular Momentum (AAM) forecast days, and Rapid Turnaround electronic Very Long Baseline Interferometry (RT e-VLBI) observations.

2. OVERVIEW OF EOP RS/PC SOLUTION

The daily EOP combination and prediction solution (finals.daily) is produced at approximately 1700 UTC each day; the weekly version (Bulletin A) is produced on Thursday at approximately 1700 UTC. Data from VLBI, Global Positioning System (GPS), Satellite Laser Ranging (SLR), and AAM are used in these solutions. Observations from the past are combined with appropriate weighting factors and used, along with AAM forecast data, to predict EOP values into the future. It is estimated there are 600 users who receive IERS RS/PC data each week, and roughly 40000 ftp downloads are made per month. Most uses of the data are for practical, non-research purposes with many users — 85 to 90 % — having limited technical skills. Details on the inputs, processes, and results of the RS/PC solution can be found at Stamatakos et al., (2008).

3. REVIEW OF AND FUTURE DEVELOPMENTS IN UTGPS PROCESSING

Each day near 1700 UTC, just after the IGS Rapid orbits are determined, a UT1-like quantity, called UTGPS, is generated. It is an estimate of UT1 at noon UTC for the previous day (Tracey et al., 2008). Not only is the UTGPS solution an accurate addition to the combination solution after the last VLBI intensives are generally available, but the last UTGPS solution also provides a good starting point for UT1 predictions.

The following is a conceptual description of the determination of UTGPS. Suppose one obtains orbit positions for GPS satellites in both celestial and terrestrial coordinates. If one also had a good estimate of the parameters for the transformation from terrestrial to celestial coordinates, except for the UT1 contribution, then one could solve for UT1 of the Earth.

On the most recent day with VLBI observations, the Earth orientation parameters are very accurately known. The GPS positions in the IGS Rapid orbit file for that day can then be transformed from

the terrestrial positions (at 15-minute intervals) for any satellite in the file to celestial coordinates. An integrated orbit (called a starting orbit) is then fit to these inertial positions. The integrated orbits always take known Earth and Solar System gravitational forces into account, and also use a Solar Radiation Force (SRF) model. The SRF model for the satellite gives very accurate perturbations for the orbit plane, as a function of Sun angle from the satellite orbit plane, since it is based on the orbit perturbations observed in previous years.

On any succeeding day near 17:00 UTC, the IGS Rapid orbits file for the preceding day becomes available. Using any reasonable a priori estimate (or prediction) of Earth orientation parameters for that day, the terrestrial positions for the satellite from the file are transformed to obtain approximate observed positions in the celestial frame. The starting orbit is then integrated to the same 24-hour time span to give accurate predicted positions in celestial coordinates at the observed position times. The position residual vectors between the observed and predicted positions are determined; in particular, the component of the residual vectors along the predicted orbit normal is computed. Lastly, the correction to the a priori UT1 value which minimizes this component is found. This correction more accurately positions the Earth in the celestial frame. This correction applied to the a priori UT1 value at 12 hr UTC gives an estimate of the true UT1 value, assuming that the modeling errors in the integrated GPS orbits are smaller than the unpredictable variations in UT1 from day to day. The above procedure is applied to multiple GPS satellites, and the median of the determined UT1 values is UTGPS. For more details the reader is referred to (Kammeyer, 2000) and (Tracey et al., 2008).

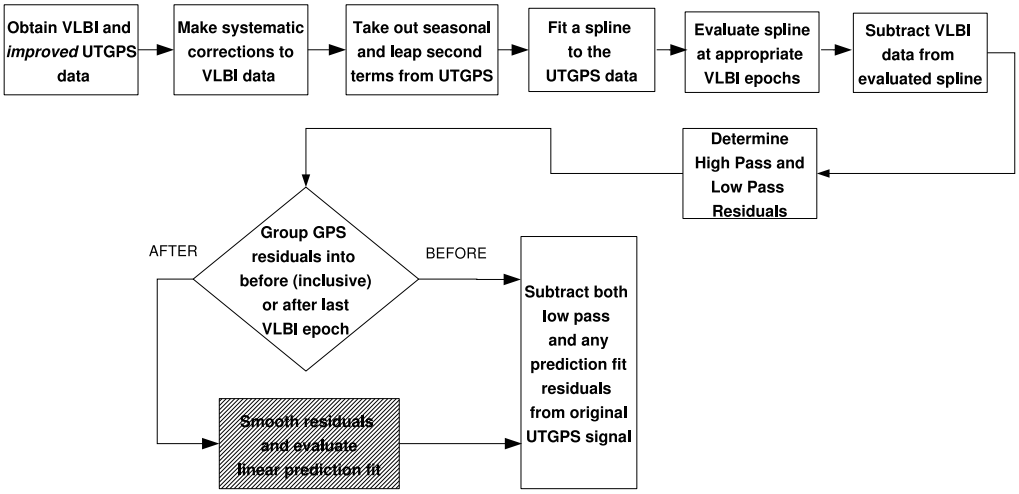

Figure 1: Future High Pass Filtering Flowchart for UTGPS

After the UTGPS estimate is made for noon UTC, it must be processed further before using it in the EOP combination software. Figure 1 contains a flowchart of the anticipated high-pass filtering process. A cubic spline is fit to several weeks of UTGPS data. VLBI data, which have had systematic corrections applied, are then subtracted from the UTGPS cubic spline. The resulting residuals are low-pass filtered and then sorted into two groups — those before (inclusive) and those after the last VLBI epoch. Currently, an auto-regressive fit is made for those points after the last VLBI epoch and then the low pass filtered residuals are subtracted from both groups. In the near future, smoothing and a linear prediction fit will be applied to the data after the last VLBI epoch, which results in improved UTPGS accuracy after the last VLBI epoch when compared to the auto-regression prediction. Finally, the low pass residuals will be subtracted from both groups.

Residuals, created by subtracting the Bulletin A UT1 data from the unfiltered UTGPS values, are shown in Figure 2(a) using both the current and new UTGPS (which is described in the next paragraph). The new UTGPS has less noise than the current version. (Note, the new UTGPS was not run continuously; it was restarted at MJD 53720, and that is the reason for the jump back to a residual of 0.0 at MJD 53720.) Figure 2(b) contains the residuals created by subtracting the Bulletin A UT1 data from the calibrated filtered UTGPS data that are used in the combination process. The 1-σ residuals computed using the current UTGPS data are 18 μsec; whereas, with the new UTGPS data, the 1-σ error is reduced to 12 μsec.

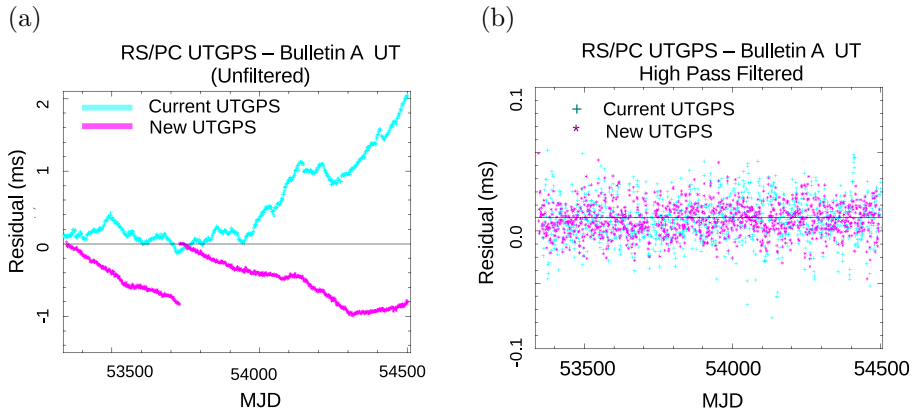

Figure 2: (a) Residuals of Unfiltered UTGPS and (b) Residuals of High-pass UTGPS

A new UTGPS solution has been developed. It uses between 15 and 25 satellites, as opposed to approximately 10 for the current UTGPS solution. Better solar force modeling has been incorporated; the JGM3 gravity model (degree 12, order 12) is still used and provides sufficient accuracy. The initial results are encouraging — there is significant improvement in the UT1 estimates. Given the better solution at the end of the combination, the UT1 predictions should also improve since there is a more accurate starting point for them. The quality of the new UTGPS solution is being monitored. It is anticipated that the new UTGPS will be incorporated into the operational procedures by early 2009.

4. REVIEW OF AAM ESTIMATION USED IN THE RS / PC SOLUTION

The flowchart in Figure 3(a) and also Figure 4 of Stamatakos et al. (2008) illustrates the AAM estimation process, except for the change in forecast length from 5 to 7.5 days. A detailed explanation of the flowcharts can be found in Stamatakos et al. (2008). The additional AAM forecast data from National Oceanographic and Atmospheric Administration (NOAA) and U.S. Navy Operational Global Atmospheric Prediction System (NOGAPS), were added to the EOP combination and prediction software beginning on October 4, 2007. The resulting prediction accuracy has improved beyond the 5-day range since this change was implemented. Figure 3(b) illustrates the improvement in the prediction accuracy during the first 10-month period when the AAM forecasts were increased from 5 to 7.5 days, with the accuracy increasing by approximately 15% at 7 days.

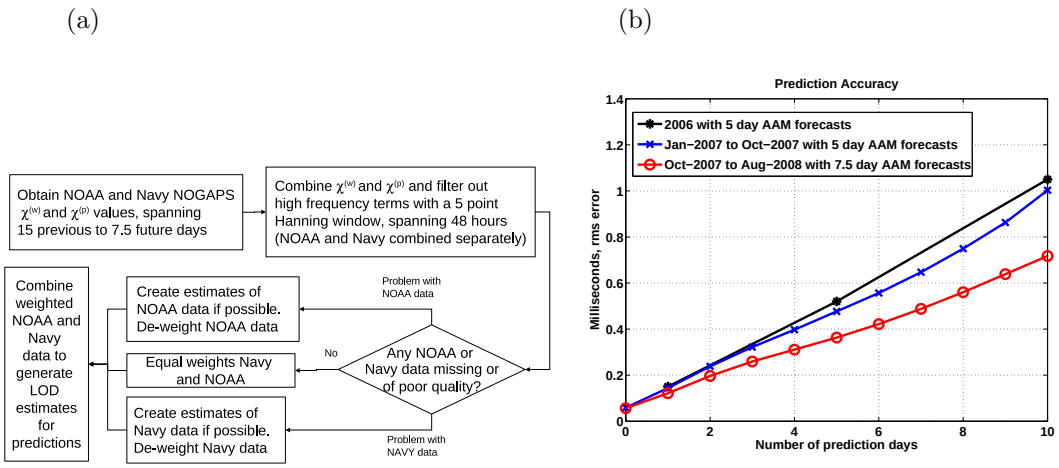

Figure 3: (a) Processing of AAM data before using it in the combination and prediction process, and (b) Recent Improvements in EOP Prediction Results before and after AAM forecast data was extended from 5 to 7.5 days

(a)

Intensive	Solution	Number of points	(μsec) Estimated Error
Rapid	Combination	21	23
Rapid	Prediction	21	99
Standard	Combination	303	57
Standard	Prediction	303	123

(b)

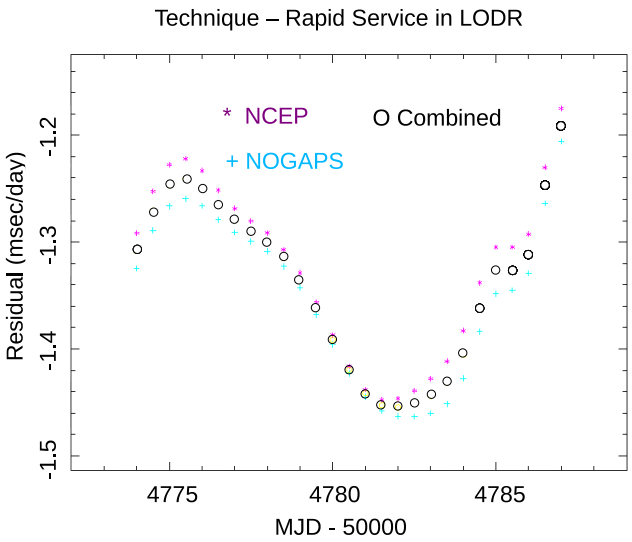

Figure 4: (a) Preliminary Results from the Rapid e-VLBI Analysis, and (b) AAM minus LODR daily diagnostic plot

5. RAPID TURNAROUND (RT) e-VLBI INTENSIVES

The RT e-VLBI intensives are observed and processed more recently than the IGS Ultra orbit observations. An analysis of the effect of the RT e-VLBI intensives on the RS/PC combination and prediction of UT1 was started on September 30, 2007, and has continued to the present. Only the last day of the combination and the 1-day prediction were analyzed. There were a limited number of solutions with the RT e-VLBI. As listed in Figure 4(a), there was a noticeable improvement in the combination solution — roughly a factor-of-2 improvement using the RT e-VLBI over the standard solution. The prediction improvement was smaller — there was only an improvement of 20% over the standard solution.

6. FUTURE DIRECTIONS

Additional monitoring of AAM residuals and statistics, for both analysis and forecast data, is being planned. Figure 4(b) contains an example of the AAM residual plot statistics being implemented at the RS / PC for monitoring of AAM analysis data. Using the European Centre for Medium-Range Weather Forecasting (ECMWF) series in addition to the NOGAPS and NCEP data, is also being investigated.

7. REFERENCES

Kammeyer, P. (2000), "A UT1—like Quantity from Analysis of GPS Orbit Planes", Celestial Mechanics and Dynamical Astronomy 77: pp. 241-272, 2000.

Stamatakos, N., Luzum, B., Wooden, W., (2008) "Recent Improvements in IERS Rapid Service/Prediction Center Products," Proceedings of the Journées 2007 "Systèmes de Référence Spatio-Temporels", N. Capitaine (ed.), Observatoire de Paris, pp. 163—166.

Tracey, J., Kammeyer, P., Stamatakos, N., (2008) "Usage of the UT1-like Quantity at the USNO", International GNSS Service, Analysis Center Workshop, 2-6 June 2008, Miami Beach, Florida, USA.

IMPROVING SHORT-TERM EOP PREDICTION USING COMBINATION PROCEDURES

Z.M. MALKIN
Central Astronomical Observatory at Pulkovo of RAS
Pulkovskoe Ch. 65, St. Petersburg 196140, Russia
e-mail: malkin@gao.spb.ru

ABSTRACT. A well known problem with EOP prediction is that a prediction strategy proved to be the best for some testing period and prediction length may not remain as such for other period of time. In this paper we consider possible strategies to combine EOP predictions made using different analysis techniques to obtain a final prediction with the best accuracy corresponding to the least prediction error between input predictions. This approach can be used to improve the short-term real-time EOP forecast.

1. INTRODUCTION

Prediction of the Earth Orientation Parameters (EOP) is a practically very important and theoretically very interesting task, one of the main fields of activity of operational EOP services. Various methods are developed to compute a highly accurate EOP forecast. However, a usual and well known problem is that different methods show different accuracy at different time intervals and prediction lengths. A method which is the best for short-time prediction may not be such for long-time prediction, and vice versa. On the other hand, a method which was proven to be the best for a testing period of time may not remain as such for the coming period. As an example, results of actual UT1 predictions are shown in Figure 1. One can see that different predictions show the best results for different years and length of prediction.

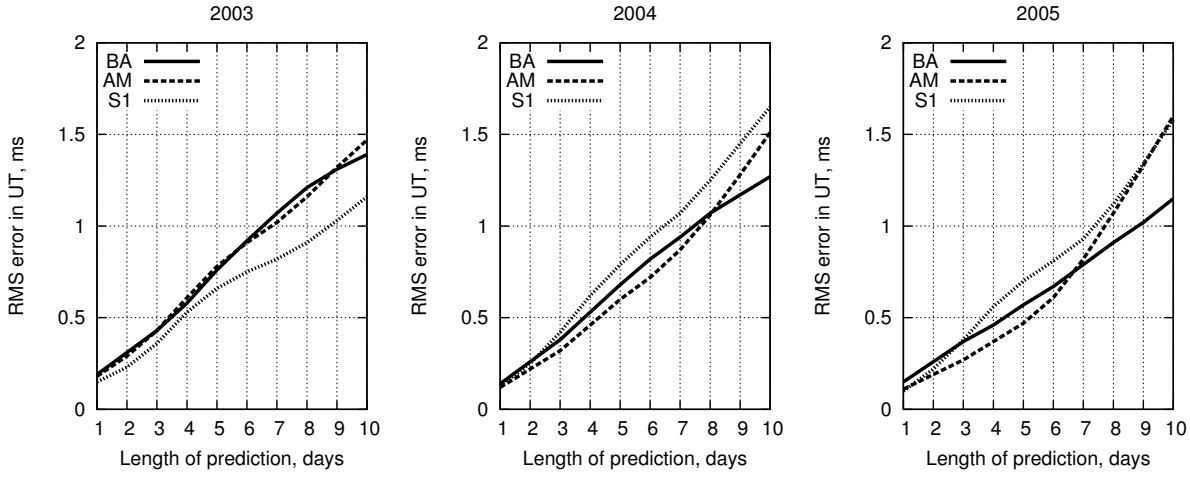

Figure 1: Results of actual UT1 predictions for three years. BA – Bulletin A prediction, AM – prediction of the same NEOS series made by the author, S1 – author's prediction of the SLR series computed at the Institute of Applied Astronomy. Last two predictions were made making use of method developed by Malkin & Skurikhina, 1996

A practical consequence is that a prediction procedure optimally adjusted for some time period may not remain the best for the following time period. Evidently, the main reason of this is that the Earth rotation is more complicated process than we are able describe by our forecast models. So, the question is whether we can improve our prediction strategy to make it more robust to unpredictable behavior of the Earth?

In this paper we try to use combining procedures to achieve this goal. We will concentrate on short-term prediction up to 5-day length as evidently the most interesting for practical needs, GNSS applications in the first place.

2. TEST PREDICTIONS

For testing purposes, nine series of everyday predictions for the period from 1 October 2006 through 31 December 2007 making use of prediction strategy developed at the Institute of Applied Astronomy (Malkin & Skurikhina, 1996). This method includes three prediction techniques:

1. Least squares fitting for trend and several harmonics,
2. Autoregression.
3. Autoregressive Integrated Moving Average.

Final prediction is composed of several segments computed using different methods and/or model parameters and merged in one continuous series using boundary conditions. The main model parameters that can be varied to adjust the prediction procedures are the following:

1. base interval,
2. number and period of harmonics,
3. trend order,
4. AR order,
5. IMA order,

Abovementioned nine prediction series were computed using various sets of listed parameters aside from item 2 which remains the same for all the predictions.

3. COMBINED PREDICTIONS

Using prediction time series computed as described above, three combined predictions were computed for the period from 1 January 2007 through 31 December 2007. They are the following:

C1 – average of input prediction as proposed and tested by Luzum et al., 2007, and Schuh et al., 2008.

C2 – best previous prediction for given length. Normally, we compute EOP prediction on the day of the last observed epoch ("today"). To compute n-day ahead prediction we examine the set of predictions made n days ago and select one that predicts today EOP most accurately. Then we compute our today n-day ahead prediction making use of the method used for computation of the best prediction made n days ago.

C3 – best yesterday prediction. To compute this prediction we examine the set of predictions made yesterday and use for today prediction the method which corresponds to the prediction made yesterday and predicts today EOP most accurately.

Note that C2 and C3 predictions also use C1 results along with the input data. The accuracy of the nine test predictions and three combinations are shown in Fig. 2.

From this test one can see that all the tested combined predictions show similar accuracy for the Pole coordinates, better than accuracy of input series. Marginal advantage of C2 and C3 can bee noticed.

There is a more complicated situation with the UT1 prediction. The average (C1) prediction does not provide a satisfactory result, probably because of presence of bad predictions (note the worst UT1 prediction in the upper left part of corresponding plots). The C3 (best yesterday prediction) is clearly the best for short-time UT1 prediction.

4. CONCLUSIONS

1. A procedure based on computation of multiply predictions with further combination/choice of the best one can provide robust accurate operational EOP forecast.

2. To achieve the best results, input predictions should be computed using the best methods.

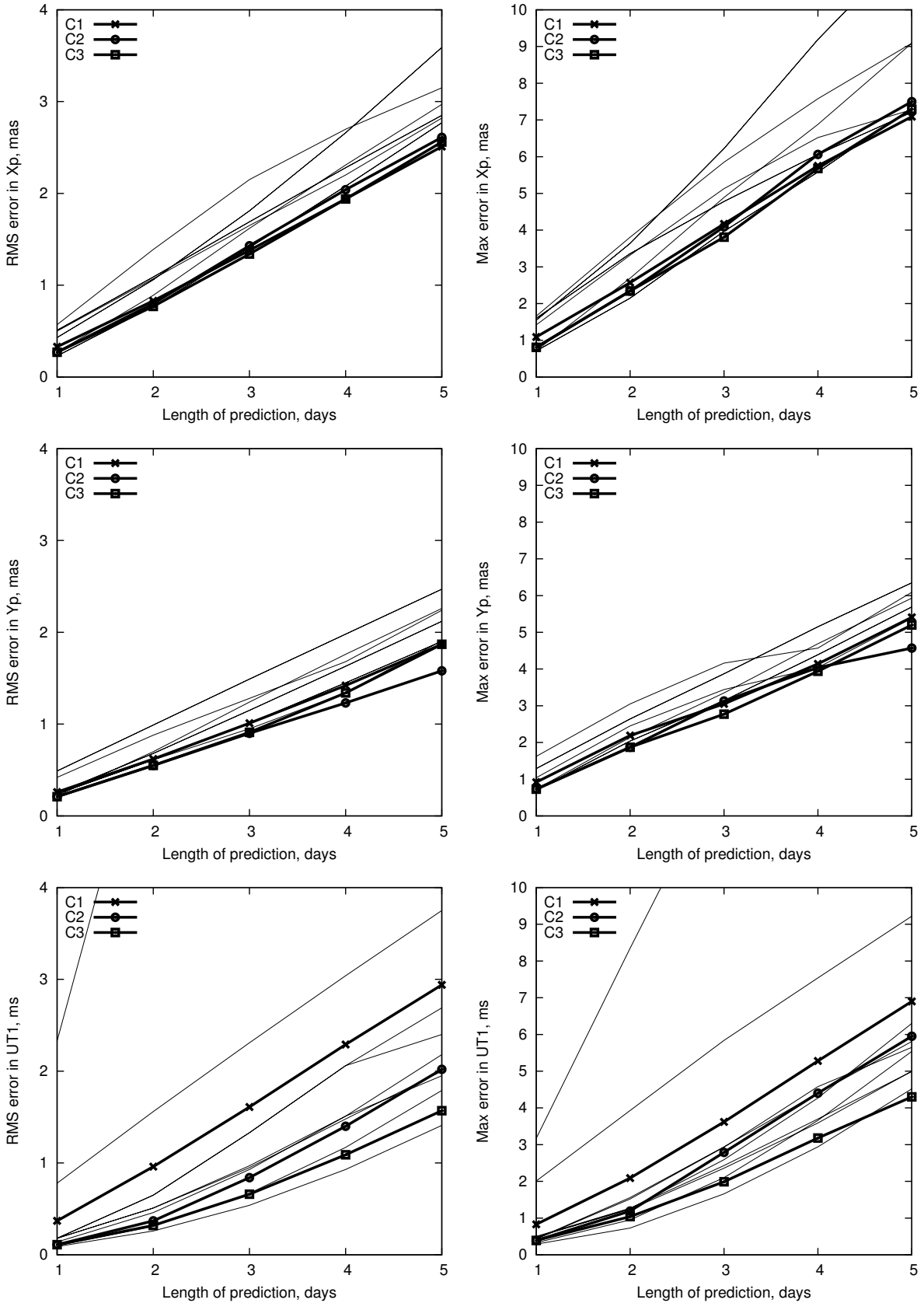

Figure 2: The RMS and maximum errors of the input and combined predictions.

5. REFERENCES

Malkin, Z., Skurikhina, E., 1996, "On Prediction of EOP", Communications of the Institute of Applied Astronomy RAS, No. 93.

Luzum, B., Wooden, W., McCarthy, D., Schuh, H., Kosek, W., Kalarus, M., 2007, "Ensemble Prediction for Earth Orientation Parameters", Geophysical Research Abstracts, 9, 04315.

Schuh, H., Kosek, W., Kalarus, M., Akyilmaz, O., Gambis, D., Gross, R., Jovanovic, B., Kumakshev, S., Kutterer, H., Mendes Cerveira, P.J., Pasynok, S.,Zotov, L., 2008, "Earth Orientation Parameters Prediction Comparison Campaign – first summary", Geophysical Research Abstracts, 10, EGU2008-A-07644.

CONTRIBUTION OF WIDE-BAND OSCILLATIONS EXCITED BY THE FLUID EXCITATION FUNCTIONS TO THE PREDICTION ERRORS OF THE POLE COORDINATES DATA

W. KOSEK[1], A. RZESZÓTKO[1], W. POPIŃSKI[2]
[1]Space Research Centre, Polish Academy of Sciences
Bartycka 18A, 00-716 Warsaw, Poland
e-mail: kosek@cbk.waw.pl; alicja@cbk.waw.pl
[2]Central Statistical Office
al. Niepodległości 208, 00-925 Warsaw, Poland
e-mail: w.popinski@stat.gov.pl

ABSTRACT. The x, y pole coordinates model data were computed by numerical integration of differential equation of polar motion using equatorial components of atmospheric, ocean, hydrologic excitation functions and their sums. Other x, y pole coordinates model data were obtained by summing different frequency components determined by the discrete wavelet transform band pass filter (DWTBPF). The IERS pole coordinates data and the pole coordinates model data were then predicted by the combination of the least-squares (LS) model extrapolation and autoregressive (AR) prediction (LS+AR). Comparison of the prediction errors of the IERS pole coordinates data and the pole coordinates model data, computed at different starting prediction epochs, has enabled examination of the influence of wide-band oscillations present in the IERS pole coordinates data as well as the fluid excitation functions on the prediction errors of the IERS pole coordinates data.

1. INTRODUCTION

Increase of accuracy of space geodetic techniques during the last decades caused increase of determination accuracy of Earth orientation parameters i.e. x, y pole coordinates, universal time UT1-UTC and precession-nutation corrections. However, the prediction errors of the x, y pole coordinates and UT1-UTC data even for a few days in the future are ten or hundred times greater than their determination errors (Kosek et. al. 2008). Since oscillations in pole coordinates data are mostly excited by joint atmospheric and ocean excitation functions these functions may be the main cause of prediction errors increase of pole coordinates data (Kosek 2005).

2. DATA

The following data sets were used in the analysis: 1) the IERS x, y pole coordinates data from the *EOPC04_05* combined solution with the sampling interval of 1 day (IERS, 2008). 2) Equatorial components of atmospheric angular momentum (AAM) from *aam.ncep.reanalysis.** data in 1948-2008.6 which are the sum of mass and motion terms with the sampling interval of 6 hours (AER, 2008). These data were interpolated with 1 day sampling interval using linear interpolation. 3) Equatorial components of ocean angular momentum (OAM) which are the sum of mass and motion terms, created after connection of two separate files with the sampling interval of 1 day: a) *c20010701.oam* (or *gross03.oam*) from Jan. 1980 to Mar. 2002, b) *ECCO_kf049f.oam* from Mar. 2002 to Mar. 2006 (JPL, 2008). 4) Equatorial components of hydrologic angular momentum (HAM) obtained by numerical integration of water storage data: *water_ncep_1979.dat, water_ncep_1980.dat,..., water_ncep_2004.dat* in 1979 - 2004 from National Centers for Environmental Prediction (NCEP) with the sampling interval of 1 day (NCEP, 2008).

3. COMPUTATION OF POLE COORDINATES MODEL DATA FROM FLUID EXCITATION FUNCTIONS

To examine the influence of fluid excitation functions on prediction errors of x, y pole coordinates data first the pole coordinates model data were computed from the equatorial components of these excitation

functions. The differential equation of polar motion is given by the following formula:

$$i \cdot \dot{m}(t)/\sigma_{ch} + m(t) = \chi(t) \tag{1}$$

in which $m(t) = x(t) - i \cdot y(t)$ are the pole coordinates data to be computed, $\chi(t) = \chi_1(t) + i\chi_2(t)$ are equatorial components corresponding to atmospheric, ocean and hydrologic excitation functions, $\sigma_{ch} = [1 + i/(2Q)]2\pi/T_{ch}$ is the complex-valued Chandler frequency, $T_{ch} = 433$ days and $Q = 170$ is the quality factor. Solution of this equation in discrete time moments can be obtained using the trapezoidal rule of numerical integration:

$$m(t + \Delta t) = m(t)exp(i\sigma_{ch}\Delta t) - i\sigma_{ch}\Delta t[\chi(t + \Delta t) + \chi(t)exp(i\sigma_{ch}\Delta t)]/2, \tag{2}$$

where Δt is the sampling interval of data.

4. COMPUTATION OF POLE COORDINATES MODEL DATA USING WAVELET TRANSFORM BAND PASS FILTER

To show the influence of wide-band oscillations in x, y pole coordinates data on the prediction errors of these data, the DWTBPF was applied to filter these oscillations. The discrete wavelet transform (DWT) j^{th} frequency component of the complex-valued signal $x(t)$ is given by the formula:

$$x_j(t) = \sum_{k=-2^{j-1}}^{2^{j-1}-1} S_{j,k}\varphi_{j,k}(t) \qquad for \qquad t = 0, 1, ..., n-1, \qquad j = j_o, j_o + 1, ..., p-1, \tag{3}$$

where $S_{j,k} = \sum_{t=0}^{n-1} x(t)\varphi_{j,k}(t)$ are the DWT coefficients and $\varphi_{j,k}(t) = \sqrt{n}2^{-j/2}\varphi_j(t - n/2 - 2^{-j}kn)$ are the discrete Shannon wavelet functions (Benedetto and Frazier 1994), $n = 2^p$ is the number of data, p is a positive integer.

For fixed lowest frequency index $0 \le j_o \le p - 2$ and time index $k = -2^{j_o}, -2^{j_o} + 1, ..., -2^{j_o} - 1$,

$$\varphi_{j_o}(t) = exp[-i\pi(t - n/2)n]\frac{sin[2^{j_o+1}\pi(t - n/2)/n]}{n \cdot sin[\pi(t - n/2)/n]}, \qquad \varphi_{j_o}(n/2) = 2^{j_o+1}/n. \tag{4}$$

For higher frequency index $j = j_o+1, j_o+2, ..., p-1$, and time index $k = -2^{j-1}, -2^{j-1}+1, ..., -2^{j-1}-1$,

$$\varphi_j(t) = exp[-i\pi(t - n/2)/n]\frac{sin[2^j\pi(t - n/2)/n]\{2cos[2^j\pi(t - n/2)/n] - 1\}}{n \cdot sin[\pi(t - n/2)/n]}, \qquad \varphi_j(n/2) = 2^j/n. \tag{5}$$

The DWTBPF enables computation of such frequency components of complex-valued time series that their sum is exactly equal to the input time series: $\sum_{j=j_o}^{p-1} x_j(t) = x(t)$.

Components with frequency indices $j < 4$ and $j > 4$ correspond to longer period and shorter period oscillations, respectively. The pole coordinates model data were computed by summing the chosen frequency components but including the frequency component $x_4(t)$ corresponding to the sum of the Chandler and annual oscillations. The frequency component $x_5(t)$ corresponds to the semiannual oscillation.

5. PREDICTION OF POLE COORDINATES MODEL DATA

To predict x, y pole coordinates data the LS+AR method was applied (Kosek et al. 2004, 2008). In this prediction algorithm first the LS model which consists of the Chandler circle, annual and semi-annual ellipses and linear trend is fit to x, y pole coordinates data. The differences between x, y pole coordinates data and their LS model give the LS model residuals. Prediction of x, y pole coordinates data is the sum of the LS model extrapolation and the autoregressive prediction of the LS residuals.

The absolute value of the differences (prediction errors) between the IERS pole coordinates data and their predictions computed by the LS+AR algorithm and prediction errors of the pole coordinates model data computed from atmospheric, ocean and hydrologic excitation functions are shown in Figure 1. Fluid excitation functions alone do not explain all the prediction errors of pole coordinates data, however some unpredictable variations after 2006 are possibly caused by atmospheric excitation. Some unpredictable variations in pole coordinates data in 1980 - 1982 and at the end of 2002 and beginning of 2003 are caused by irregular ocean excitation. The prediction errors of the pole coordinates model data computed from hydrologic excitation are very small.

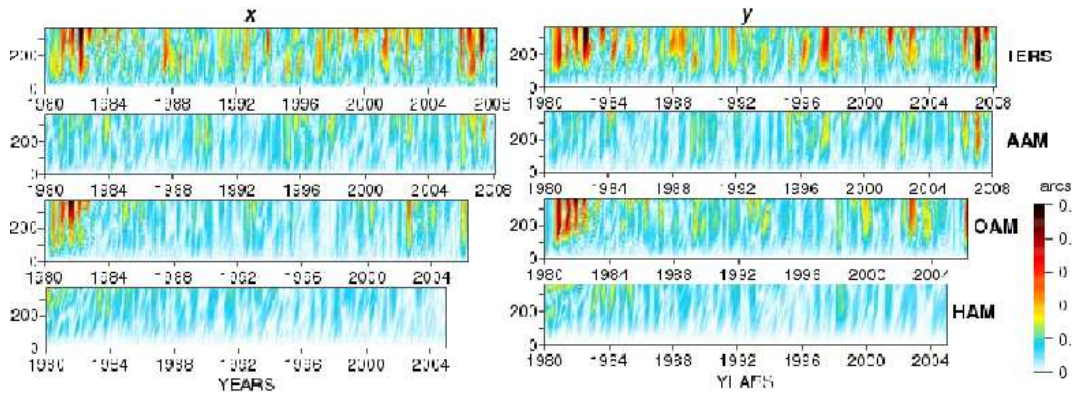

Figure 1: The LS+AR prediction errors of the IERS x, y pole coordinates data and of the x, y pole coordinates model data computed from AAM, OAM and HAM excitation functions.

The mean prediction errors of the pole coordinates model data computed from AAM, OAM and HAM excitation functions are shown for comparison with the mean prediction errors of the IERS pole coordinates data in Figure 2. The contributions of AAM or OAM excitation to the mean prediction errors of the pole coordinates data from 1 to about 100 days in the future is similar and of the order of 60% of the total error. When the prediction length increases, then the mean prediction errors caused by ocean excitation become greater than those caused by atmospheric excitation. The contribution of HAM excitation to the mean prediction errors of the IERS pole coordinates data is more than two times smaller than the contribution of AAM excitation, and it decreases with decrease of the prediction length.

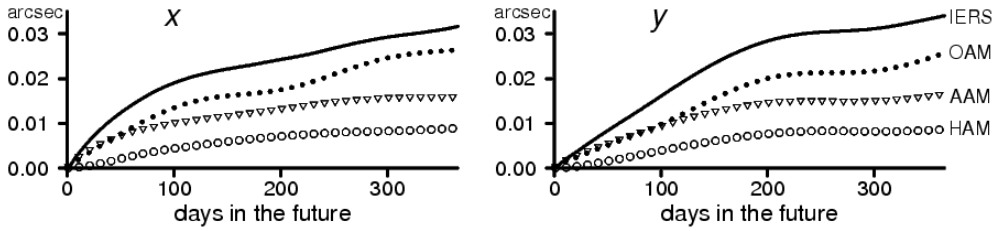

Figure 2: The mean LS+AR prediction errors of the IERS x, y pole coordinates data (thin line) and of the x, y pole coordinates model data computed from AAM (dots), OAM (triangles) and HAM (circles) excitation functions.

The mean prediction errors of the model pole coordinates data computed by summing the chosen DWTBPF frequency components are shown in Figure 3. Short term predictions errors up to about 50 days in the future can be explained by the sum of the frequency components corresponding to the Chandler, annual and other shorter period oscillations. If the pole coordinates model data consisted only of the Chandler and annual oscillations then the prediction errors up to 100 days in the future would be very small and of the order of few mas. The mean prediction errors the pole coordinates model data computed from AAM + OAM excitation functions and computed by summing the chosen frequency components corresponding to the Chandler, annual and shorter period oscillations are of the same order and explain about $80 - 90\%$ of the mean prediction error of the IERS pole coordinates data (Fig. 4).

6. CONCLUSIONS

The contributions of AAM or OAM excitation functions to the mean prediction errors of the IERS pole coordinates data from 1 to about 100 days in the future are similar and of the order of 60% of the total prediction error. The contribution of OAM excitation function to the mean prediction errors of the IERS pole coordinates data for prediction lengths greater than 100 days becomes greater than the contribution of the AAM excitation function. The contribution of the joint AAM+OAM excitation to the mean prediction errors of the IERS pole coordinates data is almost equal to the contribution of the sum of

Chandler + annual and shorter period frequency components. Both contributions explain about $80-90\%$ of the total prediction error. Big prediction errors of the IERS pole coordinates data in 1981-1982 and in 2006-2007 are mostly caused by wide-band OAM and AAM excitation functions, respectively. The prediction errors of the IERS pole coordinates data caused by HAM excitation functions are very small and they decrease with decrease of prediction length.

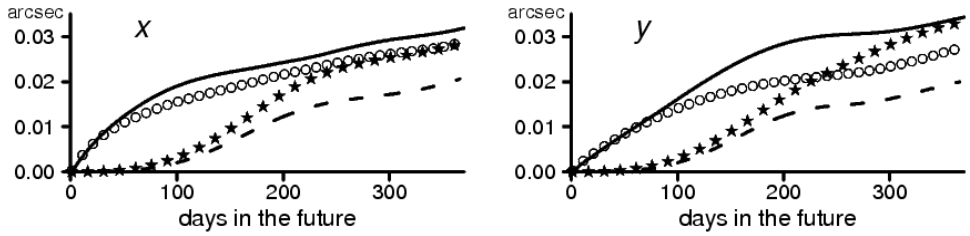

Figure 3: The mean LS+AR prediction errors of the IERS x, y pole coordinates data (thin line) and of the x, y pole coordinates model data computed by summing the DWTBPF components corresponding to Chandler + annual and shorter period oscillations (circles), Chandler + annual and longer period oscillations (stars), as well as Chandler + annual oscillations (dashed line).

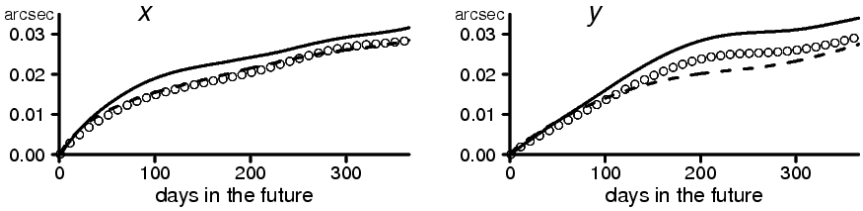

Figure 4: The mean LS+AR prediction errors of the IERS x, y pole coordinates data (thin line) and of the x, y pole coordinates model data computed from AAM+OAM (dashed line) excitation functions, as well as by summing the DWTBPF components corresponding to Chandler, annual and shorter period oscillations (circle line).

Acknowledgements. Attendance of co-authors W. Kosek and A. Rzeszótko at the Journees 2008 were supported by a conference grant. The paper was supported by the Polish Ministry of Education and Science under the project No 4 T12E 039 29.

7. REFERENCES

AER 2008, tt ftp://ftp.aer.com/pub/anon_collaborations/sba/.

Benedetto J.J. and Frazier M.W., 1994, Mathematics and Applications, LRC Press, Boca Raton, 221–245.

IERS 2008, tt http://hpiers.obspm.fr/iers/eop/eopc04_05/.

JPL 2008, tt http://euler.jpl.nasa.gov/sbo/sbo_data.html.

Kosek W., 2005, Excitation of the Chandler wobble by the geophysical annual cycle., Proc. ECGS Chandler Workshop: Cahiers du Centre Europeen de Geodynamique et de Seismologie, Vol. 24., H.P. Plag, B. Chao, R. Gross and T. van Dam (eds.), 121–126.

Kosek W., McCarthy D.D., Johnson T.J., Kalarus M., 2004, Comparison of polar motion prediction results supplied by the IERS Sub-bureau for Rapid Service and Predictions and results of other prediction methods. Proc. Journees 2003, 164–169.

Kosek W., Kalarus M., Niedzielski T., 2008, Forecasting of the Earth orientation parameters - comparison of different algorithms, Proc. Journes 2007, 155–158.

NCEP 2008, tt ftp://ftp.csr.utexas.edu/pub/ggfc/water/NCEP.

EARTH ORIENTATION PARAMETERS FROM GLONASS OBSERVATIONS

S. FETISOV, S. PETROV, S. SMIRNOV, D. TROFIMOV
St.Petersburg State University, Russia
e-mail: gnss.astrometry@gmail.com

ABSTRACT.

The GLONASS system experienced for some period of time a lack of satellites. Now, after renewal of regular launches, it is becoming more and more functional, and hence presents a possibility to solve actual astro-geodetic problems. In this work we concentrate on estimation of the Earth orientation parameters from GLONASS observables. First, we develop a procedure for estimation of pole coordinates, Universal time, and celestial pole offsets. Secondly we carry out a feasibility study in order to assess accuracy of estimated parameters. Finally, we develop a procedure for joint processing of GPS and GLONASS observations for estimation of Earth orientation parameters.

GEOPHYSICAL MASS REDISTRIBUTIONS FROM GRACE: THE CASE OF THE ANTARCTIC AND GREENLAND ICE SHEETS

M. HORWATH, R. DIETRICH
Institut für Planetare Geodäsie, Dresden Technical University, Germany
e-mail: horwath@ipg.geo.tu-dresden.de

ABSTRACT.

The GRACE (Gravity Recovery and Climate Experiment) satellite mission launched in 2002 is able to observe global geophysical mass redistributions through their gravitational effect. At a long-term scale, they are dominated by ice-related processes, i.e., ice mass changes and glacial-isostatic adjustment of the solid earth. GRACE has, indeed, proven a valuable and unique tool for assessing, in particular, the large ice sheets' mass changes. However, respective results from different analyses differ considerably. A thorough understanding of the various error mechanisms involved in the GRACE data analysis and in the geophysical reductions is necessary to ensure reliable results with realistic uncertainty assessments as well as to advance the methods of analysis.

We present our results on Antarctic and Greenland ice mass changes obtained with an adapted methodology from the Release 04 monthly GRACE solutions by GeoForschungsZentrum Potsdam for the time interval from 08/2002 to 01/2008. We consider mass changes of the entire ice sheets but also of their individual large drainage basins. For Antarctica, for example, we detect ice mass loss which is clearly dominated by changes in the Amundsen Sea Sector and Northwest Marie Byrd Land (West Antarctica) while East Antarctica appears to be near balance. We also discuss global "fingerprints" of the detected ice mass changes in terms of sea level variations and crustal load deformations.

Emphasis is put on a thorough error assessment which exceeds previous work. The obtained insights may help to resolve some of the differences between the results of different studies and open the way to even more reliable and more detailed GRACE inferences on global mass redistributions.

THE DECADAL FLUCTUATIONS IN THE EARTH'S ROTATION AND IN THE CLIMATE CHARACTERISTICS

N. SIDORENKOV[1], I.R.G. WILSON[2]
[1] Hydrometcentre of RF,
B.Predtechensky pereulok, 11-13, Moscow, 123242, Russia
sidorenkov@mecom.ru
[2] Queensland Department of Education,
Toowoomba, Australia;
irgeo@ozemail.com.au

ABSTRACT. Close correlations are found between the decades-long variations in the length of the day (LOD), variations in the rate of the westward drift of the geomagnetic eccentric dipole, and variations in some key climate parameters i.e. anomalies in the type of the atmospheric circulation, the hemisphere-averaged air temperature, the increments of the Antarctic and Greenland ice sheet masses, and the PDO.

This presentation outlines recent progress towards a better understanding of the causes of these relationships. The constraints put on the processes in the Earths interior by the decadal fluctuations of the Earth's rotation are discussed. We proposed that there is a spin-orbit coupling between the Earth's rotation rate and its motion together with the Sun about the barycentre of the solar system. Evidence in favour of this hypothesis is presented.

1. INTRODUCTION

It is well known that fluctuations in the Earth's LOD have components with characteristic time scales of the order of several decades. The origin of these decadal fluctuations of the Earth's rotation velocity are usually attributed to the Earth's core-mantle coupling. Support for this hypothesis comes from the fact that it could explain why there is a close correlation between the decadal fluctuations in the Earth's rotation and the variations in the rate of the westward drift of the geomagnetic eccentric dipole. It is reasonable to assume that the observed changes could be produced by the redistribution of angular momentum between the Earths fluid core and mantle. However, we contend that the empirical evidences and facts demand that this generally accepted assumption should be revised.

2. THE EMPIRICAL EVIDENCE

Figure 1 shows that the observed changes in the specific mass of the Antarctic ice sheet closely correspond to the specific mass variations that are needed to explain the "decadal" fluctuations in LOD. However, this correspondence is only a qualitative one. The problem is that the amplitude of the observed variations in the specific ice mass is 28 times less than the required amplitude. However, we believe that this discrepancy can be explained by a model that involves the drift of lithosphere over the asthenosphere.

Since the mass of the ice sheets in Antarctic and Greenland depend on the variations in climate, it is reasonable to assume that the decadal fluctuations in the Earth's rotation may also correlate with the fluctuations in the climatic characteristics and indices. Following this line of reasoning, we have found that the atmospheric circulation regimes are well correlated with the changes in the Earths rotation rate.

Figure 2 shows a close relationship between the decadal-long fluctuations in the Earths rotational rate (solid curve), the cumulative sum of anomalies of the circulation form C atmospheric circulation using the Vangengeim's classification (dashed curve), and the ten-year running mean of the anomalies of the Northern Hemisphere air temperature (dotted curve).

Finally, figure 3 shows the relationship between the deviation of the Earth's LOD from its long–term trend and the Pacific Decadal Oscillation (PDO) index. The upper graph shows the PDO reconstruction of D'Arrigo et al. (2001) between 1707 and 1972. The reconstruction has been smoothed with a 15–year running mean filter to eliminate short–term fluctuations. Superimposed on this PDO reconstruction is the instrumental mean annual PDO index (Mantua 2007) which extends the PDO series up to the

year 2000. The lower graph shows the absolute deviation of the Earth's LOD from its long–term trend between 1656 and 2005. The data in this figure has also been smoothed with a 15-year running mean filter. We can see from figure 3 that whenever there are large deviations in the Earth's length of day from its long–term trend, the PDO index is positive. It is important to note that the changes in the LOD precede those in the PDO by about eight years.

Hence, it is possible that the exchange of angular momentum between the Earth's mantle and its liquid core could be responsible for the decadal fluctuations in the Earth's rotation rate. And it could be argued that it is these decadal fluctuations in the Earth's rotation rate that cause the observed long-term changes in the climatic and glaciological characteristics. However, we present new evidence that shows that these tele–connections could also be explained by a spin-orbit coupling mechanism operating between the planets and the Sun that simultaneously affects both the processes in the Earth's core and the Earth's climatic systems.

3. A SPIN-ORBIT COUPLING MECHANISM

A recent paper by Ian Wilson et al. (2008) presents evidence that claims the changes in the Sun's equatorial rotation rate are synchronized with the changes in the Sun's orbital motion about the barycentre of the Solar System. This paper showed that the recent maximum asymmetries in the Solar motion about the barycentre have occurred in the years 1865, 1900, 1934, 1970 and 2007. And as we can see in Figure 4, these years of maximum asymmetry in the Solar motion closely correspond to the points of inflection in the Earth's length-of-day.

Figure 5 shows that, from 1700 to 2000 A.D., on every occasion where the Sun has experienced a maximum in the asymmetry of its motion about the centre-of-mass of the Solar System, the Earth has also experienced a significant deviation in its rotation rate (i.e. LOD) from that expected from the long-term trends. This fact indicates that the changes in the Earth's rotation rate are synchronized with a phenomenon that is linked to the changes in the solar motion about the barycentre of the Solar System.

4. SUMMARY

We have shown that there are strong correlations between the decadal-long variations in the length of the day and variations in certain climate characteristics i.e. the increments of the Antarctic and Greenland ice sheet masses, anomalies of the atmospheric circulation regimes, and changes in the hemisphere-averaged air temperature and the Pacific Decadal Oscillation.

From the empirical data, we argue that there is compelling evidence to support the idea that these correlations are due to a spin-orbit coupling between the Earth's rotation rate and its motion (that it shares with the Sun) about the barycentre of the solar system.

5. REFERENCES

D'Arrigo, R., Villalba, R., and Wiles, G. 2001, "Tree-ring estimates of Pacific decadal climate variability", Clim. Dyn., 18, pp. 219–224.

Mantua, N.J., Hare, S.R., Zhang, J.M., and Francis, R.C. 1997, "A Pacific interdecadal climate oscillation with impacts on salmon production", Bull. Am. Meteorol. Soc., 78(6), pp. 1069–1079.

Sidorenkov, N.S. 2005, "Physics of the Earth's rotation instabilities", Astronomical and Astrophysical Transactions, vol. 24, No. 5, pp. 425–439.

Sidorenkov N.S., Lutsenko O.V., Bryazgin, N.N., 2005, "Variation of the mass of the sheet of Antarctica and instability of the Earths rotation." Russian Meteorology and Hydrology, No. 8, pp. 5-13.

Wilson, I. R. G., Carter, B. D., and White, I. A., 2008, "Does a Spin-Orbit Coupling Between the Sun and the Jovian Planets Govern the Solar Cycle?", Publications of the Astronomical Society of Australia, 25, pp. 85–93.

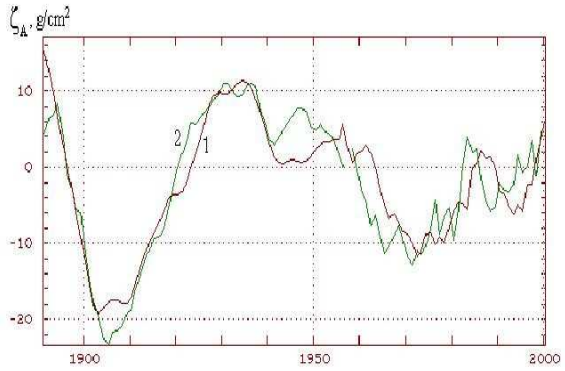

Figure 1: Temporal variations of the specific mass of ice in Antarctica, $g \cdot cm^{-2}$
1 - the theoretical value ; 2 - the empirical value (Sidorenkov et. al. 2005).

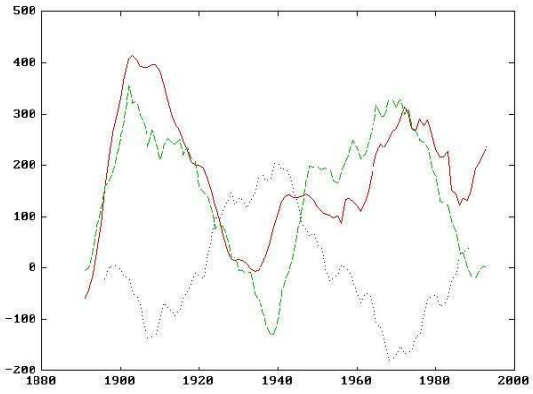

Figure 2: Synchronous changes in the length of day(solid curve), the cumulative sums of anomalies of the circulation form C (dashed curve), and of the ten-year running anomalies of the Northern Hemisphere air temperature (after elimination of a trend and a thousand fold magnification (dotted curve).

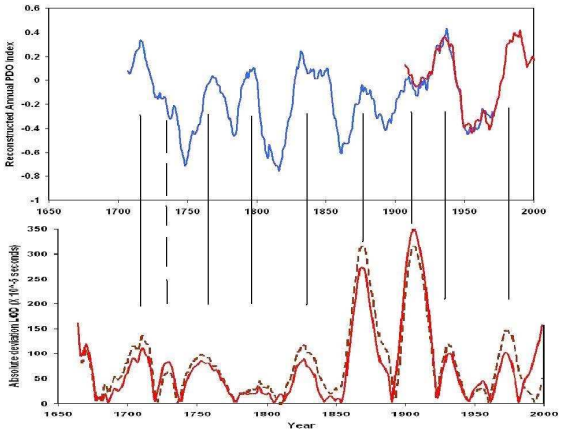

Figure 3: The upper graph shows the PDO reconstruction of D'Arrigo et al. (2001) between 1707 and 1972. The lower graph shows the absolute deviation of the Earths LOD from 1656 to 2005 (Sidorenkov 2005).

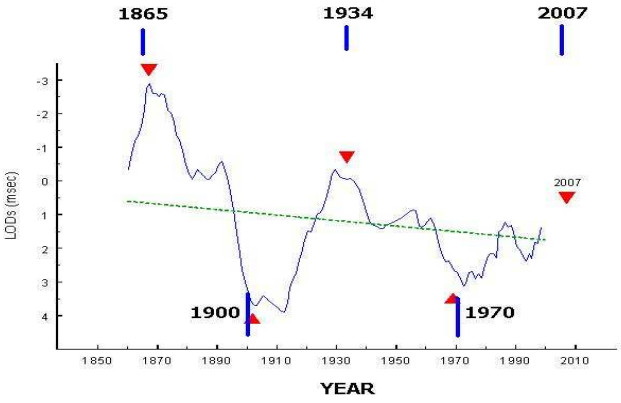

Figure 4: Wilson's asymmetries in the Solar motion (vertical lines); Landscheidt's zero phases in the solar motion (diamonds); tidal slow-down of the Earth's rotation (dashed line)

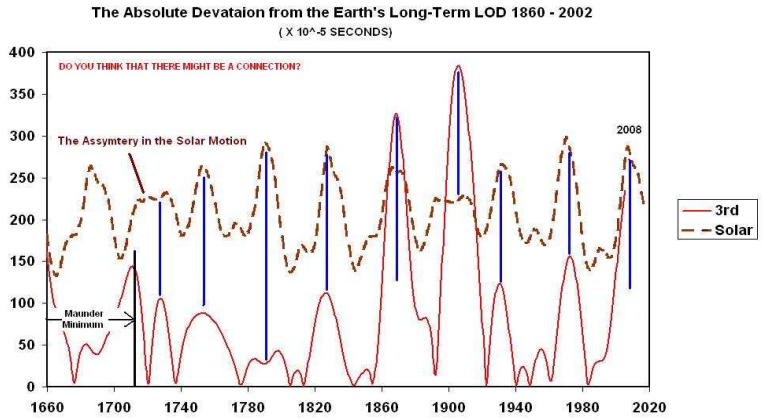

Figure 5: On every occasion where the Sun has experienced a maximum in the asymmetry of its motion about the centre-of-mass of the Solar System, the Earth has also experienced a significant deviation in its rotation rate (i.e. LOD) from that expected from the long-term trends

22-YEAR OSCILLATIONS OF UT1, CORE ANGULAR MOMENTUM AND GEOMAGNETIC FIELD

Ya. CHAPANOV[1], J. VONDRÁK[2], C. RON[2]
[1] Central Laboratory for Geodesy of Bulgarian Academy of Sciences
Acad. G. Bonchev Str., Bl.1, Sofia 1113, Bulgaria
e-mail: chapanov@clg.bas.bg
[2] Astronomical Institute of Academy of Sciences of Czech Republic
Boční II, 141 31 Prague, Czech Republic
e-mail: vondrak@ig.cas.cz, ron@ig.cas.cz

ABSTRACT.The possible interconnection between the 22-year cycles of the Earth rotation from one side and solar activity, geomagnetic field, Core Angular Momentum (CAM), global water redistribution, from the other one is investigated by means of annual UT1 data for the period 1623–2005, smoothed Wolf's numbers, AA and DST geomagnetic Indexes, Mean Sea Level (MSL) changes at Stockholm, and several solutions for CAM from the Special Bureau for the Core (SBC). The amplitude of 22-year UT1 oscillations is about 0.6s. Significant correlation exists between the 22-year cycles of UT1 and geomagnetic Index AA, most of the CAM solutions and MSL change at Stockholm. The analysis shows very small influence of the geomagnetic field on the observed 22-year UT1 cycles, whose excitation are 22-year climatic variations mainly and MSL oscillations with amplitude of about 9mm.

1. INTRODUCTION

The Earth rotation data for the period 1623.5-2005.5 are available from the IERS EOP Data Center. The annual time series of UT1-TT (Universal Time UT1 and Terrestrial Time TT) and LOD (Length of Day) are combination between the solution of Stephenson and Morrison (1984), based on lunar eclipses and star occultations before 1955 and modern determinations afterwards. These time series give good opportunity to study the long-term oscillations of UT1 and their connection with some natural phenomena as solar activity, climatic and weather variations, atmospheric and ocean circulations and conditions etc. A model of Earth rotation periodical variations, based on Fourier approximation of UT1 data, is created in (Chapanov et al., 2008). The model separates UT1 oscillations into different frequency bands, corresponding to the intrinsic cycles of the solar activity and liquid earth core. This model is used here to study interconnection between the 22-year cycles of the solar activity, geomagnetic field, core angular momentum and mean sea level.

2. UT1-TT DATA AND MODEL OF EARTH ROTATION

The UT1 data consist of visible long term oscillations and a parabolic part (Fig.1, a). According to

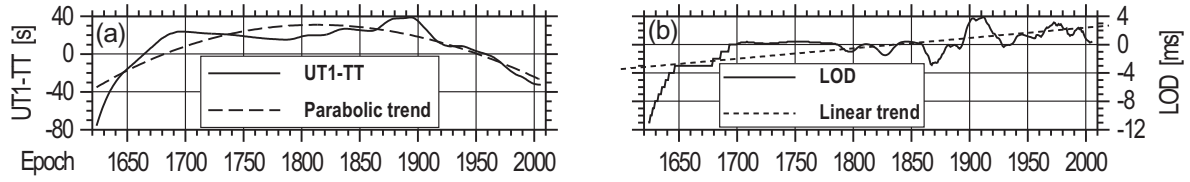

Figure 1: LOD and UT1-TT time series based on Morrison and Stevenson solution for the Earth rotation.

the LOD behavior (Fig.1, b), the data contain significant short-periodic noise for the period 1623-1700 due to step-wise variations, almost no change in the period 1700-1790 and significant decadal oscillations after 1800. The periodical part of the UT1-TT variations are determined after excluding the polynomial part of power 2 from the data (Fig.2, a). The model of the Earth rotation for the period 1623.5-2005.5 is

created by means of a Fourier approximation of the UT1-TT variations with use of 100 harmonics, which includes oscillations with periods longer than 3.8a and estimated accuracy of amplitudes about 11ms. The coefficients of the model are estimated by means of the Least Squares Method. Part of the peaks of UT1 amplitude spectrum (Fig.2, b) are connected with the cycles of some natural phenomena: 6.5-year gravity cycles (1); 11-year sunspot variations (2); 12-year core cycles (3); 18.6-year tides due to motion of lunar node (4); 22-year solar magnetic cycles (5); 45-year solar equatorial asymmetry (6), and many other signals coming from the liquid core of the Earth.

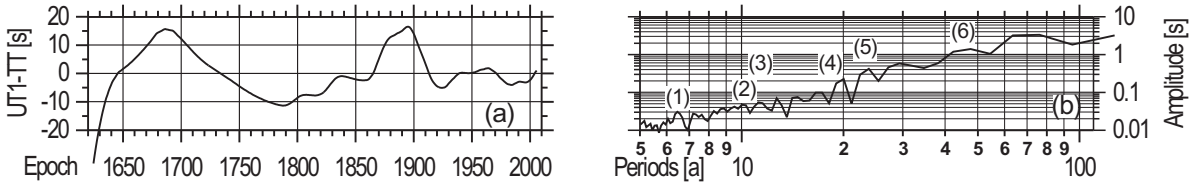

Figure 2: Periodical part of UT1-TT variations, determined by excluding of the parabolic term.

3. 22-YEAR CYCLES OF THE SOLAR ACTIVITY AND UT1

Three time series of 22-year cycles of UT1, determined by the coefficients of Fourier approximations of UT1 data since 1623, 1800 and 1868 are used here. The first time series contains three oscillations with periods from the band 21-24a (Fig.3, a) and will be used to compare common 22-year cycles between the Earth rotation and solar activity. The second time series contains three oscillations with periods from the band 20-25a, and will be used to compare common 22-year cycles between the Earth rotation, CAM and mean sea level (Fig.3, b). The last time series contains two oscillations with periods 20 and 23a and will be used to compare common oscillations of UT1 and AA geomagnetic Index (Fig.3, c).

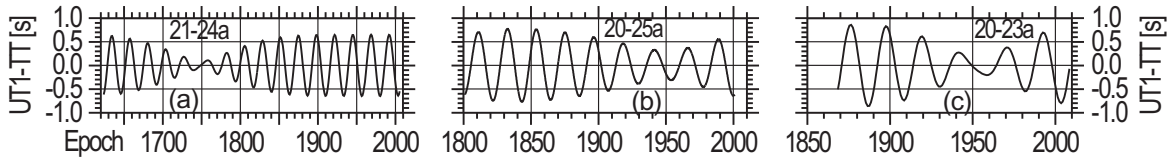

Figure 3: UT1-TT variations with periods from the band 21-24a since 1623 (a); with periods from the band 20-25a since 1800 (b); and with periods from the band 20-25a since 1868 (c).

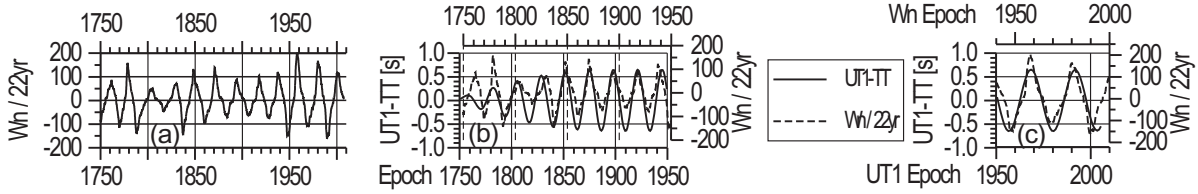

Figure 4: Extended time series of 22-year solar activity cycles, determined by sign alternation of Wolf's numbers cycles(a). Comparison between the 22-year cycles of UT1–TT and extended Wolf's numbers for the periods 1750–1950, (b) and 1950–2008, (c).

The amplitude of 22-year UT1 oscillations decreases during the Maunder minimum of the solar activity (1645-1715) and next 3 decades, when the UT1 oscillations synchronize their phase with the new solar magnetic cycles. The UT1 amplitude increases linearly during next five 22-year cycles (1750-1860) to the value of 600ms (Fig.3, a). The comparison between the 22-year cycles of the UT1 and solar activity is made by means of extended time series of solar magnetic cycles, determined by sign alternation of Wolf's numbers cycles (Fig.4, a). The correlation coefficients between these two time series are +0.71 for the period 1750–1950 with time delay of about 3 years (Fig.4, b), and +0.86 for the period 1950–2005, with significant fictitious phase delay (fig.4, c), due to variations of the periods of solar activity cycles.

4. GEOMAGNETIC INDEXES AND CORE ANGULAR MOMENTUM

The hourly geomagnetic Index AA for the period 1868–2008 (Fig.5, a) and daily equatorial DST Index for the period 1963–2005 (Fig.5, b) are used here, as well as some solutions for the Core angular momentum in LOD units for the period 1843–1990 (Fig.6, a), available at the server of the Special Bureau for the Core (`http://sbc.oma.be/`) of the IERS Global Geophysical Fluids Centre (GGFC).

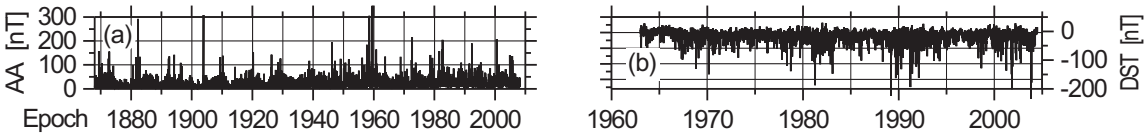

Figure 5: Geomagnetic Indexes AA – (a) and DST – (b).

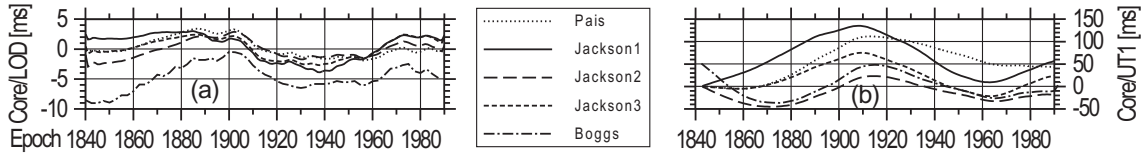

Figure 6: Core Angular Momentum in LOD units – (a) and in UT1 units – (b).

The 22-year oscillations of AA Index are determined by two oscillations with periods 20a and 23a from the Fourier approximation of the data and they are highly correlated with the 22-year cycles of UT1 with coefficient +0.92 and time advance 5a (Fig.7, a), while the long-term behavior of DST Index, determined by Vondrák's filtration reveal only partial correlation with the UT1 variations (Fig.7, b). The

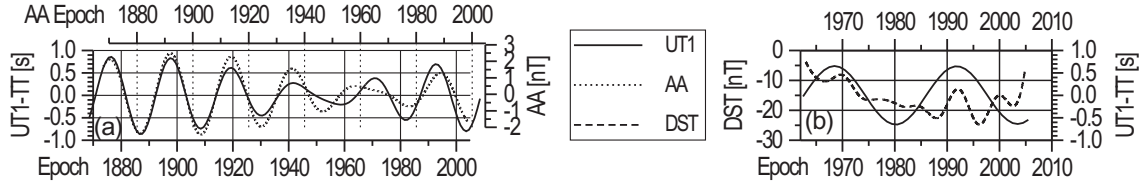

Figure 7: Comparison between 22-year cycles of UT1-TT and geomagnetic Indexes AA (a) and DST (b).

CAM in UT1 units (Fig.6, b) are determined by an integration of the following solutions for the CAM: Hide et al. (2000), Pais and Hulot (2000) and 3 solutions of Jackson (1997). The 22-year oscillations of the CAM, determined by oscillations with periods from the band 21-25a, are negatively correlated with the corresponding UT1 oscillations, but their very low amplitude of about 1-2ms is not enough to explain the amplitude of about 600ms of the observed 22-year UT1 oscillations (Fig.8, a).

5. 22-YEAR CYCLES OF THE MEAN SEA LEVEL AND UT1

The probable source of excitation of the 22-year variations of Earth rotation are 22-year climatic variations due to the solar activity and oscillations of the mean sea level connected with them. The changes of MSL, due to total solar irradiance variations and additional evaporation, followed by global water redistribution and ice thickness variations over the polar caps, are the necessary conditions to provide appropriate oscillations of the axial Earth moment of inertia with 22-year period. The UT1 and MSL oscillations should have opposite phases during the above process.

All cycles of UT1 and MSL oscillations at Stockholm with periods from the band 20-25a are highly correlated with coefficient –0.82 and delay of about 4a (Fig.8,b). The 9mm amplitude of 22-year MSL oscillations at Stockholm may explain 15% of the observed UT1 oscillations, which points out to possible resonance between the MSL change due to the solar activity (which affects Earth's inertial moment) and core oscillations.

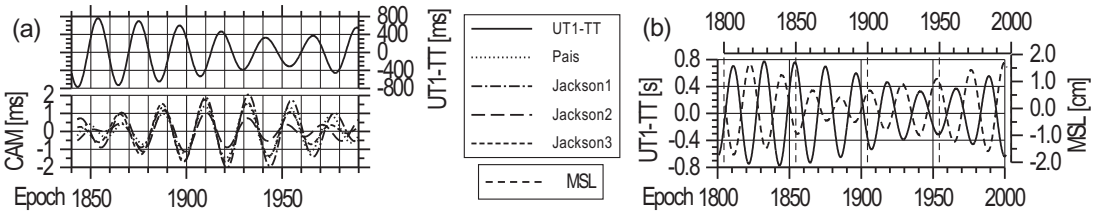

Figure 8: Comparison between 22-year cycles of the Core Angular Momentum (CAM) and UT1-TT (a); and between 22-year cycles of the Mean Sea Level at Stockholm and UT1-TT (b) .

6. CONCLUSIONS

The time series of the universal time UT1 variations for the interval 1623.5-2005.5 give good opportunity to study the long-term oscillations of UT1, corresponding to the magnetic cycles of the solar activity with period about 22a. The amplitude of 22-year UT1 oscillations decreases during the Maunder minimum (1645-1715) and next 3 decades, when the UT1 oscillations synchronize their phase with the new solar magnetic cycles. The UT1 amplitude increases linearly during next five 22-year cycles (1750-1860) to the value of 600ms.

The extended time series of 22-year cycles of the Wolf's number, determined by sign alternation, is highly correlated with the 22-year variations of UT1-TT after 1750 with a phase shift during the last 2 cycles.

The 22-year UT1 variations are in good agreement with the corresponding cycles of the AA geomagnetic Index with correlation coefficient +0.92 and time delay of about 5 year. The 22-year oscillations of CAM, determined from some solutions of SBC, are negatively correlated with the corresponding UT1 oscillations, but their very low amplitude of about 1-2ms is not enough to explain the amplitude of about 600ms of the observed 22-year UT1 oscillations.

The probable source of excitation of the 22-year variations of Earth rotation are 22-year climatic variations due to the solar activity and oscillations of the mean sea level connected with them. The changes of MSL, due to total solar irradiance variations and additional evaporation, followed by global water redistribution and ice thickness variations over the polar caps, are the necessary conditions to provide appropriate oscillations of the axial Earth moment of inertia with 22-year period. The observed amplitude of 22-year MSL oscillations at Stockholm may explain 15% of the observed UT1 oscillations, which points out to possible resonance between the MSL change due to the solar activity (which affects Earth's inertial moment) and core oscillations.

It is necessary to separate the direct influence of the solar activity on the 22-year UT1 oscillations from the core signals. Two basic approaches are available: by estimating UT1 response to the 22-year component of the Wolf's numbers variations, or by determining the Earth's inertial moment change, due to MSL oscillations and global water redistribution over the continents and polar caps.

7. REFERENCES

Chapanov, Ya. Vondrák, J., Ron, C., 2008, "Decadal Oscillations of The Earth Rotation", AIP Conf. Proc., Vol. 1043, "Exploring the Solar system and the Universe", Bucharest, 14-20 April 2008, 197–200.

Hide, R., Boggs, D. H. and Dickey, J. O., 2000, "Angular Momentum fluctuations within the Earth's liquid core and torsional oscillations of the core-mantle system", Geophys. J. Int. 143, 777–786.

Jackson A., 1997, "Time-Depency of geostrophic core surface motions", Phys. Earth Planet. Int., 103, 293–311.

Pais, A. and Hulot, G., 2000, "Length of day decade variations, torsional oscillations and inner core superrotation: evidence from recovered core surface zonal flows", Phys. Earth Planet. Int. 118, 291–316.

Stephenson, F.R. and Morrison, L.V., 1984, "Long-Term Changes in the Rotation of the Earth: 700 BC to AD 1980", Phil. Trans. R. Soc. of London, Ser. A, 313, 47–70.

LUNAR LASER RANGING AND EARTH ORIENTATION

L. BISKUPEK, J. MÜLLER
Institut für Erdmessung, Leibniz Universität Hannover
Schneiderberg 50, 30167 Hannover
e-mail: biskupek@ife.uni-hannover.de, mueller@ife.uni-hannover.de

ABSTRACT. Lunar Laser Ranging (LLR) is carried out for more than 38 years. Several parameters of the Earth–Moon system can be determined with high accuracy by dedicated data analysis. These comprise, e.g., coordinates of the stations and the reflectors, lunar gravity field, orbit and rotation of the Moon, the secular tidal acceleration but also gravitational physics parameters. Here, we focus on the determination of Earth orientation parameters. Long–term nutation coefficients for the 18.6 years period are determined in the global adjustment and compared with results from studies of other analysis centres and parameters of the MHB2000 model of (Mathews et al., 2002). Furthermore, Earth rotation $\Delta UT0$ and variation of latitude $\Delta\phi$ are determined by the daily decomposition method from post–fit residuals. In our LLR analysis, different EOP series are applied and their effect on the Earth–Moon parameters investigated. The results of this study are presented, too.

1. MODEL AND ANALYSIS

The existing model to analyse LLR data at the Institut für Erdmessung (IfE) is based on Einstein's theory of gravity. It is fully relativistic and complete up to the first post–Newtonian ($1/c^2$) level, e.g. (Müller et al., 2008). The basic observation equation for the station–reflector distance is defined in the Barycentric Celestial Reference Frame (BCRF). The station and reflector coordinates have to be transformed from their respective reference frames (the terrestrial (TRF) or selenocentric (SRF) reference frame) into the inertial frame. Here, the Earth orientation parameters (EOP) are used for the Earth and the libration angles, computed by numerical integration, for the Moon. The Earth–Moon distance is obtained by numerical integration of the corresponding equation of motion, considering Newtonian and relativistic effects.

Based on the LLR model two groups of parameters for the Earth–Moon system (ca 180 in total) are determined by a weighted least–squares adjustment of the observations. The Newtonian parameters are, e.g., initial position, velocity and physical librations of the Moon, coordinates of LLR observatories and retro–reflectors, orbit and mass of the Earth–Moon system, lunar gravity field, long–periodic nutation parameters and the lag angle, indicating the lunar tidal acceleration. These parameters are summarised in the so–called standard solution. The post–fit residuals of the solution can be further investigated for Earth orientation parameters, see below. By extending the standard solution, it is possible to solve for parameters related to general relativity, like temporal variation of the gravitational constant (Müller and Biskupek, 2007) and metric parameters. It is also possible to investigate the strong equivalence principle and preferred–frame effects (Soffel et al., 2008).

Figure 1 shows the annually averaged weighted post–fit residuals of the standard solution with data from Dec. 1969 to Mar. 2008 (16230 normal points). It reflects the precision of the LLR measurement and analysis model, about $20-30$ cm up to the middle 80ies. From 1985 on, more stations started to observe the Moon and the residuals decreased. In the last years, only two stations, one with reduced accuracy, tracked the Moon, so that the residuals increased again. For more details see (Müller et al., 2008).

2. EARTH ROTATION FROM LLR DATA BY DAILY DECOMPOSITION

To investigate the effect of different EOP series in the LLR analysis, the series IERS EOP C04 and COMB2006 were used as input for the global standard solution. Then, the post–fit residuals were analysed to determine corrections for Earth rotation $\Delta UT0$ and variation of latitude $\Delta\phi$. In a further step, the $\Delta\phi$ corrections were used to iteratively improve the results of the global standard solution.

Both EOP series were obtained from the combination of "operational" EOP series derived from the

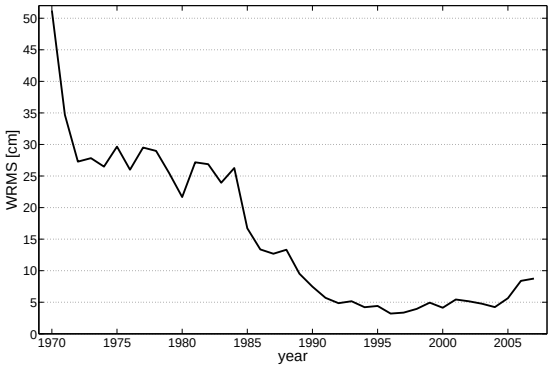

Figure 1: Weighted post–fit residuals (observed minus computed Earth–Moon distance) annually averaged

various space–geodetic techniques VLBI (Very Long Baseline Interferometry), GPS (Global Positioning System), SLR (Satellite Laser Ranging) and LLR, as well as optical observations, see (Gambis, 2004; Gross, 2007). Additionally, in the C04 series DORIS (Doppler Orbitography and Radiopositioning Integrated by Satellite) data were included. Further differences between the series on the data side are, that not exactly the same time periods were used and the filter techniques to combine the data were different. Another difference between the series is the treatment of tidal effects. In the C04 series periods from 5 days to 18.6 years are corrected by the model of (Defraigne & Smits, 1999), in the COMB2006 series periods from 5 days to 35 days are corrected using the procedure of (Yoder et al., 1981). As the comparison of the two series (C04 minus COMB2006) shows, the difference in all components (x_P, y_P and $\Delta UT1$) is large in the period between 1970 and 1982. It is between -18 and 34 mas for polar coordinate x_P and between -42 and 15 mas for polar coordinate y_P. For Earth rotation $\Delta UT1$, the difference is between -2.1 and 3.3 ms. From 1982 on, the difference decrease more and more, for polar coordinates it is near zero now. For $\Delta UT1$ it is about -0.005 ms today, because of the different treatment of the tidal effects.

The two EOP series, i.e., the pole coordinates x_P/y_P and Earth rotation $\Delta UT1$, are used in the analysis for the transformation between the celestial and terrestrial systems. In addition, the long–periodic, diurnal and sub–diurnal effects of the ocean are corrected according to the IERS Conventions 2003.

To determine Earth rotation from LLR data, the post–fit residuals are first sorted by station–reflector combinations and merged in daily sets. One set must include the minimum of three station–reflector pairs. Out of 16230 observations, 1179 daily sets for the station OCA in Grasse and 752 daily sets for the station McDonald in Texas were found. These sets are analysed in a second least–squares adjustment (daily decomposition method, see (Dickey et al., 1985) applying the following model:

$$r(t) = r_{\Delta UT0} + r_{\Delta\phi} + r_n, \tag{1}$$

where the post–fit residuals of the first least–squares fit are assumed to be caused by contributions from Earth rotation

$$r_{\Delta UT0} = 2\ \Delta UT0\ r_E\ \cos\phi\ \sin H\ \cos\delta, \tag{2}$$

from variation of latitude

$$r_{\Delta\phi} = 2\ \Delta\phi\ r_E\ (\sin\phi\ \cos\delta\ \cos H - \sin\delta\ \cos\phi) \tag{3}$$

and a part containing other effects r_n, like systematic ranging errors and model errors. $\Delta UT0$ and $\Delta\phi$ enter the respective equation as

$$\Delta\phi = x_P\ \cos\lambda - y_P\ \sin\lambda \tag{4}$$

and

$$\Delta UT0 = \Delta UT1 + \tan\phi\ (x_P\ \sin\lambda + y_P\ \cos\lambda) \tag{5}$$

with the declination δ, the hour angle H of the Moon, the latitude ϕ and the Earth's radius r_E. Figure 2 shows the result for the determination of $\Delta\phi$ from the post–fit residuals for the McDonald station by using the different EOP series. The daily solutions (dots), calculated with eq. (3), are smoothed by a spline filter. The curves of the two calculations show large differences in the 70ies and middle 80ies, the

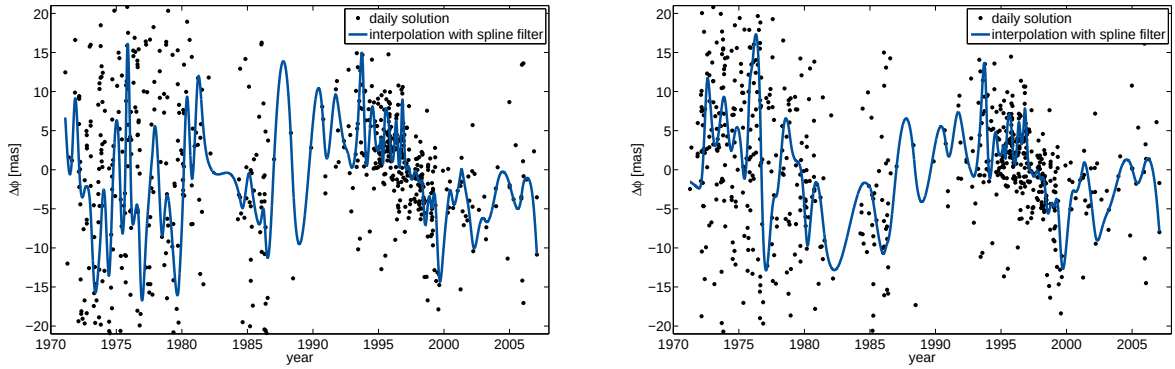

Figure 2: Results of the daily decomposition method for $\Delta\phi$ when using the EOP series C04 (left) and COMB2006 (right) as input in the global adjustment

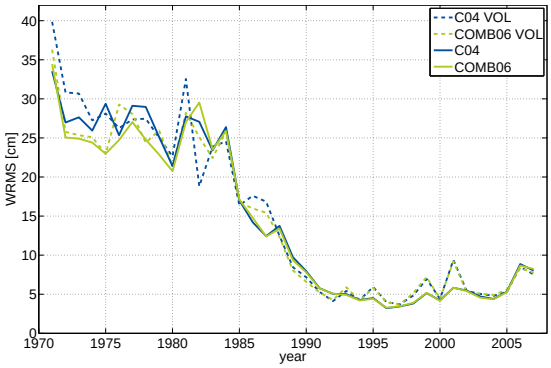

Figure 3: Results of using the $\Delta\phi$ corrections in the global adjustment

period where the two EOP series show large differences, too. From the middle 80ies on, when both EOP series are very similar, also the results are very similar here.

In the next step, these spline–interpolated $\Delta\phi$ values are iteratively used as corrections in the global adjustment, figure 3 shows the corresponding results. Here, two calculations have been made for both EOP series: One as reference without the estimated $\Delta\phi$ values (solid lines) and one with the $\Delta\phi$ correction applied (dotted lines). It can be seen, that again in the time span from the middle 80ies on, where the EOP series are very similar, also the residuals are very similar. It is furthermore obvious, that the residuals can not really be improved by using the $\Delta\phi$ correction. It seems, that the input EOP series are already very accurate. In the time span up to the 80ies, the residuals by using the COMB2006 series are smaller than that one based on the C04. But also here, the results of the global adjustment can not really be improved by applying the determined $\Delta\phi$ correction.

3. NUTATION

A further study was dedicated to the determination of nutation parameters from LLR data. In the IERS Conventions 2003 nutation is described as

$$\Delta\psi = \sum_{i=1}^{N} (A_i + A_i' t)\ \sin(ARG) + (A_i'' + A_i''' t)\ \cos(ARG) \tag{6}$$

$$\Delta\epsilon = \sum_{i=1}^{N} (B_i + B_i' t)\ \cos(ARG) + (B_i'' + B_i''' t)\ \sin(ARG) \tag{7}$$

with $ARG = \sum_j^5 N_j F_j$, N_j : multiplier, F_j : Delaunay parameter. In the global adjustment, the non–time–dependent nutation coefficients A_i, A_i'', B_i and B_i'' of the 18.6 years period were determined and compared with the values of the MHB2000 model (Mathews et al., 2002). Table 1 gives some preliminary

Table 1: Preliminary results for nutation coefficients of the 18.6 years period

	A_i[mas]	A_i" [mas]	B_i [mas]	B_i" [mas]
MHB2000 model	-17206.42	3.33	9205.23	1.54
our investigation	-17203.42	4.15	9204.49	3.81
standard deviation	0.39	0.31	0.17	0.15

results. The values of all coefficients show large differences to the values of the model, the largest in A_i and B_i''. These are also seen in the analysis of other groups (Williams, 2008).

4. CONCLUSIONS

The investigations show, that the determination of variation of latitude $\Delta\phi$ from LLR data is possible. Using these values in the next iteration step of the LLR analysis does, however, not significantly improve the residuals. Obviously, the input EOP series are already of good quality. As further work other filters, apart from the spline filter, will be tested. Also values for length of day LOD will be calculated to compare them with LOD results from VLBI.

The estimated nutation coefficients for the 18.6 years period show large differences to the MHB2000 model, which are not understood yet. Here, further investigation is needed. In a next step, the coefficients for more periods (9 years, 1 year) will be determined and compared to the model.

Acknowledgements. Current LLR data are collected, archived and distributed under the auspices of the International Laser Ranging Service (ILRS) (Pearlman et al., 2002). We acknowledge with thanks, that the more than 38 years of LLR data, used in these analyses, have been obtained under the efforts of personnel at the Observatoire de la Côte d'Azur in France, the LURE Observatory in Maui, Hawaii, the McDonald Observatory in Texas as well as the Apache Point Observatory in New Mexico.

We would also like to thank the DFG, the German Research Foundation, which funded this study within the research unit FOR584 "Earth rotation and global dynamic processes".

5. REFERENCES

Defraigne, P., Smits, I., 1999, "Length of day variations due to zonal tides for an inelastic earth in non–hydrostatic equilibrium", Geophys. J. Int. , 139, pp. 563–572.

Dickey, J.O., Newhall, X.X., Williams, J.G., 1985, "Earth Orientation From Lunar Laser Ranging and an Error Analysis of Polar Motion Services", J. Geophys. Res. (B11), 90, pp. 9353–9362.

Gambis, D., 2004, "Monitoring Earth orientation using space–geodetic techniques: state–of–the–artand prospective", J. Geod., 78, pp. 295–303.

Gross, R.S., 2007, "Combinations of Earth orientation measurements: SPACE2006, COMB2006, and POLE2006", JPL Publication, no. 07-05.

Mathews, P.M., Herring, T.A., Buffett, B.A., 2002, "Modeling of nutation and precession: New nutation series for nonrigid Earth and insights into the Earth's interior", J. Geophys. Res. (B4), 107, pp. 10.1029/2001JB000390.

McCarthy, D.D. (eds.), Petit, G. (eds.), 2004, "IERS Conventions (2003)", IERS Technical Note No. 32, Verlag des Bundesamts für Kartographie und Geodäsie, Frankfurt am Main.

Müller, J., Biskupek, L., 2007, "Variations of the gravitational constant from lunar laser ranging data", Class. Quan. Gravity, 24, pp. 4533–4538, doi: 10.1088/0264-9381/24/17/017.

Müller, J., Williams, J.G., Turyshev, S.G., 2008, "Lunar Laser Ranging Contributions to Relativity and Geodesy", in: Lasers, Clocks and Drag–Free Control: Exploration of Relativistic Gravity in Space, eds: Dittus, H., Lämmerzahl, C., Turyshev, S.G., Springer, 349, pp. 457–472.

Pearlman, M.R., Degnan, J.J., Bosworth, J.M., 2002, "The International Laser Ranging Service", Adv. Space Res., 30, pp. 135–143, doi: 10.1016/S0273-1177(02)00277-6.

Soffel, M., Klioner, S., Müller, J., Biskupek, L., 2008, "Gravitomagnetism and lunar laser ranging", Phys. Rev. D, 78, pp. 024033.

Williams, J.G., 2008, Priv. communication.

Yoder, C.F., Williams, J.G., Parke, M.E., 1981, "Tidal Variations of Earth Rotation", J. Geophys. Res. , 86, pp. 881–891.

WHAT COULD BRING LLR OBSERVATIONS IN DETERMINING THE POSITION OF THE CELESTIAL POLE

W. ZERHOUNI, N. CAPITAINE, G. FRANCOU
SYRTE, Observatoire de Paris, CNRS, UPMC
61 Avenue de l'Observatoire 75014 Paris France
e-mail: wassila.zerhouni@obspm.fr; nicole.capitaine@obspm.fr; gerard.francou@obspm.fr

ABSTRACT. It has been demonstrated that the analysis of Lunar Laser Ranging (LLR) observations could bring scientific results in various domains including astronomy, gedoynamics and gravitational physics. Here, we focus on the contribution of the LLR in determining the Earth Orientation Parameters (EOP), especially, the direction towards the Celestial Intermediate Pole (CIP) in the Geocentric Celestial reference System. The strategy we have followed, consists in : first, calculating the LLR residuals over a period of more than 37 years, using the IAU 2006-2000A model of precession-nutation (i.e MHB 2000 nutation of Mathews et al. 2002 and P03 precession of Capitaine et al. 2003) and the CIO based procedure. Second, determining the GCRS X and Y coordinates of the Celestial Intermediate Pole at regular interval (i.e in our case, every 70 days). Finally, comparing the results obtained with VLBI observations in order to evaluate the potential of LLR as compared to VLBI for estimating the X, Y quantities.

1. INTRODUCTION

The main purpose of this paper is to focus on the application of the Lunar Laser Ranging technique in the field of the Earth rotation, especially for the determination of the celestial pole coordinates.
We can divide our work into two principals parts :

- the first part consists in the calculation of the LLR residuals with respect to all the best available models,
- the second part consists in the determination of the celestial pole coordinates from LLR and analysis of the correction to the IAU precession-nutation model.

2. CALCULATION AND ANALYSIS

For the calculation of the residuals, we have used the LLR data from both stations of McDonald and CERGA over periods spanning 1969–2006 and 1984–2005, respectively. Figure 1 shows the residuals obtained for McDonald's station.

Then, we have calculated the corrections to the celestial pole coordinates with respect to the IAU 2006-2000A model of precession nutation (i.e MHB 2000 as the nutation model and P03 as the precession model) every 70 days. We have used the CIO procedure and the SOFA 2007 routines (see at `www.iau-sofa.rl.ac.uk`).
Figure 2 represents the DX, DY corrections to the celestial pole coordinates obtained with this computation.

In order to characterize the signal, we have first estimated the corrections to the long term nutation amplitudes (18.6-yr, 9.3-yr, secular term and constant term). Second, we have estimated the annual, semi-annual, secular and constant term. In this case, we have first removed the Free Core Nutation using a routine developed by S.Lambert (cf. IERS Conventions 2003 updated).
The results obtained in the first case are provided in Fig.3.
Figure 4 represents the results obtained in the second case.

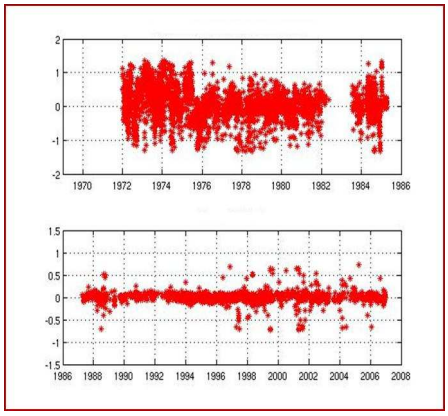

Figure 1: LLR residuals of McDonald's station from 1969 to 2006 (in meters)

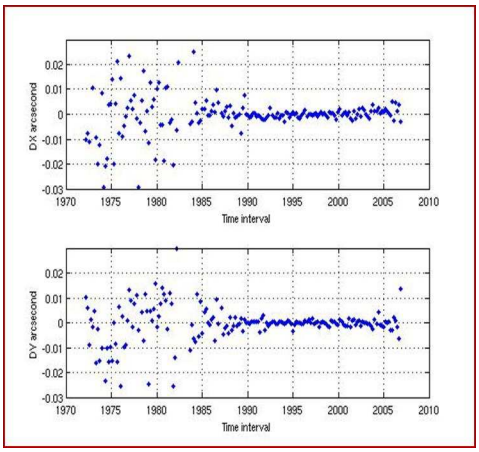

Figure 2: DX, DY corrections to the celestial pole coordinates (LLR data, IAU 2006-2000A precession nutation model)

Finally, we have calculated the VLBI celestial pole offsets with respect to the IAU 2006-2000A model of precession-nutation using the IVS combined solution (ivse08q1.eops). This solutions is given with respect to the IAU 2000A model of precession nutation. In order to be consistent with our work, i.e to refer the celestial pole offsets to the IAU2006-2000A model, we have used Eq.1 (from Capitaine & Wallace 2006, Eq.(41) after correcting a typographical error), which expresses the difference between the IAU2006 and IAU2000 model. The results are represented on Fig.5.

$$\begin{aligned} X_{IAU2006} - X_{IAU2000} &= 155t - 2564t^2 + 2t^3 + 54t^4 \\ Y_{IAU2006} - Y_{IAU2000} &= -514t - 24t^2 + 58t^3 - 1t^4 - 1t^5 \end{aligned} \quad (1)$$

It is clear from Fig.5 that the corrections to the celestial pole coordinates obtained from VLBI are determined with a better precision than with the LLR observations. This is due to the imperfect distribution of the LLR observations.

3. CONCLUSION

From LLR observations, it is possible to determine the corrections to the celestial pole coordinates with a precision of the order of 100μas, which is ten times greater than with VLBI. An appropriate combination of these two is expected probably contribute to the improvement of this determination.

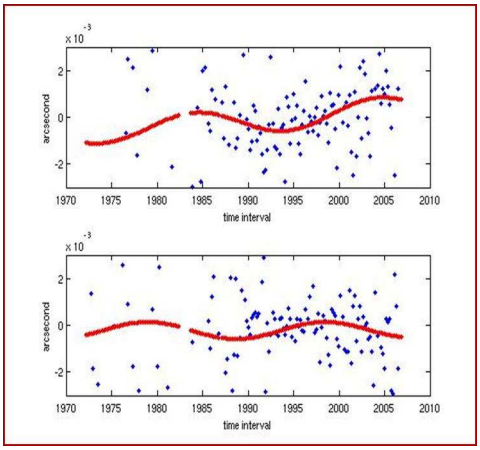

Figure 3: dots in blue: correction DX, DY to the celestial pole coordinates - lines in red: the fitted terms (18.6, 9.3, secular and constant term)

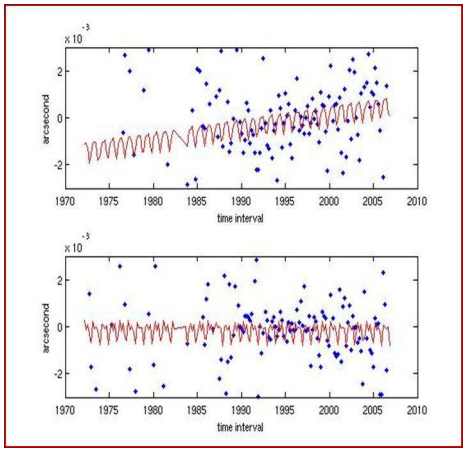

Figure 4: dots in blue: correction DX, DY to the celestial pole coordinates - lines in red: the fitted terms (annual, semi-annual, secular and constant term)

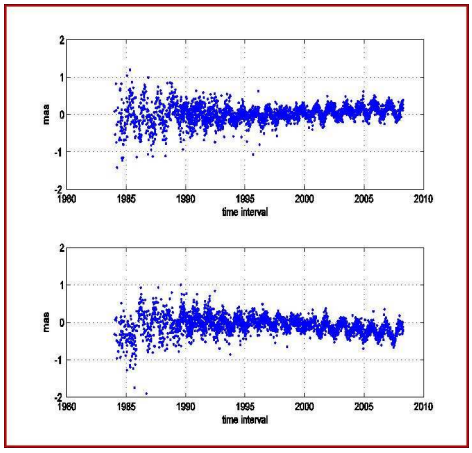

Figure 5: VLBI pole offsets with respect to the IAU 2006-2000A model of precession nutation

4. REFERENCES

Capitaine, N., Wallace, P.T 2006, High precision methods for locating the celestial intermediate pole and origin, Astron. Astrophys., 450, pp.855-872.

Capitaine, N., Wallace, P.T., and Chapront, J. 2003, Expressions for IAU 2000 precession quantities, Astron. Astrophys., 412, 567-586.

Chapront, J., Chapront-Touz, M. and Francou, G. 1999, Determination of the lunar orbital and rotational parameters and of the ecliptic reference system orientation from LLR measurements and IERS data, Astron. Astrophys., 343, 624-633.

Chapront, J., Chapront-Touz, M. and Francou, G. 2002, A new determination of lunar orbital parameters precession constant and tidal acceleration from LLR measurements, Astron. Astrophys., 387, 700-709.

Mathews, P.M., Herring, T.A., and Buffet, B.A. 2002, J.Geophys. Res, 107(B4), 10.1029/2001JB00390.

McCarthy, D. D. 1996, IERS technical Note 21: IERS Conventions (1996).

IERS technical Note 32 : IERS Conventions (2003).

SOFA : www.iau-sofa.rl.ac.uk.

website : hpiers.obspm.fr/eop-pc/models/fcn/index.html.

CONTRIBUTION OF THE COMPLETE GLONASS CONSTELLATION TO THE ESTIMATION OF NUTATION RATES

M. KUDRYASHOVA, R. WEBER, H. SCHUH, S. ENGLICH
Institute of Geodesy and Geophysics Vienna University of Technology
Gusshausstrasse 27-29, E128/1, A-1040 Wien, Austria
e-mail: mvk@mars.hg.tuwien.ac.at, robert.weber@tuwien.ac.at

ABSTRACT. It is well known that nutation rates can be derived from precise distance measurements to Global Navigation System (GPS) satellites gained within a global reference station network. The main goal of this work is to study the potential contribution of new satellite constellations (like revitalized GLONASS and upcoming GALILEO) to the estimation of nutation rates w.r.t. GPS-only based nutation rates. For this purpose two series of nutation rates have been produced: the first one is based on the GPS observations only and the second – on the observations of two satellite systems (GPS and GLONASS). In order to derive these series we used simulated observations produced by means of the Bernese v.5.0 software [1]. This investigation highlights the impact of the geometry and gain in number of observations due to new or fully upgraded constellations on the overall error budget and in special on the correlation coefficients between nutation rates and radiation pressure parameters.

1. DESCRIPTION OF SOLUTION

For our analysis we produced two series of nutation parameters: a GPS-only based solution and a GPS+GLONASS combined solution. To generate the first series we used real GPS satellite orbits and clock information delivered by the CODE AC of the IGS. The second series have been established on the basis of simulated orbits of the 24 satellites of a complete GLONASS constellation [2]. In a further step of the analysis we had to simulate observations for both solutions (to obtain comparable results also the GPS observations were simulated).

Characteristics which are common for both solutions are summarized below:

- software: BERNESE 5.0 (for simulation and processing of observations);
- network: 116 stations from IGS realisation of ITRF2005;
- nutation offsets w.r.t. IAU 2000 nutation model;
- estimated parameters: corrections to orbit parameters (Keplerian elements and radiation pressure parameters), tracking station coordinates and nutation rates;
- pre-eliminated parameters: clocks and troposphere parameters, ambiguities;
- data span: 12.09.2005 - 27.09.2005 (CONT05 campaign).

Since we processed simulated observations we had to introduce two changes into our standard procedure to estimate nutation rates from GNSS observations. The standard procedure and changes are shown in the Fig.1. Firstly, we had to adapt the orbit fitting procedure because the virtual a priori orbit information could not be fitted by Bernese force models with reliably small residuals. Secondly, due to simplifications, the produced orbits experience noticeable gaps at the day borders. As a result, the estimation of nutation rates has to be made on the basis of one-day solutions.

2. RESULTS AND DISCUSSION

As expected the introduction of a simulated GLONASS constellation increases the number of observations almost twice (by $\approx 90\%$ under the assumption of an observation network fully equipped with hybrid GPS+GLONASS receivers). This implies in case of non-existing biases (a very crude assumption) a decrease of the rms of the estimated parameters according to the square-root law. The numbers in

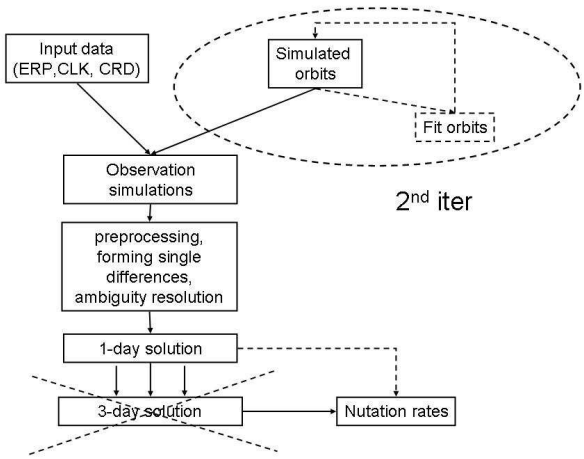

Fig1. Data-flow diagram. The solid line boxes and arrows sketch our standard procedure, the dotted line - changes have been made for simulations.

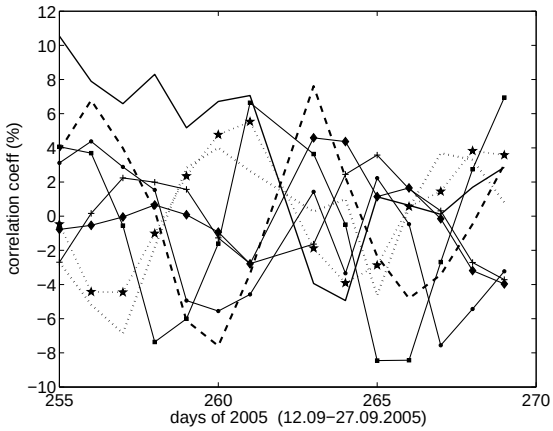

Fig2. Correlation coefficients between D0 term of the RPR parameters and daily nutation rates in obliquity for the satellites of the first GLONASS orbital plane (each line corresponds to one of the satellites) in case of GPS+GLONASS solution.

table 1 are therefore raw factors which demonstrate the relation of how the formal errors of the nutation rates might decrease in case of including observations to the GLONASS satellites and omitting of potential intersystem biases. The unit weight of the solutions is of course governed by the quality of the orbit fit which should be at the 1cm level to achieve a 0.1mas/day accuracy of the rates.

	GPS-only			GPS+GLONASS		
date	$\sigma_{\Delta\psi}$	$\sigma_{\Delta\varepsilon}$	N_{obs}	$\sigma_{\Delta\psi}$	$\sigma_{\Delta\varepsilon}$	N_{obs}
13.09	171	80	910.272	118	54	1.697.008
14.09	170	81	910.276	117	54	1.705.278
15.09	171	81	909.886	119	54	1.697.606
16.09	171	82	910.404	116	54	1.705.718
17.09	170	82	910.402	118	54	1.696.540

Table 1: Ratio of the formal errors and observation numbers of the nutation rates estimated for GPS-only and GPS+GLONASS solutions (for several days).

The correlation coefficients between nutation rates and radiation pressure parameters could serve as a real measure of the contribution of improved geometry of an additional (w.r.t. GPS) satellite system. Note, that among the estimated radiation pressure parameters (RPR), only D0, X0, Y0 and XC, XS terms have a non-negligible correlation with nutation rates. Fig. 2 presents the correlations between the nutation rate in obliquity and the D0 term for a combined GPS+GLONASS scenario. It can be seen that the correlation coefficients are about -0.1 to +0.1 for the GPS+GLONASS solution. We should note that the corresponding correlations for a GPS-only solution are in the range of up to -0.25 and +0.25.

Acknowledgements. First author express gratitude to the Descartes/Nutation Advisory Board for financial support of this work (in frame of the grant GALILEO/NUTATION).

3. REFERENCES

Bernese GPS Software v. 5.0, U.Hugentobler, R. Dach, P.Fridez(eds.), 2007.
Deep space analytic satellite propagator algorithm: http://www.coastalbend.edu/acdem/math/sats/.

Session 5

DEVELOPMENTS IN ASTRONOMICAL REFERENCE FRAMES

DÉVELOPPEMENTS CONCERNANT LES SYSTÈMES DE RÉFÉRENCE ASTRONOMIQUES

PRESENT AND FUTURE RADIO REFERENCE FRAMES

C. MA
Goddard Space Flight Center
Code 698.0
8800 Greenbelt Road, Greenbelt, Maryland, 20771, USA
e-mail: Chopo.Ma@nasa.gov

ABSTRACT. Different but overlapping sets of extragalactic radio sources provide the reference frames for several purposes, notably Earth orientation and the terrestrial reference frame, spacecraft navigation, and astrophysical phase referencing. These reference frames have differing characteristics for numbers, spatial distribution and accuracy but have been unified up to now in the use of S/X band VLBI data and common observing stations. While the frequent observations for EOP are dominated by purpose-built geodetic stations, the majority of the global network stations have an astronomical focus or a major astronomical component. The ICRF has been the basis for assuring consistency among the various uses. In the future there is likely to be a specialization of reference frames driven by developments such as VLBI 2010, with instrumentation and network geometry optimized for EOP, and Ka-band spacecraft tracking. Higher frequency observations have the potential for improving the precision and stability of source positions. While the next realization of the ICRF will use S/X data, it will be important to relate other radio frames to the ICRF. The status of the second realization of the ICRF and some of the technological developments will be discussed.

1. THE PRESENT RADIO REFERENCE FRAMES

Radio-frequency reference frames are derived from VLBI observations. Currently the best realization of the ICRS is the ICRF, which was derived originally from simultaneous S-band and X-band VLBI data through 1995. Two extensions were made utilizing data through 2002 and increasing the number of sources in the catalogue to over 700 but retaining the original 212 defining sources, uncertainty floor of 250 microarcseconds and accuracy of the axes of 30 microarcseconds. The ICRF is the basis for realizations of the ICRS at other frequencies.

In practice, however, most ICRF defining sources are used less often than certain subsets of the ICRF catalogue and a large set linked to the ICRF. The most frequent VLBI observations utilizing the ICRF as a set of fixed fiducial objects are for monitoring Earth orientation parameters (twice a week for all five angles and daily for UT1) and for maintaining the terrestrial reference frame. For these purposes 150 sources with relatively high flux and compact structure have been used throughout the history of geodetic VLBI. These sources have the highest number and density of observations, have long time histories and thus dominate the VLBI data set. Recently the number of sources used regularly for geodesy was increased from 100 to over 200 and a few strong but unstable sources were deleted from the list. Simulations show that this change should improve the geodetic results.

For astronomical observations requiring a nearby source for phase referencing a much larger set is desirable. The positions of over 2000 sources were derived from the sessions of the VLBA Calibrator Survey (VCS). The astrometric quality is not as good as the ICRF since each source was observed at a single epoch, albeit with the VLBA, i.e, with many more stations than the usual astrometric network. The VCS sources were linked to the ICRF by including a number of ICRF sources in each session.

For spacecraft navigation in the solar system using differential VLBI a set of sources along the ecliptic is necessary, especially in the region of anticipated critical maneuvers. The Deep Space Network has been most active in observing such sources.

The fundamental requirements for developing a radio reference frame for general or specific purposes

ht!

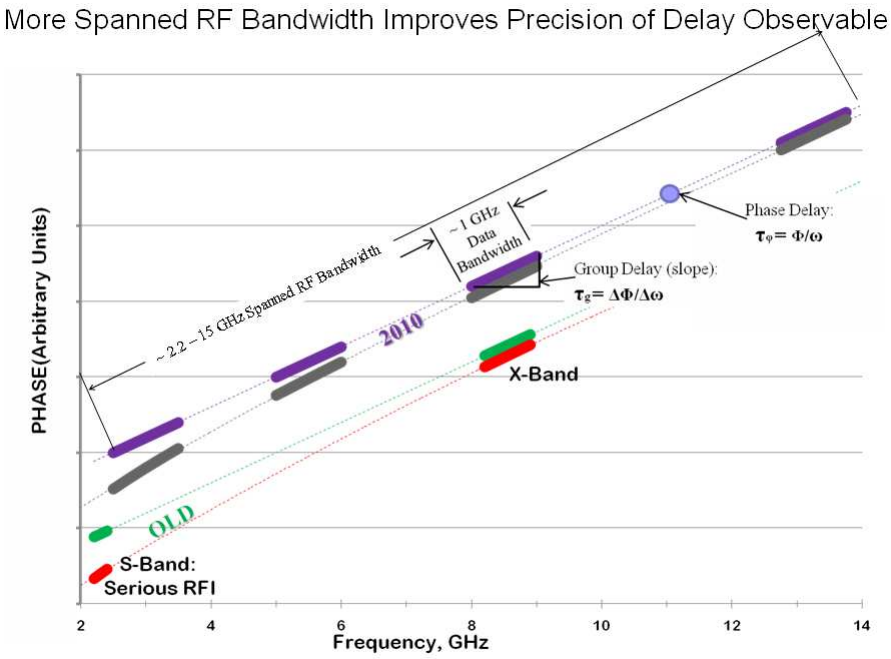

Figure 1: Schematic of the current S/X and the broadband systems

include simultaneous, dual-frequency observations to remove ionospheric effects, sufficient number, geographic distribution and sensitivity of stations, and sufficient sources over the sky and in particular regions as needed. The number of observing epochs and time span for the sources depend on the accuracy required but is also affected by the previous factors. The larger uncertainty for the VCS positions is still adequate for its purpose.

These applications have in the past all relied on dual S/X (2/8 GHz) VLBI observations. There are two developments that will lead to a proliferation of radio reference frames in the future, Ka-band space craft signals and the VLBI 2010 broadband system for geodesy. The benefits of Ka-band (32 GHz) for space craft telemetry are greater data capacity and smaller size. The DSN has already made X/Ka observations to develop a navigation catalogue but the number of X/Ka stations is very limited.

2. THE FUTURE RADIO REFERENCE FRAMES

The VLBI 2010 broadband concept is designed to meet ambitious geodetic and programmatic goals, mitigate worsening radio interference problems (especially severe at S-band) and replace ageing VLBI equipment. The goals include measurements accurate to 1 mm on a global scale, continuous measurements of Earth orientation parameters and station positions, quick data delivery and analysis, and low cost of construction and operation. The strategies include reducing random and systematic errors (particularly from the atmosphere), improving the number and distribution of stations ($>$ 20 would be desirable), significantly increasing the number of observations in total and in a given time interval, and developing new observing strategies. Simulations show that a 24-station VLBI 2010 network should improve EOP by a factor of at least 5 over the current routine results, which are hindered by non-optimal network size and geometry and practical limitations on recording rate.

Figure 1 shows the schematic of the broadband system above and the current S/X system below. The current S/X system is in fact two discrete receivers at fixed frequencies. A group delay is determined from each band and the two group delays are combined to give an ionosphere-free observable. In the

broadband system a single feed permits the sampling of multiple bands at arbitrary frequencies within the feed's bandwidth. The bands are placed to avoid interference. Each band is wider than the current S/X bandwidths and the overall spanned bandwidth is greater, so all bands are to be processed together to give an ionosphere-free phase delay with much higher precision than the group delay.

It should be noted that wide RF sampling and high rate recording are concomitant requirements. These are both needed to give sufficient sensitivity with 12-m antennas, which are smaller than the 20-30 m antennas most common in the geodetic network today. The reason for using smaller antennas is to reduce costs and for fast slewing.

The specific path under development by NASA and other organizations includes a fast, automated 12-m antenna, a broadband feed (2 - 12 GHz) and amplifiers, sampling in four, flexibly placed bands, and recording at 2 Gbps in a mode optimized for network data transmission and software correlation. Two proof-of-concept receivers and back ends have been built by NASA and installed on antennas at Westford, Massachusetts and Greenbelt, Maryland. The cryogenic receiver has a commercial, off-the-shelf broadband feed with dual linear polarization followed by broadband low noise amplifiers. Each of the four bands can be arbitrarily placed in the full RF range by a flexible up/down converter that acts as the local oscillator. Each band is split into 32 MHz channels and digitized by a digital back end (DBE) before being recorded at 2 Gbps on Mark5B+ recorders. These two systems have recorded data that have been successfully correlated.

There are two critical future steps for the proof-of-concept systems. The current feed has frequency-dependent phase center and beam pattern variations. A compact feed without these undesirable traits is under development at Chalmers University. A 12-m antenna to replace the 5-m antenna at Greenbelt has been ordered and is expected to be ready for testing by the end of 2009.

Other VLBI 2010 projects include the Twin Telescope at the Wettzell Fundamental Station, a new station at Auckland University of Technology, three new systems for Geoscience Australia at Hobart, Yaragadee and Katherine, and new stations in the Azores and Canary Islands.

In full operation the VLBI 2010 network would observe 200 sources continuously for EOP and station positions. Because of the broadband implementation the effective source positions will not be identical to the S/X positions. However, because of the density of observing and the optimized network distribution the data would provide a wealth of position and structure information about the sources used. Other sources could be observed by older, larger antennas that have been retrofitted with VLBI 2010 electronics.

THE CELESTIAL FRAME AT FOUR RADIO FREQUENCIES

C. S. JACOBS
Jet Propulsion Laboratory, California Institute of Technology/NASA
4800 Oak Grove Dr., Pasadena CA 91109
e-mail: Chris.Jacobs@jpl.nasa.gov

ABSTRACT.

The International Celestial Reference Frame was adopted by the IAU in 1997 based on VLBI measurements at S/X-band (2.3/8.4 GHz) and complemented by HIPPARCOS measurements at optical frequencies. At that time, the IAU encouraged the astrometric community to extend the ICRF to other frequencies. In response, VLBI measurements have been made at 24, 32, and 43 GHz.

This paper will discuss the programmatic and scientific motivations for extending the ICRF to these higher frequencies. A summary of results to date will be presented including evidence that these new high frequency frames are rapidly approaching the accuracy of the S/X-band ICRF. Finally, prospects for future improvements of high frequency radio reference frames will be discussed.

See the full paper at the end of the Volume, on page 251 (late paper)

ASTROMETRIC AND PHOTOMETRIC VARIABILITY IN QUASARS

A.H. ANDREI[1,2,3], S. BOUQUILLON[3], J.I.B. de CAMARGO[1], J.L. PENNA[1], F. TARIS[3], J. SOUCHAY[3], D.N. da SILVA NETO[2,4], R. VIEIRA MARTINS[1,2], M. ASSAFIN[2],
[1] Observatório Nacional/MCT
R. Gal. José Cristino 77, Rio de Janeiro, Brazil
[2] Observatório do Valongo/UFRJ
Lad. Pedro Antônio 43, Rio de Janeiro, Brazil
[3] SYRTE, Observatoire de Paris, CNRS, UPMC
61 Av. de l'Observatoire, Paris, France
[4] Centro Universitário Estadual da Zona Oeste
Av. Manuel Caldeira de Alvarenga, Rio de Janeiro, Brazil
e-mail: oat1@on.br

ABSTRACT. Quasars are the choicest objects to define a quasi-inertial reference frame. At the same time they are active galactic nuclei powered by a massive black hole. As the astrometric precision approaches the limit set by the forthcoming GAIA mission, the astrometric stability can be investigated. Though the optical emission from the core region usually exceeds the other components by a factor of hundred, the variability of those components must surely imply in some measure of variability on the astrometric barycenter. To investigate the correlation between long term optical variability and what is dubbed as the random walk of the astrometric center, a program is being pursued at the WFI/ESO2.2m. A sample of quasars was selected by the large amplitude and long term optical variability. The observations are typically made every two months. The treatment is all differential, comparing the quasar position and brightness against a basket of selected stars for which the average relative distances and magnitudes remain constant. The provisional results for four objects bring strong support to the hypothesis of a degree of relationship between astrometric and photometric variability.

1. INTRODUCTION

The rapid flux variation seen in quasars is a convincing indication of the smallness of the emitting region. And the amplitude of variation, at cosmological redshifts, tells of the enormous output being produced. At the same time, since longer, year-like, and large amplitude variation are also recorded, the same reasoning would suggest that the other quasar's elements aren't at a standstill. There are several mechanisms apt to generate the optical and positional variability. Some of such proposed mechanisms are (Cheung et al., 2003; Eliztur, 2006): opacity changes around the core regions; instabilities propagated across the accretion disk; emission from a precessing jet; variability powered by supernovae explosions; or conversely, variability triggered by tidal disruption of stellar masses; emission from regions at superluminal speeds; luminosity disturbance brought by the host galaxy; microlensing.

Whatever the causes, the goal here is to search whether an observed long term, high amplitude optical variability can relate to astrometric variability of the quasar photocentre (Johnston et al., 2003). If verified, the relationship could indicate that high photometric variation would make a given quasar less apt to materialize a stable extragalactic reference frame, as the one from the GAIA mission.

2. THE OBSERVATIONAL PROGRAM

The long term program required by the monitoring of optical fluctuations in large cycles can only be established by ground based observations. Therefore an astrometric limit is established at the level of few mas. This level, in turn, demands for good seeing and telescope imaging, as well as relative astrometry. In order to maximize the chances of register the investigated relationship, quasars from the sample of Teerkopi (2000), and light curves from Smith et al.(1993), were selected on basis of long period and large photo-variability. The observations are run under the Observatório Nacional/MCT, Brasil, telescope time contracted to ESO at the Max Planck 2.2m telescope at La Silla, Chile.

Table 1: WFI/ESO 2.2m Telescope Observational Program

QSO	RA	DEC	<V>	B-V	z	Δm	Slots
0210−5101	02:10:46.2	−51:01:02	16.9	0.56	1.003	∼1	P13,P21,P22,P33
0339−0146	03:39:30.9	−01:46:36	18.4	0.35	0.852	1.1	P13,P22,P23,P33
0407−121	04:07:48.4	−12:11:37	15.3	0.16	0.574	0.6	P22,P23
0442−0017	04:42:38.7	−00:17:43	19.2	0.37	0.850	3.2	P23,P23
0522−6107	05:22:34.4	−61:07:57	18.1	-.05	1.400	∼1	P13,P22,P23,P31,P33
0538−4405	05:38:43.5	−44:05:05	17.5	0.46	0.894	3.7	P13,P21,P22,P23,P31,P33
0739+0137	07:39:18.0	+01:37:05	16.5	0.43	0.191	0.9	P21,P23,P31
0813+0150	08:13:53.0	+01:50:50	18.0	0.18	0.402	1.4	P22,P31,P32
0858+1651	**08:58:52.6**	**+16:51:27**	**17.7**	**0.40**	**1.449**	**0.6**	**P22,P23,P31,P32**
0925+1444	09:25:07.3	+14:44:03	17.8	0.54	0.896	2.0	P22,P31
1218+0200	**12:18:55.8**	**+02:00:02**	**18.1**	**0.02**	**0.240**	**1.5**	**P22,P23,P31,P32**
1254+1141	12:54:38.3	+11:41:06	17.0	0.35	0.870	1.3	P31,P32
1512−0905	**15:12:50.5**	**−09:06:00**	**16.9**	**0.20**	**0.361**	**1.5**	**P11,P12,P13,P23,P31,P32,P33**
1620+1724	16 20 11.3	+17 24 28	16.8	0.17	0.114	2.1	P11,P13,P23,P31,P32,P33
1620+1736	16 20 21.8	+17 36 24	16.4	0.12	0.555	1.1	P11,P13,P23,P31,P32,P33
1751+0939	**17:51:32.8**	**+09:39:01**	**18.4**	**0.68**	**1.360**	**∼1**	**P11,P12,P13,P23,P31,P32,P33**

Table 1: For each object of the program are given the pointing equatorial coordinates, the reference magnitude and color index, the redshift, and the expected optical variability. The quasars here treated are shown in bold types. The slots for which were made observations of a given object are presented in the last collumn. The periods codes are, P11=April/2007; P12=June/2007; P13=September/2007; P21=October/2007; P22=January/2008; P23=February/2008; P31=April/2008; P32=May/2008; P33=August/2008.

The program started in April 2007 and it will extend till 2009, with observations nearly every two months. Table 1 brings the program sources, some of their characteristics, and the epochs for which there are already reduced observations.

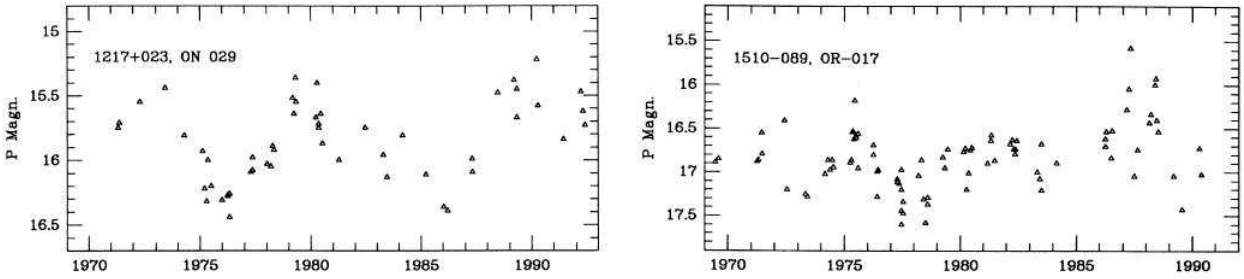

Figure 1: Examples of optical variability, as given by Smith et al. (1993)

3. DATA TREATMENT AND DATA REDUCTION

The ESO2p2 WFI direct image camera is compound of 8 CCDs, each covering a field of 7.5 × 15.0 arcmin, to scale of 0.238 arcsec/px. For all the observations the same CCD was used, keeping the quasar on a clean spot, at about 1/3 of the diagonal starting from the optical axis. The same configuration is repeated for all the observations of a same quasar, jittering allowed. The observations as a rule are made within 2h of hour angle. Red (Rc/162, peak 651.7nm, FWHM 162.2nm) and blue (BB#B/123, peak 451.1nm, FWHM 135.5nm) filters are used for each run. Depending on the quasar magnitude, typically from 3 to 5 images are taken with each filter. The integration times are never longer than 30 min., yet as long as possible to provide good imaging of the target and of the surrounding stars. The combined S/N ratio is always close to 1000 for each run.

All images are treated by IRAF MSCRED for trimming, bias, flat, bad-pixel and split. Typically

Table 2: Measures of Precision (pixel)

N(tot)	E(X)	E(Y)	E(M)	N(R)	E(X)	E(Y)	E(M)	N(B)	E(X)	E(Y)	E(M)
10229	0.017	0.017	0.001	7373	0.017	0.015	0.001	2856	0.018	0.021	0.001
24407	0.036	0.038	0.002	16527	0.034	0.034	0.002	7880	0.047	0.047	0.001

Table 2: Average precision (1512-0905 sample), in units of pixel. On the upper row are the average values for the best imaged objects, while on the second row are the averages for all imaged objects (above threshold 4). Counts and averages are for the R and B filters sets, as well as for the combined (tot) set.

the image treatment enhances the SNR by a factor of 2. IRAF DAOFIND and PHOT are employed for the determination of centroids and (instrumental) magnitudes, with the entry parameters adjusted for each frame. Centroids and fluxes are obtained from the adjustment of bi-dimensional Gaussians. The inner ring where the object counting is made and the outer ring where the sky background is counted are variable for each object and frame, but their ratio is kept constant. The plate scale and frame orientation are derived by IRAF IMCOORDS, from UCAC2 catalogue stars (though, since the astrometry is totally relative, their values are of no great deal to define the correlation under study).

4. FIRST RESULTS

The first results regard to separate R and B filter solutions, for the four sources for which the light curve is more populated. The procedure initially adjusts the frames one on top of the other, on coordinates and magnitudes, by the quasar. Next, frame after frame, on basis of the PHOT outcomes, the objects common to all frames are stored, provided that the (X,Y) coordinates and the magnitudes do not vary above a chosen threshold.

The common objects (X,Y) coordinates and magnitudes are then adjusted by a complete 3^{rd} degree polynomial to a mean frame (eq. 1). On eq.1, **C** stands either for X, Y or M.

$$C_n^m - < C >_n = C_0 + \sum_{i,j,k}^{1,3} A_{i,j,k}^m X^i Y^j M^k \qquad object\ \mathbf{n}\ of\ frame\ \mathbf{m} \qquad (1)$$

Finally, a further round of analysis discard the objects which (X,Y) or magnitude variation are above the threshold of optimum precision (Fig. 2). The averages on (X,Y) and magnitude of the remaining

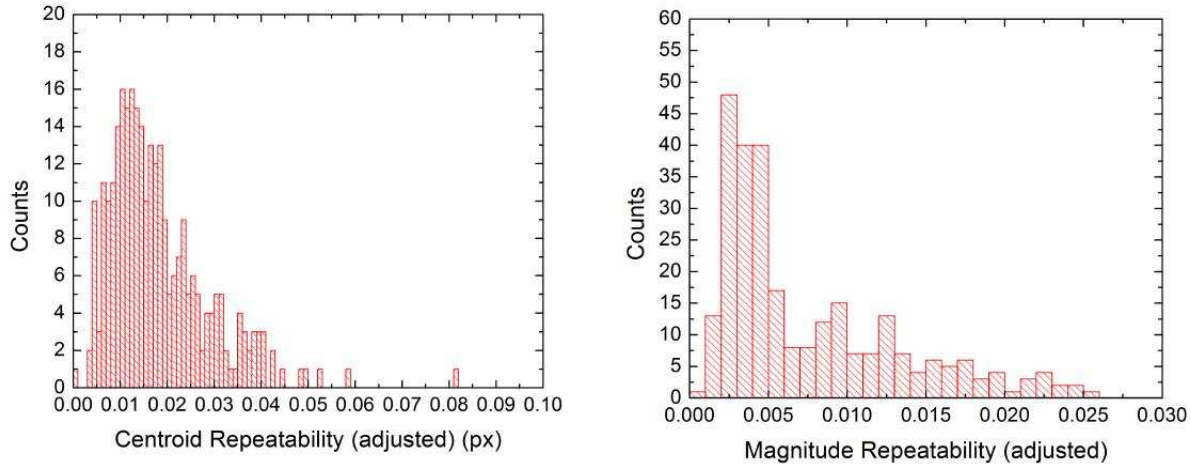

Figure 2: (X,Y) and magnitude repeatability after eq.1 adjustment to the mean frame.

objects (referred to the quasar as fixed origin) are obtained and correlated against the time-line and against each other. Table 3 summarizes the results.

Table 3: ESO2p2 program quasar's magnitude and (X,Y) coordinates time and crossed correlations.

QSO	Nf (R)	Ns	Mag×t	Amp (mag)	X×t	Xamp (mas)	Y×t	Yamp (mas)	X×Mag	Y×Mag
0858+1651	10	5	**0.82**	**0.025**	0.06	4	**0.79**	**4**	0.17	**0.61**
			(0.001)		(0.86)		**(0.002)**		(0.59)	**(0.04)**
1218+0200	4	8	**0.98**	**0.022**	**0.50**	**5**	**0.60**	**3**	0.35	**0.59**
			(0.03)		**(0.39)**		**(0.29)**		(0.57)	**(0.41)**
1512−0905	14	3	**0.94**	**0.072**	**0.41**	**4**	0.33	9	**0.52**	0.15
			(0.01)		**(0.27)**		(0.39)		**(0.16)**	(0.70)
1751+0939	8	26	**0.98**	**1.233**	**0.97**	**6**	0.23	7	**0.91**	0.04
			(0.13)		(0.15)		(0.85)		**(0.27)**	(0.98)

R filter time and cross-correlation for magnitude and (X,Y) coordinates. **Nf** brings the number of used frames, that is those in which large numbers of common stars with the other frames are found. **Ns** is the final number of common stars. The statistical significance of the correlations is given in brackets in the line below. Most significant values are marked by boldface types.

QSO	Nf (B)	Ns	Mag×t	Amp (mag)	X×t	Xamp (mas)	Y×t	Yamp (mas)	X×Mag	Y×Mag
0858+1651	8	1	**0.89**	**0.010**	**0.58**	**6**	**0.54**	**4**	**0.72**	**0.76**
			(0.007)		**(0.17)**		**(0.21)**		**(0.07)**	**(0.05)**
1218+0200	6	2	**0.66**	**0.043**	0.20	5	**0.55**	**6**	0.30	**0.90**
			(0.34)		(0.80)		**(0.45)**		(0.70)	**(0.10)**
1512−0905	13	1	**0.74**	**0.262**	0.30	5	**0.92**	**5**	**0.54**	**0.63**
			(0.02)		(0.40)		**(0.001)**		**(0.11)**	**(0.05)**
1751+0939	9	1	**0.99**	**0.438**	**0.66**	**5**	0.29	7	**0.66**	0.24
			(0.001)		**(0.11)**		(0.52)		**(0.11)**	(0.61)

Same as above for filter B. Notice that less common stars are retained.

5. CONCLUSION AND PERSPECTIVES

This program is still contemplated on five forthcoming slots of observation at the WFI/ESO2p2 telescope. They will enable to populate the variability monitoring of the remaining quasars of the program. On the reduction practice, the R and B frames can be combined in order to derive a chromatic refraction correction. Also the frames taken in sequence can be co-added to amplify the S/N ratio.

The presented results must therefore be considered as provisional. At the same time, notice that the magnitude time correlation and variation amplitude follow what was expected from previous independent programs. The photometric and astrometric process of relative treatment are the same, using successive adjustments of the frames towards a common average. It brings support to the correlations found.

The preliminary results strongly prompt for the continuation of this program. With more sources, and longer monitoring, a clearer understanding on the subject can be addressed.

6. REFERENCES

Cheung,C.C., Wardle,J.F.C., Chen,Tingdong, Hariton,S.P., 2003; "New detections of optical emission from kiloparsec-scale quasar jets", New Astronomy Reviews, Vol 7, #6, pp. 423–425.

Elitzur, M., 2006; "Unification Issues and the AGN Torus", in "The Central Engine of Active Galactic Nuclei", ASP Conference Ser., Vol 373, p. 415.

Johnston,K.J., Boboltz,D., Fey,A., Gaume,R., Zacharias,N., 2003; "Astrophysics of reference frame tie objects", in "Interferometry in Space", Proc. of SPIE, Vol 4852, pp. 143–151.

Smith, A.G., Nair, A.D., Leacock, R.J., Clements, S.D., 1993; "The longer optical time scales of a large sample of quasars", AJ, Vol 105, #2, pp. 437–455.

Teerikorpi, P., 2000; "Evidence for the class of the most luminous quasars" A&A, Vol 353, p77-91.

APPARENT MOTION OF THE RADIO SOURCES AND STABILITY OF THE CELESTIAL REFERENCE FRAME

V.E. ZHAROV, M.V. SAZHIN, V.N. SEMENTSOV, K.V. KUIMOV, O.S. SAZHINA, E.A. RASTORGUEVA
Sternberg State Astronomical Institute
Universitetsky pr. 13, Moscow 119992
zharov@sai.msu.ru

ABSTRACT. The physical basis of the apparent motion of the ICRF radio sources is discussed. All sources can be divided into four groups according their motion characteristics. We discuss here the linear and uniform motion model. The apparent velocities of the radio sources are of the order of speed of light or even more, therefore, we conclude that these radio sources are the relativistic jets or plasma clouds moving with velocities of the order of speed of light. The linear and uniform source motion can be explained by model of jet precession. In the frames of model we discuss the physical characteristics of some ICRF sources. So, for long-term stability of the ICRF new catalog of the selected radio sources has to contain both coordinates (right accession and declination) and trends (linear or quadratic).

1. INTRODUCTION

The XXIII General Assembly of the IAU recommended to adopt international celestial reference system (ICRS) as a realization of the fundamental coordinate reference system. The ICRS is the base to solve all astrometry and navigation tasks. The ICRS is defined through the kinematical characteristics, making the coordinate axis fixed with respect to the distant matter of the Universe.

A realization of the ICRF consists of a set of precise coordinates of extragalactic radio sources which are supposed to be motionless. The reason is that the proper motion of these radio sources is expected to be negligibly small because of their remoteness.

The first realization of the ICRF (International Celestial Reference Frame) catalog was constructed in 1995 by a reanalysis of the VLBI observations (Ma et al., 1998). The objects in the frame are divided in three subsets: "defining", "candidate" and "other". The defining sources should have a large number of observations over long data span; they maintain the axes of the ICRS. Sources with an insufficient number of observations or an observing time span are designated as the candidates; they could be potential defining sources in future realizations of the ICRF. The category of other sources includes objects with poorly determined positions, but they are useful to link the ICRF with other reference frames. The 212 of these are defining sources providing a core of the ICRF. The estimated source position uncertainty for the "defining" sources is about 0.25 mas. The 294 "candidate" sources have fewer observations. The 102 "other" sources were added for possible ties of reference frames. Two extensions of the ICRF have been elaborated, ICRF-Ext.1 (IERS, 1999) and ICRF-Ext.2 (Fey et al., 2004), for densification of the frame.

Other classification was proposed by Feissel-Vernier (2003). She classified a set of 362 sources as stable or unstable based on the analysis of source position time-series.

The apparent motion of a radio source (quasar) defining by its peculiar velocity, is expected to be of the order of 0.5 μas/year. This value is less than the modern observational accuracy. Therefore, quasars are considered to be fixed in space. But this is not the case. The modern observations show (MacMillan, 2003), that quasars and other objects, which the ICRF is based on, have angular velocities larger then expected, even being more that the speed of light. One of the reasons of apparent motion of this kind is a weak microlensing effect caused by stars and dark stars in our Galaxy (Sazhin et al, 2001). However, the simple estimations show that this is not the case. One needs to investigate others causes.

We analyzed the time series of the quasars coordinates that were calculated by nine centers of VLBI observations, and we also found that quasars have non-negligible motion. Model of motion was represented as polynomial with respect to time (Zharov, Rastorgueva, this issue).

According to the polynomial models we shall divide apparent motions in several types. In our work we derived the parameters of motion of the radio sources and we found that all of them show one of the

types of motion listed below.

- Group I. Linear and uniform motion (inertial motion) (Fig. 1a).
- Group II. Linear but non-uniform motion (accelerated motion) (Fig. 1b).
- Group III. Cone cutting motion with constant velocity module (Fig. 2a).
- Group IV. The common case of curvilinear motion; velocity is not constant (Fig. 2b).

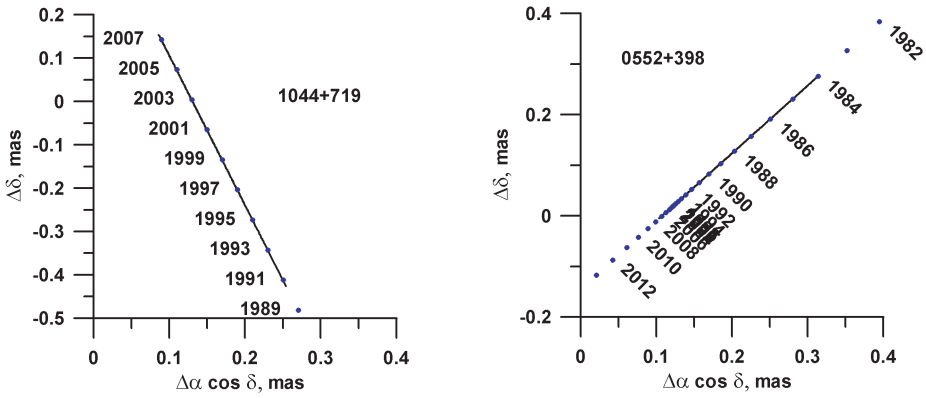

Figure 1: Uniform motion of 1044+719 and accelerated motion of 0552+398

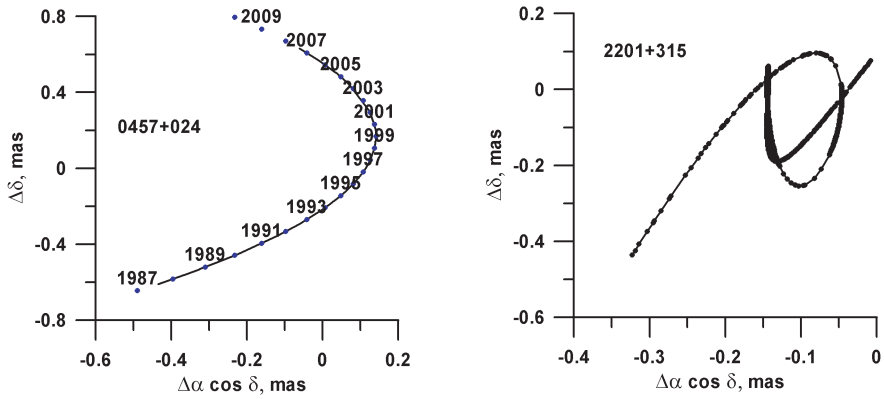

Figure 2: Motion of sources 0457+024 and 2201+315

Here we will discuss the first model of apparent motion of the quasars (group I). The linear and uniform apparent motion of the radio source is the simplest case and can be predicted with high accuracy and for a long time interval.

2. THE MODELS OF QUASAR RADIO SOURCES

The widely accepted model of quasar is a supermassive black hole surrounded by accretion disk (Begelman et al., 1984; Blandford, Znajek, 1977). This model was confirmed with microlensing observations (Koptelova et al., 2007), where it was demonstrated that distribution of brightness over the quasar disk is similar to brightness distribution over accretion disk. A central engine of quasar produces a jet of relativistic particle which emits radio waves, and the jet is radio source. As a result, one can conclude that the optical and radio sources are space separated parts of the unique source. We will follow the model discussed and elaborated in Blandford, Königl (1979) and Begelman et al.(1984).

In these papers, model of radio source with well defined internal structure (which consists of jet of high temperature relativistic plasma, bulk motion of separated clouds as hot spot etc.) is discussed. The right

example of such source is 3C345 or Cygnus A. These sources have well defined internal structures that reveal the fast motion of bright spots, and are not included into the list of ICRF sources. Radio sources which are included in the ICRF list are radio quiet quasars which reveal almost point-like unresolved structure. Nevertheless, we believe that physics of their non-stationarity is similar to radio active quasars.

Authors of papers (Blandford, Königl, 1979; Begelman et al., 1984) distinguish two main physical mechanisms. The first one is a steady jet of high temperature relativistic plasma and second is a bulk motion of separate accelerated cloud. Here we will discuss steady jet only and their effect on long-term stability of the ICRF (Zharov et al., 2009).

Jets are elongated structure with some brightness distribution along the jet. In some position of the jet, brightness has maximum. We will call it hot spot. The distance from the origin of the jet to the hot spot r_s is of the order of 1 kpc or less (according to theoretical estimations)(Blandford, Königl, 1979).

It is necessary to mention that

$$r_s \sim \frac{1}{\nu},$$

therefore, a jet which is unresolved in a frequency ν will be unresolved in whole range of radio frequencies. Distance to the hot spot increases with increase of wavelength ($\lambda = c/\nu$). If one observes in shorter wavelength, the distance to the hot spot became shorter. The resolution ability of a radio interferometer is proportional to wavelength:

$$\theta_{ang} \sim \frac{\lambda}{B},$$

here B is baseline. If the wavelength of observation decreases the resolution ability of radio interferometer increases, it means that minimal separated angle θ_{ang} became less, but the distance to the hot spot also decreases. Therefore, for the radio source of this type, one has to increase interferometer base, not decreases wavelength.

3. PRECESSION OF THE QUASAR JET AS NONSTATIONARY SOURCE

Precession of jets is observed in many celestial systems including extragalactic ones. A very good example of jet precession is QSO 2300-189 (Hunstead, et al., 1984). Precession of jet with high precession speed is observed also in black hole which is component of binary system SS434 (Davydov V.D. et al., 2008). The speed of precession is almost constant during the long time interval in binary star system. Therefore, one can expect the same stability of the speed in extragalactic systems.

The angular velocity of a hot spot and total shift of a source over sky depend on the jet precession speed and ranges into interval $10^{-4} \div 10^{-8}$ yr^{-1} depending of parameters of black hole and surrounding matter. As the jet precesses the jet hot spot moves over the sky. The angular velocity of the hot spot depends both on the precession speed and geometry of the black hole system with respect to the direction of the observer. The interval of observation is of the order of 30 years and precession period is longer than 10 000 years; so one can expect the linear and uniform motion over the observing interval. The angular velocity can be approximated as constant

$$\mu = \frac{\theta_s}{1+z}\Omega Q. \tag{1}$$

Here θ_s is the angular distance from the origin of the jet to the hot spot ($\theta_s = r_s/\rho_s$, ρ_s is the angular cosmological distance to the source), and z is the redshift of the source, and Q is the factor of the order of unity, which depends on geometry and velocity of the system. Therefore the precession period provides us with the interval of stability of the coordinate system based on these sources.

The source 1044+719 The angular distance between optical and radio coordinates is $\theta_s = 165$ mas, the rms of optical coordinates is 73.9 mas, the difference can be considered as confident with level 2.3 σ. The redshift is $z = 1.15$, the ratio of linear to angular distance for the standard cosmological model is:

$$s = 8.286\frac{kpc}{1''},$$

that corresponds to a linear distance between the origin of jet to the hot spot of $r_s = 1.37$ kpc.

The apparent angular velocity of the source is $\mu = 36$ μas/year, which corresponds to the linear apparent velocity $v = 2.1$ c. It also corresponds to the precession speed $\Omega \sim 2.3 \cdot 10^{-4}$/year. That means that for several centuries this source has to keep linear and uniform motion.

The source 1726+455 The angular distance between optical and radio coordinates is $\theta_s = 181$ mas, the rms of optical coordinates is 74.8 mas, the difference can be considered as confident with a level of 2.4 σ. The redshift is $z = 0.71$, the ratio of linear to angular distance for the standard cosmological model is:

$$s = 7.202 \frac{kpc}{1''},$$

that corresponds to a linear distance between the origin of jet to the hot spot of $r_s = 1.30$ kpc.

The apparent angular velocity of the source is $\mu = 12$ μas/year, which corresponds to the linear apparent velocity $v = 0.5c$. It also corresponds to the precession speed $\Omega \sim 2.3 \cdot 10^{-4}$/year. That means that for several centuries this source has to keep linear and uniform motion.

Below we show the complete list of the sources which demonstrated the linear and uniform motion: 0007+171(D), 0039+230(D), 0048-097(O), 0104-408(O), 0202+149(C), 0248+430(D), 0556+238(D), 0602+673(C), 0953+254(O), 1044+719(C), 1124-186(C), 1150+497(D), 1324+224(D), 1413+135(O), 1656+053(C), 1726+455(D), 1738+476(C), 1751+441(D), 1929+226(C), 1932+204(C), 2145+067(D), 2351+456(O), 2356+385(C) (D means defining source, C is candidate and O is other).

As seen from the list above, some of the sources are defining. So, the precessional motion of jet that we see as motion of source affects the stability of the ICRF. Orientation of the new catalog with respect to the ICRF will depend on time.

Acknowledgements. Research supported in part under RFBR grants 08-02-00971, 07-02-01034, 07-01-00126.

4. REFERENCES

Begelman, M.C., Blandford,R.D., Rees, M.J., 1984, Rev. Mod. Phys 56, 255.
Blandford, R.D., Znajek, R.L., 1977, MNRAS 179, 433.
Blandford, R.D., Königl, A., 1979, AJ 232, 34.
Davydov V.D., Esipov V.F., Cherepashchuk A.M., 2008, Astron.Rep., 85, 545 (russian).
R.W. Hunstead, H.S. Murdoch, J.J. Condon et al., 1984, MNRAS 207, 55.
Ma, C., Arias, E.F., Eubanks T.M., Fey A.L., Gontier A-M, Jacobs, C.S., Sovers, O.J., Archinal, B.A., Charlot, P., 1998, AJ 116, 516.
IERS, 1999, 1998 IERS Annual Report, Observatoire de Paris, 87.
Fey, A.L., Ma, C., Arias, E.F., Charlot, P., Feissel-Vernier, M., Gontier, A.-M., Jacobs, C. S., Li, J., McMillan, D.S., 2004, AJ 127, 3587.
Feissel-Vernier, M., 2003, A&A 403, 105.
Koptelova, E., Shimanovskaya, E., Artamonov, B., Yagola, A., 2007, MNRAS 381, 1655.
MacMillan, D.C., 2003, in Future Directions in High Resolution Astronomy, eds. J.D. Romney, M.J. Reid (The 10th Anniversary of the VLBI ASP Conference series).
Sazhin, M.V., Zharov, V.E., Kalinina, T.A., 2001, MNRAS 323, 952.
Zharov, V.E., Sazhin, M.V., Sementsov, V.N., Kuimov K.V., Sazhina, O.S., 2009, Astron. Rep. (accepted for publication, russian).
Zharov, V.E., Rastorgueva, E.A., this issue.

INVESTIGATION OF STABILITY OF RADIO SOURCES FROM ARC-LENGTH METHOD

S. BOLOTIN & S. LYTVYN
Main Astronomical Observatory of the NAS of Ukraine
27 Akad. Zabolotnoho St.
Kiev 03680 Ukraine
mailto:bolotin@mao.kiev.ua

ABSTRACT. Obtained by various VLBI analysis centers time series of source positions contain two types of signal: changes in coordinates of sources and corrections to an orientation of the Celestial Reference Frame. Before to start an investigation of sources variability, one has to transform a CRF solution for each session to some reference celestial frame. On the other hand, the length of arc connecting two radio sources is invariant to the chosen CRF. In this talk we present results of study of variability of arc lengths derived from available time series of radio sources.

1. INTRODUCTION

New realization of International Celestial Reference Frame (ICRF) requires that many particular tasks should be solved. One of them is selecting a set of stable radio sources which are defining the orientation of a constructed celestial reference frame (usually called DEFINING sources). There are at least two approaches to accomplish this task: 1) a physical approach, based on analysis of source characteristics, such as a red shift, type of radio source, distribution of its brightness, and so on, and 2) statistical approach, based on analysis of variability of source positions from VLBI data processing. This work belongs to the second approach.

In the frame of IERS/IVS ICRF2 project in the mid of 2007 various VLBI analysis centers produced "time series" solutions – estimations of sources positions for each session of VLBI observations. A purpose of such solutions is aimed on studies of stability of sources positions and selection of stable radio sources for the ICRF2 implementation.

2. LENGTH OF ARCS FROM TIME-SERIES SOLUTIONS

Time series of sources positions usually are estimated simultaneously with the Earth orientation parameters for each session, therefore they are presented in its own, unique for each session, Celestial reference frame. Before to start an investigation of sources variability, one has to transform a CRF solution for each session to some reference celestial frame. On the other hand, the length of arc connecting two radio sources is invariant to the orientation of chosen CRF. Therefore, studying the variability of the arcs lengths, it is possible to infer about stability of radio sources.

In the frame of one session the length of arc, ℓ_{ij}, connecting i^{th} and j^{th} sources and its standard deviation, $\sigma^2_{\ell_{ij}}$, can be expressed as:

$$\ell_{ij} = \arccos\left[\sin\delta_i \sin\delta_j + \cos\delta_i \cos\delta_j \cos\left(\alpha_i - \alpha_j\right)\right],$$

$$\sigma^2_{\ell_{ij}} = \left(\frac{\partial\ell_{ij}}{\partial\delta_i}\right)^2\sigma^2_{\delta_i} + \left(\frac{\partial\ell_{ij}}{\partial\delta_j}\right)^2\sigma^2_{\delta_j} + \left(\frac{\partial\ell_{ij}}{\partial\alpha_i}\right)^2\sigma^2_{\alpha_i} + \left(\frac{\partial\ell_{ij}}{\partial\alpha_j}\right)^2\sigma^2_{\alpha_j} + 2\frac{\partial\ell_{ij}}{\partial\delta_i}\frac{\partial\ell_{ij}}{\partial\alpha_i}\rho_i\sigma_{\delta_i}\sigma_{\alpha_i} + 2\frac{\partial\ell_{ij}}{\partial\delta_j}\frac{\partial\ell_{ij}}{\partial\alpha_j}\rho_j\sigma_{\delta_j}\sigma_{\alpha_j},$$

where

α_i, α_j, δ_i, δ_j – right ascensions and declinations of i^{th} and j^{th} sources;
σ_{α_i}, σ_{α_j}, σ_{δ_i}, σ_{δ_j} – their standard deviations;
ρ_i and ρ_j – correlation coefficients between right ascension and declination of i^{th} and j^{th} sources.

In the expression of $\sigma^2_{\ell_{ij}}$, the terms which contain correlations between coordinates of i^{th} and j^{th} sources are omitted.

For each of the sessions, we evaluated lengths of arcs and their standard deviations. Then, for each arc we computed variability of the length, and, using least square method, made estimations of variabilities of sources positions.

Eight VLBI analysis centers submitted time series solutions of source positions. In Tab. 1 general characteristics of analyzed time series are presented.

Table 1: General characteristics of time series solutions

Sol.ID	Analysis Center	Software	Estimation of		Number of		
			TRF	EOP	Src	Sess	Arcs
aus003a	GA, Australia	OCCAM6.2	Session	Session	1089	3307	3768
bkg000c	BKG, Germany	CALC/SOLVE	Global	Session	1084	3468	13294
dgf000g	DGFI, Germany	OCCAM6.1e	Global	Session	801	3083	12426
gsf001a	GSFC NASA, USA	CALC/SOLVE	Fixed	Fixed	955	4319	14333
iaa000c	IAA RAS, Russia	QUASAR	Session	Session	583	3850	11730
mao000b	MAO NASU, Ukraine	SteelBreeze	Fixed	Fixed	2485	3907	12937
opa002a	OPAR, France	CALC/SOLVE	Session	Session	644	3741	11113
usn000a	USNO, USA	CALC/SOLVE	Fixed	Fixed	849	4061	13586

In the table for each solution identifier the following fields are shown: name of analysis center; applied software; how the coordinates and velocities of stations and Earth rotation parameters were treated: fixed, estimated as global or local parameters; number of sources in a time series; number of sessions; number of arcs with number of individual epochs more than ten.

Assuming that there are no systematic effects in variations of length of arcs and variations of different sources are uncorrelated we can write a system of equations for all arcs:

$$\sigma_i{}^2 + \sigma_j{}^2 = \sigma_{ij}{}^2, \quad i < j$$

where σ_{ij} is a variability of an arc between i^{th} and j^{th} sources, evaluated from time series of length of the arc, σ_i and σ_j are unknown variabilities of the sources.

3. RESULTS

From the solution of the equation system for each of time series we estimated variations of sources. In Tab. 2 the most stable and most unstable sources with corresponding variabilities are present. For some time series, where our assumptions are not met (primarily, due to outliers in time series), the solution of the equation system gives negative signs for particular $\sigma_i{}^2$. In such cases the sign is put before σ_i. The investigations have shown that negative sign of $\sigma_i{}^2$ usually means that variations of i^{th} source position are small.

Evaluated values of variabilities of sources positions we have treated in the following way: sources from the upper third of the table (sorted by variability) we considered as stable sources in statistical sense (i.e., there are no systematic effects in their positions), while sources from the lower third of the table we considered as the unstable ones.

Based on obtained distribution of variations of sources positions we have created two lists: a list of stable radio sources (sources which have shown themselves as the stable ones in at least six of eight input time series), and a list of unstable sources (which are unstable in at least six time series). The results of such selections are summarized in Tab. 3 and Tab. 4. In the tables along with the names of sources are indicated their status and number of sessions.

As one can infer from the tables there are several radio sources with status CANDIDATE or OTHER which positions are stable enough that they could serve as the DEFINING ones in forthcoming ICRF2. On the other hand, we found that one of DEFINING sources, 1954–388, has variations which are remarkably larger than mean variations for time series. That is an indication of unstable coordinates of the source.

4. CONCLUSIONS

Investigation of time series of sources positions shows that arc lengths are independent from chosen orientation of reference frames, which in such solutions are unique for each VLBI session.

Table 2: Most stable and unstable sources per time series

aus003a		bkg000c		dgf000g		gsf001a	
Src	$\sigma, \mu as$	Src	$\sigma, \mu as$	Src	$\sigma, \mu as$	Src	$\sigma, \mu as$
$1417+385$	-278	$1057-797$	-234	$1417+385$	92	$2209+236$	-282
$0917+624$	-54	$1101+384$	-186	$2209+236$	187	$0642+449$	-82
$2209+236$	128	$2209+236$	-167	$1652+398$	224	$1101+384$	-56
$2356+385$	282	$2223-052$	-135	$0642+449$	245	$2037+511$	88
$0955+476$	292	$0743+259$	-71	$0235+164$	260	$1606+106$	114
$0808+019$	326	$1606+106$	149	$0556+238$	261	$1417+385$	163
$2136+141$	366	$1417+385$	154	$2223-052$	265	$1057-797$	177
$1357+769$	369	$2136+141$	199	$2136+141$	287	$0917+624$	184
$1300+580$	377	$1652+398$	199	$1101+384$	290	$1807+698$	186
$0642+449$	385	$2113+293$	217	$0917+624$	303	$2113+293$	192
$1128+385$	396	$0917+624$	217	$2113+293$	311	$1749+096$	196
$1611+343$	409	$0642+449$	221	$1807+698$	322	$2223-052$	269
$0804+499$	423	$1749+096$	230	$0955+476$	332	$2356+385$	293
⋮		⋮		⋮		⋮	
$2243-123$	988	$1510-089$	1026	$1954-388$	923	$1954-388$	1155
$1124-186$	1002	$0212+735$	1028	$1958-179$	945	$2149+056$	1187
$0106+013$	1014	$1954-388$	1112	$1502+106$	949	$0106+013$	1232
$0212+735$	1050	$2128-123$	1117	$1144-379$	952	$1034-293$	1233
$0402-362$	1067	$1730-130$	1118	$2128-123$	966	$2251+158$	1274
$1502+106$	1076	$1622-253$	1130	$1730-130$	979	$1730-130$	1289
$0420-014$	1096	$0104-408$	1274	$1908-201$	982	$1921-293$	1334
$0742+103$	1112	$1921-293$	1412	$1622-253$	996	$2126-158$	1352
$0454-234$	1116	$0537-441$	1429	$1921-293$	1046	$1226+023$	1379
$0208-512$	1140	$1034-293$	1434	$2149+056$	1054	$1424-418$	1379
$1908-201$	1163	$2255-282$	1557	$1034-293$	1076	$2255-282$	1382
$2149+056$	1208	$1424-418$	1879	$0104-408$	1115	$2134+004$	1434
$1144-379$	1243	$0919-260$	2305	$2255-282$	1233	$0919-260$	1796

iaa000c		mao000b		opa002a		usn000a	
Src	$\sigma, \mu as$	Src	$\sigma, \mu as$	Src	$\sigma, \mu as$	Src	$\sigma, \mu as$
$1417+385$	155	$1652+398$	253	$0642+449$	105	$0642+449$	128
$2209+236$	203	$0642+449$	306	$1652+398$	180	$0917+624$	188
$0642+449$	220	$1101+384$	310	$2209+236$	181	$0743+259$	297
$1652+398$	258	$1128+385$	382	$1101+384$	235	$2223-052$	320
$2223-052$	278	$0602+673$	384	$2136+141$	271	$1101+384$	342
$1807+698$	293	$0955+476$	386	$0955+476$	274	$1652+398$	346
$1101+384$	303	$1417+385$	402	$2113+293$	279	$1745+624$	369
$0235+164$	305	$1807+698$	420	$1606+106$	285	$1807+698$	403
$2136+141$	307	$1726+455$	421	$1417+385$	300	$2136+141$	413
$1749+096$	347	$0014+813$	426	$1745+624$	305	$2113+293$	413
$0917+624$	368	$2356+385$	427	$2223-052$	308	$1057-797$	438
$0014+813$	369	$1745+624$	428	$0917+624$	310	$0955+476$	442
$0718+792$	372	$0808+019$	434	$1749+096$	313	$2356+385$	457
⋮		⋮		⋮		⋮	
$1144-379$	961	$0208-512$	1057	$1641+399$	1051	$1954-388$	1172
$2128-123$	975	$1633+382$	1073	$0106+013$	1098	$1641+399$	1185
$1954-388$	976	$1144-379$	1099	$2128-123$	1120	$0106+013$	1193
$0402-362$	1009	$1502+106$	1104	$1908-201$	1182	$1351-018$	1212
$1921-293$	1010	$1034-293$	1120	$1622-253$	1230	$1730-130$	1215
$2149+056$	1032	$2128-123$	1134	$2126-158$	1258	$2149+056$	1253
$0104-408$	1046	$1954-388$	1212	$1730-130$	1265	$1908-201$	1257
$1730-130$	1054	$0104-408$	1215	$1034-293$	1309	$1034-293$	1264
$1034-293$	1056	$1730-130$	1262	$1958-179$	1322	$1226+023$	1373
$2251+158$	1185	$1921-293$	1284	$2251+158$	1364	$1921-293$	1408
$1641+399$	1231	$2251+158$	1373	$1921-293$	1521	$2255-282$	1547
$2255-282$	1266	$1641+399$	1406	$1226+023$	1530	$1424-418$	1822
$1226+023$	1345	$2255-282$	1509	$2255-282$	1568	$0919-260$	1952

From analysis of arcs variations it is possible to select sets of stable and unstable sources. The analysis reveals few stable sources, which have status CANDIDATE or OTHER and could be used as DEFINING sources in future. Also, one of DEFINING sources, 1954–388, shows large variation of coordinates and is

Table 3: A list of selected stable sources

Src	St	N Ses	Src	St	N Ses	Src	St	N Ses
$0014+813$	D	1007	$0917+624$	D	134	$1652+398$	C	209
$0059+581$	O	1738	$0955+476$	D	1717	$1726+455$	D	1156
$0133+476$	D	1128	$1057-797$	D	287	$1745+624$	D	597
$0235+164$	D	658	$1101+384$	C	323	$1749+096$	C	2238
$0528+134$	C	2865	$1128+385$	D	1014	$1807+698$	C	756
$0552+398$	C	3870	$1156+295$	D	1055	$2037+511$	D	877
$0602+673$	C	395	$1300+580$	O	735	$2113+293$	D	346
$0642+449$	D	1006	$1357+769$	C	1565	$2136+141$	D	843
$0718+792$	D	886	$1417+385$	C	193	$2209+236$	D	155
$0743+259$	D	476	$1519-273$	C	405	$2223-052$	C	821
$0804+499$	D	1177	$1606+106$	D	1991	$2356+385$	C	387
$0851+202$	C	3105	$1638+398$	O	1056			

Table 4: A list of selected definitely non-stable sources

Src	St	N Ses	Src	St	N Ses
$0104-408$	O	422	$1641+399$	O	1113
$0106+013$	O	1279	$1730-130$	O	458
$0402-362$	O	260	$1908-201$	C	422
$0537-441$	O	650	$1921-293$	O	1174
$0919-260$	O	217	$1954-388$	D	429
$1034-293$	O	872	$1958-179$	O	888
$1144-379$	C	385	$2126-158$	C	185
$1226+023$	O	953	$2128-123$	O	607
$1424-418$	O	424	$2134+004$	O	745
$1502+106$	O	488	$2149+056$	C	222
$1510-089$	O	222	$2216-038$	O	370
$1622-253$	O	1271	$2251+158$	O	1098
$1633+382$	O	373	$2255-282$	O	845

definitely unstable. It is interesting to note, that this source was never suspected in instability.

However, the number of detectable stable sources by this method (in this work it is 35) is small. Moreover, arcs length analysis of time series reveals systematic effects in variations of sources positions for almost all time series. Further investigations of the effects should be continued.

Acknowledgements. Our solution, mao000b, is based on the VLBI observations provided by the International VLBI Service for Geodesy and Astrometry (IVS).

The authors are grateful to the VLBI analysis centers that provided the results of estimation radio source positions.

5. REFERENCES

Ma, C., 2008, "Progress in the 2nd Realization of the ICRF", In Proc. Journées Systèmes de Référence Spatio-Temporels 2007, N.Capitaine (ed.), Paris, France, pp. 3-7.

Schlueter, W., Himwich, E., Nothnagel, A., Vandenberg, N., Whitney, A., 2002, "IVS and Its Important Role in the Maintenance of the Global Reference Systems", Advances in Space Research, Vol. 30, No 2, pp. 145-150.

VLBA IMAGING OF SOURCES AT 24 AND 43 GHZ

D.A. BOBOLTZ[1], A.L. FEY[1], P. CHARLOT[2,3]
& THE K-Q VLBI SURVEY COLLABORATION

[1] U.S. Naval Observatory
3450 Massachusetts Ave., NW, Washington, DC, 20392-5420, USA
e-mail: dboboltz@usno.navy.mil, afey@usno.navy.mil

[2] Université de Bordeaux
Observatoire Aquitain des Sciences de l'Univers, BP 89, 33271 Floirac Cedex, France

[3] CNRS, Laboratoire d'Astrophysique de Bordeaux
UMR 5804, BP 89, 33271 Floirac Cedex, France
e-mail: Patrick.Charlot@obs.u-bordeaux1.fr

ABSTRACT. We have imaged the sub-milli-arcsecond structure of 274 extragalactic sources at 24 and 43 GHz in order to assess their astrometric suitability for use in a high-frequency celestial reference frame. Ten epochs of observations with the Very Long Baseline Array were conducted over the course of ∼5 years, resulting in a total of 1339 images produced for 274 sources at K-band and 132 sources at Q-band. A detailed analysis of the images allowed us to characterized the effects of intrinsic source structure on the astrometric observations. We find that the average flux densities for the sources imaged at these higher frequencies is ∼1 Jy, with epoch-to-epoch variations of less than 20%. We also find that the intrinsic structure of the sources is reduced at 24 and 43 GHz relative to typical X-band results. Finally, we find that variations of the flux density contained within the radio core relative to the total source flux density are less than 8% on average at 24 GHz. Our results indicate that there are numerous sources available at high frequencies, and these sources persist over relatively long periods of time. In addition, the sources are more compact at these higher frequencies and should provide high-quality astrometric reference points resulting in an improved celestial reference frame.

1. INTRODUCTION

As part of a collaborative effort to extend the International Celestial Reference Frame (ICRF) to higher radio frequencies, we have observed a number of extragalactic sources at Q band (43 GHz) and K band (24 GHz) using the 10 stations of the Very Long Baseline Array (VLBA) operated by the National Radio Astronomy Observatory (NRAO). The long term goals of this program are: 1) to develop a high-frequency celestial reference frame (CRF) with a variety of applications including improved deep space navigation, 2) to provide the astronomical community with an extended catalog of calibrator sources for VLBI observations at 24 and 43 GHz, and 3) to study source structure and source stability at these higher frequencies in order to improve the astrometric accuracy of future reference frames.

Over the course of 5 years from 2002–2007, 10 epochs of VLBA observations were recorded for the high-frequency reference frame program. All 10 of these epochs included observations at 24 GHz. Additionally, four of the 10 epochs included simultaneous observations at 43 GHz and two of the epochs included observations at X-band (8.4 GHz). Details concerning the observing strategy, data calibration, astrometric analysis, and construction of a high-frequency catalog will be presented in a forthcoming paper by Lanyi et al. (2009). In these proceedings, we concentrate on the imaging aspects of the program, specifically source flux density, intrinsic source structure, and the variations of each of these quantities. In §2 we briefly summarize the data calibration and imaging process, whereas §3 and §4 contain the results of the analysis of the resulting images. A more detailed discussion of the entire high-frequency imaging program will be presented in a forthcoming paper by Charlot et al. (2009).

2. DATA CALIBRATION AND IMAGING

Data from the 10 epochs of VLBA K- and Q-band observations were calibrated and corrected for residual delay and delay rate using the NRAO's Astronomical Image Processing System (AIPS). Initial amplitude calibration was accomplished using system temperature measurements taken during the observations combined with NRAO-supplied antenna gain curves. Fringe-fitting was performed using solution intervals equal to the scan durations and a point source model in all cases. After correction for residual delay and delay rate, the data were written to FITS disk files, and subsequent image processing was carried out using the Caltech DIFMAP software package.

The visibility data for each frequency band were edited, self-calibrated, Fourier inverted, and CLEANed. Self-calibration and imaging was performed using an automatic script in an iterative procedure that corrected the data for residual amplitude and phase errors. A point source model was used at the beginning and convergence was achieved when the peak in the residual image became less than a specified factor times the root-mean-square (rms) noise of the residual image from the previous iteration. The 1–2% of sources with emission structure too complex or too extended for the automatic imaging script to handle were imaged by hand, i.e. in an interactive mode, following the same prescription as that for the automatic mode. Subsequent image analysis was performed outside of DIFMAP using the CLEAN components models resulting from the imaging of each source.

3. SOURCE FLUX DENSITY

For sources to be effective astrometric references (e.g. for spacecraft navigation and astronomical phase referencing) they should have relatively high flux densities and little variation in the flux density over time. From the CLEAN components models derived from the imaging, the total source flux densities ($S_{\rm total}$) were determined for all of the sources in all sessions in both frequency bands. From $S_{\rm total}$ we computed the mean flux density ($\bar{S}$) per source averaged over all sessions in which the source was observed. Plotted in Figure 1 are the distributions of $\bar{S}$ for all of the sources imaged in the program including 138 sources at X band, 274 sources at K band, and 132 sources at Q band. The mean (median) values of the distributions are approximately 1.5 (0.8) Jy at X band, 1.1 (0.7) Jy at K band, and 1.4 (0.9) Jy at Q band. Similar results were found for the 97 sources that were common to all three observing bands, where the mean (median) values were found to be 1.7 (0.9), 1.5 (0.9) and 1.5 (1.0) Jy at X, K and Q bands, respectively. It should be noted that the higher average Q-band flux densities (than K-band) are likely due to a selection effect, since these sources were drawn from a pool of strong sources with an X-band flux of >300 mJy. The K-band flux density results, however, contain sources for which this minimum X-band cut-off criteria was relaxed to ∼200 mJy.

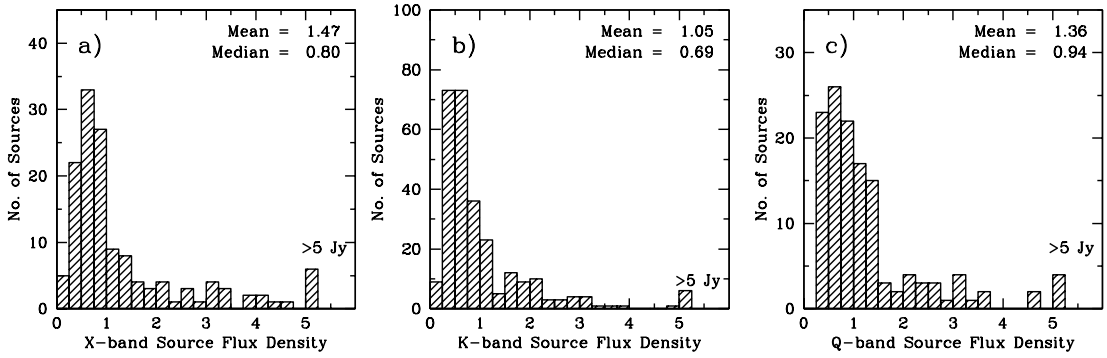

Figure 1: Distributions of the mean (averaged over all epochs) source flux density ($\bar{S}$) at a) X band, b) K band, and b) Q band. There were a total of 138, 274, and 132 sources, respectively, for which the flux density was measured at each of the three bands in our VLBA data set.

We characterized the extent to which the total flux density varied over time by computing the flux density variability index ($\sigma_S/\bar{S}$), which is the standard deviation of the measured flux densities per source divided by the mean. A minimum value, $\sigma_S/\bar{S} = 0.0$, indicates no variation in the flux density with time.

We determined $\sigma_S/\bar{S}$ for 235 sources at K band and 132 sources at Q band that were observed in two or more VLBA epochs. We computed mean (median) values of the flux density variability of 0.18 (0.16) for the K-band sources and 0.19 (0.15) for the Q-band sources. Thus we find that the average epoch-to-epoch flux density variations are less than ∼20% at both K and Q band. These results are limited to the ∼5 yr period over which our data were recorded and by the ∼10% variations in the absolute flux density scale of the data.

4. SOURCE STRUCTURE

The structure of the sources was characterized using the structure index (SI), first described in Fey & Charlot (1997). The structure index for each source at each epoch was determined using source CLEAN components models derived from the images. Structure indices were determined in a manner similar to that presented in Fey & Charlot (1997, 2000). Figure 2 compares the distributions of the source structure indices derived from our VLBA observations at the three bands, X, K, and Q. The figure plots histograms of the maximum SI drawn from all available sessions in which the structure index for a particular source was determined. There were a total of 138 sources at X band, 274 sources at K band and 132 sources at Q band for which the SI was measured. The figure shows a greater number of $SI = 1, 2$ (the most compact) sources at progressively higher frequencies. The percentage of $SI = 1, 2$ sources is 71, 85, and 92% for X-, K-, and Q-band, respectively. Similar results were found for the 97 sources common to all three frequencies, where the percentage of sources having $SI = 1, 2$ is 71% at X, 87% at K, and 93% at Q band. These results suggest that the impact of source structure should be reduced at higher frequencies.

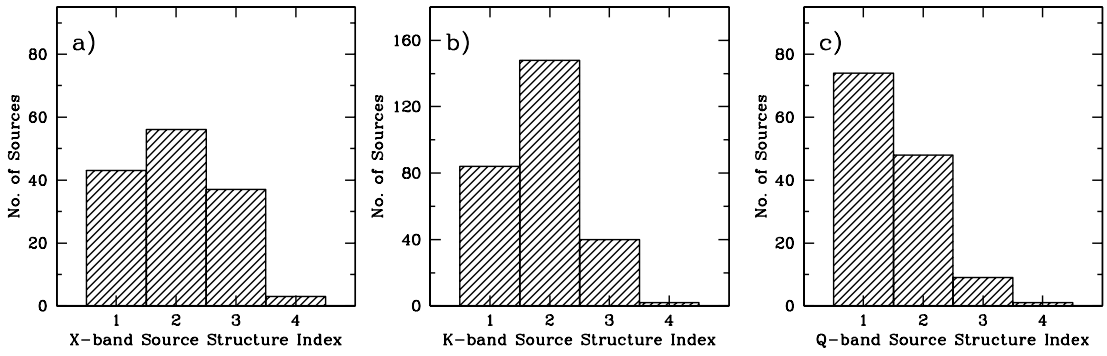

Figure 2: Distributions of values for the maximum source structure index (SI) at a) X band, b) K band and c) Q band. There were a total of 138, 274, and 132 sources, respectively, for which the maximum SI was measured at each of the three bands in our VLBA data set.

To characterize the changes in source structure over time we introduce the source compactness, C, and the compactness variability index ($\sigma_C/\bar{C}$). Both are computed on a continuous scale between 0.0 and 1.0 and are more sensitive to small changes in the structure over time. The compactness, C, is the ratio of the flux contained within the synthesized beam to the total image flux ($S_{\rm beam}/S_{\rm total}$). A value of $C = 1.0$ represents a point-like source with no extended emission. The source compactness variability index is defined as the standard deviation of the compactness divided its the mean ($\sigma_C/\bar{C}$), similar to the flux density variability index. A value, $\sigma_C/\bar{C} = 0.0$, corresponds to no variation in the compactness over time. Shown in Figure 3 are the distributions of source compactness variability index for sources imaged in more than one session at K and Q band, respectively. The mean (median) compactness variability for the 235 sources at K band is 0.08 (0.06). For the 82 sources at Q band mean (median) values of $\sigma_C/\bar{C}$ are slightly smaller 0.07 (0.05). These results indicate that, on average, the high-frequency radio emission from the core of these sources relative to the total flux density varies by no more than about 8% at either frequency. As in the case of the flux density variability, the compactness variability results are limited to the ∼5 yr period over which our VLBA data were recorded.

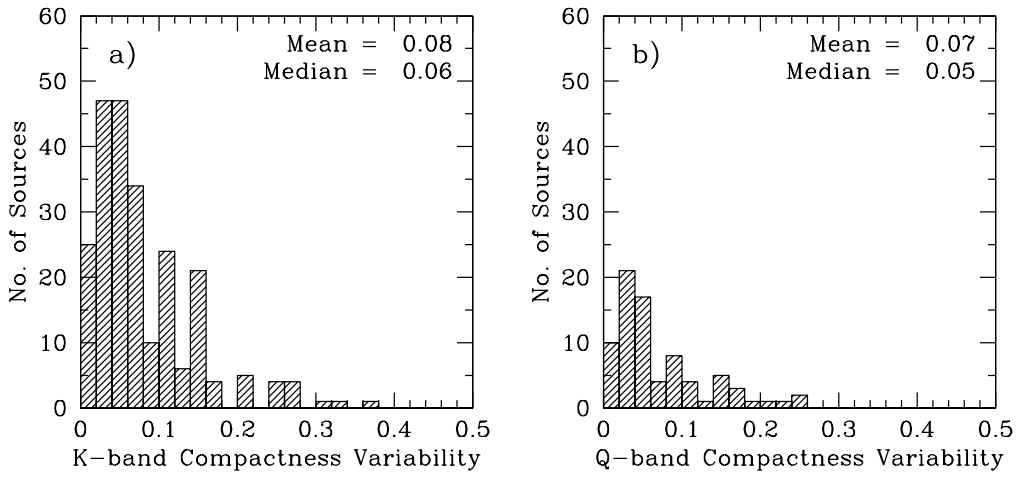

Figure 3: Distributions of the source compactness variability index ($\sigma_C/\bar{C}$) for sources at a) K band and b) Q band. There are a total of 235 sources observed in more than one epoch at K band, and a total of 82 sources observed in more than epoch at Q band. A minimum variability, $\sigma_C/\bar{C} = 0.0$, indicates no variation in the compactness over time.

5. CONCLUSIONS

We have produced a combined total of 1339 K- and Q-band images of 274 extragalactic sources from ten epochs of VLBA data observed as part of a program to select high-frequency sources for use in spacecraft navigation and future celestial reference frames. A detailed analysis of the images allowed us to characterized the strength of the sources, the intrinsic structure of the sources, and the variability of each of these quantities. We find that the distributions of source flux density at K and Q band show mean values greater than 1 Jy for each of the two high-frequency bands. Epoch-to-epoch variations are less than 20% over the ∼5 yr observing period. We also find a clear dependence of source structure index, SI, on observational frequency. The percentage of sources with $SI = 1, 2$ (the most compact) increases from ∼70% at X band, to ∼85% at K band, to ∼92% at Q band. This result suggests decreased effects due to source structure at higher frequencies. Finally, we find that variations in source structure, as measured by the source compactness variability, are less that 8% on average. Our results indicate that there are numerous sources available at high frequencies, and these sources persist over relatively long (5 years) periods of time. In addition, the sources are more compact at these higher frequencies and should provide high-quality astrometric reference points.

6. REFERENCES

Charlot et al., 2009, "The Celestial Reference Frame at Higher Radio Frequencies. II. VLBA Imaging at 24 and 43 GHz", AJ, submitted.

Fey, A. L., & Charlot, P., 2000, "VLBA Observations of Radio Reference Frame Sources. III. Astrometric Suitability of an Additional 225 Sources", ApJS, 128, 17.

Fey, A. L., & Charlot, P., 1997, "VLBA Observations of Radio Reference Frame Sources. II. Astrometric Suitability Based on Observed Structure", ApJS, 111, 95.

Lanyi, G. et al., 2009, "The Celestial Reference Frame at Higher Radio Frequencies. I. VLBA Astrometric Observations at 23 and 43 GHz", AJ, submitted.

THE LQAC (LARGE QUASAR ASTROMETRIC CATALOGUE): PRINCIPLE OF COMPILATION AND RELATED STUDIES

J.SOUCHAY[1], A.H.ANDREI[2], C.BARACHE[1], S.BOUQUILLON[1], A.M.GONTIER[1], S.LAMBERT[1], C.LE PONCIN-LAFITTE[1], F.TARIS[1], E.F.ARIAS[3], D.SUCHET[1], M.BAUDIN[1]
[1] SYRTE, Observatoire de Paris, CNRS, UPMC, France
[2] Observatório Nacional/MCT and Observatório do Valongo/UFRJ, Rio de Janeiro, Brazil
[3] Bureau International des Poids et Mesures, Sèvres, France

ABSTRACT. We have recently achieved at SYRTE (Paris Observatory) the construction of the Large Quasar Astrometric Catalogue (LQAC) including 113 666 objects (Souchay et al.,2008). The main purpose consisted in compiling all the quasars already discovered and archived in more than 200 individual catalogues, in a single file. We also added the maximum of information concerning the redshifts, the photometry and the radio fluxes. We were very careful at giving the best determination for the celestial coordinates of the quasars. We show some results related to cross-identifications and completeness of information. A catalogue like the LQAC will be undoubtedly very useful for the preparation of the GAIA mission.

1.INTRODUCTION

A new era appeared in the fields of astrometry in 1988, when the IAU decided to adopt the ICRF (International Celestial Reference Frame) as the reference frame to be conventionally chosen by the astromomical community. The ICRF in its original version is a set of 212 quasars which have been intensively studied with the VLBI (Very Long Baseline Interferometry) technique, and which offers all the guarantees of astrometric stability (Ma et al.,1998): in other words, their relative displacements perpendicular to the line of sight are negligible so that they can be considered as quasi inertial objects. This is due to their very far distance (typically of the order of several billion light-years), although their recession speed (and also their transversal one) is significant with respect to the speed of light.

Therefore any newly discovered quasar is potentially dedicated to astrometric purpose. Thus the discovery of new quasars at present time and in the future is a real challenge for modern astrometry. Generally a density of several tens of astrometric standards per square degree is required in order to determine with the best accuracy the positions of all the objects of a given field in the sky. With the dramatic sensitivity of new astronomical techniques, it is already possible to reach this density for quasars in some given selected celestial fields. Thus we believe that in the near future a good part of the celestial sphere will be covered by a large number of quasars so that a direct astrometric calibration with the help of these extragalactic quasi inertial targets will be possible at a large scale.

2. LARGE SURVEYS AND QUASARS CATALOGUES

The number of newly discovered quasars increases year after year in an exponential way thanks to the arrival of very large and deep surveys as the SDSS (Sloan Digital Sky Survey) and the 2-degree Field quasar Redshift Survey (2dF). The Sloan Digital Sky Survey (Adelman-McCarthy et al., 2007) covers one quarter of the sky observed from a dedicated 2.5 m telescope located at Apache Point, New Mexico. Images of the explored zone were obtained at seven bandwidths, namely u,b,v,g,r,i,z, that is to say from the ultraviolet cutoff to the near infrared, and the redshifts were determined precisely from spectroscopic complementary measurements. The typical accuracy per coordinate of the positions of the quasars of the SDSS are typically 45 mas (milliarcseconds) when measured against the USNO Astrograph catalogue and 75 mas when measured against Tycho 2 (Pier et al., 2003). The 5th release of the SDSS contains 74 868 objects whereas the DR6 release contains several additional thousands of objects. The 2dF quasar redshift survey, quoted as 2QZ (Croom et al.,2004) is based on a pre-selection of quasars candidates from well defined criteria based on broadband u, b,r photometric measurements obtained from plate scanning of UKST photographic plates. It contains 22 971 quasars. The SDSS and 2QZ quasars catalogues are by far the densest of a very large set of other quasars catalogues : more than 200 can be counted for which

	VV06	A–L	LQAC	% of completness
u	74 367	96 343	**99 665**	87.8
b	79 488	96 253	**106 801**	93.9
v	54 542	48 466	**75 396**	66.3
g	0	74 862	**74 862**	65.9
r	1 540	99 537	**100 811**	88.7
i	101	86 143	**86 238**	75.9
z	0	74 861	**74 861**	65.9
J	9	13 647	**13 656**	12.0
K	3	13 647	**13 650**	12.0
1.4 GHz	8 405	1 811	**8 934**	7.8
2.3 GHz	0	3 234	**3 234**	2.8
5.0 GHz	3 585	862	**3 951**	3.4
8.4 GHz	0	3 858	**3 858**	3.3
24 GHz	0	61	**61**	0.0
redshift	85 182	101 535	**110 745**	97.4

Table 1: Number of entries per item for the following catalogues: VV06, A–L, and final LQAC. The difference between the 4th and the 3rd column gives the contribution of VV06 to the LQAC.

the number of objects range from a few ones to several hundreds (see the CDS website).

3. THE L.Q.A.C. (LARGE QUASAR ASTROMETRIC CATALOGUE

We have recently achieved the construction of the Large Quasar Astrometric Catalogue (LQAC) whose details can be found in Souchay et al.(2008). The LQAC consists in compiling a large majority of the overall population of recorded quasars at the present time. One of the goals consists in selecting the best astrometric determination of the equatorial coordinates (α,δ) with respect to the ICRF. In that aim we have selected a hierarchical order according to the astrometric quality of the catalogues in which the quasar could been found. In the case of cross-identifications between two or more catalogues, the a priori most trustable coordinates have been kept, according to the supposed accuracy of the catalogues involved.

Although the various catalogues contributing to the LQAC are quite inhomogeneous in term of number of objects, quality of astrometric determinations, number of photometric bandwidths etc... we have observed that more than 90 % of the total sample of the quasars compilated are found by gathering only 8 catalogues, which insures quite a good global homogeneity. In decreasing order of accuracy we have set a flag from "A" to "H" to these catalogues which are : the ICRF-Ext2 (flag "A", Fey et al.,2004)), the VLBA (flag"B", Beasley et al,2002), the VLA (flages "C" and "H"), the JVAS (flag "D", Wilkinson et al.,1998), the SDSS(flag "E", Adelman-Mc Carthy et al.,2007), the 2QZ (flag "F", Croom et al.,2004), the FIRST (flag "G", Gregg et al.,1996), and the Hewitt and Burbridge (flag "I",1993) catalogues. Note that the first four catalogues have been constructed from very precise radio measurements, at the level of the sub-milliarcsecond, from long or very long baseline interferometry (VLBI). One of the advantages of selecting a flag is to know directly, for a given quasar, all the catalogues in which it is included, as this can be viewed directly inside the final LQAC ASCII catalogue (Souchay et al.,2008). Note that 3 further very dense catalogues, the 2MASS (flage "J"), the GSC2.3 (flag "K") and the B1.0 (flag "L") were used not for the inclusion of additional quasars, but in order to complete the gaps in photometric information. the "M" flag is reserved to the quasars which are present in the Véron-Cetty and Véron (2006) release of their compiled catalogue.

The LQAC contains 113 666 quasars, and it is the largest compiled catalogue available now. Notice that this last number corresponds roughly to the number of stars in the Hipparcos catalogue release, which means that the average number of objects per square degree is about the same in the two cases.

	A	B	C	D	E	F	G	H	I	J	K	L
A	**716**	642	582	377	72	6	27	0	327	333	500	480
B	-	**3 355**	1 598	1 577	288	33	71	1	522	911	2034	1965
C	-	-	**1700**	1 272	203	10	52	0	413	576	1 133	1 090
D	-	-	-	**2 117**	253	6	53	0	287	547	1 306	1 267
E	-	-	-	-	**74 866**	2 053	553	4	1329	11 735	69 705	62 768
F	-	-	-	-	-	**22 965**	0	0	495	619	19 504	17 274
G	-	-	-	-	-	-	**966**	2	142	527	872	796
H	-	-	-	-	-	-	-	**154**	19	17	31	35
I	-	-	-	-	-	-	-	-	**7 142**	1 175	3 306	3 014
J	-	-	-	-	-	-	-	-	-	**13 647**	13 243	12 740
K	-	-	-	-	-	-	-	-	-	-	**91 061**	78 397
L	-	-	-	-	-	-	-	-	-	-	-	**81 662**

Table 2: The various catalogues participating to the quasars compilation named LQAC (Large Quasar Astrometric Catalogue) (Souchay et al.,2008). Each flag represents one of the catalogues involved. The nomenclature is the following one : (A) Icrf-Ext.2 (radio) ; (B) VLBA (radio) (C) VLA-015 (radio) (D) JVAS (radio) ; (E) SDSS (optical) ; (F) 2QZ (optical) ; (G)FIRST ; (H)VLA+015 ; (I) Hewitt and Burbridge ; (J) 2MASS ; (K) GSC2.3 ; (L) B1.0 ; (M) Véron-Cetty and Véron. The VLA has been divided into two parts : VLA-015 and VLA+015 according to the a priori accuracy of the determination of the celestial coordinates of the quasars (with respect to the 0".15 threshold). The number of common quasars of each cross-identification must be compared with the total number of quasars in the LQAC, i.e. 133 666 objects

	Mean (mas)		σ (mas)			
	$\Delta\alpha\cos\delta$	$\Delta\delta$	$\Delta\alpha\cos\delta$	$\Delta\delta$	N_1	N_2
VLBA	−0.010	0.039	0.767	0.585	94	4
VLA	−0.054	−0.009	1.025	1.391	63	10
JVAS	−3.287	−0.081	9.793	12.629	90	5
SDSS	1.210	−12.203	52.022	51.728	96	4
2QZ	86.242	45.991	193.667	181.214	98	3
FIRST	−30.282	0.010	286.750	319.342	96	3
HB	97.800	100.152	726.512	785.789	85	5
VV06	30.393	286.513	582.571	586.322	97	3

Table 3: Determination of the astrometric accuracy of the catalogues used in the LQAC. N_1 stands for the percentage of quasars remaining after a 3σ rejection threshold algorithm, and N_2 for the number of necessary iterations. Each catalogue has been compared with a compilation of the catalogues preceding it (the first one ICRF-Ext.2 is not indicated).

Thus we can imagine that at long term the absence of proper motion of quasars will certainly constitutes a great advantage with respect to stars as ideal astrometric standards.

In Table 1 we present the number of quasars per item (magnitude band, radio flux, redshift). We compare the Véron-Cetty and Véron (2006) release(noted VV06) with our compilation gathering only the quasars belonging to the 8 dense catalogues with flags A to I above (the VLA catalogue is represented by two flags) , and with magnitude information completed with the help of the catalogues J,K,L. Notice that objects belonging to the VV06 compilation and not present in our A to L compilation where added in order to have a completeness. A new flag "M" was given for these objects, with an identification number to determine the original catalogue or survey where it has been firstly detected.

When available, photometric informations were given at u,b,v,g,r,i,z, J,K optical and infrared bandwidths, and radio flux at 1.4 GHz, 2.3 Ghz, 5.0 Ghz, 8.4 Ghz and 24 Ghz. The percentage of quasars for which radio flux is available is very small in comparison of the whole sample. Notice that for a large majority of objects (97.4 %) the redshift is given. In addition to these informations we calculated the absolute magnitudes of the quasars M_i and M_b respectively at infrared and blue bandwidths. In that aim we used a very recent model of galactic extinction, of the K correction and of determination of the luminosity distance.

In Table 2, we represent the leading catalogues with flags from A to L participating to the LQAC compilation, with the number of cross-identifications between two given catalogues of this set.

In Table 3 we present the mean values and the residuals between the positions of quasars in a catalogue with a given flag with the positions of this same quasar given by the pre-compilation of a priori better catalogues in terms of astrometric accuracy.

We think that the LQAC (Souchay et al.,2008) and its future extensions through regular updates will be very useful for future investigations towards densest and most accurate celestial reference frames as well as a good preparatory work to the GAIA mission consisting in gathering the maximum of information with respect to the quasars which constitute the ideal objects for 21th Century astrometry.

4. REFERENCES

Adelman-McCarthy, J.K., Agüeros, M.A., Allam, S.S., et al. 2007, ApJS, 172, 634
Beasley, A.J., Peck, A.B., Petrov, L., et al. 2002, ApJS, 141, 13
Croom, S.M., Smith, R.J., Boyle, B.J., et al. 2004, MNRAS, 349, 1397
Fey, A.L., Ma, C., Arias, E.F., et al. 2004, AJ, 127, 3587
Flesch E., Hardcastle, M.J., 2004,A&A,427,387
Gregg, M.D., Becker, R.H., White, R.L., et al. 1996, AJ, 112, 407
Hewitt, A., & Burbidge, G. 1993, ApJS, 87, 451
Ma, C., Arias, E.F., Eubanks, T.M., et al. 1998, AJ, 116, 516
Pier, J.R., Munn, J.A., Hindsley, R.B., et al. 2003, AJ, 125, 1559
Souchay, J., Andrei A.H., Barache,C., et al. 2008, A&A, in press
Wilkinson, P.N., Browne, I.W.A., Patnaik, A.R., et al. 1998, MNRAS, 300, 790

THE JOINT MILLI-ARCSECOND PATHFINDER SURVEY (JMAPS): INTRODUCTION AND SCIENCE POSSIBILITIES

R. GAUME[1], B. DORLAND[1], R. DUDIK[1], G. HENNESSY[1], Z. DUGAN[1], V. MAKAROV[2], P. BARRETT[1], C. DIECK[1], D. VEILETTE[1], & N. ZACHARIAS[1]
[1] U.S. Naval Observatory, 3450 Massachusetts Ave. NW Washington, DC 20392-5420, USA
[2] NASA Exoplanet Science Institute, Pasadena, CA 91125, USA

ABSTRACT. JMAPS is a small, space-based, all-sky visible wavelength astrometric and photometric survey mission for 0^{th} through 14^{th} V-band magnitude stars with a 2012 launch. The primary objective of the JMAPS mission is the generation of an astrometric star catalog with better than 1 milliarcsecond positional accuracy and photometry to the 1% accuracy level or better at 1^{st} to 12^{th} mag. A 1-mas all-sky survey will have a significant impact on our current understanding of galactic and stellar astrophysics. JMAPS will improve our understanding of the origins of nearby young stars, provide insight into the dynamics of star formation regions and associations, investigate the dynamics and membership of nearby open clusters, and discover the smallest brown dwarfs at distances up to 5 pc after a 2-year mission, and Jupiter-like planets out to 3 pc after 4 years.

1. INTRODUCTION

Over the last 10 years the U.S. Naval Observatory (USNO) has been involved in a number of space astrometry missions. The Full-sky Astrometric Mapping Explorer (FAME) (Johnston 2003) was a NASA-funded mission that was cancelled after the Preliminary Design Review (PDR) due to budget considerations. A concept study for the Origins Billions Star Survey (OBSS) mission (Johnston et al. 2006) was funded by NASA, but subsequent funding for mission development was not provided. USNO has been directly involved in the SIM PlanetQuest mission (Unwin et al. 2008). Although significant technology development has occurred for SIM PlanetQuest, at present the mission does not have a viable launch date.

All of the space astrometry missions discussed above, along with several other concepts, are (or were) proposed for NASA funding. During 2004, changing budget priorities within NASA prompted the USNO to explore alternative mission designs and funding sources. The result of this exploration is the Joint Milli-Arcsecond Pathfinder Survey (JMAPS).

2. JMAPS OVERVIEW

JMAPS is a small single aperture spacecraft, funded by the US government for launch in 2012. The principal objective of the JMAPS mission is to produce an all-sky visible wavelength astrometric and photometric catalog for 0^{th} through 14^{th} V-band magnitude stars. The accuracy objective of the JMAPS mission is to generate an astrometric star catalog with better than 1 milliarcsecond positional accuracy and photometry to the 1% accuracy level, or better, for stars in a 1^{st} to 12^{th} mag range. The final JMAPS catalog will be delivered in 2016. Astrometric positions will be reported in ICRS coordinates, tied to the ICRF though direct observations of the visible wavelength counterparts of radio wavelength ICRF sources. An artist's conception of JMAPS in orbit is depicted in Figure 1.

3. SPACECRAFT OVERVIEW

The current JMAPS spacecraft concept is shown in Figure 2. JMAPS is a single payload spacecraft consisting of a customized spacecraft bus (bottom), with solar panels, and an instrument deck (top). The solar panels fold against the bus in a stowed and locked position during launch and are deployed on-orbit. In addition to housing the power subsystem, the spacecraft bus contains communications, thermal control, avionics, reaction wheel, and inertial measurement unit subsystems. The Attitude

Determination and Control System (ADCS) is split between the bus and instrument deck. While the spacecraft is slewing, the star tracker located on the instrument deck determines spacecraft attitude to approximately 1 arcsecond. During standard observations the ADCS system holds spacecraft pointing stability to a 50 mas specification. This is accomplished by using the primary instrument to generate boresight pointing quaternions at a 5 Hz rate as derived from observations of a handful of reference stars on the primary focal plane. The total mass of the spacecraft, including contingency, is about 180 kg and the spacecraft occupies a volume of 96.5 cm (h) x 71 cm x 61 cm.

Figure 1: JMAPS in orbit

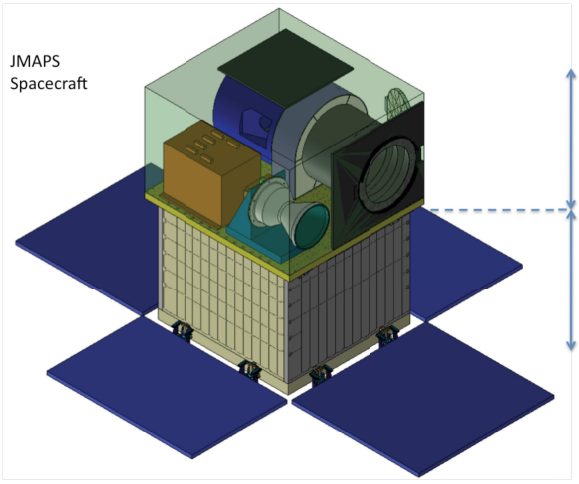

Figure 2: JMAPS Spacecraft

4. INSTRUMENT OVERVIEW

A depiction of the layout of the JMAPS instrument deck components is shown in Figure 3. The Optical Telescope Assembly (OTA) is the largest structure on the instrument deck, consisting of a single aperture, 19 cm diameter, f/20 telescope. The nominal point spread function (PSF) is 0.87 arcseconds full width half maximum (FWHM). The J-MAPS field of view is 1.24° x 1.24°. The OTA supports a JMAPS astrometric bandpass of 700-900 nm; spectroscopic observations will be conduced within a wider 450-900 nm band. During normal observations, a sun shield (not shown in Fig. 3) will protect the OTA from direct exposure to solar heating.

Tucked under the OTA (not seen in Fig. 3) is the Focal Plane Assembly (FPA). The JMAPS FPA consists of a 2 × 2 mosaic of Teledyne Imaging Sensor (TIS) H4RG-10 detectors, as shown in Figure 4. The H4RG-10 is a 10 micron pitch, 4192 × 4192 pixel CMOS-Hybrid detector. CMOS-Hybrid technology combines many of the best characteristics of CCD and CMOS technology. The nominal pixel subtense is 0.55 arcseconds, providing a sampling of approximately 1.6 pixels per PSF FWHM. USNO has sky-tested the first generation H4RG-10 detector (the A1) (Dorland et al. 2007). USNO will receive and sky-test the second generation detector (A2) in 2009. It is anticipated JMAPS flight devices will result from the third generation of the H4RG-10 detector.

Major components of the instrument deck also shown in Fig. 3 are the Instrument Electronics Box (IEB), which houses the primary on-board electronics for both the instrument and bus, the Terma star tracker, and thermal radiators. Combined with a thermoelectric cooler (TEC), the radiators will help maintain the JMAPS FPA at a temperature of 193K, with a stability of 10mK.

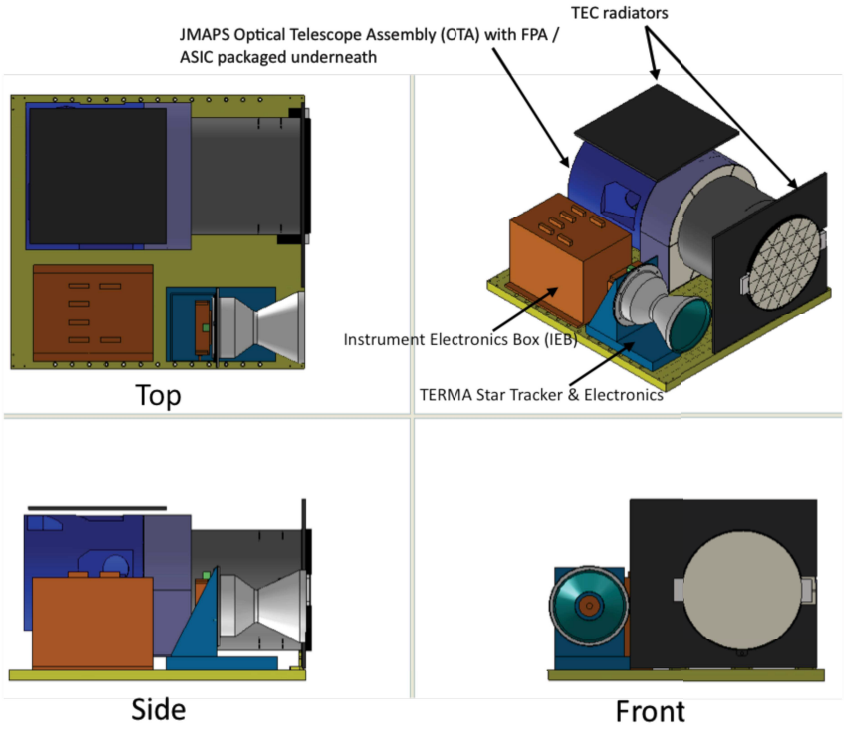

Figure 3: JMAPS Instrument—Conceptual design of the payload deck

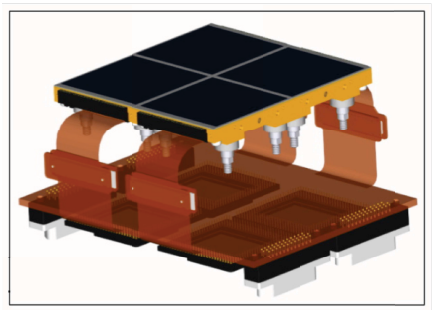

Figure 4: JMAPS FPA 4K 2 × 2 Mosaic Concept

5. JMAPS CONOPS

JMAPS will be launched into a 900 km sun-synchronous terminator orbit and operate in a step-stare mode, typically sweeping out swaths of the sky at approximately a 90° angle to the Earth-Sun line (regions of maximum parallax signal). Windowed FPA integration times of 1, 4.5 and 20 seconds will be used for the majority of stars. Shorter integration times (0.01 or 0.2 seconds) will be used for the brightest stars. In order to link the JMAPS reference frame to the ICRF, the optical counterparts of radio wavelength ICRF quasars will be directly observed by JMAPS by employing integration times of 500 seconds.

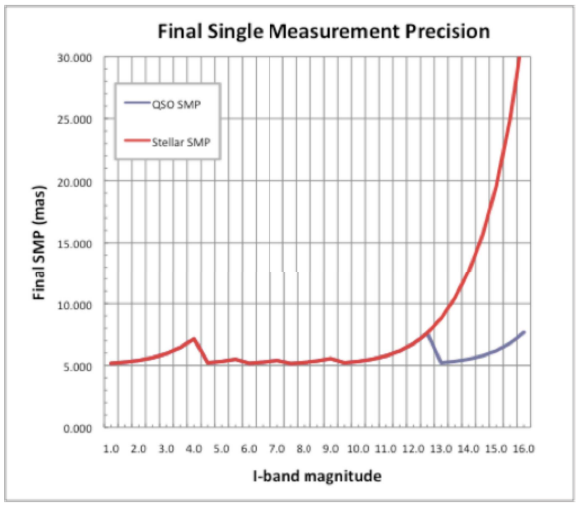

Figure 5: JMAPS **single measurement** precision predictions as a function of stellar I-band magnitude

6. JMAPS SCIENCE POSSIBILITIES

The predicted JMAPS single measurement precision (SMP) is shown in Figure 5. The sawtooth nature of the SMP plot is attributed to the various integrations times utilized for stars of different magnitudes (see §5). The objective of achieving 1 mas stellar astrometric accuracies is achieved through a global reduction of multiple (40–60) observations obtained throughout the 2–3 year mission lifetime. A 1-mas all-sky survey will have a significant impact on our current understanding of galactic and stellar astrophysics. JMAPS will improve our understanding of the origins of nearby young stars, provide insight into the dynamics of star formation regions and associations, investigate the dynamics and membership of nearby open clusters, and discover the smallest brown dwarfs at distances up to 5 pc after a 2-year mission, and Jupiter-like planets out to 3 pc after 4 years. JMAPS will provide critical milliarcsecond-level parallaxes of tens of millions of stars in the difficult 8–14^{th} magnitude range, which when combined with stellar spectroscopy and relative radii determined from exoplanet transit surveys, allows a determination of stellar radii and exoplanet densities. In addition, the 20-year baseline between the groundbreaking Hipparcos mission and the J-MAPS mission allows a combination of the JMAPS and Hipparcos catalogs to produce common proper motions on the order of 50–100 microarcseconds per year.

7. REFERENCES

Dorland, B. N., et al., 2007, "Laboratory and sky testing results for the TIS H4RG-10 4k × 4k 10-micron visible CMOS-hybrid detector", Proceedings of the SPIE, Volume 6690, pp. 66900D

Johnston, K. J. 2003, "The FAME Mission", Proceedings of the SPIE, Volume 4854, pp. 303-310.

Johnston, K. J., et al., 2006, "The Origins Billions Star Survey: Galactic Explorer", PASP, Volume 118, Issue 848, pp. 1428-1442

Unwin, S. C., et al., 2008, "Taking the Measure of the Universe: Precision Astrometry with SIM PlanetQuest", PASP, Volume 120, issue 863, pp.38-88

WAVELET ANALYSIS OF HUGE STELLAR CATALOGUES

A.S. TSVETKOV, V.V. VITYAZEV, I.I. KUMKOVA
St. Petersburg State University
University pr., Peterodvorets, St. Petersburg, 198504, Russia
e-mail: a.s.tsvetkov@inbox.ru; vityazev@list.ru

ABSTRACT. We present the wavelet technique for searching the heterogeneities of stellar density in the data of NOMAD (Naval Observatory Merged Astrometric Dataset) catalogue which contains more than a billion stars. The known and unknown globular and open clusters have been detected in various photometric bands up to V=18. A lot of artifacts in NOMAD data were found in addition. This technique can be used for catalogues of the nearest future including the products of GAIA mission.

1. NOMAD DATABASE

The huge stellar catalogues which became available in the last years require new processing procedures. At present, the world largest stellar catalogue is the Naval Observatory Merged Astrometric Dataset (NOMAD). It contains more than 1 billion stars.

The NOMAD catalogue is a compilation of six astrometric catalogues – Hipparcos, UCAC2, YB6, Tycho-2 and USNO-B. In addition, it includes the photometric data from the 2MASS project. Finally, photometry in six bands (B, V, R, J, H, K) is available for about the half of stars. The distribution of NOMAD stars via their magnitude V is shown in Fig. 1

The average stellar density of the catalogue is tens of thousand stars per square degree, in some directions it is about 1 million stars per square degree. It is interesting that the catalogue contains even the stars belonging to bright galaxies. This abundance of data poses the problem of searching the unknown stellar clusters in our Galaxy. This paper demonstrates the application of the wavelet technique for detecting the irregularities in stellar density.

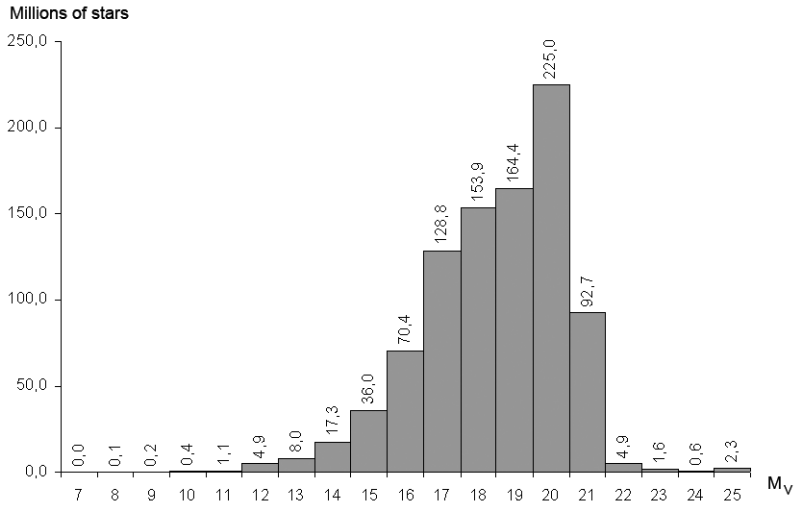

Figure 1: Distribution of NOMAD stars via magnitude V

2. ONE DIMENSIONAL WAVELET TRANSFORM

Processing the giant catalogues is severe time consuming work. To make the search of clusters as fast as possible we need to use the simplest wavelet technology. Let us consider the stellar density as a one-dimensional function of longitude along a circle of some galactic latitude. In practice, the average densities in narrow belts may be used. Since we are hunting the small scale features the 1-D wavelets may be used.

Let x_k, $k = 1...N$ are the discrete values of stellar density, Δt is the interval of sampling:

$$x_k = x(t_k), \qquad t_k = \Delta t \cdot k, \qquad k = 1, 2, \ldots, N. \tag{1}$$

We use the MHAT (Mexican hat) wavelet function

$$\psi(t) = (1 - t^2)e^{-t^2/2}. \tag{2}$$

It is important to note that the zero and first-order moments of the function (2) vanish.

The discritized wavelet transform can be written as follows:

$$W(a_i, b_j) = \frac{1}{n(a_i, b_j)} \sum_{k=1}^{N} x_k^{\circ} \psi^* \left(\frac{t_k - b_j}{a_i} \right), \qquad n(a_i, b_j) = \sum_{k=1}^{N} \exp\left(-\frac{1}{2} \left(\frac{t_k - b_j}{a_i} \right)^2 \right). \tag{3}$$

Here

$a_i = i\Delta a$ is a wavelet scale, $i = 1, \ldots, N_a$; $N_a < N$ defines the value of index i, corresponding to maximal scale;

$b_j = j\Delta b$ is a coordinate shift, $j = 1, \ldots, N$.

It is reasonable to adopt equal values for the scale and coordinate shift intervals:

$$\Delta a = \Delta b = \Delta t. \tag{4}$$

Further, the function (2) has strong localization in spatial domain. It is possible to show that

$$\int_{-L}^{+L} (1 - t^2)e^{-t^2/2}\, dt < 0.01 \tag{5}$$

for $L \approx 3.6$. It allows to decrease noticeably the number of terms in equations (3). Defining the "index-radius" of wavelet as

$$j^* = \left[\frac{La_i}{\Delta b} \right], \tag{6}$$

and taking into account (4) and (6) we finally obtain

$$W_{i,j} = \frac{1}{n_{i,j}} \sum_{k=j-j^*}^{k=j+j^*} x_k^{\circ} \psi^* \left(\frac{k - j}{i} \right), \qquad n_{i,j} = \sum_{k=j-j^*}^{k=j+j^*} \exp\left(-\frac{1}{2} \left(\frac{k - j}{i} \right)^2 \right). \tag{7}$$

The problem of edge effect (the restriction of admissible value of index j in equations (7)) is not important in our case since our functions are periodical: ($x_{k+N} = x_k$ and $x_{k-N} = x_k$). Equations (7) make the computational procedure very fast.

It is a common practice to use the squares of $W_{i,j}$. In our task we prefer the values

$$S_{i,j} = W_{i,j} \cdot |W_{i,j}, \tag{8}$$

since the positive and negative values $S_{i,j}$ help distinguish between congregation and rarefication of stars. The array of $S_{i,j}$ (or $|S_{i,j}|$) is often called the *scalogram*.

The left image in Figure 2 demonstrates the wavelet analysis of the simulated distribution of x_k. One can see the different representation of two artificial "clusters" of different size. The "diffraction" effects with negative density are noticeable near sharp boundaries of the heterogeneities.

The right image represents the results of wavelet analysis of a strip along the small circle of celestial sphere bounded by galactic latitudes $+31.5^\circ \le b \le +32.5^\circ$. The set of data x_k is the average values

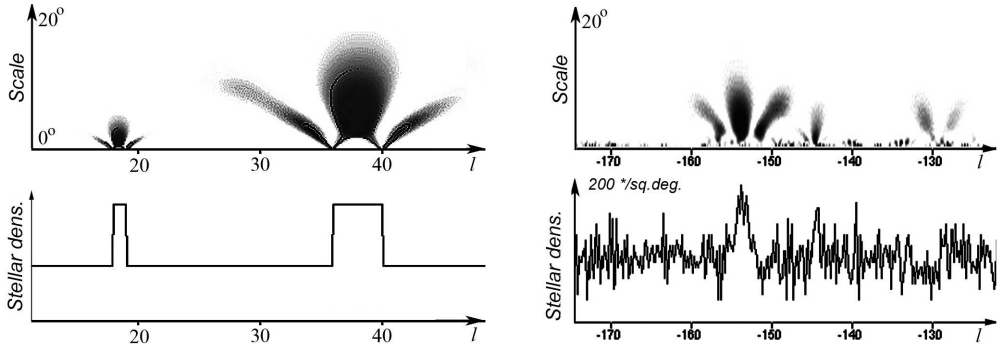

Figure 2: Wavelet transform of artificial (left) and real (right) data

of stellar density for stars $10 \leq J \leq 12$ within the interval $\Delta t = 10'$. Near $l = -153°$ one can see the distinct concentration produced by open cluster M 44 (Praecepe – "Hive"). We will see later that wavelet analysis can detect not only such obvious concentrations but substantially smaller ones.

3. WAVELET SURVEY OF THE CELESTIAL SPHERE

The fast algorithm for searching local heterogeneities in stellar density was proposed. It consists of the following steps:

- The sampling of stars from NOMAD according to some selection criteria (for example, the magnitude range);
- The forming of narrow strips (1° or 0.5° wide) along circles of equal galactic latitude. These strips are divided into small areas with constant longitude intervals ($10'$ or $5'$);
- Calculating the values x_k of average stellar density for each area in all strips;
- Application of the one dimensional wavelet technique to all strips.

The transformation of a scalogram (2-D array $S_{i,j}$) into *a scalegram* (1-D array G_j)

$$G_j = \frac{1}{i_{max} - i_{min} + 1} \sum_{i=i_{min}}^{i_{max}} S_{i,j} \tag{9}$$

allows to visualize all the celestial sphere using for example the Aitoff-projection (Fig. 3). The variation of values i_{min} and i_{max} results in the different visible details in the scalogram.

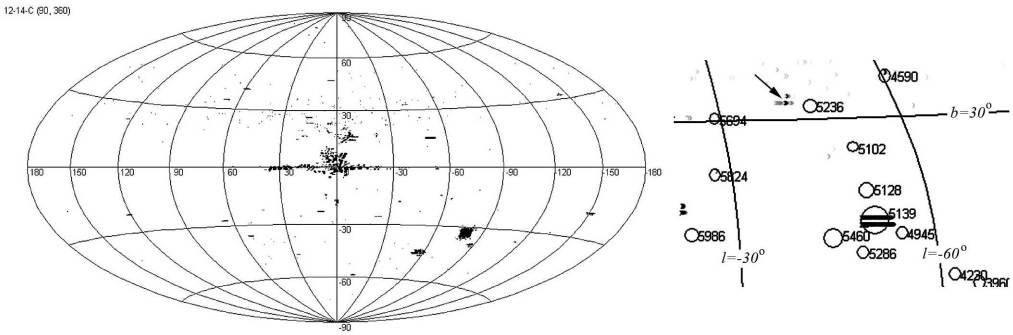

Figure 3: The general view of wavelet survey for stars of $12^m - 14^m$ (left) and its detail (right)

The analysis of an image like Fig. 3 gives evidence of three kinds of objects:

- The known clusters detected by wavelet technique;
- The known clusters which are not detected by wavelet technique;
- The unknown objects detected by wavelet technique.

The first class of objects is obvious. The explanation of the second situation is that some clusters are not visible in all magnitude ranges. For instance, the Pleiades (M 45) is imperceptible in the sample of faint stars ($12^m - 14^m$) but is easily detected in the sample of bright stars ($8^m - 10^m$).

The most interesting class of objects is the third one. Probably, we have found some unknown stellar clusters, for example, in the region near $l = -45.5°$, $b = +32°$ (Fig. 4, left). Still, we could not determine the origin of some strange objects like (Fig. 4, center).

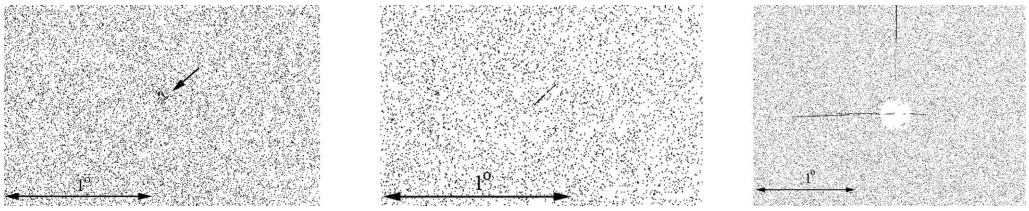

Figure 4: The unknown cluster (left), the object of unknown origin (center) and the artifact (right)

The most prevalent unknown objects are found to be the observational artifacts of the catalogue. The Fig. 4 (right) shows distinctly that the catalogue data contains even the diffraction rays near bright stars as usual stars.

4. CONCLUSION

Earlier, nebulous spots in the sky frequently fooled comet discoverers. To help them Charles Messier compiled his famous catalogue of stellar clusters, galaxies and nebulae visible in telescopes of XVIII century. Now, diffraction spikes and other artifacts in NOMAD put obstacles in the way of stellar cluster hunting. To help detecting new stellar clusters one need to have a catalogue of all known artifacts in the biggest data set of the XXI century. Our further goals are: the compilation of a catalogue for all detected aggregates in NOMAD; census of the NOMAD's artifacts and, finally, constructing the catalogue of new stellar clusters.

5. REFERENCES

NOMAD, Naval Observatory Merged Astrometric Dataset: `http://www.navy.mil/nomad` (2002).

The Hipparcos and Tycho Catalogues 1997: ESA SP-1200 (1997).

UCAC1: Zacharias, N. et al., 2000, ASP Conference 216, 427.
UCAC2: Zacharias, N. et al., 2004, AJ 127, 3043.

YB6: Monet, D.G., 2004: complete scan of NPM and SPM plates.

Tycho-2: Hog, E. et al. 2000, A&AS 355, L27

USNO-B: Monet, D. G. et al., AJ 125, 984 (2003)

2MASS: `http://www.ipac.caltech.edu/2mass/releases/allsky/`

J. D. McEwen, M. P. Hobson, D. J. Mortlock, A. N. Lasenby, 2005, IEEE Transactions on Signal Processing.

Sulentic, J.W., Tifft, W.G., 1977, Revised New General Catalogue of Nonstellar Astronomical Objects, Tuscon.

Harris W.E., 1996, A catalog of parameters for globular clusters on the Milky Way, AJ 112, 1487.

Dias W.S., Alessi B.S., Moitinho A., Lepine J.R.D., 2002, New catalog of optically visible open clusters and candidates (V2.8), A&AS 389, 871.

Vityazev, 2001, V.V. Wavelet analysis of time series, SPb (in Russian)

QSOs PHOTOMETRIC IDENTIFICATION FOR ASTROMETRIC REDUCTION OF CCD IMAGES

A. ALBERT AGUILAR[1], C. BARACHE[1], S. BOUQUILLON[1], D. GINGRAS[2], J. SOUCHAY[1], F.TARIS[1],
[1] SYRTE, Observatoire de Paris, CNRS, UPMC
61, avenue de l'Observatoire, 75014 – Paris, France
[2] GEGI/Université de Sherbrooke
2500 Bd. Université, Sherbrooke (Québec), Canada

ABSTRACT. Because of their important distances, Quasi-Stellar Objects (QSOs) seem point-like sources with no apparent proper motion. This is the reason why QSOs are quasi-ideal objects for linking a CCD image to another one or for linking directly a CCD image to the OCRF and with the forthcoming 'GAIA reference Frame'. One of the difficulties of astrometric reduction using QSOs as reference points is to distinguish QSOs from stars in CCD images. We present in this poster three distinct QSOs identification methods based only on the photometric characteristics of QSOs and we study the advantages and disadvantages of each one from an astrometric point of view.

1. QSOs IDENTIFICATION METHODS

The QSOs identification methods we have developed and tested are ones using photometric characteristics of celestial objects only, easily obtained from several CCD images of a same sky-field taken with different filters. The first method studied here is based on a Multi-Layer Perceptron Neural Network (MLP-NN). The second method is based on a parametrization of the stellar accumulation points in a three-dimensional (3D) colour space, as explained by H.J. Newberg and B. Yanny (1997). The third and last method is based on two rejection masks built from a two-dimensional (2D) mapping of high stellar density and a 2D mapping of high QSO density respectively. More details about these three methods are given in the electronic file of this poster available on the following site : `http://syrte.obspm.fr/~bouquillon/JSR/2008/poster.pdf`.

2. USED DATA SETS

We used two data sets to parametrize and test these three methods. These data sets are subsets of two catalogs of stars and QSOs coming from recent large sky-survey (the 2QZ and the SDSS surveys) and limited to the Galactic Pole regions to avoid disturbance from Milky Way stars (see figure 1). For each object found in these data sets, we have the magnitudes in three (or four) different broad optical bands and the redshift value for the celestial objects identified as QSOs. We used the redshift value only to discriminate QSOs from stars and to parametrize the learning phase of the MLP-NN method.

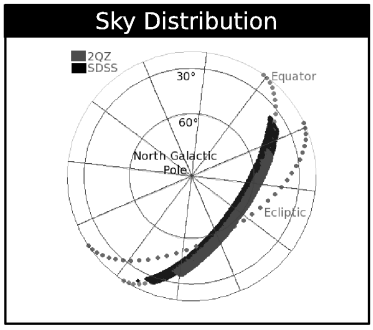

Figure 1: SDSS and 2QZ sky distribution

3. FIRST RESULTS, CONCLUSION AND PERSPECTIVES

The efficiency of each method is estimated with the help of two criteria commonly used in statistical decision theory:

• A "completeness criterion" to estimate the percentage of QSOs missed (type I error) by each algorithm.

• A "false alarm error criterion" to estimate the percentage of false QSOs (type II error) produced by each algorithm.

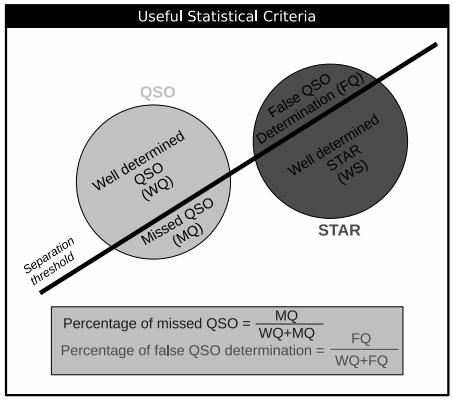

Figure 2: "Completeness criterion" and "false alarm error criterion"

With these methods, it seems that the identification of QSOs among stars, only with the help of their photometric characteristics, is reachable with some low percentage of false QSOs determination and low percentage of missed QSOs.

• With the first method (Multi-Layer Perceptron Neural Network), we obtained for the SDSS data set 25 % of missed QSO for 5.2% of false QSOs determination and for the 2QZ data set 25 % of missed QSO for 9.6% of false QSOs determination

• With the second method (Parametrization of the stellar accumulation points), we obtained for the SDSS data set 24 % of missed QSO for 5% of false QSOs determination. This method is not a suitable method for the 2QZ data set.

• With the last method (Two rejection masks), we obtained with masks build with the 2QZ data set and applied to the SDSS data set 49 % of missed QSO for 7.6% of false QSOs determination.

We also found that we could improve the efficiency of these methods by combining with one another. More details about our results are in the electronic file of this poster available on the site given before.

Nevertheless, to be used for astrometric reduction, these methods need improvements. Indeed, if we consider for instance the results obtained by applying the first method to the SDSS data set with magnitudes in three colors (25 % of missed QSO for 12.6% of false QSOs determination) and if we suppose a density around 14 QSOs by square degree (for QSOs magnitude lower than 20), to make an astrometric reduction of a CFHT CCD image, this method would provide only 10 QSOs with around two 'false QSOs determination'. This is very little.

4. REFERENCES

Newberg, H.J and Yanny, B., 1997 "Three-dimensional parameterization of the stellar locus with application to QSO color selection" The Astrophysical Journal Supplement Series, Vol 113, pp. 89-104

SEPARATION PROPER MOTIONS FROM ORBITAL ONE OF DOUBLE OR MULTIPLE STARS BY USING HIPPARCOS AND GROUND-BASED OBSERVATIONS

G. DAMLJANOVIC
Astronomical Observatory
Volgina 7, 11060 Belgrade 38, Serbia
e-mail: gdamljanovic@aob.bg.ac.yu

ABSTRACT. In my PhD thesis ("Improvement of accuracy of proper motions of Hipparcos Catalogue stars using optical latitude observations", Belgrade Univ., 2007) and few published papers, I used Hipparcos and ground-based long history optical observations of latitude, the Least Squares Method (LSM) with linear model, to get better proper motions in declination than the Hipparcos ones. After that, I continue this investigation, but with another model which can include the orbital motion (of double or multiple stars) into calculation and to separate the proper motion in declination from the orbital one of observed Hipparcos stars. Some parts of the sky (presented via Hipparcos stars data) are with bigger errors than averaged one of stars positions (which is about 1 mas) and of stars proper motions (close to 1 mas/yr), the shortness of the Hipparcos observations (less than four years) yields bigger proper motions errors of double or multiple stars than the single ones, about 15 years elapsed since the HIPPARCOS satellite observations because the epoch of Hipparcos Catalogue is 1991.25, etc. The data of latitude variations are used (covering the period 1899.7-1992.0) to improve the Hipparcos proper motions in declination of stars observed in line with the Earth orientation programmes; the method is presented here.

1. INTRODUCTION

The Hipparcos ESA mission (ESA, 1997) produced two catalogues in optical wavelength, both linked to the ICRF (the International Celestial Reference Frame): Hipparcos (118218 stars with coordinate accuracy close to 1 mas at the epoch 1991.25, 1 mas/yr accuracy of proper motions in $\mu_\alpha \cos\delta$ and μ_δ and very accurate parallaxes and photometry), and Tycho (1058332 stars with 25 mas accuracy of coordinates). The Hipparcos Catalogue was adopted to be the primary realization of ICRS (the International Celestial Reference System) in the domain of optical wavelengths. It contains stars brighter than $V = 12$ (mostly between $V = 7$ and $V = 9$).

It is evident that the combinations of Hipparcos and Tycho catalogues and the ground-based ones can improve the positions and proper motions of observed stars. During the last decade, a few problems concerning the Hipparcos data appeared: a better accuracy of the data for single Hipparcos stars than for double and multiple ones due to the short life of the satellite mission, different accuracy of the data on different parts of the celestial sphere, more inaccurate apparent star positions due to the errors of proper motions because their influence is linear in time (from the moment 1991.25) and by now the errors of apparent position has attained about 15 mas (one order of magnitude larger than the average position error in Hipparcos Catalogue), etc. All of this is the reason that a few star catalogues appeared after the Hipparcos one, such as ARIHIP (Wielen et al., 2001), and the Earth Orientation Catalogue (EOC-2) (Vondrák, 2004), with more accurate star positions and proper motions than those from Hipparcos.

The proper motion μ of the star (tangential part on the sphere) can be separated into two parts, μ_α (along the coordinate α) and μ_δ (along the δ): $\mu = (\mu_\alpha^2 \cos^2\delta + \mu_\delta^2)^{1/2}$. It is $\mu_\delta = (\delta_1 - \delta_2)/(t_1 - t_2)$, where δ_1 and δ_2 are two positions (in the same system) of the same star for the epoch t_1 and t_2, respectively. The error of μ_δ is $\epsilon_{\mu_\delta} = (\epsilon_1^2 + \epsilon_2^2)^{1/2}/|t_2 - t_1|$, where ϵ_1 and ϵ_2 are standard errors of δ_1 and δ_2, respectively. So, ϵ_{μ_δ} is proportional to $1/t$ (Eichhorn, 1974); with long observational interval t we can get very good accuracy ϵ_{μ_δ} (better than the Hipparcos one).

2. DATA AND METHOD

Here we use the results of latitude observations made with 10 PZT instruments (at 6 observatories: Mizusawa, Mount Stromlo, Ondřejov, Punta Indio, Richmond and Washington) and the Hipparcos Catalogue data in order to obtain proper motions in declination more accurate than the Hipparcos ones.

The reduction procedure concerning the latitude has been described in (Vondrák et al., 1998). We investigate the latitude variations φ_i with time around the corresponding mean latitudes. The elimination of systematic effects (polar motion, local and instrumental systematic variations) of interest for this investigation is described in the paper (Damljanović, 2005). Like that, we get the residuals (for corresponding observational epochs) r'_i, and assume that the values r'_i are mostly due to the catalogue systematic errors (influence of proper motions in declination) because of $\Delta\varphi + (d\varphi/dt)t \approx \Delta\delta + t\Delta\mu_\delta$, (Vondrák et al., 1998), where: $\Delta\delta$ is the correction of declination, $\Delta\mu_\delta$ is the correction of proper motion in declination, t is the time. For the case of single star, we process star by star by using the LSM and $r''_i = a + b(t_i - 1991.25)$, where a and b are the unknowns, the values r''_i are the averaged values of r'_i over subperiods of 1 year for each star, and the values t_i are the times (in years) corresponding to r''_i. The value a is the correction of $\Delta\delta$ and b is the correction of $\Delta\mu_\delta$; both are calculated for the epoch 1991.25. As an input value for the LSM, among the points r''_i we add one more point with the coordinates (1991.25, 0.″0). All points are with suitable weights (Damljanović et al., 2006). We add our calculated corrections b to the corresponding Hipparcos proper motions in declination. In this way we obtain the values μ_δ and their errors.

In the case of double or multiple stars, we get the model (for star by star procedure) $r'''_i = b't'_i + A\sin(2\pi t'_i/P) + B\cos(2\pi t'_i/P)$, where: the residuals $r'''_i = r''_i - a$, the values $t'_i = t_i - 1991.25$ are the time (in years), b' is the unknown corrections to the Hipparcos proper motions in declination (more or less close to the suitable values b), the unknown values A and B are useful to calculate the amplitude $am = (A^2 + B^2)^{1/2}$ of periodic part. The periodic part is $am * \cos(2\pi t'_i/P - F)$ with the period P and phase F (from the moment 1991.25). At that way, we have got three unknowns to calculate: b', A and B. The value P (in years) is from the interval $(2; 4 * m')$ with step $k = 1$ year, where m' is the number of the observed years. For each star we have got $(4 * m' - 3)$ different solutions of the unknowns b', A and B, but the best one is for the value P when the calculated curve is the best fit for the set of the input points (r'''_i points plus the Hipparcos one (1991.25, 0.″0)). The best fit is for the case $\sigma_0 = min.$, where σ_0 is the root mean square error of differences between the calculated points of the curve and suitable input ones r'''_i. Lake that, we can determine the value P, also.

Our next step is to apply this model on the data of double or multiple PZT stars, and to check the results by using the EOC-3 ones. The possible case for this model is the star H111841 (observed about 49 years at Washington and Mizusawa observatories) with the points r''_i close to the sinusoid curve.

It was evident that ground-based data are useful and can improve the reference frame (via improvement of proper motions in declination of Hipparcos stars). Because of it we continue with the investigations about the proper motions by using the ground-based data and more complex model than the linear one.

GD performed his work as a part of the Projects No 146004 "Dynamics of celestial bodies, systems and populations" supported by the Ministry of Science and Technological Development of R. Serbia.

3. REFERENCES

Damljanović, G., 2005, "Photographic zenith tubes observations to improve Hipparcos proper motions in declination of some stars", Serb. Astron. J., 170, pp. 127–132.

Damljanović, G., Pejović, N., Jovanović, B., 2006, "Improvement of Hipparcos proper motions in declination", Serb. Astron. J., 172, pp. 41–51.

Eichhorn, H., 1974, "Astronomy of star positions", Frederick Ungar Publishing Co., New York.

ESA, 1997, "The Hipparcos and Tycho Catalogues", ESA SP-1200.

Vondrák, J., Pešek, I., Ron, C., Čepek, A., 1998, "Earth orientation parameters 1899.7 – 1992.0 in the ICRS based on the HIPPARCOS reference frame", Astron. Inst. of the Academy of Sciences of the Czech R., Publ. No. 87.

Vondrák, J., 2004, "Astrometric star catalogues as combination of Hipparcos/Tycho catalogues with ground-based observations", Serb. Astron. J., 168, pp. 1–7.

Wielen, R., Schwan, H., Dettbarn, C. et al., 2001, Veröff. Astron. Rechen – Inst. Heidelberg No. 40 (Karlsruhe: Kommissions – Verlag G.Braun).

ABSOLUTE ASTROMETRY FROM VLBA RDV OBSERVATIONS

A.L. FEY, D.A. BOBOLTZ
U.S. Naval Observatory
Washington, DC 20392 USA
e-mail: afey@usno.navy.mil; dboboltz@usno.navy.mil

ABSTRACT. The Very Long Baseline Array began participating in geodetic VLBI experiments in earnest in 1997 through the Research and Development VLBI (RDV) program. These experiments involve the 10 stations of the VLBA plus several antennas of the geodetic VLBI network and have occurred about every two months since the inception of the program. The VLBA RDV experiments are part of a collaborative program of geodetic and astrometric research between the National Aeronautics and Space Administration, the National Radio Astronomy Observatory and the U.S. Naval Observatory and are scheduled to accommodate the diverse goals of the participating institutions. The catalog of radio positions derived from these data and the frame they define are compared to ICRF-Ext.2. Because the VLBA RDV data are so prolific and of such high quality, when combined with the existing database of VLBI astrometric/geodetic experiments, they will make a significant contribution to the construction of the next realization of the ICRF.

1. VLBA RDV POSITION ESTIMATION

Radio positions were estimated from VLBA RDV data based upon a global solution similar to that for the ICRF and its extensions except that only data from the VLBA RDV series of experiments were used. A total of 65 VLBA RDV sessions, each of 24-hours duration, were used resulting in 1 119 464 measurements of group delay and phase delay rate. A total of 18 geodetic antennas participated in the observations. Accurate astrometric positions were estimated using the Goddard Space Flight Center CALC/SOLVE software. Parametrization of the solution followed that of the ICRF. Astrometric positions were estimated for 732 sources. The distribution on the sky of the observed sources is shown in Figure 1.

2. COMPARISON OF CATALOG TO ICRF-EXT.2

The source positions estimated from the VLBA RDV data were compared to ICRF-Ext.2. Table 1 lists statistics of the catalog differences. Results show that the VLBA RDV catalog compares very well in $\alpha \cos\delta$ with a weighted mean offset near zero. However, the VLBA RDV catalog appears to be biased slightly with respect to ICRF-Ext.2 in δ with weighted mean offset of about 70 μas. The offset in δ may be due to the fact that the VLBA is primarily a northern hemisphere array. However, the weighted mean offsets are not significant in terms of the weighted root-mean-square (wrms) differences.

Table 1: Weighted Root-Mean-Square Differences

	Matching	Weighted Mean (μas)		wrms (μas)	
Catalogs Compared	Sources	$\alpha \cos\delta$	δ	$\alpha \cos\delta$	δ
VLBA RDV/ICRF-Ext.2	558	−15	−69	190	275
VLBA RDV/ICRF-Ext.2	191[a]	+1	−32	257	285

[a]Includes only sources designated ICRF Defining.

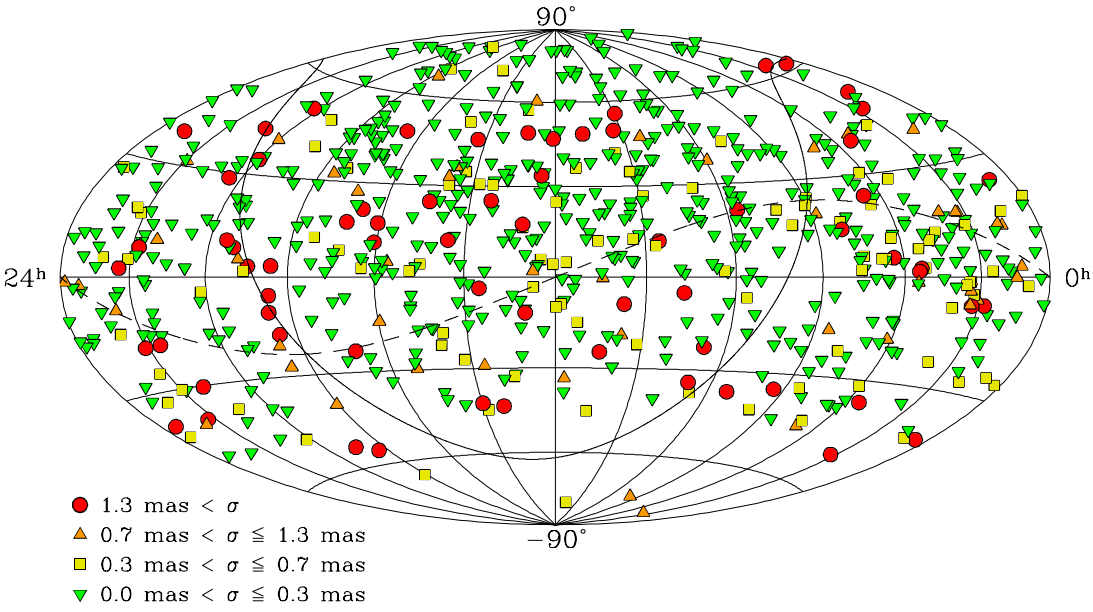

Figure 1: Distribution of the sources observed in 65 VLBA RDV sessions on an Aitoff equal-area projection of the celestial sphere. Position formal uncertainty (root-sum-square of $\sigma_{\alpha\cos\delta}$ and σ_δ) is indicated by the key. The dashed line represents the ecliptic plane and the solid line represents the Galactic equator.

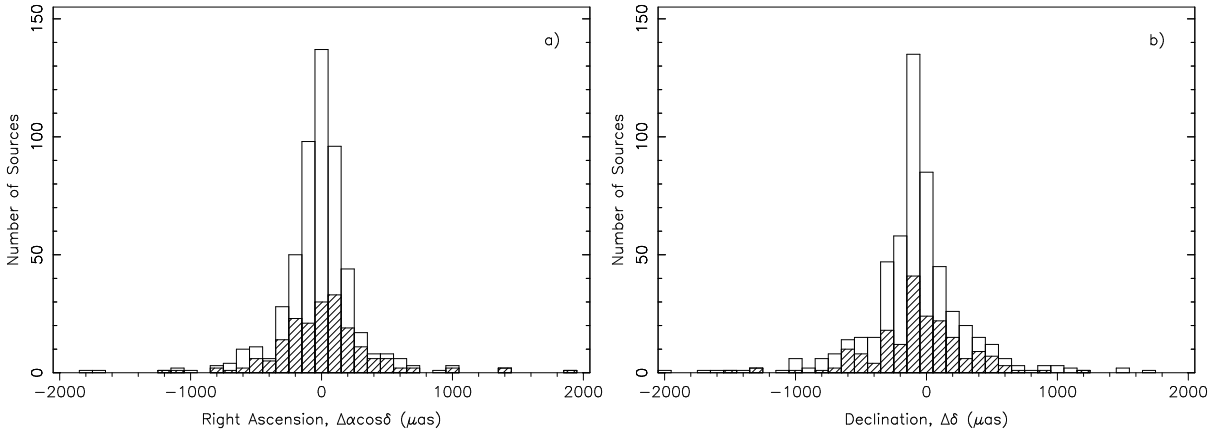

Figure 2: Distribution of differences in a) $\alpha\cos\delta$ and b) δ between positions derived from VLBA RDV data and their ICRF-Ext.2 positions. The hashed portions of the bins show the distribution for the 191 sources designated ICRF Defining. The weighted mean and wrms differences in $\alpha\cos\delta$ and δ for all 558 matching sources are -15 ± 190 μas and -69 ± 275 μas, respectively. The weighted mean and wrms differences in $\alpha\cos\delta$ and δ for just the 191 sources designated ICRF Defining are 1 ± 257 μas and -32 ± 285 μas, respectively. No fitted rotations or deformations between frames were removed for this comparison.

SOURCE SELECTION FOR ICRF DEFINING SET FROM SOURCE POSITION TIME SERIES ANALYSIS

S.L. KURDUBOV, E.A. SKURIKHINA
Institute of Applied Astronomy
nab. Kutuzova 10, St.Petersburg 191187, Russia
e-mail: ksl@ipa.nw.ru

ABSTRACT. Radio Sources Positions Time Series (TS) were analyzed with covariation analysis technique. List of the best and worse sources was used for form the set of sources for NNR constraints. The global solutions with different sets of sources for NNR constraints were obtained. Transformation parameters between this catalogues and ICRF-ext.2 were calculated and compared.

1. IAA SOURCES POSITION TIME SERIES GENERATION

Source positions TS iaa000b, iaa000c (WG ftp area) with more then 75 points were analyzed using covariance functions technique (Kurdubov, 2008). As a value indicated the stability of the time series we use the values $q(\tau_1)$ — the second point of covariance function which shows how much the TS are correlated and does not matter the origin of correlation the random walk or piece-wise linear or some else. We calculate the coefficient $k = 100 * Max(q(\tau_1)_{RA*cosDE}, q(\tau_1)_{DE})$ for each time series and use as TS stability indicator. The list of 140 sources sorted in order of increasing of the k value is presented at the Table 1 with the category of the sources in column c: "d" – defining, "c" – candidate, "o" – others.

N	*Source*	c	k	N	*Source*	c	k	N	*Source*	c	k	N	*Source*	c	k	N	*Source*	c	k
1	1351-018	c	4	29	1357+769	c	13	57	0458-020	c	18	85	1057-797	d	26	113	0014+813	d	38
2	0111+021	c	5	30	1638+398	o	13	58	1219+044	d	18	86	1923+210	c	26	114	1404+286	o	38
3	1128+385	d	5	31	1418+546	d	13	59	1308+326	d	18	87	1104-445	o	26	115	1803+784	c	39
4	2318+049	c	6	32	2136+141	d	13	60	0808+019	c	19	88	1034-293	o	26	116	0919-260	o	39
5	0201+113	c	7	33	0735+178	o	14	61	2121+053	o	19	99	2201+315	o	27	117	1548+056	o	40
6	2209+236	d	7	34	0336-019	c	15	62	1633+382	o	19	90	0814+425	c	27	118	0745+241	d	41
7	0133+476	d	7	35	0748+126	c	15	63	1611+343	c	19	91	0917+624	d	27	119	0106+013	o	41
8	1255-316	c	8	36	1101+384	c	15	64	1334-127	o	19	92	0229+131	c	28	120	2234+282	c	42
9	1606+106	d	8	37	0823+033	c	15	65	1555+001	c	19	93	1055+018	o	28	121	1510-089	o	42
10	1652+398	c	9	38	1144-379	c	15	66	0003-066	c	20	94	2216-038	o	28	122	1954-388	d	43
11	0556+238	d	9	39	2223-052	c	15	67	1124-186	c	20	95	1958-179	o	29	123	1730-130	o	44
12	1417+385	c	9	40	0805+410	d	15	68	2149+056	c	20	96	2200+420	o	29	124	1424-418	o	44
13	1144+402	o	9	41	0552+398	c	15	69	1849+670	d	21	97	0742+103	o	29	125	2134+004	o	45
14	0657+172	c	10	42	1156+295	c	15	70	2145+067	d	21	98	0528+134	c	29	126	1637+574	d	45
15	1908-201	c	10	43	1749+096	c	16	71	2255-282	o	21	99	0402-362	o	30	127	1044+719	c	48
16	0743+259	d	10	44	2113+293	d	16	72	0637-752	d	21	100	2251+158	o	30	128	1614+051	c	49
17	0642+449	d	10	45	2243-123	o	16	73	1502+106	o	21	101	0656+082	o	31	129	0954+658	d	50
18	0804+499	d	10	46	1004+141	o	16	74	0420-014	o	21	102	1610-771	o	31	130	0355+508	o	56
19	0602+673	c	10	47	0607-157	c	16	75	0119+041	c	22	103	0953+254	o	31	131	2128-123	o	57
20	0749+540	d	10	48	1726+455	d	16	76	0048-097	o	22	104	0923+392	o	32	132	1641+399	o	58
21	2356+385	c	10	49	0955+476	d	17	77	0235+164	d	22	105	1815-553	o	32	133	1226+023	o	58
22	2126-158	c	11	50	0104-408	o	17	78	0718+792	d	22	106	1145-071	c	32	134	1354+195	o	69
23	1807+698	c	11	51	1622-253	o	17	79	1741-038	o	22	107	0454-234	o	34	135	1053+815	d	73
24	1300+580	o	12	52	2037+511	d	17	80	1228+126	c	22	108	0212+735	o	35	136	2007+777	o	78
25	0059+581	o	12	53	0300+470	o	17	81	0119+115	c	24	109	0016+731	o	35	137	1313-333	c	84
26	1519-273	c	12	54	0727-115	o	17	82	0851+202	c	24	110	1823+568	d	35	138	1642+690	d	85
27	0234+285	c	13	55	0537-441	o	17	83	1514-241	c	24	111	0208-512	o	36	139	1253-055	o	121
28	1739+522	c	14	56	1745+624	d	18	84	0202+149	c	26	112	1921-293	o	37	140	0316+413	o	131

Table 1: Stability coefficients for some sources

As more unstable (K more then 50) were consider the last 11 sources, the next from which 1642+690 1053+815 0355+508 1313-333 1354+195 2128-123 need be removed from the stable 199 M. Fiessel stable sources list(MFV199) (Feissel-Vernier, 2003), this sources can be added to 163 M. Fiessel unstable sources list(MFV163): 0316+413 0355+508 1053+815 1226+023 1253-055 1313-333 1354+195 1641+399 1642+690 2128-123 and this two sources 1053+815 1642+690 are form category defining. The coefficient k value varies from 4 till 131. We consider sources with coefficient value less then 10 as the most stable. For this test the list of 212 defining sources can be supplemented by the next 14 sources: 1351-018, 0111+021, 2318+049, 0201+113, 1255-316, 1652+398, 1144+402, 0657+172, 1908-201, 0602+673, 2356+385, 2126-158, 1807+698, 1417+385. All this sources are from the category "c" and the last source is from the "other" sources. The MFV199 list can be supplemented by the next 6 sources: 1255-316, 1417+385, 2356+385, 2126-158 from the category "c" and 0556+238, 0743+259 defining ("d") sources.

solution	$A1$	$A2$	$A3$	Da	Dd	Bd
	μas	μas	μas	μas	μas	μas
$q55_1$	-7.1 ± 10.4	19.1 ± 9.7	-1.6 ± 11.6	0.0 ± 0.4	-0.2 ± 0.3	-1.7 ± 11.3
$q55_2$	-7.1 ± 10.4	30.8 ± 9.8	-7.5 ± 11.7	0.2 ± 0.4	-0.3 ± 0.3	2.0 ± 11.4
$q55_3$	-16.2 ± 10.3	17.3 ± 9.7	-6.0 ± 11.5	0.1 ± 0.4	-0.3 ± 0.3	1.9 ± 11.3
$q55_4$	-9.6 ± 10.4	18.3 ± 9.7	-6.0 ± 11.6	0.0 ± 0.4	-0.1 ± 0.3	-9.4 ± 11.3
$q55_5$	3.5 ± 10.3	16.1 ± 9.7	-14.1 ± 11.5	0.0 ± 0.4	-0.1 ± 0.3	-10.6 ± 11.3
$q65$	-7.8 ± 10.4	20.6 ± 9.7	-8.4 ± 11.6	-0.1 ± 0.4	-0.2 ± 0.3	-4.9 ± 11.3
$q75$	-1.5 ± 10.3	22.9 ± 9.7	-12.6 ± 11.5	0.4 ± 0.4	-0.2 ± 0.3	-0.5 ± 11.3
$q85$	-4.0 ± 10.4	26.4 ± 9.7	-14.5 ± 11.6	0.6 ± 0.4	-0.2 ± 0.3	-7.1 ± 11.3
$q95$	-6.4 ± 10.4	28.1 ± 9.7	-15.7 ± 11.6	0.6 ± 0.4	-0.1 ± 0.3	-13.0 ± 11.3
$q105$	-9.7 ± 10.4	25.7 ± 9.7	-20.4 ± 11.6	0.6 ± 0.4	-0.2 ± 0.3	-8.9 ± 11.3
$q115$	-9.0 ± 10.4	25.0 ± 9.7	-21.3 ± 11.6	0.6 ± 0.4	-0.2 ± 0.3	-6.2 ± 11.3
$q125$	-8.2 ± 10.4	29.1 ± 9.7	-26.4 ± 11.6	0.6 ± 0.4	-0.2 ± 0.3	-4.6 ± 11.3
$q135$	-5.5 ± 10.4	25.9 ± 9.7	-27.3 ± 11.6	0.6 ± 0.4	-0.2 ± 0.3	-3.4 ± 11.3
$q140$	-2.9 ± 10.4	23.7 ± 9.7	-25.6 ± 11.6	0.6 ± 0.4	-0.2 ± 0.3	-0.7 ± 11.3
$q212$	-4.1 ± 10.4	-41.4 ± 9.7	23.2 ± 11.6	0.6 ± 0.4	-0.5 ± 0.3	22.3 ± 11.3

Table 2: Transformation parameters from test catalogues to ICRF by MFV199

In order to test stability criteria described above, we calculated 15 VLBI global solutions uses various sets of sources from our list for NNR constraints the origin of the CRF. As input catalogues we used ICRF-Ext.2 (Fey et al., 2004) and VTRF2005. IAU2000A precession-nutation model was applied. The origin TRF was defined by the NNR/NNT constraints for 11 stations: MATERA, KOKEE, WETTZELL, FORTLEZA, WESTFORD, ALGOPARK, NYALES20, NOTO, ONSALA60, LA-VLBA, MK-VLBA. Estimated parameters: source positions (global), station positions and rates (global), Earth orientation: X_p, Y_p, $UT1-TAI$, X_c, Y_c (local), zenith troposphere delay: linear+stochastic signal (local), troposphere gradient: east and north (local), station clocks: quadratic+stochastic signal (local). The solution designed as $q65$ calculated using the first 65 sources from out list (k¿20) for NNR constraints. This sources we consider as of rather good stable. For the solutions $q55_1$ – $q55_5$ we use for 55 sources from first 65 most stable sources: without first 10 sources from our list NNR constraints was used 55 sources from first 65 most stable sources without first 10 for $q55_1$, second 10 sources for $q55_2$ etc; in the solutions $q65$ – $q140$ for NNR constraints was used from 65 to 140 sources from our list correspondingly; solution $q212$ – with the 212 ICRF defining sources for NNR constraints. The obtained 15 catalogues were compared with the ICRF original catalogue. Transformation parameters by the MFV199 list calculated using standard IERS model with 6 parameters are shown in Table 2.

2. REFERENCES

Feissel-Vernier, M., 2003, "Selecting stable extragalactic compact radio sources from the permanent astrogeodetic VLBI program", A&A 403, pp. 105-110.

Fey, A. et al., 2004, "The Second Extension of the International Celestial reference Frame: ICRF-Ext.2", AJ 127, pp. 3587–3608.

Kurdubov, S., Skurikhina, E., 2008, "Source positions time series generation and analysis", in the Proceedings of the Journées 2007, N. Capitaine (ed.), Observatoire de Paris, pp. 111–113.

ROTATION CURVE OF OUTER DISK FROM UCAC2 CATALOGUE

J. LIU, Z. ZHU
Department of Astronomy, Nanjing University
22 Hankou st. Nanjing, China, 210093
e-mail: ljconline@163.com; zhuzi@nju.edu.cn

ABSTRACT. We present a method for determination of Galactic rotation curve of the outer disk by using statistical parallax based on the USNO CCD Astrograph Catalog (UCAC2). Statistical method is used in order to obtain the heliocentric distance of selected star groups and their rotational velocity with respect to the Galactic center. An anti-galactic-center sample of 6,714 objects is picked as tracers from 48,330,571 UCAC2 stars. Solar peculiar motion component that perpendicular to Galactic plane is employed to calculate distance, and mean proper motion along galactic longitude to calculate the rotational velocity. The result is a flat rotation curve with slight decrease on the assumption that $V_0 = 220\mathrm{kms}^{-1}$.

1. INTRODUCTION

The rotation of our Galaxy for $R > R_0$ is proved hard to measure, because of the solar location in the middle of the Galactic plan. The rotation curve of outer disk has been studied using planetary nebulae, CO clusters of HII regions. The most cited work indicate that the rotation curve rise to $250\mathrm{kms}^{-1}$ at a distance of R=10kpc (Fich, 1991). According to a new classical Cepheids method (Pont, 1997), the rotation curve is flat and slightly decreasing between R_0 and $2R_0$ which has a mismatch of $30\mathrm{km}^{-1}$ compared to HII region rotation curve.

In general, radial velocity and distance must be independently provided with tracers to calculate the rotation curve. However, in UCAC2 (Zacharias, 2004), there is none of them, so we use new technique named statistical parallax in order to find the heliocentric distance of the tracers and in some special scenario the radial velocity is not necessary.

2. THE FUNDAMENTAL HYPOTHESIS AND SAMPLE FROM UCAC2

Anti-Galaxy center star groups are picked as a function of color index and UCAC2 magnitude. Stellar motion with respect to the sun can be divided into three parts: (1)stellar peculiar motion $\vec{V}$, (2)parallactic motion which reflect the solar peculiar motion and (3)components from Galactic rotation.

We suppose that stars move randomly in space, accordingly, the first part has the property that $\sum \vec{V} = 0$, equivalent to $\sum \mu_{lp} = 0$ and $\sum \mu_{bp} = 0$, where the subscript p denotes peculiar motion. In this sense, the average of the catalogue proper motions equals to the parallactic motion $-\vec{V}_{\odot}$.

For the UCAC2 stars limited in anti Galactic center area, we retain only the data which has photometry and error in proper motions smaller than 50% to confirm the precise of our results. On the other hand, the color index should be in small scope to insure the same type of stars. As a result 6,741 stars are picked from the UCAC2.

3. WORKING ON THE ROTATION CURVE

We divide up this sample into subsamples as a function of UCAC2 magnitude in red bandpass. Stars of each subsample can be considered at the same distance because they have the same color index. Let i be the number of subsamples along the anti-galaxy center and $n_1 \cdots n_i$ express the amount of stars in each group. For each star group: following quantities are calculated: (1)The mean position i.e. the geometrical center on the celestial sphere:

$$l_j = \frac{1}{n_j}\sum_{k=1}^{n_j} l_k \quad b_j = \frac{1}{n_j}\sum_{k=1}^{n_j} b_k \quad j = 1 \cdots i \tag{1}$$

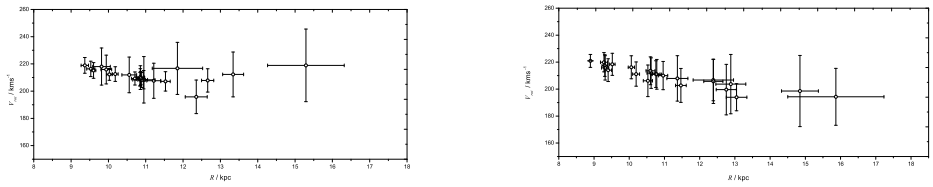

Figure 1: The rotation curve of outer disk with error bars. Each point denotes the projective mean value of corresponding star group. The sun is at the origin of X axis in case of $R_0 = 8.0$kpc and $V_0 = 220\text{kms}^{-1}$. Only groups with $n_j > 10$ are plotted on the figure in order to guarantee the statistical method effective. The left panel: the UCAC2 magnitude interval is 8.0–16.0 and we use samples with $0.3 < E = J_{2MASS} - K_{2MASS} < 0.6$; the right panel: $0.5 < E = J_{2MASS} - K_{2MASS} < 0.7$ and the same magnitude interval as before.

where l and b represent galactic longitude and latitude; (2) The projective components of proper motions on this central direction

$$\begin{pmatrix} \mu'_{lk}\cos b'_k \\ \mu'_{bk} \\ 0 \end{pmatrix} = R_1\left(90^\circ - b_j\right) R_3\left(l_j - l_k\right) R_1\left(b_k - 90^\circ\right) \begin{pmatrix} \mu_{lk}\cos b_k \\ \mu_{bk} \\ 0 \end{pmatrix} \tag{2}$$

We make an assumption that the stars move around the galaxy center along the circular track, accordingly, the radial velocity, which is the third row of velocity vector, equals zero. Because only 2-dimension projection of velocity on the celestial sphere is available in UCAC2, this is the reason why only anti-Galactic sample is picked. As above, the average proper motion of each group is:

$$\mu_{lj}\cos b_j = \frac{1}{n_j}\sum_{k=1}^{n_j}\mu'_{lk}\cos b'_k \qquad\qquad \mu_{bj} = \frac{1}{n_j}\sum_{k=1}^{n_j}\mu'_{bk} \tag{3}$$

Finally the mean distance of each group can be obtained:

$$V_z = -W_\odot = V_{bj}\cos b_j = \kappa\frac{\mu_{bj}}{\pi_j} \qquad \text{i.e.} \qquad r_j = -\frac{W_\odot}{\kappa\mu_{bj}} \tag{4}$$

where $\kappa = 4.74$ is the transition factor and we adopt $W_\odot = 7.17\text{kms}^{-1}$ (Dehnen & Binney, 1998) as the third component of peculiar velocity of the sun. The rotational velocity from statistical distance has following expression:

$$v_{rot} = V_0 + \kappa\mu_{lj}\cos b_j r_j \tag{5}$$

where $V_0 = 220\text{kms}^{-1}$ (Kerr & Lynden-Bell, 1986) is the circular speed of the sun.

It is logical to write $E = J_{2MASS} - K_{2MASS}$ although there is no magnitude in optical bandpass with UCAC2 astrometry. The resulting rotation curve is displayed in Fig.1.

Fitting the rotation curve with linear function gives

$$V_{rot} = 218.89(\pm1.89) - 2.85(\pm0.68)R \quad \text{for} \quad 0.3 < J - K < 0.6 \tag{6}$$

$$V_{rot} = 221.23(\pm1.64) - 3.76(\pm0.39)R \quad \text{for} \quad 0.5 < J - K < 0.7 \tag{7}$$

The slope is about -3$\text{kms}^{-1}\text{kpc}^{-1}$ which means a degressive rotation curve but it is not significantly away from zero. Suppose the rotational velocity is constant, the error of our result is derived from interstellar extinction and selected parameters. We have found that the statistical parallax show coherence with the distance scale of the revised Hipparcos Catalogue.

4. REFERENCES

Dehnen, W., Binney J., 1998, "Local stellar kinematics from Hipparcos data", MNRAS 298, 387–394

Fich, M., 1991, "The mass of the Galaxy", ARA&A 29, 409–45

Kerr, F.J., Lynden-Bell, D., 1986 "Review of galactic constants", MNRAS 221, 1023–1038

Pont, F., Queloz, D., et al., 1997, "Rotation of outer disc from classical cepheids", A&A 318, 416–428

Zacharias, N., Urban, S., et al., 2004, "The second US Naval Observatory CCD astrograph catalog (UCAC2)", AJ 127, 3043–3059

FORTHCOMING CLOSE APPROACHES OF JUPITER AND SATURN TO GEODETIC RADIO SOURCES

V.N. L'VOV, Z.M. MALKIN, S.D. TSEKMEJSTER
Central Astronomical Observatory at Pulkovo of RAS
Pulkovskoe Ch., 65, St. Petersburg 196140, Russia
e-mail: epos@gao.spb.ru, malkin@gao.spb.ru

ABSTRACT. In this paper[1], a list of apparent close approaches of Jupiter and Saturn to the geodetic radio sources for the years 2008-2050 has been obtained making use of the EPOS software package. We have found 79 events with distance tolerance of $10'$, including four occultations of radio sources by Jupiter and one occultation by the Saturn's ring.

1. INTRODUCTION

Very long baseline interferometry (VLBI) observations of astrometric radio sources at epochs of close approaches of greatest Solar system planets Jupiter and Saturn allow us to measure such important physical effects as light deflection and signal retardation and thus help in testing GR (see e.g. Kopeikin, 2001). Unfortunately, these events are rather rare phenomena. On the other hand, their observations need considerable resources. So, it is important to foreseen these encounters well in advance.

Although pre-computation of the approaches of Solar System bodies to radio sources with the accuracy required for scheduling of VLBI observations at a level of several arcseconds is not very difficult task for astronomers, and interested groups perform their own computation of epochs of these events, we hope that the approach list presented in this paper would be interesting for VLBI community because it allows us to have an overview of the forthcoming encounters of Jupiter and Saturn with a radio sources for better scheduling of observing experiments.

2. LIST OF APPROACHES

The list of approaches of Jupiter and Saturn to geodetic radio sources presented in Table 1 has been obtained making use of the EPOS software package (Ephemeris Program for Objects of Solar system) developed at Pulkovo Observatory (L'vov et al., 2001) which is a versatile tool for ephemeris computations in astronomy and celestial mechanics. The list of the radio sources we have checked is available at `http://www.gao.spb.ru/english/as/ac_vlbi/sou_car.dat`.

The computations were made for the period till 2050. We have chosen the distance tolerance of $10'$. Commonly speaking, such a tolerance is too large for the ground based VLBI, especially for Saturn. However we believe this extended distance range may be useful for planning of space based observations, more sensitive to the physical effects under investigation. In total, 79 events were found. It is interesting to note that due to the "loops" of the planet's apparent path on the sky some source may have up to three successive apparent approaches with various values of angular distance. Four events for Jupiter are occultations, and one event for Saturn is an occultation by the Saturn's ring; they all are marked with asterisk.

It should be mentioned that the angular distance between the planet and radio source given in Table 1 is computed for the geocenter, and may change by $1-2"$ with change of the observer's location on the Earth. As to space VLBI, the angular distance may change up to the value of relation between geocentric and planetocentric distances of the spacecraft, depending on the positional angle.

More details on events considered in this paper, as well as circumstances of other Solar System phenomena, can be computed on request.

[1]The full version of this paper is published in Solar System Research, 2009, v. 43, No. 4, p. 313.

Table 1: List of close approaches of Jupiter and Saturn to geodetic radio sources

Date Y M D	Planet	Source	Dist, arcmin	Date Y M D	Planet	Source	Dist, arcmin
2008 11 19	Jupiter	1922-224	1.4	2029 03 15	Jupiter	1333-082	7.2
2009 02 10	Saturn	1125+062	1.3	2029 09 28	Jupiter	1352-104	0.8
2009 03 08	Jupiter	2104-173	4.6	2030 11 30	Saturn	0409+188	5.1
2009 06 25	Saturn	1109+076	2.4	2031 02 23	Jupiter	1734-228	4.3
2011 07 03	Jupiter	0210+119	5.7	2031 06 07	Jupiter	1734-228	0.9
2011 09 13	Jupiter	0229+131	2.5	2031 10 05	Jupiter	1723-229	5.2
2012 02 04	Jupiter	0201+113	8.2	2032 04 03	Saturn	0503+216	1.2
2012 02 20	Jupiter	0210+119	5.7	2033 02 04 *	Jupiter	2104-173	0.3
2013 02 28	Jupiter	0420+210	3.6	2033 02 27	Jupiter	2126-158	6.9
2013 10 23	Jupiter	0723+219	2.1	2033 05 24	Saturn	0620+227	3.4
2013 11 07	Jupiter	0725+219	7.0	2034 01 28	Jupiter	2245-091	5.3
2013 11 22	Jupiter	0723+219	5.8	2034 06 15	Saturn	0723+219	0.6
2015 06 19	Saturn	1548-177	2.6	2034 07 16	Saturn	0741+214	2.6
2015 11 19	Saturn	1614-195	1.1	2035 05 13	Jupiter	0201+113	6.7
2016 11 22	Saturn	1658-217	3.2	2035 05 24	Jupiter	0210+119	2.9
2017 10 13	Jupiter	1352-104	1.1	2037 01 16	Saturn	1013+127	1.2
2017 12 13	Saturn	1752-225	1.2	2037 05 28	Jupiter	0558+234	5.1
2019 10 28	Jupiter	1723-229	3.1	2037 07 24	Saturn	1013+127	3.9
2020 08 02	Jupiter	1922-224	1.3	2037 08 27	Jupiter	0725+219	2.7
2020 10 24	Jupiter	1922-224	5.9	2037 09 19	Jupiter	0741+214	0.5
2021 02 19	Jupiter	2104-173	2.4	2041 09 11	Jupiter	1352-104	1.2
2021 08 10	Saturn	2044-188	0.3	2043 02 01 *	Jupiter	1734-228	0.0
2021 12 08	Saturn	2044-188	1.9	2043 10 18	Saturn	1459-149	3.7
2022 11 13	Jupiter	2354-021	2.7	2044 02 27	Saturn	1548-177	0.5
2022 12 04	Jupiter	2354-021	2.9	2045 01 20	Jupiter	2104-173	3.2
2023 04 13	Saturn	2221-116	0.5	2045 02 12	Jupiter	2126-158	4.7
2023 04 18	Saturn	2223-114	4.6	2045 05 29	Jupiter	2245-091	7.6
2023 06 11	Jupiter	0210+119	0.5	2045 09 20	Jupiter	2223-114	3.8
2023 11 05	Jupiter	0229+131	3.3	2045 09 20	Saturn	1614-195	0.8
2024 01 02	Jupiter	0210+119	6.6	2045 09 24 *	Jupiter	2221-116	0.3
2024 01 04	Saturn	0220-119	6.2	2045 12 04	Jupiter	2223-114	7.8
2024 03 18	Saturn	2252-090	2.6	2046 01 10	Jupiter	2245-091	1.4
2025 09 15	Jupiter	0723+219	3.6	2046 09 17	Saturn	1658-217	0.9
2025 09 18 *	Jupiter	0725+219	0.2	2047 04 28	Jupiter	0201+113	4.9
2025 10 25	Jupiter	0741+214	0.5	2047 05 08	Jupiter	0210+119	5.1
2025 11 29	Jupiter	0741+214	4.6	2047 10 17	Saturn	1752-225	6.1
2026 04 01	Saturn	0019-001	7.9	2048 11 28	Saturn	1853-226	5.4
2026 10 18	Saturn	0037+011	2.4	2049 05 11	Jupiter	0558+234	2.2
2028 05 20	Saturn	0208+106	1.3	2049 08 29	Jupiter	0741+214	3.0
2028 10 24 *	Saturn	0223+113	0.2				

3. REFERENCES

Kopeikin S.M., 2001, Testing the Relativistic Effect of the Propagation of Gravity by Very Long Baseline Interferometry. Astrophys. J., **556**, No. 1, pp. L1–L5.

L'vov, V.N., Smekhacheva, R.I., Tsekmejster, S.D., 2001, "EPOS – the software package for support of the study of the Solar system objects", Proceedings of the conference "Near-Earth Astronomy", Zvenigorod, Russia, May 21-25, 2001, pp. 235–240.

AN ANALYSIS OF SOURCE MOTIONS DERIVED FROM POSITION TIME SERIES

Z. MALKIN, E. POPOVA
Central Astronomical Observatory at Pulkovo of RAS
Pulkovskoe Ch., 65, St. Petersburg 196140, Russia
e-mail: malkin@gao.spb.ru

ABSTRACT. In this paper, an attempt is made to extract a systematic part from the source apparent motions obtained from the position time series provided by nine IVS Analysis Centers in the framework of the ICRF-2 project. Our preliminary results show that the radio source velocities and the parameters of the systematic part of the velocity field differ substantially between the source position time series.

1. INTRODUCTION

Many radio sources observed during astrometric/geodetic VLBI sessions show progressive variations in its position derived from single session solutions. Several physical effects can cause systematic apparent movement of celestial objects. Hence investigation of the radio source apparent velocity field can help in investigations in various fields, such as fundamental physics, cosmology, etc. Several analysis strategies for computation of systematic part in the radio source velocities can be used:

a) estimate source position and velocities from global solution, then fit spherical harmonics to the velocities (Gwinn et al. 1997);

b) compute the coefficients of spherical harmonics as global parameters (MacMillan 2005; Titov 2008);

c) compute velocities from position time series, then fit spherical harmonics to the velocities.

In this paper, we will test the latter approach which, hopefully, can provide a possibility for supplement comparisons and accuracy assessment. For this work, we have used 26 source position time series computed at nine VLBI analysis centers in the framework of the ICRF-2 project[1] making use of six different software, which provides a good opportunity for comparisons. For more rigorous comparison we also selected the data at common epochs for 17 series. Only the time series having at least 5 sessions and 3-year time span were used. Time series statistics is shown in Table 1.

2. COMPARISON OF VELOCITIES AND SPHERICAL HARMONICS

The source velocities were computed as weighted linear drift of the submitted source positions with weights inversely proportional to the reported variances of source positions. Since some time series contain positions with unlikely small errors (down to 1 μas in the iaa series), which leads to problems with computing the velocity as the weighted trend, it was decided to use a minimal error value of 20 μas, i.e. all errors less then this value were replaced by 20 μas. No series except iaa were substantially affected by this procedure.

At this stage we could compare both values of the source velocities and their errors obtained from different time series. Comparison of velocities showed that they can differ by several times. Median errors in velocities are shown in Table 1; they can serve as an index of the scatter of position time series. One can see that some time series are much more noisy than others.

Then we compute the coefficients of two spherical harmonics ΔH_{12} and ΔH_3 using the following formulas (Titov 2008):

$$\mu_\alpha = -\Delta H_{12} \sin 2\alpha\,, \quad \mu_\delta = -\frac{\Delta H_{12}}{4} \cos 2\alpha \sin 2\delta + \frac{\Delta H_3}{2} \sin 2\delta.$$

The results of computation are presented in Table 1. It can be noted that using more strict criteria, such as minimum 10 sessions and 10 years of observations gives statistically similar result, with smaller value of the formal error in the harmonics coefficients when more observations are used. In the last row

[1] http://ivscc.gsfc.nasa.gov/ivsmisc/ICRF2/timeseries

of the table the results are presented corresponding to the cumulative solution including all the velocity estimates in the input time series.

Table 1: Median errors in velocities $V_\alpha \cos\delta$, V_δ, and spherical harmonics ΔH_{12}, ΔH_3. Unit: μas

Series	All sessions					Common sessions				
	Nsou	$V_\alpha \cos\delta$	V_δ	ΔH_{12}	ΔH_3	Nsou	$V_\alpha \cos\delta$	V_δ	ΔH_{12}	ΔH_3
aus000a	71	7	11	-8.76±3.15	1.02±2.33	—	–	–	—	—
aus001a	343	19	28	-4.53±1.08	-2.13±0.87	—	–	–	—	—
aus002a	308	18	26	-0.34±1.22	-0.47±0.99	—	–	–	—	—
aus003a	322	18	29	-3.80±1.12	-2.47±0.90	—	–	–	—	—
bkg000c	537	14	18	-1.01±0.83	0.85±0.74	350	17	21	-0.27±0.91	-1.27±0.83
dgf000a	277	19	25	-3.84±1.44	4.88±1.49	—	–	–	—	—
dgf000b	476	15	18	-1.66±0.73	1.12±0.70	350	18	21	-1.06±0.74	-0.73±0.71
dgf000c	476	15	21	-0.27±0.90	1.23±0.76	350	19	26	0.88±0.93	-1.08±0.80
dgf000d	476	15	19	-1.94±0.75	1.14±0.72	350	19	23	-1.47±0.77	-0.71±0.73
dgf000e	476	15	19	-2.08±0.73	1.08±0.71	350	19	22	-1.71±0.77	-0.57±0.73
dgf000f	531	16	23	-0.29±0.86	1.27±0.71	350	19	26	0.85±0.97	-0.88±0.81
dgf000g	531	16	19	-2.09±0.71	1.18±0.67	350	19	23	-1.83±0.80	-0.43±0.75
gsf001a	582	13	17	-0.62±0.70	-0.09±0.64	350	15	19	-0.77±0.86	-0.76±0.78
gsf002a	592	13	17	-0.39±0.65	0.64±0.59	350	17	20	0.50±0.83	-1.46±0.76
iaa000b	458	15	22	1.23±1.37	0.80±1.16	350	18	22	3.49±1.21	1.70±1.08
iaa000c	481	16	22	1.15±1.34	2.16±1.15	350	20	23	2.75±1.24	3.44±1.17
mao000b	555	23	31	0.05±1.05	1.01±0.86	350	25	34	0.14±1.26	-0.35±1.07
opa000a	384	15	19	0.11±1.10	-0.46±0.95	—	–	–	—	—
opa000b	510	16	23	-6.14±1.09	0.46±0.88	350	19	28	-10.55±1.52	-1.01±1.21
opa001a	392	15	18	0.20±0.99	-0.37±0.87	—	–	–	—	—
opa002a	511	17	19	0.66±0.87	-0.53±0.77	350	16	20	-0.21±0.94	0.15±0.85
sai000b	501	25	37	-1.96±1.18	1.79±0.95	350	30	45	0.27±1.37	-1.39±1.14
usn000d	572	13	18	-0.70±0.78	0.18±0.70	350	17	20	-0.25±0.90	-1.44±0.81
usn001a	572	21	29	-5.94±1.22	1.53±1.02	350	25	34	-6.57±1.67	-0.28±1.38
All data				-1.24±0.19	0.62±0.17				-0.54±0.23	-0.51±0.21

3. CONCLUDING REMARKS

Although most results obtained in this paper are formally statistically reliable, they differ substantially between input time series, and also between various sets of data selected. This fact, along with results of velocity comparison, may indicate that source position time series should be used with care for analysis of the fine effects in the source motions.

Further study is needed to investigate a possibility to use combined or cumulative solution as the most reliable estimate of spherical harmonics. In particular, careful selection of input series should be performed. For instance, in our cumulative solution dgf data are clearly overweighted due to 6 series used, often with very similar position estimates. On the other hand, it seems to be inappropriate to use only one series from one analysis center because some centers compute two and more series using quite different approaches, and this would be important to compare all of them, because there is no indisputable proof in favor of only one approach.

4. REFERENCES

Gwinn, C.R., Eubanks, T.M., Pyne, T., Birkinshaw M., Matsakis D.N., 1997, "Quasar proper motions and low-frequency gravitational waves", ApJ 485, pp. 87-91.

Macmillan, D.S., 2005, "Quasar Apparent Proper Motion Observed by Geodetic VLBI Networks", In: Future Directions in High Resolution Astronomy: The 10th Anniversary of the VLBA, ASP Conference Proceedings, V. 340. Eds. J. Romney, M. Reid, San Francisco, 2005, pp. 477–481.

Titov. O., 2008, "Proper motions of reference radio sources", In: Proc. Journées Systèmes de Référence Spatio-temporels 2007, Meudon, France, 17-19 Sep 2007, N. Capitaine (ed.), pp. 16–19.

SPECIFIC STUDY OF THE GRAVITATIONAL EFFECTS OF CERES, PALLAS AND VESTA ON MARS AND THE EARTH'S ORBITAL PARAMETERS

J. SOUCHAY[1], D. GAUCHEZ[1], A. NEDELCU[2], D. GINGRAS[3], C. TOULOUSE-MALIFAUD[1]
[1]SYRTE, Observatoire de Paris, CNRS, UPMC, France
[2] Institul Astronomic Academiei Romanei, Bucuresti, Romania
[3]Université de Sherbrooke, Canada

ABSTRACT. The drastic evolution of computing tools and the necessity to take into account small effects has led the specialists of ephemerides to include a large number of asteroids in their computations. For this reason it looks appropriate to model in details the individual specific effects of these asteroids (at least the largest ones). In this paper we present our work (Souchay et al., in prep.) concerning the effects of Ceres, Pallas and Vesta on the orbital parameters of the Earth Moon Barycenter (EMB) and Mars , as well as on the longitude and distance of Mars with respect to the EMB , which are important in term of space navigation. A least-square analysis has been carried out to model in details the effects of the asteroids, thus allowing a precise determination of the largest sinusoidal terms, at the level of the kilometer.

1. INTRODUCTION

The construction of modern ephemeris as the recent INPOP (Fienga et al.,2008), EPM2006 (Pitjeva,2007) and DE414 (Konopliv et al.,2006) requires to take into account the gravitational effects of a large number of asteroids. Considering up-to-date space navigation, a lot of asteroids (about three hundreds) have enough mass to perturb significantly terrestrial planets such as Mars and the Earth. Nevertheless, because of the large uncertainty on the determination of the asteroids' mass, it is difficult, or impossible, to evaluate the effect with enough accuracy. An important step to evaluate the accuracy limits in the ephemerides of the four inner planets was made by Standish and Fienga(2002) carrying out a Monte Carlo analysis and adjusting the ephemerides to fit the observational data with a suitable set of asteroid masses. In addition, to clearly understand the influence of a given asteroid in the orbital motion of a terrestrial planet, an interesting way consists in determining the differences of motion when considering or not this asteroid in the computations. In a recent study (Souchay et al., A & A in prep.) we restricted our attention on the three largest asteroids Ceres, Pallas and Vesta.

2. COMPUTATIONS AND RESULTS

Our work is similar but to previous calculations done by Williams (1984), but with an extended analysis of the effects of asteroids . At first we integrate a classical N-bodies problem for the solar system, by taking 9 bodies into account (the Sun and the eight planets). Then we carry out the same integration, but by the sole addition of the perturbing asteroid (Ceres, Pallas or Vesta). Subtracting the two signals gives a direct determination of the effect of the single asteroid considered on the EMB or Mars.

We have carefully investigated the effects of each of the 3 asteroids on the 6 orbital parameters (a,e,i, Ω,$\tilde{\omega}$, L) of the 2 bodies (EMB and Mars), which are consequently represented by 36 curves at total. The effects on the EMB are naturally much smaller than for Mars, for two reasons : the comparatively small mass of the planet and its proximity to the asteroids. In addition we have also investigated the influences of Ceres, Pallas and Vesta on the distance and the longitude of Mars which are important in astrometry and space navigation. As an example, we show in **Fig.1** the variations of Mars distance with respect to the EMB due to each of the three asteroids. It is possible to model the total curve (obtained by summing the effects) as a sum of Fourier and Poisson components in the form : $\Delta d_{EMB-Mars} = \sum_i A_i \sin \omega t + B_i \cos \omega_i t + C_i \times t \sin \omega t + D_i \times t \cos \omega_i t$, where the frequencies ω_i are obtained through a Fast Fourier Transform (FFT), and the amplitudes A_i etc... are obtained by least mean squares analysis. The 7 leading components are shown in Table 1. The signal is dominated by

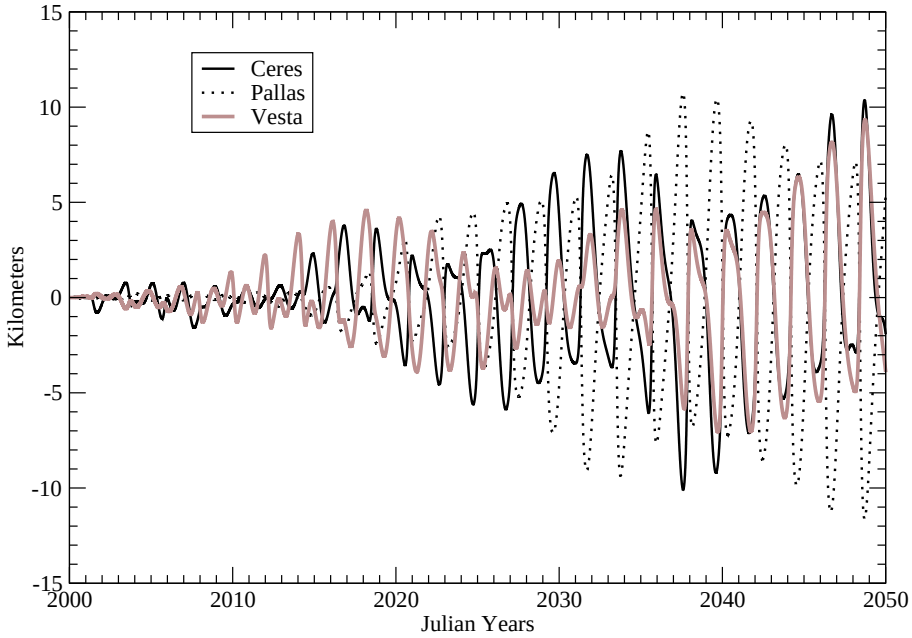

Figure 1: Variations of Mars distance from the Earth Moon Barycenter (EMB) due to Ceres, Pallas and Vesta

Poisson terms reaching 18 km peak to peak in a 100 years time span. This can be explained by the fact that the linear trend of Δe, Δi etc... are gradually affecting the amplitudes of the components of Mars orbital motion.

Table 1: Leading sinusoidal components (Fourier and Poisson terms) in the distance between the Earth-Moon barycenter and Mars, due to the influence of the combined effects Ceres, Pallas and Vesta

Period (day)	A_j $\sin \omega t$ (m)	B_j $\cos \omega t$ (m)	Amplitude total (m)	C_j $t \times \sin \omega t$ (m)	D_j $t \times \cos \omega t$ (m)	Amplitude total (m)
1170.0	56.05	-115.07	127.99	-715.23	1095.97	1308.70
891.0	-217.55	-302.32	372.45	2263.06	709.70	2371.73
777.8	250.44	735.28	776.76	-2374.90	-17534.05	17746.06
687.0	. 78.82	-473.69	480.21	-4781.23	857.05	4857.44
389.5	417.46	-304.41	516.66	-27.93	5781.76	5781.83
356.0	25.37	737.52	737.95	3081.31	-6485.06	7179.86
315.0	-127.92	153.02	199.44	1211.37	-1665.16	2059.17

3. REFERENCES

Fienga, A., Manche, H., Laskar,J., Gastineau,M., 2008, A & A 477, 315

Konopliv, A.S., Yoder, C.F., Standish,E.M., Yuan,D.N., Sveshnikova,E.S., 2006, Icarus 182,23

Pitjeva E.V., 2007, in: Proc. Journées Systèmes de Référence Spatio-temporels 2007, N. Capitaine (ed.), pp. 65–68.

Standish,E.M., Fienga,A., 2002, A & A 384,322

Williams, J.G, 1984, Icarus 57,1

ASTROMETRY WITH GROUND BASED OPTICAL TELESCOPES

F. TARIS[1], S. BOUQUILLON[1], J. SOUCHAY[1], A. H. ANDREI[2,3], F. COLAS[4], D. GINGRAS[5]
[1] SYRTE, Observatoire de Paris, CNRS, UPMC
61 Av. de l'Observatoire, Paris, France
[2] Observatório Nacional/MCT, R. Gal. José Cristino 77, Rio de Janeiro, Brasil
[3] Observatório do Valongo/UFRJ, Lad. Pedro Antônio 43, Rio de Janeiro, Brasil
[4] IMCCE/Observatoire de Paris, France
[5] Université de Sherbrooke, Canada
2500, Boulevard de l'Université, Sherbrooke (Québec), Canada

ABSTRACT. Astrometry with ground based optical telescopes is a newly developed theme in the Paris Observatory SYRTE Department. It recovers some activities like: - the observation of the WMAP probe with optical telescopes for the future astrometric monitoring of GAIA, - the realization of an ecliptic catalog of quasars (using the CFHT images), - the link between radio and optical positions of quasars. In the case of WMAP we will detail more particularly the observations made with the ESO 2.2 m telescope and with the 105 cm telescope of the Pic du Midi. Our goal is to be able to obtain the position of GAIA on its orbit with an uncertainty of 150 m in position and 2.5 mm/s in velocity. We will give the first results for the astrometric reduction of the images of WMAP obtained with these two telescopes.

1. INTRODUCTION

In the domain of astrometry, SYRTE is involved in the realization of the International Celestial Reference Frame (ICRF) which is necessary to know with optimal precision the location of all the bodies in the Universe. One of the tasks consists in establishing the coordinates of quasars as accurately as possible. These quasars are assumed to provide fixed (quasi-inertial) directions in space, which make it possible to determine the coordinates of moving objects: stars in galactic rotation, planets and asteroids rotating around the Sun etc... Because of the increasing number of sources in the catalogues of quasars, it is necessary to make their intercomparison as well as the analysis of the extremely accurate observation data obtained by very long baseline interferometry (VLBI) in the radio domain, or by CCD images in the focal plan of large telescopes at optical wavelengths. Another research theme is the link between the International Celestial Reference System and the dynamical system represented by the trajectories of the mobile bodies in the solar system. At SYRTE, the analysis of lunar laser ranging data, of pulsar chronometry, and the use of optical observations lead to the determination of this link.

2. PREPARING THE GAIA MISSION

The requirements, due to astrometric reasons, about the position and velocity of the spacecraft on its orbit are very stringent. It has been shown (Perryman 2005, Mignard 2005) that the uncertainty must be, at most, 150 m (20 mas) and 2.5 mm/s (1 mas/h) respectively. To achieve that high level of requirements the Ground Based Optical Tracking (GBOT) must be used together with the classic Doppler and ranging techniques (these two last techniques can only deliver 6 km and 8 mm/s). GAIA's location roundabout the L2 Lagrange point is approximately 1.5 million km from the Earth, facing roughly opposite of the Sun. Its visual magnitude would be approximately 18 (this value can be off by a huge amounts, +/-1mag). In order to prepare the GBOT of GAIA, the Wilkinson Microwave Anisotropy Probe (WMAP) has been chosen. That probe is also located around the L2 Lagrange point and its magnitude (roughly 19) is very near from the expected magnitude of GAIA. WMAP is then a reasonable model for the brightness and observability of GAIA. The precise astrometric position of WMAP has been provided by Dale Fink, Navigator of WMAP Spacecraft Control Team at NASA.

3. ESO 2.2M + WFI

Sebastien Bouquillon (SYRTE-OP), Ricky Smart (INAF/OATo, Torino) and Alexandre Andrei (Observatorio Nacional, Rio de Janeiro) have used the 2.2 m telescope of the European Southern Observatory at La Silla, Chile, to take several images of NASA's WMAP satellite in its orbit. Sextractor (Terapix) or Daofind (IRAF) have been used to obtain the (x, y) positions of the sources on the CCD. The standard deviation of the difference between the computed and the observed positions of stars gives the best available information about the standard deviation of WMAP. Results obtained with three independent softwares are given here:

	Home made	TERAPIX	IRAF
Right asc. (α)	70.1 mas	70.5 mas	69.7 mas
Dec. (δ)	80.8 mas	77.0 mas	72.2 mas

Table 1: Results on astrometric reduction obtained with three independant softwares

4. T105 PIC DU MIDI (FRANCE)

The astrometric reduction has been done with the same three independent softwares that for the ESO CCD. A plate solution was determined with a second order polynomial in x and y leading to the following residuals:

Time of observ.	$\sigma(\alpha)$	$\sigma(\delta)$
23h05m33s	64 mas	48 mas
23h09m00s	65 mas	61 mas
23h12m25s	65 mas	57 mas

Table 2: Results on astrometric reduction obtained at the Pic du Midi

The results obtain were compared with the theoretical ephemeride. Moreover the brightness of WMAP has been calibrated with respect to the UCAC2 reference stars (UCAC2 stars are not photometric standards). The results are as follows:

Time of observ.	diff(α)	diff(δ)	mag($\pm -1\sigma$)
23h05m33s	21.104"	3.234"	18.620(+/-0.249)
23h09m00s	21.297"	3.141"	18.661(+/-0.257)
23h12m25s	21.530"	3.231"	18.757(+/-0.251)

Table 3: Comparison between observed/theoretical coordinates and magnitude determination

The difference between the observed position and the ephemeride is relatively large but quite constant. This can be due to the ephemeride itself (constant offset), to the inaccuracy of the position of the telescope (10 m), to the time synchronisation of the Pic du Midi (0.1 s) or to other effects...

The fluctuation of the magnitude can be explained by the ambient conditions (clouds, bad seeing and Moon's age). The rapid changes in object brightness due to varying illumination of spacecraft must also be taken into account.

5. CONCLUSION

In the frame of the GBOT-GAIA, first observations of WMAP have been done with the 2.2 m ESO and 1.05 m Pic du Midi telescopes. Preliminary results show that it is possible to obtain the position of WMAP with the uncertainty of the UCAC2 stars. Hence when the GAIA early-catalogue will be accessible to the GBOT community the uncertainty about the GAIA position could be better than 20 mas. It will permit to reach the very stringent requirements of the GAIA mission.

6. REFERENCES

Mignard, F., 2005, Ephemeris requirements for GAIA, GAIA-FM-023

Perryman, M., 2005, Specifications for absolute time and orbital ephemeris for ESOC, GAIA-CA-TN-ESA-MP-012-2

THE KINEMATICAL ANALYSIS OF PROPER MOTIONS AND RADIAL VELOCITIES OF STARS BY MEANS OF THE VECTOR SPHERICAL HARMONICS

A.S. TSVETKOV, V.V. VITYAZEV, I.I. KUMKOVA
St. Petersburg State University
University pr., Peterodvorets, St. Petersburg, 198504, Russia
e-mail: a.s.tsvetkov@inbox.ru; vityazev@list.ru

ABSTRACT. The paper describes the application of the 3-D vector spherical harmonics (henceforth VSH) to the investigation of stellar kinematics. The VSH technique is suitable for present and future catalogues which contain all three components of velocity vector: proper motions and radial velocities. In general, the VSH allows to detect all the systematic components in the stellar velocity field and does not depend on any model. If some physical model is used, the VSH not only determines the parameters of the model, but detects the systematic components which are beyond the model. The application of the VSH to the Hipparcos data complimented with radial velocities discovers the systematic components which are beyond the linear Ogorodnikov-milne model.

1. OUTLINE OF THE METHOD

It is widely known that in the linear approximation the stellar velocity field may be described with the Ogorodnikov-milne model

$$\vec{V} = \vec{V}_0 + M^+ \vec{r} + M^- \vec{r}, \tag{1}$$

where $\vec{V}_0$ — taken with opposite sign velocity of the Sun with respect to given centroid of stars. This velocity is defined by components U, V, W in the directions of the principal galactic axes x, y, z; M^+ — the diverging matrix with the dilation coefficients M^+_{11}, M^+_{22}, M^+_{33}, and M^+_{12}, M^+_{13} M^+_{23} standing for shears in the galactic planes (x, y), (x, z), (y, z), M^- — the rotation matrix with the components ω_1, ω_2 ω_3 of the angular rotation vector in the proper motions about axes x, y, z;

Let $\mathbf{e}_l, \mathbf{e}_b, \mathbf{e}_r$ be the unit vectors in longitude, latitude and radial velocity directions. Using notation $K_{nkp}(l, b)$ for spherical harmonics, introduce Vectorial Spherical Functions as follows:

$$\mathbf{V}_{nkp}(l, b) = K_{nkp}(l, b)\mathbf{e}_r. \tag{2}$$

$$\mathbf{T}_{nkp} = \frac{1}{\sqrt{n(n+1)}} \left(\frac{\partial K_{nkp}(l,b)}{\partial b}\mathbf{e}_l - \frac{1}{\cos b}\frac{\partial K_{nkp'}(l,b)}{\partial l}\mathbf{e}_b \right), \tag{3}$$

$$\mathbf{S}_{nkp} = \frac{1}{\sqrt{n(n+1)}} \left(\frac{1}{\cos b}\frac{\partial K_{nkp}(l,b)}{\partial l}\mathbf{e}_l + \frac{\partial K_{nkp}(l,b)}{\partial b}\mathbf{e}_b \right). \tag{4}$$

We have shown that with $M^*_{11} = M^+_{11} - M^+_{22}$; $x = M^+_{33} - \frac{1}{2}(M^+_{11} + M^+_{22})$; $y = \frac{1}{3}(M^+_{11} + M^+_{22} + M^+_{33})$; r standing for distance in $[ps]$ and proper motions expressed in $[km\ s^{-1}\ kps^{-1}]$ the equations of condition may be written in terms of VSF as follows:

$$\mu_l \cos b\, \mathbf{e}_l + \mu_b\, \mathbf{e}_b = -U/r\, \frac{\mathbf{S}_{111}(l,b)}{\rho_{11}} - V/r\, \frac{\mathbf{S}_{110}(l,b)}{\rho_{11}} - W/r\, \frac{\mathbf{S}_{101}(l,b)}{\rho_{10}} +$$
$$+\omega_1\, \frac{\mathbf{T}_{111}(l,b)}{\rho_{11}} + \omega_2\, \frac{\mathbf{T}_{110}(l,b)}{\rho_{11}} + \omega_3\, \frac{\mathbf{T}_{101}(l,b)}{\rho_{10}} +$$
$$+\frac{M_{13}^+}{3}\, \frac{\mathbf{S}_{211}(l,b)}{\rho_{21}} + \frac{M_{23}^+}{3}\, \frac{\mathbf{S}_{210}(l,b)}{\rho_{21}} + \frac{M_{12}^+}{6}\, \frac{\mathbf{S}_{220}(l,b)}{\rho_{22}} +$$
$$+\frac{M_{11}^*}{12}\, \frac{\mathbf{S}_{221}(l,b)}{\rho_{22}} + \frac{x}{3}\, \frac{\mathbf{S}_{201}(l,b)}{\rho_{20}}, \tag{5}$$

$$V_r/r = -U/r\, \frac{K_{111}(l,b)}{R_{11}} - V/r\, \frac{K_{110}(l,b)}{R_{11}} - W/r\, \frac{K_{101}(l,b)}{R_{10}} +$$
$$+M_{13}^+\, \frac{2K_{211}(l,b)}{3R_{21}} + M_{23}^+\, \frac{2K_{210}(l,b)}{3R_{21}} + M_{12}^+\, \frac{K_{220}(l,b)}{3R_{22}} + \tag{6}$$
$$+M_{11}^*\, \frac{K_{221}(l,b)}{6R_{22}} + x\, \frac{2K_{201}(l,b)}{3R_{20}} + y\, \frac{K_{001}(l,b)}{R_{00}},$$

where

$$R_{nk} = \sqrt{\frac{2n+1}{4\pi}} \begin{cases} \sqrt{\frac{2(n-k)!}{(n+k)!}}, k > 0; \\ 1, \quad k = 0, \end{cases} \tag{7}$$

$$\rho_{nk} = \frac{R_{nk}}{\sqrt{n(n+1)}}\ . \tag{8}$$

This apparently new result gives possibility to use decomposition of the velocity field on VSF for two goals: determination of the Ogorodnikov-Milne parameters and searching the systematics beyond the model.

Application of this method to the proper motions and parallaxes from HIPPARCOS catalogue complimented with known radial velocity gave evidence that beside the classical components the real velocity field does contain extramodel systematic components partial explanation of which may be given in frames of generalized kinematical model of the second order. The further details of the FSF method will be published elsewhere.

Acknowledgements. The authors appreciate the support of this work by the grant 1323.2008.2 of the President of Russian Federation and by the grant 2.1.1.5077 of the Ministry of Education and Sciences.

2. REFERENCES

Mignard F., Morando B., 1990, "Analyse de catalogues stellaires au moyen des harmoniques vectorielles, Journés 1990 "Systèmes de référence spatio-temporels", Paris, pp. 151-158.

du Mont B., 1997, "A three-dimensional analysis of the kinematics of 512 FK4 Sup. stars. A&A, 61, N 1. pp. 127-132.

Vityazev V., Shuksto A. Ed. G.Byrd et al., 2004, ASP, v.316, pp.230-233.

COMPARISON OF THE TIME SERIES OF COORDINATES OF THE ICRF SOURCES

V.E. ZHAROV, E.A. RASTORGUEVA
Sternberg State Astronomical Institute
Universitetsky pr. 13, Moscow 119992
zharov@sai.msu.ru

ABSTRACT. The time series of $\Delta\alpha\cos\delta$ and $\Delta\delta$ obtained by various IVS centers were analyzed. These series for each source were fitted by the best polynomial regression model to estimate the motions of the sources. It was shown that variations of coordinates of the sources can be both linear and curvilinear, and motions have to be taken into account during generation of new ICRF catalog.

1. MODEL OF MOTION

Model of motion was represented as polynomial with respect to time.

It is necessary to find the best multiple linear regression model:

$$y_i = \beta_0 + \beta_1 x_i + \beta_2 x_i^2 + \beta_3 x_i^3 + \varepsilon_i,$$

where x_i is the time of i's observation, y_i is the correction $\Delta\alpha\cos\delta$ or $\Delta\delta$ to the adopted coordinates, β_j are the regression coefficients, and the ε_i's are independently distributed normal errors, each with mean zero and variance σ^2.

The "best" model (or degree of polynomial) is defined by the criteria:

$$R^2 = 1 - \frac{\sum w_i(y_i - \widetilde{y})^2}{\sum w_i(y_i - \overline{y})^2},$$

where w_i is the weight of y_i and $\overline{y}$ is the weighted mean. The best fitting function $\widetilde{y}$ has to maximize the value of the multiple-correlation coefficient R^2.

The highest degree of polynomial was chosen as "three" to guarantee predictability of motion: we can expect that extragalactic radio sources have small motions.

2. ANALYSIS OF MOTION

Nine time series obtained by the IVS centers: AUS, BKG, DGF, GSFC, IAA, MAO, OPA, SAI, USNO were used to analyze the sources' motions.

On Fig. 1 histograms $\beta_i/\sigma(\beta_i)$ for i=1,2,3 are shown ($\sigma(\beta_i)$ are uncertainties of the regression coefficients). If use criteria $\beta_i/\sigma(\beta_i) > 2$, then approximately 40% of observed sources show significant motion.

New classification of sources can be proposed based on this conclusion: the best fitting function $\widetilde{y}$ is used to predict position of source, for example, at 2025. Prediction intervals D_α for α and D_δ for δ depend on trend and noise of corresponding time series. The criteria $D = \sqrt{D_\alpha^2 + D_\delta^2} < n$ can be used for selection of "stable" sources. In our analysis we used $n = 2.5$ mas.

According this criteria only 32 sources: 0014+813, 0059+581, 0133+476, 0202+149, 0212+735, 0234+285, 0528+134, 0552+398, 0556+238, 0602+673, 0727-115, 0749+540, 0804+499, 0851+202, 0923+392, 0955+476, 1044+719, 1101+384, 1300+580, 1308+326, 1357+769, 1418+546, 1611+343, 1638+398, 1726+455, 1739+522, 1741-038, 1803+784, 2037+511, 2145+067, 2200+420, 2356+385 show predictable motion with small noise. One can note that these sources are observed very frequently: from 350 (0602+673) to 3500 times (0552+398).

According the polynomial models one can divide apparent motions in several types: linear, uniform motion; linear, non-uniform motion; motion on conic section with constant velocity module; curvilinear motion with variable velocity. Motion of part of sources ($\sim 70\%$) can be explained by simple physical

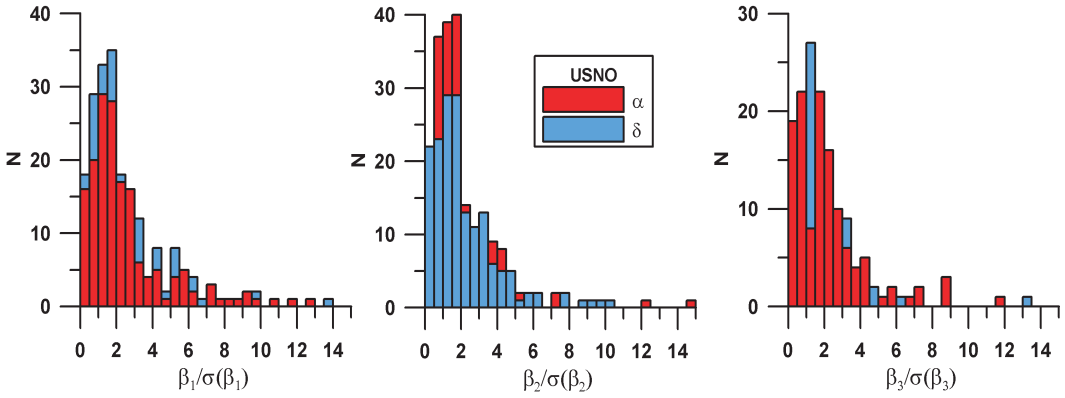

Figure 1: Statistics of motion (USNO)

models of motion and evolution of quasar (Zharov et al., this issue). Polynomial models of motion of rest sources are too complicated to be explained now. Their non-predictable motions lead to noise in orientation of ICRF.

In our model corrections $\Delta\alpha$ or $\Delta\delta$ to adopted coordinates depend on time. So, catalog of sources must contain both their coordinates and motions, sometimes including quadratic term. Because coordinates depend on time orientation of new catalog relative the ICRF depends on time too. Three rotation angles $\theta_1, \theta_2, \theta_3$ around the axes of the equatorial coordinate system are shown on Fig. 2. Sources observed more than 100 times were selected at first (black line). Then the defining sources were used for estimation of $\theta_1, \theta_2, \theta_3$ (red line). As seen from Fig. 2 in order to improve stability of the ICRF, the no-net-rotation condition has to be applied to well observed sources without dividing them in different categories. Among defining sources there are many sources observed only 15-50 times; it is not enough to determine reliable parameters of motion.

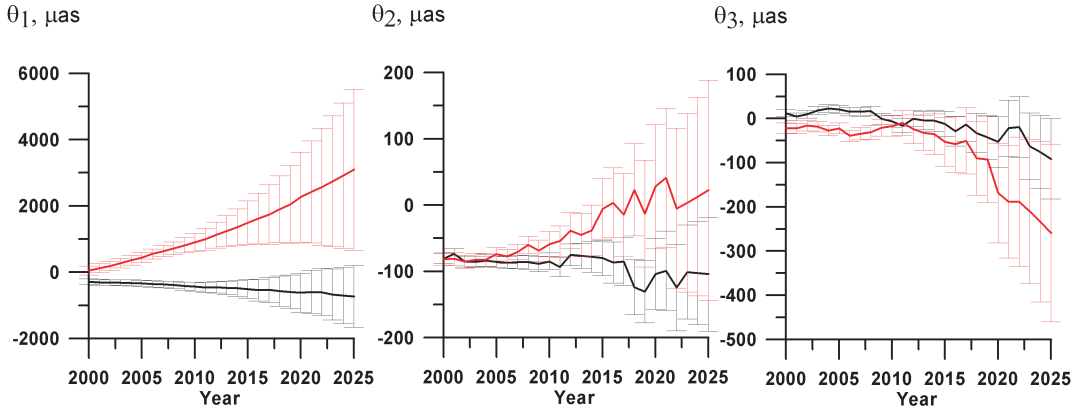

Figure 2: The rotation angles based on the USNO time series

Acknowledgements. Research supported in part under RFBR grants 08-02-00971 and 07-01-00126.

3. REFERENCES

Zharov, V.E., Sazhin, M.V., Sementsov, V.N., Kuimov, K.V., Sazhina, O.S., Rastorgueva, E.A., this issue.

RECONSIDERING THE DEFINITION OF GALACTIC COORDINATE SYSTEM AND GALACTIC CONSTANTS

Z. ZHU, J. LIU
Department of Astronomy, Nanjing university
22 Hankou st., Nanjing, China
e-mail: zhuzi@nju.edu.cn; e-mail:ljconline@163.com

ABSTRACT. The galactic coordinates were originally defined by the IAU in 1958 and thereafter transformed from the B1950.0 system to the J2000.0 system after the new astronomical constants and celestial reference system have been introduced by the IAU as of 1984. In 1994, the IAU GA in the Hague recommended that the celestial reference system FK5 be replaced by the ICRS. Therefore, the present Galactic coordinates may be problematic due to their original definition and transformation, which have led to some confusion in their application and misunderstanding of the concept of the corresponding reference system. On the other hand, the Galactic constants as recommended by the IAU in 1985 have usually been adopted. Various observations in the last decades show that these constants should be updated, including the Galactic distance scale and Galactic rotation. These fundamental constants play a crucial role for the observation and theory of the Galaxy. In this work, we carefully investigate the questions of the Galactic coordinates, and suggest that the relevant IAU commissions set up a new working group in order to reconsider the redefinition of the IAU Galactic constants and coordinates.

1. CONFUSED SITUATION ON THE GALACTIC COORDINATE SYSTEM AND CONSTANTS

At the 16th General Assembly of the International Astronomical Union, held in Grenoble in 1976, the IAU recommended several changes in the fundamental reference frame (FK4) which were brought into effect from January 1 1984. Afterwards, the standard coordinate frame was changed from the equinox and equator of B1950.0 to that of J2000.0 and synchronously the unit of time for precession and star proper motions was changed from tropic centuries to Julian centuries. From 1991, IAU agreed to adopt a fundamental reference system based on distant extragalactic sources in order to replace the nearby bright stars (IAU 1991, IAU 1998, IAU 2001). The 23th IAU General Assembly (IAU 1997) adopts that, from 1 January 1998, the IAU celestial reference frame shall be the International Celestial Reference System (ICRS) as defined by the International Earth Rotation Service (IERS).

However, in the past decades, the definition of the Galactic coordinate system has never been changed but has been transfered from one system to another (e.g. from FK4 to FK5, or from B1950.0 to J2000.0, or to ICRS). Various comparisons provide evidence that there exit some misunderstandings during these transformations, which can lead to some confusion. Various works are still on the B1950.0 System: the KPNO international spectroscopic survey for extragalactic emission-line objects (Jangren, 2005); the westerbork northern sky survey for giant radio galaxies (Schoenmakers, 2001); the catalogue of galactic supernova remnants (Green, 1998), etc.

For the general practice of research on the Galaxy, a transformation from the equatorial reference system to the Galactic reference system is necessary. This transformation is given by:

$$[\mathbf{x}_G \quad \mathbf{y}_G \quad \mathbf{z}_G] = [\mathbf{x} \quad \mathbf{y} \quad \mathbf{z}]\,\mathbf{G}\,, \tag{1}$$

where the matrix $\mathbf{G}$ is related to the definition of North Galactic pole (NGP) and Galactic center (GC) in the equatorial reference system. For the matrix $\mathbf{G}$ applied to the B1950.0 FK4-based reference system and the J2000.0 FK5 reference system, Murray (1983 and 1989) gives:

$$\mathbf{G}_{B1950.0} = \mathbf{N}_{B1950.0} \begin{bmatrix} -0.066988739 & +0.492728466 & -0.857600811 \\ -0.872755766 & -0.450346958 & -0.188374602 \\ -0.483538915 & +0.744584633 & +0.460199785 \end{bmatrix}\,, \tag{2}$$

and:

$$\mathbf{G}_{J2000.0} = \mathbf{N}_{J2000.0} \begin{bmatrix} -0.054875539 + 0.494109454 - 0.867666136 \\ -0.873437105 - 0.444829594 - 0.198076390 \\ -0.483834992 + 0.746982249 + 0.455983795 \end{bmatrix} . \quad (3)$$

in which $\mathbf{N}$ is the equatorial triad at the epoch. According to Murray's work, the B1950.0 Galactic coordinates is considered to be absolute and should be unaffected by aberration. The procedure is problematic at the current precision level because of the existence of the E-term that cannot be eliminated during the transformation from the FK4 system to the FK5 system:

$$\mathbf{S}_{FK5} = \mathbf{S}_{FK4} - \frac{1}{c}\mathbf{S}_{FK4} \times (\mathbf{S}_{FK4} \times \mathbf{V}_E) \ . \quad (4)$$

The vector $\mathbf{S}_{FK4}$ and $\mathbf{S}_{FK5}$ are the arbitrary direction in the reference system denoted by the subscript FK4 and FK5, respectively, and $\mathbf{V}_E$ is the E-term in the aberration. The Galactic axes will no longer be mutually orthogonal, with an error of 0.33 arcsecond, which means a distortion of the Galactic plane if a direct transformation is applied. On the other hand, in ICRS, the Hipparcos and VLBA observations of Sgr A* give incoherent value for the transition matrix $\mathbf{G}$.

Based on different Galactic reference systems and methods, Galactic constants have been investigated by many authors. In 1964 and 1985, the IAU recommended two sets of constants. In order to understand the possible confusion on these constants, we take the galactocentric distance of our solar system as an example. Another example about the confused situation on Galactic constants is the mass of the Galaxy.

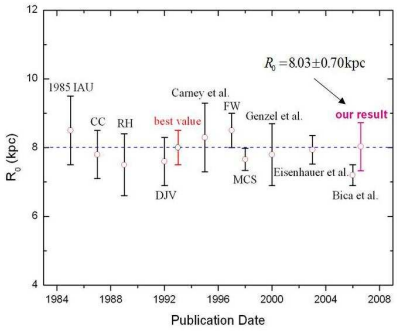

Figure 1: Individual measurements of R_0 in the last decades. Typical values of R_0: 10 kpc (IAU 1964), (8.5 ± 1) kpc (IAU 1985), (8.0 ± 0.5) kpc (Reid 1993), and our result derived from open cluster (8.03 ± 0.70) kpc.

Based on the assumption of both axisymmetry and equilibrium dynamics, the Galactic mass is expressed as (Rohlfs and Kreitschmann, 1998):

$$M(R) = 2.5 \times 10^5 R V_0^2(R) M_\odot \quad (5)$$

Adopting for the circular speed of the Sun, $V_0 = 220\,\mathrm{kms}^{-1}$ (Kerr or Lyden-Bell, 1986), or $V_0 = 270\,\mathrm{kms}^{-1}$ (Mendez 2000), implies for the mass interior to the solar circle, an increase by as much as 50% for the latter V_0 value as compared to the former.

Since various high precision observations have given more reliable and consistent Galactic constants in the last decades, a new recommendation of Galactic constants would be needed in order to avoid confusion in modeling Galactic physics.

2. RECONSIDERING THE IAU DEFINITION

As mentioned in the previous section, the present work, which is based on the Galactic coordinate system, suffers from some confusion in the definition of the reference system and constants. It is necessary to redefine the Galactic reference system and constants for uniform practical applications and exact concept of the coordinate system. For high precise observation at micro-arc-second level, the Galactic coordinate system should be directly connected to the ICRS.

THE CELESTIAL FRAME AT FOUR RADIO FREQUENCIES

C. S. JACOBS
Jet Propulsion Laboratory, California Institute of Technology/NASA
4800 Oak Grove Dr., Pasadena CA 91109
e-mail: Chris.Jacobs@jpl.nasa.gov

ABSTRACT: The International Celestial Reference Frame (ICRF) adopted by the IAU in 1997 was based on VLBI measurements at S/X-band radio frequencies of 2.3/8.4 GHz and complemented by HIPPARCOS measurements at optical frequencies. At that time, the IAU encouraged the astrometric community to extend the ICRF to other frequencies. In response, VLBI measurements have been made at 24, 32, and 43 GHz. We discuss the programmatic and scientific motivations for extending the ICRF to these higher frequencies. This paper reviews results to date including evidence that these new high frequency frames are rapidly approaching the accuracy of the S/X-band ICRF. Prospects for future improvements of high frequency radio reference frames are also discussed.

1. INTRODUCTION

For about three decades now, radio frequency work in global astrometry, geodesy, and deep space navigation has been done at S/X-band (2.3/8.4 GHz) and has been tremendously successful in producing 100 μas level global astrometry (e.g. Ma et al, 1998; Fey et al, 2004; Petrov, 2008) and sub-cm geodesy. In response to the IAU's call to extend the ICRF to new frequencies (IAU, 1997), development work over the last decade has enabled astrometric observing at 24, 32, and 43 GHz. This paper is a review of global astrometric frames at 24, 32, and 43 GHz with comparison to the traditional 2.3/ 8.4 GHz frames.

Why these new frequencies? Increasing observing frequencies by factor of 3 to 5 has several advantages. For tracking of spacecraft in deep space, the driver is the potential for higher telemetry data rates to and from probes. Other advantages include 1) the spatial distribution of flux becomes significantly more compact lending hope that the positions will be more stable over time (Charlot et al, 2008), 2) Radio Frequency Interference (RFI) at S-band would be avoided, 3) Ionosphere and solar plasma effects on group delay are reduced by a factor of 9 to 25!

While these are very significant advantages, there are also disadvantages. Observing above 8.4 GHz moves one closer to the water vapor line at 22 GHz and thus increases the system temperature from a few Kelvins per atmospheric thickness up to 10–15 Kelvins per atmosphere or more. Thus one becomes much more sensitive to weather. Furthermore, the sources themselves are in general weaker and many sources are resolved. Also, with the observing wavelengths shortened by a factor of 3 to 5, the coherence times are shortened so that practical integration times are a few minutes or less—even in relatively dry climates. The shorter wavelengths also imply that the antenna pointing accuracy requirements must be tightened by the same factor of 3 to 5. The combined effect of these disadvantages is to lower the system sensitivity. Fortunately, recent advances in recording technology make it feasible and affordable to offset these losses in sensitivity by recording more bits.

This paper is organized as follows: We will describe the observations & modelling, and review the resulting frames. Next, we will estimate the accuracy by comparing the X/Ka frame to a recent S/X frame. This will be complemented by a discussion of the error budget. Finally, we will provide conclusions and anticipated directions for further research.

2. OBSERVATIONS & RESULTS

At the time of this report, celestial reference frames have been produced at four radio frequencies: S/X-band (2.3/ 8.4 GHz), K-band (24 GHz), Q-band (43 GHz), and X/Ka-band (8.4/ 32 GHz). All these frames cover the full 24 hours of right ascension. Only the S/X frames cover the full range of declinations. The original S/X-band ICRF (Ma et al, 1998) was produced in 1995 based on 1.6M observations resulting in 608 source positions (Fig. 1). More recent S/X frames benefit from much larger data sets. For example,

the 2008b-astro frame (Petrov, 2008) uses about 5M observations from a variety of networks around the globe to produce a frame of $\approx$ 3500 sources of which $\approx$ 2400 have position uncertainties of less than 1 mas (Fig 2). At K-band 82K observations (Lanyi et al, 2008) are used to produce a frame of 275 sources covering down to about -40° declination (Fig. 3). At Q-band 19K observations (Lanyi et al, 2008) produce a frame of 132 sources covering down to roughly -30°. (Fig 4). At X/Ka-band 7K observations (Jacobs & Sovers, 2008) produce a frame of 321 sources covering down to -45° (Fig. 5). As can be seen from Figs. 1–5, all current radio frames are significantly weaker in the southern hemisphere. This is due to the scarcity of southern stations. In particular, the K and Q-band frames are based on the all-northern VLBA and the X/Ka frame uses only one southern station. Even the S/X frame with its full sky coverage has a very limited number of observations in the far south. In Figs. 1–5, the sources are coded according to their 1-σ formal declination uncertainties with the value ranges indicated in the figure's legend. Note that on average, the declination precision decreases as one moves toward the south for all frames.

While there are some modelling variations amongst the various catalogs, the description of Sovers *et al* (1998) is a fair first approximation. For further details the reader is referred to the papers cited for each frame described above.

3. ACCURACY

Experience shows that formal uncertainties tend to underestimate true errors. External estimates of errors were obtained by comparing X/Ka-band RA and declinations to estimates from analysis of S/X data. For the 273 sources in common, the weighted RMS (wRMS) differences are 235 μas in RA cos(dec) and 285 μas in declination. These differences reveal decreasing accuracy RA and declination as one moves south. For K and Q-band accuracy see Lanyi et al (2008).

In astrometry, it is usually much easier to measure the relative positions of nearby sources than to accurately measure sources that are separated by long arcs. In order to investigate this tendency, we calculated for both X/Ka and S/X the arclengths between all pairs of sources, binned them in 5 deg bins and then differenced the arcs. We then took the mean arclength difference for each bin. As expected, arclengths agree better for short arcs and gradually worsen as arcs grow longer out to a mean difference of 70 μas at arcs of 90 deg. This is one measure of the level of zonal errors in our comparison.

4. ERROR BUDGET

Having assessed the size of errors in X/Ka positions using the much larger S/X data set as a standard of accuracy, we now discuss the major contributions to the errors of the X/Ka measurements: SNR, instrumentation, and troposphere. Figure 6 shows the weighted RMS group delay vs. log10 of the Ka-band SNR. We conclude that for SNR < 30, the thermal error dominates the error budget. For higher SNRs, troposphere and instrumentation errors become important. Binning of wRMS delay vs. airmass thickness shows that troposphere is not the dominant error due to the generally low SNRs just mentioned. However, the phase rates (which carry much less weight in the fit) are dominated by errors from tropospheric mismodelling, thus hinting that troposphere will become more important as our SNR improves (Treuhaft & Lanyi, 1987; Bar-Sever et al 2007). The last major category of errors comes from un-calibrated instrumentation. A proto-type phase calibrator has been developed for calibrating from the feed to the digitizer (Hamell et al, 2003). Test data indicate an approximately diurnal instrumental effect with $\approx$180 psec RMS. Although the data themselves can be used to partially parameterize this effect, we believe that phase calibrators will be needed in order to achieve accuracy of better than 200 μas in a timely manner.

5. CONCLUSIONS

The challenge has been met to extend the S/X-based ICRF to 3 to 5 times higher frequencies with frames now being produced at 24, 32, and 43 GHz. For now, S/X frames still have better global coverage and better formal uncertainties and in all likelihood better true accuracy. However, the frames at 24, 32, and 43 GHz now have accuracies on the order of 1/4 mas. At K-band, incomplete calibration of plasma and tropospheric effects limits accuracy. Compared to K-band, at Q-band plasma errors are 4 times less, but weaker sources and shorter atmospheric coherence times lead to SNR limited accuracy. Like Q-band, X/Ka-band has SNR issues and has worse instrumental errors due to the lack of instrumental

phase calibrations. We expect the instrinsic source structure at frequencies above 8 GHz to become more compact thereby enticing observers with the potential for frames which are more stable and perhaps eventually more accurate than the S/X-based ICRF.

Acknowledgements. The research described in this paper was performed at the Jet Propulsion Laboratory of the California Institute of Technology, under a contract with the National Aeronautics and Space Administration. Copyright © 2009 by California Institute of Technology. Government sponsorship acknowledged. X/Ka data were collected with NASA's Deep Space Network. K and Q-band data were acquired an analyzed by the KQ VLBI Collaboration using data from the NSF's VLBA instrument (see Lanyi et al [2008] for a full list of collaborators). We thank the staff from both the DSN and the VLBA.

6. REFERENCES

Bar-Sever, Y. E., et al, 2007, 'Atmospheric Media Calibration for the Deep Space Network,' Proceedings of the IEEE (Special issue), 95, 11.

Charlot, P., et al, 2008, 'The Celestial Reference Frame at Higher Radio Frequencies II. VLBA Imaging at 24 and 43 GHz,' submitted to AJ .

Fey, A. L., et al, 2004, 'The Second Extension of the ICRF: ICRF-Ext.2', AJ , 127, pp. 3587-3608.

Hamell, R., Tucker, B., & Calhoun, M., 2003 'Phase Calibration Generator,' JPL IPN Prog. Report 42-154, pp. 1-14.

IAU General Assembly XXIII, Resolution B2-d, Kyoto, Japan, August 1997.
iau.org/static/resolutions/IAU1997_French.pdf

Jacobs, C.S., & Sovers, O. J., 2008, 'Extending the ICRF to Higher Radio Frequencies: Global Astrometric Results at 32/8 GHz,' IVS 2008 General Meeting Proc., St. Petersburg, Russia., D. Behrend and K. D. Baver, eds.

Lanyi, G. E. et al, 2008, 'Extraglactic Celestial Reference Frames at 24 and 43 GHz: Global Astrometric Results from the VLBA', submitted to AJ .

Ma, C., et al, 1998, 'The International Celestial Reference Frame as Realized by Very Long Baseline Interferometry', AJ , 116, 1, pp. 516-546.

Petrov, L., 'VLBI global solution 2008b_astro,' *modified to use uninflated errors as provided by D. Gordon of NASA Goddard Space Flight Center.*
http://vlbi.gsfc.nasa.gov/astro/

Sovers, O. J., J. L. Fanselow, C. S. Jacobs, 1998, 'Astrometry and Geodesy with Radio Interferometry: Experiments, Models, Results,' Rev. Mod. Phys., 70, 4.

Treuhaft, R. N. & Lanyi, G.E., 1987, 'The Effect of the Dynamic Wet Troposphere on Radio Interferometric Measurements,' Radio Science, 22, pp. 251-65.

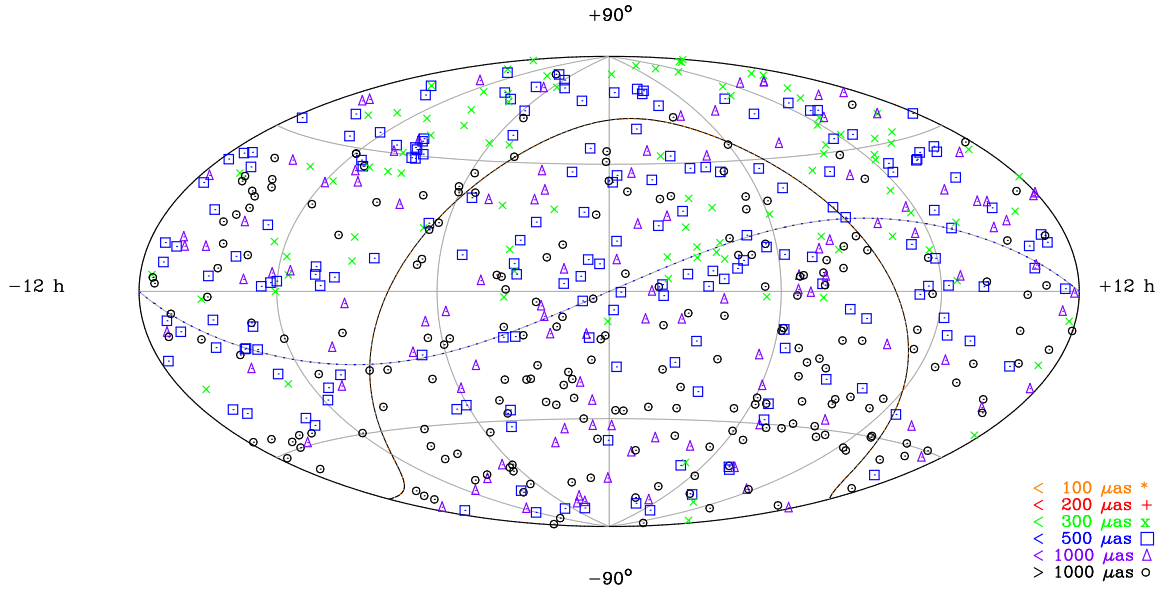

Figure 1: 608 S/X-band sources of the original ICRF based on a 1995 solution (Ma et al, 1998). Symbols indicate 1-σ formal declination uncertainties with size bins defined in the legend at lower right. (α, δ) = $(0, 0)$ is at the center. The ecliptic plane is indicated by a dashed line. The galactic plane is indicated as a black line approximately shaped like an Ω.

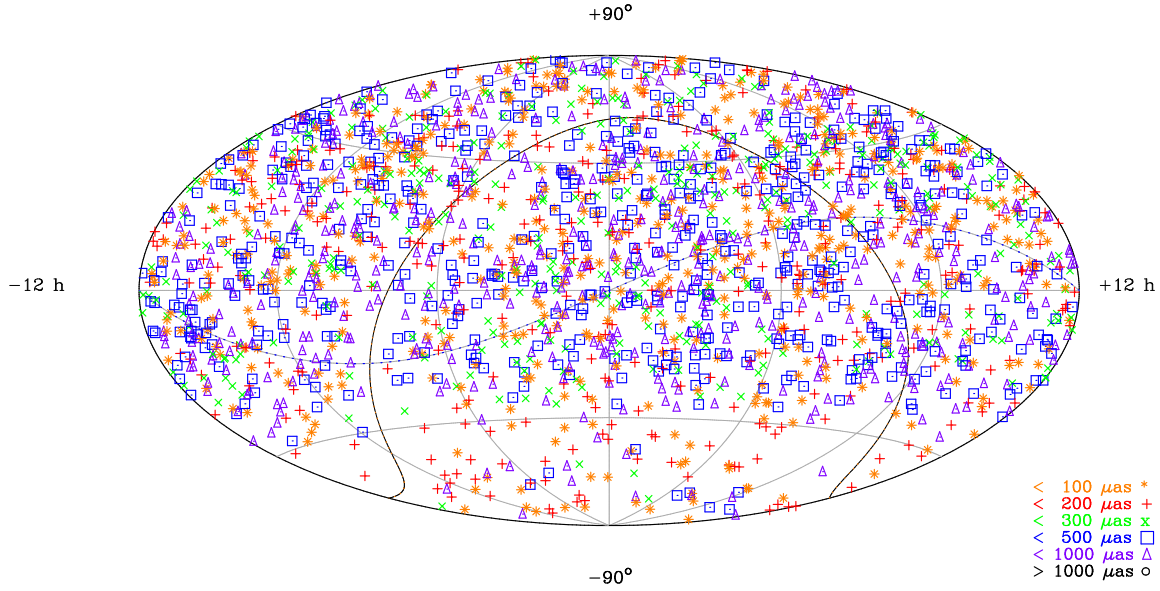

Figure 2: $\approx$ 2400 S/X sources from the 2008b-astro catalog with uncertainties < 1 mas (Petrov, 2008) . Symbols indicate 1-σ formal declination uncertainties with size bins defined in the legend at lower right. (α, δ) = $(0, 0)$ is at the center. The ecliptic plane is indicated by a dashed line. The galactic plane is indicated as a black line approximately shaped like an Ω.

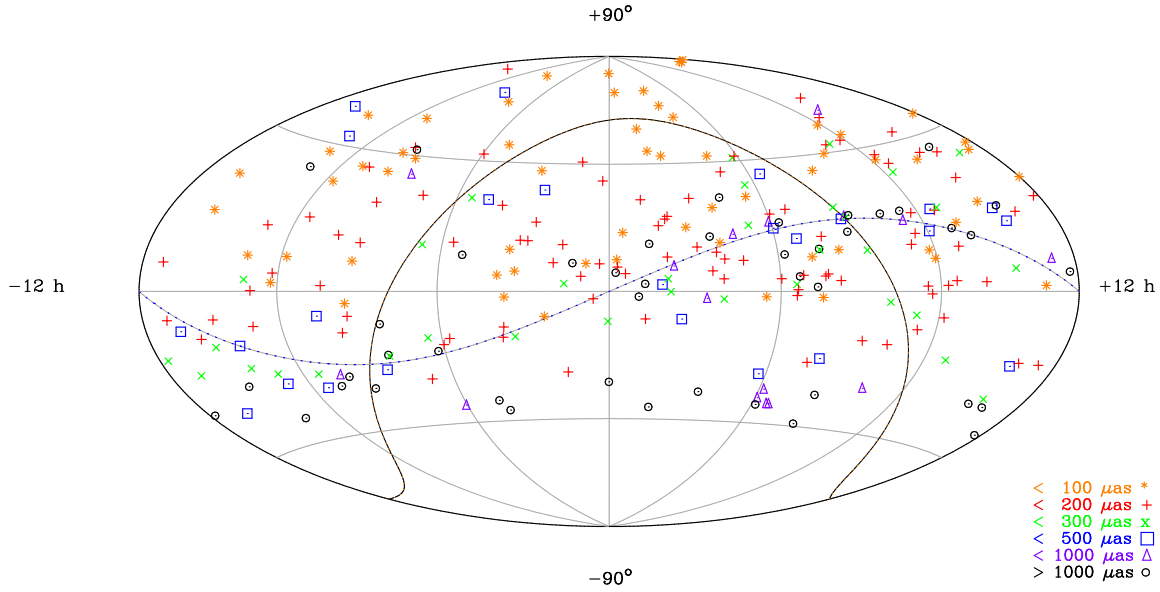

Figure 3: Distribution of 275 K-band sources detected to date (Lanyi et al, 2008). Symbols indicate 1-σ formal declination uncertainties with size bins defined in the legend at lower right. $(\alpha, \delta) = (0, 0)$ is at the center. The ecliptic plane is indicated by a dashed line. The galactic plane is indicated as a black line approximately shaped like an Ω.

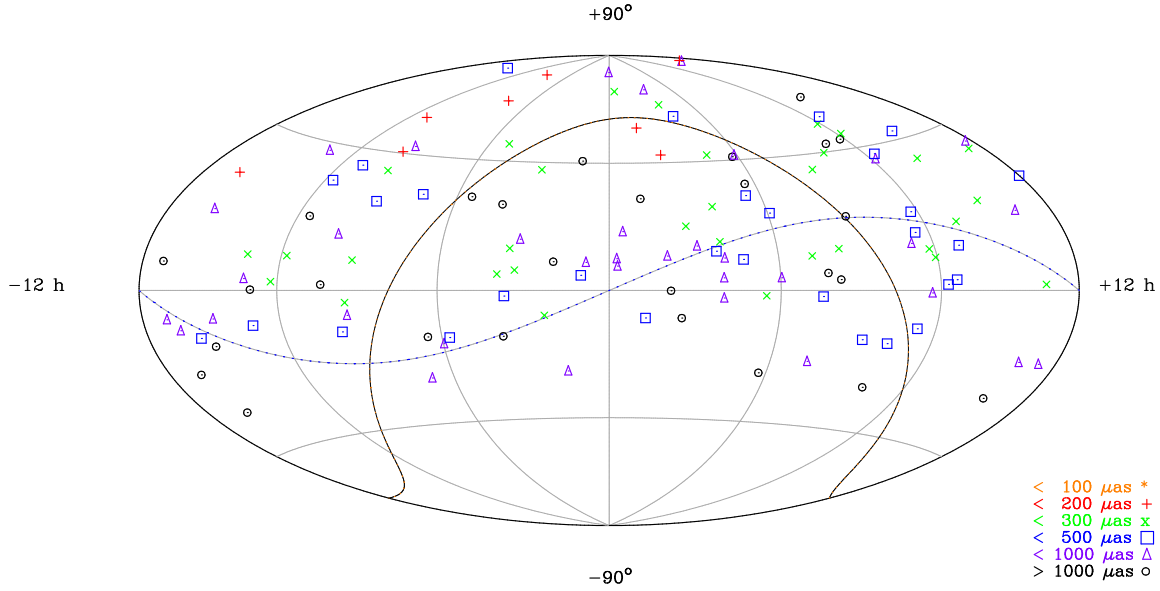

Figure 4: Distribution of 132 Q-band sources detected to date (Lanyi et al, 2008). Symbols indicate 1-σ formal declination uncertainties with size bins defined in the legend at lower right. $(\alpha, \delta) = (0, 0)$ is at the center. The ecliptic plane is indicated by a dashed line. The galactic plane is indicated as a black line approximately shaped like an Ω.

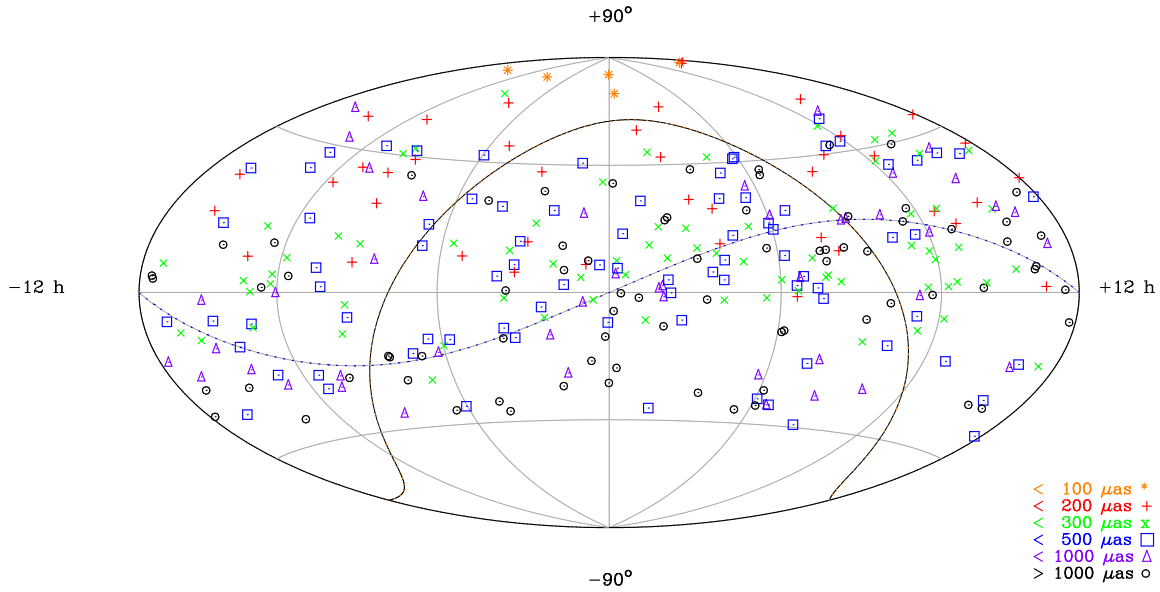

Figure 5: Distribution of 321 X/Ka-band sources detected to date (Jacobs & Sovers, 2008). Symbols indicate 1-σ formal declination uncertainties with size bins defined in the legend at lower right. (α, δ) = $(0, 0)$ is at the center. The ecliptic plane is indicated by a dashed line. The galactic plane is indicated as a black line approximately shaped like an Ω.

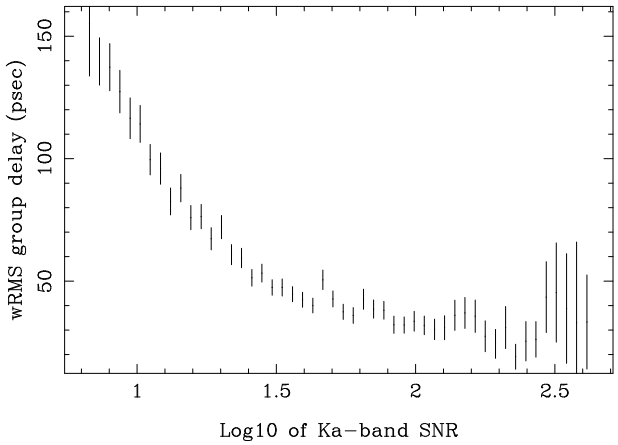

Figure 6: The wRMS residual group delay vs. the log10 of the Ka-band SNR. Note the noise floor of ≈30 psec as other error sources such as troposphere and instrumentation begin to dominate once the SNR becomes > 30.

POSTFACE

JOURNÉES 2010 SYSTÈMES DE RÉFÉRENCE SPATIO-TEMPORELS
"New challenges for reference systems and numerical standards in astronomy"
Observatoire de Paris (France), 20-22 September 2010 (dates to be confirmed)

Scientific Organizing Committee
A. Brzeziński, Poland; N. Capitaine, France (Chair); V. Dehant, Belgium; D.D. McCarthy, USA; M. Soffel, Germany; J. Souchay, France; J. Vondrák, Czech R.; Ya. Yatskiv, Ukraine

Local Organizing Committee
Chair: N. Dimarcq (SYRTE, Observatoire de Paris)

Conference location : Observatoire de Paris, Paris, France

Scientific objectives

The Journées 2010 "Systèmes de référence spatio-temporels", with the sub-title "New challenges for reference systems and numerical standards in astronomy", will be organized at Paris Observatory, from 20 to 22 September 2010 (dates to be confirmed). These Journées will be the twentieth conference in this series whose main purpose is to provide a forum for advanced discussion in the fields of space and time reference systems, Earth rotation, astrometry and time.

The Journées 2010 will be focused on the issues related to the recent developments and new challenges in astronomical space and time reference systems and their relativistic aspects, astrometric catalogs, Earth orientation, astronomical constants and numerical standards, planetary ephemerides and modern astrometry.

There will be presentations and discussions related to the IAU Working Groups, such as "Numerical Standards for Fundamental astronomy" (NSFA), or Division 1 commissions.

Scientific programme

The scientific programme of the Journées 2010 will include sessions devoted to:

Recent achievements and challenges for:
- astrometric catalogues (optical and radio)
- SI units, astronomical constants and numerical standards
- relativity and reference systems
- planetary ephemerides and their comparison
- pulsars timing and time transfer
- theory and observations of Earth orientation
- educational efforts in relativistic astrometry and celestial mechanics

Contact : Journées 2010, Nicole Capitaine, SYRTE, Observatoire de Paris,
61, avenue de l'Observatoire, 75014, Paris, France;
phone : 33 1 40 51 22 31; fax : 33 1 40 51 22 91; e-mail : n.capitaine@obspm.fr (Subject: Journees 2010)
or see the web page of the Journées 2010 at: `http://syrte.obspm.fr/journees2010/`
(that will be regularly updated)